SUPPLEMENTO

AL VOLUME II, SERIE X,

DEL

NUOVO CIMENTO

1955

(2° Semestre)

SUPPLEMENTO

AL VOLUME II, SERIE X,

DEL

NUOVO CIMENTO

A CURA DELLA SOCIETÀ ITALIANA DI FISICA

1955

2° Semestre

NICOLA ZANICHELLI EDITORE
BOLOGNA

Digitized by the Internet Archive
in 2024

https://archive.org/details/supplemento-al-nuovo-cimento_1955_2_1

SUPPLEMENTO
AL VOLUME II, SERIE X, DEL
NUOVO CIMENTO
A CURA DELLA SOCIETÀ ITALIANA DI FISICA

1955 — 2° Semestre — N. 1

QUESTO FASCICOLO

CONTENENTE

I RENDICONTI

DEL

CORSO CHE NELLA VILLA MONASTERO A VARENNA

DAL 18 LUGLIO AL 7 AGOSTO 1954

FU TENUTO A CURA

DELLA SCUOLA INTERNAZIONALE DI FISICA

DELLA SOCIETÀ ITALIANA DI FISICA

È DEDICATO ALLA MEMORIA

DI

ENRICO FERMI

RISTAMPA

SUPPLEMENTO AL VOLUME II, SERIE X
DEL NUOVO CIMENTO

N. 1, 1955
2° Semestre

INDICE

INTRODUZIONE

G. POLVANI – Discorso inaugurale . . . . . pag. 4
G. PUPPI – Prolusione . . . . . » 8

PARTE PRIMA – **Fisica delle particelle elementari.**

SEZIONE I: Questioni relative alla Fisica dei pioni e nucleoni . . . . . pag. 17

E. FERMI – Lectures on Pions and Nucleons . . . . . » 17
W. HEISENBERG – The production of Mesons in very High Energy Collisions . . . . . » 96

SEZIONE II: Questioni relative alla fotoproduzione e fenomeni connessi pag. 104

G. BERNARDINI – Lectures on Photoproduction . . . . . » 104
B. T. FELD – Photomeson Production from Hydrogen . . . . . » 139
B. T. FELD – The Photodisintegration of the Deuteron at High Energies and Associated Phenomena . . . . . » 145
S. LOKANATHAN and J. STEINBERGER – Search for the β-Decay of the Pion . . . . . » 151

SEZIONE III: Questioni riguardanti i mesoni pesanti prodotti dai raggi cosmici o dal cosmotrone. . . . . pag. 163

B. ROSSI – Lectures on Fundamental Particles . . . . . » 163
M. CECCARELLI – Results on Heavy Mesons . . . . . » 227
A. BONETTI – On the Identification of Charged Hyperons and the Establishment of Their Decay Schemes in Nuclear Emulsions . » 231
C. DILWORTH and B. ROSSI – Comparison of Results on K-Particles Disintegrating at Rest in Cloud Chambers and Photoemulsions . » 239
N. DALLAPORTA – Statistical Evidence Concerning the χ-Meson Decay » 247
A. DE BENEDETTI, C. M. GARELLI, L. TALLONE and M. VIGONE – Two Examples of a Star Emitting Two Heavy Unstable Particles » 249

E. Amaldi – On the Measurement of the Mean Life-Time of Strange Particles . . . . . pag. 253
R. Levi Setti – Unstable Fragments . . . . . » 263

Sezione IV: Questioni relative all'origine dei raggi cosmici . . . . . pag. 275

B. Rossi – Lectures on the Origin of Cosmic Rays . . . . . » 275
U. Haber-Schaim – The Energy Spectrum of the Primary Cosmic Radiation. . . . . » 336

Parte Seconda – **Progetti di macchine acceleratrici.**

Sezione I: Progetto di macchina acceleratrice per il Centro Europeo di Ricerche Nucleari . . . . . pag. 339

E. Amaldi – CERN, the European Council for Nuclear Research . . » 339
J. B. Adams – The Alternating Gradient Proton Synchrotron . . . » 355
A. Citron and M. G. Hine – Experimental Facilities of the CERN Proton Synchrotron . . . . . » 375
G. Lüders – Theory of Particle Orbits in the Alternating Gradient Synchrotron . . . . . » 392
T. G. Pickavance – Synchrocyclotrons and the CERN 600 MeV Machine . . . . . » 403

Sezione II: Progetto inglese di macchina acceleratrice . . . . . pag. 413

T. G. Pickavance – Proton Linear Accelerators for Nuclear Research and the A.E.R.E. 600 MeV Project . . . . . » 413

Sezione III: Progetto francese di macchina acceleratrice . . . . . pag. 423

H. Bruck et R. Lévi-Mandel – Sur le projet du Synchrotron à protons de Saclay . . . . . » 423

Sezione IV: Progetto italiano di macchina acceleratrice . . . . . pag. 442

G. Salvini – The Italian Design of a 1000 MeV Electronsynchrotron. A Comparisons between the Strong and the Weak Focusing . . . . . » 442
E. Persico – A Theory of the Capture in a High Energy Injected Synchrotron . . . . . » 459

Discorso inaugurale.

DI

G. POLVANI

Presidente della Società Italiana di Fisica

Un anno fa, pronunciando il discorso inaugurale del 1° Corso estivo organizzato dalla Scuola Internazionale di Fisica della nostra Società, qui a Villa Monastero a Varenna, riportavo la domanda, che molti mi avevano effettivamente rivolto e sulla bocca dei più si intuiva pronta ad essere pronunciata, se cioè quest'anno e gli anni prossimi la Scuola Internazionale di Fisica avrebbe riaperto i battenti, organizzando nuovi Corsi, rispondevo che il Consiglio di Società non avrebbe potuto non considerare senza estremo favore ed interesse, non ostante le difficoltà e le fatiche che accompagnano una siffatta impresa, il ripetersi di essa.

La cerimonia che oggi qui si svolge è la conferma della mia, del resto assai facile, previsione.

Già durante il Corso dell'anno passato si era infatti vista l'opportunità di tenere un nuovo Corso quest'anno, trattando — come più diffusamente vi dirà il Direttore del Corso, prof. PUPPI — questioni relative alla rivelazione di particelle elementari e alle loro interazioni con particolare riguardo alle particelle artificiali prodotte; ed anzi i professori POWELL, BLACKETT, che l'altr'anno furono qui come docenti, ben favorevolmente si erano espressi ed avevano sollecitato la istituzione di un secondo Corso; come questo già suggerisce e confermerà l'opportunità di tenerne un terzo per lo studio delle particelle di bassa energia.

Ma anche dal di fuori dell'ambiente ristretto della Scuola ci sono pervenute calorose sollecitazioni a proseguire in questa nostra iniziativa.

Il successo estremamente proficuo del 1° Corso è stato il nostro migliore fautore; ed io non potrei, senza mancare alla più elementare regola del dovere e senza tradire il mio sentimento, non esternare l'espressione della riconoscenza

mia e della Società a tutti coloro che l'anno passato ci aiutarono ad iniziare l'impresa dando il loro lavoro, il loro danaro e i loro mezzi, la loro dottrina, la loro saggezza e soprattutto il conforto del loro appoggio morale.

* * *

Il lavoro dell'anno passato è stato sintetizzato in un volume di *Rendiconti* di ben 310 pagine. E a loro, Eccellenza SCAGLIA, e avv. BOSISIO, che qui, intervenuti solleciti al nostro invito, impersonano con la loro autorità i due organismi, il Ministero della Pubblica Istruzione e il nuovo Ente Villa Monastero, tra i quali ha mosso i suoi primi passi la nostra pupilla Scuola Internazionale di Fisica, e nei quali si sintetizzano in sede nazionale e locale, il consenso e l'appoggio dati alla nostra impresa, giunga gradito l'omaggio di questi *Rendiconti* che a nome del Consiglio della nostra Società ho l'onore di offrire in testimonianza tangibile della nostra fatica e dell'affettuosa nostra riconoscenza.

* * *

Quest'anno il debito di riconoscenza già grave, si estende ed aumenta; e noi vogliamo qui ricordarli, questi nostri creditori cui tanto dobbiamo: molti sono ancora quelli dell'anno passato, amici fedeli, altri nuovi si sono aggiunti. E vogliamo ricordarli — se essi ce lo permettono — senza differenze di graduazione, perchè tutti ci hanno aiutato con ugual entusiasmo ed ugual cuore, permettendo così di attuare, con concordia d'animi e d'intenti, questo 2° Corso della nostra Scuola. Eccoli i nomi scritti nel grosso libro del nostro debito.

Il Ministro della Pubblica Istruzione, sua Eccellenza il prof. GAETANO MARTINO; il Presidente del Consiglio Nazionale delle Ricerche, prof. GUSTAVO COLONNETTI; il Prefetto della Provincia di Como, dott. MARIO GAIA; il Presidente del Comitato Nazionale della Fisica, prof. ELIGIO PERUCCA; il Presidente del Comitato Nazionale per le ricerche Nucleari, prof. FRANCESCO GIORDANI; il Rettore Magnifico della Università di Milano, prof. GIUSEPPE MENOTTI DE FRANCESCO; i direttori generali del Ministero della Pubblica Istruzione, dott. MARIO DI DOMIZIO, prof. ATTILIO FRAIESE, ing. MARIO PANTALEO, qui rappresentati dal dott. GARULLI e dall'ing. CAVALLI; i direttori degli Istituti di Fisica di Padova e di Milano; il Direttore dell'Istituto Nazionale di Idrobiologia, prof. VITTORIO TONOLLI; il Commissario governativo del medesimo Istituto, dott. CARLO BACCARINI; il Presidente dell'Ente Villa Monastero, avv. GIBERTO BOSISIO, che tanto a cuore ha preso questa nuova istituzione; il Presidente dell'Ente Provinciale per il Turismo nella Provincia di Como, dott. GIUSEPPE RUSSO; il Presidente dell'Unione Industriali Lecchesi, sen. PIERO AMIGONI; il Presidente della Società Radiomarelli, conte BRUNO QUINTAVALLE;

il Presidente della Società Badoni, ing. GIUSEPPE BADONI; il Presidente della Fabbrica Italiana Lampade Elettriche sig. LUIGI BUTTI; il Presidente della Società Metalgraf, cav. EGISTO BIFFI; il Presidente delle Acciaierie Caleotto, comm. ERNESTO BONAITI; il Consigliere delegato della Società Orobia, ing. ARTURO FERRARIO e l'ing. EUGENIO SOMAINI di LOMAZZO, amico sicuro dei fisici d'Italia.

A tutti che ho nominato il ringraziamento più vivo.

* * *

A nulla sarebbe valso però l'aiuto di tanti uomini se fossero mancate la fiducia, la collaborazione, anche il sacrificio degli scienziati invitati a salire sulla cattedra di questa Scuola: a tutti loro quindi, per la preziosità stessa del loro alto sapere, va una particolarmente devota parola di gratitudine.

A FERMI soprattutto, gloria della nostra terra, il quale presente nel cuore ammirato degli italiani, ha voluto accogliere, come già nel 1949, l'invito della nostra Società e sodisfare un po', con la sua presenza, la nostra nostalgia, che poi purtroppo sarà più acerba che mai.

E con lui una lunga schiera di docenti che verranno o per tenere lezioni o conferenze o seminari o discussioni, ecc.: J. B. ADAMS, M. G. HINE e G. LÜDERS del Centro Europeo Ricerche Nucleari di Ginevra; E. AMALDI, E. PERSICO dell'Università di Roma; G. BERNARDINI dell'Università di Roma, attualmente all'Università di Illinois a Urbana; A. BONETTI, C. DILWORTH e R. LEVI SETTI dell'Università di Milano; H. BRUCK e R. LÉVY-MANDEL del Commissariat à l'Énergie Atomique; M. CECCARELLI e N. DALLAPORTA dell'Università di Padova; B. T. FELD e B. ROSSI del Massachusetts Institute of Technology; C. M. GARELLI dell'Università di Torino; U. HABER-SCHAIM della Università di Berna; W. HEISENBERG dell'Università di Göttingen; L. LEPRINCE RINGUET dell'École Polytechnique di Parigi; T. G. PICKAVANCE dell'Atomic Energy Research Establishment di Harwell; G. SALVINI dell'Università di Pisa; J. STEINBERGER della Columbia University di New York. Molto probabilmente qualche altro fisico si aggiungerà a questa già lunga lista di docenti.

A loro tutti, e con loro al prof. PUPPI, dell'Università di Padova, Direttore del Corso, fedele e prezioso collaboratore, il ringraziamento più vivo della Società tutta e mio personale, al quale aggiungo, sicuro di interpretare i sentimenti degli allievi, il ringraziamento anche di questi.

I quali dovevano essere solo trenta, secondo il bando, e sono invece ben quarantacinque. Ed io, che mi sono fatto la fama di essere un po' il cerbero che ostacola l'ingresso ai soprannumerari, debbo sinceramente dichiarare che, se l'aver ricevuto un notevolissimo numero di domande di ammissione al Corso è stata ragione di sodisfazione, se l'avere aumentato notevolmente il numero

degli allievi è stato ed è gradita preoccupazione, il sapere che di molti è rimasta vana la richiesta è stata ed è tuttora per me, veramente ragione di rammarico e di angustia.

Anche quest'anno i nostri allievi provengono da tutte le parti del mondo; permettete che ve li presenti: J. L. Berthelot (proveniente da Parigi), M. Bruin (da Amsterdam), C. W. Clark (da Cambridge, USA), G. von Dardel (da Stoccolma), V. P. Duggal (da Bombay), J. Fujimoto (da Tokio), Y. Goldschmidt-Clermont (da Ginevra), U. Haber-Schaim (da Berna); J. Brizot (da Parigi), K. Kandiah (da Harwell), L. L. Kothari (da Bombay), D. Keefe (da Dublino), L. Kowarski (da Ginevra), M. Menon (da Bristol), S. C. Nassar (da Beirut), A. Orkin-Lecourtois (da Parigi), N. Porter (da Dublino), M. Reinharz (da Vienna), J. G. Röderer (da Göttingen), A. Rogozinski (da Parigi), L. Rosendorff (da Rehovoth), J. Trembley (da Parigi), G. Vanderhaege (da Bruxelles), R. Weill (da Lausanne), e ancora B. Bosco, D. Brini, B. Brunelli, C. Castagnoli, M. Ceccarelli, G. Cini, A. M. Conforto, F. Duimio, S. Jannelli, A. Lovati, A. Milone, C. Milone, S. Mora, G. Poiani, G. Quareni, O. Rimondi, A. Rossi, L. Scarsi, P. G. Sona, G. Stoppini, B. Vitale (dall'Italia).

È verosimile che altri allievi occasionali si aggiungano durante il Corso.

A tutti, maestri ed allievi il benvenuto di cuore della Società Italiana di Fisica, quello del Consiglio della Società e quello mio personale.

* * *

Un anno fa chiudevo il mio discorso inaugurale con l'augurio che gli eventi fossero alla nostra Scuola Internazionale di Fisica, così favorevoli, come favorevoli erano i voti sotto i quali essa nasceva.

Il breve passato mostra propizie le stelle del mattino. Possa la nostra Scuola pervenire a luminoso meriggio.

SUPPLEMENTO AL VOLUME II, SERIE X
DEL NUOVO CIMENTO

N. 1, 1955
2° Semestre

Prolusione.

DI

G. PUPPI

Direttore del Corso

Il contributo delle macchine acceleratrici alla Fisica delle particelle elementari.

È costume di questa Scuola che alla cerimonia ufficiale di inaugurazione il Direttore illustri le finalità del Corso che si svolgerà, e tragga spunto da questa illustrazione per informare il pubblico intervenuto dello stato della Fisica, almeno per quella parte che nel Corso verrà trattata. L'anno passato parlai del contributo dato dallo studio dei raggi cosmici alla Fisica delle particelle elementari; dirò quest'anno del contributo che ad essa hanno dato i risultati ottenuti con particelle artificialmente accelerate o prodotte con le macchine: due argomenti, quindi, e due Corsi strettamente connessi, nei quali le informazioni provenienti da entrambi i campi di indagine si uniscono e reciprocamente si completano.

L'avere organizzato due corsi successivi sulla Fisica delle particelle elementari potrebbe prestarsi a qualche critica, onde mi propongo di parlarvi delle ragioni contingenti ed obbiettive che a questo ci hanno indotto. Non si può negare, infatti, che in Italia il numero dei ricercatori che si dedicano alla Fisica delle particelle elementari è preponderante rispetto al numero di quelli che si dedicano ad altri campi della Fisica: ne può far fede l'indice del *Nuovo Cimento*. Pertanto, dovendo varare una istituzione nuova, come questa Scuola, e volendo innestarla in modo vitale nella vita scientifica nazionale, ci è sembrato opportuno iniziare con le particelle elementari. È vero, inoltre, che le nazioni europee e con esse l'Italia, sono impegnate in uno sforzo, anche economicamente non indifferente, per attrezzarsi in modo soddisfacente, sia individualmente, sia attraverso il CERN per tale tipo di Fisica, con la costruzione di una serie di grandi macchine acceleratrici di particelle, e che non si deve aspettare che le macchine funzionino per pensare

al loro impiego scientifico. Ed è vero anche, infine, che, in questo momento, per un complesso di circostanze, lavorare in particelle elementari significa più che mai, anche nel campo dei raggi cosmici, lavorare su un piano di collaborazione internazionale. Di tale collaborazione si è avuto nel 1953 un bellissimo esempio, in occasione dei voli di Sardegna per le lastre nucleari; ed il Corso tenuto l'anno passato, qui a Varenna, è appunto servito per chiarire gli obbiettivi di ricerca, unire personalmente i ricercatori, e standardizzare i metodi di misura.

Questi sono gli elementi di giudizio che ci hanno guidato nella scelta del tema dei primi due Corsi e che ugualmente guideranno nel Corso dell'anno prossimo da dedicarsi alla Fisica nucleare di bassa energia, ai modelli nucleari, alle pile. Da una parte quindi, necessità di innestarsi nel connettivo della ricerca odierna nazionale, dall'altra, di suscitare interesse, studio, discussione e fantasia su quelli che saranno i maggiori obbiettivi di ricerca dell'immediato futuro. Resta insoluto ed intoccato, il problema di fondo, se effettivamente la Fisica delle particelle elementari meriti questa posizione preminente che essa ha in effetti assunto. Per conto mio penso che si possa essere soddisfatti della semplice conferma a posteriori, indicata dal rapido sviluppo assunto dalle ricerche in questo campo. D'altra parte noi non possediamo princìpi generali di Filosofia naturale che ci dicano se altra Fisica sia più importante della Fisica delle particelle elementari. Si potrebbe però anche aggiungere, e mi sembra difficile negarlo, che tutta la Fisica deve il suo enorme e rapido sviluppo proprio allo studio delle particelle elementari, e che solo dalla conoscenza delle proprietà di queste deriva la possibilità di una chiara descrizione dei fatti macroscopici, e la possibilità di enunciare proposizioni sensate anche in fenomeni inaccessibili al nostro controllo, sia nel mondo microscopico, sia su scala universale.

Tanto per fare degli esempi, non vi è chi non ricordi che il legame chimico e il ferromagnetismo hanno atteso, per una loro descrizione soddisfacente, fino a che non è stato possibile definire le proprietà dell'elettrone, e che, solo dopo raggiunta la conoscenza delle reazioni nucleari, si è vista la possibilità di comprendere l'evoluzione delle stelle.

E aggiungerò che, per quello che è il nostro modo consueto di pensare, e fino a che questo modo si dimostrerà fecondo, il ridurre i fenomeni più complessi alle proprietà di poche particelle elementari soddisfà alla esigenza di unità e di semplicità del nostro sapere.

Ma se pure questi primi corsi sono dedicati alle particelle elementari e alla Fisica nucleare di alta, media e bassa energia, non mancheranno negli anni futuri corsi su altri argomenti. Già si è avuto quest'anno un breve convegno sulla Fisica dei solidi, sempre qui a Varenna, quasi a stabilire una ipoteca sul futuro, forse sul prossimo futuro, ed altro programmerà e farà la Società Italiana di Fisica.

Per ora accontentiamoci delle particelle elementari e più propriamente seguiamole nei fenomeni di grande energia, in quel fantastico mondo nel quale tutto si svolge in volumetti di spazio incredibilmente piccoli e in intervalli di tempo straordinariamente brevi, ma portando in gioco energie tali che, se si potessero ridurre in scala, macroscopicamente, risulterebbero spaventose.

* * *

Di che cosa più particolarmente ci occuperemo quest'anno? Quali saranno gli argomenti trattati nelle nostre lezioni e nei nostri seminari?

Un gruppo di lezioni, affidato al prof. Bruno Rossi, tratterà del problema dell'origine dei raggi cosmici e del problema delle nuove particelle instabili pesanti. Si può dire che sono questi i due grandi problemi che tengono desto l'interesse dei fisici per lo studio dei raggi cosmici. Il primo argomento va ad innestarsi nell'affascinante problema del comportamento dell'Universo, dato che, se pur il Sole ha una grande importanza per i fenomeni dei raggi cosmici, il problema della loro origine sembra non si possa porre soltanto in termini di un problema solare, ma almeno di un problema che interessi la nostra Galassia.

Il problema delle particelle instabili pesanti, che ha formato l'oggetto principale del Corso dell'anno passato, ha ricevuto nuova luce dalle esperienze di laboratorio, che solo recentemente si sono potute incominciare con le più grosse macchine acceleratrici, quelle macchine che, per le energie che sono capaci di imprimere alle particelle accelerate, si dicono bevatroni. Inoltre molti aspetti di questo problema, che interessa i nostri maggiori laboratori, hanno avuto in quest'anno notevole sviluppo. Ci è parso pertanto opportuno riprenderlo ora per un aggiornamento ed un nuovo tentativo di sintesi. Su questo argomento avremo quindi seminari e discussioni alle quali sono stati invitati ad intervenire anche diversi specialisti stranieri e italiani.

Un altro gruppo di lezioni, questo sulla Fisica dei mesoni π e dei nucleoni, sarà svolto dal prof. Fermi, mentre il prof. Bernardini ed altri tratteranno particolarmente il problema della fotoproduzione di mesoni. L'altr'anno alla Fisica dei mesoni π e dei nucleoni potemmo solo opportunamente fare qualche accenno. Quest'anno invece essa forma il tema principale del Corso, ed avrà, nella terza settimana di questo, una trattazione su base più strettamente sperimentale e tecnica, con una discussione generale sulle caratteristiche delle macchine acceleratrici in uso e in progetto, in Europa e fuori d'Europa, e sul loro modo di impiego. Anche questa parte del Corso, che si svolgerà sotto forma di lezioni, seminari e discussioni si gioverà del contributo di numerosi specialisti di fama riconosciuta.

Programma intenso, vario e, non ve lo nascondo, un poco faticoso; ma

l'alto grado di preparazione di tutti gli allievi, che qui mi piace segnalare, permetterà certo di svolgerlo integralmente.

* * *

È di questa Fisica dei nucleoni e dei mesoni π che desidero parlarvi oggi, della sua evoluzione, delle prospettive future, della sua importanza nella economia del nostro Universo e del nostro sapere.

Si parla ormai di una unica Fisica dei nucleoni e dei mesoni π perchè lo studio di queste particelle elementari e delle loro proprietà si considera come un unico problema, che si chiama problema delle forze nucleari. Almeno così, come è a noi dato oggi di intuirlo, con la limitata fantasia che possediamo nel dominio delle particelle elementari, questo problema delle forze nucleari ci sembra sostanzialmente dipendere dalle proprietà della interazione tra mesoni π e nucleoni, sebbene, come al solito, già nell'enunciare questa proposizione formuliamo una riserva mentale a proposito dei mesoni pesanti.

Come si può comprendere questo legame tra il problema delle forze nucleari e le proprietà della interazione tra mesoni π e nucleoni? Si tratta di una storia già vecchia, giudicandolo con il metro con cui la Fisica parla di vecchiezza e di attualità: una storia di circa vent'anni fa e che molti di voi conoscono. Si diceva allora che, se i princìpi generali della Fisica, stabiliti in base ai fenomeni della Meccanica e dell'Elettromagnetismo, potevano essere estesi anche ai fenomeni nucleari, allora la descrizione di questi ultimi doveva potersi ricondurre alla conoscenza delle proprietà di una particella nuova, il mesone. Il filo del discorso è presso a poco il seguente. Lo studio dell'Elettromagnetismo, della Meccanica celeste e della Meccanica in laboratorio, ci ha portati a considerare tra le leggi più generali della natura, oltre al principio di azione e reazione e al principio di inerzia, anche il principio di relatività, e a considerare, come moto campione, il moto della luce nei sistemi inerziali. Su questi princìpi, molto generali, è costruita la teoria della relatività ristretta, che è il nostro quotidiano strumento di indagine nel mondo delle particelle elementari. Ora, i fenomeni sono determinati dalle forze che agiscono tra i corpi. Di tali forze la Fisica classica conosceva solo due tipi: forze gravitazionali e forze elettromagnetiche. Le forze gravitazionali sono responsabili del moto dei corpi celesti e, in genere, del comportamento su larga scala dell'Universo. Inoltre nell'ambito della Fisica della Terra, sono responsabili del peso dei corpi, delle maree e così via. Le forze elettromagnetiche invece determinano il comportamento dell'atomo e con esso tutti i fenomeni chimici, la struttura dei solidi, l'assorbimento ed emissione della luce e così via. Per chi ama le immagini e le rispondenze tra il grande e il piccolo, potrei aggiungere che, come le forze gravitazionali nel sistema solare tengono la Terra e gli altri pianeti intorno

al Sole, così le forze elettromagnetiche tengono, nell'atomo, gli elettroni intorno al nucleo. Però non ci si può fermare qui, perchè il nucleo è un sistema complesso quanto l'atomo e anzi più ancor dell'atomo, e soggetto anch'esso, come l'atomo, i corpi, l'Universo stesso a modificazioni, a fenomeni che non si possono interpretare in base all'azione dei due tipi di forze citati.

Più precisamente voi sapete che il nucleo è formato di nucleoni, cioè protoni e neutroni, e che questi nucleoni sono tenuti insieme da forze che non sono nè gravitazionali nè elettromagnetiche. Non che questi tipi di forze non siano presenti nel nucleo, ma il comportamento di esso esige almeno un terzo tipo di forze che è stato definito appunto come « forze nucleari ».

Vediamo ora che cosa dicono i nostri princìpi generali a proposito delle forze che si esercitano, nel caso più semplice, tra coppie di corpi, siano poi esse newtoniane o coulombiane; e precisamente vediamo cosa dice a questo proposito la teoria della relatività.

Una teoria relativistica delle forze che si esercitano tra corpi non può mai contemplare un'azione istantanea a distanza, perchè le interazioni tra corpo e corpo non si possono propagare con velocità infinita: la velocità della luce nel vuoto costituisce infatti un limite superiore per la velocità di propagazione di un qualsiasi segnale.

Questo discorso deve farsi quindi anche per le forze nucleari, se i citati princìpi generali sono estendibili ai fenomeni nucleari. Come facciamo a sapere se tale estensione è valida? C'è un unico modo coerente con la metodologia scientifica che noi seguiamo, per saperlo: accettare l'estensione e verificare a posteriori le conseguenze.

Ora la costruzione di una teoria che non sia di azione a distanza, ma di campo, risolta dalla teoria di Maxwell, ha portato, per i fenomeni elettrodinamici, a considerare come veicolo essenziale delle azioni elettromagnetiche tra cariche e cariche, le onde elettromagnetiche; l'analogo problema per i fenomeni gravitazionali, risolto dalla relatività generale, porta alla previsione delle onde gravitazionali; la teoria di campo per le forze nucleari porta a prevedere le proprietà di quelle che sono state dette « onde mesoniche ». Questo in una teoria puramente classica; in una teoria quantistica questi vari tipi di onde, di veicoli cioè delle interazioni tra carica e carica, sieno esse cariche elettriche, gravitazionali o nucleari, diventano altrettanti quanti, altrettante particelle elementari: fotone, gravitone, mesone. Il fatto che fotone e gravitone abbiano massa nulla e il mesone massa diversa da zero, non costituisce per la teoria della relatività alcuna differenza di principio, ed il fatto dipende dalle caratteristiche delle forze che le dette particelle rappresentano e trasmettono tra carica e carica: a lungo raggio d'azione le prime due, a corto raggio d'azione le terze. Purtroppo, la teoria della relatività, così esplicita nell'affermazione della necessità di una teoria di campo delle forze di qualsiasi natura tra corpo e corpo, non è più di alcun aiuto per quanto riguarda la scelta del particolare tipo

di teoria di campo, tra le varie che si possono costruire, e che sono state effettivamente proposte da una ventina di anni a questa parte.

Questa scelta deve essere fatta, al solito, a posteriori, indagando quale delle possibili teorie che si possono costruire prevede, per il nucleone e per il mesone, proprietà tali che si trovino effettivamente realizzate in natura.

La cronaca dello sviluppo della Fisica nucleare nel ventennio passato, riporta entusiasmi e delusioni: fasi di ottimismo, quando qualitativamente un fatto veniva ad inquadrarsi nella previsione teorica, fasi di pessimismo quando, andando a fare i conti, ci si accorgeva che la previsione quantitativa non corrispondeva ai dati sperimentali. Anche oggi, nonostante abbiamo un già ampio panorama dei fenomeni e una lunga esperienza critica, dobbiamo essere molto prudenti nell'enunciare una qualsiasi proposizione definitiva su questo argomento.

Voi vi chiederete la ragione di questo prolungato stato di incertezza, e ve ne meraviglierete, pensando alla concentrazione di uomini e di mezzi che si è avuta per indagare questi problemi.

La ragione è che fino a pochi anni fa, prima che le grandi macchine acceleratrici entrassero in funzione, i dati sperimentali su cui si doveva ragionare derivavano in gran parte dal comportamento di sistemi estremamente complessi, come sono i nuclei; mentre le informazioni sul sistema più semplice, quello costituito da due nucleoni, erano limitate al caso di energie molto basse, e mancavano inoltre e, si può dire completamente, le informazioni sul comportamento del sistema mesone-nucleone. Ora è ovvio che, dovendo studiare le forze che si esercitano tra nucleone e nucleone e sospettando che responsabili di queste forze siano i mesoni π, è più facile avere in proposito informazioni, non da sistemi complessi, ma da sistemi semplici, nucleone-nucleone, mesone-nucleone; anche perchè, confessiamolo, l'unico problema meccanico che sappiamo risolvere rigorosamente è il problema di due corpi e questo è anche l'unico caso in cui si può, almeno a priori, sperare di fare una previsione teorica ben definita.

Ebbene, le macchine acceleratrici hanno permesso in sostanza di realizzare questo: fornendo fasci estremamente intensi di particelle, in condizioni geometriche ideali e con energia definita, esse hanno dato finalmente la possibilità di realizzare una serie di esperienze particolarmente semplici come la diffusione elastica nucleone-nucleone, quella mesone-nucleone, la produzione di mesoni per urto nucleone-nucleone e la produzione di mesoni per urto fotone-nucleone.

Queste esperienze semplici, nel senso che in esse interviene il minor numero possibile di parametri e particolarmente intense, nel senso che i dati si ricavano da numerosissimi processi elementari, permettono di costruire una descrizione fenomenologica delle forze nucleari che la teoria dovrà interpretare. Questo punto ha forse bisogno di chiarimento, perchè può non essere immediato il

comprendere come i risultati delle esperienze non si debbano immediatamente mettere a raffronto con le previsioni delle varie teorie mesoniche. In realtà questo avviene nella pratica, perchè il raffronto con la teoria può essere fruttifero solo quando si abbia già un ampio panorama dell'andamento dei fenomeni. La costruzione di una teoria fenomenologica è pertanto il primo passo nell'ordinamento dei dati dell'esperienza e in essa bisogna far uso, oltre che dei risultati sperimentali, del più ristretto numero possibile di ipotesi, perchè quando ci si muove su di un terreno che non si conosce, con mentalità e metodi stabiliti in altri domini della Fisica, è bene procedere solo con l'ausilio di poche proposizioni, molto generali e di facile controllo. Facciamo uso della meccanica relativistica e dei suoi princìpi di conservazione, ma questo non basta perchè i corpi di cui stiamo trattando, non sono puri punti materiali, ma possiedono coordinate interne. Allora si dove scoprire quali sono queste coordinate interne e quindi enunciare per esse un principio di conservazione.

I princìpi di conservazione sono, si può dire, il punto di confluenza tra una descrizione fenomenologica e una teoria formale, solo che il modo con cui vi si giunge è differente.

Una teoria formale infatti, deduce i princìpi di conservazione dalla equazione o dalle equazioni fondamentali che regolano i fenomeni sotto forma di integrali primi; una descrizione fenomenologica, che parte dai dati, cioè dai risultati della esperienza, intesa nel senso più lato, diretta o indiretta, pratica o concettuale, deve scoprire i princìpi conservativi, ricercando i parametri che descrivono i fenomeni.

La teoria fenomenologica delle forze nucleari si sta costruendo stabilmente, per la prima volta, forse solo in questi giorni, ed essa ci dice che questi nucleoni e mesoni sono degli oggetti piuttosto complessi e che oltre alla loro massa, carica elettrica e carica nucleare, spin, momento magnetico, bisogna tener conto, solo per il problema delle forze nucleari, almeno di due altre coordinate interne e cioè della parità intrinseca e dello spin isotopico e dei relativi princìpi di conservazione. Si assiste nella Fisica moderna ad uno strano dramma, che non so quali sviluppi avrà in futuro; più si riduce la descrizione della natura, cioè più si riduce il numero di particelle responsabili dei fenomeni e più crescono gli attributi di quelle, le quali, pertanto, mentre, per un certo ordine di fenomeni possono venir considerate elementari, per altri e nella realtà appaiono sistemi estremamente complessi. E sebbene il parlare di una struttura del nucleone sia prematuro, perchè non si sa cosa esattamente ciò significhi, possiamo però dire che il nucleone, che entra come elemento semplice nella descrizione del nucleo, ha già una sua Fisica ed ha già perduto la sua semplicità.

Io credo che a voi sia chiaro cosa significhi dire che il nucleone ha una massa, una carica elettrica, una carica nucleare: questo significa che due nucleoni interagiscono tra di loro sia con forze gravitazionali, sia con forze elettriche,

sia con forze nucleari. È anche noto, perchè se ne è parlato per gli elettroni, cosa significhi avere uno spin e un momento magnetico. Anche la parità è un concetto sorto dalla Fisica molecolare. Nuovo e tipico delle particelle nucleari è invece, o attualmente sembra lo sia, il concetto di spin isotopico. Entrato per via teorica nella Fisica nucleare, esso veramente sembra il parametro chiave per la costruzione della teoria fenomenològica delle interazioni tra particelle nucleari. Il mondo nucleare appare dunque veramente complicato.

Come voi sapete, dei nucleoni ve ne sono di due varietà, il protone e il neutrone, dei mesoni π ve ne sono di tre varietà, con carica elettrica rispettivamente positiva, negativa, nulla. Ora l'interrogativo che si pone è se queste cinque differenti varietà, e le molte che si possono formare combinando tra loro e nucleoni e mesoni e fotoni, hanno, nei riguardi delle interazioni nucleari, proprietà tutte distinte. In altre parole ci si può domandare se lo stato di carica elettrica dei nucleoni e dei mesoni è determinante per le interazioni nucleari. La risposta è no: protone e neutrone non hanno proprietà distinte, per quanto riguarda la interazione nucleare, ma possono veramente considerarsi come due stati di una unica particella; ed altrettanto può dirsi per i tre tipi di mesoni. Lo stato di carica elettrica è un attributo non sostanziale per le interazioni nucleari: per esse c'è solo nucleone e mesone.

Mi resta da dire in particolare qualche cosa sulle forze nucleari, che rivelano caratteristiche molto peculiari, anche nella loro versione statica. Le forze gravitazionali statiche e le forze elettrostatiche sono centrali: a definirle basta la distanza tra i due corpi interagenti. Le forze nucleari non sono certamente forze centrali: inoltre il loro comportamento in funzione della distanza tra due nucleoni è molto vario, infinitamente repulsive a piccolissima distanza, divengono fortemente attrattive a distanza dell'ordine di 10^{-13} cm per poi ridursi rapidamente a zero con l'aumentare della distanza in modo all'incirca esponènziale. I termini non statici in queste forze hanno una notevole importanza e il loro andamento con la velocità dei nucleoni è da precisare.

Con la progressiva definizione delle caratteristiche delle forze nucleari e con la costruzione della descrizione fenomenologica, viene progressivamente gettata luce anche sulla possibile teoria che in futuro renderà conto di questi fatti. Se questo futuro sia molto prossimo non sappiamo, perchè non si sa mai, nè si può prevedere a quale punto la descrizione fenomenologica permetta di intravedere la teoria finale. Alcuni risultati si sono però già avuti, ed è oggi opinione diffusa, che quanto si sa sulle forze nucleari abbia ristretto le possibili teorie mesoniche, almeno in termini di quei parametri che oggi pensiamo esauriscano la descrizione del nucleone, praticamente ad una sola. Si può forse già oggi dire che una sola versione delle teorie mesoniche, quella pseudoscalare è possibile, nel senso che le sue previsioni non sono contraddette da nessun punto essenziale della fenomenologia a noi nota. Molto diversa sarebbe la proposizione che si dovrebbe enunciare ove chiedeste se le previ-

sioni quantitative di questa teoria sono in perfetto accordo con i risultati sperimentali: questo dipende ancora troppo e in modo non facilmente valutabile, da difficoltà tecniche insite nella teoria.

* * *

E qui termino. Il mio è un prologo: ho detto dei personaggi ed ho detto del soggetto. Spero di aver suscitato in voi l'interesse per quanto si farà a questa Scuola.

Qui finisce, oggi, il mio compito.

Varenna, Villa Monastero – Gruppo di partecipanti al 2° Corso della Scuola Internazionale di Fisica della Società Italiana di Fisica.

1. M. Cresti. - 2. M. Deutschmann - 3. B. Puppi - 4. J. Steinberger - 5. N. Dallaporta - 6. I. Polvani - 7. S. C. Nassar - 8. A. Orkin-Lecourtois - 9. G. Salvini - 10. C. Castagnoli - 11. G. Poiani - 12. A. Rogozinsky - 13. J. Brizot - 14. J. Trembley - 15. M. Ceccarelli - 16. M. Porter - 17. P. Giacometti - 18. K. Kandiah - 19. G. Wataghin - 20. U. Haber-Schaim - 21. J. G. Röderer - 22. B. Locatelli - 23. K. Gottstein - 24. C. M. Garelli - 25. C. Dilworth-Occhialini - 26. Y. Fujimoto - 27. L. Tallone - 28. G. Tomasini - 29. R. Levi-Setti - 30. A. Rostagni - 31. B. Brunelli - 32. A. Borsellino - 33. G. Fidecaro - 34. P. Caldirola - 35. B. Rossi - 36. G. Polvani - 37. D. Keefe - 38. G. Cini - 39. M. G. K. Menon - 40. E. Fermi - 41. Y. Goldschmidt-Clermont - 42. M. Bruin - 43. G. Bernardini - 44. G. Puppi - 45. G. Occhialini - 46. L. Scarsi - 47. B. Vitale - 48. M. Conversi - 49. G. Quareni - A. Bonetti - 51. L. Leprince-Ringuet - 52. B. T. Feld.

sioni quantitative di questa teoria sono in perfetto accordo con i risultati sperimentali: questa dipende ancora troppo e in modo non facilmente valutabile, dalla difficoltà tecniche insite nella teoria.

E qui termino. Il mio è un prologo: ho detto dei personaggi ed ho detto del soggetto. Spero di aver suscitato in voi interesse per quanto si farà a questa Scuola.

Qui finisce, oggi, il mio compito.

Varenna, Villa Monastero – Gruppo di partecipanti al 2° Corso della Scuola Internazionale di Fisica della Società Italiana di Fisica.

PARTE PRIMA

SEZIONE I

Questioni relative alla Fisica dei pioni e nucleoni.

Lectures on Pions and Nucleons.

E. FERMI †

(Edited by B. T. FELD)

CONTENTS. – **Preface.**

A) **Isotopic spin.**
B) **Experiments Involving Pions and Nucleons.**
C) **Experiments with Polarized Nucleons.**

PREFACE

It was with considerable misgiving that I agreed to edit this set of notes, based on the lectures of ENRICO FERMI *at Varenna. The notes were originally prepared by students at the school, making liberal use of tape recordings of the lectures. Many portions are, essentially word-for-word, in the original form. This is certainly not the form in which* FERMI *would have written them for publication, for his methods of oral and of written presentation were very different. In their present form, however, they illustrate (subject to the limitations of those who transcribed and edited them) the unique qualities of* FERMI *as an expositor and teacher.*

In the hope of preserving this quality, I have tried to minimize the changes from the original notes, confining my role of editor to the occasional correction of obvious errors on the part of the transcribers and to occasional interpolations, mostly to fill in omissions on the part of the transcribers.

In working on these notes, I have been rewarded by frequently encountering sections which are so unique in their language and approach as to evoke for me, again, the picture of FERMI *as he lectured during those lovely mornings in the beautiful setting of the Villa Monastero on Lake Como. It is to be hoped that these notes have succeeded, in some small measure, in capturing the spirit of those unforgettable lectures.*

12 Feb. 1955. B. T. FELD

A) Isotopic Spin.

1. – Nucleons.

The isotopic spin notation was invented by HEISENBERG [1] in the early 30's almost immediately after the discovery of the neutron. The neutron appeared to be a particle with properties similar to those of the proton, and the idea was that they could both be described as different states of the same particle. Thus we can say that a particular nucleon, which I shall indicate by the symbol $\mathcal{N}$ can have two forms p or n, proton or neutron. The idea at this stage is purely formal and it could be adapted, though probably not fruitfully, to distinguish any two objects. As time went on, the fruitfulness of the notation became apparent, because the properties of nucleons are such that they make the notation more valuable than a purely formal device. However, just for a short time, let me pursue the purely formal consequences of this notation. We are here presented with what is usually called a dichotomic variable, i.e., a variable that can take on essentially two values. If we represent, as is usual, a function of a dichotomic variable by a vertical slot containing the two values a and b, $f = \left| \begin{matrix} a \\ b \end{matrix} \right|$, then this is a function which for the first of the variables takes the value a and for the second takes the value b.

There is in Physics a wide amount of experience as to the behaviour of these functions of dichotomic variables. They were encountered for the first time when PAULI [2] worked out the theory of the spin $\frac{1}{2}$, which is also a dichotomic variable. The state may be specified by saying that the spin is « up » or « down ». There are certain standard linear operators that operate on variables of this type, and they are essentially the Pauli operators. We may con-

---

[1] W. HEISENBERG: *Zeits. f. Phys.*, **77**, 1 (1932).
[2] W. PAULI: *Zeits. f. Phys.*, **43**, 601 (1947).

sider adding the unity operator $\begin{vmatrix} 1 & 0 \\ 0 & 1 \end{vmatrix}$ to the three Pauli operators:

$$\begin{vmatrix} 0 & 1 \\ 1 & 0 \end{vmatrix}, \quad \begin{vmatrix} 0 & -i \\ i & 0 \end{vmatrix}, \quad \begin{vmatrix} 1 & 0 \\ 0 & -1 \end{vmatrix}.$$

We then have a list of four operators which are linear and have the following property. They and their linear combinations are all the possible linear operators on any function of a dichotomic variable. Whether this is a spin, or a variable which tells us whether the particle is a proton or a neutron, makes no difference whatsoever. We shall define:

$$2\tau_1 \equiv \begin{vmatrix} 0 & 1 \\ 1 & 0 \end{vmatrix}; \quad 2\tau_2 \equiv \begin{vmatrix} 0 & -i \\ i & 0 \end{vmatrix}; \quad 2\tau_3 \equiv \begin{vmatrix} 1 & 0 \\ 0 & -1 \end{vmatrix}.$$

The factors 2 here introduced will prove convenient later.

What is, for instance, the significance of the operator $2\tau_1$, when applied to a proton p? The function which represents the proton state, is in this notation

$$p = \begin{vmatrix} 1 \\ 0 \end{vmatrix}.$$

Similarly we shall introduce another function $n = \begin{vmatrix} 0 \\ 1 \end{vmatrix}$, which defines the neutron. Now,

$$\begin{vmatrix} 0 & 1 \\ 1 & 0 \end{vmatrix} p = \begin{vmatrix} 0 & 1 \\ 1 & 0 \end{vmatrix} \begin{vmatrix} 1 \\ 0 \end{vmatrix} = \begin{vmatrix} 0 \\ 1 \end{vmatrix} = n.$$

means a linear operation with coefficients indicated by the square matrix $\begin{vmatrix} 0 & 1 \\ 1 & 0 \end{vmatrix}$ applied to the function $\begin{vmatrix} 1 \\ 0 \end{vmatrix}$ and this yields $\begin{vmatrix} 0 \\ 1 \end{vmatrix}$. So, we see that $2\tau_1$ changes p to n and, as can be shown, also changes n into p. $2\tau_1$ is thus the operator that interchanges a proton and a neutron. Similarly one can show the operational significance of the others.

Now let me consider just one application, which would make this notation worth considering even if all our problems were concerned with only a single nucleon. (To be sure, in this case, the notations would be somewhat superfluous.) Suppose we consider the operators $(\frac{1}{2} + \tau_3)$ and $(\frac{1}{2} - \tau_3)$.

(1.1)

$$\text{Now} \quad (\tfrac{1}{2} + \tau_3) = \begin{vmatrix} \frac{1}{2} & 0 \\ 0 & \frac{1}{2} \end{vmatrix} + \begin{vmatrix} \frac{1}{2} & 0 \\ 0 & -\frac{1}{2} \end{vmatrix} = \begin{vmatrix} 1 & 0 \\ 0 & 0 \end{vmatrix}$$

$$\text{therefore} \quad (\tfrac{1}{2} + \tau_3)\, p = p\,; \quad (\tfrac{1}{2} + \tau_3)\, n = 0;$$

$$\text{similarly} \quad (\tfrac{1}{2} - \tau_3) = \begin{vmatrix} \frac{1}{2} & 0 \\ 0 & \frac{1}{2} \end{vmatrix} - \begin{vmatrix} \frac{1}{2} & 0 \\ 0 & -\frac{1}{2} \end{vmatrix} = \begin{vmatrix} 0 & 0 \\ 0 & 1 \end{vmatrix}$$

$$\text{therefore} \quad (\tfrac{1}{2} - \tau_3)\, n = n\,; \quad (\tfrac{1}{2} - \tau_3)\, p = 0\,.$$

These are called projection operators.

Now consider a nucleon which may be a proton with a certain amplitude a and a neutron with a certain amplitude b, $\mathcal{N} = \begin{vmatrix} a \\ b \end{vmatrix} = ap + bn$. If we apply our operator $(\frac{1}{2} + \tau_3)$ to the wave function $ap + bn$; the result is

$$(\tfrac{1}{2} + \tau_3)(ap + bn) = ap\,.$$

In other words this operator projects out of a mixture of states, that part which is a proton. For this reason $(\frac{1}{2} + \tau_i)$ is called a projection operator. It is a projection operator for protons. Similarly $(\frac{1}{2} - \tau_i)$ is a projection operator for neutrons.

Suppose that we want to write the Hamiltonian for a nucleon without specifying whether this nucleon is a neutron or a proton. How can we do that? Let H_p and H_n be the Hamiltonians for a proton and a neutron, respectively. In a simple case, for example, they may have the form:

$$H_p = \frac{p^2}{2M_p} + U_p(x)\,, \qquad H_n = \frac{p^2}{2M_n} + U_n(x)\,. \tag{1.2}$$

In general these Hamiltonians are different because $U_n \neq U_p$ since the forces acting on a proton will be different from the forces acting on a neutron. This is seen to be true if we consider that there are, for example, electrical forces. Part of the potential may be the Coulomb potential, which leaves the neutron unaffected and acts on the proton only. The kinetic energy parts are different, too, because of the small but appreciable difference in mass of the proton and neutron.

Now our task is to write a Hamiltonian for the nucleon, valid whether the particle is a proton or a neutron, or also, in the case which at present may seem meaningless, that the particle is both a neutron and a proton. In terms of the projection operators, it is very easy to do this. Let me write as an expression for the Hamiltonian H without index for the nucleon,

$$H = H_p(\tfrac{1}{2} + \tau_3) + H_p(\tfrac{1}{2} - \tau_3) = \frac{H_p + H_n}{2} + (H_p - H_n)\tau_3\,. \tag{1.3}$$

Now I claim that this is the right Hamiltonian for the nucleon.

This can be shown as follows: The nucleon wave function is a function of the coordinates; we summarise by x not only the positional coordinates but also the spin coordinates. In addition there will be what, for the time being, I will call the charge coordinate, which specifies whether the particle is a proton or a neutron. The isotopic spin operators τ operate on functions of the charge coordinates. Such a wave function can always be written in the

following manner:

$$(1.4) \qquad \psi(x, c) = \begin{vmatrix} \psi_1(x) \\ \psi_2(x) \end{vmatrix} = \psi_1(x) \begin{vmatrix} 1 \\ 0 \end{vmatrix} + \psi_2(x) \begin{vmatrix} 0 \\ 1 \end{vmatrix} = \psi_1(x)p + \psi_2(x)n ,$$

$\psi_1(x)$ and $\psi_2(x)$ is a pair of functions of the variable x only.

After these preliminaries, let us try to decide what this Hamiltonian operator does when applied to a function of this type

$$H\{\psi_1(x)p + \psi_2(x)n\} = H_p\psi_1(x)p + H_n\psi_2(x)n .$$

Thus the effect of H on the wave function is to operate on the proton part with the Hamiltonian H_p and on the neutron part with H_n. If our wave function consists of a proton part only, then it treats it just as a proton. If the wave function consist of the neutron part only, it treats it as a neutron.

2. – The Two-Nucleon System.

Up to this point it may be only a matter of curiosity that one can write a Hamiltonian which is ready to treat any nucleon whether it is a proton or a neutron. This is purely formal, and there is no physics involved in it. Incidentally, up to this point we could have taken, for example, a proton and an electron, introduced a variable which would tell us whether the particle were a proton or an electron (two very different particles), used the same type of formalism, and written a Hamiltonian which would act correctly on a particle whether it is a proton or an electron. We may begin to see the fruitfulness of this notation if we go on to the case of two nucleons, and this is the next case we will want to investigate. Let us denote the variables related to one of the two nucleons with one prime (x', c') and to the other, with two primes (x'', c''). Similarly with the operators, $\tau'(\tau_1', \tau_2', \tau_3')$ and $\tau''(\tau_1'', \tau_2'', \tau_3'')$. The wave function of our system will be $\psi(x', x'', c', c'')$. Let us concentrate especially on the meaning involved in the various possible values of the two charge coordinates, (c', c'') which tell us whether the two particles are protons or neutrons. An immediate generalisation of what we have done in the previous case leads us to recognise that the charge possibilities of two nucleons are 4 (nn, pp, np, pn) so we see that a wave function of this kind can be written as

$$(2.1) \qquad \psi(x', x'', c', c'') = p(c')p(c'')\psi_1(x', x'') + n(c')n(c'')\psi_2(x', x'') + \\ + p(c')n(c'')\psi_3(x', x'') + n(c')p(c'')\psi_4(x', x'') .$$

In this case, then, the general wave function consists of four parts, which contain four functions of the space and spin coordinates of the two nucleons.

The next point is to try to do for two nucleons what we have done for one, namely, to write down a Hamiltonian that operates correctly on all charge possibilities. In doing this I want to begin by making a simplification; I propose to ignore the difference of the masses of proton and neutron. We shall call the common value M. This simplification is not essential but makes certain details simpler. In the Hamiltonian there will enter terms containing the potential energy. We will call the potential energy between two protons U_{pp}, and the potential energy between two neutrons U_{nn}. U_{nn} will certainly be different from U_{pp}, since, for instance, in U_{pp} there is a Coulomb part which is missing in U_{nn}. In the case that one particle is a proton and the other a neutron it is known that the simple idea of potential is not applicable because there are also exchange potentials. We know that in the nuclear force between a neutron and a proton there are essentially two terms: one that acts in a straightforward way as a potential energy term, and the other that acts as a potential energy term combined with an exchange of the two particles. In the discussion of nuclear forces one considers various types of exchange (e.g., MAJORANA: exchange of the positional coordinates leaving the spin coordinates unchanged; HEISENBERG: exchange of both position and spin coordinates). For our discussion it does not really matter what kind of exchange we consider. However, since we do not distinguish in our notation between the position and spin coordinates, it will be more convenient to use the Heisenberg exchange. We shall call the exchange operators E_x; thus

$$E_x\psi(x', x'') = \psi(x'', x') . \tag{2.2}$$

If we have two particles, of which one is a proton and one a neutron, we may write the potential U in two parts,

$$U = V + WE_x , \tag{2.3}$$

thus

$$U\psi(x', x'') = V\psi(x', x'') + W\psi(x'', x') . \tag{2.4}$$

Suppose $\psi(x', x'')$ in symmetric, i.e. $\psi(x', x'') = \psi(x'', x')$; then $U\psi = (V + W)\psi$. Or assume $\psi(x', x'')$ is anti-symmetric; then $U\psi = (V - W)\psi$.

We now note that any function can be written as a sum of a symmetric and an anti-symmetric part, as can be seen from the identity

$$\psi(x', x'') = \underbrace{\frac{\psi(x', x'') + \psi(x'', x')}{2}}_{\text{Symmetric}} + \underbrace{\frac{\psi(x', x'') - \psi(x'', x')}{2}}_{\text{Anti-symmetric}} . \tag{2.5}$$

Thus if we divide our function into symmetric and anti-symmetric parts we can write the potential in a simple way, namely

$$U_s = V + W, \qquad U_a = V - W, \tag{2.6}$$

which are the potentials to be adopted if ψ is symmetric or anti-symmetric respectively.

This leads us naturally to the discussion of the symmetry properties of the nucleon wave functions. In arriving at the symmetry properties we shall apply the Pauli Principle, which tells us that the over-all wave function is anti-symmetric, provided that all the coordinates of one nucleon are interchanged at the same time with all the coordinates of the other. We must include in this exchange also the charge coordinate c. The demand of the Pauli Principle is that an acceptable wave function changes its sign under interchange of all of its coordinates; i.e.

$$\psi(x', x'', c', c'') = -\psi(x'', x', c'', c') . \tag{2.7}$$

Using the previous expression for ψ, we obtain for the anti-symmetry condition

$$\begin{aligned} p(c')p(c'')\psi_1(x', x'') + n(c')n(c'')\psi_2(x', x'') + p(c')n(c'')\psi_3(x', x'') + \\ + n(c')p(c'')\psi_4(x', x'') = -\{p(c')p(c'')\psi_1(x'', x') + n(c')n(c'')\psi_2(x'', x') + \\ + p(c'')n(c')\psi_5(x'', x') + n(c'')p(c')\psi_4(x'', x')\} . \end{aligned} \tag{2.8}$$

This identity is required by the Pauli Principle, which is one of the best established laws of Quantum Mechanics. The conditions under which this identity is satisfied are

$$\left\{ \begin{array}{lll} a) & \psi_1(x', x'') = -\psi_1(x'', x') & \text{for the coefficients of } p(c')p(c'') , \\ b) & \psi_2(x', x'') = -\psi_2(x'', x') & \text{for the coefficients of } n(c')n(c'') , \\ c) & \psi_3(x', x'') = -\psi_4(x'', x') & \text{for the coefficients of } p(c')n(c'') , \\ d) & \psi_4(x', x'') = -\psi_3(x'', x') & \text{for the coefficients of } n(c')p(c'') . \end{array} \right. \tag{2.9}$$

This set of equations represents the complete symmetry requirement. The first two correspond to both particles being either protons or neutrons, respectively. The last two correspond to the particles being a proton and a neutron, and vice versa. The last two conditions are not immediately useful. However adding and subtracting equations c) and d), we obtain something simpler.

If we define

$$\psi_5 = \frac{1}{\sqrt{2}}(\psi_3 + \psi_4) \qquad \text{and} \qquad \psi_6 = \frac{1}{\sqrt{2}}(\psi_3 - \psi_4) , \tag{2.10}$$

it follows from the above equations that

$$\psi_5(x', x'') = -\psi_5(x'', x') \quad \text{(anti-symmetric)} \tag{2.11}$$

and

$$\psi_6(x', x'') = \psi_6(x'', x') \quad \text{(symmetric)}. \tag{2.12}$$

Now we can simplify the expression for $\psi(x', x'', c', c'')$. By substituting $\psi_3 = (1/\sqrt{2})(\psi_5 + \psi_6)$ and $\psi_4 = (1/\sqrt{2})(\psi_5 - \psi_6)$, we obtain

$$\psi(x', x'', c', c'') = pp\psi_1 + nn\psi_2 + \frac{pn + np}{\sqrt{2}}\psi_5 + \frac{pn - np}{\sqrt{2}}\psi_6\,, \tag{2.13}$$

where ψ_1, ψ_2, ψ_5 are anti-symmetric, ψ_6 is symmetric. Note that the pp, nn, and pn+np parts which are symmetric, are multiplied respectively by ψ_1, ψ_2 and ψ_5 which are anti-symmetric. In addition the pn — pn part which is anti-symmetric is multiplied by ψ_6 which is symmetric.

If the particles are two protons, then the Hamiltonian which would act on the part of the wave function containing the factor pp would be

$$H_{pp} = \frac{p'^2 + p''^2}{2M} + U_{pp}\,. \tag{2.14}$$

For the part with the factor nn the two neutron Hamiltonian,

$$H_{nn} = \frac{p'^2 + p''^2}{2M} + U_{nn}\,, \tag{2.15}$$

applies. The Hamiltonian we want to act on ψ_5 is

$$H_a = \frac{p'^2 + p''^2}{2M} + U_a \tag{2.16}$$

and the Hamiltonian we want to act on ψ_6 is

$$H_s = \frac{p'^2 + p''^2}{2M} + U_s\,. \tag{2.17}$$

All that is needed is a device for writing the general form of the Hamiltonian that automatically does the appropriate switching, namely applies to each part of the wave function the kind of Hamiltonian which is applicable to it. This requires the use of projection operators that select out of these mixtures

of charge states the various parts. It is very easy to see that the projection operator which selects pp is

$$O_{pp} = (\tfrac{1}{2} + \tau_3')(\tfrac{1}{2} + \tau_3'') . \tag{2.18}$$

Similarly

$$O_{nn} = (\tfrac{1}{2} - \tau_3')(\tfrac{1}{2} - \tau_3'') . \tag{2.19}$$

We note that $(\frac{1}{2}+\tau_3')(\frac{1}{2}-\tau_3'')$ projects out pn. But we need an operator which projects out $(pn+np)/\sqrt{2}$ and one which projects out $(pn-np)/\sqrt{2}$.

I will just write down these operators and leave the proof as an exercise. The operator which projects out the part with anti-symmetric ψ_5 is

$$O_a = \tfrac{1}{4} + \tau_1'\tau_1'' + \tau_2'\tau_2'' - \tau_3'\tau_3'' . \tag{2.20}$$

The operator which projects out the part with symmetric ψ_6 is

$$O_s = \tfrac{1}{4} - \tau_1'\tau_1'' - \tau_2'\tau_2'' - \tau_3'\tau_3'' . \tag{2.21}$$

So the Hamiltonian of 2 nucleons is

$$H = H_{pp}O_{pp} + H_{nn}O_{nn} + H_aO_a + H_sO_s . \tag{2.22}$$

The only physical condition which has been introduced so far (aside from the Pauli Principle) has been the near equality of the masses of neutron and proton. Now we shall introduce the physical principle of the charge independence of nuclear forces. We shall postulate that the forces between two protons or two neutrons or also between a proton and a neutron are the same, provided in the latter case that the wave function of the two nucleons is of the anti-symmetric type $\psi_a(x', x'')$. This assumption is supported to some extent by experiment. The only major difference that is known to exist among these forces is the Coulomb force, which in many nuclear phenomena, especially in light nuclei, plays only a secondary role. Thus we have

$$H_{pp} = H_{nn} = H_a . \tag{2.23}$$

In the other Hamiltonian, H_s, the potential energy is unmistakably different. The potential that corresponds to an antisymmetric state observed, for example, in the virtual state of the deuteron, is about 10 MeV; the potential that corresponds to the symmetric state, the state of the bound deuteron, is about 20 MeV. So the difference between the two potentials is about a factor of 2.

The Hamiltonian can then be written

$$H = H_a(O_{pp} + O_{nn} + O_a) + H_s O_s \tag{2.24}$$

and if we put in the projection operators this becomes

$$H = H_a\left(\frac{3}{4} + \tau' \cdot \tau''\right) + H_s\left(\frac{1}{4} - \tau' \cdot \tau''\right) = \frac{3H_a + H_s}{4} + (H_a - H_s)\tau' \cdot \tau'', \tag{2.25}$$

where we have put

$$\tau' \cdot \tau'' = \tau_1' \tau_1'' + \tau_2' \tau_2'' + \tau_3' \tau_3''. \tag{2.26}$$

The first part is independent of the charge operators; the second term involves the analogue of the scalar product $\tau' \cdot \tau''$ which is a scalar not in ordinary space but corresponds to a scalar with respect to an orthogonal transformation of the axes 1, 2, and 3 of the charge space. Many consequences derive from this invariant structure of the Hamiltonian with respect to rotations in charge space. eq. (2.25) is an approximation because we have neglected the Coulomb forces.

τ for a nucleon is compounded of $\tau_1 \tau_2 \tau_3$ which are the Pauli operators apart from a factor 2. These operators were introduced to represent the spin angular momentum; as such, they obey the angular momentum commutation rules and have all the formal properties of the angular momentum. So we may say that, as regards their mathematical properties, $\tau_1' \ldots \tau_3''$ obey all the same rules as the angular momentum components. But the three directions labeled 1, 2 and 3 are now not three directions in ordinary space, but in a fictitious space which we can call charge space or isotopic spin space.

The properties of angular momentum in ordinary space can be adapted then to the properties in this I.S. space. For example τ is a vector in charge space and in the same way one may define the scalar product of two vectors for 2 nucleons $\tau' \cdot \tau''$ and their sum $\boldsymbol{T} \quad \tau' + \tau''$, $\boldsymbol{T}$ beeing called the total isotopic spin of the system. With respect to changes of the coordinate system in I.S. space (e.g. rigid rotations) the Hamiltonian (2.25) is invariant, i.e. it is a scalar. Then the total isotopic spin and its components will be constants of motion, in the same sense as the angular momentum vector is a constant of motion when the Hamiltonian is invariant under rotation in ordinary space. Further $\tau_1 \tau_2 \tau_3$, in the same manner as the Pauli spin operators, obey the following commutation rules:

$$\begin{cases} \tau' \wedge \tau' = i\tau', \\ \tau'' \wedge \tau'' = i\tau'', \\ \boldsymbol{T} \wedge \boldsymbol{T} = i\boldsymbol{T}. \end{cases} \tag{2.27}$$

Making use of (2.27) one finds that the following operators commute with the Hamiltonian: T_1, T_2, T_3, T^2; thus

$$[HT_1] = 0\,, \quad [HT_2] = 0\,, \quad [HT_3] = 0\,, \quad [HT^2] = 0 \tag{2.28}$$

and so T_1, T_2, T_3, T^2 are constants of the motion.

Since the same formal considerations apply and since H is a scalar, the properties of ordinary angular momentum can be applied to the isotopic spin dependence of the two nucleon wave function. One can choose a diagonal representation of T^2 and T_3, where

$$\begin{cases} T^2_{\text{op}} = T\,(T+1) \\ T_{3\text{op}} = T,\ T-1,\ \ldots - T \end{cases} \quad (T = \text{integer or half-integer}). \tag{2.29}$$

As in the case of the angular momentum for a system of 2 electrons, T then takes the values 0, 1. Another property which also follows is that all states of constant T should have the same energy and, in fact, are the same state viewed from different directions in I.S. space.

Before leaving the 2-nucleon system, we discuss a correction to the scheme of charge independence which indicates where this scheme is defective. One can write down immediately one term, at least, which has been neglected and must be added to the Hamiltonian (2.25). This term describes the coulomb interaction and will, of course, be present only if both nucleons are protons. This additional term may be expressed as

$$+\frac{e^2}{r}\,O_{\text{pp}}\,,$$

where e^2/r is the Coulomb energy of the two charges and the projection operator O_{pp} is that defined in Eq. (2.18), which selects the case in which both nucleons are protons. Writing it out, we obtain the following additional term to the Hamiltonian (2.25)

$$\frac{e^2}{r}\,O_{\text{pp}} = \frac{e^2}{r}\left\{\frac{1}{4} + \frac{\tau_3' + \tau_3''}{2} + \tau_3'\tau_3''\right\}. \tag{2.30}$$

The new Hamiltonian is no longer an isotopic scalar invariant. Considering the commutators of H with the components of the total isotopic spin vector it is clear that

$$[HT_1] \neq 0\,, \qquad [HT_2] \neq 0\,,$$

but even in this case $[HT_3] = 0$ (charge conservation), since $T_3 = \tau_3' + \tau_3''$ commutes with all the terms in the new Hamiltonian.

3. – The Many-Nucleon System.

The generalization to a system of many nucleons is a straight-forward extension of the previous considerations. Consider a collection of A nucleons, all of which have their associated isotopic spin vectors $\boldsymbol{T}^{(1)}$, $\boldsymbol{T}^{(2)}$, ..., $\boldsymbol{T}^{(A)}$. As regards the Hamiltonian, we do not know very much even about 2 nucleons let alone about a many-nucleon system. For example, 3-body forces may well play a large part. As in the case of 2 nucleons we will postulate that the Hamiltonian for A nucleons is also invariant under rotation in I.S. space, i.e. a scalar. Then the total isotopic spin vector,

$$\boldsymbol{T} = \boldsymbol{T}^{(1)} + \boldsymbol{T}^{(2)} \ldots + \boldsymbol{T}^{(A)}\,, \tag{3.1}$$

will have all the properties of an angular momentum vector and will be a constant of the motion.

The charge operator which in the case of a single nucleon has the form $(\frac{1}{2}+\tau_i)$ and the eigen-values 1 (proton) and 0 (neutron) may be extended to the present system, if one defines the charge operator of a nucleus as the sum of the charge operators of all the nucleons:

$$Q = \sum_{j=1}^{A}\left(\frac{1}{2} + \tau_3^{(j)}\right) = \frac{A}{2} + T_3\,. \tag{3.2}$$

Since the charge of the nucleus and the number of nucleons are both constant it follows that T_3 must remain constant. For this reason T_3 is a true constant of the motion. The other isotopic spin components are only approximately constants of the motion. In this respect T_3 has a special position that has no analogue for angular momentum vectors for which all components are essentially equivalent.

Next, one may classify states of the nucleus in isotopic spin multiplets. The possible values of T are

$$T = \begin{cases} A/2 \\ \vdots \\ 0 \end{cases}, \quad A \text{ even}, \qquad T = \begin{cases} A/2 \\ \vdots \\ \frac{1}{2} \end{cases}, \quad A \text{ odd}. \tag{3.3}$$

Each state of the system of nucleons may be characterised by a particular value of T and for a chosen value of T the possible values of T_3 are then T, $T-1$, ... $-T$. For example in the case of $T=1$, T_3 may have the values 1, 0, -1, forming an isotopic spin triplet composed of 3 neighbouring isobars with respective charges $(A/2)+1$, $A/2$, and $(A/2)-1$. For $T=\frac{1}{2}$ there occurs an isotopic spin doublet.

One of the first doublets to be recognised was the $^7Li_3 - {}^7Be_4$ pair:

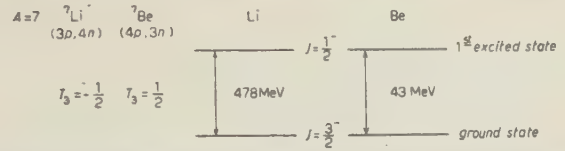

Fig. 1. – The energies and angular momenta of the ground and first excited states of the ^7Li-^7Be isotopic spin doublets.

The ground states of these nuclei are in fact closely similar (neglecting correction terms such as that due to the Coulomb potential) while the first excited states of these nuclei form another well known I.S. doublet.

Before leaving this question of I.S. as applied to a nucleus, it is interesting to remark that many reactions (e.g. α-particle emission) which, on grounds of energy, angular momentum, and parity, one would expect to occur strongly, often take place very slowly. This is frequently due to the fact that isotopic spin is not conserved in these reactions.

4. – Systems Containing Nucleons and π-Mesons.

The possible values for the isotopic spin of the pion can be obtained from the basic Yukawa reaction

$$\mathcal{N} \rightleftarrows \mathcal{N} + \pi \,. \tag{4.1}$$

We assume that isotopic spin is conserved in this reaction. From the fact that $\mathcal{N}$ has isotopic spin $\frac{1}{2}$ it follows from the usual rules for the addition of angular momentum vectors that the pion can have only either $T = 1$ or $T = 0$. The fact that the pion is known to exist in three charge states, positive, neutral and negative, which behave like an isotopic triplet, suggests that the choice for the pion must be $T = 1$.

Observe that the relationship between the charge operator for a pion and a nucleon is different. For a pion T_3 gives directly the charge without the addition of the $\frac{1}{2}$ term:

$$\text{meson charge} = T_3 = \begin{cases} +1 & \text{for } \pi^+ \\ 0 & \text{» } \pi^0 \\ -1 & \text{» } \pi^- \end{cases} \tag{4.2}$$

Then for a system of A nucleons and B pions the total charge is

$$\sum_{A \text{ nucleons}} \left(\frac{1}{2} + \tau_3\right) + \sum_{B \text{ pions}} \tau_3 = \frac{A}{2} + T_3 \,, \tag{4.3}$$

where T_3 is the 3-rd component of the total I.S. of the system and is again conserved since both the charge and the number of nucleons are constant.

We now introduce the postulate that even for a system of nucleons and pions the Hamiltonian is approximately a scalar invariant in charge space. As for the case of nucleons only, this hypothesis will apply only if the Coulomb forces are neglected and the mass differences between proton and neutron on the one hand and charged and neutral pions on the other are also neglected.

From this postulate it follows that the resultant isotopic spin (i.e. its three components and its magnitude) are time constants and have in addition all the formal properties of angular momentum vectors.

We consider a system composed of a nucleon and a pion: $(\mathcal{N}, \pi)$. We have already seen that for a nucleon $\tau(\mathcal{N}) = \frac{1}{2}$ and for a pion $\tau(\pi) = 1$.

The total isotopic spin T can then take on the two values

$$T = \tfrac{3}{2}\,, \qquad T = \tfrac{1}{2}\,.$$

The following notation will be used for charge states:

$$\mathrm{n}^+ \quad \text{means} \quad \mathrm{n} + \pi^+, \quad \text{etc.}$$

So we have six possible charge states:

$$\mathrm{p}^+, \quad \mathrm{p}^0, \quad \mathrm{p}^-, \quad \mathrm{n}^+, \quad \mathrm{n}^0, \quad \mathrm{n}^-,$$

that we shall call « physical charge states », directly accessible to observation. [Remember, for analogy, that a given combination of an orbital and spin angular momentum forms a mixture of states of the different possible total angular momenta].

We use the function χ_3 as indicating a state with $T = \frac{3}{2}$, and in order to fix the charge state we use the superscript $(2T_3)$ on it.

For $T = \frac{3}{2}$

$$T_3 = \begin{cases} \frac{3}{2} \\ \frac{1}{2} \\ -\frac{1}{2} \\ -\frac{3}{2} \end{cases} \qquad \text{charge} = \frac{A}{2} + T_3 = \begin{cases} 2 \\ 1 \\ 0 \\ -1 \end{cases} \tag{4.4}$$

we obtain four functions

$$\chi_3^{(3)}, \quad \chi_3^{(1)}, \quad \chi_3^{(-1)}, \quad \chi_3^{(-3)}.$$

$\chi_{2T}^{2T_3}$ in general is the wave function corresponding to isotopic spin T and charge-state T_3 .

The wave functions for the case of a nucleon and a pion are as follows:

$$
\begin{array}{lll}
 & T=\frac{3}{2} & T=\frac{1}{2} \\
(4.5)\quad \left\{\begin{array}{ll} (a) & \chi_3^{(3)}=p^+ \\ (b) & \chi_3^{(1)}=\sqrt{\frac{2}{3}}\,p^0+\sqrt{\frac{1}{3}}\,n^+ \\ (c) & \chi_3^{(-1)}=\sqrt{\frac{2}{3}}\,n^0+\sqrt{\frac{1}{3}}\,p^- \\ (d) & \chi_3^{(-3)}=n^- \end{array}\right. & \begin{array}{ll} (e) & \chi_1^{(1)}=\sqrt{\frac{1}{3}}\,p^0-\sqrt{\frac{2}{3}}\,n^+ \\ (f) & \chi_1^{(-1)}=-\sqrt{\frac{1}{3}}\,n^0+\sqrt{\frac{2}{3}}\,p^- \end{array}
\end{array}
$$

The coefficients of combination here used are the Clebsch-Gordon coefficients. The χ's are all orthogonal.

We can experimentally realise a final state of $T=\frac{3}{2}$ by the bombardment of hydrogen by π^+, and, in principle, it is possible to obtain in a similar way the $T=\frac{3}{2}$ state as an n^- state. The $T=\frac{1}{2}$ state, however, cannot be obtained in a pure form in any single nucleon-meson combination.

B) Experiments Involving Pions and Nucleons.

5. – Meson-Nucleon Scattering.

Let us now introduce the scattering amplitudes S_3 and S_1, corresponding to scattering in the different isotopic spin states, in the following way

$$
(5.1)\qquad \left\{\begin{array}{l} e^{ikz}\,\chi_1 \to S_1\chi_1 \\ e^{ikz}\,\chi_3 \to S_3\,\chi_3\,, \end{array}\right.
$$

where there first terms correspond to initial (plane wave incident pion) states, and the others to final (scattered pion) states.

In the scattering of positive pions on protons only the charge state p^+ is involved. Therefore the amplitude for this case is S_3.

For the case of π^- scattered by protons the initial state is a mixture of $\chi_3^{(-1)}$ and $\chi_1^{(-1)}$.

From (*c*) and (*f*) of (4.5) we have the following expressions

$$
(5.2)\qquad \left\{\begin{array}{l} n^0=\sqrt{\frac{2}{3}}\,\chi_3^{(-1)}-\sqrt{\frac{1}{3}}\,\chi_1^{(-1)}\,, \\ p^-=\sqrt{\frac{1}{3}}\,\chi_3^{(-1)}+\sqrt{\frac{2}{3}}\,\chi_1^{(-1)}\,. \end{array}\right.
$$

So we can write (omitting the common upper index -1)

$$(5.3)\quad (p^-)\exp[ikz] = \sqrt{\tfrac{1}{3}}\chi_3 \exp[ikz] + \sqrt{\tfrac{2}{3}}\chi_1 \exp[ikz] \to \sqrt{\tfrac{1}{3}}\chi_3 S_3 + \sqrt{\tfrac{2}{3}}\chi_1 S_1 =$$
$$= \sqrt{\tfrac{1}{3}}(\sqrt{\tfrac{2}{3}}\, n^0 + \sqrt{\tfrac{1}{3}}\, p^-)\, S_3 + \sqrt{\tfrac{2}{3}}\,(-\sqrt{\tfrac{1}{3}}\, n^0 + \sqrt{\tfrac{2}{3}}\, p^-)\, S_1 =$$
$$= n^0 \sqrt{2}\ (S_3 - S_1)/3 + p^-(S_3 + 2S_1)/3\,.$$

In this relation the first term describes the charge exchange scattering and the second one the elastic scattering.

At present it is experimentally possible to bombard protons with positive and negative pions. For instance, the cyclotron of Chicago accelerates protons to an energy of 460 MeV. These strike a Be target, producing positive and negative pions. (A Be target is particularly suitable for obtaining pions.)

About 10% of the protons colliding with the target give rise to nuclear collisions, and only a few percent of these collisions give pions. The number of these is of the order of $10^{10} \div 10^{11}$ s^{-1}.

In the collisions neutral pions are also produced, but these decay within $\sim 10^{-14}$ s, and their disintegration products can be eliminated before reaching the measuring devices.

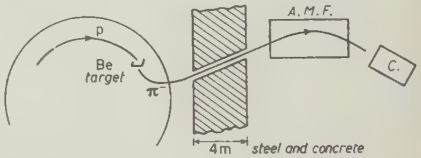

Fig. 2. – Schematic diagram of the method for producing negative pion beams at the University of Chicago synchrocyclotron.

Negative pions are deviated by the magnetic field of the cyclotron, pass through a hole in a shield of 4 m concrete and steel, then are purified, before reaching the measuring equipment, by an auxiliary magnetic field (A.M.F.), as shown in Fig. 2.

Positive pions are obtained in a rather similar way by reversing the magnetic field of the cyclotron, but in this case it is not possible to reach the same intensity and energy as for negative pions since the pions observed are those emitted in the backward direction.

The techniques of observations use counters, diffusion cloud chambers and photographic plates.

A typical arrangement with scintillation counters is shown in Fig. 3.

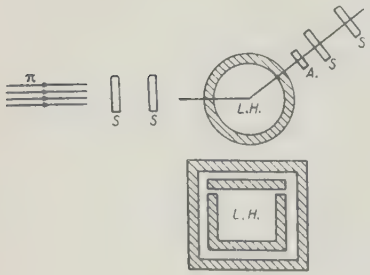

Fig. 3. – A typical arrangement for the observation of pion scattering from protons.

L.H., Liquid hydrogen; *S*, Scintillation counters; *A*, Anticoincidence, used when one wants to discriminate photons from charged pions. A convenient liquid hydrogen container can be made from styrofoam, having a specific gravity of only 0,03 and very easy to machine.

The beam of pions is not really pure, because there is always a rather large contamination of muons; but these are readily distinguished, as they have, for the same magnetic rigidity, a different range from the pions. This also applies to the electron component that is sometimes present.

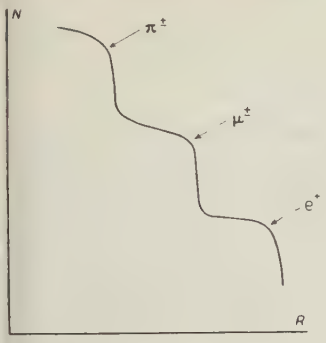

Fig. 4. – Counting rate vs. absorber thickness for a « pion » beam. The heights of the steps are proportional to the amounts of the various components in the beam.

If we plot in a diagram the intensity of the beam as a function of absorber thickness, R, we obtain a curve like the one shown in Fig 4, which enables us to determine the amount of contamination in the beam.

Photographic plates are also a convenient means of detection: they have a concentration of hydrogen comparable to that in liquid hydrogen. The technique used is that of « area scanning » to find events like that shown in Fig. 5.

At the place where one observes this event it is possible that one has a case of pion-proton scattering. One then tests the coplanarity and the relationship between the angles α, β.

One may also use in these measurements a hydrogen filled diffusion cloud chamber, which has the advantage that it contains only hydrogen.

Bubble chambers are being developed now, and this technique too is very promising. Good tracks have been obtained by HILDEBRAND in Chicago, using pentane in the bubble chamber.

The three scattering processes shown in column 1 of Table I can be directly investigated experimentally. Now, we have seen that the scattering amplitudes of these three processes are expressible in terms of S_3 and S_1; the amplitudes for scattering in the states with isotopic spin $T=\frac{3}{2}$ and $\frac{1}{2}$, respectively, are shown in Table I.

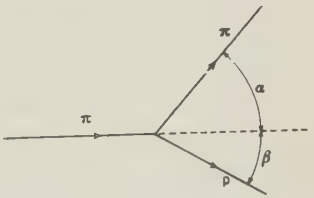

Fig. 5. – An event observed in a photographic emulsion which could correspond to a pion-proton scattering.

TABLE I. – *Scattering amplitudes for the possible processes involving charged mesons on hydrogen.*

Process	Amplitude
$p^+ \to p^+$	S_3
$p^- \to p^-$	$\frac{1}{3} S_3 + \frac{2}{3} S_1$
$p^- \to n^0$	$(\sqrt{2}/3)(S_3 - S_1)$

The process $p^+ \to p^+$ is controlled directly by the amplitude S_3, because p^+ is a pure state of $T=\frac{3}{2}$. Since p^- and n^0 are mixtures of the states $T=\frac{3}{2}$ and $\frac{1}{2}$, the amplitude $((S_3/3)+(2S_1/3))$ describes the elastic scattering of negative pions by protons and the amplitude $(\sqrt{2}/3)(S_3 - S_1)$ describes the charge-exchange scattering. So in order to complete the scattering analysis and to find the cross-sections, it is necessary to obtain expressions for S_1 and S_3.

The expressions that we will arrive at for S_3 and S_1 are, however, obtained under the simplifying assumption that only s and p states are present. There is much discussion of the legitimacy of this assumption but it seems fairly clear that at sufficiently low energy this approximation should by justified.

In principle the waves of increasing angular momentum make contributions to the scattering which vary with increasing powers of the momentum; so, at sufficiently low energy one might say that the s-state should dominate and that only at somewhat higher energy the p-state will contribute significantly. At still higher energies one expects the d-wave and higher angular momentum states to become increasingly important.

We will see that there is good evidence that the interaction in the p-state is abnormally strong, so there is perhaps some point in including both s- and p-states in the analysis. One of course hopes that the d-state will not yet contribute appreciably at the energies of interest, not only because this is in accordance with the general sequence of importance of the various terms, but also because there is no reason to suspect that the interaction in the d-state is intrinsically as strong as that in the p-state.

Now if we make this assumption, the problem of expressing S_1 and S_3 becomes a rather conventional problem of collision theory in which all effects are interpreted in terms of phase shifts.

The only complication which remains to be taken into account is the spin of the nucleon; for example, S_3 should be labelled by another index indicating the direction of the spin of the nucleon in the initial state. We shall consider the scattering of a pion wave which is incident along the z-direction. The target nucleon may have its spin parallel or anti-parallel to this direction. We shall distinguish these two possibilities by means of superscripts α, β, corresponding to spin up and spin down, respectively. So instead of only S_3, we now need the expressions for S_3^α and S_3^β.

Next let us introduce the phase shifts for the various angular momentum states. In the case of the s-state the resultant angular momentum is controlled by the spin of the nucleon only and thus there occurs only one angular momentum state, that with $J=\frac{1}{2}$. For p-states, on the other hand, the spin of the nucleon may be parallel or anti-parallel to the orbital angular momentum $l=1$ of the p-wave, giving two possibilities, namely $J=\frac{1}{2}, \frac{3}{2}$, as in ordinary doublet states. Therefore we have three different states, differing in orbital and total angular momentum, to each of which we must assign

a phase shift. This number of states must be doubled when one considers that we are dealing with two possible values of the isotopic spin. Altogether, then, we have the six combinations of three possible angular momentum states and two possible charge states. The corresponding phase shifts are also six, and the notation usually adopted for them is shown in Table II.

TABLE II. – *Notation adopted for the scattering phase shifts, assuming s- and p-wave scattering only.*

	$s_{\frac{1}{2}}$	$p_{\frac{1}{2}}$	$p_{\frac{3}{2}}$
$T = \frac{3}{2}$	α_3	α_{31}	α_{33}
$T = \frac{1}{2}$	α_1	α_{11}	α_{13}

We expect that all scattering phenomena in a certain low energy range will be described by the set of these six α's. In particular S_3 will be described in terms of α_3, α_{31} and α_{33} and S_1 in terms of α_1, α_{13} and α_{11}. The expressions for S_3^α and S_3^β are the following:

$$\begin{pmatrix} S_3^\alpha \\ S_3^\beta \end{pmatrix} = \frac{\exp[ikr]}{kr} \cdot \left[\left\{ e_3 + (2e_{33} + e_{31}) \cos\theta \right\} \begin{pmatrix} \alpha \\ \beta \end{pmatrix} \pm (e_{31} - e_{33}) \sin\theta \exp[\pm i\varphi] \begin{pmatrix} \beta \\ \alpha \end{pmatrix} \right], \tag{5.4}$$

where e^{ikr}/kr describes the outgoing spherical wave, while the e's are the following quantities:

$$\begin{cases} e_{31} = \exp[2i\alpha_{31}] - 1 , \\ e_{33} = \exp[2i\alpha_{33}] - 1 , \\ e_3 = \exp[2i\alpha_3] - 1 . \end{cases} \tag{5.5}$$

The first term of (5.4) corresponds to no spin-flip, and the second to spin-flip. The expressions for S_1^α and S_1^β are the same, except that in place of e_{31} we must write e_{11}, and so forth.

We can obtain the intensity of the scattered wave by taking the square modulus of the coefficient in (5.4) of the term corresponding to one spin direction, and adding to it the square modulus of the coefficient for the other spin direction. So we have one term independent of the angle θ, another proportional to $\cos\theta$, another to $\cos^2\theta$. We are thus led to an angular distribution of the type

$$\frac{d\sigma}{d\Omega} = a + b\cos\theta + c\cos^2\theta . \tag{5.6}$$

If we had included, for example, d-states but no higher angular momentum states, then terms in $\cos^3\theta$ and $\cos^4\theta$ would have appeared in (5.6). In general each additional angular momentun state considered will result in the introduction of two further terms in this expansion in powers of $\cos\theta$.

There is a further complication which has been neglected in the above discussion of the scattering in s- and p-states. This is the perturbation due to the Coulomb scattering, resulting in an interference with the pure nuclear scattering. Let us consider the $p^+ \to p^+$ scattering as a simple example in which we are not troubled with the complication of charge exchange scattering. Suppose for a moment that we could switch on and off alternatively either the Coulomb force or the purely nuclear interaction. When we have only the Coulomb interaction, we get Rutherford scattering. This has an extremely large cross-section at small angles but decreases very rapidly, as the fourth power of the angle θ. Therefore $(\mathrm{d}\sigma/\mathrm{d}\Omega)_{\text{Coulomb}}$ is very important in the forward direction and becomes practically negligible at angles greater than say, 30° or 40°.

Now the question arises as to the effect of interference when both modes of scattering occur. The exact formula has been obtained by VAN HOVE [3], but the effect can be demonstrated in good approximation by the following considerations: we shall split $(\mathrm{d}\sigma/\mathrm{d}\Omega)$ into two nuclear parts, $(\mathrm{d}\sigma/\mathrm{d}\Omega)_1$ which is coherent with the Coulomb scattering and $(\mathrm{d}\sigma/\mathrm{d}\Omega)_2$ which is incoherent.

Then since the cross-section is proportional to the square of the amplitude, we have,

$$\frac{\mathrm{d}\sigma}{\mathrm{d}\Omega} = \left[\sqrt{\left(\frac{\mathrm{d}\sigma}{\mathrm{d}\Omega}\right)_1} + \sqrt{\left(\frac{\mathrm{d}\sigma}{\mathrm{d}\Omega}\right)_{\text{Coulomb}}}\right]^2 + \left[\sqrt{\left(\frac{\mathrm{d}\sigma}{\mathrm{d}\Omega}\right)_2}\right]^2. \tag{5.7}$$

The coherent part of the amplitude $\sqrt{(\mathrm{d}\sigma/\mathrm{d}\Omega)_1}$ corresponds to « no spin-flip » of the nucleon, while the incoherent part $\sqrt{(\mathrm{d}\sigma/\mathrm{d}\Omega)_2}$ corresponds to « spin-flip », because in Coulomb scattering it is known that the major contribution arises from the « no spin-flip » process. The interference of nuclear and Coulomb scattering may be positive or negative depending on the sign of the amplitude of nuclear scattering and this enables one to determine this sign, as we shall see later.

Forgetting for the moment the effects of the Coulomb forces, which in most cases are a minor correction, we can make the comparison with experiment. Many experiments of the type in which we are interested, e.g.

$$p^+ \to p^+, \qquad p^- \to p^- \qquad \text{and} \qquad p^- \to n^0,$$

have been carried out at a variety of energies.

---

[3] L. VAN HOVE: *Phys. Rev.*, **88**, 1358 (1952).

The angular distributions in these reactions have been studied separately and each has been fitted by an expansion of the form $a+b\cos\theta+c\cos^2\theta$. The experimental results therefore yield, essentially, sets of quantities a^+, b^+, c^+ obtained from the angular distribution in the $p^+ \to p^+$ reaction; a^-, b^-, c^- from that of $p^- \to p^-$, and a^0, b^0, c^0 from the charge exchange scattering $p^- \to n^0$. These nine quantities constitute the maximum information that experiment can give provided of course that the assumed formula is correct. There have been many attempts to determine whether the contribution from higher angular momentum states appears in a significant way, especially at high energies. But so far, because of rather limited experimental accuracy, it has been impossible to draw any significant conclusion. Therefore we may say that even if higher angular momentum terms are present, they are too small to be observed at present.

For this reason I propose to ignore such terms, so that at each energy, the experimental distributions give us the value of the nine quantities a^+, b^+, c^+, etc.. To determine the six phase shifts α_3, α_1, α_{33}, ..., from the nine experimental coefficients is an overdetermined problem, which has a solution, provided that the theory is correct. Of course it could be solved within the experimental error, which is quite large, even if there where some appreciable deviation from isotopic spin conservation.

The method we could adopt is, for example, to consider first only the data on negative pion scattering. In other words, consider only the six coefficients a^-, b^-, c^-, a^0, b^0, c^0, and from them determine the six phase shifts. Then we can compute the coefficients a^+, b^+, and c^+ of the positive pion scattering and compare them with the direct measurements. This is, in a certain sense, an honest way of checking the theory, and it turns out to work fairly well. But there are unfortunately various ambiguities which are of the following kind. Suppose I follow this scheme, and try to solve the six equations for the six unknown quantities. Then I find a number of solutions, all of which give very similar values for the p^+ coefficients a^+, b^+, c^+, so that this procedure does not appear to yield a unique solution.

As long as the Coulomb scattering is neglected there is, in particular, the ambiguity that a change of sign of all phase shifts does not change the angular distribution. It is especially in this respect that the Coulomb forces are important. Because the Coulomb scattering is well known and completly understood, one has the possibility of determining the sign of the nuclear phase shifts by observing the sign of the interference term. This has been done to some extent by many people. I cannot say that the results which have been obtained on this point are final. But they warrant the conclusion that the probability, that the signs that I am going to give are correct, is perhaps 90%. I am now going to present a set of phase shifts that is compatible with the experimental data. It is not by any means the only solution but is the one

which, for a variety of reasons, appears at present to be the most probable.

These solutions were first published by GLICKSMAN (4) and are obtained by assuming that only α_3, α_1 and α_{33} are different from 0. This rather drastic assumption is perhaps not quite justified but yields a very simple fit of the experiments. With this simplification GLICKSMAN found that α_{33} is approximately proportional to η^3 (*).

The coefficient of η^3 is not quite constant but ranges from 0.26 radians at low energy to 0.31 at higher energy. This expression becomes equal to 90°, which is the conventional definition of a resonance, at about $\eta=1.7$, corresponding to a laboratory energy a little below 200 MeV.

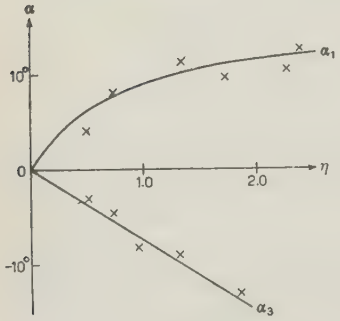

Fig. 6. – Experimental s-wave phase shifts as a function of $\eta = p/\mu c$ of the pion in the c.m.s.

The experimental evidence concerning the phase shifts α_3 and α_1 is a bit confused. The experimental points are shown in Fig. 6 with « reasonable » curves drawn through them.

Previous indications, reported at the Rochester conference in 1953 (5), appeared to indicate that α_3 could be positive at very low energy and become negative at somewhat higher energies. However, more recent data seem to favor the simpler solution shown in Fig. 6.

OREAR (6) has collected all pertinent data at low energy and proposes the following formulas for α_3 and α_1 at low energy:

$$\begin{cases} \alpha_3 = -.11\eta\,, \\ \alpha_1 = +.16\eta\,; \end{cases} \tag{5.8}$$

$|\alpha_3|$ apprently increases linearly with η over a rather long interval, although it is difficult to predict what will happen at higher energies; α_1 instead reaches a plateau of about 10° and its behaviour becomes rather unclear at high energies (see Fig. 6).

I should mention in this connection that in the Orear analysis somewhat more weight was given to the pion scattering experiments than to the photoeffect experiments. There exists a relation (7) between the photoeffect and

(4) M. GLICKSMAN: *Phys. Rev.*, **94**, 1335 (1954).

(*) η is the meson momentum, in the c.m.s., in units of μc (μ is the pion rest-mass).

(5) *Proceedings of the Fourth Annual Rochester Conference on High Energy Physics* (New York, 1954).

(6) J. OREAR: *Phys. Rev.*, **96**, 176 (1954).

(7) H. L. ANDERSON and E. FERMI: *Phys. Rev.*, **86**, 794 (1952).

the difference between α_1 and α_3 near $\eta=0$. With the best data on the photoeffect $(\alpha_1 - \alpha_3)/\eta$ should be about 0.21 instead of 0.27 according to OREAR. This corresponds to a discrepancy in the intensities by the factor $(0.27/0.21)^2=1.65$.

6. – Interpretation of the Phase Shifts.

We have described our experimental knowledge of the phase shifts in pion-nucleon interactions. The question now arises as to what quantitative conclusions we can draw from these phase shifts. Consider a system of two particles, say a pion and a nucleon. When they are far apart, our understanding of the system is as complete as that of any other two body problem; however, when the distance between them is small, say less than the interaction range, r_0, our understanding is very limited.

In order to obtain a simplified picture let us assume that a potential of short range, r_0, acts between the two particles. For a state of definite charge and angular momentum, we can write the equation for $r\psi = u(r)$. $u(r)$ obeys the radial Schrödinger equation,

$$u'' + \left[p^2 - \frac{l(l+1)}{r^2} - 2m\,U(r)\right] u = 0\,, \tag{6.1}$$

where we have used a system of units in which $\hbar=c=1$, m is the reduced mass, and $p^2=2mE$. An exact solution of (6.1) may be obtained for values of $r > r_0$; for values $r < r_0$, this is not possible unless we know the potential. So, let us divide the equation into an inside part $(r < r_0)$ for which we can say very little and an outside one $(r > r_0)$.

For the outside (6.1) becomes

$$u'' + \left[p^2 - \frac{l(l+1)}{r^2}\right] u = 0\,. \tag{6.2}$$

The general solution of (6.2) is a linear combination of two fundamental solutions. Written in a normalized form they are:

$$\sqrt{\frac{\pi}{2}\,pr}\,J_{l+\frac{1}{2}}(pr) \equiv J(pr)\,, \tag{6.3}$$

$$\sqrt{\frac{\pi}{2}\,pr}\,N_{l+\frac{1}{2}}(pr) \equiv N(pr)\,, \tag{6.4}$$

where J and N are Bessel funotions. J is regular at $r=0$. On the other hand N is singular at $r=0$.

The asymptotic expressions for these two solutions are, for large values of r,

$$J \to \sin\left(pr - \frac{\pi l}{2}\right) \quad \text{and} \quad N \to \cos\left(pr - \frac{\pi l}{2}\right), \tag{6.5}$$

for small values of r,

$$J \to \frac{(pr)^{l+1}}{(2l+1)!!} \quad \text{and} \quad N \to \frac{(2l-1)!!}{(pr)^{l}}. \tag{6.6}$$

The !! means that in the factorial multiplication, only odd numbers are included, i.e. $1 \cdot 3 \cdot 5 \cdot 7 \cdot \ldots (2l+1) \equiv (2l+1)$!! If there were no interaction the solution should be regular at the origin and it would be J. When there is an interaction, however, we expect that for $r > r_0$, $u(r)$ will be a linear combination of the two asymptotic solutions, of the form $aJ + bN$.

This mixture can be determined if the phase shift is known. For a phase shift, α, we have the asymptotic solution $\sin(pr - (\pi l/2) + \alpha)$, instead of $\sin(pr - \pi l/2)$ which corresponds to zero phase shift. [It must be remembered that α is added to $(pr - \pi l/2)$ and not to (pr) alone.]

The asymptotic form of the phase-shifted solution is then

$$\sin\left(pr - \frac{\pi l}{2}\right)\cos\alpha + \cos\left(pr - \frac{\pi l}{2}\right)\sin\alpha .$$

Its exact form in the region $r > r_0$ is then

$$u(r > r_0) = J\cos\alpha + N\sin\alpha \tag{6.7}$$

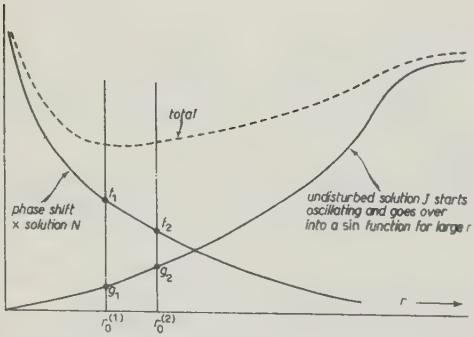

Fig. 7. – Schematic representation of the radial wave function $u(r)$ for an interaction of range r_0.

and since α is known experimentally, we can determine the coefficients. In the vicinity of r_0, for low meson momenta and thus small pr (we assume for simplicity $pr_0 \ll 1$) we may use (6.6). The solution is then:

$$u(r) \cong \cos\alpha \frac{(pr)^{l+1}}{(2l+1)!!} + \\ + \sin\alpha \frac{(2l-1)!!}{(pr)^{l}} \tag{6.8}$$

For small α, with $\cos\alpha \cong 1$, $\sin\alpha \cong$ $\cong \alpha$, Fig. 7 shows schematically

the undisturbed solution J (in the absence of any phase shift), the phase shift correction αN, and the actual solution obtained by adding the two. For $r < r_0$ the above solution has no physical significance.

The question now arises: what is the magnitude of the perturbation arising from the phase shift? Clearly this is dependent on the magnitude of r_0. Thus (see Fig. 7) if $r_0 = r_0^{(1)}$, the perturbation is measured by $(f_1/g_1)^2$ and if $r_0 = r_0^{(2)}$, it is $(f_2/g_2)^2$; these are very different.

We shall now demonstrate that, for an angular momentum l, the phase shift α, at low energy, is proportional to p^{2l+1}.

Consider a potential function $U(r)$ of range r_0, the exact nature of which is unknown for $r < r_0$. In the vicinity of r_0 the solutions $u(r)$ of (6.2) computed for $r < r_0$ and $r > r_0$ must have equal values and derivatives

$$u(r_0 + \varepsilon) = u(r_0 - \varepsilon), \qquad u'(r_0 + \varepsilon) = u'(r_0 - \varepsilon). \tag{6.9}$$

Because our equation (6.1) is linear, what is required is to match, on the two sides of r_0, the ratio $u(r)/u'(r)$. Put

$$\varrho \equiv \frac{u_l(r_0)}{u_l'(r_0)} = \varrho(E) \tag{6.10}$$

and assume that $\varrho(E)$ is computed from the inside solution. Assuming for the outside solution the form (6.8) we obtain, by matching at r_0,

$$\varrho(E) = \frac{\cos\alpha \dfrac{(pr_0)^{l+1}}{(2l+1)!!} + \sin\alpha \dfrac{(2l-1)!!}{(pr_0)^l}}{(l+1)\cos\alpha \dfrac{p^{l+1}r^l}{(2l+1)!!} - l\sin\alpha \dfrac{(2l-1)!!}{p^l r_0^{l+1}}}. \tag{6.11}$$

From this follows

$$\operatorname{tg}\alpha = \left[\frac{(l+1)\varrho(E) - r_0}{l\varrho(E) + r_0}\right] \frac{(pr_0)^{2l+1}}{(2l+1)!!\,(2l-1)!!}, \tag{6.12}$$

which expresses the phase shift α in terms of $\varrho(E)$.

Near the threshold $\varrho(E)$ can be substituted for, by its values for zero energy $\varrho(0)$. For small values of E this is an adequate approximation. Also for small values of p and consequently small α, $\operatorname{tg}\alpha \cong \alpha$. We then have $\alpha = \text{constant} \cdot p^{2l+1}[Q\varepsilon D]$.

As the energy E is increased, the dependence of α on p will contain terms of higher power than $(2l+1)$. Thus, we may express the coefficient of (6.12)

as an expansion in powers of E

$$\text{tg}\,\alpha \cong [Y_0 + Y_1 E + \ldots] \frac{(pr_0)^{2l+1}}{(2l+1)!!\,(2l-1)!!}. \tag{6.13}$$

We note that the first correction to the phase shift gives a term proportional to p^{2l+3} (and not to p^{2l+2}).

It is clear that α cannot be computed as long as ϱ is unknown. However for most values of ϱ the coefficient in (6.12) is of the order of one (*).

Only over a relatively small range of ϱ values, in the region of $\varrho \approx -r_0/l$, does the coefficient become very large. For this reason a value of

$$\alpha \gg \frac{(pr_0)^{2l+1}}{(2l+1)!!\,(2l-1)!!},$$

would indicate an exceptional condition well worth looking into.

(*) This is, of course, only true for $l > 1$. For $l = 0$, (6.13) becomes

$$\text{tg}\,\alpha = \left[\frac{\varrho(E) - r_0}{r_0}\right] pr_0 . \tag{6.14}$$

The behavior of the coefficient in (6.12) and (6.14) is shown in Fig. 8 for a number of l-values.

$$\text{tg}\,\alpha = Y \frac{(pr_0)^{2l+1}}{(2l+1)!!\,(2l-1)!!}, \qquad Y \equiv \frac{(l+1)\varrho(E) - r_0}{l\varrho(E) + r_0}.$$

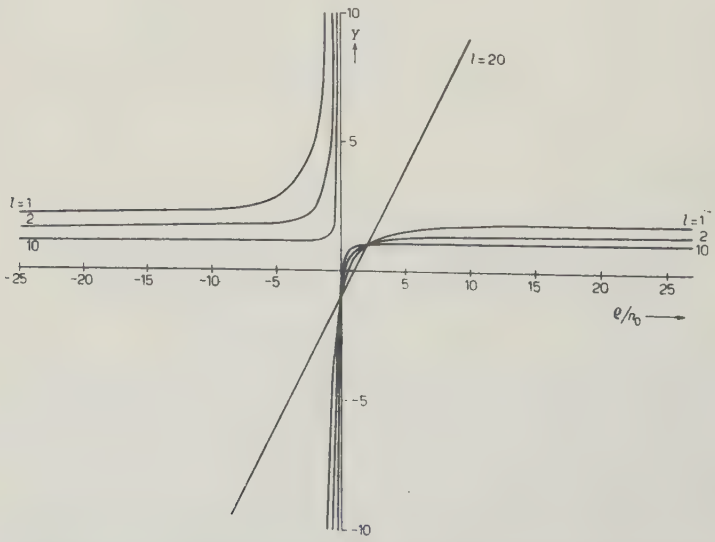

Fig. 8. – Dependence of the phase shift on the wave function at the interaction boundary.

The importance of the factorials in the denominator of (6.12) is shown in the following Table III.

TABLE III. – *The factorials in the denominator of the dependence of phase shift on momentum, eq.* (6.12).

l	$(2l+1)!!\,(2l-1)!!$
0	1
1	3
2	45
3	1575

The rapid increase in the denominator with increasing l is another reason why we expect the phase shifts near threshold to be negligible for $l \geqslant 2$.

We can now try to estimate from the phase shifts the actual magnitude of the perturbation introduced by the interaction. For this purpose let us evaluate the ratio of the total disturbed wave function (6.7) to the undisturbed wave function $J(pr)$. The square of this ratio may be referred to as the « enhancement factor ». It represents the increase in probability, due to the interaction, for the two particles to be « in contact ».

For small values of p

$$\cos\alpha \cong 1\,, \qquad \sin\alpha \cong \alpha \cong ap^{2l+1}\,,$$

$$\text{the undisturbed wave function} \cong \frac{(pr)^{l+1}}{(2l+1)!!}\,,$$

$$\text{the perturbation term} \cong ap^{2l+1}\frac{(2l-1)!!}{(pr)^{l}}\,.$$

The phase-shifted wave function, which is the sum of the two expressions given above, is

$$\frac{(pr)^{l+1}}{(2l+1)!!} + ap^{2l+1}\frac{(2l-1)!!}{(pr)^{l}}\,.$$

The enhancement factor is, then

$$\text{E.F.} = \left\{1 + \frac{a(2l+1)!!\,(2l-1)!!}{r_0^{2l+1}}\right\}^2. \tag{6.15}$$

For the s and p waves we have previously obtained the phase shifts at low energies for $T=\frac{3}{2}$ and $T=\frac{1}{2}$ given in Table IV.

TABLE IV. – *Experimental pion-nucleon scattering phase shifts at low energies.*

Wave \ T	$\frac{3}{2}$	$\frac{1}{2}$
$s_{\frac{1}{2}}$	$\alpha_3 = -0.11\,\eta$	$\alpha_1 = 0.16\,\eta$
$p_{\frac{1}{2}}$	$\alpha_{33} = 0.26\,\eta^3$	—

Substituting these values we obtain for the enhancement factors:

$$(6.16)\quad \text{E.F.}(\alpha_3) \cong \left[1 - \frac{0.11}{r_0}\right]^2,\quad \text{E.F.}(\alpha_1) \cong \left[1 + \frac{0.16}{r_0}\right]^2,\quad \text{E.F.}(\alpha_{33}) \cong \left[1 + \frac{0.78}{r_0^3}\right]^2,$$

r_0 is measured in units of $\hbar/\mu c$.

For $r_0 \cong 1$, the enhancement factors are ~ 1 for α_3 and α_1 and ~ 3 for α_{33}. However, the « 3,3 » p-wave appears, from experimental observations, to be more important than is indicated by the enhancement factor 3. In fact, the experimental evidence from photomeson production suggest that the factor is probably ~ 10. This would be the case for $r_0 \approx 0.7$, which may be taken as an indication that the range of the interaction is somewhat $< \hbar/\mu c$.

Table V shows the enhancement factors for the (3,3) scattering as a function of relative meson momentum η, calculated for the measured α_{33} phase shifts and using the correct Bessel function solutions for the wave functions, for a number of assumed values of the interaction range, r_0.

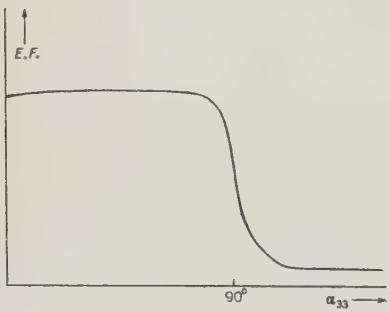

Fig. 9. – General behaviour of the enhancement factor in the (3,3) state as a function of the phase shift α_{33}.

TABLE V. – *Enhancement factors for the wave function at $r = r_0$ corresponding to p-wave scattering in the (3,3) state.*

		E. F.			
η	α_{33}	$r_0 = 0.5$	$r_0 = 0.6$	$r_0 = 0.7$	$r_0 = 1.0$
0	($15^\circ\,\eta^3$)	53	22	10.8	3.2
0.5	1.88°	49	26	10.4	3.8
1.	15°	62	36	12.5	4.6
1.5	58°	68	31	16.9	4.1
1.7 (*)	90°	57	19	11.0	1.6
2.0 (**)	145°	3.4	0.8	0.2	0.1

(*) This is the momentum corresponding to the « resonance » energy, at which $\alpha_{33} = 90°$.

(**) The values of the E.F. for $\eta = 2$ are small and probably the exact values do not have any physical significance. For $r_0 = 1$, there is actually a node between $\eta = 1.7$ and $\eta = 2.0$. The general dependence of the E.F. on the value of α_{33} is indicated in Fig. 9, from which we may see that the « resonance » behavior of the processes involving the (3,3) state is due to two factors: the rapid rise at low energies comes from the p^3 dependence of α_{33}; the rapid decrease above the resonance energy comes from the rapid falling off of the E.F..

7. – Photomeson Production.

We have heard from BERNARDINI's lectures that at low energies, close to the threshold for the photoproduction of positive pions from hydrogen, the transition is to a state in which the pion is emitted in an s-state. This is indicated by the flatness of the angular distribution as well as by the excitation function, which seems to be proportional to the momentum of the pion. I would like now to discuss in a simplified form the mechanism of this photopion production and begin with an approach that does not lead to an adequate solution. We may argue as follows. According to YUKAWA the nucleon alternates between a state of the bare nucleon, say a proton, and a state, which may be described as a neutron plus a positive pion which surrounds the neutron in some sort of a cloud

$$\text{p} \rightleftarrows \text{n} + \pi^+ . \tag{7.1}$$

The incoming photon may catch the system in the latter state and produce a photo-disintegration by ejecting the pion. What estimate can we make of the intensity of this effect? We know that the initial state has $J=\frac{1}{2}$ and even parity, being just a proton. (A nucleon is, by definition, treated as a particle with even parity.)

In the final state, the pion, of intrinsic spin 0, is emitted in an s-state, i.e., with no orbital angular momentum. The spin of the system is thus essentially the spin of the remaining neutron, i.e. $\frac{1}{2}$. The pion is pseudoscalar and therefore the parity of the system in an orbital s-state will be odd. The transition is thus from a $J=\frac{1}{2}$ (+) to $J=\frac{1}{2}$ (—) state, a transition which is classified as an electric dipole (El) transition.

Now, what will happen to the direction of the nucleon spin in this transition? Let us take the z-axis in the direction of propagation of the photon and assume that the spin of the nucleon is up in the initial state; i.e. the initial spin state is α. After the transition the proton will change to a neutron and the pion can be considered as free. In this process the spin of the nucleon will be flipped so that the final spin state is β (spin down). The reason for this spin flip can be seen if we consider the angular momentum carried by the photon. The photon may be described by a scalar function, e^{ikz}, which we may call the orbital part, and a polarization vector, which plays the role of an object with spin $s=1$. The orbital part e^{ikz} can be expanded in spherical harmonic functions $Y_{l,m}$, which have the orbital angular momentum l. The z-component m of the orbital angular momentum is always zero, since e^{ikz} only depends on z.

The polarization state of the photon can be described in terms of two

circularly polarized states of opposite directions, which in the case of a linearly polarized photon are mixed in equal proportions. The angular momentum of these two polarization states corresponds to a spin $s=1$, with the z-component $s_z=\pm 1$. Since the z-component of the orbital angular momentum is $m=0$, the total angular momentum has the z-component, $j_z=\pm 1$. The magnitude of the total angular momentum $\boldsymbol{j}=\boldsymbol{l}+\boldsymbol{s}$ can take all integral values, zero excluded. To each value of j there correspond three values of l, namely $l=j\pm 1$ and $l=j$ and two parities corresponding to an electric or a magnetic multipole interaction.

Since the spin in our initial state was stipulated as being up, i.e. $j_z=+\frac{1}{2}$, and the photon transfers an angular momentum component ± 1 in the z-direction, it follows that in the final state we must have $j_z=+\frac{3}{2}$ or $-\frac{1}{2}$. Since the final state is $S_{\frac{1}{2}}$, it follows that $j_z=-\frac{1}{2}$ is the only possibility. The spin of the nucleon is thus flipped in the transition and the final spin state must be a β-state.

We now try to account for the observed intensity of the photoeffect using the naive picture of a Yukawa nucleon, sometimes surrounded by a cloud of pions, which may the be ejected by the photon. For this we first have to write down the wave function of the initial state. We are interested only in that part of the initial state which has the form n^+ since in our simple picture the proton is photoelectrically active only in this form. In the expression for the wave function of the initial state

$$\psi_i=f(\sqrt{\tfrac{2}{3}}n^+-\sqrt{\tfrac{1}{3}}p^0)(\sqrt{\tfrac{2}{3}}\beta Y_{1,1}-\sqrt{\tfrac{1}{3}}\alpha Y_{1,0})g(r) \tag{7.2}$$

the factor f is the amplitude of this state. f is smaller than unity but probably not very much smaller. The next factor in (7.2) is the isotopic spin function $\chi_1^{(1)}$ (6.5), for the system $(\mathcal{N}+\pi)$ in the $T=\frac{1}{2}$, $T_z=\frac{1}{2}$ state. The next term specifies the spin and orbital angular momentum state of the system. In the decomposed form of the proton, this state must have angular momentum $\frac{1}{2}$ and even parity. To make the parity even the pion must be moving in a P-orbit around the neutron. The angular momentum $\frac{1}{2}$ of the system is obtained by combining the spin $s=\frac{1}{2}$ of the neutron with the orbital angular momentum $l=1$ of the pion. Stipulating the initial state of the system as an α-state with the total spin up, $J_z=+\frac{1}{2}$, we can have $m=1$ and the neutron in a β-state, or $m=0$ and the neutron in the α-state. The term in the wave function represents the proper mixture of these spin and angular momentum states according to CONDON and SHORTLEY ([8]).

([8]) E. U. CONDON and G. H. SHORTLEY: *The Theory of Atomic Spectra* (Cambridge, 1935).

We finally have the radial part $g(r)$ of the wave function on which we have very little information.

The final state also contains a pion and a nucleon. The pion is in a positive energy state, in the form of an outgoing wave. In the final state the isotopic state may be either $T=\frac{1}{2}$ or $T=\frac{3}{2}$, since the interaction with the photon may lead to $\Delta T=0$ or $\Delta T=\pm 1$. We therefore have two wavefunctions for the final state:

$$\left| \begin{array}{l} \psi_3 = (\sqrt{\tfrac{1}{3}}\, n^+ + \sqrt{\tfrac{2}{3}}\, p^0)\, \beta \dfrac{u_3(r)}{r}\,, \\ \psi_1 = (\sqrt{\tfrac{2}{3}}\, n^+ - \sqrt{\tfrac{1}{3}}\, p^0)\, \beta \dfrac{u_1(r)}{r}\,. \end{array} \right. \tag{7.3}$$

These contain the isotopic spin functions $\chi_3^{(1)}$ and $\chi_1^{(1)}$ from (4.5) corresponding to $T_3=+\frac{1}{2}$ and $T=\frac{3}{2}$ or $\frac{1}{2}$, respectively. The total spin of the final state is required to be down. Since the pion is in an s-state and has no intrinsic spin, the neutron spin must also be down, i.e. be in a β-state.

Since the pion is in an s-state we have no angular part of the wave function. Finally we have the radial parts $u_3(r)/r$ and $u_1(r)/r$ of the wavefunction in the final state.

We must now compute the matrix element corresponding to the interaction of the photon with the system. The interaction of a particle with a photon is described by the term: $e\boldsymbol{A}\cdot\boldsymbol{v}$, where $\boldsymbol{A}$ is the vector potential of the electromagnetic field. We should thus calculate the matrix element of the velocity $\boldsymbol{v}$ or, in the non relativistic case, the momentum $\boldsymbol{p}$ of the pion.

In the special case of electrons in an atom it is proved that this amounts to taking the matrix element of the coordinates, but this is not permitted in the present case.

Before we write down the matrix element we note that in the initial and final states the terms containing p^0 do not contribute since the neutral pions give no current to interact with the photon.

Furthermore, since the interaction with the pion current does not change the spin of the nucleon, the part of the initial wavefunction containing the spin state α is irrelevent since the final spin state of the nucleon is a β-state.

We obtain e.g. for the x-component of the matrix element to the final state with $T=\frac{3}{2}$

$$\langle \text{final}|p_x|\text{initial}|\rangle = \text{const}\cdot f \int Y_{1,1}\, g(r)\, \frac{\partial}{\partial x}\frac{u_3(r)}{r}\, \mathrm{d}^3\boldsymbol{r}\,. \tag{7.4}$$

For the spherical harmonic function $Y_{1,1}$ we have

$$Y_{1,1}(\vartheta,\varphi) \sim \sin\vartheta\cdot e^{i\varphi} = \frac{x+iy}{r}. \tag{7.5}$$

In order to estimate the magnitude of the matrix element we must know something about $g(r)$ and $u(r)$. Of $g(r)$ we do not know anything at small distances, but for $r \gtrsim \hbar/\mu c$ it decreases rapidly with the distance from the nucleon, approximately as $\exp[-r\mu c/\hbar]$.

For the wavefunction $u(r)$ of the emitted pion we can use the previously given asymptotic expressions (6.5). For the case $l=0$,

$$u_3(r) \sim \sin(\eta r + \alpha_3) \tag{7.6}$$

and

$$u_1(r) \sim \sin(\eta r + \alpha_1)\,, \tag{7.7}$$

if we limit ourselves to low energies of the emitted pion.

We use the experimental values of OREAR [6] for the phase shifts α_3 and α_1 which, for small values of η, are:

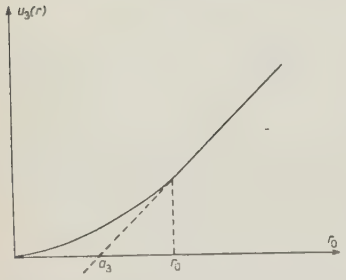

Fig. 10. – Shape of the radial function $u_3(r)$ for small values of r.

$$\alpha_3 = a_3\eta \quad \text{with} \quad a_3 = -0.11\,, \tag{7.8}$$

and

$$\alpha_1 = a_1\eta \quad \text{with} \quad a_1 = +0.16\,. \tag{7.9}$$

The asymptotic expressions for u_3 and u_1 are valid outside the range r_0 of the potential. Inside r_0 we do not know the shape of $u(r)$ except that it should go to zero for $r=0$ (see Fig. 10). However the volume inside r_0 is small and does not contribute very much to the matrix element, the main part of the electromagnetic interaction being in the region of and outside r_0, so we can use the above expressions (7.6)-(7.9) for u_3 and u_1 in calculating the matrix elements. This conclusion will of course be valid only if the wavefunction $g(r)$ in the initial state has an appreciable tail, so that there is a fair probability for the pion to be found outside r_0. Using as an approximation, (7.6) with (7.8) the derivative of u_s becomes (for $\eta r \ll 1$)

$$\frac{\partial}{\partial x}\frac{u_3(r)}{r}\frac{\partial}{\partial x}\left(\eta + \eta\frac{a_3}{r}\right) = -\eta\frac{a_3}{r^3}x\,. \tag{7.10}$$

The matrix element (7.4) now becomes (after integrating over the angles)

$$\langle \text{final}|p_x|\text{initial}\rangle = \frac{\hbar}{i}\frac{2f}{9\sqrt{L}}\begin{Bmatrix} a_3 \\ a_1 \end{Bmatrix}\eta\int g(r)\,\mathrm{d}r\,. \tag{7.11}$$

The factor $1/\sqrt{L}$ comes from the normalization of the wavefunctions (7.6), (7.7) of the final unbound state, the normalization volume being a sphere of radius L. L, of course, disappears in the final result. The essential feature of (7.11) is that the matrix element is proportional to the phase shifts $a_3\eta$ and $a_1\eta$ respectively. To get numerical values we must make a guess at the function $g(r)$. It turns out that the result is not very different if we assume various reasonable forms. (E.g., one can take an exponential or a Bessel-function, K_1).

From these matrix elements one calculates the cross-section for the transition $p^\gamma \to n^+$. A numerical calculation gives:

$$\sigma(p^\gamma \to n^+) = 1.0 \cdot 10^{-27} \cdot f^2 \eta \left(\frac{a_3 + 2a_1}{3}\right)^2 \text{cm}^2 . \tag{7.12}$$

For the probability f^2 that the proton is n a state consisting of a neutron and a pion, ready to be « photo-electric-effected », we can assume unity, an assumption which may be too large by perhaps a factor of 2.

The numerical part of (7.12), $1.0 \cdot 10^{-27}$ cm^2 comes from the assumption that the wavefunction $g(r)$ has a range of the order of $\hbar/\mu c$, which gives a cross-section of nuclear dimensions. The remaining part of (7.12) consists of pure numbers since the momentum η is expressed in units of μc and the lengths a_s and a_1 in units of $\hbar/\mu c$. If we introduce the experimental values (7.8), (7.9) for a_1 and a_3 we find

$$\sigma(p^\gamma \to n^+) = 5 \cdot 10^{-30} \cdot \eta \text{ cm}^2 . \tag{7.13}$$

This cross-section is much too small, the experimental value being about $150 \cdot 10^{-30}\eta$ cm^2, a factor of 30 larger.

Even though the above theoretical argument is very approximate, a drastic modification would be needed to account for a factor of 30. It should however be pointed out that the predicted energy dependence, proportional to the momentum η of the emitted particle, is correct. A more correct procedure would be to apply pseudoscalar meson theory to the problem as first suggested by WENTZEL (unpublished). It does not make much difference if the pseudoscalar or pseudovector coupling is used for the calculation. We will, for simplicity, assume PV-coupling following CHEW ([9]). However $PS - PV$ theory is not renormalizable, as $PS - PS$ theory is, and it is therefore frowned upon by the high priests of field theory.

There is a hope, somewhere between ~ 5 and 95%, that $PS - PS$ theory is the truth.

CHEW takes a higly common sense approach to the problem, and is tem-

([9]) G. F. CHEW: *Phys. Rev.*, **95**, 1669 (1954).

porarily satisfied with a partial solution, which does not take into account, for example, relativistic effects. Within its limitations the theory appears to be fairly self-consistent and essentially convergent in the sense that the various terms in the approximation grow smaller as one proceeds with the evaluation.

CHEW introduces the simplification that the mass M of the nucleon is very large compared to the pion mass so that the nucleon will remain at rest. This is really a weak point of the theory. The nucleon has then only its spin and its charge as dynamical variables. In addition CHEW gives the nucleon a finite size in order to avoid convergence difficulties. The interaction between the nucleon and the surrounding pion field is taken as

$$H_{\text{int}} = \sqrt{4\pi}\frac{f}{\mu}\sum_{\lambda=1}^{3}\tau_\lambda\int \varrho(\boldsymbol{r})\boldsymbol{\sigma}\cdot\boldsymbol{\nabla}\varphi_\lambda\,\mathrm{d}^3\boldsymbol{r}\,, \tag{7.14}$$

f is a coupling constant. The units are such that $\hbar=c=1$. The interaction is written in an isotopic spin invariant form. In PV-coupling the interaction is between the spin $\boldsymbol{\sigma}$ of the nucleon and the gradient of the pion fields φ_λ. φ_3 is the neutral meson and φ_1 and φ_2 the charged meson field. The interaction has the form of a scalar product in charge space and is thus invariant.

Since CHEW assumes the nucleon to have a finite size the interaction has to be averaged over the volume of the nucleon, using a weight function $\varrho(\boldsymbol{r})$, normalized as follows

$$\int \varrho(\boldsymbol{r})\,\mathrm{d}^3\boldsymbol{r} = 1\,. \tag{7.15}$$

Actually, for what we are discussing at present, photo-production near the threshold, we could omit the weighting function $\varrho(\boldsymbol{r})$ and take a point interaction. For this particular problem, the result is essentially identical. However, we may as well leave it in the form (7.14).

The general idea of this type of explanation, as it was first proposed by WENTZEL, is the following. Let us introduce in (7.14) the gauge-transformation, making this expression gauge-invariant when the e.m. field is introduced. This will add two terms, which are very suitable to describe directly the photo-effect. If the field φ had a definite charge, e, the gauge-transformation would consist in writing $(\boldsymbol{\nabla} - ie\boldsymbol{A})$ instead of $\boldsymbol{\nabla}$.

Now, there is a slight extra complication for the following reason. We have to deal with a field φ with its 3 real components φ_1, φ_2 and φ_3, which correspond to different charge states. In fact, the normal convention is to associate the field φ_3 to π^0. So, for example, in so far the φ_3 part of (7.14) is concerned, $e=0$, and the transformation for the third component will be just no trans-

formation at all ($\nabla \to \nabla$). There are however complications for φ_1 and φ_2 because φ_1 and φ_2 are not the amplitudes of the plus and minus pions field, but are linear combinations of the two. In fact, the easy way to remember the rule is the following. Let us consider the spherical harmonics of order 1, since we are describing a system of isotopic spin 1 which behaves in charge space essentially as a spherical harmonic of order 1. They are, apart from a common normalisation factor,

$$(7.16)\qquad \begin{cases} Y_{11} \to \varphi^+ \alpha \dfrac{-\sin\vartheta \cdot \exp[i\varphi]}{\sqrt{2}} & \text{corresponding to } \pi^+, \\ Y_{10} \to \varphi_0 \alpha \cos\vartheta & \text{corresponding to } \pi^0, \\ Y_{1-1} \to \varphi^- \alpha \dfrac{\sin\vartheta \cdot \exp[-i\varphi]}{\sqrt{2}} & \text{corresponding to } \pi^-. \end{cases}$$

These spherical harmonics are respectively proportional to the expressions

$$(7.17)\qquad \frac{-x-iy}{\sqrt{2}}, \qquad z, \qquad \frac{x-iy}{\sqrt{2}}.$$

The three components φ_1, φ_2 and φ_3 form, essentially, a vector in charge space (not in the true space), like the Pauli operators σ_1, σ_2 and σ_3 of the spin of the nucleon, which also act as the components of a vector. Substituting in (7.17) φ_1, φ_2, φ_3 for x, y, z, we obtain the expressions

$$(7.18)\qquad \begin{cases} \varphi^+ = \dfrac{-\varphi_1 - i\varphi_2}{\sqrt{2}} & \text{corresponding to } \pi^+ \text{ amplitude}, \\ \varphi_0 = \varphi_3 & \text{corresponding to } \pi^0 \text{ amplitude}, \\ \varphi^- = \dfrac{\varphi_1 - i\varphi_2}{\sqrt{2}} & \text{corresponding to } \pi^- \text{ amplitude}. \end{cases}$$

The expressions $\nabla\varphi^\pm$ is to be transformed into $(\nabla \mp ie\boldsymbol{A})\varphi^\pm$. In (7.14) we have the gradients of φ_1, φ_2, φ_3. When we apply the gauge transformation, extra terms will be added. They are

$$(7.19)\qquad H' = \sqrt{4\pi}\frac{fe}{\mu}\int \boldsymbol{\sigma}\cdot\boldsymbol{A}\,(\tau_1\varphi_2 - \tau_2\varphi_1)\,\varrho(\boldsymbol{r})\,\mathrm{d}^3\boldsymbol{x}\,.$$

These extra terms, added in order to satisfy to gauge condition, are precisely the terms which are responsible for the photo-production. Now, this should be fairly evident because, apart from nucleon spins and such things, (7.19)

includes essentially the products of the vector $\boldsymbol{A}$ and one of the φ (φ_1 or φ_2) that correspond to the charged pion field. We know that in field theory the vector potential or its components are creation or destruction operators of photons. Similarly the operators φ_1, and φ_2 create or destroy a charged pion. In the reaction

$$\mathcal{N} + \gamma \rightarrow \mathcal{N} + \pi \tag{7.20}$$

we must destroy a photon (operator A) and create a pion (operator φ_1 or φ_2). Both operators are present in (7.19).

In order to arrive at a quantitative result, we need the matrix element of (7.19) corresponding to this transition. From it the cross-section can easily be computed. The easiest way is to go from the components φ_1 and φ_2, that are not definitely charge components, back to the φ^+ and φ^-, which are operators representing the creation o π^+ and π^-. Let me call, according to the usual notation,

$$\begin{cases} \varphi^+ = \varphi^* \\ \varphi^- = -\varphi\,. \end{cases} \tag{7.21}$$

Expression (7.19) becomes

$$H' = \sqrt{4\pi}\, i \sqrt{2}\, \frac{fe}{\mu} \int \boldsymbol{\sigma} \cdot \boldsymbol{A}\, (\tau^* \varphi + \tau \varphi^*)\, \varrho(r)\, \mathrm{d}^3\boldsymbol{x}\,, \tag{7.22}$$

where

$$\begin{cases} \dfrac{\tau_1 + i\tau_2}{2} = -\tau^* & \text{is the operator which transforms n in p}\,, \\ \dfrac{\tau_1 - i\tau_2}{2} = \tau & \text{is the operator which transforms p in n}\,, \\ \varphi^* & \text{is the operator which creates } \pi^+ \text{ and destroys } \pi^-\,, \\ \varphi & \text{is the operator which creates } \pi^- \text{ and destroys } \pi^+\,. \end{cases} \tag{7.23}$$

The matrix element for the reaction

$$\gamma + \mathrm{p} \rightarrow \mathrm{n} + \pi^+ \tag{7.24}$$

is, then, near the threshold

$$ME = i\, \sqrt{8\pi}\, \frac{ef}{\mu}\, \sigma_\varepsilon \sqrt{\frac{2\pi}{\nu}}\, \frac{1}{\sqrt{2\omega}} \int \varrho(r)\, \exp\left[i\nu x\right] \mathrm{d}^3\boldsymbol{x}\,, \tag{7.25}$$

in which

σ_s is the component of the $\boldsymbol{\sigma}$ vector in the polarisation direction of $\boldsymbol{A}$ ($\boldsymbol{\epsilon}$ is a unit vector in this direction);

e^{ipx} is the propagation term introduced, by the electro-magnetic field; the pion near the threshold (small pion momentum) does not contribute a corresponding propagation factor;

$\sqrt{2\pi}/\sqrt{\nu}$ is the normalisation factor of $\boldsymbol{A}$, corresponding to one photon per unit volume; likewise $1/\sqrt{2\omega}$ is a similar normalization factor for the pion; ν and ω are the energies, in appropriate units, of the photon and pion, respectively.

The form factor $\varrho(r)$ has, in the most recent version of the Chew's theory, the radius: $\frac{1}{5}\cdot\hbar/\mu c$; on the other hand, $1/\nu$ is, at threshold, about $\hbar/\mu c$ and is therefore much longer than the range of ϱ. The integral in (7.25) is therefore ≈ 1.

Equation (7.25) has been obtained on the assumption that the meson wave-function can be expressed as a plane wave. Actually, the outgoing meson is in an s-state, with $r\psi(r) = u(r) = \sin(kr+\alpha) \cong kr + \alpha \approx kr$. (The term due to the phase shift, $\alpha = ka$, leads to a small correction, essentially that calculated in the preceding approximation, and is therefore neglected in the following.) Using this wave function, appropriately normalized in a sphere of radius L, we obtain

$$\langle n^+|H'|p^\gamma\rangle = \pm i\sqrt{\frac{4\pi}{L}}\frac{ef}{\mu}\frac{k}{\sqrt{\nu\omega}}, \tag{7.26}$$

where the $\pm$ sign corresponds to the nucleon spin antiparallel and parallel, respectively, to the photon polarization vector.

The passage from the matrix element to the cross-section is carried out by the usual formula

$$c\sigma = \frac{2\pi}{\hbar}|ME|^2\varrho_{\text{final}}, \tag{7.27}$$

where the density of final s-states is

$$\varrho_{\text{final}} = \frac{L}{\pi v} = \frac{L}{\pi\eta}. \tag{7.28}$$

Near threshold, putting $\nu = \omega = \mu$, $k/\mu = \eta$, and converting from the $\hbar = c = 1$ to

the ordinary CGS system, we obtain

$$\sigma = 8\pi\left(\frac{\hbar}{\mu c}\right)^2\left(\frac{e^2}{\hbar c}\right)\left(\frac{f^2}{\hbar c}\right)\eta \cong 0.15\cdot 10^{-27}\eta \text{ cm}^2 . \quad (*) \tag{7.29}$$

From (7.29) we derive the value of the coupling constant $f^2/\hbar c \cong 0.04$. This value can be improved upon by making use, instead of (7.29), of a similar expression in which certain nucleon recoil corrections are introduced. According to BERNARDINI and GOLDWASSER [10] this new analysis of the data yields

$$f^2/\hbar c = 0.058 . \quad (**)$$

This values coincides with the one adopted by CHEW [9] to account for the pion-nucleon scattering properties. It is certainly gratifying that the same value of the coupling constant is adequate to interpret both phenomena.

There is one point, however, on which I am not clear. The constant $f^2/\hbar c$, according to CHEW [9] is a « renormalized » coupling constant. It is precisely because of this renormalization that Chew's scattering theory is fairly rapidly convergent. Now it would appear at first sight that a different renormalization should apply for the scattering than for the photo-effect. I do not know of any simple explanation why this, as indicated by the experimental evidence, does not appear to be the case.

8. – Connections between Scattering and Photoproduction.

We want to establish certain formal relations which are useful for the phenomenological treatment of problems on which we have little theoretical information. The method itself has general applicability. We shall discuss the photo-effect as an example.

Thus the reaction we consider is

$$\gamma + \mathcal{N} \to \mathcal{N} + \pi . \tag{8.1}$$

(*) The same cross section could have been obtained by using the plane wave approximation (7.25) for the matrix element, and using for the density of final states (for unit normalization volume)

$$\frac{dN}{dW} = \frac{p^2}{2\pi^2\hbar^3 v} . \tag{7.30}$$

[*Note by* B. T. FELD]

(10) G. BERNARDINI and E. L. GOLDWASSER: *Phys. Rev.*, **95**, 857 (1954).

(**) The authors give $.066 \pm .008$ in ref. (10).

We shall restrict ourselves to such low energies that s and p-states give a sufficient description of the phenomena. In the following Table VI the possible states for this reaction are catalogued.

TABLE VI. – *Possible states involved in photomeson production from nucleons.*

a) Initial states				*b*) Final states		
nucleon		photon		nucleon+pion		
I	parity		I parity	state	I	parity
$\frac{1}{2}$	+	$E1$	1 —	$s_{\frac{1}{2}}$	$\frac{1}{2}$	—
		$M1$	1 +	$p_{\frac{1}{2}}$	$\frac{1}{2}$	+
		$E2$	2 +	$p_{\frac{3}{2}}$	$\frac{3}{2}$	+

The possible transitions are shown in Table VII.

TABLE VII. – *Possible states in photomeson production leading to the emission of s- or p-wave mesons.*

photon	state		meson
$E1$	$\frac{1}{2}$ —	→	$s_{\frac{1}{2}}$ —
$M1$	$\frac{1}{2}$ +	→	$p_{\frac{1}{2}}$ +
$M1$	$\frac{3}{2}$ +	→	$p_{\frac{3}{2}}$ +
$E2$	$\frac{3}{2}$ +	→	$p_{\frac{3}{2}}$ +

One should note that all final states are double because of the two possible I-spin values, $T = \frac{3}{2}$ and $\frac{1}{2}$. Linear combinations of these states will give us the physical states p^0 and n^+, in which we are ultimately interested. The resulting eight possibilities are described by eight complex amplitudes; i.e. sixteen real numbers have to be determined. Now one can prove that the 16 numbers can be reduced to 8, because it is possible to determine the phases of these 8 complex numbers. This may be done by making use of the formal properties of the S-matrix.

We shall restrict ourselves to a set of states with definite values of I, I_z, and parity. Then, for the wave function of each physical state, only the radial part of the wave function will remain to be determined.

We will make use of the channel picture, as described in BLATT and WEISSKOPF ([11]).

Consider a system of particles that may transform into each other on col-

([11]) J. M. BLATT and V. F. WEISSKOPF: *Theoretical Nuclear Physics* (New York, 1952).

liding. For example the transformations may be

$$p + \gamma \longleftrightarrow n + \pi^+ \longleftrightarrow p + \pi^0 . \tag{8.2}$$

In general

$$A_1 + B_1 \longleftrightarrow A_2 + B_2 \longleftrightarrow A_3 + B_3 \longleftrightarrow \dots . \tag{8.3}$$

Confining ourselves to states of definite angular momentum and parity we assign a « channel » to each set of two colliding particles. Channel I will describe the colliding particles A_1+B_1 channel 2 the particles A_2+B_2, and so forth. These channels may be pictured (see Fig. 11) as converging into a « black box » in which we may consider that the reactions take place which change one type of particle into others. We may describe for example a collision between A_1+B_1 as a wave packett heading along channel 1 for the black box. After the collision is completed there will be outgoing wave packets, not only in the original channel 1 but also in the others. (The collision may have changed the nature of the particles to A_3+B_3, for example). What describes the essential properties of the reaction is the ensemble of all « reflection coefficients » including cross reflection from one channel into another.

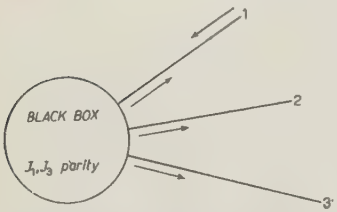

Fig. 11. – Schematic representation of the channels available for the reaction

$$A_i + B_i \rightleftarrows A_j + B_j .$$

These coefficients are n^2 in number for a black box with n channels, and may be ordered in the form of a matrix with n rows and n columns.

The S-matrix is essentially such a matrix. One must, however use a special type of normalization. Instead of normalizing the ingoing or outgoing waves to amplitude one, they are normalized to flux = 1.

For example an ingoing wave on channel λ will be

$$\frac{\exp[-ik_\lambda r_\lambda]}{\sqrt{v_\lambda}} \qquad (\text{units } \hbar = c = 1) , \tag{8.4}$$

where k_λ and v_λ are the momentum (in c.m.s.) and velocity of the incident particles A_λ at the given energy of the system. This ingoing wave may be reflected with the reflection coefficient $S_{\lambda\mu}$ into the channel μ (particles $A_\mu+B_\mu$) This reflected wave is

$$S_{\lambda\mu} \frac{\exp[ik_\mu r_\mu]}{\sqrt{v_\mu}} \equiv a_{\lambda\mu} \exp[ik_\mu r_\mu] . \tag{8.5}$$

The S-matrix is then

$$S = \begin{vmatrix} S_{11} & S_{12} & S_{13} & \dots \\ S_{21} & S_{22} & S_{23} & \dots \\ \dots & \dots & \dots & \dots \\ \dots & \dots & \dots & \dots \end{vmatrix} \tag{8.6}$$

If the incoming wave had an amplitude 1, the outgoing waves would have the coefficients $a_{\lambda\mu}$. However, for reasons of convenience we do not normalize the waves to amplitude 1, but to $1/\sqrt{v}$. This normalization corresponds to unit flux instead of unit particle density. Thus if we enter with one particle per second through a certain channel, through all channels there will emerge one particle per second.

We then call the S-matrix that matrix which consists of the coefficients $S_{\lambda\mu}$ of the waves, thus normalized. To describe the complete phenomenology of our three possible reactions (8.2) we need an S-matrix with 3 rows and 3 columns.

The are *two* formal properties of the S-matrix which will be quite useful.

(8.7) 1) The S-matrix is a *unitary* matrix. We denote by $\tilde{S}$ the Hermitian conjugate of S, $\tilde{S}_{ik} = S^*_{ki}$. Then this property means the matrix equation $S\tilde{S} = \tilde{S}S = 1$ (identity matrix).

(8.8) 2) Within certain limits, which are valid in a large number of cases, the S-matrix is *symmetric*; that is $S_{ki} = S_{ik}$.

The proof of these theorems can be found in BLATT and WEISSKOPF [11], and we will only look at the physical reasons for these properties.

1) We consider again the black box. We may enter this box with a very long but finite wave packet, which at the time $t = 0$ is heading for the box. A certain time after, it has entered the box and will be reflected into the various channels as outgoing packets moving out along the various channels. When the incoming flux is normalized to 1, the sum of the outgoing fluxes must also be 1. An analysis of this « conservation of flux » property shows that it is expressed mathematically by the fact that the S-matrix is unitary.

2) The symmetry of S has its origin essentially in the property of time reversibility. This enters into the S-matrix in the following manner: we consider an incoming wave in channel 1, and an outgoing wave in channel 2, which have, respectively, the forms $\exp[-ik_1 r_1]/\sqrt{v_1}$ and $\exp[+ik_2 r_2]/\sqrt{v_2}$.

Let us restrict ourselves to the case where the Hamiltonian describing the process is real. Then $H\psi=E\psi$, and also $H\psi^*=E\psi^*$. By going from ψ to ψ^* one interchanges ingoing and outgoing waves.

This establishes a relationship between the reflection coefficients S_{12} and S_{21}. A complete discussion shows that the relationship is $S_{12}=S_{21}$, which expresses the symmetry of the S-matrix.

Before we are ready to use these properties, I must still say what this matrix is like in the simple case where there is just one channel. What the black box does is to reflect the incoming wave to the outside with unchanged amplitude. So $|S_{11}|=1$. We can write for the incoming wave $\exp[-ikr]/\sqrt{v}$ and for the outcoming wave $S_{11}\exp[ikr]/\sqrt{v}$.

It is clear that S_{11} has modulus 1 because all that goes in must come out, as there is only one channel. Thus, for S_{11} we can write $\exp[2i\alpha]$, α being a real number.

The overall wave function containing the incoming and outgoing part has the structure $\exp[2i\alpha]\cdot\exp[ikr]+\exp[-ikr]$ (the normalisation factor $\sqrt{v}$ is left out for convenience). Dividing by $\exp[i\alpha]$ we obtain $\exp[i(kr+\alpha)]+$ $+\exp[-i(kr+\alpha)]=2\cos(kr+\alpha)$. We call α the phase shift. If α is equal to 0 it means that the box acts as an inert thing.

Suppose that we have not one but several channels, for instance three, but that there are no cross links. (The box is divided in black compartments). This is essentially the same thing as before, so we can write

$$S_0=\begin{vmatrix} \exp[2i\alpha_1] & 0 & 0 \\ 0 & \exp[2i\alpha_2] & 0 \\ 0 & 0 & \exp[2i\alpha_3] \end{vmatrix}, \tag{8.9}$$

α_1, α_2, α_3 being the phase shifts which determine the reflection coefficients of each compartment. The 0's indicate that there are no cross links.

Let us assume now that we have 3 channels and that in first approximation we have the same situation as before, i.e. no cross connections between the various channels (photon goes out as photon, π as π, etc.). But, as a second approximation, let us assume that there are weak interconnections between the channels i.e. that the cross reflectivity is there but it is small.

In this case, we may write for the overall matrix

$$S=S_0+i\varepsilon\,, \tag{8.10}$$

where S_0 represents the unconnected matrix (8.9), with the phase shifts α_1, α_2, α_3, and where ε contains all the cross links. The elements of ε are small

and their squares shall be neglected. The factor i has been put in for convenience.

Now we shall apply to the overall S-matrix the 2 properties (8.7), (8.8). In doing this we shall neglect the quadratic terms in ε.

So we write

$$S = S_0 + i\varepsilon\,.$$

The hermitian conjugate is

$$\tilde{S} = \tilde{S}_0 - i\tilde{\varepsilon}\,. \tag{8.11}$$

Applying the unitary property, we obtain

$$1 = S\tilde{S} = S_0\tilde{S}_0 + i(\varepsilon\tilde{S}_0 - S_0\tilde{\varepsilon})\,. \tag{8.12}$$

Now, as $S_0\tilde{S}_0 = 1$ it follows

$$\varepsilon\,\tilde{S}_0 = S_0\tilde{\varepsilon}\,, \tag{8.13}$$

where the matrix $\tilde{S}_0$ is given by

$$\tilde{S}_0 = \begin{vmatrix} \exp[-2i\alpha_1] & 0 & 0 \\ 0 & \exp[-2i\alpha_2] & 0 \\ 0 & 0 & \exp[-2i\alpha_3] \end{vmatrix} \tag{8.14}$$

Remember that the general form of an element (m, n) of the product of 2 matrices A and B is

$$(AB)_{mn} = \sum_l A_{ml}B_{ln}\,. \tag{8.15}$$

In the products $S\cdot\tilde{\varepsilon}$ the first factor is diagonal, which means that we can write,

$$\sum_l A_{ml}B_{ln} = A_{mm}B_{mn}\,, \tag{8.16}$$

since only the elements with $l = m$ are different from 0.

So we can write

$$(S_0\tilde{\varepsilon})_{mn} = \exp[2i\alpha_m]\cdot\tilde{\varepsilon}_{mn} = \exp[2i\alpha_m]\cdot\varepsilon^*_{nm}\,, \tag{8.17}$$

$\varepsilon\tilde{S}_0$ has, similarly, the mn element $\varepsilon_{mn}\exp[-2i\alpha_n]$. We can rewrite the previous identity (8.13) $\exp[2i\alpha_m]\varepsilon^*_{nm} = \varepsilon_{mn}\exp[-2i\alpha_n]$. Now we will use the

symmetry condition. As S_0 is symmetric, ε must also be symmetric and therefore $\varepsilon_{nm} = \varepsilon_{mn}$.

The above relation now becomes $\exp[2i\alpha_m]\varepsilon^*_{nm} = \varepsilon_{nm} \exp[-2i\alpha_n]$.

If we now multiply both sides by $\exp[i(\alpha_n - \alpha_m)]$ we obtain

$$\varepsilon_{mn} \exp[-i(\alpha_m+\alpha_n)] = (\varepsilon_{mn} \exp[-i(\alpha_m+\alpha_n)])^* . \tag{8.18}$$

Therefore $\varepsilon_{mn} \exp[-i(\alpha_m+\alpha_n)]$ is real and we can write

$$\varepsilon_{mn} = \varrho_{mn} \exp[i(\alpha_m+\alpha_n)] , \tag{8.19}$$

where ϱ_{mn} is a real number. This applies generally to the case in which there are weak cross links between the channels (i.e., where most of the phenomenon is straight scattering in each of the channels, with the phase shifts α_1, α_2, α_3 in the various channels).

ε_{mn} represents one of the cross-links, which generally is a complex number. In order to determine it, experimentally or otherwise, we must usually determine two things: the real and the imaginary parts. Our procedure however saves us part of this labour: the phase parts being determined by the scattering, we have only to determine the real number ϱ_{mn} (which can be positive or negative).

So now we can write schematically the matrix

$$S = \begin{vmatrix} \exp[2i\alpha_1] & i\varrho_{12} \exp[i(\alpha_1+\alpha_2)] & i\varrho_{13} \exp[i(\alpha_1+\alpha_3)] \\ i\varrho_{12} \exp[i(\alpha_1+\alpha_2)] & \exp[2i\alpha_2] & i\varrho_{23} \exp[i(\alpha_2+\alpha_3)] \\ i\varrho_{13} \exp[i(\alpha_1+\alpha_3)] & i\varrho_{23} \exp[i(\alpha_2+\alpha_3)] & \exp[2i\alpha_3] \end{vmatrix} \tag{8.20}$$

or the equivalent

$$S_{mn} = \delta_{mn} \exp[2i\alpha_m] + i\varrho_{mn} \exp[i(\alpha_m+\alpha_n)] ,$$

with

$$\varrho_{mn} = \varrho_{nm} . \tag{8.21}$$

Now let us see how this simplification works in the case of the photo-effect. First let us consider the following reactions in the case of very low energy (near the threshold):

$$\begin{cases} p + \gamma \to n + \pi^+, \\ p + \gamma \to p + \pi^0. \end{cases} \tag{8.22}$$

The reaction $p + \gamma \to p + \pi^0$ is practically absent and only builds up very slowly with energy, which indicates that most of the π^0 effect is in p-wave pion production. We may ask why, in the presence of fairly strong exchange scattering, the internal exchange interaction of the π does not give rise to the second reaction, even if the first process occurs primarily.

First let us see whether any of these formal properties contradicts the experimental result. Let us consider specifically, the s-wave production caused by the electric dipole transition $E1$ having three channels, p^γ, n^+ and p^0 in a state of $J = \frac{1}{2}$, $J_z = \frac{1}{2}$ and odd parity.

We may expect, and this is supported by theory and experiment, that the electromagnetic interactions are weak (the electromagnetic coupling constant is small (1/137) so the cross-section for the photo-effect is of the order of 10^{-4} barns while the scattering cross-sections are of the order of several millibarns). Then we can, as a zero'th approximation, switch off the electromagnetic interaction. In this case, we have for the interaction matrix

(8.23)
$$S_0 = \begin{array}{c|ccc} & p^\gamma & n^+ & p^0 \\ \hline & 1 & 0 & 0 \\ & 0 & X & X \\ & 0 & X & X \end{array}$$

The p^γ channel is not effective as we have switched off the electromagnetic interaction. But even if this is not assumed, the p^γ channel will hardly be important because, as we know, the electromagnetic field is hardly influenced by the charge of the proton, and the photon scattering is very small. So we can put the phase shift α_γ equal to 0 and can write:

(8.24)
$$\exp[2i\alpha_\gamma] = 1 .$$

Now, a condition for applying the above formalism is that we have only diagonal elements in S_0. This is not the case for our choice of channels because the exchange scattering between n^+ and p^0 involves cross links.

In order to avoid this difficulty, we choose our channels not in terms of pure charge states but as linear combinations of them. We shall take as pure states the isotopic spin states corresponding to $\frac{3}{2}$ and $\frac{1}{2}$

(8.25)
$$\begin{cases} \chi_3 = \sqrt{\frac{1}{3}}n^+ + \sqrt{\frac{2}{3}}p^0 \\ \chi_1 = -\sqrt{\frac{2}{3}}n^+ + \sqrt{\frac{1}{3}}p^0 \end{cases}$$

since there are no cross links between these.

We can now write:

$$S_0 = \begin{vmatrix} 1 & 0 & 0 \\ 0 & \exp[2i\alpha_3] & 0 \\ 0 & 0 & \exp[2i\alpha_1] \end{vmatrix} \tag{8.26}$$

and

$$S = \begin{vmatrix} 1 & i\varrho_3 \exp[i\alpha_3] & i\varrho_1 \exp[i\alpha_1] \\ i\varrho_3 \exp[i\alpha_3] & \exp[2i\alpha_3] & X \\ i\varrho_1 \exp[i\alpha_1] & X & \exp[2i\alpha_1] \end{vmatrix} \tag{8.27}$$

We are not interested in the off-diagonal scattering elements.

Now we can go back to the physical states. The charge state that is produced in the photo-effect is described by

$$i\varrho_3 \exp[i\alpha_3](\sqrt{\tfrac{1}{3}}n^+ + \sqrt{\tfrac{2}{3}}p^0) + i\varrho_1 \exp[i\alpha_1](-\sqrt{\tfrac{2}{3}}n^+ + \sqrt{\tfrac{1}{3}}p^0) .$$

If we pick out the coefficients of the physical states, and get rid of the factor i, we obtain:

$$n^+(\sqrt{\tfrac{1}{3}}\varrho_3 \exp[i\alpha_3] - \sqrt{\tfrac{2}{3}}\varrho_1 \exp[i\alpha_1]) + p^0(\sqrt{\tfrac{2}{3}}\varrho_3 \exp[i\alpha_3] + \sqrt{\tfrac{1}{3}}\varrho_1 \exp[i\alpha_1]) .$$

Now we are faced with the experimental fact that the coefficient of (n^+) is large and that of (p^0) is small, or at least not measurable.

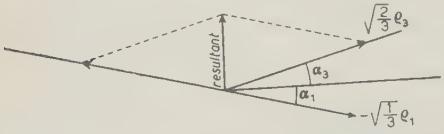

Fig. 12. – Diagram illustrating the effective cancellation of amplitudes giving rise to the small value of the p^0 electric dipole photoproduction.

If we first put the phase shifts equal to 0, it follows that $\sqrt{\frac{1}{3}}\varrho_3 - \sqrt{\frac{2}{3}}\varrho_1$ is large and $\sqrt{\frac{2}{3}}\varrho_3 + \sqrt{\frac{1}{3}}\varrho_1$ is very small.

Our formalism therefore leads to no contradiction; it only tells us that ϱ_3 and ϱ_1 have opposite signs and that $\sqrt{2}\varrho_3 \approx -\varrho_1$. It would, however, be a real contradiction if the coefficient of p^0 were exactly zero. In fact since the two complex vectors have different phase shifts, they will give us a residual vector different from 0, as shown in Fig. 12.

If α_3 and α_1 are small, one obtains the following result for the ratio of the two cross-sections:

$$\frac{\sigma(\to p^0)}{\sigma(\to n^+)} \geqslant \frac{2}{9}(\alpha_1 - \alpha_3)^2 . \tag{8.28}$$

In others words, there is some justification for the assumption of aninternal exchange scattering. So, if the two scattering cross-sections are known (we refer only to the s-wave part) and if $\alpha_1 \neq \alpha_3$ (as we know, they are unequal and of opposite sign) then there exists a minimum value of the cross-section for the p^0 process.

Near the threshold, $\alpha_3 - \alpha_1$ is approximately $10^o\eta$, which corresponds to $\sim 2 \cdot 10^{-1}\eta$ in radians. Thus the ratio of the cross-sections is

$$\frac{\sigma(\to p^0)}{\sigma(\to n^+)} \geqslant 10^{-2}\eta^2 . \tag{8.29}$$

This value is too small and would not be observable at present.

There is another point. We know that near the threshold the phase shifts are proportional to the momentum and therefore $(\alpha_1 - \alpha_3)^2 \sim \eta^2$. But also the cross-section $\sigma(\to n^+) \sim \eta$, from which follows

$$\sigma(\to p^0) \geqslant c\eta^3 . \tag{8.30}$$

This energy dependence is like the one for p-wave photomeson production and makes it extremely hard to distinguish experimentally a small s-wave contribution (*).

9. – Meson Production in Nucleon-Nucleon Collisions.

We consider the reaction

$$2\mathcal{N} \rightleftarrows 2\mathcal{N} + \pi . \tag{9.1}$$

Experimentally, it has been observed in considerable detail up to a bombarding energy of the incident nucleon of approx. 450 MeV. For this bombarding energy, the pion energy is about 70 MeV in the centre of mass system. This energy is small compared to μc^2 and, consequently, we can apply some simplifications which are valid only near the threshold. The reaction takes a

(*) The presence of this small s-wave photoproduction has been detected by the observation of a small asymmetry ($\cos\theta$ term) in the angular distribution of the p^0 reaction, arising from interference between the s-wave and the dominant p-wave production [Y. Goldschmidt-Clermont, L. S. Osborne and M. Scott: *Phys. Rev.*, **97**, 188 (1955)] [*Note by* B. T. Feld].

variety of forms:

(9. 2) $$\mathrm{p}+\mathrm{p} \rightarrow \begin{cases} \mathrm{p}+\mathrm{p}+\pi^0 \\ \mathrm{p}+\mathrm{n}+\pi^+ \end{cases} \quad (\mathrm{d})$$

(9.3) $$\mathrm{n}+\mathrm{p} \rightarrow \begin{cases} \mathrm{p}+\mathrm{p}+\pi^- \\ \mathrm{p}+\mathrm{n}+\pi^0 \quad (\mathrm{d}) \\ \mathrm{n}+\mathrm{n}+\pi^+ \end{cases}$$

(9.4) $$\mathrm{n}+\mathrm{n} \rightarrow \begin{cases} \mathrm{n}+\mathrm{n}+\pi^0 \\ \mathrm{p}+\mathrm{n}+\pi^- \end{cases} \quad (\mathrm{d})$$

The symbol (d) indicates that the proton and the neutron, after the reaction, may be bound as a deuteron. Not all of these reactions have been observed. In particular, experiments on the processes (9.4) cannot be carried out directly, and have been performed using the loosly bound neutron of deuterium. However, the information obtained is not abundant and we may just as well disregard these processes. Actually reactions (9.2) and (9.4) are charge symmetric and we have good reason for expecting that these reactions will have essentially the same features.

In attempting to put some order into the rather abundant but still quite incomplete experimental material concerning the reactions (9.2) and (9.3), one may take isotopic spin conservation as the main guiding principle.

We observe that in the initial state we have 2 nucleons, which can form states with total I-spins. $T=1$ or 0. So we have, for the initial state, essentially 2 possibilities. In the case $T=1$, depending on the orientation of the I.S. vector in charge space, the actual physical state may be pp, nn, or pn: the principle, however, is that the orientation of the I.S. vector in charge space is immaterial and the properties of the processes are controlled by the values of the vector and not by the values of its 3-rd component.

In the final state, the system consists of a pion, with $T=1$, and 2 nucleons, of which the resultant total I.S., $T_{2\tau\eta}$, may again be 1 or 0. Naturally, the resultant I.S. of the 3 particle system, $\pi+2\eta$, must be equal to the initial I.S. This suggests a classification of the possible processes by means of 2 indices, which represent the I.S. of the initial state ($T=0$ or 1) and the I.S. of the 2 nucleons in the final state. So we would expect the possible combinations shown in Table VIII.

TABLE VIII. – *Classification of the isotopic spin states of the two nucleons* $\mathcal{N}+\mathcal{N} \to \mathcal{N}+\mathcal{N}+\pi$.

Initial T	Final $T_{2\mathcal{N}}$	Classification
1	1	11
1	0	10
0	1	01
(0)	(0)	(00)

(For example, 01 indicates the reaction that occurs when 2 nucleons collide in the initial state in the combination $T=0$ and in the final state the 2 nucleons form a system with $T=1$, which is combined with the $T=1$ of the π to give the resultant 0).

The hypothesis of I.S. conservation evidently excludes the $T=0$, $T_{2\mathcal{N}}=0$ combination. So the possibilities are reduced to 3. An important experimental question is to see whether, in fact, the variety of physical reactions can really be reduced to 3 by these considerations. This analysis has been performed by ROSENFELD ([12]). In the following discussion I shall make use of these results. Let us introduce the following notation: we indicate with A_1, A_0, A_{-1} the charge states of the system of 2 nucleons having total I.S.$=1$ and with B the only charge state corresponding to total I.S.$=0$. We have

$$
(9.5) \qquad \begin{cases} A_1 = pp \\ A_{-1} = nn \\ A_0 = \dfrac{pn+np}{\sqrt{2}} \qquad \text{(symmetric combination)} \\ B = \dfrac{pn-np}{\sqrt{2}} \qquad \text{(antisymmetric combination).} \end{cases}
$$

Suppose e.g. that we start with a B state ($T=0$). If we look at Table VIII, if $T=0$ the final state must be $T_{2\mathcal{N}}=1$; so after the collision has taken place, the state will go into a state containing 2 nucleons in an A state and a pion, which has total I.S.$=1$. We represent this final state with $(A\pi)_0$, where the subscript 0 indicates that the total I.S. is 0.

So we write

$$
(9.6) \qquad \begin{cases} B \to \Gamma_{01}(A\pi)_0 \\ A \to \Gamma_{10}(B\pi)_1 + \Gamma_{11}(A\pi)_1 , \end{cases}
$$

([12]) A. H. ROSENFELD: *Phys. Rev.*, **96**, 139 (1954).

where Γ_{01}, Γ_{11}, Γ_{10} are the transition amplitudes which control the intensity of the processes. (In the second equation (9.6) we have 2 terms because the 2 nucleons in the final state may have I.S. = 0 or 1).

In this manner the phenomenon is described in terms of the 3 transition amplitudes Γ_{01}, Γ_{11}, Γ_{10}. Using the standard rules for angular momentum vector combination, we have

$$
(9.7)\qquad
\begin{cases}
(A\pi)_0 = \dfrac{1}{\sqrt{3}}\,(A_1\pi^- + A_{-1}\pi^+ - A_0\pi^0) \\
(A\pi)_1 = \begin{cases}
\dfrac{1}{\sqrt{2}}\,(A_1\pi^0 - A_0\pi^+) & T_3 = +1 \\
\dfrac{1}{\sqrt{2}}\,(A_1\pi^- - A_{-1}\pi^+) & T_3 = 0 \\
\dfrac{1}{\sqrt{2}}\,(A_0\pi^- - A_{-1}\pi^0) & T_3 = -1
\end{cases} \\
(B\pi)_1 = \begin{cases}
B\pi^+ & T_3 = +1 \\
B\pi^0 & T_3 = 0 \\
B\pi^- & T_3 = -1
\end{cases}
\end{cases}
$$

where A_1, A_{-1}, A_0 may be expressed in terms of the physical states by use of (9.5). For example, let us consider an initial state with 2 protons ($T=1$, $T_3=1$). According to (9.6) and (9.7) we have

$$
(9.8)\qquad (pp) \to \Gamma_{10}(B\pi^+) + \Gamma_{11}\left(\frac{A_1\pi^0 - A_0\pi^+}{\sqrt{2}}\right).
$$

The Γ coefficients are, in general, functions of the initial energy, the energy of the pion and its angle of emission. Eq. (9.8) may be written, by use of (9.5),

$$
(9.9)\qquad (pp) \to \left(\frac{\Gamma_{10}}{\sqrt{2}} - \frac{\Gamma_{11}}{2}\right)(pn+) - \left(\frac{\Gamma_{10}}{\sqrt{2}} + \frac{\Gamma_{11}}{2}\right)(np+) + \frac{\Gamma_{11}}{\sqrt{2}}\,(pp0)\,.
$$

In both the cases $(p\tilde{n}+)$ and $(np+)$, there is a proton, a neutron and a π^+, but in the first case the proton comes first. There is actually a distinction between these 2 states, that depends on which we call the first and which the second nucleon. We shall call the first nucleon that one whose momentum in the c.m.s. (Fig. 13) has algebraically the largest projection on the direction of the pion momentum.

As long as we are interested in the cross-section integrated over all angles, the distinction between first and second nucleon has no meaning. Using the expression (9.9) we obtain, when we do not distinguish between $(pn+)$ and $(np+)$ states:

$$\sigma(pp) = \sigma(pp \to pp0) + \sigma(pp \to pn+)$$

with

$$\left\{\begin{aligned} &\sigma(pp \to pp0) = \tfrac{1}{2}\int |\Gamma_{11}|^2 \mathrm{d}x \\ &\sigma(pp \to pn+) = \int |\Gamma_{10}|^2 \mathrm{d}x + \tfrac{1}{2}\int |\Gamma_{11}|^2 \mathrm{d}x\,, \end{aligned}\right. \tag{9.10}$$

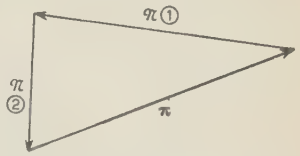

Fig. 13. – Diagram illustrating the method of classifying two identical nucleons in the reaction

$$\mathcal{N} + \mathcal{N} \to \mathcal{N} + \mathcal{N} + \pi.$$

where the integration variable x summarizes all angular, energy, and other appropriate variables. We can, in a quite similiar way, analyse all the other processes and express all the cross-sections in terms of the 3 following cross- sections:

$$\left\{\begin{aligned} \sigma_{11} &= \tfrac{1}{2}\int |\Gamma_{11}|^2 \mathrm{d}x \\ \sigma_{10} &= \int |\Gamma_{10}|^2 \mathrm{d}x \\ \sigma_{01} &= \tfrac{1}{3}\int |\Gamma_{01}|^2 \mathrm{d}x\,. \end{aligned}\right. \tag{9.11}$$

One finds

$$\left\{\begin{aligned} \sigma(pp \to pp0) &= \sigma_{11} \\ \sigma(pp \to pn+) &= \sigma_{10} + \sigma_{11} \\ \sigma(np \to pp-) &= \tfrac{1}{2}(\sigma_{01} + \sigma_{11}) \\ \sigma(np \to np0) &= \tfrac{1}{2}(\sigma_{01} + \sigma_{10}) \\ \sigma(np \to nn+) &= \tfrac{1}{2}(\sigma_{01} + \sigma_{11}) \end{aligned}\right. \tag{9.12}$$

where σ is, in general, a function of the energies

$$\sigma = \sigma(E_{in}, E_\pi)\,. \tag{9.13}$$

In the two reactions

$$\mathrm{pp} \to \mathrm{pn}+$$

$$\mathrm{np} \to \mathrm{np0}$$

there is a considerable probability (of the order of 50 %) that the two nucleons come out bound as a deuteron. In these cases, the cross-sections are expressed by

$$\text{(9.14)} \qquad \begin{cases} \sigma(pp \to d+) = \sigma_{10}(d) \\ \sigma(np \to d0) = \frac{1}{2}\sigma_{10}(d) \end{cases}$$

(the simpler expressions are due to the fact that the deuteron has $T=0$). $\sigma(d)$ is a function of the initial energy only, since we are dealing with a 2-body reaction.

We have a considerable amount of experimental information on various of these processes at various energies. Following ROSENFELD's work ([12]), we will try to determine from the experimental data the values of σ_{11}, σ_{10} and σ_{01} as functions of the parameters upon which they depend. If we measure the π^0-production in pp collisions we obtain directly σ_{11}; also σ_{10}(d) appears isolated in reactions (9.14).

The experimental data on the reaction $pp \to d\pi^+$ are rather complete. Some of them are obtained from the direct, some from the inverse reaction.

The information on the other reactions is, on the other hand, rather meager.

Let us consider now in detail the angular momenta for the three processes 11, 10, 01. In Table IX are listed the possible angular momentum states compatible with the Pauli principle for two nucleons in a $T=0$ or a $T=1$ state.

TABLE IX. – *Angular momentum states permitted by the Pauli principle for two nucleons in the two possible isotopic spin states.*

$T=0$	$T=1$
$^3S_1$	$^1S_0$
$^1P_1$	$^3P_{0,1,2}$
$^3D_{1,2,3}$	$^1D_2$
$^1F_3$	$^3F_{2,3,4}$

The subscripts are the values of J. Let us consider first the process 10, on which the experimental information is most abundant; the possible final states of the two nucleons are shown in the left hand column of Table IX. For instance, we can have the 2 nucleons in the state $^3S_1$. In addition, we have a pion in the final state. For this we specify the angular momentum (s, p, d, ...) with respect to the c.m. system.

We indicate, for example, by the symbol $(^3S_1 p)$ a final state in which the 2 nucleons are in a $^3S_1$ state and the pion in a p-orbit.

In Table X we have collected the most important initial and final states for the (1,0) process.

TABLE X. – *Angular momentum states possible in the reaction* $\mathcal{N}+\mathcal{N} \rightarrow \mathcal{N}+\mathcal{N}-\pi$, *in which the nucleons are initially in the* $T=1$ *state and finally in the* $T=0$ *state.*

Process	Initial state	Final state	I parity
(1,0)	$^3P_1$	$(^3S_1, s)$	1 —
	$^1S_0$	$(^3S_1, p)$	0 +
	$^1D_2$	$(^3S_1, p)$	2 +

In constructing this Table we have listed only the final state of the types (Ss) and (Sp). Higher angular momenta of the pion are improbable at low energy. The nucleons, in addition, are very probably emitted in an S-state because of the large enhancement of this state due to nucleon-nucleon forces. Observe that in Table X, the $(^3S_1 p)$ final state with $J=1$ is missing. The erason is that no initial state with $T=1$ has the required angular momentum and parity.

We have previously found that the cross-sections, for the various processes of pion production considered, may be written as linear combinations of the quantities σ_{01}, σ_{10}, σ_{11}, which are functions of the initial energy of the two nucleons and of the energy of emission of the pion. The coefficients in the combination of these σ's for the various processes of interest are summarized in Table XI.

TABLE XI. – *Summary of the isotopic spin states involved in the various reactions leading to pion production by nucleon-nucleon collision.*

Reaction	Coefficient of		
	σ_{01}	σ_{10}	σ_{11}
pp → pp0	0	0	1
→ np +	0	1	1
→ d +	0	1	0
np → pp —	$\frac{1}{2}$	0	$\frac{1}{2}$
→ np0	$\frac{1}{2}$	$\frac{1}{2}$	0
→ d0	0	$\frac{1}{2}$	0
→ nn +	$\frac{1}{2}$	0	$\frac{1}{2}$

Consider, now, the experimental data on these various reactions. Except in the two cases in which a deuteron is produced in the final state, the pion emerges with a continuous spectrum of energies.

In Fig. 14, taken from the quoted paper of ROSENFELD [12], are presented curves consistent with the observed cross-sections for the various processes plotted against the maximum value of the pion momentum in the c.m.s. in μc units. (This momentum is denoted by η.) These curves are based on the following considerations

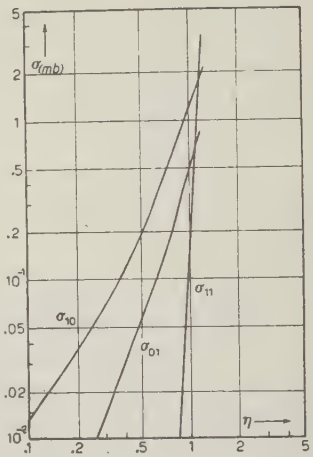

Fig. 14. – Cross-sections for the three fundamental reactions which govern pion production in nucleon-nucleon collisions, plotted against the maximum c.m.s. momentum of the pion.

a) The experimental cross-sections for the reaction $pp \to d+$ agree quite well with an expression of the form $0.14\eta + 1.0\eta^3$. This formula has a semi-theoretical justification, which we shall consider later. From the table one can see that the cross-section involves only the term σ_{10}, and we indicate this by $\sigma_{10}(d)$ to remind us that it arises in the reaction in which a deuteron occurs in the final state.

b) Another experimental cross-section measured is that for $pp \to np+$, in which the neutron and proton emerge unbound. Experimentally it is often easier to detect just the emergent pion, without knowing whether the nucleons remain bound or unbound. The curve of σ_{10} in Fig. 14 represents the sum of the two cross-sections $pp \to pn+$ and $pp \to d+$. The intensities of the two processes are roughly comparable.

c) At present there are only two experimental points known for $\sigma_{11}(\eta)$, the cross-section for $pp \to pp0$. In the absence of further information, the best we can do to describe the excitation function is to join the two points (at 350 MeV and 450 MeV) by a straight line on our log — log graph. The equation for this line is $\sigma_{11} \cong 0.2\eta^8$.

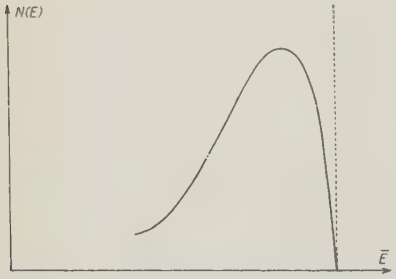

Fig. 15. – Neutron spectrum from the bombardment of a beryllium target by monoenergetic, high energy protons.

d) We now discuss briefly the experimental techniques for studying the neutron-proton collision reactions, from which one obtains σ_{01}. A beam of neutrons may be obtained from the proton beam in an accelerator by charge-exchange scattering in a suitable target, e.g. Beryllium. The neutrons are not monochromatic and the spectrum of the emergent neutrons is about like the one plotted in Fig. 15.

Essentially, two techniques have been used in the experiments we are consider-

ing. These are due to i) YODH (unpublished), ii) WRIGHT and SCHLUTER ([13]).

i) The Yodh technique has been used in studying the two np reactions in which positive and negative pions emerge. A liquid hydrogen target is used and photographic plates are suitably positioned to record the pion tracks, as shown in Fig. 16. In this manner the total cross-section and angular distribution can be studied, for the reactions

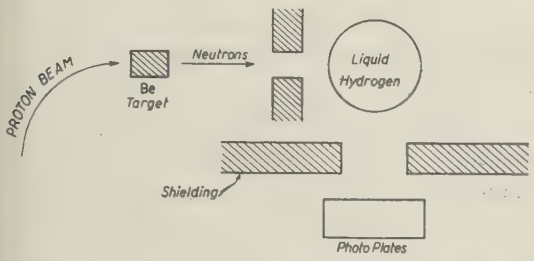

Fig. 16. – Method of Yodh for observing the pions produced in n-p collisions.

$$\mathrm{np} \nearrow \mathrm{pp}- \quad \searrow \mathrm{nn}+ .$$

ii) WRIGHT and SCHLUTER have used, instead, a hydrogen filled diffusion cloud chamber operating at a pressure of 30 atmospheres in conjunction with a magnetic field. With the neutron beam, one can use a high flux of primary neutrons since they are not detected in the chamber unless they interact. Most of the events observed are neutron-proton scatterings and these are used to calibrate the primary neutrons both as to intensity and energy spectrum. The collimation in this experiment is extremely good, since the target and chamber can be separated by about ten metres, so that angular measurements can be carried out very accurately. By using a rather low pulse rate (~ one every half-minute), to avoid local depletions of alcohol vapour, and strict temperature control, these workers have found it possible to distinguish between proton and deuteron tracks unambiguously on the basis of track density and curvature (see Fig. 17). In this manner they separated the neutron-proton scattering events from some 100 cases corresponding to the reaction $n + p \to d + \pi^0$, and so derived the cross-section for this process.

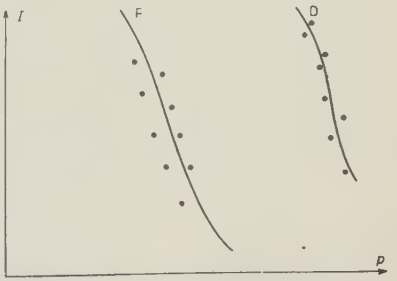

Fig. 17. – Plot of ionization vs. momentum for the tracks observed in a hydrogen-filled diffusion chamber bombarded by fast neutrons (in the experiment of WRIGHT and SCHLUTER).

([13]) R. A. SCHLUTER: *Phys. Rev.*, **95**, 639 (A) (1954).

This cross-section is given in Table XI as $\frac{1}{2}\sigma_{10}$. According to the theory therefore one should have

$$2\sigma(\mathrm{np} \to \mathrm{d0}) = \sigma(\mathrm{pp} \to \mathrm{d}+) \,. \tag{9.15}$$

This was actually found to be the case.

In the same set of pictures, WRIGHT and SCHLUTER have many cases of the reactions $\mathrm{np} \to \mathrm{pp}-$ and $\mathrm{np} \to \mathrm{nn}+$. The first of these is very easily recognized as a three prong event. A peculiarity of the reaction $\mathrm{np} \to \mathrm{pp}-$ is the angular asymetry of the pion emission. In the c.m.s., the negative pions are emitted preferentially in the direction of the original neutron. The positive pions, instead, are more abundant in the opposite direction.

The cross-section σ_{01} has been measured at one energy only (average bombarding energy ~ 400 MeV). From Table XI, it follows that

$$\sigma(\mathrm{np} \to \mathrm{nn}+) + \sigma(\mathrm{np} \to \mathrm{pp}-) - \sigma(\mathrm{pp} \to \mathrm{pp0}) = \sigma_{01} \,. \tag{9.16}$$

It is expected that the excitation function for σ_{01} should be $\sim \eta^4$. On the basis of a single experimental point the coefficient of η^4 is about 0.5 mb.

We summarize the approximate values and energy dependences of the three basic processes:

$$\left\{ \begin{array}{l} \sigma_{10} = \left\{ \begin{array}{ll} \mathrm{d}\,; & 0.14\eta + 1.0\eta^3 \\ \mathrm{np}\,; & 1.0\eta^4 \end{array} \right. \\ \sigma_{01} = 0.5\eta^4 \\ \sigma_{11} = 0.2\eta^8 \,. \end{array} \right. \tag{9.17}$$

The dependences of the above cross-sections on η are in qualitative agreement, as far as the present experimental information goes, with the theoretical scheme of BRUECKNER, SERBER and WATSON [14] who stress the consequences of the hypothesis that pions are normally emitted into p-states. Consider the basic Yukawa reaction,

$$\mathcal{N} \rightleftarrows \mathcal{N} + \pi \,, \tag{9.18}$$

and assume that the nucleon, owing to its large mass, is effectively at rest. The angular momentum and parity of the state represented on the left hand side of (9.18) is $(\frac{1}{2}+)$. Because the pion is a pseudoscalar, the parity of the right hand state is $(-1)^{l+1}$. The pion, therefore, must be emitted into a state

[14] K. BRUECKNER, R. SERBER and K. WATSON: *Phys. Rev.*, **84**, 258 (1951).

of odd l in order to conserve parity. The angular momentum $J = \frac{1}{2}$ can then be obtained *only* with $l = 1$, which combines with the spin $\frac{1}{2}$ of the final nucleon to give a resultant spin of $\frac{1}{2}$.

The conclusion is, therefore, that a nucleon at rest emits pions in p-states only. The extension of this conclusion to pions emitted in the collision of two nucleons is not necessarily correct. The two nucleons in some of the intermediate states of the process may have large relative velocity, in which case the above argument breaks down. Moreover virtual formation of nucleon-antinucleon pairs may also play a role, and when this is the case pions may be emitted preferentially into s- rather than p-states.

It appears, however, that the preferential emission of pions into p-states is fairly well supported by experiment, at least at energies not too far from the threshold for pion production.

The energy dependence near the threshold of the excitation function for a reaction in which n particles are produced is controlled by the energy dependence of the transition matrix element and by the statistical weight of the final state. The statistical weight S near the threshold is

$$S = \text{const} \cdot p^{3n-5}, \tag{9.19}$$

where p is the maximum momentum of the emitted particles at the given energy. This result can be obtained by observing that S is dimensionally proportional to the ratio between the volume V_p in momentum space and the energy E. For n independent particles the momentum space has $3n$ dimensions. Because of the conservation of the center of mass, however, only the momenta of $n-1$ particles can be assigned arbitrarily and the dimensions of V_p are therefore reduced to $3(n-1)$.

Therefore

$$V_p \propto p^{3n-3}. \tag{9.20}$$

Also near the threshold, where the emitted particles are non relativistic,

$$E \propto p^2. \tag{9.21}$$

Thus

$$S \propto V_p/E \propto p^{3n-5}. \tag{9.22}$$

If all particles were emitted into s-states, the matrix element near the threshold would be approximately energy independent and the reaction cross-section would be proportional to (9.19)

$$\sigma \propto p^{3n-5} \qquad (s\text{-states only}). \tag{9.23}$$

If particles are emitted preferentially into p-states, however, additional powers of p appear. The matrix element in this case is proportional to p^q where q is the number of particles emitted in p states.

In this case, then, (9.22) must be multiplied by the extra factor p^{2q}, since the cross-section is proportional to the square of the matrix element. We thus have

$$\sigma \propto \eta^{2q+3n-5} \qquad (q \text{ particles in } p\text{-states}). \tag{9.24}$$

We apply this formula to the reaction $\sigma_{10}(\mathrm{d})$ in which two particles, d and π, are produced. According to (9.24), the excitation function should be proportional to η or to η^3, depending on whether the pion is emitted into an s- or a p-state. Actually in (9.17) this reaction has been represented by two terms, of which the first corresponds to s-wave pion emission and the second (which is usually the largest) to p-wave pion emission.

The reactions $\sigma_{10}(\mathrm{np})$ and σ_{01} have a different energy dependence. For three particles, of which only one (the pion) is in a p-state, we would expect, according to (9.24) $\sigma \propto \eta^6$. But the two nucleons are not completely free, because they tend to have very low relative energy. This is due to the nucleon forces which tend to form a quasi bound, « virtual state » of two nucleons. If this were completely true and the two nucleons were in a bound state, we would expect a two particle reaction, with energy dependence η^3. In fact, the situation is intermediate and an empirical interpolation between the two extremes, η^3 and η^6, yields approximately $\sigma \propto \eta^4$.

The steep excitation function of the σ_{11} process will be discussed later.

Let us consider the reaction

$$2\mathrm{p} \rightarrow \mathrm{d}+ \tag{9.25}$$

in greater detail. Its cross-section is given by (9.17)

$$\sigma(\mathrm{pp} \rightarrow \mathrm{d}+) = 0.14\eta + 1.0\eta^3 \text{ mb.}$$

which fits very smoothly the experimental data. The first term corresponds to the pion going into an s-state and the second, into a p-state. In the range of energy where there is experimental information, the main contribution is from the second term, the first one giving rise to a small deviation from the second. For this reason a fit to the experimental data does not give a reliable value of the coeficient of η. The adopted value 0.14 has been obtained by Rosenfeld [12] using a procedure introduced years ago by Brueckner, Serber and Watson [15], in the interpretation of an experiment by Panofsky [16].

---

[15] K. Brueckner, R. Serber and K. Watson: *Phys. Rev.*, **81**, 575 (1951).

[16] W. K. H. Panofsky, R. L. Aamodt and J. Hadley: *Phys. Rev.*, **81**, 565 (1951).

In the Panofsky experiment a π^- stops in deuterium gas and attaches itself to a deuteron, forming a mesic atom; the meson has time enough to fall in the k orbit of the system. We have a system containing a d and a π^- at very low energy (slightly negative). According to PANOFSKY, two reactions occur

(9.26) (9.27)
$$\mathrm{d} + \pi^- \begin{cases} \nearrow 2\mathrm{n} \\ \searrow 2\mathrm{n} + \gamma \end{cases}$$

PANOFSKY's conclusion is that in 70% of the cases the first reaction takes place and in 30% of the cases, the second.

The inverse of the first reaction

(9.28)
$$2\mathrm{n} \to \mathrm{d} + \pi^-$$

is the charge symmetric twin of the reaction $2\mathrm{p} \to \mathrm{d}+$. We may expect, from general principles, that the intensities of these two reactions are comparable. From the rate of transition in the first branch (9.26) we could compute the cross-section for the inverse reaction by detailed balancing, and this would give the cross-section for the very similar reaction (9.25). In the Panofsky experiment, however, the two reactions (9.26) and (9.27) are too fast (of the order of 10^{-14} s) so that are we not able to determine their rates, but only the ratio of the two rates. We will try to estimate the rate of (9.27) and to deduce from it, and the known branching ratio between (9.26) and (9.27) a value for the rate of (9.26). We use the fact that the deuteron is a very loosely bound system of a proton and a neutron and instead of computing the rate of (9.27), we will compute the rate of

(9.29)
$$(\mathrm{p} + \mathrm{n}) + \pi^- \to 2\mathrm{n} + \gamma\,,$$

which is closely related to

(9.30)
$$\mathrm{p} + \pi^- \to \mathrm{n} + \gamma\,.$$

(The extra neutron plays only a relatively minor role.) An estimate of the ratio in the rates of (9.29) and (9.30) has been given by BRUECKNER, SERBER and WATSON ([15]), who find that it is $\frac{2}{3}$.

The reaction (9.30) is the inverse of the photo-effect $\mathrm{n} + \gamma \to \mathrm{p} + \pi^-$, which is related to $\mathrm{p} + \gamma \to \mathrm{n} + \pi^+$ by a factor of about 1.5; the last reaction was measured near the threshold by BERNARDINI and GOLDWASSER ([10]). We have thus, all the information that is needed in order to compute the cross-section of (9.25) near the threshold. By carrying out the calculation one finds the term 0.14η millibarns of (9.17).

We consider, now, the angular distribution of the reaction (9.25). If we make the assumption that the π can be emitted in an s- or a p-state, we have only the three possibilities shown in Table XII.

TABLE XII. – *Angular distributions in the reaction* $\mathcal{N}+\mathcal{N} \rightarrow \mathrm{d}+\pi$ *on the assumption of s- and p-wave pion emission only.*

Initial		Final	Ang. distribution
$^3P_1$	$\rightarrow$	$(^3S_1, s)_{1-}$	isotropic
$^1S_0$	$\rightarrow$	$(^3S_1, p)_{0+}$	isotropic
$^1D_2$	$\rightarrow$	$(^3S_1, p)_{2+}$	$\frac{1}{3} + \cos^2\theta$

The angular distributions given in the last column correspond to the case that only one value of the angular momentum contributes to the reaction. Otherwise, interference of different angular momentum states may take place.

The angular distribution in the first row of Table XII is isotropic because the π is emitted in an s-state. Also, in the second row we have an isotropic distribution because the state in question has $J=0$.

In the third row of the table the angular distribution is $\frac{1}{3}+\cos^2\theta$, as may be seen by the following argument. The initial state $^1D_2$ is a state with $J=2$ and no spin. The z-component of the angular momentum is equal to 0, as is found by expanding in spherical harmonics the plane wave e^{ikz}. Then, the final state must also have $J=2$ and $m=0$. The angular momentum of this state is the resultant of the deuteron spin $S=1$ and the orbital angular momentum 1 of the pion emitted as a p-wave. From CONDON and SHORTLEY ([8]) one finds that the appropriate linear combination of spin function $S=1$ and spherical harmonic $L=1$ to give $J=2$, $m=0$, is

$$s_{+1}L_{-1} + s_{-1}L_{+1} + 2s_0L_0$$

where

$$(9.31)\quad L_{+1} = Y_{11} \propto -\frac{\sin\theta e^{i\varphi}}{\sqrt{2}}, \quad L_0 = Y_{10} \propto \cos\theta, \quad L_{-1} = Y_{1,-1} \propto \frac{\sin\theta e^{-i\varphi}}{\sqrt{2}}.$$

The angular distribution is given by the sum of the square moduli of the coefficients of the three spin functions and is therefore proportional to

$$2\cdot\frac{\sin^2\theta}{2} + 4\cos^2\theta = 1 + 3\cos^2\theta \propto \frac{1}{3} + \cos^2\theta.$$

If all the three states of Table XII contribute to the reaction, the angular distribution expected is not simply the sun of the three distributions, because

of interference. We observe that the initial state $^3P_1$, does not interfere with the other two states in the table, which are singlet states ($^1S_0$ and $^1D_2$). These two are however capable of interfering. One finds that the interference of these two states results in the angular distribution of the pion of the form

$$\frac{\mathrm{d}\sigma}{\mathrm{d}\Omega} \propto A + \cos^2\theta\,, \tag{9.32}$$

with

$$A = \frac{1 - 2\varepsilon_1 + \varepsilon_1^2 + \varepsilon_2^2}{3 + 6\varepsilon_1}\,, \tag{9.33}$$

where $\varepsilon = \varepsilon_1 + i\varepsilon_2$ is the ratio of the (complex) transition amplitudes of the second and third processes of Table XII. To $A + \cos^2\theta$ we add the isotropic intensity B due to the first process of the table and we obtain the final angular distribution.

$$\frac{\mathrm{d}\sigma}{\mathrm{d}\Omega} \propto C + \cos^2\theta \qquad \text{where} \qquad C = A + B\,. \tag{9.34}$$

One can measure C at various energies and plot C vs. the pion momentum η. One obtains a plot in which the points scatter widely because of the large experimental error. The points indicate, however, that at most energies C is not far from $\frac{1}{3}$. This suggests that the third process of Table XII is strongly dominant. Following ROSENFELD [12], one might attempt to separate the contributions to the total intensity of the three processes of Table XII. Due to the very low accuracy of the measurements of C this involves very great arbitrariness. However a set of relative intensities of the three processes that fits the data is the following

$$0.14\eta \;:\; 0.04\eta^3 \;:\; 0.96\eta^3$$

in the order in which the processes are listed in the Table.

The most striking feature is the relative importance of the third process in Table XII. One might conjecture that this feature is related to the strong enhancement factor of the p-state of the pion-nucleon system, with $J = \frac{3}{2}$ $T = \frac{3}{2}$ (the state (3,3)). In order to test this conjecture, we postulate that, in the dominant process, the pion π and the nucleon $\mathcal{N}_1$ that emits it are in the (3,3) state. The other nucleon $\mathcal{N}_2$ will be in an s-state with respect to $\mathcal{N}_1$. The final state of (9.25) consists therefore of two parts:

part 1	$(\mathcal{N}_1 + \pi)$	has	$T = \frac{3}{2}$	$J = \frac{3}{2}$	parity +
part 2	the nucleon $\mathcal{N}_2$	has	$T = \frac{1}{2}$	$J = \frac{1}{2}$	parity + .

The possible values of the resultants for this kind of final state are, according to the quantum mechanical rules of vector addition:

$$T = 1 \text{ or } 2$$

$$J = 1 \text{ or } 2$$

$$\text{parity } +$$

These values of T, J and the parity of the final state must be the same as for the initial state consisting of two nucleons. The T-value for two nucleons is either 0 or 1; only $T = 1$ matches.

For $T = 1$, the possible states of two nucleons are the following:

$$^1S_0\,, \quad ^3P_{0,1,2}\,, \quad ^1D_2\,, \quad ^3F_{2,3,4}\,, \quad \ldots\,.$$

Of these only

$$^1D_2$$

has the proper parity and J-value. Thus, we see that the hypothesis that the strong enhancement factor of the (3,3) state determines the dominant process of reaction (9.25) leads naturally to the conclusion that the process of line 3 of Table XII should be dominant.

We now discuss the reaction

(9.35) $$\mathrm{p} + \mathrm{p} \rightarrow \mathrm{p} + \mathrm{n} + \pi^+\,.$$

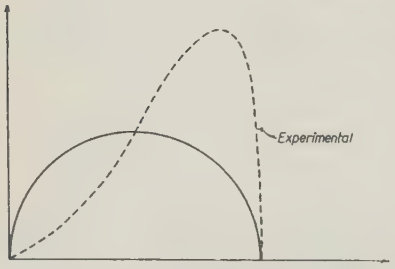

Fig. 18. – Experimental pion energy distribution in the reaction $\mathrm{p} + \mathrm{p} \rightarrow \mathrm{p} + \mathrm{n} + \pi^+$, compared to the theoretical distribution based on the assumption that the cross-section is determined only by the statistical weight of the final state.

In this reaction, the pion has a continuous spectrum of energies, with a peak in the high energy region. What are the qualitative elements which enter into this energy distribution? The best way of discussing this is to compare the observed energy distribution with the one that would be expected near threshold (non-relativistic region) on the assumption that the shape of the spectrum is controlled only by the statistical weight of the final state. If this were the case the spectral distribution would be represented by the semicircular line in Fig. 18.

Now, two factors tend to modify this shape: the first is an enhancement factor, coming from the forces between the two nucleons, which favors a small relative energy of the nucleons, that is a

large energy of the pion. The second factor comes from the fact that the pion is emitted in a p-state. This means that the transition matrix element is proportional to the pion momentum, and the intensity to its square. Both factors tend to modify the actual shape of the spectrum as shown in Fig. 18.

By a more quantitative argument, WATSON [17] found that this phenomenological description is in qualitative agreement with experiment. Quantitatively, however, the theory fails to predict correctly the ratio of the two branches of the reaction

$$\text{(9.36)} \qquad \mathrm{p} + \mathrm{p} \begin{cases} \nearrow \mathrm{d} + \pi^+ \\ \searrow \mathrm{p} + \mathrm{n} + \pi^+ . \end{cases}$$

The ratio of the second to the first branch is experimentally about twice the ratio predicted by the theory. This discrepancy could well be due to a perturbation of the enhancement factor of the two nucleon wave function, due to the presence of the pion.

We have still to discuss the reactions 11 and 01. There is very little experimental information on them.

The first one apparently has a very steep excitation curve, which is approximately proportional to η^8; this is based mainly on data on the reaction

$$\text{(9.37)} \qquad \mathrm{p} + \mathrm{p} \to \mathrm{p} + \mathrm{p} + \pi^0 ,$$

in which the process σ_{11} appears alone. There are only two experimental measurements: one made at a bombarding energy of ~ 345 MeV, at Berkeley, and the other at a bombarding energy of ~ 450 MeV, at Chicago. The two experimental points are fitted by the expression

$$\text{(9.38)} \qquad \sigma_{11} \sim 0.2\eta^8 ,$$

but this formulae may be modified by subsequent, more extensive and precise experiments.

Regarding the 01 process, even less is known. Information on this process is obtained from the two reactions

$$\text{(9.39)} \qquad \mathrm{n} + \mathrm{p} \to \mathrm{p} + \mathrm{p} + \pi^- ,$$

$$\text{(9.40)} \qquad \mathrm{n} + \mathrm{p} \to \mathrm{n} + \mathrm{n} + \pi^+ .$$

They have been observed at only one energy, at Chicago by YODH. He bombarded hydrogen with neutrons having a continuous spectrum, centered

---

[17] K. M. WATSON: *Phys. Rev.*, **88**, 1163 (1952).

at about 400 MeV. The cross-section thus obtained is due to the combined effect of the 01 and 11 processes, $\frac{1}{2}\sigma_{01} + \frac{1}{2}\sigma_{11}$. σ_{01} can be obtained from the difference between this cross-section and the corresponding one on the σ_{11} curve. As there is only one experimental point, there is no question of drawing an excitation curve. But if one assumes than σ_{01} follows a η^4 law, as it should according to the following very rough arguments, then the coefficient should be about 0.5 millibarns,

$$\sigma_{01} \cong 0.5\eta^4 . \tag{9.41}$$

This excitation function corresponds to the hypothesis that only two angular momentum states contribute to the 01 process, precisely the only two that are « favored » because, in the final state, the pion is in a p-state and the two nucleons in an S-state. The two possibilities are

$$\begin{cases} {}^3S_1 \to ({}^1S_0 p)_1 , \\ {}^3D_1 \to ({}^1S_0 p)_1 . \end{cases} \tag{9.43}$$

The η^4 dependence then represents a compromise between the η^3 dependence for a bound ${}^1S_0$ state and the η^6 dependence for uninteracting nucleons (see eq. (9.24)).

The apparently much steeper excitation function for the 11 process, proportional to η^8, could be due to the fact that for this process there are no « favored » angular momenta. This process must then be due to the contributions of many unfavored processes. The excitation function suggests that most of them are of the (Pp)-type, which would lead to $\sigma \propto \eta^{4+9-5} = \eta^8$.

10. – Multiple Production of Pions.

Multiple production of pions has been observed at Brookhaven. Several experiments have been made with the Brookhaven beam, but much more work is needed to give a clear picture. The situation at high energies is more complicated than that at low energies because more particles are emitted.

As a basis for comparison we might use the statistical theory ([18]). In many cases we will find very drastic deviations from this theory and then we must look for an explanation. Unfortunately, few data have been obtained directly from nucleon-nucleon collisions or pion-nucleon collisions. Most of the data have been obtained from nucleon- or pion-nucleus collisions. The interpretation of these data is obviously less simple.

([18]) E. FERMI: *Phys. Rev.*, **92**, 452 (1953); **93**, 1434 (1954).

In this category are the experiments of YUAN and LINDENBAUM [19] relating to the emission of π^+ in the collision of protons, of 1.0 and 2.3 GeV, on beryllium. They observe the spectrum of emitted pions and the ratio of positive to negative pion production. The spectrum is of the shape indicated in Fig. 19, in which the observed pion energies have been converted to their energies in the center of mass system, computed on the assumption of production in nucleon-nucleon collisions. The results of YUAN and LINDENBAUM are summarized in Table XIII.

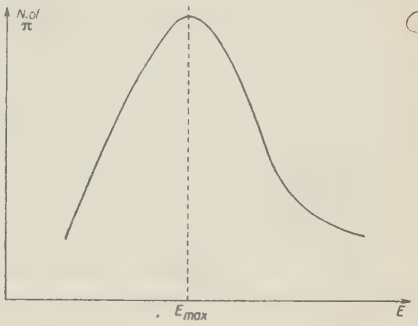

Fig. 19. – Pion energy distribution from bombardment of Be by protons from the Brookhaven Cosmotron, from the experiments of YUAN and LINDENBAUM. The pion energies are in the c.m.s., computed on the assumption of production in a nucleon-nucleon collision.

TABLE XIII. – *Summary of the results of Yuan and Lindenbaum on meson production from the bombardment of* Be *by protons from the Brookhaven Cosmotron.*

Primary GeV	π	E_{max} (MeV)	π^+/π^-
2.3	+	130	1.8
2.3	−	90	
1.0	+	90	4.5
1.0	—	80	

The statistical predictions, according to calculations made by YANG (unpublished) are, summarized in Table XIV.

TABLE XIV. – *Predictions of the statistical theory for the properties of meson production from proton bombardment of* Be *at Cosmotron energies, according to Yang.*

GeV	Production	E_{max}	π^+/π^-
2	double	100	1.7
	single	450	
1	double	90	3.5
	single	170	

[19] L. C. L. YUAN and S. J. LINDENBAUM: *Phys. Rev.*, **93**, 1431 (1954); S. J. LINDENBAUM and L. C. L. YUAN: *Phys. Rev.*, **95**, 638 (A) (1954).

The experimental figure are closer to the theoretical values of E_{max} for double pion production. This is in contradicton with the theoretical expectation of the statistical theory, that single production should still be dominant at these energies.

A set of data that can be compared more directly with theory was obtained in experiments carried out with a hydrogen filled diffusion cloud chamber by SHUTT *et al.* ([20]), who investigated the reactions of protons bombarded by the Cosmotron neutron beam (of about 1.7÷1.8 GeV mean energy and 2.3 GeV maximum energy). For technical reasons, only the three-prong events were recorded. There are many possible reactions, with end produets such as those given in Table XV.

TABLE XV. – *Some possible end products of the bombardment of hydrogen by fast neutrons.*

End products	Observable prongs
n p	1
p p —	3
n n +	1
p n 0	1
n p + —	3
p p — 0	3
n n + 0	1
.....	.....
p p + — —	5

No five-prong events were observed out of some hundred events; so, the probability of such an event is of the order of a fraction of 1%. Three-prong events are rather abundant and attempts have been made to classify them in detail. This is not always feasible and the statistics given in Table XVI may still include some wrong assignments.

TABLE XVI. – *Preliminary results of Shutt et al. on the events produced in a hydrogen filled diffusion chamber by Cosmotron neutron beam.*

Event	Number observed
p p —	24
p p — 0	30
n p + —	95

([20]) W. B. FOWLER, R. P. SHUTT, A. M. THORNDIKE and W. L. WHITTEMORE: *Phys. Rev.*, **95**, 1026 (1954).

The ratio of the observed single pion production (p p —) to the observed double production (n p + —) is, experimentally, $24/95 \cong 1/4$, whereas the expectation of the statistical theory is 4/1. The discrepancy is about a factor 16 in favor of double pion production.

There are some elements of the angular distribution of the (n p + —) reaction that are worth noting. In the c.m.s. the neutron and the π^- are emitted preferentially in the original direction of the neutron; the proton and the π^+ tend to go off in the original direction of the proton.

One must look for the reason for such an angular distribution and, also, for the drastic deviation from the relative intensities expected from the predictions of the statistical model. It has been suggested by many people that they are related to the « resonant » state (3,3). For example PEASLEE ([21]) and others consider as a first step of the reaction.

$$\text{n} + \text{p} \rightarrow \text{n}^* + \text{p}^* , \tag{10.1}$$

where n^* and p^* are excited (resonant) states, $\text{n}^* = (\text{n} + \pi^-)$ and $\text{p}^* = (\text{p} + \pi^+)$, that almost istantaneously disintegrate into a nucleon and a pion (*).

From measurements of the momenta of the charged particles one can compute the relative momentum of the proton and π^+ in their center of mass system and also, although with less certainty, of the neutron and π^-. One can then examine the energy of the $(\text{p} + \pi^+)$ or $(\text{n} + \pi^-)$. If the resonance were sharp, this energy should be well defined (of the order of 200 MeV). But, in fact the resonance is not at all sharp. Perhaps a better picture is given by the enhancement factor as a function of the energy of $(\text{p} + \pi^+)$ or $(\text{n} + \pi^-)$. This factor, as shown in Table V, is large up to the « resonance » energy and drops sharply beyond it. On this basis, one expects, then, that a plot of the observed values of the energies of $(\text{p} + \pi^+)$ and $(\text{n} + \pi^-)$ should yield most values in the energy range up to ~ 200 MeV. There is some small experimental confirmation of this prediction.

The diffusion cloud chamber group has also studied the interactions of 1.37 GeV π^- with protons. (The interactions of the 1.37 GeV π^- beam in nuclear emulsions has also been investigated by WALKER *et al.* ([22]).) On the basis of 94 events, THORNDIKE (unpublished) find the following tentative results:

$$\sigma_{\text{total}}(1.37 \text{ GeV } \pi^- + \text{p}) = 34 \text{ mb} , \tag{10.2}$$

([21]) D. C. PEASLEE: *Phys. Rev.*, **94**, 1085 (1954).

(*) We have, of course, also the possibilities $\text{n}^* = (\text{p} + \pi^-)$ and $\text{p}^* = (\text{n} + \pi^+)$. However, since the states $(\text{n} + \pi^-)$ and $(\text{p} + \pi^+)$ are pure $T = \frac{3}{2}$ states, the probability of their resonant formation is greater than for the mixed states $(\text{p} + \pi^-)$ and $(\text{n} + \pi^+)$. [*Note of* B. T. FELD].

([22]) W. D. WALKER, J. CRUSSARD and M. KOSHIBA: *Phys. Rev.*, **95**, 852 (1954).

for events of all types, including $p \rightarrow p^-$, n^0, p^{-0}, p^{-00}, n^{+-}, etc.. A special study has been made of the elastic scattering events (52 in number). Of these, 43 are scattered through an angle $\theta < 20°$, while 9 are more or less uniformly scattered over the rest of the angular range. This indicates an appreciable « shadow » scattering with, roughly, $\sigma_{\text{shadow}} \approx 7.2$ mb, and $\sigma_{\text{real elastic}} \approx 1.5$ mb. Since $\sigma_{\text{shadow}} < \frac{1}{2}\sigma_{\text{total}}$, we conclude that the nucleon is partially transparent to 1.37 MeV pions. The above values indicate a nucleon transparency of $\sim 20\%$.

C) Experiments with Polarized Nucleons.

11. – Polarization in Nuclear Scattering.

The most detailed information which can be obtained at present on nuclear forces comes from scattering experiments. In the past, cross-sections and angular distributions for nucleon-nucleon scattering have been available up to energies of about 10 MeV; at these energies only *s*-states are involved. More recently, however, it has been possible to extend the range of observation up to about 400 MeV in the laboratory system. The most important information which has been obtained in this energy region is that concerning exchange forces, but in general, little progress has been made, and spin analyses of the various particles involved are still not normally possible.

In the last year or two, however, some progress has been made, particularly in the study of polarization phenomena in the scattering of protons in the high energy range. The attempts to discover such effects are, of course, not new and some early work was done at Berkeley ([23]) with neutrons. The polarization effects observed were only a few percent, and within the experimental uncertainties. The first really successful experiments on polarization in this energy range were performed by OXLEY and co-workers ([24]) at Rochester, who worked with protons. Their experiment is typical of the methods used by later workers, aside from practical modifications rendered necessary by geometrical conditions in the different laboratories. The proton beam inside the synchro-cyclotron strikes a target (carbon, beryllium, and copper have been used; the material of the target is not critical for this experiment) and some of the protons are scattered. Several types of scattering occur, of which we shall consider three.

([23]) L. F. WOUTERS: *Phys. Rev.*, **84**, 1069 (1951).

([24]) C. L. OXLEY, W. F. CARTWRIGHT, J. ROUVINA, E. BASKIR, D. KLEIN, J. RING and W. SKILLMAN: *Phys. Rev.*, **91**, 419 (1953).

a) Coulomb scattering, which, at these energies, is limited to very small angles, and may be neglected.

b) Nucleon-nucleon scattering, in which the interaction may be regarded approximately as a nucleon-nucleon collision, and a recoil nucleon appears at roughly 90° to the direction of the scattered proton. Since the nucleons in the nucleus are not at rest and other nucleons are always involved in the collision, the angular distribution will not show a sharp maximum at 90°. Nevertheless, this type of collision will occur, and may be regarded as pp or pn scattering.

c) Shadow (elastic) scattering. This always occurs if absorption processes are present, because of wave conservation theorems. It is appreciable up to an angle $\theta \sim \lambda\!\!\!^{-}/R$, where R is the radius of the nucleus.

Other types of scattering will also occur, in which the incident nucleon collides several times within the nucleus, imparting considerable excitation energy, and giving rise to a diffuse beam of low energy particles.

We assume that the initial protons are unpolarized, so that half of them will have spin orientation « up » and half spin orientation « down ». On striking the target, the protons will be scattered by each of these processes. If we consider scattering at an angle θ to the right or to the left of the incident direction, particles of one spin orientation will tend to be scattered preferentially to one side or the other; but it is not possible to predict from symmetry considerations alone the sign or amount of polarization in a given direction.

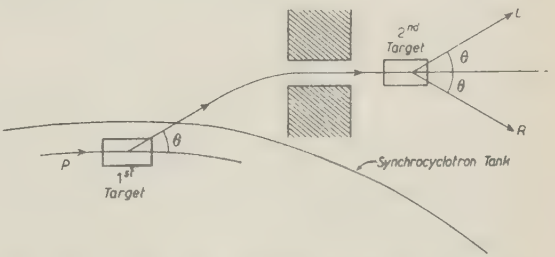

Fig. 20. – Typical arrangement used in the production and analysis of beams of polarized protons from a synchro-cyclotron.

The degree of polarization can be measured by means of the azimuthal asymmetry in the scattering by a second scatterer.

The usual arrangement of first and second scatterers is shown in Fig. 20. The fringing field of the cyclotron will deviate the scattered protons so that the direction of observation does not point directly at the target, and this will reduce contamination by secondary neutrons. The magnetic field does not disturb the polarization of the scattered protons because the spin orientation is parallel or anti-parallel to the magnetic field. If the primary beam is unpolarized, there will be no difference in the intensities of the left and right scattered beams, at a given angle, after the first scattering. These two beams will, however, be partially polarized.

The ratio of spin-up protons going into left and right beams will be

$$\frac{\text{Left}}{\text{Right}} = \frac{1+\varepsilon}{1-\varepsilon}, \tag{11.1}$$

and the ratio of spin-down protons in the two beams will be

$$\frac{\text{Left}}{\text{Right}} = \frac{1-\varepsilon}{1+\varepsilon}. \tag{11.2}$$

If we consider the beam scattered to the left the proportion between spin-up and spin-down is $(1+\varepsilon)$ to $(1-\varepsilon)$. We define the polarisation as

$$P = \frac{\text{Number up} - \text{Number down}}{\text{Number up} + \text{Number down}} = \frac{(1+\varepsilon)-(1-\varepsilon)}{2} = \varepsilon, \tag{11.3}$$

Now if we carry out a second scattering as closely as possible identical with the first, the ratio of the left to right intensities will be:

$$\frac{\text{Left}}{\text{Right}} = \frac{(1+\varepsilon)(1+\varepsilon)+(1-\varepsilon)(1-\varepsilon)}{(1+\varepsilon)(1-\varepsilon)+(1-\varepsilon)(1+\varepsilon)} = \frac{1+\varepsilon^2}{1-\varepsilon^2}. \tag{11.4}$$

This allows the calculation of the polarization of the first scattered beam from

$$\frac{L-R}{L+R} = \varepsilon^2, \tag{11.5}$$

though the sign of ε cannot be determined in this way. The ratio observed experimentally for the intensities of the second scattering to the left and to the right is about 1.5-2, quite a large difference, and the corresponding ratio of spin-up to spin-down may be as high as 3.

A variant of this experiment had been attempted previously ([25]), in which neutrons were observed from the first target, having undergone exchange scattering. In order to study the anisotropy of the neutron beam, protons were then observed from the second target. This method is experimentally simpler, since the path of the neutrons is unaffected by the field of the magnet; but the polarization observed is very much less than that for protons, the observed differences being in most cases comparable to the experimental error. We shall limit ourselves, therefore, to p-p scattering in both scatterers.

We start with a partially polarized beam of protons, whose degree of polarization is known approximately, and can use this to investigate proton-nuclear

([25]) H. BRADNER and R. E. DONALDSON: *Phys. Rev.*, **95**, 663 (A) (1954).

forces, correcting the results to correspond to 100% initial polarization. Any kind of target material can be used now as the second scatterer, and the angular distributions of the left-right asymmetry can be investigated.

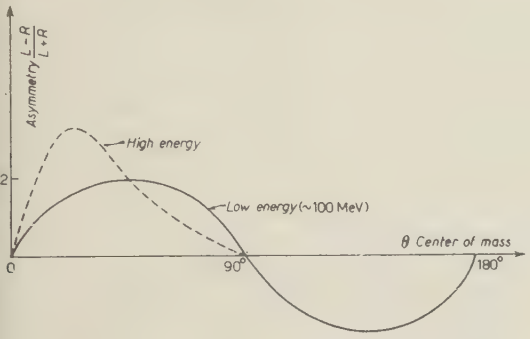

Fig. 21. - Summary of the experimental results on the left-right asymmetry in the scattering of polarized protons by hydrogen.

Consider first scattering of polarized protons by liquid hydrogen. The experimental results ([26,27]) are shown in Fig. 21. The maximum asymmetry occurs, for low energies, at about 45° in the c.m.s. At higher energies the maximum is shifted to smaller angles. Most of the experimental points are for values of θ between 0 and 90°, and the results are corrected to 100% polarization. The experimental data are not yet very accurate, however.

Similar experiments may be carried out on the scattering of polarized protons by nuclei. A higher degree of asymmetry is observed here and $(L-R)/(L+R)$ may be about 0.5-0.6 (Fig. 22). The results here are plotted in the laboratory system. The asymmetry becomes quite small at about 30°, and we have little information about the behaviour at larger angles.

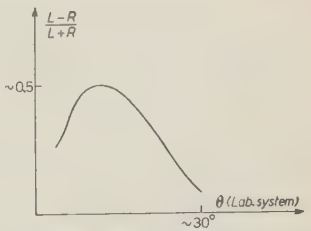

Fig. 22. - Left-right asymmetry observed in the scattering of polarized protons by complex nuclei.

In considering the theoretical interpretation of the polarization effects in proton-proton scattering, we may adopt either of two methods. The first is to calculate the polarization expected on the basis of various proposed potentials, e.g. those of JASTROW, LEVY, CHEW and other workers. It is found that most of these models predict polarization effects smaller than those observed. This may be due to the fact that static potentials are used, in which velocity dependent forces are not included. It is not unlikely that velocity dependent forces are important, and this may vitiate any comparison, even with a valid form of the static potential.

([26]) O. CHAMBERLAIN, E. SEGRÈ, R. TRIPP, C. WIEGAND and T. YPSILANTIS: *Phys. Rev.*, **93**, 1430 (1954).

([27]) J. MARSHALL, L. MARSHALL and H. G. DE CARVALHO: *Phys. Rev.*, **93**, 1431 (1954); H. G. DE CARVALHO, E. HEIBERG, J. MARSHALL and L. MARSHALL: *Phys. Rev.*, **94**, 1796 (1954).

The second method, which also has had little success so far, aims only at an empirical description of the facts. One may try to analyse the experimental data in terms of phase shifts. Due to the Pauli principle, the even l states S, D, ... have total spin zero (singlets) and odd l-states P, F, ... have total spin 1 (triplets). This limits the number of possible states, but not sufficiently.

Attempts in this direction have shown that the data available at present are inadequate to determine a unique set of phase shifts. In part this is due to the fact that in the high energy collision of two nucleons very many angular momentum states are of importance. For this reason a much higher experimental accuracy than is available at present would be needed.

If we consider only the angular momentum states S and P, we require the 4 scattering phase shifts α_{lj} shown in Table XVII.

TABLE XVII. – *States and phase shifts involved in* p-p *scattering at relatively low energies.*

State	Phase shift
$^1S_0$	α_{00}
$^3P_0$	α_{10}
$^3P_1$	α_{11}
$^3P_2$	α_{12}

So far, attempts to describe the nucleon-nucleon scattering in this manner have been remarkably unsuccessful, and this is due to the great ambiguity in fitting the various parameters involved: one can find solutions, but not convincing ones, because they allow the phase shifts to be varied almost at will. There is some expectation that, by adding a new experimental fact to be explained, namely data on the polarization, the problem will become somewhat more confined.

The assumption that only the S and P-states contribute to the phenomena is, in this case, particularly unjustified since, for colliding nucleons of energies $200 \div 300$ MeV, it is to be expected that quite appreciable angular momenta will contribute. We make here this assumption only to get an idea of the form of the dependence of the scattering parameters on the phase shifts.

On this assumption, the angular distribution may be given by the formula (where λ is taken in the c.m. system):

$$\frac{1}{\lambda^2}\frac{\mathrm{d}\sigma}{\mathrm{d}\Omega} = A + B\cos^2\vartheta + C\sin\vartheta\cos\vartheta\cos\varphi\,, \tag{11.6}$$

when the nucleons are travelling along the z axis, with the spin direction parallel to the y-axis. The dependence on φ is what gives the right-left asymmetry in polarization phenomena; the coefficient C is the important one

for the asymmetry. The coefficients A, B and C are expressible in terms of the phase shifts, in the following forms:

$$
\left\{
\begin{aligned}
A &= \sin^2\alpha_{00} + \sin^2\alpha_{10} + \frac{9}{4}\sin^2\alpha_{11} + \\
&\quad + \frac{13}{4}\sin^2\alpha_{12} - 2\cos(\alpha_{10}-\alpha_{12})\sin\alpha_{10}\sin\alpha_{12} - \\
&\quad - \frac{9}{2}\cos(\alpha_{11}-\alpha_{12})\sin\alpha_{11}\sin\alpha_{12}\,, \\
B &= \frac{9}{4}\sin^2\alpha_{11} + \frac{21}{4}\sin^2\alpha_{12} + 4\cos(\alpha_{10}-\alpha_{12})\sin\alpha_{10}\sin\alpha_{12} + \\
&\quad + \frac{27}{2}\cos(\alpha_{11}-\alpha_{12})\sin\alpha_{11}\sin\alpha_{12}\,, \\
C &= 6\sin(\alpha_{10}-\alpha_{12})\sin\alpha_{10}\sin\alpha_{12} + 9\sin(\alpha_{11}-\alpha_{12})\sin\alpha_{11}\sin\alpha_{12}\,.
\end{aligned}
\right. \tag{11.7}
$$

Experimentally we know, in the case of p-p scattering, the total cross-section and the angular distribution averaged over right and left, so that the polarization terms disappear. What is remarkable about this distribution is that it is almost spherically symmetric, which would indicate that B is very small. Then one has the polarization factor or asymmetry that can be used to determine the magnitude of the coefficient C.

There is one point that indicates that the assumption made (only S and P-waves) is not very good, at least at the higher energies (about 250 MeV or greater). The asymmetry predicted by (11.6) would have a shape like curve B of Fig. 23, with a maximum at 45°; instead, at higher energies, the asymmetry seems to have a shape like curve A, with the maximum shifted towards smaller angles.

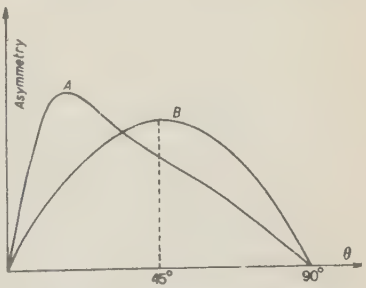

Fig. 23. - Comparison of shape of observed asymmetry, in the scattering of polarized protons by protons, with the prediction of the simple theory assuming S- and P-wave scattering only.

The coefficient C is controlled only by the P-phase shifts, since only the triplet part of the scattering is coupled with the spin. Also, if all the P-phase shifts were equal, $C = 0$.

The above theory could be expanded, as more precise data become available on p-p scattering and, with some principle of charge independence, extended to n-p scattering.

When a polarized beam of nucleons hits a scatterer, three scattering processes can take place: elastic scattering (or shadow scattering); nucleon-nucleon scattering, and nucleon evaporation from excited nuclei. The resulting energy

spectrum of the scattered nucleons is shown in Fig. 24, where part *a*) represents the elastically scattered nucleons (with energy a little smaller than the primary energy, because of the small amount of energy that is taken up by the nucleus); part *b*) represents the nucleons from nucleon-nucleon collisions; and part *c*) represents the evaporation nucleons.

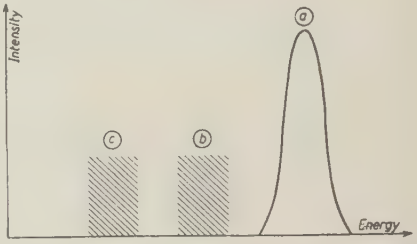

Fig. 24. – Spectrum of scattered nucleons for an incident high energy nucleon on a complex nucleus.

It is experimentally difficult to study the degree of polarization of the various components of this spectrum; in principle, it may be done by using a counter telescope with various absorbers, in order to isolate the various energy bands. Some experimental data (MARSHALL ([27])) are summarized in Fig. 25. We can conclude that the elastically scattered component is polarized, and that the polarization is higher for this component than for the other ones.

Of course, this pattern is some function of the angle θ, because the elastically scattered component has a sharp forward distribution; so, if we go to $\theta = 40^\circ \div 45^\circ$ (depending on the energy) the polarization effect becomes much harder to observe.

Fig. 25. – Asymmetry in the scattering of polarized protons from complex nuclei as a function of the thickness of absorber in the telescope used to detect the scattered protons.

We will now, give a rapid interpretation of the polarization of the elastically scattered component. The polarization of the elastically scattered component is probably due to a spin-orbit coupling of the same nature as that present in the shell model of the nucleus (MAYER ([28])). This model of the nucleus is essentially based on the observed shell structure, in which the assumption, that there is a strong spin-orbit coupling, is very important. We describe the orbit as that of a particle in a potential well, characterized by the quantum numbers l and $j = l + s = l \pm \frac{1}{2}$ (the plus or minus indicating spin parallel or antiparallel to the orbital angular momentum). To fit the experimental values, we have to assume that there is a considerable splitting between $l + \frac{1}{2}$ and $l - \frac{1}{2}$ levels, the coupling making the larger value of j more stable than the smaller value. This indi-

([28]) M. G. MAYER: *Phys. Rev.*, **74**, 235 (1948); **75**, 1969 (1949); **78**, 16, 22 (1950).

cates that the energy corresponding to the « parallel » state is lower than that corresponding to the « antiparallel » state.

One may say that the energy is proportional to $l \cdot s$, with a negative coefficient, i.e. $E = -cl \cdot s$. This is the type of spin-orbit coupling suggested by the nuclear structure.

What sort of interactions between spin and orbit are plausible in nuclear matter? Consider the extreme view of a nucleus where the density ϱ as a function of the distance from the center is constant up to the edge of the nucleus, and then dropping to zero. The nuclear forces are of very short range (say a), as indicated in the Fig. 26. Consider the large sphere of Fig. 27*a* to be the nucleus hit by the nucleon, travelling through nuclear matter of density ϱ; the small circle inside represents the range of the nuclear forces. There will be essentially no forces on the average acting on the nucleon or its spin, at least as long as the nucleon travels in the uniform part of the nuclear matter. There will be, however, some attenuation of the beam in the direction of incidence, equivalent to an absorption due to collisions with other nucleons.

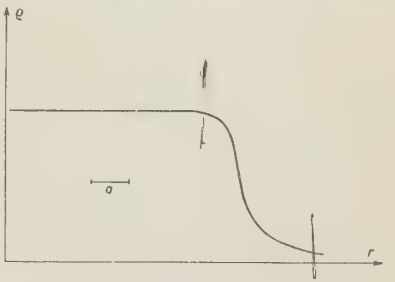

Fig. 26. – Schematic plot of the density of nuclear matter in a nucleus; the range of the nuclear forces is indicated by the distance a.

The situation differs as soon as the nucleon comes to the edge of the nucleus, where ϱ decreases sharply, going to zero outside; the nucleon is then in a sphere of action where on one side the density is ϱ and on the other 0 (see Fig. 27*b*).

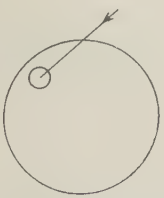

Fig. 27*a*. – Nucleon passing through a nucleus in a region of essentially no net force.

Fig. 27*b*. – Nucleon passing through a nucleus in a region of strong forces.

At this point, the spin-orbit coupling is controlled essentially by the following vector elements: the momentum $\boldsymbol{p}$ of the nucleon, the spin vector $\boldsymbol{\sigma}$ and finally a vector that is the gradient of the nuclear density; the spin-orbit coupling energy is a scalar, and can be fabricated from the 3-vectors by the following combination: $\boldsymbol{\sigma} \cdot \boldsymbol{p} \wedge \nabla \varrho$. Other terms (functions of momentum, gradient of ϱ, ϱ) may be included, but will be neglected for the moment.

Taking into account the shape of the function ϱ, we can transform the previous expression into:

$$(11.8) \qquad (\text{coeff.}) \frac{\varrho'}{r} \boldsymbol{\sigma} \cdot \boldsymbol{x} \wedge \boldsymbol{p} ,$$

where $\boldsymbol{X} \wedge \boldsymbol{p} = \boldsymbol{l}$ (in units of $\hbar$); the coefficient has a negative sign, which satisfies the conditions of the shell model.

Using (11.8) we can try to find out what polarization arises from the spin-orbit coupling. ϱ' is peaked around the edge of the nucleus, where ϱ goes to zero; if we assume a sharp drop for ϱ at the edge, then ϱ' can be represented by a delta-function.

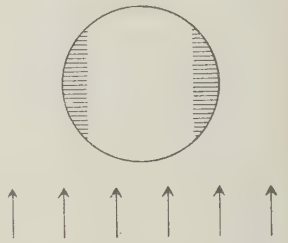

Fig. – 28. Beam of polarized protons (spin up) impinging on a spherical nucleus. The shaded areas represent the regions where the nuclear potential is distorted by the spin-orbit coupling.

Now, we may try to see, without formulae, the effects of such an interaction. Assume a nuclear potential (for instance with sharp corners) and a beam of particles completely polarized as in Fig. 28.; there will be a potential of the $\boldsymbol{\sigma} \cdot \boldsymbol{l}$ type; on the right hand side $\boldsymbol{\sigma} \cdot \boldsymbol{l}$ is positive, and, on the left side, negative. Then the potential well will be deformated as shown in Fig. 29.

Another datum of importance in describing the potential is the main potential well depth (20÷30 MeV). In addition, there is absorption. If the observation is confined to the elastically scattered part of the beam, any particles that suffer non-elastic collisions will be be considered as lost to the beam. This loss of particles (for example, by collisions against nucleons in the nucleus) manifests itself by an attenuation of the beam. The standard way to describe these absorption properties is to add an imaginary component to the potential:

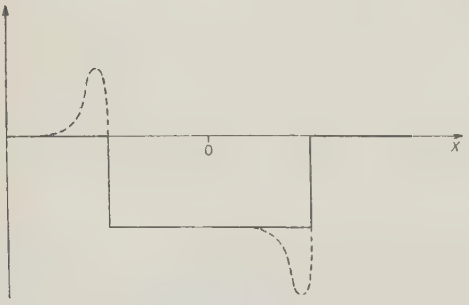

Fig. 29. – Deformation of the nuclear potential due to a spin-orbit coupling of the form of eq. (11.8).

$$(11.9) \qquad U = U_1 + iU_2 .$$

Then the Schrödinger equation takes the form

$$(11.10) \qquad i\hbar \frac{\partial \psi}{\partial t} = (E_{\text{kin}} + U_1 + iU_2)\psi .$$

If we consider only the part depending on U_2, we get

$$(11.11) \qquad \psi \propto \exp\left[(U_2/\hbar)t\right],$$

which, for $U_2 < 0$, represents an absorbed wave.

The magnitude of U_2 is controlled by the mean free path for collisions with nucleons in nuclear matter, which can be computed from the nuclear density and the nucleon-nucleon cross-sections at the given energy; for an energy of 200÷300 MeV, U_2 has a value of about — 7 MeV.

What happens when a particle beam encounters a potential with a real and an imaginary part, and with a depression and a rise, is essentially a diffraction problem. The action of the central part of the potential is clearly symmetric; that of the depression and rise clearly asymmetric.

For a first description of the problem, consider a first approximation corresponding to the Born approximation: this corresponds essentially to considering each element of the potential as acting on the wave with an amplitude proportional to the local value of the potential. Consider scattering through a certain angle θ; the amplitude, after taking into account interference due to the path difference or phase difference resulting from scattering in different regions of the nucleus, is

$$(U_1 + iU_2)\exp[ikr] - D\exp[ik(r - R\vartheta) + D\exp[ik(r + R\vartheta)] = \tag{11.12}$$
$$= [(U_1 + iU_2) + 2iD\sin kR\vartheta]\exp[ikr],$$

where D is the volume of the depression and rise, relative to the total volume of the nucleus, and R the radius of the nucleus.

The amplitude of the scattered wave is therefore (removing the common factor $\exp[ikr]$)

$$U_1 + iU_2 + 2iD\sin kR\vartheta . \tag{11.13}$$

Now look for the terms that may make a right-left difference in the amplitudes for $+\vartheta$ and $-\vartheta$. It is evident that U_1 makes no difference in the intensity, which is the square of the modulus of the amplitude, i.e.

$$U_1^2 + (U_2 + 2D\sin kR\vartheta)^2 = \tag{11.14}$$
$$= U_1^2 + U_2^2 + 4D^2\sin^2 kR\vartheta - 4|U_2|D\sin kR\vartheta .$$

This expression for the intensity is symmetric, except for the term containing $\sin kR\vartheta$; since U_2 is negative, this term means that the intensity to the left is greater than that to the right.

One may now argue as to the validity of this Born approximation procedure. It is medium good for light elements, and medium bad for heavy elements. The reason is the following: The condition for validity of the Born appr. is that the primary wave be not too strongly disturbed by the potential in question. Now, if one considers one element only (and the others

are of comparable importance), namely the effect of U_2, one sees that the wave is absorbed and its intensity reduced in traversing the nuclear matter. It turns out that for a rather large nucleus the intensity drops by about a factor 2, or that the wave loses about 30% of its amplitude. Now, 30% may be considered as small, or as large: we are in an intermediate situation, which may indicate that the Born approximation gives at least a qualitatively correct result for light nuclei, but probably we should make a more accurate calculation for the quantitative details.

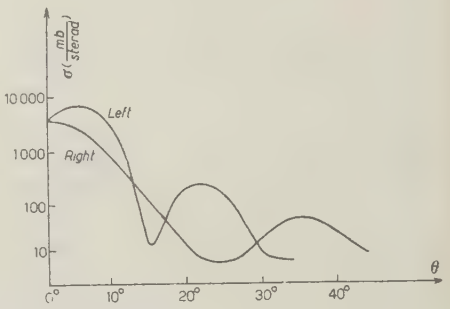

Fig. 30. – Differential elastic scattering cross-sections for 340 MeV polarized protons on carbon calculated for a square well complex potential with spin-orbit coupling.

More detailed calculations can be carried out on this wrong model (sharp potential well ([29])): the results for 340 MeV protons on carbon are showed in Fig. 30.

Interference maxima and minima occur at different angles for left and right scattering; in the region of small angles the left curve is higher than the right one, as was already foreseen in the previous more simple considerations. The right curve has maxima less sharp and shifted towards larger angles than the left one.

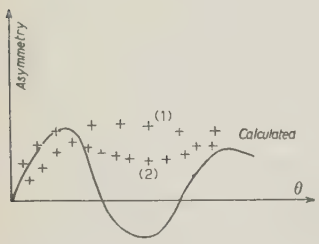

Fig. 31. – Comparison of observed asymmetries in the scattering of polarized protons from C (1) and Al (2) with the predictions from Fig. 30.

Experimentally, the situation is not yet quite clear. The values for the asymmetry, compared with those calculated from Fig. 30, are shown in Fig. 31. (SEGRÈ at Berkeley, on C (1) and Al (2) ([30])).

We should remember that this theory applies only to the elastically scattered protons; as the angle ϑ increases the competition with the non-elastically scattered protons becomes more and more important (the cross-section varies by a factor 100 from 0° to 30°), and it is difficult experimentally to separate the elastically scattered protons from the other components.

The aluminium curve shows a minimum, but no reversal of the polarization. An experimental situation of this kind is not unexpected, because of

([29]) See, for example, G. A. SNOW, R. M. STERNHEIMER and C. N. YANG: *Phys. Rev.*, **94**, 1073 (1954); B. J. MALENKA: *Phys. Rev.*, **95**, 522 (1954); W. HECKROTTE and J. V. LAPORE: *Phys. Rev.*, **95**, 1109 (1954).

([30]) O. CHAMBERLAIN, E. SEGRÈ, R. TRIPP, C. WIEGAND and T. YPSILANTIS: *Phys. Rev.*, **95**, 1105 (1954); **96**, 807 (1954).

the extreme model used: in the sharp-edged nucleus model, with the δ-function in the l-s coupling, the interference terms are very strongly exagerated. Presumably, if one eliminates the sharp boundary, one will wash out these interference patterns.

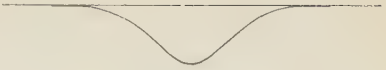

Fig. 32. – Density distribution in a light nucleus, showing the inadequacy of a model which assumes a sharp boundary.

In a small nucleus the edges of the nucleus are something like in Fig. 32; if one takes a nucleus with a larger radius (with the radius large compared to the diffuseness of the edges) then one can get a potential corresponding to something like Fig. 33; here, interference effects presumably begin to appear. One can try to introduce a suitable degree of diffuseness to account for the experimental results.

Fig. 33. Particle density distribution in a heavy nucleus.

Now two final remarks.

1) Sign of the polarization: a theory of this kind predicts that at small angles the particles with spin up go preferentially to the left; for this, there is no experimental confirmation. The sign of the polarization can be detected by two methods:

a) studying the interference with coulomb scattering;

b) slowing down a polarized beam, by ionization loss, to a few MeV, and detecting the sign of the polarization by means of processes of ordinary nuclear physics, which are sufficiently understood to give the sign of the polarization; there is sufficient reason to believe that during ionization loss there is very little probability of spin flip (*).

2) In the Born approximation, the polarization phenomena appear as due only to the U_2 part of the potential; this is just a trick used in Born approximation, because the potential scatters with an amplitude given directly by the potential; if you go to higher approximations, things become more complicated.

What we have learned from the polarization effects is the following: there is good evidence that the l-s coupling of conventional nuclear physics persists with essentially the same strength at higher energies; this can presumably be tied to the primary origin of the l-s coupling, already present in a latent form in the nucleon-nucleon forces.

(*) This has recently been done at Chicago (L. MARSHALL and J. MARSHALL: *Nature*, fasc. 1 (1955)), and the sign turns out to be as predicted by the theory of Fermi. [*Note of* B. T. FELD].

SUPPLEMENTO AL VOLUME II, SERIE X
DEL NUOVO CIMENTO

N. 1, 1955
2° Semestre

The Production of Mesons in Very High Energy Collisions (*).

W. HEISENBERG

Max-Planck-Institut für Physik - Göttingen

When nuclear encounters take place at very high energies, say of 100 GeV or more, then usually many mesons are produced. This does not necessarily mean that already in a nucleon-nucleon collision many mesons are produced because it might be that a production of many mesons takes place through a cascade process inside a nucleus. This was the view which was for a long time held by HEITLER. On the other hand, I think there has recently been pretty good evidence that also in a single nucleon-nucleon collision many mesons can be produced. Best evidence for this are perhaps the jets which are occasionally observed and in which there are great numbers of shower tracks without the appearance of any heavy tracks. Although it is in most cases not probable that these events are actually simple nucleon-nucleon collisions one may say that even if they constitute reactions with nucleons at the surface of a nucleus the nucleus cannot have participated in the process very much since else one would have observed the evaporation of particles. That such events are possible has been emphasized by the theory long ago and the attempts have also started very early to connect the theoretical estimates with experiment. I remind you of the papers by WATAGHIN — but it was only in recent years that one has tried to give a more detailed theoretical description. Such description was given by FERMI and myself and recently by LANDAU. In the following I shall not repeat the details of FERMI's and my own papers but I will give a survey of LANDAU's work which is perhaps not generally accessible since it was published in Russian. At the end I will compare the results of the three theories with recent experiments. LANDAU's paper appeared after those of FERMI and myself and tries to improve on the angular distribution of the particles as found by FERMI.

We describe everything in center of mass system. To begin with we have two

(*) Reproduced from the magnetophone-tape after the lecture of the Author.

nucleons which are pictured in Fig. 1 as very thin disks (Lorentz-contraction). Where the two disks collide we have a region of very high energy density and of extremely strong interaction and therefore one can assume that a large proportion of the proton energy goes into the mesonic field. As well in Fermi's as in Landau's theory the assumption is made that the whole kinetic energy is transferred into the mesonic field, whereas I assumed that this proportion depends on the degree of interaction. It is small when the impact parameter is large, whereas the total energy goes into the mesonic field when the particles collide head-on.

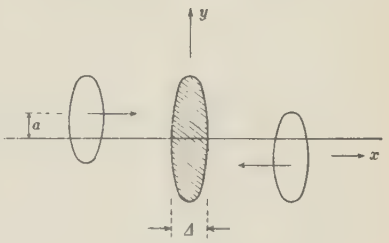

Fig. 1.

Now at the beginning we have a very high energy density of the mesonic field concentrated in a small region and we must ask what happens. In Fermi's theory the interaction in the meson field in supposed to be so strong that we can consider this as a state of temperature equilibrium, the temperature simply being calculated from the energy density. It is assumed that the mesons are a kind of Bose gas, the energy density is given by the initial energy of the process, and thereby one can calculate the temperature from Boltzmann's law. FERMI then assumes that when the region of the meson field starts expanding the temperature equilibrium is at once frozen in, the energy distribution and the number of particles stay constant.

In my paper I did not consider the mesons as a Bose gas but rather as a wave-field which obeyes a non-linear wave-equation, the non-linearity representing the strong interaction. So I simply had to calculate how such a nonlinear-wave equation would lead to an expansion and to what kind of expansion.

LANDAU tries to improve the Fermi theory. He is not satisfied with the assumption that the particles spread out without any further interactions isotropically into space. For some time, he says, there will still be interaction because the energy density is still very high. When the energy density has fallen below a certain critical value, only then one may expect the interactions to become so weak that they do not affect the energy distribution. Now LANDAU has defined this point as the one at which the temperature reaches the order of $\mu c^2/k$ (where μ is the rest mass of π-meson and k is the Boltzmann constant). In the region of strong interaction the particles will be accelerated by hydrodynamic pressure almost only in the x-direction (Fig. 1) and therefore the angular distribution will be much less uniform than in Fermi's theory. LANDAU distinguishes three steps of the whole development:

1) A hydrodynamic state of affairs where the gas which is first concentrated in a small region, expands nearly linearly to the sides. Therefore

we can treat this as a two-dimensional problem in x and t. The process is still non-adiabatic, i.e. the interaction is so strong that heat-transfer will take place from one element to another with the total entropy slightly increasing. When the linear expansion has reached a certain degree than also the expansion sidewards will come into play and then he considers the expansion as an adiabatic process. Finally a state is reached in which the temperature in that part of the volume which is considered goes down to the order of $\mu c^2/k$. From this moment on the interaction is broken off, LANDAU assumes that then the energy and angular distribution remain constant. He arrives in this way at angular and energy distributions which are different from FERMI's.

He assumes, however, that the total number of particles is the same as in the Fermi theory, he actually normalized his number of particles so as to fit the Fermi theory. We now consider the steps in detail:

First, the period from t_0 to t_1 (Fig. 1). LANDAU starts from the energy-momentum tensor

$$T^{ik} = pg^{ik} + (\varepsilon + p)u^i u^k \ ;$$

p (hydrodynamic pressure in the system where the gas is at rest) equal to, $\varepsilon/3$ for pure Bose gas, neglecting the rest mass,

ε energy density in the rest system,

$\vec{u}$ four dimensional velocity with which a volume-element in the gas is moving

$$g^{ik} = \begin{pmatrix} -1 & & & 0 \\ & 1 & & \\ & & 1 & \\ 0 & & & 1 \end{pmatrix} \qquad u = \left\{ \frac{1}{\sqrt{1-\beta^2}}, \frac{\vec{\beta}}{\sqrt{1-\beta^2}} \right\}.$$

In this bose-gas the temperature T is proportional to $\varepsilon^{\frac{1}{4}}$, therefore the entropy goes as $\varepsilon^{\frac{3}{4}}$.

He now applies to the tensor T^{ik} the ordinary rules

$$\frac{\partial T^{ik}}{\partial x^k} = 0 \ ,$$

For our two-dimensional problem this reduces to two equations. If one considers only those parts of the gas which move approximately with the velocity of light ($u = u^0 \gg 1$) these equations can be replaced by the following:

$$\frac{\partial}{\partial t}(\varepsilon u^2) = -\frac{1}{4}\frac{\partial \varepsilon}{\partial \zeta}, \qquad \frac{\partial \varepsilon}{\partial t} = -\frac{\partial}{\partial \zeta}\left(\frac{\varepsilon}{u^2}\right); \qquad \zeta = t - x$$

of course such hydrodynamic equations have very many solutions and it is not quite easy to pick out such solutions which represent the phenomenon well;

therefore I feel that the solution LANDAU picked out is perhaps somewhat arbitrary, but at least one can check that it is actually an approximate solution. Here it is

$$\varepsilon = \varepsilon_0 \exp\left[-\tfrac{4}{3}(\eta + \tau - \sqrt{\tau\eta})\right] \qquad \text{where} \quad \tau = \lg(t/\Delta) \quad \eta = \lg(\zeta/\Delta).$$

For the above ε, u^2 must be of the following form:

$$u^2 \approx \frac{t}{2\zeta}\sqrt{\frac{\tau}{\eta}},$$

ε and u^2 are solutions only if we neglect the differential quotient of τ and η at this point.

Because of $T^{00} = \varepsilon u^2$ and $u^2 \sim t/\zeta$ we obtain for the energy $\mathrm{d}E$ in a layer of thickness $\mathrm{d}\zeta = \zeta\,\mathrm{d}\eta$

$$\mathrm{d}E = \varepsilon a^2 u^2 \mathrm{d}\zeta\,,$$

where a is the radius of the disk. Therefore

$$\mathrm{d}E \sim \exp\left[-\tfrac{1}{3}(\sqrt{\tau} - 2\sqrt{\eta})^2\right]\mathrm{d}\eta\,.$$

In this manner one finds for the entropy

$$\mathrm{d}S \sim \exp\left[-\tfrac{1}{2}(\sqrt{\tau} - \sqrt{\eta})^2\right]\mathrm{d}\eta\,.$$

If you plot the energy density as a function of ζ you obtain qualitatively Fig. 2.

2) We now come to the period $t_1 \to t_k$. The instant t_1 depends on the position of the volume element in the gas, it is not the same all over the gas.

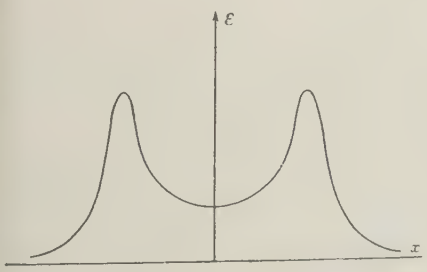

Fig. 2.

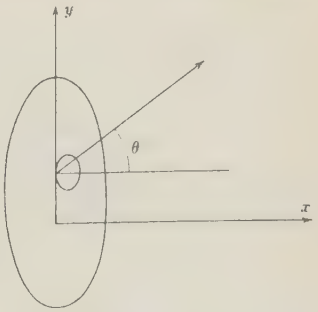

Fig. 3.

Let us now assume in this step ($t_1 \to t_k$) that the expansion can take place in all directions. The question is under what direction the different volume

elements are emitted. LANDAU says that the velocity of any volume element is caused by the acceleration due to hydrodynamic pressure.

The angle θ (compare Fig, 3) is then determined by,

$$\theta = \left(\frac{\partial T_{yy}}{\partial y}\right) \Big/ \left(\frac{\partial T_{xx}}{\partial x}\right),$$

which is the ratio of force in y-direction to that in x-direction. In y-direction the energy density decreases smoothly and the derivative $\partial T_{yy}/\partial y$ will be of the order of magnitude ε/a. While $\partial T_{xx}/\partial x$ will be of the order ε/ζ. Therefore we have

$$\theta \sim \zeta/a\,.$$

Now it seems easy to calculate the value of t_1. The one-dimensional solution is valid if $t\zeta \ll a$; therefore it has the time limit $t_1 = a^2/\zeta$.

Thus in the middle the volume elements start to spread out to all directions soon, but at the outer edge they are always pressed in the forward direction by hydrodynamic pressure.

Beyond the time t_1 Landau assumes that the process is adiabatic.

$$\varepsilon u^2 t^2 = \text{const}\,.$$

This means that the energy density times volume is constant. Whereas the relation $sut^2 \sim \text{const}$ follows from the fact that the entropy density times volume is constant. From these two equations we have

$$u \sim t$$

$$\varepsilon \sim 1/t^4\,.$$

Just at the time t_1, we introduce $\tau_1 = L + \lambda$ and $\eta_1 = L - \lambda$, where

$$\lambda = \lg\,(a/\zeta) \qquad \text{and} \qquad L = \lg\,(a/\Delta) = \lg\,(E/2Mc^2)\,.$$

Therefore one obtains for the entropy

$$\mathrm{d}s \sim \exp\,[\sqrt{L^2 - \lambda^2}]\mathrm{d}\lambda\,.$$

Because of the proportionality between the entropy and the number of particles in the volume elements ($\mathrm{d}N \sim \mathrm{d}s$) this is equivalent to

$$\mathrm{d}N \sim C\,\exp\,[\sqrt{L^2 - \lambda^2}]\,\mathrm{d}\lambda\,.$$

Having introduced $\lambda = -\lg \operatorname{tg}(\theta/2)$ one obtains the angular distribution in the center of mass system:

$$\mathrm{d}N \sim \exp\left[\sqrt{L^2 - \lambda^2}\right](\mathrm{d}\theta/\sin\theta) .$$

The constant factor is gained by normalization:

$$\int \mathrm{d}N = N .$$

3) *Determination of time* t_k. The solution having the required properties for $t \geqslant t_1$, is

$$\varepsilon = \varepsilon_0 \left(\frac{t_1}{t}\right)^4 \exp\left[-\frac{4}{3}(2L - \sqrt{L^2 - \lambda^2})\right] .$$

the instant t_k of the free spreading-out of the particles is given by

$$t_k = t_1 \left(\frac{\varepsilon_0}{\varepsilon_k}\right)^{\frac{1}{4}} \exp\left[-\tfrac{1}{3}(2L - \sqrt{L^2 - \lambda^2})\right] ,$$

where

$$\varepsilon_k \sim \frac{\mu c^2}{(\hbar/\mu c)^3} ,$$

ε_k being the energy density for which $T_k = \mu c^2/k$. t_k again is different for the different volume elements.

Let us now calculate the velocity u of the volume element at the instant t_k, i.e. the velocity with which the mesons are left when the interaction has stopped

$$u = \frac{t_k}{t_1} u_{t_1} = \frac{t_k}{t_1}\sqrt{\frac{t_1}{\zeta}} = \frac{t_k}{a} .$$

The energy-distribution is therefore:

$$\mu u \sim M \exp\left[-\frac{L}{6} + \lambda + \tfrac{1}{3}\sqrt{L^2 - \lambda^2}\right] ,$$

(μ, meson mass; M, proton mass).

Passing over to the angles one gets

$$\mu u \sim \frac{\text{const}}{\theta} \qquad \text{for small } \theta.$$

Having finished this short report on Landau's calculations, let us now go into the physics of these equations. One important result is that mesons of high energy are emitted only under small angles θ. I.e., the angular distribution is very anisotropic in the sense that only slow mesons can be emitted in all directions.

The energy distribution is not very different from Fermi's and is essentially given by

$$\mathrm{d}E \sim \exp\left[-\tfrac{1}{3}(\sqrt{\tau} - 2\sqrt{\eta})^2\right].$$

This energy distribution has however a high energy tail in such a manner that the number of particles of high energy E decreases as $\mathrm{d}E/E$.

This high energy tail is longer than in Fermi's or my theory. We shall now make a detailed comparison of the three theories.

In both the Fermi and Landau theories we have in the initial state a Bose gas with a fixed number of particles and very strong interacton. In my theory we have a mesonic field of very high energy concentration. It is a well defined field, not a statistical assembly like a Bose gas, which will obey a non-linear wave equation. In the Fermi and Landau theory practically all kinetic energy of the nucleons goes into the meson field, whereas in my theory the possibility of glancing collisions is taken into account where only a small part of the kinetic energy goes into the meson field.

For the transition $t_0 \to t_1$ all the 3 theories are rather different. Perhaps Landau's theory here resembles mine more than Fermi's since it takes into account the interaction between the particles at this stage. Both theories also give a strong dependency of the number of high energy mesons on the angle of emission, that is a strong anisotropy, contrary to Fermi's theory.

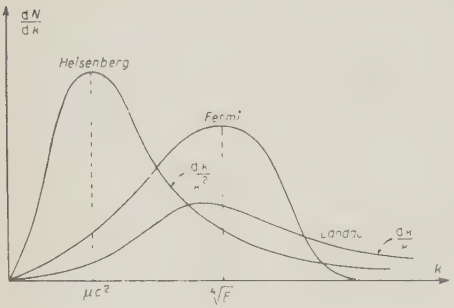

Fig. 4.

From t_k onwards the 3 theories make the same assumption of no further interactions taking place.

The energy distributions resulting from the theories are qualitatively given in Fig. 4.

As to the comparison with experiment there seems to be good evidence that the multiplicities are rather low at high energies. If one assumes the energy distribution of my theory to be correct it is possible to get the right multiplicities only by making plausible assumptions on the fraction of the energy going into the meson field. If, on the other hand, the glancing collisions should not play an important role one would have to conclude from the small number of mesons that the energy distribution as given by Fermi or Landau is better.

Which of the two alternatives is true has not yet been decided by the experiments. I might mention that in the one case which so far still seems to be the most useful one (20 shower particles being spread out over an angle of about 50 degrees) the average measured energy of the secondaries is much smaller than given by the Fermi theory and seems to fit quite well my theory. But one case is really no case and one has to wait for further experimental results.

Now with regard to the angular distribution the famous shower of Schein shows a strong anisotropy in the center of mass system. This has been interpreted by Fermi by taking into account angular momentum conservation.

Still the anisotropy is so marked, that it may be taken as an argument in favour of Landau's or my theory.

There is another argument which comes from the observation of large air showers. There, too, seems to be the indication of a very strong anisotropy

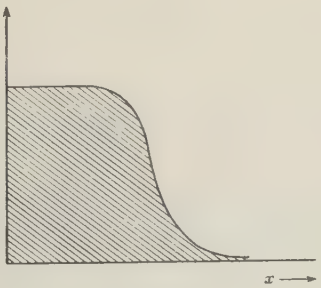

Fig. 5.

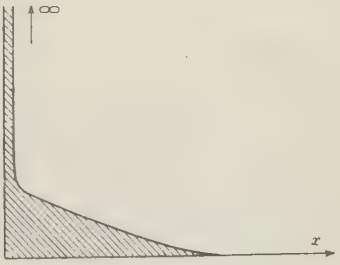

Fig. 6.

since the shower cones are always distributed within distances only of the order of 10 or 20 cm.

In conclusion I should like to mention that the angular distribution is very important for the study of the structure of elementary particles.

It is easy to see that the angular distribution depends on the distribution in space of the mass density of the nucleon. In Landau's and my theory a smooth distribution (Fig. 5) was assumed which gives a strong anisotropy whereas in current theories like quantum electrodynamics one uses distribution functions of δ-function type (with a tail) (Fig. 6) which would result in rather isotropic angular distributions. For these reasons it is important to study the angular distributions in order to obtain information about the structure of elementary particles.

PARTE PRIMA

Sezione II

Questioni relative alla fotoproduzione e fenomeni connessi.

Lectures on Photoproduction.

G. Bernardini (*)

Istituto Nazionale di Fisica Nucleare - Sezione di Roma
Physics Department University of Illinois, Urbana, Ill.

1. – Total Cross-Sections.

1·1. – The photoelectric production of pions by nucleons is more complicated than the pion-nucleon scattering.

This last one may be analized in terms of phase shifts only, i.e. in terms of partial waves depending upon the two good quantum numbers: angular and isospin momenta.

The first instead involves also the photon absorption which from one side destroys the conservation of the isospin and from the other introduces a nucleon « electromagnetic structure » which can be correlated to the scattering only by a definite nucleon model. However the so-called « *phenomenological* » approach is almost indipendent of any model.

Recently, mainly through the works of Feld [1], Fermi [2], Watson [3] and Gell-Mann and Watson [4], this interpretation of the photopion processes reached a rather complete and satisfactory agreement with the more reliable experimental results, both for charged as well as for neutral pions. The term « phenomenological », especially in the latest works Watson's, means a rather deep analysis based on conservative principles, as those implied by the S-matrix formalism and time-reversal. It is phenomenological in the sense that for instance the strong interaction in the $I = \frac{3}{2}$, $J = \frac{3}{2}$ state is accepted

---

(*) Now professor at the University of Illinois, Urbana, Ill.

(1) B. T. Feld: *Phys. Rev.*, **98**, 330 (1953).

(2) E. Fermi: Unpublished, see *Varenna lectures*, 1954.

(3) K. Watson: *Phys. Rev.*, **95** 228 (1954): see also K. A. Brueckner and K. M. Watson: *Phys. Rev.*, **92**, 1023 (1953).

(4) M. Gell-Mann and K. M. Watson: *Annual Review of Nuclear Sciences*, **4**, 219 (1954).

as an experimental fact from the pion-nucleon scattering experiments and then introduced in the interpretation of pion-photoproduction. This analysis based on general principles cannot be erroneous but in some over-simplifications introduced in dealing with the several processes. One of these for instance, and the main one, may be the limitation to the two lowest angular momentum states.

Prof. FERMI has shown in his lectures the essential lines of this analysis. In this and in the following lectures the most recent and reliable experimental results, both on charged and neutral photopions, will be summarized and then, for a better understanding, « phenomenologically » discussed. Step by step, explicit reference to FERMI's lectures will be made and, occasionally, only some additional explanatory arguments will be introduced.

1·2. – The four photoelectric reactions of the nucleon are

$$(1)\qquad \gamma + \mathrm{p} \begin{cases} \nearrow\ \mathrm{n} + \pi^+ = \mathrm{n}^+ & a) \\ \searrow\ \mathrm{p} + \pi^0 = \mathrm{p}^0 & b) \end{cases}$$

$$(2)\qquad \gamma + \mathrm{n} \begin{cases} \nearrow\ \mathrm{p} + \pi^- = \mathrm{p}^- & a) \\ \searrow\ \mathrm{n} + \pi^0 = \mathrm{n}^0 & b) \end{cases}$$

Reactions (2*a*) and (2*b*) have been studied mostly using deuterium and their interpretation needs some assumptions on the influence of the binding forces. Reaction (2*b*) has not yet been directly measured and studied.

Reaction (1*b*) at energies sufficiently above threshold (250 ÷ 300 MeV) has a cross-section comparable with (1*a*). As it will be seen this fact would hardly be understandable without the idea of a strong charge-independent pion nucleon interaction. Actually at these energies the branching ratio between (1*a*) and (1*b*) is essentially determined by the angular and isospin pion-nucleon momenta. We shall be concerned with reactions (1) and (2) at not too high energies. By « not too high energies », we mean energies such that the multiple photo-production of pions is certainly impossible or negligible. According to the results of some preliminary experiments at Cal. Tech. and Stanford that means at least energies of about 400 MeV. For this energy interval, the corresponding interaction distance is then expected to be the pion-Compton wave length $\lambda\!\!\!^{-}_{\mathrm{C}} = \hbar/\mu c$. Because the pion wave length $\lambda\!\!\!^{-} = \hbar/p_\pi$ at $\simeq$ 400 MeV is about twice $\lambda\!\!\!^{-}_{\mathrm{C}}$, the expected dominant pion angular momenta occurring in photopion phenomena up to 400 MeV are $\lesssim 2$.

Precisely up to 400 MeV the pion angular momentum l_π will be

$$(3)\qquad \hbar l_\pi \simeq p_\pi \cdot \lambda\!\!\!^{-}_{\mathrm{C}} \lesssim 2\hbar\,.$$

1·3. – As it has been already mentioned the phenomenological analysis is mostly a correlation between pion-nucleon scattering and photo-pion pro-

duction. The correlation has sense only when comparing the same pion energies and momenta in the center of mass system (c.m.s.).

The relativistic transition between the laboratory system (l.s.) and the center of mass system is well known. A very general and neat presentation of all the more interesting formulae on this subject can be found in BLATON: *Mathematisk fysiske Meddelelser*, **24**, n. 20.

We shall designate by indexes L and B the quantities referring respectively to l.s. or c.m.s.

For the special cases in which we are now interested (nucleon at rest); the total energy available in the c.m.s. is

$$W = \sqrt{E^2 - \mathbf{K}^2} \nearrow \begin{matrix} \sqrt{M^2 + \mu^2 + 2ME_L} & \text{(incident pion)} \\ \searrow \sqrt{M^2 + 2Mv_L} & \text{(incident photon)} \end{matrix} \tag{4}$$

where

E = total energy,
$\mathbf{K}$ = total momentum,
M = nucleon mass ($M_p = M_n$),
μ = pion mass = 140 MeV/c^2,
E_L = total pion energy,
v_L = energy, momentum incident photon ($h = c = 1$).

It is useful to remember that

$$v_B = \left(\frac{M}{M + 2v_L}\right)^{\frac{1}{2}} v_L \tag{5}$$

and that the velocity of the *center of mass* is

$$\beta = \frac{\mathbf{K}}{E} = \frac{v_L}{v_L + M}. \tag{6}$$

The pion momentum in the pion nucleon system is

$$p_B = \frac{p_L}{\sqrt{1 + (\mu/M)^2 + 2(E_L/M)}} \tag{7}$$

or with

$$\eta = p_B/\mu, \qquad \omega_L = E_L/\mu = \sqrt{\eta^2 + 1}$$

$$\eta^2 = \frac{\omega_L^2 - 1}{1 + 2(\mu/M)\omega_L + (\mu/M)^2} \simeq \frac{\omega_L^2 - 1}{1 + 2(\mu/M)\omega_L}. \tag{8}$$

With the preceding formulae we can find some very useful relationships. Comparing a pion-nucleon scattering with a photopion production leading to the

same energy in the c.m.s., we have by (4)

$$(9) \qquad \nu_L = E_L + \frac{\mu^2}{2M}.$$

Introducing the kinetic energy T_L of the pion we get

$$(9') \qquad \nu_L = T_L + \mu + \frac{\mu^2}{2M} = T_L + \nu_0$$

where ν_0 is in the l.s. the threshold energy

$$(10) \qquad \nu_0 = \mu\left(1 + \frac{\mu}{2M}\right).$$

With

$$M_p = 938.2\,, \qquad \mu^{\pm} = 140\,, \qquad \mu^0 = 135.5\,.$$

it is found for (1*a*), i.e. for

$$p^{\gamma} \to n^+: \qquad \nu_0^+ = 151.1 \text{ (132.1 in the c.m.s.),}$$

and for (1*b*)

$$p^{\gamma} \to p^0: \qquad \nu_0^0 = 146.0 \text{ (127.9 in the c.m.s.).}$$

For instance it was found by WALKER *et al.* [5] that the total cross-section of the reaction (1*b*) has a well defined maximum ($\sigma_T^0 \cong 2.3 \cdot 10^{-28}$ cm^2) between 300 and 340 MeV photon energy. With the use of (9′) this photon energy corresponds to a pion energy $T_L \cong 320 - 150 = 170$ MeV which is the « resonance » energy of the pion-nucleon scattering.

1·4. – Reactions (1) and (2) have been studied rather extensively in all laboratories where an electron accelerator above pion threshold was available. Of course, all measurements have been performed with the continuous bremsstrahlung spectrum. However as far as we are concerned with the reactions (1*a*) and (1*b*) in hydrogen (nucleon at rest in the l.s.) we have to deal with a two body problem in which all initial energies and momenta are defined. Thus the measurement of emission angle and energy of one of the final two particles determines completely the energy of the incident photon. The determination of the cross-section requires an absolute calibration of the photon beam. This

---

[5] R. L. WALKER, D. C. OAKLEY and A. V. TOLLESTRUP: *Phys. Rev.*, **89**, 1301 (1953).

has been done by a calorimetric method by KERST and EDWARDS (6), with the 300 MeV Illinois betatron. The more elaborate Cornell calibration (7) agrees, within 2%, with KERST's. The Cal. Tech. monitoring system seems to give a value higher than the Cornell one for about 7%. Thus for comparison with other data the Cal. Tech. data should probably be multiplied by a factor ~ 1.1. The shape of the bremsstrahlung spectrum has been checked rather carefully in the several laboratories with pair spectrometers. It agrees, in the limits of the pair-spectrometer resolution, with the Schiff spectrum. As an example, in Fig. 1 the results of LEISS, YAMAGATA and HANSON (9) are plotted versus the evaluated Schiff spectrum (*).

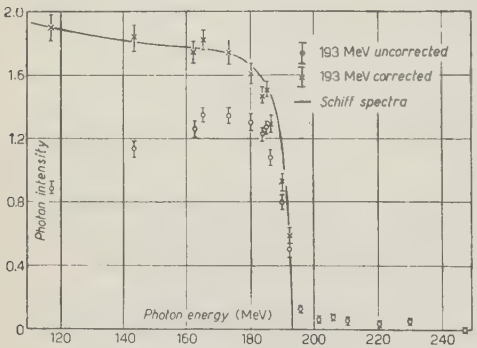

Fig. 1.

The energy region above 300 MeV has been investigated by a series of very careful and complete measurements only at Cal. Tech. Below 300 MeV experiments carried out at Berkeley, Cornell, Illinois and M.I.T. overlap each other and agree, almost systematically, in the error limits. The region around the pion threshold has been studied mostly at Illinois (**).

The techniques used have been mostly fast counter coincidences at photon-energies above 200 MeV and mostly plates at energies below this limit.

In all cases the main problem is the efficiency of the detection. It might be that all figures obtained up to now are affected by systematic errors of this type of the order of 10 %.

1·5. – In Fig. 2 the trends of the total cross-sections σ_τ^+ and σ_τ^0 of the two reactions

(1*a*) $$\gamma + p \to n^+$$

(2*a*) $$\gamma + p \to p^0$$

(6) P. D. EDWARDS and D. W. KERST: *Rev. Scient. Instr.*, **24** 490 (1953).

(8) R. LITTAUER: *Rev. Scient. Instr.*, **24**, 1113 (1953).

(9) J. LEISS, T. YAMAGATA and A. HANSON: *Illinois Reports* (1954); J. LEISS: *Thesis, University of Illinois*, 1954.

(*) i. e. using the Schiff formula (*Phys. Rev.*, **83**, 252 (1951)) for the spectrum in the forward direction using the constant C as 191.

(**) A large part of the experimental results used in these lectures and in the figures here presented has been not yet published. A list of references will be very incomplete The author expresses his deep appreciation to his friends and colleagues of the other laboratories who gave him the privilege of knowing these results prior to publication.

are plotted versus photon energies. They are given just to visualize the main features of the two processes.

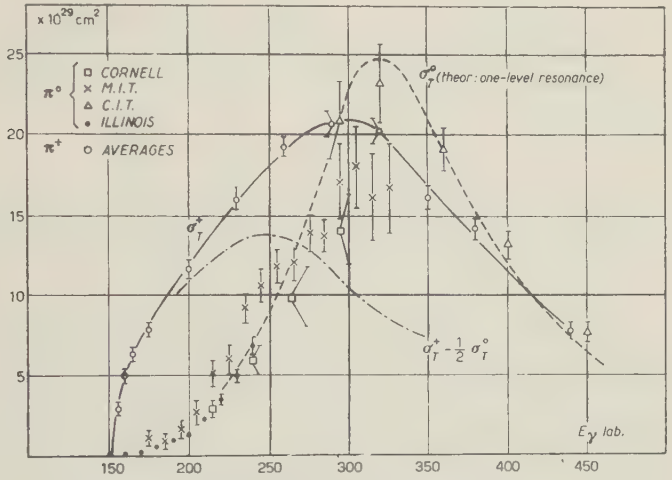

Fig. 2.

The plotted points have been evaluated integrating over the angular distributions (see following Section), that is, assuming that these angular distributions may be expressed by parabolae in cos ϑ. This procedure is probably crude but does not introduce large errors in the final results.

Fig. 3 shows in detail the behaviour of σ_T^0 up to 300 MeV.

The following characteristics are obvious: 1) both curves show a pronounced maximum, but not quite at the same photon-energy; 2) the energy dependence near threshold is completely different. Approximately, if $(\nu - \nu_0)$ is the photon energy above threshold, σ_T^+ varies as $(\nu - \nu_0)^{\frac{1}{2}}$ while σ_T^0 varies roughly as $(\nu - \nu_0)^{2.2}$ ([10]).

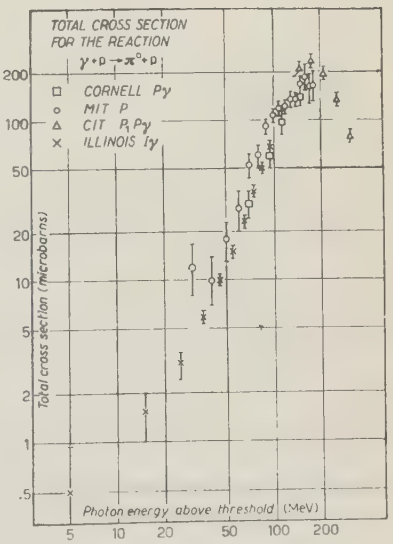

Fig. 3.

The phenomenological theory offers a qualitative interpretation of the maximum. As it has already been mentioned, *it occurs at an energy which cor-*

([10]) L. Koester and F. Mills: to be published in *Phys. Rev.*.

responds very closely to the « resonance » (*) energy of the pion-nucleon scattering. The main difference between scattering and photoproduction is that now the pion-nucleon system is not brought directly and automatically into the state of strong interaction $I=\frac{3}{2}$, $J=\frac{3}{2}$ (see FERMI's lectures) by the incident pion, but by the previously absorbed photon. The two pions, the positive and the neutral one, come out then as the two modes of decaying of the excited $(\frac{3}{2}, \frac{3}{2})$ state.

Now it has been shown by BRUECKNER, and BRUECKNER and WATSON [11], that the simple « one level » resonance formula represents very well the behavior of the $(\frac{3}{2}, \frac{3}{2})$ scattering. It is expected that a quite similar representation will fit photoproduction as well. That should be true at least as far as the strong interaction state is *really the predominant one.*

This seems to be the case for the *neutral* pion as it is shown in Fig. 2 (**). It is assumed that the observed neutral pions are predominantly emitted by a $T=\frac{3}{2}$, $J=\frac{3}{2}$ wave; the same as in the « resonance » scattering. The curve traced in Fig. 2*b* is not an « experimental » curve but that « evaluated » by GELL-MANN and WATSON [1] and the agreement could not be better.

One may say, as it will be shown later, even better than it should. The evaluation has been done assuming that

$$\sigma_T^0 = 2\pi \left(\frac{\hbar}{\mu c}\right)^2 \frac{\Gamma_\gamma \Gamma}{(E - E_0)^2 + \Gamma^2/4}, \tag{11}$$

where the parameter Γ (resonance width) and $E_0 = 159$ MeV (resonance energy) are those which fit the pion-scattering around the resonance. E is the actual pion-energy in c.m.s. and finally Γ_γ depends upon the photon energy and is the reduced width (see FELD's lectures).

Also the energy dependence of the reaction $p^\gamma \to p^0$ near threshold is the expected one. The reaction is dominated by the « resonance » that is by only one angular momentum. In that case as it has been indicated by FERMI the expected energy dependence ($l = 1$) is

$$d\sigma \cong (\sin^2 \alpha_{33}/\eta^2)\, d\eta, \tag{12}$$

where $\eta = p_\pi/\mu c$ is the pion momentum in μc units. This, expressed by the

---

[11] K. S. BRUECKNER and K. M. WATSON: *Phys. Rev.*, **76**, 923 (1952).

(*) Here and then the word « resonance » will be essentially a short cut to indicate a strong attractive interaction.

(**) Here and there the interpretation of the π^0-photoproduction will be simpler than that of the π^+. This is due to the fact, previously mentioned, that the π^0 does not interact directly with the e.m. field. As a consequence the π^0 exhibits more directly the structure of the pion-nucleon interaction.

photon energy ν, gives (α_{33} is proportional to η^3 and $\nu \simeq \sqrt{\eta^2+1}$)

$$d\sigma \cong (\nu^2 - 1)^{\frac{3}{2}} \nu \, d\nu$$

in agreement with the value found by KOESTER and MILLS.

It is worth of note that an energy dependence of the type

$$d\sigma \simeq (\sin^{2l} \delta l / \eta^2) \, d\eta , \tag{13}$$

where δl is the phase-shift of the partial wave corresponding to the angular momentum l, is quite general and it is based on very general arguments ([12]).

1·6. – For the *charged pions* we do not expect such simple and straightforward correlation, because they have a charge and also interact directly with the incident photons; instead neutral pions, even if initially present in the cloud surrounding the nucleon-source, are emitted by the nucleon system only when it gets excited as a whole by the preceding absorption of the photon.

The cross-section σ_T^+ for charged pions is thus quite different from σ_T^0. Near threshold the energy dependence is typical of an S-wave. We will see soon, also by the angular distribution, that effectively up to about 230 MeV, the positive pions are emitted predominantly in a S state. According to the odd parity of the pion with respect to the nucleon and the conservation of the total angular momentum, a single pion may be thought to be around the nucleon source in a P state. Then it might appear that this S wave could find a simple explanation in a $P \to S$ transition of a naive pion-nucleon orbital model. As it has been shown by FERMI, that is not the case. The S wave of the charge pion has certainly another origin as will be discussed in a following lecture.

In spite of the large S-wave term, σ_T^+ exhibits a maximum in a position close to that of σ_T^0 and which is certainly due to the $(\frac{3}{2}, \frac{3}{2})$ state. It is not easy to understand why it is at lower energy than that of the π^0.

The branching ratio between the two final states $\langle n^+|$ and $\langle p^0|$ is determined by charge independence. As shown by FERMI the isospin parts of these final states are:

$$\begin{aligned} \langle n^+| &= \sqrt{\tfrac{1}{3}}\, \chi + \sqrt{\tfrac{2}{3}}\, \chi_1 \\ \langle p^0| &= \sqrt{\tfrac{2}{3}}\, \chi_3 - \sqrt{\tfrac{1}{3}}\, \chi_1 \end{aligned} \tag{12}$$

([12]) K. M. WATSON: *Phys. Rev.*, **88**, 1163 (1952). Formula (13) is certainly valid when as in our case the end products of the reaction are strongly interacting in one definite angular momentum state and the range of forces is small in comparison with the particle wave lengths.

The ratio between the *partial* cross-sections *which are* « *enhanced* » (see FERMI's lectures) by the strong interaction should then be

$$\sigma_T^+/\sigma_T^0 = \tfrac{1}{2}\,. \tag{13}$$

In Fig. 2, $\frac{1}{2}\sigma_T^0$ has been subtracted from σ_T^+ to indicate the amount of σ_T^+ which may be considered as due to « non-enhanced » processes. This subtraction implies an oversimplification; however the dropping down of this non-enhanced part around the « resonance » is quite interesting. Obviously around the resonance, the $(\frac{3}{2}, \frac{3}{2})$ state competes vigorosouly with all other possible states.

2. – Survey on Photopion-Production. The Angular Distributions.

2·1. – We want now to consider the angular distribution of the photopions.

It is obvious that it is always possible to write the differential cross-section $\mathrm{d}\sigma/\mathrm{d}\Omega$ as a function of photon-energy ν and scattering angle θ in terms of a series (*)

$$\frac{\mathrm{d}\sigma}{\mathrm{d}\Omega}(\nu, \theta) = A_0(\nu) + A_1(\nu)\cos\theta + A_2(\nu)\cos^2\theta + \dots\,. \tag{1}$$

The argument mentioned in Sec. **1** about the angular momenta being involved in photopion production, suggests that the terms after the third are very likely rather small. In other words (up to ~ 400 MeV) the series will drop off rather quickly because only S-, P- and, at most, D-waves will be present with large amplitudes.

This argument is somewhat emphasized by the consideration of the statistical factors automatically involved. Consequently, we will analyze the experimental results on photopions on the basis of a simplified angular dependence as given by (1) with the higher terms definitely dropped.

2·2. – *The angular distribution of the* π^0 is not as well determined as that of the charged ones. The experimental difficulties encountered are essentially due to the two-photon decay of the π^0 This decay destroys the simplicity

(*) It is probably very well known that (1) is equivalent to an expansion in spherical armonics, that is in partial waves corresponding to the various angular momenta. It is also obvious that the second term A_1 is an interference term and therefore depends also upon the relative phases of the partial waves. We will see later some more about this expansion. See also FERMI's lectures.

of the two-body problem leaving us only one possible simple angular correlation, that of the recoiling proton. But the condensation of recoiling angles in the foreward directions (which are usually heavily loaded with the electron background) makes also the detection of recoiling protons somewhat difficult.

Starting with the pioneer work of STEINBERGER, PANOFSKY and STELLER [13] there have been four methods used to measure the reactions

$$p^{\gamma} \to p^{0}, \qquad \pi^{0} \to 2\gamma .$$

1) Detect the recoiling proton only [14].

2) Detect one gamma only [15].

3) Detect both gammas in coincidence [16].

4) Detect a coincidence between the recoiling proton and one of the two gammas [17].

But all of them have some very definite difficulties in getting either good statistics or a good angular definition. Method 2) could be used only for determining the total cross-section; method 1) suffers either from the condensation of recoiling protons in the forward direction or from the rather low energies at larger angles; method 3) and 4) suffer from low counting rates and difficulties in getting an accurate estimate of solid angles, detection-efficiency, etc..

In agreement with what has been mentioned in the first Section concerning the production of π^0 by « resonance » it is expected that, up to about 400 MeV, a P wave will be largely the predominant one.

That means that for the reaction $p^{\gamma} \to p^{0}$, the expressions (1) will be simply

$$\left(\frac{d\sigma}{d\Omega}\right)^{0} \simeq A_0 + A_2 \cos^2\theta = A_0\left(1 + \frac{A_2}{A_0}\cos^2\theta\right). \tag{2}$$

Actually with the data available up to now, the analysis of angular distribution of neutral pions gives, for the coefficients A_j, the following values listed in Table I.

---

[13] J. STEINBERGER, W. K. H. PANOFSKY and J. S. STELLER: *Phys. Rev.*, **86**, 180 (1952).

[14] Y. GOLDSCHMIDT-CLERMONT, L. S. OSBORNE and M. B. SCOTT: *Phys. Rev.*, **89**, 329 (1953), and preprint; D. C. OAKLEY and R.W. WALKER: preprint; L. J. KOESTER: preprint.

[15] G. COCCONI and A. SILVERMAN: *Phys. Rev.*, **88**, 1230 (1952); F. E. MILLS and L. J. KOESTER: to be published.

[16] J. STEINBERGER, W. K. H. PANOFSKY and J. S. STELLER: loc. cit..

[17] A. SILVERMAN and M. STEARNS: *Phys. Rev.*, **88**, 1225 (1925); R. L. WALKER, D. C. OAKLEY, A. V. TOLLESTRUP: preprint.

TABLE I. – *Values of the coefficients A_j as a function of the photon energy E_γ.* (E_γ *in* MeV, A_j *in* 10^{-30} cm²/ster).

A_j \ E_γ	200	240	270	300	340	380	420	460
A_0^0	1.4	7.9	14.0	24.0	24.5	18.0	12	7
$-A_2^0$	—	∼7	∼11	∼18	∼21	∼ 16	∼10	—
$-A_1$	—	∼2	—	—	—	—	—	∼—2

They are plotted in Fig. 4 which shows also some of the experimental values and the corresponding estimated errors. The smallness of the interference term A_1 is a clear indication of the actual smallness of the S-wave. This S-wave should be at any rate very small with respect to the P-wave. Because the neutral pion does not interact directly with the photon, a π^0 in a S state would be photoelectrically produced either by a (virtual) S exchange scattering or by the interaction of the photon with the recoiling proton which emits the π^0. Both processes have a small yield, in comparison with the emission by « resonance ». Recently at Illinois KOESTER (18) has been able to show the existence of the S-wave near threshold by finding that around 200 MeV it is really at least 10 times smaller than the corresponding P-wave. At higher energies the enhancement of the P-wave probably makes this proportion even less.

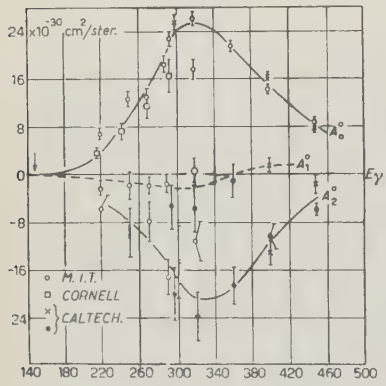

Fig. 4.

A simple electric dipole model (19) may be used to estimate the amount of S-wave due to the nucleon recoil. If one considers that the current $\boldsymbol{j}_p$ of the recoiling nucleon adds its contribution to the general interaction $\boldsymbol{j} \cdot \boldsymbol{A}$ ($\boldsymbol{A}$ is the vector potential) then the matrix elements of the four nucleon photodisintegrations which connect the following initial-final states

$$\langle p^- | \; | n^\gamma \rangle : \langle n^+ | \; | p^\gamma \rangle : \langle p^0 | \; | p^\gamma \rangle : \langle n^0 | \; | n^\gamma \rangle \tag{3}$$

are proportional to

$$\left(1 + \frac{\mu}{M}\right) : 1 : \frac{1}{\sqrt{2}}\left(\frac{\mu}{M}\right) : 0 \,. \tag{3'}$$

(18) L. J. KOESTER: to be published in *Phys. Rev.*
(19) K. M. WATSON: *Phys. Rev.*, **95**, 228 (1954).

Thus, as far as the partial cross-sections due to the recoiling currents are concerned (*), we should have

$$\sigma_s^0/\sigma_s^+ \simeq \frac{1}{2}\left(\frac{\mu}{M}\right)^2 \tag{4}$$

which is very small. But also the π^0 S-wave due to the internal (virtual) charge-exchange scattering is supposed to be very small. Precisely, if we remember the discussion on this subject given by FERMI in his lectures, this S-wave part should be of the order of $(\alpha_1 - \alpha_3)^2\sigma_T^+$.

But both α_1 and α_3 are and remain rather small and σ_T^0 is always certainly $\lesssim \frac{1}{10}\sigma_T^+$. Concluding we may say again that up to $\simeq$ 400 MeV the reaction $p^\gamma \to p^0$ ends mostly in a P state. The S-wave part will be evident mainly through its interference effects, for instance, changing with increasing energy the angular distribution from a backward to a forward one around the resonance. That seems to be the case. Hence, the coefficients A_0 and A_2 characterize fairly well the type of the P-wave. Table I suggests that $\frac{4}{5} \lesssim A_2/A_0 \lesssim \frac{5}{6}$. As will be seen later, this ratio is in agreement with an appreciable electric quadrupole contribution in the nucleon photon-absorption.

2·3. *The angular distribution of charged photopions* is pretty well known and again the agreement among the several laboratories is quite remarkable.

Usually the deviations between determinations obtained in two different experiments performed with completely different techniques (for instance counter coincidences and nuclear emulsions) are always, except in a very few cases, of the order of the estimated errors.

Hence there are good reasons to believe that the curves shown in Fig. 5 represent rather well the trends of the angular distributions of the photoproduction of π^+ from 160 up to about 300 MeV.

The experimental points here indicated are the weighted averages of all reliable experiments (**). The energy-intervals have been selected just to make the most direct use of all available data. From time to time, the data have been interpolated. The indicated errors have been evaluated directly from those given in the original works. In the very few cases in which the spreading of the results was inconsistent with the size of the errors, the maximum spreading was taken as an estimate of the error itself.

For energies higher than 300 MeV, the results recently obtained at Cal.

(*) For the S-wave due to the exchange scattering see FERMI's, lectures.

(**) Among the results which have been considered there are those recently obtained by BENEVENTANO, LEE, STOPPINI and TAU (to be published in *Il Nuovo Cimento*). At low energies they offer the more complete set of data now available.

Tech. (*) give a very complete picture of the situation. This picture is expressed by the curves of Fig. 6. They correspond to a better fit of the data *assuming a parabolic distribution in* $\cos\theta$ than that indicated by (1).

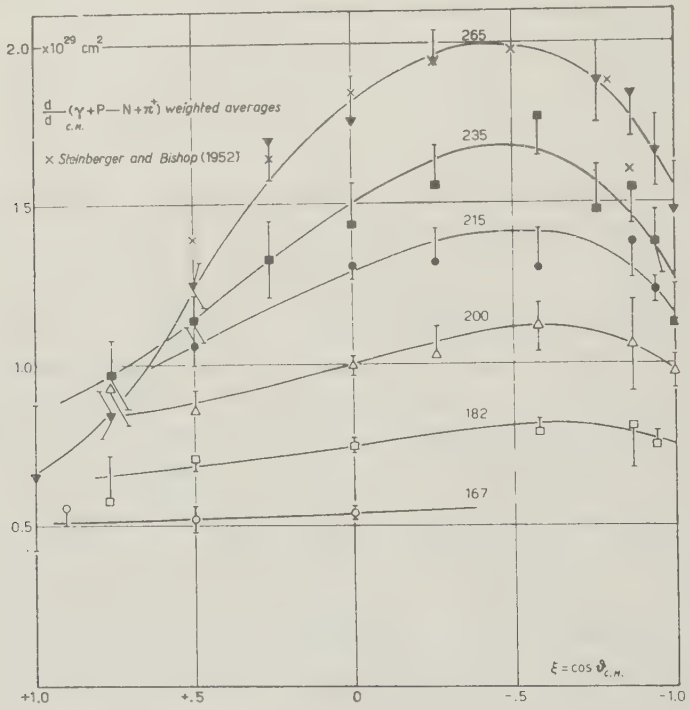

Fig. 5.

Instead the solid lines in Fig. 5 follow the experimental points more closely. The plot has been done versus $\cos\theta$ just to show to what extent one may pretend to visualize in these lines a family of parabolae.

The deviations from a parabolic fit of all curves are appreciable, but rather small. It is thus possible to represent fairly well also $(d\sigma/d\Omega)^+$ with only three terms in $\cos\theta$. Table II and fig. 7 give the corresponding coefficients as functions of photon energies in the laboratory system.

Up to 260 MeV the indicated errors are conventionally evaluated from the experimental errors of the points reported in Fig. 5.

Beyond 260 MeV the errors are those quoted by the Cal. Tech. group. The behaviour of these coefficients will be later discussed on the basis of the multi-

---

(*) The writer is deeply indebted to all his colleagues of the Cal. Tech. group for all of the information kindly sent to him.

pole analysis already mentioned and introduced by FERMI in his lectures. This behaviour is given in Fig. 7. It is quite interesting to note the change of sign of A_1 around 320 MeV which is the « resonance » energy and the fact that A_2 becomes negligible around 440 MeV.

In Fig. 7 is also indicated the part A_s^+ of A_0 which one may attribute to the S-wave and for further discussions, the sum $A_s^+ + A_2^+$ in comparison with A_0.

TABLE II. – *Values of the coefficients A_j as a function of the photon energy E_γ.* (E_γ in MeV; A_j in 10^{-30} cm²/ster.)

A_j \ E_γ	175	200	230	260 (*)	290	320	350	380	440
A_0^+	6.3±.3	10.0±.4	14.0±.5	17.9±.4	18.9±.5	18.4±.5	15.3±.5	11.3±.4	6.2±.3
$-A_1^+$	.9±.4	2.2±.6	3.6±.7	6.1±.7	3.8±1.2	1.1±.9	1.1±.6	2.5±.6	3.5±.7
$-A_2^+$	.4±.5	2.2±1.1	4.3±.7	9. ±.8	7.9±.9	7.2±.9	5.4±.9	3.0±.7	-0.4 ±.8

(*) The values and the errors above 260 are those given by WALKER, TEASDALE, PETERSON and VETTE from two different experiments; the magnet and the telescope. The values given here are the averages. The corresponding errors are somewhat smaller than one may guess from the spreading of the experimental points.

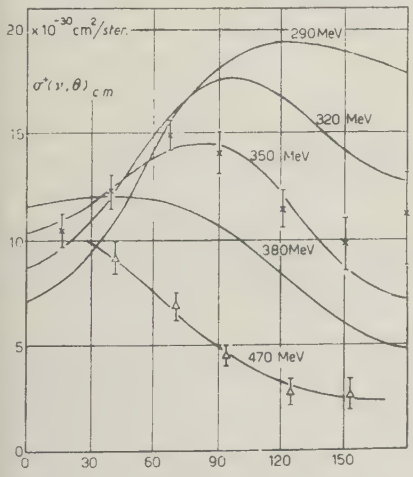

Fig. 6.

In abscissae the pion angle in c.m.s.

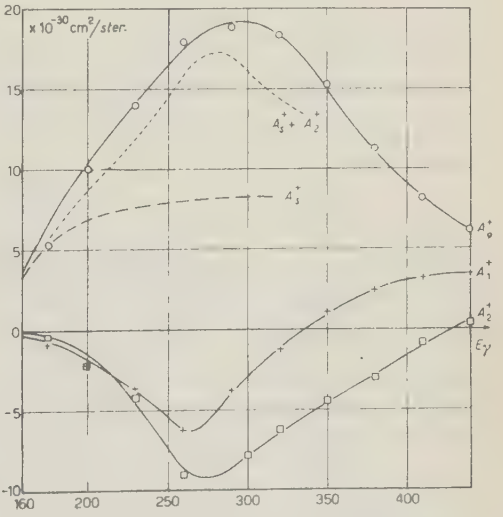

Fig. 7.

In abscissae the values of E_γ in l.s.

The total cross-sections were determined from the activation curves [23] corrected for the counting efficiency. Very near threshold all angular mo-

[23]) L. KATZ, A. G. W. CAMERON: *Can. Journ. Phys.*, **29**, 518 (1951); A. S. PENFOLD and J. E. LEISS: *Phys. Rev.*, **95**, 637 (1954).

menta, except $l = 0$ are vanishing. The total cross-sections multiplied by $\frac{1}{4}\pi$ give then the S-cross-sections per unit solid angle, as a function of the incident photon energy.

We will now confine our attention to the 90° angle in the c.m.s.. Results obtained (up to 230 MeV) at other angles in the experiments described have been used to build up the family of curves plotted in Fig. 5.

At 90° $\mathrm{d}\sigma/\mathrm{d}\Omega = A_0(\nu)$. The energy dependence of A_0, more conveniently expressed with the pion momentum $\eta = p_\pi/\mu c$, may be rather complicated.

For one of the arguments developed by FERMI and already called upon in the previous Section, the S-wave should be present in A_0 as a term varying as $\cong \eta$, the P-wave as another term varying as $\cong \eta^3$, etc.; and this beside other factors depending upon the photonenergy ν, etc. As far as concerns the S-wave only, these other factors can be taken into account correctly. We want to see this in detail. The cross-section for photopion production may be, of course, written in the usual form

$$\frac{\mathrm{d}\sigma}{\mathrm{d}\Omega} = \chi' |H|^2 , \tag{5}$$

where $|H|^2$ is the matrix element and χ' is the density of final states divided by the unitary flux of incident particles multiplied by 2π ($\hbar = c = 1$). It is easily found (see Appendix I) that

$$\chi' = \frac{2}{\mu^2} \frac{\eta\omega}{(1 + \nu/E_i)(1 + \mu\omega/E_f)} , \tag{6}$$

where $\omega = \sqrt{\eta^2 + 1}$ is the total pion energy in μ units and E_i and E_f are the initial and final total nucleon energies. Near threshold $E_i \simeq E_f \simeq M$ and $\nu \simeq \omega\mu$, then

$$\chi' \simeq \frac{2}{\mu^2} \frac{\eta\sqrt{\eta^2 + 1}}{(1 + \nu/M)^2} . \tag{6'}$$

These factors (see Appendix I) take account of the relative motion of the nucleon referred to the center of mass system. The matrix element H, as far as we consider the S-wave only, has been already discussed by FERMI in his lectures.

2·4. – *The S-wave of charged photopions*, its origin and amplitude as a function of energy has been discussed in full in FERMI's lectures. Thus I will limit myself to the description and discussion of the threshold experiment which has been initiated at Illinois by GOLDWASSER and myself

and extended and completed by BENEVENTANO, LEE, STOPPINI and TAU in Rome ([20]).

The pions were detected in photographic emulsions which were arranged around the target at laboratory angles of 30°-150° in 15° steps. A liquid hydrogen target built by HANSON, WHALIN and REITZ ([21]), has been used. The vertical cylindrical liquid hydrogen container was $1\frac{1}{4}''$ in diameter and its walls, in the region crossed by the X-rays beam, were .005" brass. The angular resolution was always better than $\pm 3°$.

Since the purpose of the experiment was to measure an absolute cross-section, many precautions were taken to check the efficiency of detection. Actually two different experiments have been made. The first with G5 600 μm Ilford plates mounted on the target equatorial plane in such a way that they faced the target with a mean angle of 7°. Meson tracks have been identified and measured by grain counting and plural scattering.

The second experiment was made using 500 μm G5 unsupported emulsions (pellicles) immersed (effectively) in an infinite medium of emulsion. These pellicles (*) have been volume scanned for π-μ decays. All plates and pellicles were scanned twice. The percentages of tracks not in common for the two scannings were used to estimate the effective scanning efficiency. It turned out to be between 93% to 99% and the results have been accordingly corrected.

Plates and emulsions can not be used for laboratory pion-energy below 10 MeV. To extend the threshold measurements down to the very lowest energies in an experiment performed by LEISS, ROBINSON and PENNER ([22]) a completely different technique has been used.

π^+-mesons and their μ^+-decay mesons were stopped in a carbon absorber surrounding the hydrogen target. Since the positrons from the decay of the stopped μ^+-mesons are emitted with an energy spectrum peaked around 36 MeV a large fraction will escape with considerable energy and can be counted. These positrons leaving the absorber will be essentially isotropic, regardless of the angular distribution of the emitted π^+-mesons. Practically, except for few corrections, the spectrum and angular distribution of positrons leaving the absorber are independent of the energy of the photon which initiated the reaction, and thus the yield of positrons is proportional to the yield of π^+. In this way activation curves were obtained in 2 MeV steps from 140 to 200 MeV.

([20]) G. BERNARDINI and E. L. GOLDWASSER: *Phys. Rev.*, **94**, 729 (1954); **95**, 857 (1954): The other results will be published in a forthcoming paper in *Il Nuovo Cimento*.

([21]) To be published in *Rev. Scient. Instr.*

(*) Underdeveloped to minimize the electron background.

([22]) J. E. LEISS: *Thesis, University of Illinois*, 1954. A report on this experiment will be published soon in *Phys. Rev.*

The only difference is to retain the dependence on ν and ω in the final expressions of $\langle n^+ | H | p\gamma \rangle$. Then in the evaluation of the cross-section the factor ω is eliminated by the same factor present in (6) and instead of (7.29) of FERMI's lectures one has

$$\frac{\mathrm{d}\sigma}{\mathrm{d}\Omega} = 2\left(\frac{\hbar}{\mu c}\right)^2\left(\frac{e^2}{\hbar c}\right)\left(\frac{f^2}{\hbar c}\right)\frac{\eta}{\nu}\left[\left(1+\frac{\nu}{M}\right)\left(1+\frac{\omega}{M}\right)\right]^{-1}. \tag{7}$$

As was shown by FERMI, this is really the cross-section for an S-wave (*). It comes out by the combined operation of $\boldsymbol{\sigma}$, which flips the spin of the nucleon, with $\boldsymbol{A}$ which in this case is effective only through the electric-dipole component $\boldsymbol{\epsilon}/\sqrt{2\nu}$ (see Section 3) and which destroys the incident photon while the charged components of the pion field create the emitted pion. We should also remember, that f^2 is here the dimensionless unrationalized coupling constant. This, according to the Chew theory, should be considered as the « renormalized » coupling constant, that is, as the constant which expresses the interaction of a pion with a physical nucleon.

2·5. – The *higher angular momenta* will also contribute to $A_0(\nu)$, i.e. to the 90° cross-section. Near threshold, beside the S-wave previously discussed, the dominant term will be that of the P-wave. As has been shown ([24]) it is due either to the magnetic dipole, or to the electric quadrupole (see also Section 3).

Both (for the general argument already mentioned) near threshold will have the pion-momentum dependence typical of a P-wave, i.e. η^3. As far as concerns the ν dependence we may argue that $\nu \simeq \sqrt{\eta^2+1} \simeq 1 + \frac{1}{2}\eta^2 + \ldots$ and consequently any factor in ν will introduce in the energy dependence a multiplying power series in η^2.

Finally following CHEW ([25]), we may consider the contribution of the direct interaction between e.m. field and charged pion current, i.e. the interaction term:

$$H' = -\int (\boldsymbol{j}_\pi \cdot \boldsymbol{A})\,\mathrm{d}v \tag{8}$$

(*) It might be worth noting that this term is an S-wave because it is originated by the gauge invariance interaction, $ie\boldsymbol{\sigma}\cdot\boldsymbol{A}$, which does not contain either the pion momentum or any angular dependence. It is also clear that the statistical factor in (7) is the right one when the nucleon motion is taken into account, but here it is merely a suitable correction to the Chew interaction. This interaction is indeed non relativistic in the approximation of an infinitely heavy nucleon.

([24]) B. T. FELD: *Phys. Rev.*, **89**, 330 (1953).

([25]) G. F. CHEW: *Phys. Rev.*, **95**, 285 (1954).

Near threshold any subsequent enhancement of the pion state is certainly small. Then this term near threshold contributes mainly directly through a classic photoelectric effect. Precisely it gives rise to an additional term in the cross-section which is a mixture of all multipoles and gives all orders of outgoing pion angular momenta because of the influence of the Sommerfeld « *retardation* », factor in the denominator.

This additional term is ([25]),

$$(9) \qquad -\frac{\mu^2}{2\nu^2}\frac{\beta^2\sin^2\theta}{(1-\beta\cos\theta)^2}, \qquad \beta=\frac{v_\pi}{c}=\text{pion velocity},$$

which at 90° in the c.m.s. becomes

$$(9') \qquad -\frac{\mu^2}{2\nu^2}\beta^2\simeq\frac{\mu^2}{2}\frac{\eta^2}{(\eta^2+1)^2}\simeq\frac{\mu^2}{2}\frac{\eta^2}{\nu^4},$$

and again introduces terms in powers of η^2.

We may then conclude that the matrix element H in (5) is not known, but that the cross-section at 90° in the c.m.s. can almost certainly be expressed as follows:

$$(10) \qquad \left(\frac{d\sigma}{d\Omega}\right)_{90^\circ}=$$

$$=\chi\{A_0^{\pm}+A_2^{\mp}\eta^2+\ldots\},$$

with

$$\chi=\frac{\eta}{\nu}\left(1+\frac{\omega}{M}\right)^{-1}\left(1+\frac{\nu}{M}\right)^{-1},$$

where the coefficients depend upon the sign of the pion.

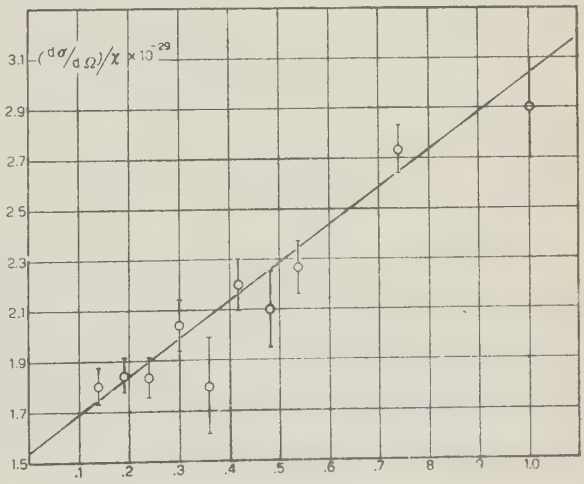

Fig. 8.

Exploring the possibility that near threshold the higher order terms in η^2 may be negligible within the accuracy of the (now available) experiments, the experimental data previously mentioned have been plotted in Fig. 8, versus η^2.

Within the indicated errors a straight line seems to be a very good fit to the experimental points, at least up to $\eta^2\simeq 1$ ($E=230$ MeV).

The best least-square fit straight line passes through the experimental points, yielding

$$(11) \qquad A_0^+=(1.54\pm.13)\cdot10^{-29}: \qquad A_2^+=(1.49\pm.25)\cdot10^{-29}.$$

The value of A_0^+ gives the following total cross-section for S-wave photoproduction at threshold,

$$\sigma_{\text{c.m.s.}} = (1.93 \pm .16)\chi \cdot 10^{-28} . \tag{12}$$

2·6. – As already indicated by FERMI, the extrapolation toward $\eta^2 \to 0$, i.e. the value of the coefficient A_0^+ may be used to obtain a value of the interaction constant f^2, the only factor which remains indeterminate in (10). This determination, as far as the experiment can be considered substantially correct, is of particular interest because of a theorem due to KROLL and RUDERMAN ([26]) which proves that for any relativistic covariant meson theory, at threshold (i.e. for $\eta \to 0$) we can write

$$A_0^{\pm} = 2\left(\frac{e^2}{\hbar c}\right)\left(\frac{f^2}{\hbar c}\right)\left(\frac{\hbar}{\mu c}\right)^2\left\{1 \pm \frac{\mu}{M} C + \left(\frac{\mu}{M}\right)^2 D^{\pm}(M/\mu) + \ldots\right\} \tag{13}$$

where f is the P-wave coupling constant and the plus-minus sign refers respectively to positive-negative pion. In (12) C is a constant and $D^{\pm}(\mu/M)$ are functions of the masses ratio μ/M. These functions are unknown, but the theorem states that at limit, for $\mu/M \to 0$, also $D \to 0$. Because $(\mu/M)^2 \cong 1/40$ it seems plausible that the third term in D is small in comparison to $(\mu/M)C$.

If $(\mu/M)^2 D$ is neglected, then

$$\left(\frac{e^2}{\hbar c}\right)\left(\frac{f^2}{\hbar c}\right)\left(\frac{\hbar}{\mu c}\right)^2 = \frac{A_0^+ + A_0^-}{2} = \frac{A_0^+}{2}\left(1 + \frac{A_0^-}{A_0^+}\right) \tag{13'}$$

and now the ratio A_0^-/A_0^+ is simply the limiting value, at threshold of the ratio $\mathrm{d}\sigma(\pi^-)/\mathrm{d}\sigma(\pi^+) = r$ between the cross-sections for charged photo-pions on the neutron and the proton.

This ratio should be determined with free nucleons. Instead we have this ratio for the two loosely bound nucleons of deuterium. The available data, near threshold ([27]) indicate that

$$r = 1.51 \pm .1 . \tag{14}$$

This value would require some corrections for the effects due to the final states (alternatively two protons for the negative pion and two neutrons for the charged one). Because they do not exceed 10% we neglect them.

([26]) N. M. KROLL and M. A. RUDERMAN: *Phys. Rev.*, **93**, 239 (1954).

([27]) M. BENEVENTANO G. BERNARDINI, D. CARLSON-LEE, G. STOPPINI and L. TAU: to be published.

Using this value of r, one finds $f^2=.067$ with an error which is supposed to be of the order of 15%, as far as all possible systematic errors can be considered properly estimated and as far as the value of r is not too much affected by the influence of the Coulomb forces on the final pion-nucleon state.

3. – Analysis of photo-pion-production.

3·1. *Expansion of an e.m. wave into multipoles.* – The analysis of the production of pions by high energy photons implies the expansion of a plane e.m. wave into multipoles. This is the analogue of the well known partial waves expansion. The main difference and source of complication is due to the fact that the e.m. field is a vector field and more particularly a « transversal » vector field ([28]).

The expansion reflects this fact. The e.m. waves are *vector* waves and the corresponding partial waves are called « vectorial spherical harmonics ».

We are here only interested in seeing semiqualitatively the use of these vector spherical harmonics in the multipole expansion of an e.m. monocromatic wave. Taking into account the gauge condition $\operatorname{div} \boldsymbol{A}=0$ such a wave may be conveniently ([29]) expressed by a potential vector

$$\boldsymbol{A}(\boldsymbol{r}, t) = \boldsymbol{A}_0 \exp[i(\boldsymbol{k}\cdot\boldsymbol{r} - \omega t)] + \text{compl. conj.}, \tag{1}$$

where $\boldsymbol{A}_0 = |\boldsymbol{A}_0| \exp[i\alpha]$ is a complex vector, $|\boldsymbol{A}_0|$ a real vector (polarization vector) and

$$\boldsymbol{k} = \frac{\omega}{c}\boldsymbol{n} = \frac{\boldsymbol{n}}{\lambda}$$

is the wave vector in the propagation direction $\boldsymbol{n} = \boldsymbol{k}/k$.

If we normalize and write $\boldsymbol{A}_0 = (1/\sqrt{2})(\boldsymbol{\epsilon}_x \pm i\boldsymbol{\epsilon}_y)$ where $\boldsymbol{\epsilon}_x$ and $\boldsymbol{\epsilon}_y$ are *two* real vectors, they must be mutually perpendicular ([30]). Thus we may choose the axes X and Y parallel to them and (1) can be written

$$\boldsymbol{A}(\boldsymbol{r}, t) = \frac{1}{\sqrt{2}}(\boldsymbol{\epsilon}_x \pm i\boldsymbol{\epsilon}_y) \exp[i(kz - \omega t)] + \text{compl. conj.}, \tag{2}$$

the upper sign referring to the right circular polarization, the lower to the left one.

([28]) See, for instance, J. M. Blatt and V. F. Weisskopf: *Theoretical Nuclear Physics* (New York, 1953), p. 796 and foll.

([29]) See, for instance, L. I. Schiff: *Quantum Mechanics* (New York, 1949), Chapter X.

([30]) $\boldsymbol{\epsilon}_x \cdot \boldsymbol{\epsilon}_y = 0$ because $|A|^2$ is real.

In this way, the plane wave has been decomposed into two parts; the first of which $(1/\sqrt{2})(\boldsymbol{\epsilon}_x \pm i\boldsymbol{\epsilon}_y)$ is the circular polarization or spin vector [31]. The corresponding spin eigenvalues are ± 1. The eigenvalue 0 is missing because the propagating e.m. field is transversal.

The exponential factor in (2) is then treated as in the partial waves analysis. Neglecting the time dependent part (which, as well known, for the following considerations is inessential)

$$\exp[ikz] = \exp[ikr\cos\theta] = \sum_{l=0}^{\infty}(2l+1)i^l j_l(kr)P_l(\cos\theta)$$

where [32]

$$(3)\qquad j_l(kr) = \left(\frac{\pi}{2kr}\right)^{\frac{1}{2}} J_{l+\frac{1}{2}}(kr) \begin{cases} \dfrac{1}{kr}\sin\left(kr - \dfrac{\pi l}{2}\right) & kr \gg l, \\ \dfrac{kr}{(2l+1)!!} & kr \ll l, \end{cases}$$

or alternatively, because

$$(4)\qquad P_l(\cos\theta) = \left(\frac{4\pi}{2l+1}\right)^{\frac{1}{2}} Y_{l,0}(\theta)$$

$$\exp[ikr\cos\theta] = \sum_{l=0}^{\infty} i^l \sqrt{4\pi(2l+1)}\, j(kr)\, Y_{l,0}(\theta)\,.$$

It follows

$$(5)\qquad \boldsymbol{A}(\boldsymbol{r}) = \sum_{l=0}^{\infty} \alpha_l(r)\, Y_{l,0}(\theta)\chi_{\pm 1} + \text{compl.. conj.},$$

where

$$\alpha_l(r) = i^l\sqrt{4\pi(2l+1)}\, j_l(kr)\,.$$

In the expansion

$$(6)\qquad \chi_{\pm 1} = \frac{1}{\sqrt{2}}(\boldsymbol{\epsilon}_x \pm i\boldsymbol{\epsilon}_y)$$

are the spin eigenfunctions $\begin{cases} s = 1 \\ m = \pm 1 \end{cases}$ and $Y_{l,0}(\theta)$ the eigenfunctions of th-

[31] To show this point rigorously and clearly would require first, the classic consideration of the angular momentum of an e.m. field given by the integral $\int(\boldsymbol{r}\times\boldsymbol{G})\,\mathrm{d}^3\boldsymbol{r}$ where $\boldsymbol{G}$ is the linear momentum density, i.e. the Poynting vector, and second, its quantization with the usual commutation rules. This argument is extensively discussed in G. WENTZEL: *Quantum Theory of Fields* (New York, 1949), §§ 12 and 16.

[32] See f.i., L. I. SCHIFF: *Quantum Mechanics* (New York, 1949), Sec. 15.

analogous of an angular (orbital) momentum $l = 0, 1, 2, \ldots$; $m = 0$. Hence each component of the expansion is a vector corresponding to one of the spin values and one of the l values. Thus it may be considered as a *vector*-wave function of a single total angular momentum $\boldsymbol{J} = \boldsymbol{L} + \boldsymbol{S} = \boldsymbol{j} + \boldsymbol{j}'$ obtained adding the two momenta $\boldsymbol{j} = \boldsymbol{L}$ and $\boldsymbol{j}' = \boldsymbol{S}$ [33].

The actual momentum involved is then $\boldsymbol{J}$ and it is convenient to substitute to the expansion (5) an expansion in functions which are simultaneously eigenfunctions of J_z and J^2 and have definite parity. Because $\boldsymbol{L}$ and $\boldsymbol{S}$ are commuting operators these new eigenfunctions are linear combinations of the products $\chi_{\pm 1} Y_{l,0}(\theta)$. In other words using the quantum-mechanical vector addition laws these eigenfunctions are *vector* functions which can be written

$$(7)\quad \begin{cases} \boldsymbol{Y}^{M=+1}_{J,l,1} = C_{l,1}(J, +1; 0, +1)\chi_1 Y_{l,0}(\theta, \varphi) + \\ \qquad\qquad + C_{l1}(J, +1; 2, -1)\chi_{-1} Y_{l,2}(\theta, \varphi)\,, \\ \boldsymbol{Y}^{M=-1}_{J,l,1} = C_{l,1}(J, -1; -2, +1)\chi_1 Y_{l,2}(\theta, \varphi) + \\ \qquad\qquad + C_{l,1}(J, -1; 0, -1)\chi_{-1} Y_{l0}(\theta, \varphi)\,, \end{cases}$$

where the C's are the vector addition coefficients or « Clebsch Gordon coefficients » [34]. Conversely making use of the symmetry relations holding for the C's coefficients, the products $\chi_{\pm 1} Y_{l,0}(\theta)$ may be expressed in terms of these vectorial eigenfunctions $\boldsymbol{Y}^{\pm 1}_{J,l,1}$

$$(8)\quad Y_{l,0}(\theta)\chi_{\pm 1} = \sum_{J=l-1}^{l+1} C_{l,1}(J, \pm 1; 0, \pm 1)\boldsymbol{Y}^{\pm 1}_{J,l,1}\,,$$

where the C's are the Clebsch-Gordon coefficients suitable for our case, i.e.

$$(9)\quad \begin{cases} C_{l,1}(l+1, \pm 1; 0, \pm 1) = \left(\dfrac{(l+1)(l+2)}{(2l+1)(2l+2)}\right)^{\frac{1}{2}}, \\ C_{l,1}(l, \pm 1; 0, \pm 1) = \mp\sqrt{\dfrac{1}{2}}\,, \\ C_{l,1}(l-1, \pm 1; 0, \pm 1) = \left(\dfrac{l-1}{2(2l+1)}\right)^{\frac{1}{2}}. \end{cases}$$

---

[33] To make more explicit reference to the usual notation of the Clebsch-Gordon coefficients we put $\boldsymbol{L} = \boldsymbol{j}$, $\boldsymbol{S} = \boldsymbol{j}'$. Beside to J. M. Blatt and V. F. Weisskopff (op. cit.) we refer to the classic treatises E. P. Wigner: *Gruppentheorie und ihre Anwendung auf die Quantenmechanik der Atomspektren* (Braunschweig, 1931); E. U. Condon and G. H. Shortley: *Theory of Atomic Spectra* (Cambridge, 1935), and to G. Racah's papers (*Phys. Rev.*, **61**, 186 (1942); **62**, 438 (1942)).

[34] E. U. Condon and G. H. Shortley: loc. cit. The symbol $C_{jj'}(J, M; m, m')$ exibits the addition of the two angular momenta j, j': $j_z = m$, $j'_z = m'$ into the total $J, J_z = M$.

Hence for each J there are three terms: $l = J+1$, J, $J-1$ and (2) becomes

$$(10) \qquad \boldsymbol{A}(\boldsymbol{r}) = \sum_{l=0}^{\infty} \alpha_l(r) \sum_{J=l-1}^{l+1} C_{l,1}(J, \pm 1; 0, \pm 1)\, \boldsymbol{Y}^{\pm 1}_{J,l,1} + \text{compl. conj.}$$

i.e. expressing everything by l

$$(10') \qquad \boldsymbol{A}(\boldsymbol{r}) = \sum_{l=1}^{\infty} i^l \sqrt{4\pi} j_l(kr) \left\{ \left[\frac{(l+1)(l+2)}{(2l+2)} \right]^{\frac{1}{2}} \boldsymbol{Y}^{\pm 1}_{l+1,l,1} \mp \left[\frac{2l+1}{2} \right]^{\frac{1}{2}} \boldsymbol{Y}^{\pm 1}_{l,l,1} + \right.$$
$$\left. + \left[\frac{l-1}{2} \right]^{\frac{1}{2}} Y^{\pm 1}_{l-1,l,1} \right\},$$

or instead expressing by J

$$(11) \qquad \boldsymbol{A}(\boldsymbol{r}) = \sum_{J=1}^{\infty} i^J \sqrt{4\pi} \left\{ -i \sqrt{\frac{J+1}{2}}\, j_{J-1}(kr) \boldsymbol{Y}^{\pm 1}_{J,J-1,1} \mp \right.$$
$$\left. \mp \sqrt{(2J+1)/2}\, j_J(kr) \boldsymbol{Y}^{\pm 1}_{J,J,1} + i \sqrt{\frac{J}{2}}\, j_{J+1}(kr) \boldsymbol{Y}^{\pm 1}_{J,J+1,1} \right\} + \text{compl. conj.}$$

These expansions hold for an e.m. plane wave when the propagation occurs along the axis. In other words when the angular momenta are quantized in the direction of the beam. In the more general case of a propagation in an arbitrary direction the allowed values of M are not only ± 1 but also 0.

Now for any arbitrary function of r the following identity holds

$$\nabla \times [f(r) \boldsymbol{Y}^{\pm 1}_{J,J,1}] = f_+(r) \boldsymbol{Y}^{\pm 1}_{J,J+1,1} + f_-(r) \boldsymbol{Y}^{\pm 1}_{J,J-1,1},$$

where $f_+(r)$ and $f_-(r)$ are deduced from $f(r)$ and are functions of r only. If $f(r) = j_l(kr)$ (only regular Bessel functions are allowed in the expansion of a plane wave) it is possible to write, instead of (11)

$$(11') \qquad \boldsymbol{A}(\boldsymbol{r}) = \sum_{J=1}^{\infty} i^J \frac{\sqrt{2\pi(2l+1)}}{k} \left\{ \mp \nabla \times [j_J(kr) \boldsymbol{Y}^{\pm 1}_{J,J,1}] + k j_J(kr) \boldsymbol{Y}^{\pm 1}_{J,J,1} \right\}.$$

The term under the $\nabla\times$ operator contains the not explicitely written spherical harmonics with $l = J \pm 1$.

Now it can be shown that $\boldsymbol{Y}^{\mp 1}_{J,J,1}$ has the parity of spherical harmonics $Y_{J,\pm 1}$ (*); i.e. the parity $(-1)^J$.

Instead

$$(13) \qquad \nabla \times \left\{ j_J(kr) \boldsymbol{Y}^{\pm 1}_{J,J,1} \right\}$$

has the opposite parity, i.e. $-(-1)^J$ because $\nabla\times$ is an odd operator. It leaves J unaltered, but changes the parity.

(*) See Appendix II.

We see then clearly that a plane wave *is neither a definite angular momentum state nor a definite parity state*. But it may be *formally* decomposed in states of definite angular momentum and parity.

This decomposition, as in the partial waves method for scattering, acquires a meaning by interaction with the charged system. This as far as the absorption (or emission) goes, may be replaced by a suitable superposition of *electric and magnetic multipoles*, with adequate strengths.

As it is well known, classically or quantically they come out from the expansion of the interaction term $\boldsymbol{j}\cdot\boldsymbol{A}$ ([35]).

Each term or pole of the expansion represents a mode of absorption of a quantum of definite angular momentum and parity. This last is defined according to the dependence of the pole from the charge coordinate. Thus, for instance, the electric dipole is odd, the magnetic dipole and electric quadrupole are even, etc.

The associated operators (expansion terms of the operator $\boldsymbol{j}\cdot\boldsymbol{A}$) may be considered as projection operators which select from the plane wave expansion (11′) those terms which fit the projection operator as J-value and parity.

Concluding it can be shown that the (pure J and parity pure) substates in which the e.m. wave may be decomposed are those assembled in the following Table I ([36]).

TABLE I.

J		l
0	never	
1	dipole terms	$\begin{cases} J\pm 1 = 0, 2 & \text{odd} \quad \text{component} \quad E_1 \quad \text{(electric)} \\ J \quad\quad = 1 & \text{even} \quad\quad\; » \quad\quad M_1 \quad \text{(magnetic)} \end{cases}$
2	quadrupole terms	$\begin{cases} J\pm 1 = 1, 3 & \text{even} \quad \text{component} \quad E_2 \quad \text{(electric)} \\ J \quad\quad = 2 & \text{odd} \quad\quad\; » \quad\quad M_2 \quad \text{(magnetic)} \end{cases}$

In the next paragraph these qualitative considerations will be made a little more clear and definite.

([35]) A complete treatment of this matter may be found, for instance, in P. M. MORSE and H. FESHBACH: *Methods of Theoretical Physics* (New York, 1953), p. 1276 and 1875.

([36]) One should remember that the electric field has the same parity of $\boldsymbol{A}$. Instead the magnetic field has parity opposite to $\boldsymbol{A}$. Actually in a plane wawe $\boldsymbol{E} = i\boldsymbol{k}\,\boldsymbol{A}$ and $\boldsymbol{H} = i\boldsymbol{k}\times\boldsymbol{A}$.

3·2. *The e.m. interaction of a nucleon.* – We now turn back to the photoproduction of pions by hydrogen. As in the classic nuclear photoeffect the emission or absorption of a photon constitutes a transition between an initial state i and a final state f of the system, nucleon plus (quantized) radiation field. This transition is caused by an interaction due to the nucleon-radiation field coupling. This is

$$H_{\text{em}} = -\int \boldsymbol{j}\cdot\boldsymbol{A}\,\mathrm{d}^3\boldsymbol{x}\,, \tag{13}$$

where $\boldsymbol{j}$ means the total current density of all particles, real or virtual, in *charged* states. The operator $\boldsymbol{j}$ contains the pion current density operator, i.e. (the pion spin = 0) [37]

$$\boldsymbol{j}_\pi = e\boldsymbol{v} = e\frac{\boldsymbol{p}}{\omega}\,; \qquad \omega = \sqrt{p^2 + \mu^2 c^4}\,. \tag{14}$$

It contains also the nucleon current

$$\boldsymbol{j}_{\mathcal{N}} = \tfrac{1}{2}e(1 + \tau_3)\boldsymbol{\alpha}\,, \tag{15}$$

where $\boldsymbol{\alpha}$ is the Dirac matrix and τ_3 the third nucleon isospin component. $\boldsymbol{A}$ is the vector potential in the gauge $\Phi = 0$. The expression (15) is relativistic To avoid the complications involved in a relativistic treatment of the nucleons we rather use a non relativistic nucleon current operator, i.e. an operator a in (14). That means that in this approximation formula (13) does not include the magnetic moment interaction which does not arise from the pion clouds However, the nucleon magnetic moment can be split [38] into the « normal » and the « anomalous » part, and the normal part can be added. For the multipole analysis it is very clear that the type of transition determined by this purely magnetic interaction is a magnetic dipole.

The « normal » part (belonging to a static property of the nucleon, i.e. to the Pauli magnetic moment) in terms of the proton and neutron magnetic momenta μ_n and μ_p is

$$H_m = -\boldsymbol{\mu}\cdot\boldsymbol{\mathcal{H}} = -\left\{\frac{\mu_n}{2}(1 - \tau_3) + \frac{\mu_p}{2}(1 + \tau_3)\right\}\boldsymbol{\sigma}\cdot\boldsymbol{\nabla}\times\boldsymbol{A}\,. \tag{16}$$

[37] Actually the operator $\boldsymbol{j}_\pi$ averages the initial and final pion current. In terms of pion field Φ it is

$$j_\mu = ie\{\Phi^*\partial_\mu\Phi - (\partial_\mu\Phi^*)\Phi\} = ie\sqrt{\frac{1}{2\omega_i}}\sqrt{\frac{1}{2\omega_f}}\,i(\boldsymbol{k}_i + \boldsymbol{k}_f) = \frac{e}{2}\frac{1}{\sqrt{\omega_i\omega_f}}(\boldsymbol{k}_i + \boldsymbol{k}_f)\,,$$

where $\boldsymbol{k}_i$ and $\boldsymbol{k}_f$ are the initial and final momenta: see G. Wentzel, *Quantum Theory of Fields* (New York, 1949), p. 66.

[38] L. L. Foldy: *Phys. Rev.*, **87**, 688 (1952 .

It is also clear that in this approximation formula (13) does not include the extra term obtained when the gauge transformation is applied to the wave pion-nucleon interaction ([39]).

However, we known from the discussion in previous sections, that this term, which is introduced « a priori » for gauge requirements, induces necessarily a transition to a final pion S state. Because the absorbed angular momentum is 1, this term is a dipole and, as already mentioned, should flip the nucleon spin. Finally, for conservation of parity, it has to be an electric dipole. In the following, we will not discuss this term again. It may be added at the right moment, assuming that all that can be said about it has been said. We want only to observe that if the addition of the gauge term is associated (as it is) with an appreciable strength, then also the contribution due to (16) is expected to be evident and determined by the strength μ. Actually the two interactions are proportional to the operators,

$$\begin{cases} \varepsilon \boldsymbol{\sigma} \cdot \boldsymbol{A} \\ \boldsymbol{\mu} \cdot \boldsymbol{\mathcal{H}} = \mu \boldsymbol{\sigma} \cdot (\boldsymbol{\nabla} \wedge \boldsymbol{A}) \end{cases} \tag{17}$$

where the constants ε and μ are the electric and magnetic strengths of the nucleon corresponding to these interactions ([40]).

3·3. *The multipole expansion of the interaction density* $\boldsymbol{j} \cdot \boldsymbol{A}$, is what remains to be considered. In this operator, the potential vector $\boldsymbol{A}$ works only on the teld of the incident e.m. plane wave. The operator $\boldsymbol{A}_{\text{op}}$ can be expanded in fierms of progressing plane wave field operators ([41]).

Precisely ([42]):

$$\boldsymbol{A}_{\text{op}} = \sum_{\boldsymbol{k}} \frac{1}{2} \left(\frac{2\pi\hbar^2 c}{\Omega k} \right)^{\frac{1}{2}} \left\{ (c_{\pm} + d_{\pm}^{*}) \exp\left[i\boldsymbol{k} \cdot \boldsymbol{r} \right] + (d_{\pm} + c_{\pm}^{*}) \exp\left[- i\boldsymbol{k} \cdot \boldsymbol{r} \right] \right\}, \tag{18}$$

where Ω is the normalization volume and where the operator $c_{\pm}$ *destroys* a right polarized photon of linear momentum $\boldsymbol{k}$ travelling in the $\pm \boldsymbol{k}/k$ direction; the operator $c_{\pm}^{*}$ *creates* instead such a photon, etc..

The matrix elements of $\boldsymbol{A}_{\text{op}}$ are given by the matrix elements of $c_{\pm}$ and $c_{\pm}^{*}$ multiplied by the corresponding coefficients; namely for the destruction or

([39]) Actually this term could be obtained, in a relativistic nucleon theory starting with the creation by a photon of a nucleon-antinucleon pair.

([40]) Naively one may consider the two interactions as the electric and magnetic contributions to the interaction due to the possible oscillations (flippings) of the nucleon spin.

([41]) E. FERMI: *Elementary Particles* (New Haven, 1951), Appendix I.

([42]) See Appendix III.

creation of a right polarized photon, they are

$$A\{R_+ \to R_+ - 1\} = \left(\frac{2\pi\hbar^2 c}{\Omega k}\right)^{\frac{1}{2}} \exp[i\boldsymbol{k}\cdot\boldsymbol{r}]\sqrt{R_+}\,, \tag{19}$$

$$A\{R_+ \to R_+ + 1\} = \left(\frac{2\pi\hbar^2 c}{\Omega k}\right)^{\frac{1}{2}} \exp[i\boldsymbol{k}\cdot\boldsymbol{r}]\sqrt{R_+ + 1} \qquad \text{etc.}, \tag{19'}$$

where R_+ is the number of right polarized photons travelling along the $+\boldsymbol{k}/k$ direction, etc.

The matrix elements (19) and (19'), apart from a constant factor, can be regarded as the eigenfunction of a polarized photon of momentum $\boldsymbol{k}$. The matrix element of the transition is then proportional to the amplitude (eigenfunction) of the photon which has been created or destroyed. This, as is well known, is a particular case of a general rule.

Let us consider the operator $\boldsymbol{j}$. This instead works on the pion-nucleon wave function and should reveal the e.m. characteristics of the possible states of such a system. As already mentioned, it is just the nucleon with its e.m. structure which emphasizes those angular momenta and parity substates in which the plane wave ($\exp[i\boldsymbol{k}\cdot\boldsymbol{r}]$) may be decomposed. In the Schrödinger representation [43]

$$j_\pi = -ihe\{\Phi^*\nabla\Phi - (\nabla\Phi^*)\Phi\}$$

and for the nucleon (not relativistic)

$$j_\mathcal{N} = -\frac{ihe}{2m}\{\psi^*\nabla\psi - (\nabla\psi^*)\psi\}\,.$$

What follows is standard procedure. Considering only the essentials, let us pick up, in the matrix element of the transition, the product

$$ihe\,(\exp[i\boldsymbol{k}\cdot\boldsymbol{r}])\nabla\,,$$

and expand the exponential such that

$$ihe\{1 + i\boldsymbol{k}\cdot\boldsymbol{r} + \ldots\}\nabla\,. \tag{20}$$

The initial state function, p^γ, (incident photon + nucleon) is simply (see FERMI's lectures)

$$|p^\gamma\rangle = \left| p \rightleftarrows \begin{pmatrix} n + \pi^+ \\ p + \pi^0 \end{pmatrix} \cdot \gamma \right\rangle .$$

[43] We neglect any e.m. interaction between pion and nucleon.

Remembering FERMI's lectures the first term of the expansion gives

$$ihe\nabla|[\gamma\cdot f(\sqrt{2/3}\,n^{+}-\sqrt{1/3}\,p^{0})(\sqrt{2/3}\,\beta Y_{11}-\sqrt{1/3}\,\alpha Y_{10})g(r)]\rangle \tag{21}$$

where also e should be considered as a projection operator which selects charged particles. Then

$$ih\cdot e\nabla\,|\,p^{\gamma}\rangle\sim|ihefn^{+}Y_{11}\nabla g(r)\rangle$$

and this is the small electric dipole part due to the pion current, estensively discussed by FERMI in his lectures.

Similarly, the second term of (20) is, apart from the coefficients

$$e(\boldsymbol{k}\cdot\boldsymbol{r})\nabla=\frac{e}{2}\{[(\boldsymbol{k}\cdot\boldsymbol{r})\nabla+\boldsymbol{r}(\boldsymbol{k}\cdot\nabla)]+[(\boldsymbol{k}\cdot\boldsymbol{r})\nabla-\boldsymbol{r}(\boldsymbol{k}\cdot\nabla)]\}. \tag{22}$$

But

$$\boldsymbol{k}\cdot\boldsymbol{r}=z\qquad\text{and}\qquad\boldsymbol{k}\cdot\nabla=\frac{\partial}{\partial z}.$$

Hence the components of the vector operator of the second term into curly brackets are

$$\frac{e}{2}[(\boldsymbol{k}\cdot\boldsymbol{r})\nabla-\boldsymbol{r}(\boldsymbol{k}\cdot\nabla)]=\frac{e}{2}\begin{vmatrix} z\dfrac{\partial}{\partial x}-x\dfrac{\partial}{\partial z}\\ z\dfrac{\partial}{\partial y}-y\dfrac{\partial}{\partial z}\\ 0\end{vmatrix}=\frac{e}{2}\begin{vmatrix} -L_y\\ L_x\\ 0\end{vmatrix} \tag{23}$$

i.e. the components of the operator which selects magnetic dipoles normal to to the propagation ([44]). Analogously, the first symmetric term is

$$\frac{e}{2}\begin{vmatrix} z\dfrac{\partial}{\partial x}+x\dfrac{\partial}{\partial z}\\ z\dfrac{\partial}{\partial y}+y\dfrac{\partial}{\partial z}\\ z\dfrac{\partial}{\partial x}+z\dfrac{\partial}{\partial z}\end{vmatrix} \tag{24}$$

i.e. the electric quadrupole ([45]).

According to their symmetry respect to the coordinates magnetic dipole and electric quadrupole are both *even* operators.

([44]) See, for example, D. BOHM: *Quantum Theory* (New York, 1951), Sec. 18, 23, p. 436.

([45]) D. BOHM: op. cit., p. 435.

3·4. *Angular distributions for pure states.* – We want now to apply the previous considerations to determine the *angular* distributions expected in the simplest case of photoproduction; i.e. when the transition involves only one state of J and parity ([46]).

The procedure is the same used by FERMI in his discussion of the E_1 (electric dipole) transition.

As in the electric dipole case discussed by FERMI, the matrix-element of the transition contains the product of the final amplitude of the pion nucleon state multiplied by that of the pole which fits the conservative rules. The estimate of the pole strenght rests on the knowledge of the nucleon structure and needs a theory or a model of the pion-nucleon system as for example, that developped by FERMI in is lectures.

As far as we are concerned with the angular distribution only vector-spherical harmonics (for the initial state) and spherical harmonics (for the final one) are involved. The appropriate C coefficients are taken into account ([47]).

Let us consider for instance the meson dipole (M_1) transition from the initial state p^γ to a final state n^+ of total angular momentum $J = 3/2$ ([48]). We have:

$$
\begin{array}{lll}
\text{initial state} & & \text{final state} \\
p^\gamma & \rightarrow & n^+ \\
M_1(j=1)\times S\left(j'=\frac{1}{2}\right) & \rightarrow & \{\text{pion } P\text{-wave } (l=1)\}\times S\left(j'=\frac{1}{2}\right) \\
m_\gamma = \pm 1, \quad m_p = \pm\frac{1}{2} = \left|\begin{matrix}\alpha\\ \beta\end{matrix}\right| & \rightarrow & m_\pi = \begin{matrix}+1\\ 0\\ -1\end{matrix}, \qquad m_n = \left|\begin{matrix}\alpha\\ \beta\end{matrix}\right|
\end{array}
\tag{25}
$$

i.e.

Initial state			C coeff.	n^+	Product
m_γ	m'_p	M	$C_{1,\frac{1}{2}}(3/2, M; m, m')$		
$+1$	α	$+3/2$	1	$P^+_{\frac{3}{2},\frac{3}{2}}$	$P^+_{\frac{3}{2},\frac{1}{2}}$
-1	α	$-1/2$	$\sqrt{1/3}$	$P^+_{\frac{1}{2},-\frac{1}{2}}$	$\sqrt{1/3}\,P^+_{\frac{3}{2},-\frac{1}{2}}$
$+1$	β	$+1/2$	$\sqrt{1/3}$	$P^+_{\frac{1}{2},\frac{1}{2}}$	$\sqrt{1/3}\,P^+_{\frac{3}{2},\frac{1}{2}}$
-1	β	$-3/2$	1	$P^+_{\frac{3}{2},-\frac{3}{2}}$	$P^+_{\frac{3}{2},-\frac{3}{2}}$

([46]) See B. T. FELD: *Phys. Rev.*, **89**, 330 (1953).

([47]) This, as first pointed out by D. R. HAMILTON: *Phys. Rev.*, **58**, 122 (1940), is a quite general statement. Provided a reaction can be thought as going through states of definite angular momenta and parities, the angular distribution of the reaction is indipendent of the specific nature of the interaction.

([48]) It is obvious that now J is not anymore the photon angular momentum but the total momentum including the nucleon spin.

Now

$$P^{+}_{\frac{3}{2},\frac{3}{2}} \sim -\frac{\alpha \sin\theta e^{i\varphi}}{\sqrt{2}},$$

$$P^{+}_{\frac{3}{2},\frac{1}{2}} \sim \sqrt{\frac{2}{3}}\,\alpha\cos\theta - \sqrt{\frac{1}{3}}\,\beta\,\frac{\sin\theta\, e^{i\varphi}}{\sqrt{2}},$$

etc. Then squaring and averaging on the photon and nucleon spins (the incident plane wave, as well as the target nucleon are unpolarized) we have that the M_1 $(J=3/2)$ induced transition has an angular dependence proportional to

$$W(\theta) = \frac{\sin^2\theta}{2} + \frac{1}{3}\left(\frac{2}{3}\cos^2\theta + \frac{\sin^2\theta}{6}\right) = 2 + 3\sin^2\theta\,.$$

Similarly for example for the E_2 $(J=3/2)$ transition one has

Initial state			C coeff.	n^+	Product
m_γ	m_p	M	$C_{2,\frac{1}{2}}(3/2, M; m, m')$		
$+1$	α	$+3/2$	$-\sqrt{1/5}$	$P^{+}_{\frac{3}{2},\frac{3}{2}}$	$-\sqrt{1/5}\,P^{+}_{\frac{3}{2},\frac{3}{2}}$
-1	α	$-1/2$	$-\sqrt{3/5}$	$P^{+}_{\frac{3}{2},-\frac{1}{2}}$	$-\sqrt{3/5}\,P^{+}_{\frac{3}{2},-\frac{1}{2}}$
$+1$	β	$+1/2$	$+\sqrt{3/5}$	$P^{+}_{\frac{3}{2},\frac{1}{2}}$	$+\sqrt{3/5}\,P^{+}_{\frac{3}{2},\frac{1}{2}}$
-1	β	$-3/2$	$+\sqrt{1/5}$	$P^{+}_{\frac{3}{2},-\frac{3}{2}}$	$+\sqrt{1/5}\,P^{+}_{\frac{3}{2},-\frac{3}{2}}$

Averaging on photon and pion spins

$$W(\theta) \sim \tfrac{1}{2}\sin^2\theta + \tfrac{1}{2}\sin^2\theta + 2\cos^2\theta = 1 + \cos^2\theta\,.$$

We may conclude now with the following Table II (B. T. Feld, op. cit).

Table II

γ-ray pole absorbed	Total J and parity	l_π	Spin flipping	Pion angular distribution
E_1 (electric dipole)	$(1/2)^-$	0	yes	const.
	$(3/2)^-$	2	yes	$2 + 3\sin^2\theta$
M_1 (magnetic dipole)	$(1/2)^+$	1	yes + no	const.
	$(3/2)^+$	1	yes + no	$2 + 3\sin^2\theta$
E_2 (electric quadrupole)	$(3/2)^+$	1	yes + no	$1 + \cos^2\theta$
	$(5/2)^+$	3	yes + no	$1 + 6\cos^2\theta - 5\cos^4\theta$

which summarizes the angular momenta and parity correlation between initial and final pure states in photopion-production.

Inspection of this Table makes evident the conservation of angular momentum and parity (compare with Table I).

Consider, for instance, the absorption of a magnetic dipole. The parity is even and the total $J = 1/2$ or $3/2$. Let say $J = 3/2$. Because the pion has odd intrinsic parity, the parity of the final orbital state must be odd, i.e. $l = 1, 3, \ldots$. But the value of J rules out anything higher than $l = 1$.

The previous considerations holds for transitions between pure states. In the actual case we have a mixture of states and the situation is more complicated because the relative phases come in.

Those phases may be determined by the scattering experiments. This is one of the basic points of the correlation between photopion production and nuclear pion scattering which may be established quite generally with the S-matrix formalism. We refer for this point to Fermis's lectures.

Appendix I

The final energy in c.m.s. (and $\hbar = c = 1$) is

$$E_f = \sqrt{\mu^2 + p_\pi^2} + \sqrt{M^3 + p_\pi^2}\,,$$

where p_π is the proton and pion momentum.

The density of final states is

$$\varrho = \frac{p_\pi^2 \, \mathrm{d}p_\pi}{2\pi^2 \mathrm{d}E_f} = \frac{p_\pi^2}{2\pi^2}\left(\frac{\mathrm{d}E_f}{\mathrm{d}p_\pi}\right)^{-1},$$

where

$$\frac{\mathrm{d}E_f}{\mathrm{d}p_\pi} = \frac{p_\pi}{E_\pi} + \frac{p_\pi}{E_p} \simeq \frac{p_\pi}{\mu\omega}\left(1 + \frac{\mu\omega}{M}\right)$$

hence with usual notations

$$\varrho = \frac{1}{2\pi^2} \frac{\eta\omega}{\mu^2\left(1+\frac{\mu\omega}{M}\right)}$$

The incident flux in the c.m.s. is

$$\text{flux}_{\text{c.m.s.}} = \text{flux}_{\text{l.s.}} \cdot (1 + \text{rel. vel. of nucleon})$$

$$= \text{flux}_{\text{l.s.}} \cdot \left(1 + \frac{v}{M}\right).$$

Because $\text{flux} \times d\sigma/d\Omega = \frac{2\pi}{\hbar}\left|H\right|^2 \varrho$ (note that the formula given by FERMI is the *total* cross-section) the formula in text follows.

APPENDIX II

In this Appendix some points concerning the expansion of a wave vector-field in vector spherical harmonics are briefly presented. This presentation by no means can be considered adequate for a full understanding of the matter. The subject is estensively discussed in J. M. BLATT and V. F. WEISSKOPFF ([49]).

Any vector field $\boldsymbol{A}(\boldsymbol{r})$ defined by differential equation and boundary conditions invariant under rotations of the coordinate system around an arbitrary axis z is associated to an operator $J_z = L_z + S_z$ where L_z is the normal angular momentum

(1) $$L_z = -i\hbar\left(y\frac{\partial}{\partial x} - x\frac{\partial}{\partial y}\right),$$

and S is defined by the property

(2) $$S_z\begin{pmatrix}A_x\\A_y\\A_z\end{pmatrix} = \begin{pmatrix}-iA_y\\+iA_x\\0\end{pmatrix} \quad ([50]).$$

([49]) See op. cit.

([50]) $i\vartheta S_z = i\vartheta \begin{vmatrix}0 & -1 & 0\\1 & 0 & 0\\0 & 0 & 0\end{vmatrix}$ is the operator of an infinitesimal rotation ϑ around z of an angular momentum vector equal 1.

The main property of J_z is that it commutes with the differential operator in the equation defining $\boldsymbol{A}(\boldsymbol{r})$. It may really be an angular momentum operator according to the physical meaning of $\boldsymbol{A}$. The form $J_z = L_z + S_z$ is pourpously chosen to break up the angular momentum J into orbital and spin moments. The operator identity $S_z(S_z^2 - 1) = 0$ which follows from (2) shows that S_z has the eigenvalues 1, 0, -1 only.

The corresponding normalized eigenvectors of S_z are

$$\chi_1 = -\frac{1}{\sqrt{2}}(\boldsymbol{u}_x + i\boldsymbol{u}_y), \qquad \chi_{-1} = \frac{1}{\sqrt{2}}(\boldsymbol{u}_x - i\boldsymbol{u}_y), \qquad \chi_0 = \boldsymbol{u}_z, \tag{3}$$

where $\boldsymbol{u}_x$, $\boldsymbol{u}_y$, $\boldsymbol{u}_z$ are the three unit vectors. Together with the operator J_z one may as well consider the other components J_x, J_y. The vector $\boldsymbol{J}$ has then, formally, the properties of an angular momentum. The simultaneous eigenfunctions of $J_z = M$ and $J^2 = (\boldsymbol{L} + \boldsymbol{S})^2$ depending upon the polar angles ϑ, φ only, are then obtained following the addition rules of angular momenta. That is possible because $\boldsymbol{L}$ and $\boldsymbol{S}$ commute. The eigenfunctions of $\boldsymbol{S}$ in any direction being of the (3) type and those of each component of $\boldsymbol{L}$ being the usual spherical harmonics.

According to the general rule for the addition of the quantum mechanical vectors these vector functions are linear combinations of the products of the eigenfunctions of $\boldsymbol{S}$ and $\boldsymbol{L}$, i.e. of the product $Y_{lm}(\vartheta, \varphi)\chi_{m'}$; $m' = 1, 0, -1$.

They are

$$\boldsymbol{Y}^M_{J,l,1} = \sum_{\substack{m=-l \\ (m=M-m')}}^{l} C_{l1}(J, M; m, m')\, Y_{l,m}(\vartheta, \varphi)\chi_{m'} \tag{4}$$

the three components of $\boldsymbol{Y}$ being $\boldsymbol{Y}\begin{cases} m+1 \\ m \\ m-1 \end{cases}$.

Because the scalar spherical harmonics are characterized by l, for each J there are three different spherical harmonics. Precisely

$$\boldsymbol{Y}^M_{J,J-1,1}, \qquad \boldsymbol{Y}_{J,J,1}, \qquad \boldsymbol{Y}_{J,J+1,1}.$$

Only for $J = 0$ we get only one spherical harmonic $\boldsymbol{Y}^0_{0,1,1}$. It corresponds to $\boldsymbol{L}$ and $\boldsymbol{S}$ opposite and equal to unity.

According to the parity of scalar spherical harmonics the vector functions $\boldsymbol{Y}^M_{J,l,1}$ have parity $(-1)^l$. Thus for a definite J the parity of $\boldsymbol{Y}_{J,J,1}$ is $(-1)^J$ and the parity of $\boldsymbol{Y}_{J,J+1,1}$ is $(-1)^{J+1}$.

The simplest of the vector function is $\boldsymbol{Y}^M_{J,J,1}$ where $J = l$.

With the use of (4) ([51]) one has

$$\boldsymbol{Y}^M_{J,J,1} = \frac{M}{\sqrt{J(J+1)}}\, Y_{J,M}\chi_0 - \frac{1}{\sqrt{2}}\sqrt{\frac{(J+M)(J-M+1)}{J(J+1)}}\, Y_{J,M-1}\chi_{+1} + \tag{5}$$

$$+ \frac{1}{\sqrt{2}}\sqrt{\frac{(J-M)(J+M+1)}{J(J+1)}}\, Y_{J,M+1}\chi_{-1}.$$

([51]) For the value of C see J. M. Blatt and V. F. Weisskopff (op. cit., p. 792), or E. U. Condon and G. H. Shortley (op. cit., p. 76).

This, for the e.m. plane wave previously considered reduces ($X_0 = 0$, $M = \pm 1$) to

$$Y^{\pm 1}_{J,J,1} = \mp \frac{1}{\sqrt{2}} Y_{J,0}\chi_{+1} \pm \sqrt{\frac{(J-1)(J+2)}{J(J+1)}}\, Y_{J,2}\chi_{-1}.$$

Appendix III

The potential vector of a plane wave is usually expressed in terms of a linearly polarized progressive waves operator as follows [52]

$$(1)\quad \boldsymbol{A}(x, y, z) = \left(\frac{2\pi\hbar c}{\Omega k}\right)^{\frac{1}{2}} \left[\left\{\boldsymbol{\epsilon}_x (a_{k+} + a^*_{k-}) \exp[i\boldsymbol{k}\cdot\boldsymbol{r}] + \boldsymbol{\epsilon}(b_{k+} + b^*_{k-}) \exp[i\boldsymbol{k}\cdot\boldsymbol{r}]\right\} + \right.$$
$$\left. + \left\{\boldsymbol{\epsilon}_y(a^*_{k+} + a_{k-}) \exp[-i\boldsymbol{k}\cdot\boldsymbol{r}] + \boldsymbol{\epsilon}_y(b^*_{k+} + b_{k-}) \exp[i\boldsymbol{k}\cdot\boldsymbol{r}]\right\}\right].$$

Where $\boldsymbol{\epsilon}_x$, $\boldsymbol{\epsilon}_y$ are the two polarization directions such that $\boldsymbol{\epsilon}_x$, $\boldsymbol{\epsilon}_y$ and $\boldsymbol{k}/n$ form a right handed orthogonal system of unit vectors. As it is well knowd $a_{k\pm}$, $a^*_{k\pm}$, $b_{k\pm}$, etc., are (non hermitian) operators called destruction ans. creation operators, since for instance a_{k-} induces transition in which disappeark a photon linearly polarized in the zx plane and progressing in the negative direction; while b^*_{k+} induces a transition in which appears a photon polarized on the zy plane and progressing in the positive direction. The positive and negative directions along the line of propagation correspond to photons associated to the same energy and opposite momenta. They are the equivalents of two degrees of freedom.

The operators a_{k+}, b_{k+} etc. (in full analogy with the equivalent classic procedure) can be rearranged such that the potential vector turns out to be expressed by circularly polarized photons. To do that we have, for example, to add a^*_{k+} and b^*_{k+} in the operator

$$c^*_{k+} = \frac{1}{\sqrt{2}} (a^*_{k+} + ib^*_{k+}).$$

Actually a^*_{k+} creates a photon $\cos \boldsymbol{kr} - i \sin \boldsymbol{k}\cdot\boldsymbol{r}$ linearly polarized along X; ib^*_{k+} creates a photon $i\cos \boldsymbol{kr} + \sin \boldsymbol{kr} = \cos(\boldsymbol{kr} + \pi/2) + \mathrm{i}\sin(\boldsymbol{kr} - \pi/2)$ polarized along the Y axis. Then c^*_{k+} creates a circularly polarized photon in $+\boldsymbol{k}/a$ direction turning toward rignt (R).

([52]) E. Fermi: *Elementary Particles*, Appendix I, formula (19).

Similarly

$$c^* = \frac{1}{\sqrt{2}}(a^*_{k-} - ib^*_{k-}) \quad \text{creates photon pol. } R \text{ in } -\boldsymbol{k}/k \text{ direction},$$

$$d^*_+ = \frac{1}{\sqrt{2}}(a^*_{k+} + ib^*_{k+}) \quad \text{creates photon pol. } L \text{ in direction } +\boldsymbol{k}/k,$$

$$c_+ = \frac{1}{\sqrt{2}}(a_{k+} + ib_{k+}) \quad \text{destroys photon pol. } R \text{ in direction } +\boldsymbol{k}/k\,,$$

etc....

Substituting in (1), formula (18) in text follows.

SUPPLEMENTO AL VOLUME II, SERIE X
DEL NUOVO CIMENTO

N. 1, 1955
2° Semestre

Photomeson Production from Hydrogen.

B. T. FELD

Physics Department - Massachusetts Institute of Tecnology - Cambridge Massachusetts (*)

The reactions

(1) $$\gamma + \mathrm{p} \to \mathrm{n} + \pi^+$$

(2) $$\gamma + \mathrm{p} \to \mathrm{p} + \pi^0$$

have been studied in a number of laboratories [1] in the energy range between threshold ($E_\gamma \cong 150$ MeV) and $E_\gamma = 450$ MeV. Writing for the cross-section in the center of mass system

(3) $$\mathrm{d}\sigma/\mathrm{d}\Omega = A_0 + A_1 \cos\theta + A_2 \cos^2\theta + \ldots$$

the coefficients A_0, A_1, A_2 exhibit the following characteristics.

a) The constant term, A_0, increases rapidly above threshold for reaction (1) — directly in proportion to the meson momentum in the c.m. system — while for reaction (2) the increase is much slower, in proportion to the cube of the meson momentum. A_0 has its maximum value, for both reactions, in the region ot $E_\gamma \cong 300$ MeV, and falls off rapidly above this energy. The value of A_0 for reaction (2) exceeds that for reaction (1) for $E_\gamma \gtrsim 250$ MeV.

b) For reaction (1), A_1 starts out negative, has its maximum amplitude at $E_\gamma \cong 270$ MeV, and changes sign at $E_\gamma \cong 320$ MeV. For reaction (2), A_1 is small below $E_\gamma \approx 400$ MeV.

c) For reaction (1), below $E_\gamma \approx 200$ MeV, $A_2 \ll A_0$. Above this energy, A_2 is negative, increases in magnitude rapidy to a maximum value at

(*) This lecture is based on work performed, while on leave from M.I.T., at the Universities of Rome and Padua, with the aid of a fellowship from the « John Simon Guggenheim Memorial Foundation ».

$E_\gamma \cong 300$ MeV,and then falls rapidly, changing sign at $E_\gamma \cong 420$ MeV. For reaction (2) the value of A_2 is, at all energies, approximately twice that of reaction (1). In addition for reaction (2) $|A_2/A_0| = 0.5\text{-}1$, more or less independent of energy.

d) None of the existing data require, for their fitting by equation (3), powers of $\cos\theta$ higher than the second.

The main features of reactions (1) and (2) have previously been interpreted [2] as indicating, in the first place, a predominance of magnetic dipole photon absorption (meson emission in the *p*-state) into an intermediate state of angular momentum $J = 3/2$ and isotopic spin $T = 3/2$, with the possibility of a resonance in the region of $E_\gamma \approx 300$ MeV and, in the second place, an appreciable electric dipole photon absorption (*S*-wave mesons) near threshold for reaction (1) which is, however, absent in reaction (2). This interpretation is in qualitative agreement with the experiments as described above, below $E_\gamma \sim 300$ MeV. In particular, the fact that A_1, which arises from interference between electric and magnetic dipole absorption in reaction (1), changes sign is a strong indication that the phase of the magnetic dipole absorption amplitude goes through 90°, i.e., through a resonance.

This simple interpretation meets with difficulty when applied for $E_\gamma < 300$ MeV. In particular, the behaviour of A_2 cannot be understood in terms of magnetic dipole absorption alone. This is not unexpected, when we observe [3] that an intermediate state with $J = T = 3/2$ and positive parity can also be formed through electric quadrupole photon absorption, and that the photon wavelengths involved are sufficiently small so that there is no *a priori* reason to exclude this effect. If we include all terms leading to the emission of mesons of angular momentum $l \leqslant 1$, the coefficients of equation (3) may be written

$$(4a) \qquad A_0 = |a_{\frac{1}{2}}^{ED}|^2 + |a_{\frac{1}{2}}^{MD}|^2 + \tfrac{5}{2}|a_{\frac{3}{2}}^{MD}|^2 + \tfrac{3}{2}|a_{\frac{3}{2}}^{EQ}|^2 + \\ + \operatorname{Re}\{a_{\frac{1}{2}}^{MD*}(a_{\frac{3}{2}}^{MD} + \sqrt{3}\, a_{\frac{3}{2}}^{EQ}) - \sqrt{3}\, a_{\frac{3}{2}}^{MD*}\, a_{\frac{3}{2}}^{EQ}\}$$

$$(4b) \qquad A_1 = 2 \operatorname{Re}\{a_{\frac{1}{2}}^{ED*}(-a_{\frac{1}{2}}^{MD} + a_{\frac{3}{2}}^{MD} + \sqrt{3}\, a_{\frac{3}{2}}^{EQ})\}$$

$$(4c) \qquad A_2 = -\tfrac{3}{2}|a_{\frac{3}{2}}^{MD}|^2 + \tfrac{3}{2}|a_{\frac{3}{2}}^{EQ}|^2 - 3 \operatorname{Re}\{a_{\frac{3}{2}}^{MD*}(a_{\frac{3}{2}}^{MD} + \sqrt{3}\, a_{\frac{3}{2}}^{EQ}) - \sqrt{3}\, a_{\frac{3}{2}}^{MD*}\, a_{\frac{3}{2}}^{EQ}\}\ .$$

Each of the above amplitudes is a complex quantity; they may be written $a_{\frac{1}{2}}^{ED} = Ae^{i\alpha}$, $a_{\frac{1}{2}}^{MD} = Be^{i\beta}$, $a_{\frac{3}{2}}^{MD} = Ce^{i\gamma}$, $\sqrt{3}\, a_{\frac{3}{2}}^{EQ} = De^{i\delta}$ in which the (real) quantities A, B, C, D, are restricted only in that they must have the proper dependence on meson momentum [2] near threshold (*), and the (real) phases α, β, γ, δ bear a simple relationship to the phases-hifts involved in meson-nucleon scat-

(*) These also contain the common factor $\lambda\!\!\!^{-}/\sqrt{8}$, where $\lambda\!\!\!^{-}$ is the Dirac wavelength of the photon.

tering [4]. Even with these restrictions, there still remain more parameters than are required to fit the data.

However, by assuming that the most important contribution to the photoproduction at higher energies comes from the intermediate state of $J=T=3/2$, it is possible to fit all of the experimental data for reaction (1) with the parameters shown in Fig. 1. For this fit we have assumed $A<0$, $B=0$, $\gamma=\delta=\alpha_{33}$ (the « Fermi » phase shift for meson scattering in the state $J=T=3/2$), and $0<x\equiv D/C<1$.

The noteworthy features of this « fit » are: *a*) The rapid increase and relatively large magnitudes of A and α (the electric dipole absorption parameters) at low energies; *b*) the « resonances » of C and γ at energies consistent with the observations on meson scattering [5]; *c*) the necessity for appreciable electric quadrupole absorption above $E_\gamma\approx 300$ MeV. Of these, only the behavior of α presents any new or surprising aspects (+).

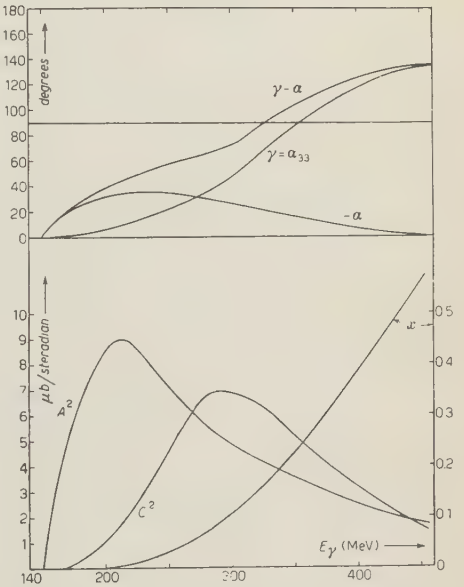

Fig. 1. – « Fermi » fit for the reaction $\gamma+p\rightarrow n+\pi^+$; The lower portion gives the magnitudes and the upper portion the phases of the amplitudes required to fit the available experiments with equations (4).

The experimental data for reaction (2) are much more scanty. Assuming that, for this reaction, $A=0$, and that C (reaction 2) $=\sqrt{2}C$ (reaction 1), which is required by the assumption of charge independence [2], the parameters of Fig. 1 give a cross-section whose energy dependence seems to agree with experiment, but whose magnitude is too great by a factor between 1 and 2. The reasons for this discrepancy are at present unclear although it is not out of the question that the absolute cross-section determinations may be in error by such a factor.

This interpretation of photomeson production on hydrogen is, as pointed out above, not unique. In particular, there exists a « Yang » type solution [3] for which $B>C$ (not, however, negligible) and for which $\beta\approx 4\gamma$ goes through 90° at $E_\gamma\approx 350$ MeV. It is interesting to note that the « Fermi » and the « Yang » type solutions can be distinguished, experimentally, on the basis of

(+) The values of α at low energy are based mainly on data which are now known to yield too large values of α.

the polarization of the recoil nucleons. This possibility is discussed by me in a recent article [6].

It is of interest to look somewhat more closely at the aforementioned « fit » in order to see if the parameters adopted have a reasonable dependence on the photon energy.

1) If we consider A^2/η (η is the π-meson momentum in units of $\hbar/\mu c$ in the c.m. system) we observe that it remains roughly constant up to ~ 200 MeV, above which energy it falls off rapidly. The fall-off, which is more rapid than $\lambda\!\!\!^{-2}_{\gamma}$, may be indicative of a « form factor » effect.

2) The behaviour of α appears rather unreasonable at low energies on the following grounds: we may write (see the lectures of FERMI on the properties of the scattering matrix)

$$Ae^{i\alpha} = A_3 e^{i\alpha_3} + A_1 e^{i\alpha_1} \tag{5}$$

whence

$$\operatorname{tg}\alpha = \frac{A_3 \sin\alpha_3 + A_1 \sin\alpha_1}{A_3 \cos\alpha_3 + A_1 \cos\alpha_1}\,. \tag{6}$$

For small α, α_3, α_1 (near threshold)

$$\alpha \approx \frac{A_3\alpha_3 + A_1\alpha_1}{A_3 + A_1}\,. \tag{7}$$

Now, from the π^0 production near threshold

$$A_3 \approx \tfrac{1}{2}A_1 \tag{8}$$

$$\alpha \approx \frac{\alpha_3 + 2\alpha_1}{3} \approx 0{,}07\eta \text{ radians}\,, \tag{9}$$

from the scattering data. This is much smaller than our assumed α, and of the wrong sign. At higher energies, however, α_3, which is negative, predominates, and our values are reasonable. The above discrepancy will probably be removed if we use the new Illinois data (see BERNARDINI) which give larger C^2 and smaller interference near threshold (*).

3) The behaviour of C can be understood in terms of a resonance at $E_\gamma \approx 350$ MeV. Using the « Breit-Wigner » formulation for the resonance, we write

---

(*) *Note added in proof*: It now appears that the major portion of the asymmetry at low energies arises from kinematical recoil effects, which have been disregarded in the above analysis [G. F. CHEW: *Phys. Rev.*, **95**, 1669 (1954)].

(10) $$C^2 = \frac{\lambda_\gamma^2 \Gamma_\gamma}{4E_r}\mathcal{R},$$

where

(11) $$\mathcal{R} = \frac{\Gamma_\pi/2E_\pi}{(1-E/E_r)^2+(\Gamma_\pi/2E_r)^2},$$

and

(12) $$\frac{\Gamma_\pi}{2E_\pi} = \left(\frac{0.3\eta^3}{1+\eta^2}\right),$$

is taken to fit the α_{33} scattering phase-shift. We then find that $C^2\mathcal{R}$ shows a similar energy dependence as A^2/η—i.e., a form factor effect. If we assume that the form factor ~ 1 for $E_\gamma \approx 200$ MeV, we obtain $\Gamma_\gamma \approx 1$ MeV. It is interesting to note that extrapolation of the low energy formula of BLATT and WEISSKOPF [7] for the probability of magnetic dipole absorption

(13) $$\Gamma(MD) = \frac{5}{2}\cdot\frac{1}{137}\left(\frac{\hbar}{mc}\right)^2\left(\frac{\hbar\omega^3}{c^2}\right),$$

gives $\Gamma(MD) \approx 5$ MeV for $m = \mu$, and $\Gamma(MD) \approx \frac{1}{8}$ MeV for $m = M$.

REFERENCES

[1] *Reaction* (1): J. STEINBERGER and A. S. BISHOP: *Phys. Rev.*, **86**, 171 (1952); R. S. WHITE, M. J. JACOBSON and A. G. SCHULZ: *Phys. Rev.*, **88**, 836 (1952); N. JARMIE, G. W. REPP and R. S. WHITE: *Phys. Rev.*, **91**, 1023 (1953); Y. GOLDSCHMIDT-CLERMONT, L.S. OSBORNE and A.WINSTON: *Phys. Rev.*, **91**, 468-A (1953); T. JENKINS, D. LUCKEY, T. R. PALFREY and R. R. WILSON: *Phys. Rev.*, **95**, 179 (1954); R. F. BACHER, J. C. KECK, V. Z. PETERSON, J. G. TEASDALE, A. V. TOLLESTRUP, R. L. WALKER and R. M. WORLOCK: *Phys. Rev.*, **92**, 1090-A (1953); G. S. JANES and W. L. KRAUSHAAR: *Phys. Rev.*, **93**, 900 (1954); G. BERNARDINI and E. L. GOLDWASSER: *Phys. Rev.*, **94**, 729 (1954); **95** 857 (1954).

Reaction (2): A. SILVERMAN and M. STEARNS: *Phys. Rev.*, **88**, 1225 (1952); Y. GOLDSCHMIDT-CLERMONT, L. S. OSBORNE and M. G. SCOTT: *Phys. Rev.*, **97**, 188 (1955); R. L. WALKER, D. C. OAKLEY and A. V. TOLLESTRUP: *Phys. Rev.*, **97**, 1279 (1955); D. C. OAKLEY and R. L. WALKER: *Phys. Rev.*, **97**, 1283 (1955). I am especially grateful to G. BERNARDINI, L. S. OSBORNE, R. L. WALKER and R. R. WILSON for private communication of the work in their respective laboratories.

[2] K. A. Brueckner and K. Watson: *Phys. Rev.*, **86**, 923 (1953); B. T. Feld: *Phys. Rev.*, **89**, 330 (1953).
[3] B. T. Feld in *Report on the Third Annual Rochester Conference* (New York, 1953).
[4] K. M. Watson: *Phys. Rev.*, **95**, 228 (1954).
[5] M. Glicksman: *Phys. Rev.*, **94**, 1335 (1954).
[6] B. T. Feld: *Nuovo Cimento*, **12**, 425 (1954).
[7] J. M. Blatt and V. F. Weisskopf: *Theoretical Nuclear Physics* (New York, 1952).

SUPPLEMENTO AL VOLUME II, SERIE X
DEL NUOVO CIMENTO

N. 1, 1955
2° Semestre

The Photodisintegration of the Deuteron at High Energies and Associated Phenomena.

B. T. FELD

Physics Department - Massachusetts Institute of Technology - Cambridge Massachusetts (*)

The reaction $\gamma + d \to n + p$ is one of the most extensively studied of nuclear reactions, mainly because of its importance in the understanding of the neutron-proton interaction. At low energies (say, between threshold, $E_{\gamma_t} = 2.23$ MeV, and $E_\gamma = 10$ MeV) the reaction is well understood and the experiments (after many discrepancies, due to experimental difficulties, have finally been removed) are in very good agreement with the theoretical predictions based on the same (static) potential between neutron and proton as is derived from other low energy phenomena. The results are summarized in a recent article in *Progress in Nuclear Physics* [1].

Briefly, the situation at low photon energies may be summarized as follows: There are two types of processes. 1) Photomagnetic disintegration (magnetic dipole photon absorption), for which the cross-section rises rapidly to a max. at about 65 keV above threshold and then falls off very rapidly at higher energies; the angular distribution is isotropic in the c.m. system; 2) photoelectric disintegration (electric dipole photon absorption) for which the cross-section has a max at about 2.2 MeV above threshold and then falls off like $\sim E^{-\frac{3}{2}}$ at higher energies. The angular distribution is $\sin^2\theta$.

Thus, near threshold $W(\theta) = \alpha + \sin^2\theta$ with $\alpha \ll 1$ as soon as E_γ is a few MeV above E_{γ_t}.

Now, at immediate energies (10 MeV $\lesssim E_\gamma \lesssim$ 50 MeV) the experiments show two new effects:

1) the appearence of an appreciable isotropic term;

(*) This lecture is based on work performed, while on leave from M.I.T., at the Universities of Rome and Padua, with the aid of a fellowship from the « John Simon Guggenheim Memorial Foundation ».

2) the appearence of an asymmetry about 90°; in this range, the angular distributions can be represented by the expression:

$$(1) \qquad W(\theta) = \frac{(\alpha + \sin^2\theta)}{(1 - \beta\cos\theta)^2} \approx (\alpha + \sin^2\theta)(1 + 2\beta\cos\theta)\,.$$

as has been demonstrated by the experiments of HALPERN and WEINSTOCK [2] and ALLEN [3]. The anisotropy is understandable as being due to a retardation effect (due to the c.m. motion, the protons emitted in the forward direction see photons of longer wave length) or, alternatively and essentially equivalently, to an interference between electric dipole and electric quadrupole photon absorption.

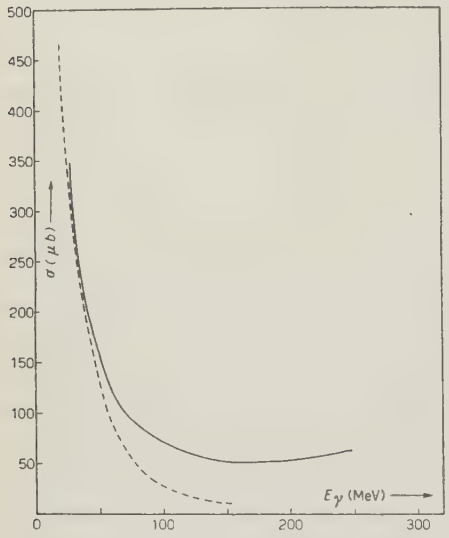

Fig. 1. – Cross-section for the reaction $\gamma + d \rightarrow n + p$. The solid curve represents the experimental values. The broken curve is the theoretical prediction [4], based on the low-energy potential.

The isotropic term has been attributed to the effect of non-central forces (such as the tensor forces which lead to the quadrupole moment of the deuteron) and follows from various types of meson theories. In this energy range, the experiments are in fair agreement with the theoretical predictions of SCHIFF [4] and of MARSHALL and GUTH [5], based on a central force (50% ordinary, 50% exchange) with a long-tailed potential. Actually, as can be seen from Fig. 1, the agreement is excellent for the total cross-section. However, since these theories predict $\alpha \approx 0$, this agreement is, to a certain extent, illusory.

Above $E_\gamma \cong 50$ MeV, the trends indicated below 50 MeV continue. In this range, experiments have been performed by BENEDICT and WOODWARD [6] and by KECH *et al.* [7] at Cornell, using counter techniques, by GILBERT and ROSENGREN [8] at Berkeley, using counters, and by SCHRIEVER, WHALIN and HANSON [9] at Illinois, using photoplate detectors. All of these investigators are in reasonable agreement as to angular distribution, but the absolute cross-section values frequently differ, mainly as a result of the difficulties involved in the absolute calibration of X-ray beams. The most recent and probably most reliable of these results, mainly from HANSON's group at Illinois, indicate a cross-section as shown in Figs. 1 and 2.

The main features of these results are:

1) essential constancy of σ_{tot} above $E_\gamma \approx 100$ MeV;

2) the great decrease of the $\sin^2\theta$ term above $E_\gamma \approx 100$ MeV;

3) the continued asymmetry which, however, does not increase with energy as would be expected if $\beta = v_p/c$ in eq. (1);

4) the large value of σ_{tot}, which is of the same order of magnitude as the photomeson production cross-section (actually, a few times smaller).

There is at present no theory which explains all the above features. Most, if not all of these features, probably result from the fact that at high energies the photodisintegration of the deuteron is undoubtedly meson-connected. Thus, for instance, the large cross-section has been ascribed by WILSON [10] to meson production when the two nucleons are closer than $\hbar/\mu c$, in which case, for purely statistical reasons, it is more probable that the meson will be reabsorbed and a nucleon emitted.

The fact that $\beta < v_p/c$ indicates that the asymmetry cannot be explained as a pure retardation effect, although it is probable that this is, at least, part of the story. On the other hand, if there exists appreciable magnetic dipole absorption, in addition to electric dipole, we would also expect an interference term proportional to $\cos\theta$ provided that both processes lead to the same final spin state for the two nucleons.

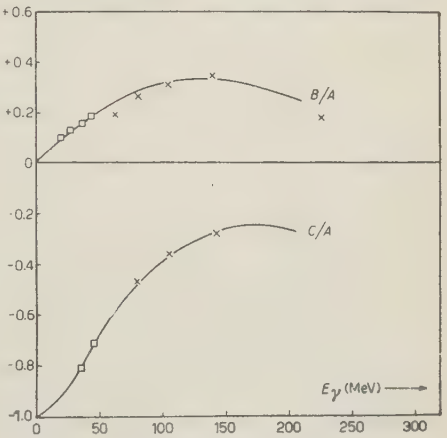

Fig. 2. – Angular Distribution in the reaction $\gamma + d \rightarrow n + p$.
The data have been fitted to $d\sigma/d\Omega = A + B\cos\theta + C\cos^2\theta$.

One possible mechanism for appreciable magnetic dipole absorption could be as follows.

If, as is indicated by photomeson production from hydrogen, there is a resonance in the $P_{\frac{3}{2}}$ state (magnetic dipole absorption) then we may consider the following mechanism for the reaction:

$$\gamma + d \rightarrow \mathcal{N}^* + \mathcal{N} \rightarrow n + p\,. \tag{2}$$

The same intermediate state would be involved in the following reactions:

$$\pi^0 + d \rightarrow n + p \tag{3}$$

$$\gamma + p \rightarrow p + \pi^0 \tag{4}$$

$$\pi^0 + p \rightarrow p + \pi^0 \tag{5}$$

of which (3), (4) and (5) or their equivalent reactions (assuming charge-independence) have all been observed and their cross-sections measured. Then, for the same c.m. energies, we can write

$$\sigma_2 = \sigma_3 \cdot (\sigma_4/\sigma_5) \,. \tag{6}$$

It is easily shown that, if all the reactions proceed through the same intermediate state of the nucleon, σ_2 is essentially independent of the photon energy for energies not too far from the meson-production threshold (both above and below the threshold). Using the observed cross-sections we obtain $\sigma_2 \approx 25$ μb. The difficulty with this model (aside from the relatively minor objection that the observed cross-section is by a factor of two larger than estimated) is that it predicts an angular distribution of the form

$$W(\theta) = [2 + 3 \sin^2 \theta] \,. \tag{7}$$

The experiments indicate much less $\sin^2 \theta$ term.

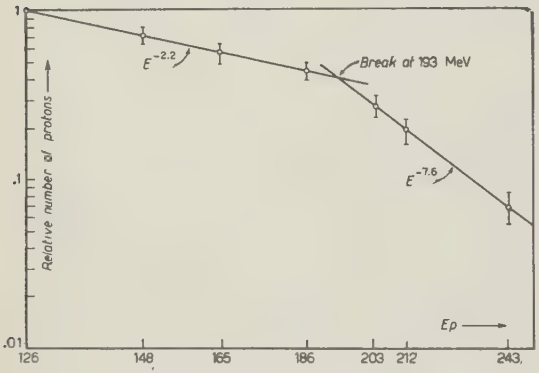

Fig. 3. – The energy distribution of photoprotons from carbon at 30°. Both scales are logarithmic. The original data have been corrected for the attenuation in the telescope and the energy spread accepted by the telescope. All the data are normalized to the value at 126 MeV.

It would also be possible to account for a symmetrical angular distribution by an electric dipole absorption process, provided that this absorption would lead to the $^3P_0$ final nucleon state. It will be interesting to see what the theory of Chew has to say on this point.

Finally, it is of interest to observe that the photodisintegration of the deuteron also appears to be the process primarily responsible for the photoproduction of high energy neutrons and protons from heavier nuclei. This is demonstrated in Figs. 3 and 4 in which are shown examples, more or less typical, of the energy and angular distributions of high energy photoprotons from carbon and beryllium produced by a 325 MeV X-ray beam at M.I.T. The characteristic feature of the energy distribution is the sharp break, which occurs at the proton energy corresponding to the photodisintegration of a deuteron by the maximum energy photon.

The sharpness of the angular distribution is due essentially to the same reason. It is of some interest to note that, assuming the deuteron model for this process, the angular distribution is an additional indication that the $\sin^2 \theta$

term in the deuteron photodisintegration is small. For a pure $\sin^2\theta$ distribution, the angular distribution shown should have a maximum at $\sim 30° \div 50°$. Actually, the observed distribution fits well with either an isotopic or a forward-peaked distribution for the deuteron process.

However, until rather recently, there were a number of discrepancies and contradictions between the various experiments and the deuteron model. Now,

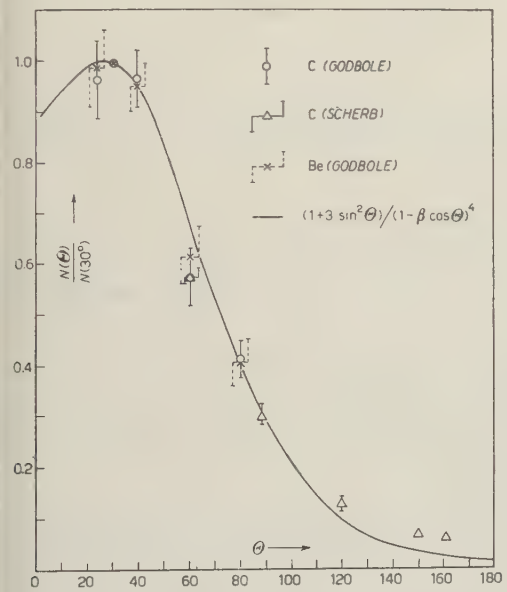

Fig. 4. – The angular distribution in the laboratory of 126 MeV photoprotons from beryllium and carbon. The data marked « Scherb » were obtained at a later date than that marked « Godbole ». The data are normalized to the value at 30°. The curve is a semiempirical fit to the data with $\beta = v/c$ of the protons.

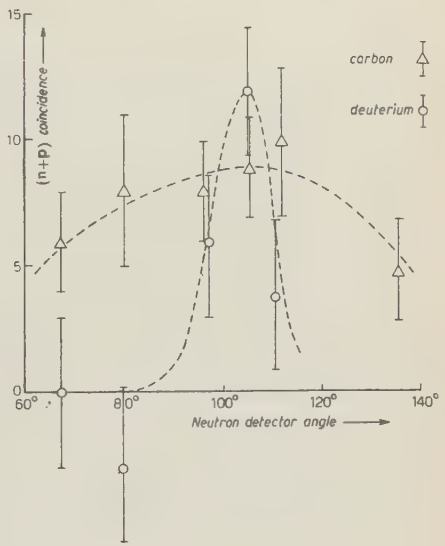

Fig. 5. – Neutron proton coincidences from carbon an deuterium as a function of the angle of the neutron counter for a fixed proton angle and energy. The coincidences are expressed in relative counts per atom per monitor unit. From MYERS, ODIAN, STEIN and WATTENBERG [9].

however, the model has been strikingly confirmed by the work of WATTENBERG *et al.* [11] at M.I.T. and BARTON and SMITH [12], at Illinois, who have observed neutron-proton coincidences at the appropriate correlation angles and in such numbers as to indicate that essentially every high energy proton is accompanied by a high energy neutron. Fig. 5 compares the angular correlation for n-p coincidences from carbon with that from d. The large angular spread from carbon is due to the preponderance of higher momenta in the relative nucleon motion within the carbon nucleus. This feature, as a matter of fact, explains most of the apparent discrepancies between previous observ-

ations on high energy photoprotons and the deuteron model of LEVINGER [13].

A complete history and set of references on these questions is given in FELD *et al.* [14].

REFERENCES

[1] G. L. SQUIRES: *Progress in Nuclear Physics* (London, 1952), vol. II, p. 89.
[2] J. HALPERN and E. V. WEINSTOCK: *Phys. Rev.*, **91**, 934 (1953).
[3[L. ALLEN, Jr.: *Phys. Rev.*, **98**, 705 (1955).
[4] L. I. SCHIFF: *Phys. Rev.*, **78**, 733 (1950).
[5] J. F. MARSHALL and E. GUTH: *Phys. Rev.*, **78**, 738 (1950).
[6] T. S. BENEDICT and W. M. WOODWARD: *Phys. Rev.*, **85**, 924 (1952).
[7] J. KECK R. M. LITTAUER, G. K. O'NEILL, A. M. PERRY, and W. M. WOODWARD: *Phys. Rev.*, **93**, 827 (1954).
[8] W. S. GILBERT and J. W. ROSENGREN: *Phys. Rev.*, **88**, 901 (1952).
[9] E. A. WHALIN, Jr.: *Phys. Rev.*, **95**, 1362 (1954)l.
[10] R. R. WILSON: *Phys. Rev.*, **86**, 125 (1952).
[11] A. WATTENBERG *et al.*: *Phys. Rev.*, **95**, 576 (1954).
[12] M. R. BARTON and J. H. SMITH: *Phys. Rev.*, **95**, 573 (1954).
[13] J. S. LEVINGER: *Phys. Rev.*, **84**, 43 (1951).
[14] B. T. FELD., R. D. GODBOLE, A. ODIAN, F. SCHERB, P. C. STEIN and A. WATTENBERG: *Phys. Rev.*, **94**, 1000 (1954).

SUPPLEMENTO AL VOLUME II, SERIE X
DEL NUOVO CIMENTO

N. 1, 1955
2° Semestre

Search for the β-Decay of the Pion. (*)

S. LOKANATHAN and J. STEINBERGER (**)

Nevis Cyclotron Laboratories, Columbia University
Department of Physics - New York

1. – Introduction.

1·1. *Theoretical.* – Normally the charged pion decays into a muon and a light neutral particle, usually assumed to be the neutrino. The possible competing decay into electron and neutrino is not without interest, and we recall here some theoretical points:

a) *Connection with nuclear β-decay.* – YUKAWA postulated the meson β-decay in a two step theory of nucleon β-decay. This hypothesis fails on the one hand because the transition rate of pion-electron decay if non-zero, is at any rate too small to account for the nuclear β-lifetimes, and on the other hand because the observed properties of β-decay require FERMI couplings [1] which are not a consequence of a two step theory with pseudoscalar mesons.

The argument may be reversed, and it may be supposed that the pion can transform into an intermediate nucleon-antinucleon pair which annihilates with normal β-decay:

$$\pi^+ \to p + n \to e^+ + \nu \,. \tag{1}$$

The pion being pseudoscalar, this transition is forbidden except in pseudoscalar and axial vector β-coupling theories. It may then be recalled that it is possible to account for the bulk of β-decay data using only scalar and tensor

(*) This research was supported by the Joint Program of the Atomic Energy Commission and the Office of Naval Research.

(**) Lecture given by J. STEINBERGER.

(1) See for instance, S. J. WU: *Proceedings of the 1954 Glasgow Conference on Nuclear and Meson Physics* (London, 1955).

interactions ([1]). The smallness of π-electron decay is therefore not in conflict with experiment. It is however in principle possible to learn about the possible role of pseudoscalar coupling in β-theory from pion-β-decay. Unfortunately the computation of process (1) not only involves divergent integrals, but different cutoff procedures have led to transition probabilities which differ by several orders of magnitude ([2,3]).

b) Symmetrical coupling of pion to muon and electron. – If the pion were coupled symmetrically to muon and electron, either directly, or by means of an intermediate nucleon anti-nucleon pair, then the relative transition probability $(\pi \to e + \nu)/(\pi \to \mu + \nu)$ depends only on kinematical factors (masses), field theoretical uncertainties cancel. One then obtains ([2,3]) for pseudoscalar coupling of the fermions .

$$\frac{\pi \to e + \nu}{\pi \to \mu + \nu} = \left[\frac{M_\pi^2 - M_e^2}{M_\pi^2 - M_\mu^2}\right]^2 = 5.4 \; ;$$

and for axial vector coupling

$$\frac{\pi \to e + \nu}{\pi \to \mu + \nu} = \left[\frac{M_\pi^2 - M_e^2}{M_\pi^2 - M_\mu^2}\right] \cdot \frac{M_e^2}{M_\mu^2} = \frac{1}{8\,000} \; .$$

The pseudoscalar result is roughly equal to the ratio of phase space. It favors $\pi \to e$ decay and is well known to be wrong. The axial vector coupling however discriminates strongly against low mass particles. If it could be established experimentally that the ratio $(\pi \to e)/(\pi \to \mu)$ is indeed less than 1/8 000, it would be possible to rule out the possibility of symmetrical coupling of the pion to the muon and electron.

1·2. *Experimental.* – In previous attempts to find this decay ([4]), photographic plates were exposed to well collimated meson beams close to the cyclotron target which was bombarded by high energy protons. It was concluded as unlikely that the electron decay of the pion should account for more than one in a thousand pion decays. Recently external meson beams of reasonable intensity have made it possible to use counters as detectors and obtain greater sensitivity. The pion beam is stopped in absorber and the decay electron detected in a counter telescope.

The chief experimental problem is that of distinguishing between π-decay

([2]) M. RUDERMAN and R. FINKELSTEIN: *Phys. Rev.*, **76**, 1458 (1949).
([3]) J. STEINBERGER: *Phys. Rev.*, **76**, 1180 (1949)
([4]) H. L. FRIEDMAN and J. RAINWATER: *Phys. Rev.*, **84**, 684 (1949).

electrons and μ-decay electrons. This is accomplished by making the detector sensitive to the shorter lifetime and higher energy of the π-decay electron.

2. – Experimental Procedure.

The experimental arrangement is shown in Fig. 1. The 60 MeV π^+ beam of the Columbia University Nevis Cyclotron is collimated and monitored by counters no. 1 and no. 2. Counter no. 1 is a plastic scintillator $4\frac{1}{2}$ inches in diameter and $\frac{3}{8}$ inches thick and counter no. 2 is a stilbene crystal $2\frac{1}{2}$ inches in diameter and $\frac{1}{8}$ inches thick. The beam is further collimated by a 2 inch diameter aperture in a 2 inch thick lead shield directly preceding counter no. 2 and is slowed by carbon absorbers inserted between no. 1 and no. 2.

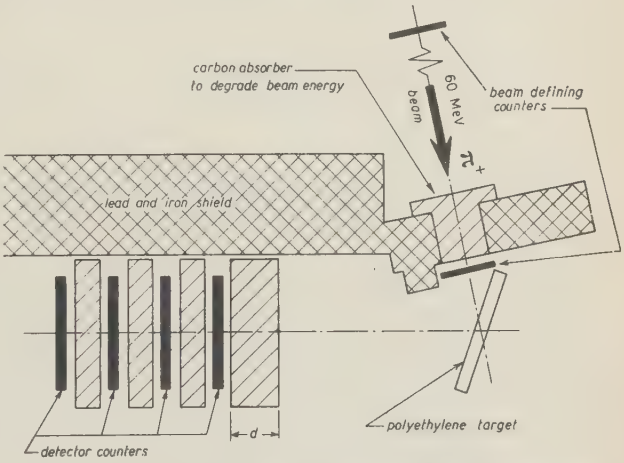

Fig. 1. – Arrangement of counters and absorbers.

The target is a $\frac{1}{2}$ inch thick piece of polyethylene (1.7 g/cm²) mounted at approximately 30° to the incident beam. Of the order of 500 pions stop in the target per second and this represents somewhat more than half of the 1-2 rate. Of these roughly 1 in 300 will decay with the charged decay product within the acceptance angle of the detector. This detector consists of four plastic scintillators, each $4\frac{1}{2}$ inches in diameter, the first three $\frac{3}{8}$ inches thick and the last $\frac{1}{4}$ inch thick. The counters no. 3,

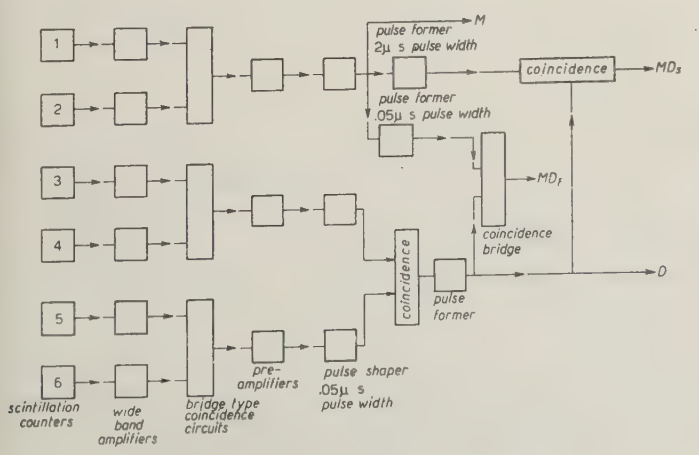

Fig. 2. – Block diagram of circuits.

4, 5 and 6 are arranged so that it is possible to insert 1 inch thick sheets of absorber between each pair of counters and an additional 6 inches in front of counter no. 3.

A block diagram of the electronics is shown in Fig. 2. The following events are recorded:

M = Monitor coincidences 1-2.

D = Detector coincidences 3, 4, 5, 6 with a resolving time of 10^{-8} s.

MD_f = « Fast » coincidences MD when D occurs within 10^{-7} s after the arrival of M.

MD_s = « Slow » coincidences MD when D occurs within $1.8 \cdot 10^{-6}$ s after the arrival of M.

Of the π^+-mesons which stop in the target, and decay with a mean life of $2.6 \cdot 10^{-8}$ s ([5]), the vast majority produce μ-mesons. The muons have a range of 2 mm in the polyethylene, about $\frac{1}{6}$ of its thickness. Approximately 95 percent of these μ-mesons therefore stop and decay in the same target piece. The mean-life of this decay is $2.2 \cdot 10^{-6}$ s ([6]), two orders of magnitude longer than the parent process, and results in a continuous β-spectrum with 53 MeV maximum energy ([7]).

With small absorber thicknesses therefore the events D are due to the μ-electrons. Of these 56 percent $= 1 - \exp[-1.8/2.2]$ are expected to be counted with the long gate of MD_s. Between 4 percent and $3\frac{1}{2}$ percent of these are counted in the short gate, MD_f. The rate D may therefore be used to determine the product of the rate of stopping π's multiplied by the acceptance solid angle of D. The ratios MD_f/D and MD_s/D may be used to determine the effective gate width of these channels.

Two sets of observations were made. In run no. 1 rates were observed with thicknesses of polyhethylene in 1 inch steps from zero arbsorber thickness (in addition to the counters and target) to 9 inches of absorber. In run no. 2 only 3 inches and 9 inches of polyethylene were used. In both runs data were obtained with and without the target, and the bulk of the observation was made with 9 inches of absorber. This latter thickness corresponds to an energy

([5]) C. WIEGAND: *Phys. Rev.*, **83**, 1085 (1951).

([6]) W. E. BELL and E. P. HINCKS: *Phys. Rev.*, **88**, 1424 (1952).

([7]) See for instance, P. SARGENT, M. RINEHART, L. LEDERMAN and K. ROGERS: in press.

loss for relativistic particles of 55 MeV due to ionization alone. μ-decay electrons cannot penetrate this absorber; however, some are nevertheless detected through the conversion of their bremsstrahlung. The geometry of counters and absorbers in D is chosen to minimize this effect. Experimentally we find 1/500 of the decay spectrum detected in this manner. This is a rate which might reasonably be expected for bremsstrahlung conversion. The μ-decay background in MD_f with 9 inches of polyethylene is therefore approximately $.04 \cdot 1/500 = 8 \cdot 10^{-5}$ of the total μ-decay rate.

3. – Experimental Results.

The experimental results were obtained in 2 three-day runs and are presented in Table I and II and in Fig. 3.

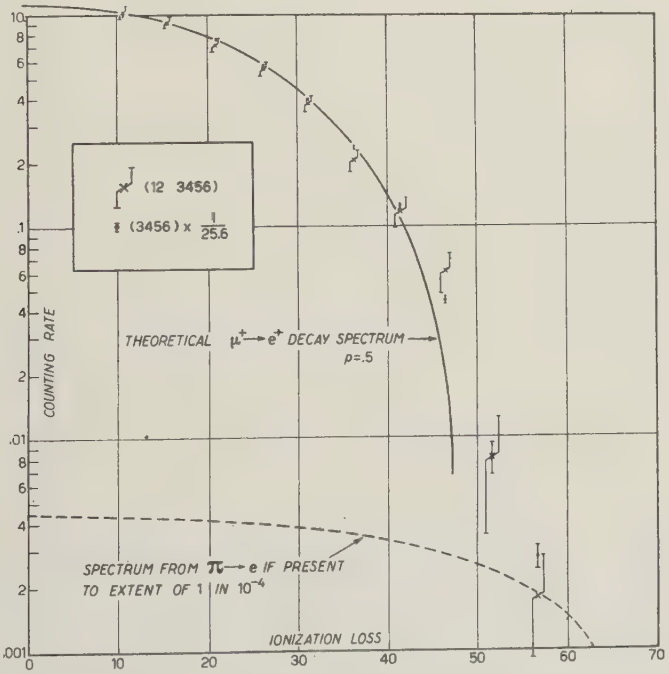

Fig. 3. – Counting rates MD_s and MD_f as a function of the absorber thickness in the detector D, obtained in run no. 1. The rates MD_f have been multiplied by the factor 25.6 so that the two curves coincide for small absorber thicknesses. The solid curve is the expected range dependence of μ-decay electrons ($\frac{1}{2} - \varrho$). The dotted curve is the expected $\pi \rightarrow$ e range dependence, and should be compared with the *difference* between the experimental curves MD_f and MD_s.

TABLE I.

Absorber		Target in			Target out			Net Monitor Counts per 10^6	
Thickness of CH_2 in inches	Total ionization loss in MeV	$M\cdot10^6$	D	MD_f	$M\cdot10^6$	D	MD_f	D	MD_f
0	7.5	4.26	14453	541	1.54	364	1	3164	126
1	12.5	4.10	11964	468	1.54	149	1	2811	113
2	17.5	3.07	7510	274	1.54	94	3	2389	87
3	22.5	3.07	5602	212	1.54	66	2	1787	68
4	27.5	3.08	3878	143	1.54	37	4	1246	44
5	32.5	3.07	2318	78	1.54	28	0	738	25.4
6	37.5	3.07	1257	45	1.54	29	1	392	14.1
7	42.5	3.07	471	23	1.54	23	0	139	7.5
8	47.5	3.07	122	3	1.54	21	1	26.1	.38
9	52.5	29.4	606	15	15.5	206	2	7.3	.38±.16

TABLE II.

Absorber		Target in				Target out				Net Monitor Counts per 10^6		
Thickness of CH_2 in inches	Total ionization loss in Mev	$M\cdot10^6$	D	MD_f	MD_s	$M\cdot10^6$	D	MD_f	MD_s	D	MD_f	MD_s
3	—	1.38	1957	56	1021	0.28	97	0	8	1320	46	741
9	—	23.6	238	6	61	11.3	27	0	13	1.4'8	.2'54 ±.10	1.4

4. – Analysis of the Data.

4·1. *Product K of stopped meson flux and detector solid angle.* – K is obtained by extrapolating the observed rate D from small absorber thickness to zero absorber thickness, as discussed in the introduction. For run no. 1 this can be done using Fig. 3, and $K_1 = 3330 \pm 50$ per 10^6 monitor counts. For run no. 2 we multiply the rate observed with 3 inches of polyethylene by the ratio of counts D extrapolated to zero absorber to counts D with 3 inches of polyethylene as determined in Fig. 3. This ratio being 2.0, $K_2 = 2640 \pm 50$ per 10^6 monitor counts.

b) Acceptance time λ for the detection of decay positrons in MD_f. – This can be determined from the counting rates of the μ-decay positrons using small

absorber thickness:

$$\lambda = \lambda_{\mu \to e} \exp\left[\ln\left(D/(D - MD_f)\right)\right].$$

We find

$$\lambda_1 = 8.6 \cdot 10^{-8} \text{ s for run no. 1,}$$

$$\lambda_2 = 6.7 \cdot 10^{-8} \text{ s for run no. 2.}$$

c) Detection probability of positrons from the decay of $\pi^+ \to e^+ + \nu$. These positrons will have an energy of 71 MeV, one half of the rest energy of the pion. With 9 inches of polyethylene, the average ionization loss of a minimum ionizing particle is 45 MeV in the 21 g/cm² of polyethylene, about 7 MeV in the four detection-counters (3.5 g/cm² CH_2) and 2.5 MeV in one half of the meson stopping target (1.1 g/cm² CH_2) for a total loss of 54.5 MeV through ionization. In the appendix we calculate the probability with which electrons of given energies will penetrate absorbers of given ionization loss taking radiation and multiple scattering into account. From Fig. 4, we interpolate that 71 MeV electrons will be detected with a probability $E = 0.48$ when 9 inches of polyethylene are present. However, this will not be quite true in the case of positrons for these can annihilate in flight. This is in large measure balanced by a similar effect on the positrons from the μ-e decay which serve as calibration. We estimate that this effect reduces the probability E by about 2 to 3 percent and therefore use the value $E = .46$.

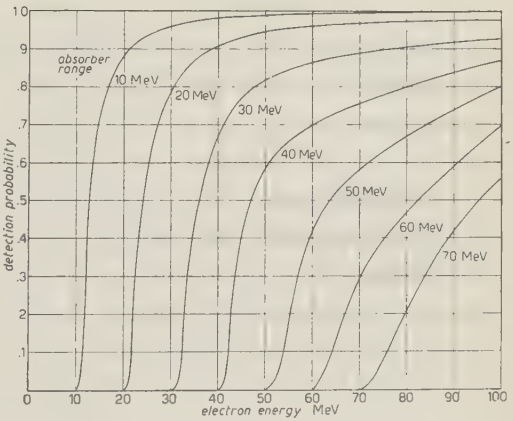

Fig. 4. – Smooth curve presentation of the results of the Monte Carlo calculations. Detection probability vs. energy in polyethylene. The range parameter is given in units of MeV ionization loss.

d) Correction for the μ*-decay positrons.* – The μ-decay positrons which are counted in MD_f with 9 inches of absorber through the conversion of the brehmsstralung radiation are directly determined from the rates D or MD_s which are almost entirely due to this effect.

Thus the number which has to be subtracted from MD_f is

$$\delta = (MD_s)_{9 \text{ inches}} \frac{\left(1 - \exp\left[(\lambda/2.2) \cdot 10^{-6}\right]\right)}{\left(1 - \exp\left[-(1.8/2.2) \cdot 10^{-6}\right]\right)},$$

or

$$\delta = (D)_{9\text{ inches}} \left(1 - \exp\left[-(\lambda/2.2)\cdot 10^{-6}\right]\right).$$

We find

$$\delta = (.18 \pm .025) \text{ per } 10^6 \text{ monitor counts for run no. 1,}$$
$$\delta = (.089 \pm .02) \text{ per } 10^6 \text{ monitor counts for run no. 2.}$$

e) Correction for inverse photomeson production and charge exchange scattering. – The target is traversed by a flux of pions measured in M. Only one half of these actually stop in the target, the average energy in the target may be approximately 25 MeV, and the average thickness of carbon traversed is ~ 1.5 g/cm^2. The meson has a finite probability for nuclear interaction with subsequent γ-emission, either from the inverse of photomeson production, or from charge exchange scattering. The former process may be estimated to have a cross-section of 2 ± 1 mb in this energy range, from observations [8] on the reaction $\gamma + C \to B^* + \pi^+$, which shows a certain resemblance to its inverse. The γ-rays emitted are of the order of 130 MeV and will have a detection probability of approximately 0.35 in D. The counting rate due to this effect is therefore approximately:

$$MD_f/M = (2 \pm 1)\cdot 10^{-27}\cdot[1.5\cdot 6\cdot 10^{23}/12]\cdot[.049/4\pi]\cdot .35 = (2.2 \pm 1.1)\cdot 10^{-7}.$$

The charge exchange cross-section in carbon has not been measured, however, it appears to be less than 1 mb for positive pions under 30 MeV [9]. The efficiency for detecting these γ-rays is somewhat less, because of the lower energy; it is approximately 0.2. The corresponding rate should therefore be

$$MD_f/M \leqslant 2\cdot 1\cdot 10^{27}\cdot[1.5\cdot 6\cdot 10^{23}/12]\cdot[.049/4\pi]\cdot 0.2 = 1.25\cdot 10^{-7}.$$

The charge exchange correction is therefore less than one half of the inverse photo process correction, but will not be made, since only an upper limit for this correction exists.

f) Fraction of π's decaying to electrons. – The net counting rate MD_f/M after subtraction for μ-decay electrons and inverse photoprocess is

$$(.38 \pm .16) - (.18 \pm .025) - (.22 \pm .11) = (-.02 \pm 21)$$

per 10^6 monitor counts for run no. 1.

[8] J. STEINBERGER and A. S. BISHOP: *Phys. Rev.*, **86**, 171 (1952).
[9] J. TINLOT: private communication.

and

$$(.254 \pm .10) - (.089 \pm .02) - (.22 \pm .11) = (-.055 \pm .15)$$

per 10^6 monitor counts for run no. 2.

The fraction of π-mesons undergoing β-decay is

$$(MD_f/M)_{\text{corrected}} \cdot 1/K \cdot 1/E = f$$

$$f_1 = -.13 \pm 1.36 \cdot 10^{-4} \text{ for run no. 1 ,}$$

$$f_2 = -.45 \pm 1.23 \cdot 10^{-4} \text{ for run no. 2 .}$$

Combining these two results, our experiment yields the ratio:

$$\frac{\pi \to e}{\pi \to \mu} = f = (-.3 \pm .9) \cdot 10^{-4} .$$

The quoted error is the standard deviation and includes the statistical uncertainty as well as an estimate of the error in the subtraction for the inverse photomeson production.

It is therefore not likely that the actual $\pi \to e$ decay fraction is greater than $.6 \cdot 10^{-4}$ or one in 17 000. The experiment is approximately twenty times more sensitive than previous attempts to find this decay mode, but no positive evidence is obtained. It seems therefore improbable that the pion is coupled symmetrically to the muon.

Appendix

Straggling of Electrons with Energies of the Order of the Critical Energy.

In this energy range the straggling is primarily due to radiation and multiple scattering. This problem has not been solved analytically, although the processes are well understood. We have solved the problem with an accuracy sufficient for our purposes by making Monte Carlo calculations for the radiation straggling and combining these with similar calculations ([1]) on the reduction in range due to the irregularity of the trajectory (multiple scattering) chiefly near its end.

The radiation straggling calculations were carried out at 6 energies: $E = 25$, 35, 50, 70, 85 and 100 MeV. The Bethe-Heitler radiation loss formula is approximated by the form which corresponds to uniform energy loss over the spectrum:

$$\mathrm{d}N(E)/\mathrm{d}x = 1/EX .$$

TABLE III. – *Results of the Monte Carlo calculations on the ranges of electrons in polyethylene. 100 trials are presented for each of six energies. The ranges in the column « Range Interval » are given in units of ionizations loss in* MeV.

Range Interval E	25	35	50	70	85	100
0 ÷ 2.5	—	—	—	—	—	—
2.5 ÷ 5	—	—	—	—	—	—
5 ÷ 7.5	1	—	—	—	—	—
7.5 ÷ 10	—	1	—	—	—	—
10 ÷ 12.5	3	—	2	—	1	—
12.5 ÷ 15	3	—	—	2	1	—
15 ÷ 17.5	6	2	—	—	2	1
17.5 ÷ 20	11	5	2	—	1	1
20 ÷ 22.5	7	4	1	—	2	1
22.5 ÷ 25	69	6	1	—	1	2
25 ÷ 27.5	—	3	1	1	1	—
27.5 ÷ 30	—	8	1	5	1	3
30 ÷ 32.5	—	6	5	2	1	1
32.5 ÷ 35	—	65	5	3	1	—
35 ÷ 37.5	—	—	6	1	3	1
37.5 ÷ 40	—	—	5	6	5	—
40 ÷ 42.5	—	—	8	2	3	2
42.5 ÷ 45	—	—	8	4	2	3
45 ÷ 47.5	—	—	17	3	3	1
47.5 ÷ 50	—	—	38	4	3	1
50 ÷ 52.5	—	—	—	6	2	1
52.5 ÷ 55	—	—	—	4	6	1
55 ÷ 57.5	—	—	—	6	3	2
57.5 ÷ 60	—	—	—	8	5	2
60 ÷ 62.5	—	—	—	6	4	3
62.5 ÷ 65	—	—	—	6	4	4
65 ÷ 67.5	—	—	—	10	6	3
67.5 ÷ 70	—	—	—	12	5	5
70 ÷ 72.5	—	—	—	—	5	5
72.5 ÷ 75	—	—	—	—	5	1
75 ÷ 77.5	—	—	—	—	5	7
77.5 ÷ 80	—	—	—	—	8	3
80 ÷ 82.5	—	—	—	—	7	5
82.5 ÷ 85	—	—	—	—	7	3
85 ÷ 87.5	—	—	—	—	—	6
87.5 ÷ 90	—	—	—	—	—	5
90 ÷ 92.5	—	—	—	—	—	5
92.5 ÷ 95	—	—	—	—	—	7
95 ÷ 97.5	—	—	—	—	—	7
97.5 ÷ 100	—	—	—	—	—	5

$N(E)$ is the number of quanta of energy E radiated per unit energy interval and X is the radiation length; in our case of CH_2 this is 65 g/cm². The absorber is then divided into sections of 5 MeV ionization loss. In CH_2 the ionization loss of minimum out-going particles is 2.18 MeV/c², so that each section corresponds to .0354 radiation length. The radiation loss probability distribution is then divided into 100 regions of equal probability and two digit random numbers are chosen for each interval. The calculation proceeds by allowing a trial electron to penetrate to the center of the first section by losing 2.5 MeV through ionization. It then radiates according to the loss picked from the radiation probability distribution by the random number of the section, loses 5 MeV by ionization to get to the center of section two, radiates according to its luck in this section and so on. We calculate for 100 trajectories at each of the six energies. The results are tabulated in Table III.

In Fig. 4 these results are plotted after the statistical irregularities are smoothed. In the same figure we alsc show the results of folding the multiple

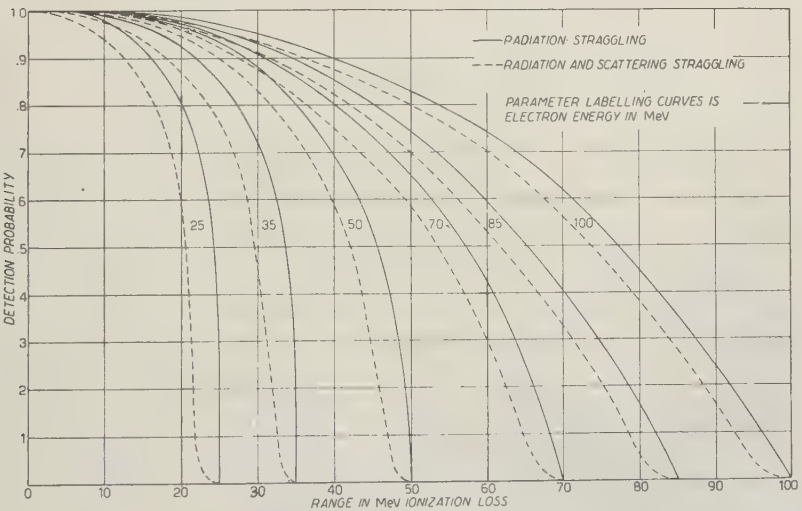

Fig. 5. – Smooth curve presentation of the results of the Monte Carlo range calculations: Detection Probability vs. Range in Polyethylene.

scattering distribution into these results ([10]). The range is given in units of ionization loss. For the purposes of the experiment it is necessary to know the detection probability (probability that the range be in excess) as a function of energy for different absorber thicknesses, and this is plotted in Fig. 5. The data of Fig. 5 are derived from Fig. 4.

([10]) The multiple scattering affects the trajectory chiefly near the end. We neglect the energy dependence of this straggling, and use the calculations made earlier for the multiple scattering of 50 MeV electrons; J. STEINBERGER: *Phys. Rev.*, **75**, 1135 (1949).

We wish to point out here that the results presented in Table I and Figs. 1 and 2 may also be used to predict the behavior in other materials, if the energy scale is converted by the factor:

$$\bar{E} = \bar{I}/I \,,$$

where I is the ionization loss per radiation length, in this case 142 MeV.

The computations have received some confirmation by comparing the observed $\mu \to e$ range curve with a computation of this range distribution using the calculated electron ranges and a spectrum for the decay electrons given by Michel's parameter $\varrho = \frac{1}{2}$ ([7]). This is shown in Fig. 3.

Lectures on Fundamental Particles.

B. ROSSI

Department of Physics and Laboratory for Nuclear Science
Massachusetts Institute of Technology - Cambridge, Massachusetts

1. – General Considerations.

1'1. – The Conservation Laws.

The expression « fundamental particle » describes a physical entity that, at the present stage of our knowledge, we find convenient to consider as a unit rather than as an aggregate of smaller and perhaps simpler parts. This definition is admittedly vague and imprecise, but I shall not attempt here to propose a more rigorous one.

Fundamental particles disappear either by interacting with other fundamental particles, or by spontaneous decay. Fundamental particles are born out of the interactions between other fundamental particles, or out of their decay processes. Thus, for example, the collision between two nucleons may produce a π-meson, which then decays into a μ-meson, which then decays into one electron and two neutrinos.

Of all the processes in which fundamental particles are born or die, only those of an electromagnetic character (e.g., pair production by photons) come within the framework of a consistent and fairly complete theoretical scheme. The theoretical description of the other processes is still non-existent, or in a very rudimentary stage. Thus, we are usually not in a position to describe what happens when fundamental particles change their identity, either by spontaneous decay, or by coming into close and strong interaction with one another. However, we shall assume that these processes do not violate the fundamental conservation laws, which are known to hold for isolated particles on systems of weakly interacting particles; i.e., the laws of conservation

of *energy*, of *linear momentum*, of *angular momentum* and of *parity*. The law of conservation of *isotopic spin* has been applied with some success to the phenomena of production of π-mesons (see lectures of E. FERMI at the Varenna Summer School, 1954). Attempts have been made to apply this law to the processes of production and decay of other fundamental particles (see GELL-MANN and PAIS, 1954), but I do not propose to discuss these still tentative theoretical developments in the present lectures.

The conservation laws of energy and linear momentum do not need any elucidation. For an isolated system composed of particles, these laws are expressed by the equations

$$U_1 + U_2 \ldots U_n + W = \text{const.} \tag{1.1}$$

$$\boldsymbol{p}_1 + \boldsymbol{p}_2 + \ldots + \boldsymbol{p}_n = \text{const. vector}. \tag{1.2}$$

In these equations U_1, $U_2 \ldots U_n$ are the total energies (including rest energy); $\boldsymbol{p}_1$, $\boldsymbol{p}_2 \ldots \boldsymbol{p}_n$ are the corresponding momenta of the particles, and W represents the interaction energy. For an individual particle, the total energy U and the momentum $p = |\boldsymbol{p}|$ are given in terms of the mass, m, the velocity of light, c, and the particle velocity, $c\beta$, by the equations

$$U = \frac{mc^2}{\sqrt{1-\beta^2}}, \tag{1.3}$$

$$p = \frac{mc\beta}{\sqrt{1-\beta^2}}. \tag{1.4}$$

The kinetic energy, E, is

$$E = U - mc^2. \tag{1.5}$$

Between U and p there exists the relation

$$U^2 = p^2c^2 + m^2c^4. \tag{1.6}$$

The above equations have a clear meaning only when the particles are isolated or weakly interacting with one another. For only then can the particles be regarded as separate physical entities. Here, we shall deal with processes that proceed through three stages. One starts from a system of weakly interacting particles; one then passes through a stage of strong interaction, not yet amenable to a theoretical description; at the end one has again a system of weakly interacting particles. The conservation laws of energy and momentum signify that the total energy and the total momentum of the system are the same in the initial and in the final state.

From the law of conservation of momentum it follows that there exists an inertial frame of reference in which the momentum of an isolated system of particles is zero at all times. This frame of reference is called the center-of-mass system, or c.m.s..

In the c.m.s., the total angular momentum of the particles has a value independent of the point with respect to which it is computed. This value also remains constant in time (principle of conservation of angular momentum).

The total angular momentum of a system of particles, $\boldsymbol{J}$, results from the *orbital angular momentum*, $\boldsymbol{L}$ (due to the relative motion of the particles considered as mass points), and of the intrinsic angular momentum, or *spin*, of the particles, $\boldsymbol{S}$. The general formalism of quantum mechanics requires that the total angular momentum, $J=|\boldsymbol{J}|$ be an integer or half-integer multiple of $\hbar$. For a system with total angular momentum $J=j\hbar$, the component, J_z, of the total angular momentum in a given direction may have the values: $j\hbar$, $(j-1)\hbar$, ..., $-j\hbar$.

The orbital angular momentum is always an integral multiple of $\hbar$. The spin, however, may be an integer or a half-integer multiple of $\hbar$. Particles with integer spin are referred to as *bosons*; particles with half-integer spin as *fermions*. From the law of conservation of angular momentum, it follows that the total number of fermions cannot change from odd to even, or vice versa, while no such restriction exists in the case of bosons.

A system containing two or more identical particles is unchanged if the two identical particles change place. Thus, if in the wave function that describes the system one interchanges the coordinates of two identical particles, the new wave function can differ from the old one only by a constant factor k (space coordinates, as well as those describing the orientation of the spin must be interchanged). If one interchanges a second time the coordinates of the two identical particles, one multiplies again the wave function by the same factor k. On the other hand, the system is now back in the initial condition. One thus concludes that $k^2=1$ and that, therefore, either $k=1$ or $k=-1$. In other words, interchanging the coordinates of two identical particles may either leave the wave function unchanged (symmetric wave function) or it may change its sign (antisymmetric wave function). It turns out that bosons have symmetric wave functions and fermions have antisymmetric wave functions.

The concept of parity arises from a symmetry property of space whereby nature does not distinguish left from right. Consider an isolated system of particles in the frame of reference where the center of mass is at rest. Suppose that the system is in a non-degenerate state characterized by given values of the energy, the angular momentum and the z-component of the angular momentum.

Assume first that the behavior of the system is described by Schrödinger's

wave equation, so that the eigenfunction under consideration is a scalar function, ψ, of the coordinates of all the particles of the system, which we shall indicate with x for short.

We now invert the direction of all three coordinate axes, so that if the original frame of reference was right-handed, the new one will be left-handed. In the new frame of reference, the function $\psi(x)$ will become a new function, $\bar{\psi}$ of the new coordinates $\bar{x}$. Since $\bar{x} = -x$, we have

$$\bar{\psi}(\bar{x}) = \psi(-x) . \tag{1.7}$$

Since the energy is a scalar quantity, it remains unchanged as one changes the direction of the coordinate axes. The same is true of the components of the angular momentum because the angular momentum is an axial vector. Quantum mechanically one can say that the operators representing the energy, the angular momentum and the z-component of the angular momentum are invariant with respect to the inversion of the coordinate axes. Thus $\bar{\psi}(\bar{x})$ and $\psi(x)$ are two eigenfunctions of the system corresponding to the same eigenvalues of the energy, the momentum, and the z-component of the momentum. Since we have assumed no-degeneracy, $\bar{\psi}(\bar{x})$ and $\psi(x)$ must represent the same state of the system, and can only differ by a constant quantity

$$\bar{\psi}(\bar{x}) = k\psi(x) ; \tag{1.8}$$

or, on account of Eq. (1.7),

$$\psi(-x) = k\psi(x) . \tag{1.9}$$

If we again change the direction of the coordinate axes, we return to the original frame of reference, and therefore to the original eigenfunction, $\psi(x)$. On the other hand, one finds as before

$$\psi(x) = k\bar{\psi}(\bar{x}), \ (*) \tag{1.10}$$

and therefore

$$\psi(x) = k^2\psi(x) . \tag{1.11}$$

(*) Notice that k in Eq. (1.10) must have the same value as in Eq. (1.8) because the process of changing from a left-handed to a right-handed system of coordinates must be undistinguishable from the process of changing from a right-handed to a left-handed system.

Thus the proportionality constant k is either $+1$ or -1 and we have to consider the two possibilities

$$\psi(-x) = \psi(x) \tag{1.12}$$

and

$$\psi(-x) = -\psi(x)\,. \tag{1.13}$$

In the first case the eigenfunction is said to have *even parity*; in the second case, *odd parity*.

For a two-body system there exists a simple relation between angular momentum and parity. Indeed, one finds that the space eigenfunctions corresponding to values of the orbital angular momentum equal to zero or to an *even* multiple of $\hbar$ have *even parity*. Instead, the eigenfunctions corresponding to values of the orbital angular momentum equal to an *odd* multiple of $\hbar$ have *odd parity*.

No such simple relation between angular momentum and parity exists for systems containing three or more particles. One finds that the eigenfunctions corresponding to $L = 0$ have always even parity. However, there exist both odd and even eigenfunctions corresponding, for example, to states of angular momentum $L = 1$.

The situation is a little more complicated in the case of particles whose behavior cannot be described in terms of a single scalar wave function. We shall consider here the case of fermions, obeying Dirac's wave equation. In this case, the wave function has four components, that we may call $\psi_1(x)$, $\psi_2(x)$, $\psi_3(x)$ and $\psi_4(x)$. Of these, two (e.g., ψ_1 and ψ_2) remain finite, and the other two (e.g., ψ_3 and ψ_4) vanish as the velocity of the particle goes to zero. Thus, for small velocities, ψ_1 and ψ_2 are large; ψ_3 and ψ_4 are small.

If, now, one changes as we have done before, the direction of all three coordinate axes, the four functions are represented in the new frame of reference by four new functions obtained from the old functions with a change in the sign of all variables. These four new functions do not satisfy Dirac's equation. However, one obtains a set of functions which again satisfy Dirac's equations if one makes the following transformation

$$\begin{cases} \bar{\psi}_1(\bar{x}) = \psi_1(-x) \\ \bar{\psi}_2(\bar{x}) = \psi_2(-x) \\ \bar{\psi}_3(\bar{x}) = -\psi_3(-x) \\ \bar{\psi}_4(\bar{x}) = -\psi_4(-x)\,. \end{cases} \tag{1.14}$$

The situation encountered here is similar to the situation arising in the case of electromagnetic fields. An electromagnetic field is described by six scalar quantities, E_x, E_y, E_z, H_x, H_y, H_z satisfying Maxwell's equations. If one changes the sign of the coordinates, one has to change simultaneously the sign of the three components of electric vectors, but not those of the magnetic vector (one says that $\boldsymbol{E}$ is a true vector, while $\boldsymbol{H}$ is an axial vector). One thus finds a new set of variables:

$$\begin{aligned} \bar{E}_x(\bar{x}) &= -E_x(-x) & \bar{H}_x(\bar{x}) &= H_x(-x) \\ \bar{E}_y(\bar{x}) &= -E_y(-x) & \bar{H}_y(\bar{x}) &= H_y(-x) \\ \bar{E}_z(\bar{x}) &= -E_z(-x) & \bar{H}_z(\bar{x}) &= H_z(-x) \end{aligned}$$

which satisfy again Maxwell's equations in their original form.

If the system is in a non-degenerate eigenstate of the energy, the angular momentum and the z-component of the angular momentum, we conclude, as before, that $\bar{\psi}_1(\bar{x})$, $\bar{\psi}_2(\bar{x})$, $\bar{\psi}_3(\bar{x})$, and $\bar{\psi}_4(\bar{x})$ must describe the same state as $\psi_1(x)$, $\psi_2(x)$, $\psi_3(x)$ and $\psi_4(x)$, so that

$$\text{(1.15)} \qquad \begin{cases} \bar{\psi}_1(\bar{x}) = k\psi_1(x) \\ \bar{\psi}_2(\bar{x}) = k\psi_2(x) \\ \bar{\psi}_3(\bar{x}) = k\psi_3(x) \\ \bar{\psi}_4(\bar{x}) = k\psi_4(x) \end{cases}$$

We again find that k can only have the values $+1$ or -1, and that accordingly the two following possibilities exist

$$\text{(1.16)} \qquad \begin{cases} \psi_1(-x) = \psi_1(x) \\ \psi_2(-x) = \psi_2(x) \\ \psi_3(-x) = -\psi_3(-x) \\ \psi_4(-x) = -\psi_4(-x) \end{cases}$$

or

$$\text{(1.17)} \qquad \begin{cases} \psi_1(-x) = -\psi_1(-x) \\ \psi_2(-x) = -\psi_2(-x) \\ \psi_3(-x) = \psi_3(x) \\ \psi_4(-x) = \psi_4(x)\,. \end{cases}$$

Since ψ_1 and ψ_2 are the two components that remain finite as the velocity goes to zero, we say that the four-component wave function has even parity in the first case, odd parity in the second.

For all systems of weakly interacting particles that can be described by the known quantum mechanical formalism, the parity is a constant of motion.

The situation is more complicated if the system goes through a stage of strong interaction, in which particles appear or disappear. Consider, for example, the production of π^0-mesons in the collision between two protons:

$$\mathrm{p} + \mathrm{p} \rightarrow \mathrm{p} + \mathrm{p} + \pi^0 . \tag{1.18}$$

One finds that if the two protons were initially in a state described by a space wave function of *even* parity, the system of two protons and one π^0-meson at the end of the interaction is in a state described by a space wave function of *odd* parity, and vice versa. If, instead, two π^0-mesons are created,

$$\mathrm{p} + \mathrm{p} \rightarrow \mathrm{p} + \mathrm{p} + \pi^0 + \pi^0 , \tag{1.19}$$

the space wave functions of the initial and the final states have the same parity.

In these and in all other examples of particle production or absorption, one finds the correct relation between the parities of the space wave functions of the initial and final states by introducing the concept of *intrinsic parity* and generalizing the law of conservation of parity so as to include both the parity of the space wave function and the intrinsic parities of the particles. In particular, to the π^0-meson one assigns odd intrinsic parity. Thus one immediately sees, for example, that if in reaction (1.18) the two protons were initially in an even state, the final state will be even by virtue of the odd parity of the space wave function and of the odd intrinsic parity of the π^0-meson.

In some cases there may be some degree of arbitrariness in the assignment of the parity of a fundamental particle. Consider, for example, the reaction

$$\mathrm{p} + \mathrm{p} \rightarrow \mathrm{p} + \mathrm{n} + \pi^+ . \tag{1.20}$$

Here one finds again that the parities of the space wave functions in the initial and final states are opposite. One can say that neutrons and protons have the same intrinsic parity, and the π^+-meson has odd intrinsic parity. Or one can say that the neutron and the proton have opposite intrinsic parity and that the π^+-meson has even parity. The first choice is the most natural one, because of the close relationship between π^+ and π^0.

Since the total number of fermions in an isolated system cannot change from even to odd or vice versa, fermions are produced and disappear in pairs, or one fermion may disappear and another fermion appear. Therefore, the

parity of a single fermion has no physical meaning. One can, however, speak of the *relative parity* of two fermions, so that a system of two fermions may have even or odd intrinsic parity.

The case of photons requires some further elucidation. The photon has angular momentum $+1$ or -1 in the direction of propagation. It can be absorbed or emitted in different states of orbital angular momentum. By combining the intrinsic angular momentum of the photon with different orbital angular momenta, L, one obtains states of different total angular momenta, J, and different parities, such as

L	J	Parity	
0	1	odd	electric dipole
1	1	even	magnetic dipole
1	2	even	electric quadrupole
2	2	odd	magnetic quadrupole, etc.

We wish to point out one more consequence of the concept of parity. Consider a system of two identical bosons. Interchanging the coordinates of the two particles is equivalent to changing the signs of all coordinates. The first operation must leave the wave function unchanged. Thus we conclude that the two bosons are in a state of *even parity*. States of odd parity are forbidden for systems consisting of two identical bosons.

1·2. – Classification of Particles.

a) Fundamental particles may be listed in order of increasing mass, as follows.

1) *Photon* (γ): the quantum of the electromagnetic field; $m = 0$, spin $= 1$. The spin can be oriented only in a direction parallel or anti-parallel to the direction of motion.

2) *Neutrino* (ν): mass 0, spin $\frac{1}{2}$.

3) *Electron* (e^+, e^-): mass $m_e = 9.1 \cdot 10^{-28}$ g; $m_e c^2 = 0.51$ MeV; charge $\pm e = \pm 4.90 \cdot 10^{-10}$ e.s.u.; spin $\frac{1}{2}$.

4) *Light mesons* (L-particles; see SMITH, BIRNBAUM and BARKAS, 1953).
μ-mesons (μ^+, μ^-): $m = 207\ m_e$; $mc^2 = 106$ MeV; charge $\pm e$; spin $\frac{1}{2}$.
π-mesons (π^+, π^-): $m = 273\ m_e$; $mc^2 = 139$ MeV; charge $\pm e$, spin 0; odd parity.

π^0-*meson* (π^0): $m = 264\ m_e$; $mc^2 = 135$ MeV; charge 0; spin 0, odd parity.

5) *Heavy mesons* (K-particles): masses between the π-meson mass and the proton mass.

6) *Nucleons*:
Proton (p): $m = 1836\ m_e$; $mc^2 = 938$ MeV; charge $+e$; spin $\frac{1}{2}$,
Neutron (n): $m = 1838\ m_e$; $mc^2 = 939$ MeV; charge 0; spin $\frac{1}{2}$.

7) *Hyperons* (Y-particles): masses between the neutron mass and the deuteron mass.

b) A more meaningful classification, based on the spin, is the following.

1) *Light fermions*: electron, neutrino, μ-meson, possibly some of the heavy mesons.

2) *Heavy fermions*: nucleons, hyperons.

3) *Bosons*: photon, π-meson, most of the heavy mesons.

As already noted, light fermions appear and disappear in pairs, or one light fermion can produce another light fermion.

A heavy fermion can change into another heavy fermion. Supposedly heavy fermions can appear or disappear in pairs. It seems that there is no possibility for a heavy fermion to disappear by producing a light fermion, for otherwise it would be difficult to explain the stability of matter.

The photon, the neutrino, the positive and negative electron, the nucleons and the light mesons have been known for some time. The heavy mesons and the hyperons, instead, have been discovered only recently. Their nature and properties form the main subject of the present lectures.

1·3. – Decay Processes of the Neutron and of the Light Mesons.

Neutrons and light mesons are unstable particles. Their decay processes are described below:

$n \to p + e + \nu + 0.8$ MeV	(mean life: 18 min; ROBSON, 1951)
$\pi \to \mu + \nu + 32$ MeV	(mean life: $2.65 \cdot 10^{-8}$ s)
$\pi^0 \to 2\gamma$	(mean life: $5 \cdot 10^{-15}$ s; ANAND, 1953)
$\mu \to e + 2\nu + 105$ MeV	(mean life: $2.1 \cdot 10^{-6}$ s).

According to field theory, there exists a correspondence between fundamental particles and fields of forces; thus the photon corresponds to the electro-

magnetic field of forces, the π-meson corresponds to the nuclear field of forces. Decay processes are described as interactions between the various fields. A short mean life indicates a strong interaction. A long mean life indicates a weak interaction, or it may be due to limitations imposed by the conservation principles or by special selection rules (*). For example, π-mesons interact strongly with nucleons; thus a π-meson could be expected to produce virtual nucleon-antinucleon pairs. However, since there is no particle lighter than the π-meson and strongly coupled with nucleons, the virtual pair cannot readily change into other particles. This explains the comparatively long mean life of π-mesons. The fact that the neutral π-meson has a shorter mean life than the charged one is accounted for by the fact that the photon field is more strongly coupled to the nucleon field than either the electron-neutrino or the μ-meson-neutrino field.

1·4. – Methods of Observation.

a) *Cloud Chambers in Magnetic Field.* – From the curvature of the tracks, one can determine the sign and the momentum of charged particles.

From the density of ionization, I, one can estimate the velocity, β. I is connected to β by an equation of the type

$$I = z^2 f(\beta)\,, \tag{1,21}$$

where z is the charge (in terms of e) and f a function depending only on the nature and pressure of the gas. For values of β considerably smaller than 1, $f(\beta)$ varies approximately as $1/\beta^2$. As β approaches 1, f passes through a minimum and then increases again. When f is plotted against $p\,mc = \beta\sqrt{1-\beta^2}$, the minimum occurs at about $\beta/\sqrt{1-\beta^2} = 3$ and the subsequent increase is very slow. The experimental determination of I is usually not very accurate.

b) *Multiplate Cloud Chambers.* – When the particle stops in the chamber, one can determine the range with an error of the order of the thickness of the plates. The range, R, is related to the momentum, p, by an equation of the type

$$\frac{R}{m} = \frac{1}{z^2} F\left(\frac{p}{m}\right), \tag{1.22}$$

where m is the mass and F a function depending only on the absorber material.

(*) « Short » means not much greater than $\hbar/mc^2 \approx 10^{-23}$ s; « long » means much greater than this characteristic time.

From the density of ionization one can estimate the velocity (Eq. (1.21)).

When the track traverses a number of plates, one can measure the root mean square angle of scattering, $\sqrt{(\vartheta^2)_{\mathrm{av}}}$. From this quantity one can compute the product $p\beta$ of the velocity and the momentum. On a first approximation, the following equation holds:

$$\sqrt{(\vartheta^2)_{\mathrm{av}}} = \frac{E_s}{p\beta c}\sqrt{\frac{x}{x_0}}, \tag{1.23}$$

where $E_s = 21$ MeV, x is the thickness of each plate in g cm^{-2} (measured in the direction of the track) and x_0 the radiation length of the plate material. The analysis is more complicated when the momentum loss in the plates cannot be neglected.

A photon or an electron of sufficiently high energy will produce in a multiplate cloud chamber an electronic shower, which develops through a number of plates. By counting electron tracks in successive sections of the chamber one obtains the number of electrons at different distances from the origin. Neglecting fluctuations, one can then determine the *shower curve*. According to shower theory, the energy E_0 of the initiating particle is proportional to the area under the shower curve, the proportionality constant depending on the material of the plates and on the minimum energy of the electrons detected (electrons of very small energy fail to emerge from the plates because their effective range is strongly reduced by multiple scattering). The area under the shower curve is proportional to the total number, N, of electron tracks counted in the various sections of the chamber (we assume here that the shower does not escape from the chamber before dying out). Thus we have

$$E_0 = bN, \tag{1.24}$$

where the constant b can be estimated theoretically, or determined experimentally. The main uncertainty arises from statistical fluctuations in the shower development, which are particularly serious when the energy is low ($\lesssim 200$ MeV).

c) Photoemulsions. – The grain density in a photoemulsion track (like the ionization density in a cloud chamber track) depends on the velocity of the particle. An equation similar to Eq. (1.21) holds. The measurement usually yields more accurate results than the corresponding cloud chamber measurement.

One can measure the scattering along a track either by subdividing the track into a number of segments and measuring the angles between the average directions of successive segments, or by determining, at regular intervals, the

distance of the track from a straight reference line. Scattering measurements yield the quantity $p\beta$ (see Eq. (1.23)). When the track is sufficiently long, one can achieve a greater accuracy than in the corresponding measurement in a multiplate cloud chamber.

If the particle stops in the emulsion, one can determine its range accurately.

d) Mass Determination. – The measurement of any two of the following quantities: p, β, $p\beta$, R determines the mass of a charged particle. Methods have been developed to obtain the mass of particles from range and scattering and from range and grain density, taking into account the gradual change of momentum and velocity along the track.

2. – Neutral V-Events. The Λ^0 and the θ^0-Particles.

2·1. – Formulae for the Analysis of the Data.

A neutral particle, decaying in flight into a positive and a negative particle, gives rise to a characteristic « V-track ».

V-tracks were observed for the first time in a cloud chamber by ROCHESTER and BUTLER (1947). Most of the data on these events come from cloud chamber observations. Recently photoplates have also yielded important results, although the occurrance of neutral V-events in photoplates is obscured by the common occurrence of two-prong neutron stars (YASIN, 1954).

The following mathematical relations are useful for the analysis of neutral V-events.

a) Q-value for a two-body decay from momentum measurements. – Consider a particle of mass m_0, energy U_0, momentum $\boldsymbol{p}_0$ disintegrating into two charged particles of masses m_1, m_2, energies U_1, U_2, and momenta $\boldsymbol{p}_1$, $\boldsymbol{p}_2$.

In the frame of reference in which the primary particle is at rest (center-of-mass system) the total kinetic energy of the secondary particles (Q-value) is given by the equation

$$m_0c^2 = m_1c^2 + m_2c^2 + Q\,. \tag{2.1}$$

Conservation of momentum and energy yields:

$$U_0 = U_1 + U_2$$

$$\boldsymbol{p}_0 = \boldsymbol{p}_1 + \boldsymbol{p}_2$$

and therefore

$$m_0^2c^4 = U_0^2 - p_0^2c^2 = (U_1 + U_2)^2 - (\boldsymbol{p}_1 + \boldsymbol{p}_2)^2c^2 \tag{2.2}$$

or

$$m_0^2c^4 = m_1^2c^4 + m_2^2c^4 + 2U_1U_2 - 2p_1p_2c^2\cos\theta\,, \tag{2.3}$$

where θ is the angle between the two secondary tracks, and p_1, p_2 indicate the magnitude of the vectors $\boldsymbol{p}_1$, $\boldsymbol{p}_2$. Equation (2.3) determines m_0 and therefore Q, if the masses and the momenta of the secondary particles are known.

b) Apparent Q-value in the case of a 3-body decay (see LEIGHTON, WANLASS and ALFORD, 1951). – Consider a particle of mass m_0 energy U_0, momentum $\boldsymbol{p}_0$, disintegrating into two charged and one neutral particle, of masses m_1, m_2, m_3, energies U_1, U_2, U_3, and momenta $\boldsymbol{p}_1$, $\boldsymbol{p}_2$, $\boldsymbol{p}_3$. We have

$$\left\{\begin{aligned} &m_0c^2 = m_1c^2 + m_2c^2 + m_3c^2 + Q \\ &U_0 = U_1 + U_2 + U_3 \\ &\boldsymbol{p}_0 = \boldsymbol{p}_1 + \boldsymbol{p}_2 + \boldsymbol{p}_3\,. \end{aligned}\right. \tag{2.4}$$

If we ignore the neutral particle (m_3) we obtain from the observations an *apparent* Q-value, Q', corresponding to an *apparent* mass, m_0', for the primary particles m_0' is given by

$$(m_0')^2c^4 = (U_1 + U_2)^2 - (\boldsymbol{p}_1 + \boldsymbol{p}_2)^2c^2\,,$$

(see Eq. (2.2)); the corresponding value of Q' is

$$Q' = (m_0' - m_1 - m_2)c^2\,.$$

The quantity $m_0'c^2$ is relativistically invariant. If we compute it in the c.m.s. where:

$$U_1^* + U_2^* = m_0c^2 - U_3^*\,,$$

$$\boldsymbol{p}_1^* + \boldsymbol{p}_2^* = -\boldsymbol{p}_3^*\,,$$

we have

$$\begin{aligned}(m_0')^2c^4 &= (m_0c^2 - U_3^*)^2 - p_3^2c^2 \\ &= m_0^2c^4 + m_3^2c^4 - 2m_0c^2U_3^*\,,\end{aligned}$$

or

$$(m_0')^2c^4 = (m_0 - m_3)^2c^4 - 2m_0c^2E_3^*\,, \tag{2.5}$$

where $E_3^* = U_3^* - m_3c^2$ is the *kinetic energy of the neutral secondary particle in the c.m.s.*. Thus the distribution of the apparent primary mass is related in a simple manner to the distribution of kinetic energy of the neutral decay product in the c.m.s..

The maximum value of m_0' corresponds to $E_3^* = 0$. It is (see Eqs. (2.4) and (2.5))

$$(m_0')_{\max} = m_0 - m_3 = m_1 + m_2 + Q/c^2 ,$$

and therefore

$$Q'_{\max} = Q . \tag{2.6}$$

The minimum value of Q' is zero. One has a $Q' = 0$ when the two charged particles are emitted in the same direction and with the same velocity in the c.m.s..

c) *Q-value for a two-body decay when the origin is known.* – If one can determine the interaction from which the neutral primary particle originates, one can measure the angles, ϑ_1 and ϑ_2, between the line of flight of the primary particle and the trajectories of the two secondary products.

In this case if one knows *one* of two the secondary momenta, e.g., p_1, one can determine the second from the equation:

$$p_1 \sin \vartheta_1 = p_2 \sin \vartheta_2 , \tag{2.7}$$

which follows from the conservation of momentum. One can then compute the Q-value as in *a*).

d) *Transverse momentum and α for a two-body decay.* – In the c.m.s. both decay products have the same momentum, p^*, and are emitted in opposite directions. Let ϑ_1^* and ϑ_2^* be the angles of emission of the two decay products in the c.m.s., measured from the line of flight of the primary particle ($\vartheta_2^* = \pi - \vartheta_1^*$). The probability of an event for which ϑ_1^* lies between ϑ_1^* and $\vartheta_1^* + \mathrm{d}\vartheta_1^*$ is proportional to the solid angle $2\pi \sin \vartheta_1^* \, \mathrm{d}\vartheta_1^* = 2\pi \, \mathrm{d}(\cos \vartheta_1^*)$.

In the laboratory system, let ϑ_1 and ϑ_2 be, as before, the angles of emission of the two secondary particles with respect to the line of flight of the primary particle. Since the component of the momentum perpendicular to the line of flight, p_T, is relativistically invariant, we have

$$p_T = p_1 \sin \vartheta_1 = p_2 \sin \vartheta_2 = p^* \sin \vartheta_1^* . \tag{2.8}$$

From these equations one can determine p_T if the origin of the V⁰-particle is known. If the origin is not known, so that one can measure only the total

angle

$$\vartheta = \vartheta_1 + \vartheta_2$$

between the two secondary particles, one can determine p_T from the value of ϑ and from the values of the two secondary momenta, p_1 and p_2. In fact, from the triangle formed by the vectors $\boldsymbol{p}_0$, $\boldsymbol{p}_1$, and $\boldsymbol{p}_2$ one obtains

$$\frac{p_1}{p_0} = \frac{\sin \vartheta_2}{\sin \vartheta} .$$

This equation, together with Eq. (2.8) yields

$$p_T = \frac{p_1 p_2}{p_0} \sin \vartheta . \tag{2.9}$$

From the fact that all values of $\cos \vartheta_1^*$ between -1 and $+1$ are equally probable one can determine the expected distribution of transverse momenta.

Another quantity related to the angle of emission in the c.m.s. (and introduced by the Manchester group) is the following:

$$\alpha = \frac{p_1 \cos \vartheta_1 - p_2 \cos \vartheta_2}{p_0} . \tag{2.10}$$

From the Lorentz transformation we obtain:

$$p_1 \cos \vartheta_1 = \frac{U_0}{m_0 c^2} p^* \cos \vartheta_1^* + \frac{p_0}{m_0 c^2} U_1^*$$

$$p_2 \cos \vartheta_2 = \frac{U_0}{m_0 c^2} p^* \cos \vartheta_2^* + \frac{p_0}{m_0 c^2} U_2^* = - \frac{U_0}{m_0 c^2} p^* \cos \vartheta_1^* + \frac{p_0}{m_0 c^2} U_2^* ,$$

where U_1^* and U_2^* are the energies of the two decay products in the c.m.s. With the help of these equations, Eq. (2.10) becomes

$$\alpha = \frac{U_1^* - U_2^*}{m_0 c^2} + 2 \frac{U_0}{p_0 m_0 c^2} p^* \cos \vartheta_1^* ,$$

or, remembering that $U_1^* + U_2^* = m_0 c^2$ and that $(U_1^*)^2 - (U_2^*)^2 = m_1^2 c^4 - m_2^2 c^4$

$$\alpha = \frac{m_1^2 - m_2^2}{m_0^2} + 2 \sqrt{\frac{1}{m_0^2 c^2} + \frac{1}{p_0^2}}\ p^* \cos \vartheta_1^* . \tag{2.11}$$

One sees that the average value of α is

$$\bar{\alpha} = \frac{m_1^2 - m_2^2}{m_0^2} , \tag{2.12}$$

and is positive, zero or negative depending on whether $m_1 > m_2$, $m_1 = m_2$, or $m_1 < m_2$. For relativistic velocities of the primary particle ($p_0 \gg m_0 c$), Eq. (2.11) becomes

$$\alpha = \bar{\alpha} + 2\frac{p^*}{m_0 c}\cos\vartheta_1^* . \tag{2.13}$$

One sees that in this case all values of α between the limits $\bar{\alpha} - 2(p^*/m_0 c)$ and $\bar{\alpha} + 2(p^*/m_0 c)$ are equally probable.

When the origin of the V⁰-particle is known, one can measure ϑ_1 and ϑ_2 and determine α from Eq. (2.10). When the origin is not known, one can use the equation

$$\alpha = \frac{p_1^2 - p_2^2}{p_0^2} . \tag{2.14}$$

One obtains this equation from Eq. (2.10) and from the following equations:

$$p_0 = p_1\cos\vartheta + p_2\cos\vartheta_2 ,$$

$$p_1\sin\vartheta_1 = p_2\sin\vartheta_2 .$$

These equations give

$$\alpha = \frac{p_1^2\cos^2\vartheta_1 - p_2^2\cos^2\vartheta_2}{p_0^2} = \frac{p_1^2\cos^2\vartheta_1 + p_1^2\sin^2\vartheta_1 - p_2^2\cos^2\vartheta_2 - p_2^2\sin^2\vartheta_2}{p_0^2}$$

which is equivalent to (2.14).

2·2. – The Λ^0-Particle.

Work performed at various laboratories, mainly at Manchester, California Institute of Technology and Indiana, has established the fact that neutral V-events include cases where the charged decay products are a proton and a light meson, and cases in which both decay products are light mesons. The former event represents the decay of a hyperon; the latter event represents the decay of a heavy meson.

We consider first the decay of the neutral hyperon.

a) *Identity of the decay products.* – Measurements of ionization and magnetic curvature indicate that the positive particle is a proton and the negative

particle is a π-meson. On some occasions the characteristic π-μ decay of the negative particle has been observed (ARMENTEROS, BARKER, BUTLER and CACHON, 1951; LEIGHTON, WANLASS and ALFORD, 1951).

b) Coplanarity. – Observations with multiplate cloud chambers (particularly of the M.I.T. group, see BRIDGE, PEYROU, ROSSI and SAFFORD, 1953) have yielded many examples of neutral hyperons that appear to originate from nuclear interactions occurring in the plates of the chamber. In these cases the plane of the V-track contains the presumed origin of the neutral hyperon. This is what one should expect if the decay is a two-body process because in such case the vector sum of the momenta of the two charged decay products must lie along the trajectory of the primary particle. If the decay were a three-body process instead (i.e., if there were a neutral decay product in addition to the two visible charged decay products) the line of flight of the primary particle should often lie outside the plane of the V-track. Thus the above result is a strong argument in favor of the assumption that the neutral hyperon undergoes a two-body decay.

c) Q-value. – Under the assumption of a two-body decay, one can determine the Q-value from the experimental observations on the tracks (see Sec. 2·1). If the assumption of a two-body decay is correct, one will find from different events, consistent values of Q. If, instead, the assumption is incorrect and one is dealing actually with a 3-body decay, one will find a continuous distribution of apparent Q-values.

In some cases it is difficult to separate a true spread from an apparent spread due to errors of measurements. The whole of the experimental evidence, however, establishes beyond doubt the existence of a group of events giving a unique Q-value: $Q = 37$ MeV (ROCHESTER and BUTLER, 1953; BRIDGE, PEYROU, ROSSI and SAFFORD, 1953; THOMPSON, BUSKIRK, COHN, KARZMARK, and REDIKER, 1953) (*). Confirming evidence obtained by means of photo emulsions has been reported (YASIN, 1954). We thus conclude that *there exists a neutral hyperon undergoing a two-body decay into a proton and a* π*-meson with an energy release of approximately* 37 MeV. This hyperon is called a Λ^0 particle. Some of its properties are listed below:

$$
(2.15) \qquad \begin{cases} \Lambda^0 \to \mathrm{p} + \pi^- + 37 \text{ MeV}, \\ m_{\Lambda^0} = 2181\ m_e, \\ m_{\Lambda^0} c^2 = 1112 \text{ MeV}, \\ \text{Spin: half integer}. \end{cases}
$$

(*) A recent paper by the group at the California Institute of Technology gives $Q = 34.7 \pm 1$ MeV (VAN LINT, TRILLING, LEIGHTON and ANDERSON, 1954).

Since the Λ^0-particle can change into a proton, it is natural to regard it as a member of the nucleon family, i.e., to consider the Λ^0-particle as some sort of an « excited state » of the neutron.

The question as to whether or not neutral hyperons different from Λ^0-particles exist will be discussed in Part **6.**

d) *Mean life.* – One can determine the mean life of Λ^0-particles from the mean distance they travel before decay. In translating distances into times one must, of course, take into account the relativistic dilation of time intervals. A complication arises from the fact that usually the path length before escape from the chamber is not long compared to the mean path before decay, so that one must make a correction for the particles that escape before decaying and that are, therefore, not detected. The results obtained so far yield the following value of the mean life (PAGE, 1954):

$$\tau_0 = (3.7^{+.6}_{-.5}) \cdot 10^{-10} \text{ s} .$$

e) *Mode of production.* – Λ^0-particles are produced in the nuclear interactions of high-energy cosmic-ray particles. SCHEIN, KASKIN, GLASSER, FAINBERG and BROWN (1953) have reported the production of Λ^0-particles by the 227 MeV π^--meson beam of the Chicago cyclotron.

Λ^0-particles have been produced at the Brookhaven Cosmotron Laboratory by the nuclear interactions of protons (3 GeV kinetic energy), neutrons (mean kinetic energy 1.7 GeV, maximum kinetic energy 2.2 GeV) and π^--mesons (1.37 GeV kinetic energy) (*). Particularly interesting are some events observed by SHUTT, by which a Λ^0 and a θ^0-particle are simultaneously produced by the interactions of π^--mesons in hydrogen.

We shall return to this and other similar observations later. Here we wish to point out that Λ^0-particles often arise from interactions where the available energy is not large enough to create their total mass. Thus we must conclude that one can produce Λ^0-particles by adding energy to existing nucleons.

Of course, one cannot rule out the possibility that Λ^0-particles may be produced also by materialization of energy. However, if this process, which has never been observed, actually occurs, each Λ^0-particle must be created together with a corresponding anti-particle. Otherwise, through the production and subsequent decay of a Λ^0-particle, one would create a proton without creating simultaneously an anti-proton or an anti-neutron, an event contrary to accepted theoretical ideas.

(*) In the case of the proton and of the neutron production, the interactions occurred outside the cloud chamber. Thus one cannot rule ont the possibility of an intermediate π-meson link.

f) *Alternate mode of decay.* – One should expect that the Λ^0-particle has the alternate mode of decay:

$$\Lambda^0 \to n + \pi^0 + 40 \text{ MeV} .$$

Observations by means of the Brookhaven cosmotron have provided some evidence for this decay process (RIDGWAY and COLLINS, 1954).

2·3. – The θ^0-Particle.

We consider next the decay of the neutral heavy meson.

a) *Mode of decay and Q-value.* – The most illuminating results on this subject come from the work of THOMPSON at Indiana.

In some cases, one of the secondary particles has been identified as a π-meson from magnetic curvature and ionization measurements. It seems likely that both secondary charged particles are π-mesons, even though one cannot yet rule out the possibility that one of them is a μ-meson.

No stringent coplanarity arguments can be made to decide the question as to whether the decay is a two-body or a three-body process. The reason is that very few identifiable K^0-decays with clear origins have been found so far. However, if one analyzes V^0-events in which both decay particles are light mesons under the assumption of a two-body decay: $K^0 \to \pi^+ + \pi^-$ one finds, in most cases, a unique Q-value of 214 ± 5 MeV (THOMPSON, 1953). We thus conclude thar *there exists a neutral heavy meson, undergoing a two-body decay into two π-mesons, with a* 214 ± 5 MeV *energy release.* This heavy meson is called a θ^0-particle. Some of its properties are listed below:

$$\left\{\begin{array}{l} \theta^0 \to \pi^+ + \pi^- + (214 \pm 5) \text{ MeV} , \\ m_{\theta^0} = (966 \pm 10)\ m_e , \\ m_{\theta^0} c^2 = (493 \pm 5) \text{ MeV} . \end{array}\right. \tag{2.16}$$

One should emphasize that some K^0-decays cannot be interpreted according to the above decay scheme. The interpretation of these events shall be discussed in Part **6**.

b) *Spin and Parity.* – If the two secondary π-mesons are produced in a state of angular momentum 0 (and therefore even parity) the θ^0-particle has *spin zero* and *even parity*. If the two secondary π-mesons are produced in a state of angular momentum 1 (and therefore odd parity) the θ^0-particle has *spin* 1 and *odd parity*. Of course, higher spin values are also possible.

c) *Mean life.* – The mean life of θ^0-particles can be determined with a procedure similar to that described in connection with Λ^0-particles. The results are not yet very accurate. The mean life is (BARKER, 1953)

$$\tau_{\theta^0} = (1.5^{\pm.5}_{-.3}) \cdot 10^{-10} \text{ s} .$$

d) *Mode of production.* – There is evidence that, in some cases at least, θ^0- and Λ^0-particles are produced simultaneously. The Brookhaven group (FOWLER, SHUTT, THORNDIKE and WHITTEMORE, 1954) have observed the following event:

$$\pi^- + p \rightarrow \Lambda^0 + \theta^0 . \tag{2.17}$$

Examples of simultaneous production of Λ^0 and θ^0-particles by cosmic-ray interactions have also been reported. In most cases it is difficult to decide whether the two particles are produced in two successive interactions within the same complex nucleus, or in the same interaction with an individual nucleon. However, THOMPSON, BURWELL, HUGGETT and KARZMARK (1954) have recently described an event where the latter interpretation appears virtually certain. Indeed, they obtained perfect balance of energy and momentum by assuming that the primary particle is a π^--meson, producing a Λ^0, θ^0 pair according to the reaction (2.17). Notice that in this event the identification of the Λ^0- and θ^0-particles is more certain than in the Brookhaven event.

If we accept the evidence for the production of Λ^0, θ^0 pairs by the interactions of π-mesons with nucleons, we must conclude, from conservation of angular momentum, that the θ^0-particle has integral spin. This rules out the possibility that the decay products of a θ^0-particle may be a π- and a μ-meson, and confirms the assumption of the decay scheme (2.16).

Theoretical arguments have been presented in favor of the assumption that Λ^0 and θ^0-particles (as, indeed, all other hyperons and heavy mesons) are always produced in pairs. These arguments are based upon the apparent contradiction between the abundant production of these particles (in nuclear interactions) and their relatively long mean life. Indeed, if hyperons and heavy mesons are strongly coupled to the nuclear field, they could disappear producing virtual nucleon-antinucleon pairs. Each virtual pair would then promptly annihilate producing π-mesons because of the strong coupling of the nucleons to the π-meson field. The mean life for decay through such a process should be of the order of 10^{-23} s. One can, however, postulate that heavy mesons and hyperons interact strongly with nuclei only when they are in pairs. Then the simultaneous production of two such particles would be a likely process, but the decay of a single particle would be highly forbidden, unless the rest energy is sufficiently large so that there could be a hyperon

or a heavy meson among the decay products. The possible relation of this selection rule to the principle of conservation of isotopic spin has been discussed by various authors (see GELL-MANN and PAIS, 1954).

c) Alternate mode of decay. – If the θ^0-particle has spin 0 it may be expected to have the following alternate mode of decay:

$$\theta^0 \to 2\pi^0 + 223 \text{ MeV} .$$

If the θ^0-particle has spin 1, this mode of decay is forbidden because two identical bosons cannot be in a state of spin 1 (see Sec. 1·1).

2·4. – The α-p_T Plot.

A graphical presentation of the data, devised by THOMPSON, brings out convincingly the fact that most V^0-events represent either Λ^0 or θ^0-decays.

This plot is useful in the case that the V^0-particles have relativistic velocities. In this case, from Eqs. (2.8) and (2.13) one obtains:

$$(2.18) \quad \left(\frac{\alpha - \bar{\alpha}}{2p^*/m_0c}\right)^2 + \left(\frac{p_T}{p^*}\right)^2 = 1 .$$

Since all quantities except α and p_T are constant, Eq. (2.18) is the equation of an ellipse in the α, p_T plane. Each decay scheme corresponds to a different ellipse. The center of the ellipse lies on the α-axis, at $\alpha = \bar{\alpha} = (m_1^2 - m_2^2)/m_0^2$. The semiaxis parallel to the p_T axis is equal to p^*. The semiaxis parallel to the α-axis is equal to $2p^*/m_0c$.

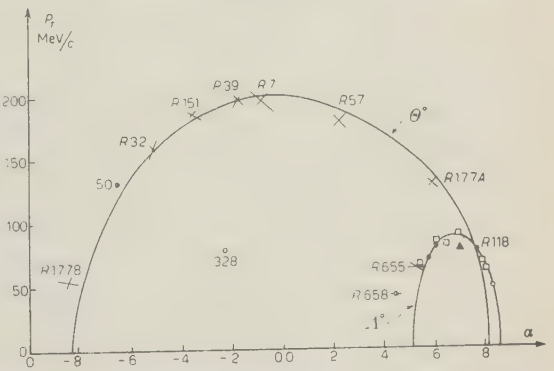

Fig. 1. – Ellipses representing the Λ^0-decay and the θ^0-decay, with several of the experimental points obtained by the Indiana group (from the report of THOMSON at the Bagnères Conference). The diagram shows only one anomalous event (328). Another anomalous event was reported later by the same group (R429; see Table IX).

Fig. 1 shows the two ellipses corresponding to the Λ^0-decay and to the θ^0-decay. With only two exceptions the neutral V-events observed by THOMPSON have representative points that lie on one or the other of the two ellipses.

3. – The τ-Meson (*).

3·1. – Decay Scheme and Q-Value.

In 1949 the Bristol Group (Brown, Camerini, Fowler, Muirhead, Powell, Ritson, 1949) discovered a particle which, upon coming to rest in a photographic emulsion, decayed into 3 light mesons, one of which was certainly a π^--meson (it produced a nuclear star). About 40 examples of such events have been observed to date in photo-emulsions. About 10 events of a similar nature have been observed in cloud chambers.

Most informative are several events observed with stacks of stripped emulsions, where one sees the secondary particles come to rest and one can recognize their nature from their behaviour at the end of the tracks.

In such cases one finds that one of the 3 decay products is a negative π-meson (it undergoes nuclear absorption, usually producing a star) and the other two are positive π-mesons (they undergo π-μ decay).

The three secondary particles of a τ-meson decaying at rest are coplanar, which indicates that there is not fourth neutral decay product (+). The energies of the secondary particles can be determined from range measurements. The resulting calculated Q-values are consistent with one another and center about 75 MeV. Thus one can conclude that *there exists a charged heavy meson which decays into* 3 *charged* π*-mesons*. This particle is called a τ-meson. Some of its properties appear below:

$$\left\{\begin{array}{l} \tau^{\pm} \to \pi^{\pm} + \pi^{\pm} + \pi^{\mp} + (74.6 \pm .3)\ \text{MeV} \\ m_{\tau} = (965.5 \pm 0.7)\ \mathrm{m_e} \\ m_{\tau}c^2 = 493\ \text{MeV}\,. \end{array}\right. \tag{3.1}$$

All τ-mesons which have been found to decay at rest in photo-emulsions and for which the sign could be determined were positive. This is consistent with the view that negative τ-mesons undergo nuclear absorption upon coming to rest in matter (see Part 3). Some of the τ-mesons that were observed to decay in flight in cloud chambers are negative.

(*) The experimental data here quoted are taken from the proceedings of the Padua Conference (April 1954), to which the reader is referred for details.

(+) An event in which this is not the case has been reported recently (Daniel and Yash Pal, 1954). This event probably represents the decay of a τ-meson into 3 π-mesons ad 1 photon.

3·2. – Other Properties of the τ-Meson.

a) Spin and parity. – Recalling that the π-meson has odd intrinsic parity, one finds that, among others, the following possibilities exist:

τ-particle		Space wave function of the 3 π-mesons	
Spin	Parity	Angular momentum	Parity
0	−	0	+
1	+	1	−
1	−	1	+

Of course, spin values greater than 1 are also possible. In the case of spin 0, even parity is ruled out by the fact that there is no space wave function of the three secondary π-mesons with odd parity and 0 angular momentum.

In principle, one could distinguish between the various possible spins and parities by determining the energy distribution of the secondary π-mesons. The data available so far do not yet lead to any very definite result.

b) Mean life. – From the fact taht almost all τ-mesons observed in photo-emulsions come to rest before disintegrating (*), it has been possible to conclude that the mean life of the τ-meson cannot be much shorter than about 10^{-8} s (see paper by AMALDI in these *Proceedings*). On the other hand, the fact that τ-mesons have been observed to decay in flight in cloud chambers shows that the mean life cannot be much longer than about $2 \cdot 10^{-8}$ s. Thus it seems that the mean life of the τ-meson must be of the order of 10^{-8} s.

c) Alternate mode of decay. – One should expect that the τ-meson can also decay according to the scheme:

$$\tau^{\pm} \to \pi^{\pm} + 2\pi^{0} + 84 \text{ MeV} .$$

Possible evidence for this decay scheme was first presented by the Rochester group and will be discussed in Part 4.

d) Mode of production. – τ-mesons arise directly from high-energy nuclear interactions, i.e., they are not, at least ordinarily, the decay products of other particles. Indeed, most of the τ-mesons found in stacks of stripped emulsions

(*) Only one case of decay in flight in photo-emulsions has been reported so far (BALDO, BELLIBONI, CECCARELLI, GRILLI, SECHI, VITALE and ZORN, 1954).

could be traced back to stars in the emulsion. τ-meson have been also produced by the cosmotron beam in Brookhaven (HILL, SALANT and WIDGOFF, 1954).

4. – Charged Heavy Mesons with a Single Charged Secondary Product.

4·1. – General Considerations.

Observations with cloud chambers and photo-emulsions have demonstrated the existence of heavy mesons which decay, each producing a single charged light meson and presumably one or more neutral particles. In some cases the decay occurs at rest (S-events), in some cases it occurs in flight (charged V-events). Tables II, III, IV, V, VI and VII contain a large sample of the available experimental data.

The interpretation of the experimental results is still uncertain. It is clear that one must invoke more than one disintegration process to explain the observed events, if for no other reason because in some cases the secondary charged decay product is a π-meson, in other cases it is a μ-meson. But how one approaches the problem of analyzing the data is still largely a matter of choice. One may be inclined to postulate the existence of many discrete mass states for fundamental particles, corresponding perhaps to different values of the spin, and characterized by different mean lives and different modes of decay. Or one may try to reduce the observed phenomena to the least possible number of different disintegration processes. Here we shall follow the latter approach, mainly because the first cannot lead to any concrete results at the present stage of our experimental knowledge. At first, we shall also leave the question open as to whether the various disintegration processes that we shall consider correspond to different particles, or whether some of them are alternate modes of decay of the same particle.

It may be pointed out from the outset that direct mass measurements on the primary particles are not of great help in the classification of the events. Usually these measurements are affected by large errors. Within the errors, most mass values appear to be compatible with the τ-meson mass. Thus, on this basis alone, there would not be any strong indication for the existence of different groups of charged K-particles. On the other hand, one can say that if several different kinds of K-particles exist, their masses must lie within a fairly narrow band around the τ-meson mass. This statement, of course, does not rule out the possible existence of K-particles with mass considerably different from the τ-meson mass, observed only on very rare occasions either because they are produced seldom or because they have a very short mean life.

4·2. – Formulae for the Analysis of S-Events or Charged V-Events.

a) Consider a charged particle of mass m_0 that decays *after coming to rest* in a photo-emulsion or in a multiplate cloud chamber (S-event).

If the particle undergoes a two-body decay into a charged particle of mass m_1, momentum $\boldsymbol{p}_1$, kinetic energy E_1, and a neutral particle of mass m_2, momentum $\boldsymbol{p}_2$, kinetic energy E_2, with an energy release Q, the following relations hold:

$$m_0c^2 = m_1c^2 + m_2c^2 + Q \; ;$$

$$\boldsymbol{p}_1 = \boldsymbol{p}_2 \; ; \qquad E_1 + E_2 = Q \; .$$

The charged particle always has the same kinetic energy, E_1. From the above equations, one obtains the following equivalent expressions for E_1:

$$E_1 = \frac{(m_0 - m_1)^2 - m_2^2}{2m_0}c^2 \; , \tag{4.1}$$

$$E_1 = Q\frac{m_2c^2 + Q/2}{m_0c^2} = Q\frac{m_2c^2 + Q/2}{(m_1 + m_2)c^2 + Q} \; . \tag{4.2}$$

For any known or assumed values of m_1 and m_2, these equations give E_1 as a function of m_0 (or Q), or conversely, m_0 (or Q) as a function of E_1.

If the particle undergoes a 3-body decay into one charged particle of mass m_1 and two neutral particles of masses m_2 and m_3, with an energy release Q, the charged particle has an energy that can vary from zero to a maximum value given by either one of the following equations:

$$(E_1)_{\max} = \frac{(m_0 - m_1)^2 - (m_2 + m_3)^2}{2m_0}c^2 \; , \tag{4.3}$$

$$(E_1)_{\max} = Q\frac{(m_2 + m_3)c^2 + Q/2}{m_0c^2} = Q\frac{(m_2 + m_3)c^2 + Q/2}{(m_1 + m_2 + m_3)c^2 + Q} \tag{4.4}$$

b) Consider a charged particle that decays in flight in a cloud chamber (charged V-event). Suppose that one can measure the momentum of the secondary charged particle and the ionization (and therefore the velocity) of the primary particle. For a known or assumed mass of the secondary charged particle, one can then compute its kinetic energy E_1 in the frame of reference of the primary particle (center of mass system). One can then apply Eqs. (4.1) to (4.4) as in the case of an S-event.

Suppose instead that the velocity of the primary particle is not known, but its momentum $\boldsymbol{p}_0$ is. In the case of a two-body decay, from the equations

$$\boldsymbol{p}_2 = \boldsymbol{p}_0 - \boldsymbol{p}_1 ,$$

$$U_2 = U_0 - U_1 ,$$

one finds

$$m_2^2 c^4 = U_2^2 - p_2^2 c^2 = (U_0 - U_1)^2 - (\boldsymbol{p}_0 - \boldsymbol{p}_1)^2 c^2 ,$$

or

$$m_2^2 c^4 = m_0^2 c^4 + m_1^2 c^4 - 2 U_0 U_1 + 2 p_0 p_1 c^2 \cos\vartheta , \tag{4.5}$$

where ϑ is the angle between the trajectory of the *primary particle* and that of the charged secondary particle. Since $U_0 = \sqrt{m_0^2 c^4 + p_0^2 c^2}$, Eq. (4.5) determines m_0 (and therefore Q) in terms of the measured quantities p_0, p_1, and ϑ, for any given value of m_2.

Notice that in any case the transverse component of the momentum, of the secondary charged particle, p_T, represents a lower limit for the momentum of this particle in the c.m.s.

4·3. – Quantities Characteristic of Four Suggested Decay Processes.

It may simplify our exposition if we list from the beginning some of the decay processes that have been suggested to account for the observed events, and discuss their properties. These processes are the following ones.

1) *The* $K_{\pi 3}$*-decay*: a three-body decay with a π-meson as the charged decay product. Already in Section 3.2 we have been led to envisage the possibility of a process of this kind as an alternate mode of decay of the τ-meson. We shall therefore discuss this $K_{\pi 3}$-decay under the assumption that the primary mass is identical to the τ-meson mass and that the two neutral decay products are two π^0-mesons:

$$K_{\pi 3}^{\pm} (\equiv \tau^{\pm}) \to \pi^{\pm} + 2\pi^0 . \tag{4.6}$$

2) *The* $K_{\mu 3}$*-decay*: a three-body decay with a μ-meson secondary. A particle with this mode of decay was first observed by O'Ceallaigh (1951) at Bristol, and was named $\varkappa$-meson. We shall arbitrarily assume that the two neutral products are two neutrinos; thus

$$K_{\mu 3}^{\pm} (\equiv \varkappa^{\pm}) \to \mu^{\pm} + 2\nu . \tag{4.7}$$

We wish to emphasize that there is no solid foundation for this assumption and that the neutral secondary products could include, for example, photons or π^0-mesons.

3) *The* $K_{\pi 2}$*-decay*: a two-body decay with a π-meson secondary. A particle with this mode of decay was first suggested by the Bristol group, with the name of χ-meson. There is reason to believe that the neutral decay product is a π^0-meson. Thus we shall assume

$$K^{\pm}_{\pi 2} (\equiv \chi^{\pm}) \rightarrow \pi^{\pm} + \pi^0 . \tag{4.8}$$

4) *The* $K_{\mu 2}$*-decay*: a two-body decay with a μ-meson secondary first suggested by the group at the Ecole Polytechnique. There is experimental evidence for the assumption that the neutral decay product is a neutrino; thus

$$K^{\pm}_{\mu 3} \rightarrow \mu^{\pm} + \nu . \tag{4.9}$$

In Table I we list the properties of the secondary charged particles of the decay processes mentioned above, computed under the assumption that the mass of the primary particle is identical to the τ-meson mass.

TABLE I. – *Properties of the secondary charged particles.*

Quantities characteristic of four different decay processes, computed under the assumption that the primary particle has a rest energy $m_0c^2 = 493$ MeV. In the case of two-body decay ($K_{\pi 2}$ and $K_{\mu 2}$) E, p, $p\beta$, and R are actual values of the kinetic energy, the momentum, the momentum times velocity and the range of the secondary particle. In the case of three-body decay ($K_{\pi 3}$ and $K_{\mu 3}$) the *maximum* values of the above quantities are listed. All quantities refer to the case that the primary particle decays at rest.

Properties of the secondary	$K^{\pm}_{\pi 3} \rightarrow \pi^{\pm} + 2\pi^0$	$K^{\pm}_{\pi 2} \rightarrow \pi^{\pm} + \pi^0$	$K^{\pm}_{\mu 3} \rightarrow \mu^{\pm} + 2\nu$ $K^{\pm}_{\mu 2} \rightarrow \mu^{\pm} + \nu$
Q-value	84	219	387
E (MeV)	53	108.5	152
p (MeV/c)	133	205	235
$p\beta$ (MeV/c)	92	170	214
R (g cm^{-2} Pb)	20	60	105
$dE/d(m_0c^2)$	—	.5	.48
$dp/d(m_0c^2)$	—	.60	.52
$d(p\beta)/d(m_0c^2)$	—	.65	.56
$dR/d(m_0c^2)$	—	.30	.32

Since there is no reason to assume *a priori* that this is so (except for the case of the $K_{\pi 3}$-decay) we also list in the table the derivatives of the various quantities with respect to the rest energy of the primary particle. One can thus readily obtain the values of these quantities corresponding to other values of the primary mass not too far from the τ-meson mass. One should keep in mind that, to a greater or lesser degree, the four decay processes considered here are still hypothetical and that other decay processes may well exist.

4·4. – Experimental Evidence for the $K_{\pi 3}$-Decay.

Table II summarizes the results on charged K-particles with a single charged secondary that have been obtained in various laboratories with the photo-emulsion technique.

TABLE II. – *Some of the most interesting examples of* K*-particles stopped in emulsions, giving rise to single charged secondary particles.*

Masses are given in terms of the electron mass; when several values are listed, they were determined with different methods, such as scattering and range, grain density and range, etc. Energies are given in MeV. Momenta and $p\beta$ are given in MeV/c. The symbols $\mu \to e$ and $\pi \to \mu \to e$ indicate that the particle has been seen to undergo $\mu \to e$ or $\pi \to \mu \to e$ decay. Interpretation: A) likely; B) possible.

Reference		Primary mass	Secondary particle				Interpretation				Remarks
			Mass or identity	$p\beta$	E_π	E_μ	$K_{\pi 2}$	$K_{\pi 3}$	$K_{\mu 2}$	$K_{\mu 3}$	
Bristol											
[1, 4]	K_1	1260±260 1380±180	< 400	235±35	160±30	170±31	—	—	B	B	
	K_2	1125±230 1125±150	$\mu \to e$	11.8	—	5.9	—	—	—	A	
	K_3	1000-2000	175±20	144±12	—	94±9	—	—	—	A	
	K_5	1200±400 950±400	200±15	66±11	—	37±8	—	—	—	A	
	K_7	~1000	μ (π)	170±29	110±20	113±25	A	—	B	B	
	K_8	1460±320 900±200	π	187±17	123±12	—	A	—	—	—	
	K_9	~1000	π	162±9	104±6	—	A	—	—	—	
	K_{14}	925±190	μ (e, π)	120±44	72±45	75±50	B	B	—	B	
	K_{15}	1100±170	π (μ, e)	184±30	121±24	125±25	A	—	B	B	
	K_{16}	~1100	μ (π)	153±24	97±17	102±16	B	—	—	A	
	K_{17}	1200±230	π	172±17	110±13	—	A	—	—	—	
	K_{18}	~1500	μ (π, e)	315±70	230±60	242±61	—	—	B	B	
	K_{19}	1000-2000	μ (π, e)	125±35	76±26	78±27	B	B	—	B	

TABLE II (*continued*).

Reference		Primary mass	Secondary particle				Interpretation				Remarks
			Mass or identity	$p\beta$	E_π	E_μ	$K_{\pi 2}$	$K_{\pi 3}$	$K_{\mu 2}$	$K_{\mu 3}$	
Bristol (*continued*)											
[4]	K_{21}	—	μ	205 ± 5	—	—	—	—	B	B	*
	K_{22}	780 ± 90	280 ± 20	170 ± 20	—	—	A	—	—	—	*
	K_{24}	1400 ± 200 1200 ± 200	203 ± 8	119 ± 9	—	—	—	—	—	A	*
	K_{31}	900 ± 200	—	145 ± 25	—	—	B	—	—	B	*
	K_{33}	850 ± 200		112 ± 20	—	—	—	—	—	B	*
Cornell											
[2]	K_2	—	280 ± 50	172 ± 26	110 ± 20	114 ± 22	A	—	—	B	
	K_3	—	191 ± 30	24.5 ± 5	—	12.8 ± 1.2	—	—	—	A	
	K_7	—	190 ± 60	111 ± 35	65 ± 25	68 ± 26	—	B	—	A	
	K_8	—	$\pi \to \mu \to e$	—	4.3	—	—	A	—	—	
Oslo											
[3, 4]	K_1	1090 ± 180	200 ± 20	126 ± 21	—	80 ± 14	—	—	—	A	*
Kopenhagen											
[4]	K_1	1680^{+760}_{-520}	—	190 ± 20	—	—	B	—	B	B	*
	K_3	1100 ± 300 1110 ± 160	(π)	223 ± 22	—	—	B	—	B	B	*
	K^5	970 ± 210	(π)	167 ± 8	—	—	A	—	—	B	*
Manchester											
[5]	K_3	1250 ± 300 1000 ± 300	(μ)	124^{+14}_{-11}	—	70 ± 11	—	—	—	A	
Brussels											
[6]	K_4	1100 ± 100	—	200 ± 30	132 ± 27	140 ± 34	B	—	B	B	
Paris											
[6, 7]	K_1	1025 ± 212	μ	197 ± 13	—	138 ± 10	—	—	B	B	Av
	K_6	966 ± 124	π, μ	290 ± 60	208 ± 47	223 ± 49	—	—	B	A	Av
[7]	K_{13}	894 ± 49	(μ)	166 ± 27	—	—	B	—	B	B	Av *
	K_{14}	933 ± 165 1300 ± 175	$\mu \to e$	—	—	33 ± 1	—	—	—	A	*
	K_{17}	1039 ± 113	(μ)	161 ± 12	—	—	B	—	—	B	Av *
	K_{22}	961 ± 62	(μ)	181 ± 15	—	—	B	—	B	B	Av *
	K_{23}	902 ± 51	(π)	166 ± 24	—	—	B	—	B	B	Av *
	K_{32}	930 ± 100	$\pi \to \mu \to e$	—	22.5	—	—	A	—	—	*

* From star.

Av. Primary mass value is the average of several determinations.

TABLE II (*continued*).

Reference		Primary mass	Secondary particle: Mass or identity	Secondary particle: $p\beta$	Secondary particle: E_π	Secondary particle: E_μ	Interpretation: $K_{\pi 2}$	Interpretation: $K_{\pi 3}$	Interpretation: $K_{\mu 2}$	Interpretation: $K_{\mu 3}$	Remarks
Milan, Genoa											
[4]	K_1	1270 ± 290	—	150 ± 27	—	98 ± 22	B	—	B	A	
	K_3	1540 ± 380 1170 ± 270	190 ± 32	108 ± 18	—	67 ± 13	—	—	—	A	*
	K_4	1360 ± 340	300 ± 50	200 ± 33	132 ± 30	140 ± 37	A	—	B	B	
	K_9	1015 ± 160	—	135 ± 7	—	—	—	—	—	A	*
	K_{10}	1025 ± 200	—	150 ± 10	—	—	B	—	—	A	*
	K_{11}	900 ± 125	—	190 ± 15	—	—	B	—	B	B	*
	K_{12}	850 ± 120	—	146 ± 10	—	—	B	—	—	B	*
	$K^{(\tau)}$	—	$\pi \to \mu \to e$	—	41.5	—	—	A	—	—	*
Rome											
[4, 7]	K_1	1120^{+220}_{-170} 1020 ± 65	π^-	—	38.5 ± 2.5	—	—	B	—	—	*–
	K_3	970^{+150}_{-110} 860 ± 35 980 ± 60	—	230 ± 30	—	—	B	—	B	B	*
	K_4	750^{+110}_{-90} 950 ± 50 1000 ± 60 980 ± 330	$\mu \to e$	—	—	$13.6 \pm .3$	—	—	—	A	*
Padua											
[4]	$K^{(\tau)}$	966 ± 100	$\pi \to \mu \to e$	—	6.0	—	—	A	—	—	*
	K_3	964 ± 60	275 ± 33	160 ± 10	—	—	A	—	—	B	*
	K_4	961 ± 122 975 ± 200	—	110 ± 11	—	—	—	B	—	B	*
	K_5	920 ± 330 1006 ± 100	—	70 ± 16	—	—	—	B	—	B	*
	K_6	865 ± 290 850 ± 100	—	52 ± 20	—	—	—	B	—	B	*
	K_7	949 ± 90 943 ± 60	278 ± 30	159 ± 9	—	—	A	—	—	B	*
	K_8	895 ± 225 1180 ± 140	175 ± 50	190 ± 15	—	—	—	—	B	B	*
	K_9	1420 ± 360 1060 ± 100	—	153 ± 36	—	—	B	—	B	B	*
	K_{10}	1100 ± 160	—	67 ± 15	—	—	—	B	—	B	*
	K_{11}	1056 ± 225	283 ± 27	172 ± 8	—	—	A	—	—	B	*

* From star.

*– Secondary appears to be π^- because it undergoes nuclear capture after stopping. The event probably represents the nuclear absorption of a K^- (see Table X).

TABLE II (*continued*).

Reference	Primary mass	Secondary particle				Interpretation				Remarks
		Mass or identity	$p\beta$	E_π	E_μ	$K_{\pi 2}$	$K_{\pi 3}$	$K_{\mu 2}$	$K_{\mu 3}$	
Tata										
[10] K_1	955 ± 140 950 ± 100	—	226 ± 20	—	—	—	—	B	B	*
[4]	1050^{+280}_{-200}	—	240 ± 25	—	—	—	—	B	B	*
Rochester										
[8]	1550 ± 280 995 ± 100	$\pi \to \mu \to e$	—	$15.2 \pm .3$	—	—	A	—	—	*
	975 ± 170 940 ± 100	$\pi \to \mu \to e$	—	$14.7 \pm .3$	—	—	A	—	—	
[9] K_2	1020 ± 300	—	—	—	—	B	B	B	B	*+
K_5	968 ± 220	272 ± 25	140 ± 10	87 ± 15	—	B	—	—	B	
K_7	982 ± 130	$\mu \to e$	—	—	28.0	—	—	—	A	
K_{12}	940 ± 235	$(\pi), \mu, e$	261 ± 34	—	—	—	—	B	B	*−
Cosmotron										
[11]	—	π	163 ± 10	—	—	A	—	—	—	
[12]	850 ± 150	(μ, e)	180 ± 13	—	—	—	—	B	B	
[13]	~ 1000	(π, μ)	177 ± 10	—	—	B	—	B	B	
	~ 1000	(π, μ)	143 ± 12	—	—	B	—	—	A	

* From star.

*+ K-particle suffers nuclear scattering.

*− Secondary followed through 7 emulsions. Energy loss slightly favors identification of secondary as an electron.

REFERENCES

[1] M. G. K. MENON and C. O'CEALLAIGH: *Proc. Roy. Soc.*, **221**, 292 (1954).

[2] P. H. BARRETT: *Phys. Rev.*, **94**, 1328 (1954).

[3] N. ISACHSEN, P. VANGEN and S. O. SÖRENSEN: *Phil. Mag.*, **44**, 224 (1953).

[4] *Proceedings of the Padua Conference*, 1954.

[5] K. H. BARKER: *Proceedings of the Duke Conference*, 1953.

[6] *Proceedings of the Bagnères Conference*, 1953 (p. 223).

[7] *Varenna Summer School*, 1954.

[8] M. F. KAPLON: *Proceedings of the Duke Conference*, 1953.

[9] M. F. KAPLON, J. CRUSSARD, J. KLAMSANN and J. NOON: *Washington Meeting A.P.S.*, 1954; also private communication.

[10] D. LAL, Y. PAL and B. PETERS: *Phys. Rev.*, **92**, 438 (1953); S. BISWAS., E. C. GEORGE and B. PETERS: *Ind. Acad. Sci.*, **38**, 418 (1953).

[11] R. D. HILL, E. O. SALANT and M. WIDGOFF: *Chicago Meeting A.P.S.*, 1954.

[12] W. F. FRY and M. S. SWAMI: *Phys. Rev.*, **96**, 235 (1954).

[13] D. RITSON: private communication (1954).

This Table lists 6 events in which the secondary particle is unmistakably a π-meson because, after coming to rest in the emulsion, it undergoes the characteristic $\pi \rightarrow \mu \rightarrow e$ decay. The values of the secondary kinetic energy are different in the six cases, being, in order of increasing magnitude: 4.3 (Cornell K_8); 6 (Padua $K^{(\tau)}$); 14.7 (Rochester); 15.2 (Rochester); 22.5 (Paris K_{3_2}) and 41.5 MeV (Milan $K^{(\tau)}$). This spread in the energy values is a clear indication for a three-body decay process.

If such a decay process is the alternate mode of decay of the τ-meson (Eq. (4.6)) the maximum secondary energy is 53 MeV (see Table I). The fact that in none of the six cases mentioned above the energy exceeds 53 MeV is in itself not very meaningful because obviously only π-meson secondaries of fairly low energy are likely to come to rest in the emulsion and thus reveal their nature by their mode of decay. However, mesons of energy somewhat greater than 53 MeV can often be reliably identified by grain density and scattering even if they do not stop in the emulsion. It is thus significant that no single example of π-meson secondary with energy between 53 and about 90 MeV has been reported so far (see Table II). Indeed, all particles in this energy range whose mass could be measured appear to be μ-mesons.

The wide gap in the energy distribution of the secondary π-mesons, appearing just beyond the computed energy limit for the alternate mode of decay of the τ-meson, lends considerable support to the assumption that this decay process is actually responsible for the low-energy group of π-meson secondaries. Notice that direct measurements indicate a mass of $(1030 \pm 35)\ m_e$ for the K-particles that undergo this mode of decay. This value is consistent with the τ-meson mass of $965\ m_e$.

Not much evidence for the $K_{\pi 3}$-decay does one find in cloud chamber pictures. A number of S- and charged V-events can be interpreted as $K_{\pi 3}$-decays, as well as according to other decay schemes. There is, however, one $V^{\pm}$-event (Paris 14435; Table IV) for which the interpretation in terms of a $K_{\pi 3}$-decay appears very likely. The secondary particle has mesonic mass and is almost certainly a π-meson because it undergoes nuclear scattering. For an assumed primary mass of $965\ m_e$, the momentum of the π-meson is the c.m.s. is 106^{+40}_{-10} MeV/c. This value is within the allowed range of momenta for the $K_{\pi 3}$-decay, but is inconsistent with the momentum corresponding to the $K_{\pi 2}$-decay (205 MeV/c). There is no primary mass measurement, so that the event could represent a Y^+-decay, but in this case the Q-value would be less than 77 MeV and therefore smaller than what appears to be the most likely value of Q for this process (see Part 5).

4·5. – Experimental Evidence for the $K_{\pi 2}$-Decay.

Aside from the 6 events ascribed to the $K_{\pi 3}$-decay, one finds in Table II a number of events in which the secondary particle appears to be a π-meson from direct mass measurement on the track. If one now examines the corresponding values of $p\beta$, one sees that they cluster around a mean value $(p\beta)_{av} = 167 \pm 6$ MeV/c, with no individual determination deviating from the mean by more than one should expect on account of statistical fluctuations (*) (for a more detailed discussion of this point, see the papers by DALLAPORTA and CECCARELLI in these *Proceedings*).

Mass measurements in photographic emulsions are always subject to some uncertainty and one cannot be sure that some of the secondary particles classified as π-mesons are not μ-mesons. Even so, the existence of a seemingly-mono-energetic group of π-meson secondaries appears to be strongly indicated.

Direct mass measurements on the primary particles of three of the clearest examples of $K_{\pi 2}$-decays give a mean value of $(972 \pm 46)\, m_e$ (see paper by CECCARELLI in these *Proceedings*). On the other hand, taking into account the measured value of $p\beta$ for the secondary π-meson, one finds that the primary mass should be 860 if the neutral decay product is a γ-ray or a neutrino, and 953 if it is a π^0-meson. There is thus here evidence in favor of the assumed decay scheme: $K^{\pm}_{\pi 2} \to \pi^{\pm} + \pi^0$. Moreover, the mass of the $K_{\pi 2}$-particle does not appear to be significantly different from the τ-meson mass.

Additional and more direct evidence on the nature of the neutral product of the $K_{\pi 2}$-decay comes from cloud-chamber observations. The M.I.T. group, working with a multiplate cloud chamber, has found many examples of electronic showers associated with the decay of K-particles at rest (see Table III). The showers appear to be produced by photons because there often is a non-ionizing link between the point of decay of the K-particle and the origin of the shower.

The observations are not consistent with a two-body decay into a photon and a light meson, because often the direction of emission of the charged secondary particle and that of the photon are not colinear. The observations would be consistent with a three-body decay, e.g. of the type: $K^{\pm} \to \mu^{\pm} + \gamma + \nu$. However, the assumption of a two-body decay with a π^0-meson as the neutral secondary particle provides the most natural explanation for the observed events. Under this assumption, the observed photons would be the decay products of the π^0-meson. The fact that in only one case both decay photons were detected can be easily accounted for by the geometry of the chamber.

(*) One possible, but not very convincing, exception is Rochester event K_5 (see Table II) which gives $p\beta = 140 \pm 10$.

TABLE III. – *Experiments of the MIT Group showing electronic showers associated with decay of* K*-particles.*

Origin of S. *a*) undetermined, outside the chamber, *b*) apparent nuclear interaction outside the chamber, *c*) nuclear interaction inside the chamber. *Charged Secondary.* The letters « *f* » and « *b* » in the fourth column indicate whether the secondary particle has been emitted in the forward or backward hemisphere with respect to the direction of the primary particle. Events H-1 through 70589 were observed using lead plates in the cloud chamber. Events 76734 through 106168 were obtained using brass plates. For these latter events the equivalent ranges in lead can be obtained by multiplying the observed ranges by 4/3. The potential range is the minimum range at production that would allow the particle to escape from the chamber with practically minimum ionization. Actual ranges are given for the particles that stop or appear heavily ionizing in the last visible section. The ionization is taken into account in the estimate of the actual ranges. The range limits indicated do not include statistical fluctuations in range (of the order of 3 percent). *Photon Secondary.* The fifth column (n. i. l.) indicates whether or not there is a non-ionizing link between the point of stopping of the S-particle and the origin of the shower. ϑ is the angle between the axis of the shower and the trajectory of the charged secondary particle. N is the total number of electron tracks in the shower. The last column lists estimated values of the individual π^0-detection probabilities. (These are calculated on the assumption of two body decay giving rise to a π^0-meson of 200 MeV/c momentum).

LEAD PLATES								
Event	Origin of S	Charged Secondary			Photon Secondary			
		Direction	Pot. Range	Actual Range g cm^{-2} Pb	n.i.l.	ϑ	N	π^0 det. prob.
H-1	*a*	*f*	67	23 ÷ 29.5	yes	180°	3	.87
TR-2	*a*	*b*	99		—	—	—	.1
S-1	*a*	*f*	41		—	—	—	.63
S-2	*a*	*f*	33		—	—	—	.82
02877	*b*	*b*	50		yes	127°	3	.69
03246	*b*	*f*	18		no	147°	4	.38
12668 (S3) *	*a*	*f*	83	66.4 ÷ 78.2	—	—	—	.38
25178	*a*	*f*	34		no	180°	5	.1
26049	*a*	*f*	52		no	157°	8-9	.48
26110 (S4)	?	*b*	72	55.2 ÷ 57.5	yes	163°	3	.19
26653	*b*	*b*	79		—	—	—	.75
29428	*c*	*f*	59		—	—	—	.74
30122 (S5)	*c*	*f*	41		—	—	—	.29
30654	*b*	*b*	22		—	—	—	.67
32531	*a*	*b*	5		yes	180°	5	.52
39567	*a*	*b*	65		—	—	—	0.0
42166 (S8)	*a*	*f*	48		—	—	—	.66

* Stopping questionable.

TABLE III (*continued*).

Even	Origin of S	Charged Secondary		Photon Secondary			
		Direction	Pot. Range / Actual Range g cm^{-2} Pb	n.i.l.	ϑ	N	π^0 det. prob.
46796	*a*	*b*	36	—	—	—	.51
53688	*a*	*b*	57	—	—	—	.69
56409	*a*	*b*	62	—	—	—	.20
58070	*a*	*b*	24	—	—	—	.38
58649	*a*	*b*	71	—	—	—	.39
61641	*c*	*f*	33	—	—	—	.55
64228	*a*	*f*	22	—	—	—	.77
64700	*c*	*f*	37	no	—	2	.39
64888	*a*	*f*	54	yes	123°	4	.75
65479	*c*	*f*	69	—	—	—	.06
66672	*a*	*b*	46	—	—	—	.87
70557	*a*	*b*	40	—	—	—	.51
70589	*a*	*b*	24	—	—	—	—

BRASS PLATES

Event	origin of S	Charged Secondary		Photon Secondary			
		Direction	Pot. Range / Actual Range g cm^{-2} Brass	n.i.l.	ϑ	N	π^0 det. prob.
76734	*b*	*b*	47	—	—	—	.62
77039	*b*	*b*	61	—	—	—	.79
77074	*b*	*f*	34	—	—	—	.60
77509	*b*	*f*	46	—	—		.58
78003	*c*	*f*	48	—	—	—	.53
78405	*b*	*f*	26	—	—	—	.66
78475	*a*	*b*	49	—	—	—	.62
80015	*c*	*f*	65	—	—	—	.73
81558	*b*	*f*	144	77.0÷107.2	—	—	—	.02
82203	*b*	*f*	50	39.2÷46.6	yes	170°	7*	.72
84965	*a*	*f*	56		—	—	—	.73
85380	*a*	*b*	143	70.9÷81.7	—	—	—	.20
85415	*a*	*f*	68		—	—	—	.56
85494	*c*	*f*	27		—	—	—	.69
85751	*b*	*f*	53		—	—	—	.73
87415	*b*	*b*	61		—	—	—	.62
87981	*c*	*f*	67	40.2÷49.2	yes	151°	3	.55
88405	*c*	*f*	55		—	—	—	.82
88515	*a*	*b*	62		—	—	—	.73
90713	*b*	*b*	57		—	—	—	.65
90912	*a*	*b*	116	20.5÷33.0	no	—	4	.70
91256	*c*	*f*	54		—	—	—	.73

* A second shower was apparently associated with this event.

TABLE III (*continued*).

Event	Origin of S	Charged Secondary			Photon Secondary			
		Direction	Pot. Range g cm^{-2} Brass	Actual Range g cm^{-2} Brass	n.i.l.	ϑ	N	π^0 det. prob.
91829	*b*	*f*	39		—	—	—	.30
92136	*c*	*b*	76	40.7	—	—	—	.50
92329	*c*	*f*	81	76.4÷79.4	—	—	—	.72
96787	*c*	*b*	81	68.6÷75.9	—	—	—	.80
98367	*c*	*f*	64		—	—	—	.76
98529	*a*	*b*	59		—	—	—	.40
99319	*b*	*b*	38		—	—	—	.28
99705	*b*	*b*	51		—	—	—	.40
100846	*a*	*f*	49		no	112°	3	.72
102209	*b*	*f*	82	77.1÷77.6	—	—	—	.56
102565	*c*	*f*	33		—	—	—	.82
105345	*b*	*b*	31		—	—	—	.68
105596	*a*	*f*	58	44.8	yes	166°	3	.69
105711	*a*	*f*	66		—	—	—	.40
106168	*c*	*f*	36		—	—	—	.66

Notice that if the primary mass is equal to that of the τ-meson, the range of the secondary π-meson in the $K_{\pi 2}$-decay should be 60 g cm^{-2} of lead. From Table III one sees that none of the S-events in which the range of the secondary charged particle is greater than 60 g cm^{-2} Pb had associated showers. In 8 out of the 15 S-events with associated showers, the secondary charged particle left the illuminated region of the chamber at practically minimum ionization, after traversing less than 60 g cm^{-2} Pb.

In events 26110, 82203, 87981, 92136 and 105596 the secondary particle stopped in a plate. Moreover, in the last two events the electron arising from the $\pi \to \mu \to e$ decay was visible and afforded a particularly accurate estimate of the point of stopping and therefore of the range. Considering errors of reconstruction and statistical fluctuations in energy loss, one sees that in these five cases the ranges of the secondary particles at production are consistent with a unique value of about 57 g cm^{-2} Pb.

In the two remaining cases (events H-1 and 90912) the charged particle entered a plate at minimum ionization after traversing 19 and 22.1 g cm^{-2} Pb, respectively, and failed to emerge from this plate. It seems likely that in these cases the apparent stopping was due to nuclear interaction.

Another convincing piece of evidence in favor of the decay process: $K^{\pm}_{\pi 2} \to \pi^{\pm} + \pi^0$ is found in a picture obtained recently by the Princeton group with a magnetic cloud chamber (HODSON, BALLAM, ARNOLD, HARRIS, RAU, REYNOLDS, TREIMAN, 1954). This picture shows the decay in flight of a *positive* particle into five charged particles, which appear to be one positive light

meson and two electron pairs. One interprets this event as a $K_{\pi 2}$-decay into a $\pi^{\pm}$ and a π^0-meson, with the subsequent decay of the π^0-meson into two electron pairs. The measured momenta of the secondary particles and their angles of emission are perfectly consistent with this interpretation. They yield for the energy release in the decay process: $Q = 213^{+15}_{-10}$ MeV, and for the corresponding value of the primary mass: $m = (954^{+30}_{-20})\ m_e$:

Of course, the direct conversion of a π^0-meson into two electron pairs is a very rare event. Usually a π^0-meson decays into two photons. According to a theoretical computation that appears to agree with experimental data, the probability of decay into one photon and one electron pair is $160/2 = 80$ times smaller than the probability of decay into two photons, and the probability of decay into two electron pairs is $(160)^2 = 25\,600$ times smaller.

A π^0-meson decaying into two photons, of course, is not detected in a magnet chamber, but a π^0-meson decaying into a photon and one electron pair is a very noticeable event. It is thus very peculiar that one should have observed the decay of a $K_{\pi 2}$-particle into a π-meson and two electron pairs before observing any example of the much more likely disintegration process into a π-meson, one photon, and one electron pair.

4·6. – Experimental Evidence for the $K_{\mu 3}$-Decay.

In Table II, one finds four events in which the secondary particle stops in the emulsion and then decays into an electron. It is natural to assume that this particle is a μ-meson, since the direct decay of π-mesons into electrons has never been observed. The ranges of the four secondary μ-mesons are different from one another, and correspond to kinetic energies of 5.9 (Bristol K_2), 13.6 (Rome K_1), 28.0 (Rochester K_7), and 33 MeV (Paris K_{14}), respectively. There is thus a spread in energy indicating a three-body decay.

Just as in the case of π-meson secondaries, only comparatively slow μ-mesons will stop in the emulsion and permit an identification on the basis of their characteristic decay. To investigate the actual energy spectrum of the $K_{\mu 3}$-decay, one must rely on the identification of the secondary particles by the scattering and the grain density along their tracks. This identification is always somewhat doubtful, the more so the higher the energy. Nevertheless, an examination of Table II leaves little doubt as to the existence among the secondaries of K-particles of a number of μ-mesons, with energies extending to about 100 MeV at least. For energies greater than about 100 MeV, μ- and π-meson are very difficult to separate, and the continuous spectrum of the $K_{\mu 3}$-decay becomes confused with the monoenergetic π-meson group arising from the $K_{\pi 2}$-decay.

Cloud-chamber observations of charged V-events provide some additional evidence for the $K_{\mu 3}$-decay. In two such events presented at the Varenna Summer School by LEPRINCE-RINGUET, the secondary particles were identified as μ-mesons, and had momenta equal to 108 MeV/c (V^+ 35467) and greater than 195 MeV/c (V^+ 24912), respectively, in the c.m.s.

In most other charged V-events no direct mass measurement on the secondary particle is available. One observes, however, a spread in the values of the secondary momenta in the c.m.s. (see Tables IV, V and VI), and one may argue that it is difficult to explain this spread by an admixture of $K_{\pi 3}$-particles. The reason is that $K_{\pi 3}$-particles presumably are τ-mesons undergoing the alternate mode of decay: $\tau^{\pm} \rightarrow \pi^{\pm} + \pi^0$, and that in cloud chambers τ-mesons are very seldom observed to decay in flight according to their normal mode: $\tau^{\pm} \rightarrow \pi^{\pm} + \pi^{\pm} + \pi^{\mp}$.

Particularly interesting is event RP993 of the Manchester Group (see Table V), which is clearly incompatible with either the $K_{\pi 3}$- or the $K_{\pi 2}$-decay If one ascribes this event to a $K_{\mu 3}$-decay, and one assumes that the two neutral products have zero mass, one finds a lower limit of $(125 \pm 90)\ m_e$ for the primary mass.

The significance of cloud-chamber observations of S-events with regard to the problem of the $K_{\mu 3}$-decay will be discussed in the next section. Here we wish to repeat that no experimental information exists as to the nature of two neutral particles in the three-body decay under discussion. The assumption that these two particles are neutrinos is thus an arbitrary one.

TABLE IV. – *Selected charged V-events observed in cloud chambers.*

θ indicates the angle of decay; p_T indicates the transverse momentum; p^* indicates the momentum in the c.m.s.. The figures in parenthesis indicate limiting values of p^* obtained by taking limiting values of p (primary) and p (secondary).

Reference	Primary			Secondary					
	p MeV/c	I/I_0	Mass (m_e)	θ	p MeV/c	p_T MeV/c	Mass or identity	p_π^* MeV/c	p_μ^* MeV/
Manchester									
[5] V−3	—	4-8	—	103°	185 ± 20	180 ± 20	—	221	217
									(184-2
V−6	1100 ± 400	1	—	12.5°	550 ± 80	119 ± 17	—	129	138
									(104-3
V−9	800 ± 260	1	—	15°	530 ± 80	138 ± 20	—	164	193
									(118-2
V−12	1500 ± 300	1	—	27.5°	440 ± 110	204 ± 50	—	252	236
									(166-2
V+13	5000 ± 200	1	—	15°	620 ± 120	162 ± 35	—	324	280
									(134-3

TABLE IV (*continued*)

ference	Primary			Secondary					
	p MeV/c	I/I_0	Mass (m_e)	θ	p MeV/c	p_T MeV/c	Mass or identity	p_π^* MeV/c	p_μ^* MeV/c
chester *tinued*)									
V+ 15	600 ± 150	1	—	9.5°	540 ± 180	89 ± 30	—	181	216 (97-325)
V− 16	—	1	—	22.5°	650 ± 130	250 ± 40	—	—	—
V− 17	—	1	—	20.5°	670 ± 70	240 ± 20	—	—	—
V+ 20	—	1	—	34°	510 ± 10	285 ± 57	—	—	—
V− J2	230 ± 50	2.5-5	600-1 500	95°	—	—	—	—	—
V− J6	350 ± 50	2-4	800-1 800	55°	280 ± 60	230 ± 50	—	221 ± 40	221 ± 40
V+ P38	130 ± 24	5-15	550-1 500	145°	—	—	—	—	—
V+ P33	368 ± 52	2-3	800-1 500	70°	170 ± 25	101 ± 24	—	118 ± 30	129 ± 35
V+ P11	590 ± 74	< 2	< 1 600	20°	—	—	—	—	—
V+ P22	420 ± 42	< 2	< 1 200	63°	—	—	—	—	—
V− P3	—	4-8	—	—	194 ± 8	—	—	227 ± 15	227 ± 15
V− P12	—	< 2	—	—	448 ± 61	—	—	208 ± 35	206 ± 35
is									
V+14435	1150^{+400}_{-230}	—	—	18.5°	273 ± 27	87 ± 9	π	106^{+40}_{-16} (*)	—
V−23322	—	—	—	3.6°	3750^{+1500}_{-750}	235^{+100}_{-50}	π	—	—
V+24912	—	—	—	54°	240^{+5}_{-2}	195^{+4}_{-2}	235 ± 15	—	—
iana									
V+R112	270 ± 10	—	< 1 200	49.2°	300 ± 20	230 ± 15	—	231 ± 15	235 ± 15
V+R390	104 ± 10	—	< p	56.7°	248 ± 6	207 ± 6	—	222 ± 6	223 ± 6
V−R423	—	—	—	—	228	101 ± 4	$\pi \to \mu$	—	—
V R521	—	—	—	—	—	—	—	219 ± 8	—
Tech. V−	185 ± 20	6-10	1200 ± 300	—	150 ± 15	—	250 ± 50	175 ± 20	170 ± 20

(*) For assumed primary mass = 965.

REFERENCES

[1] B. GREGORY, A. LAGARRIGUE, L. LERPINCE-RINGUET, F. MULLER and CH. PEYROU: *Nuovo Cimento*, **11**, 292 (1954).

[2] R. W. THOMPSON, J. R. BURWELL, H. O. COHN, R. W. HUGGETT, C. J. KARZMARK and Y. B. KIM: *Proceedings of the Rochester Conference*, 1953.

[3] Y. B. KIM, J. R. BURWELL, H. O. COHN, C. J. KARZMARK and R. W. THOMPSON: *Washington Meeting A.P.S.*, 1954.

[4] R. B. LEIGHTON and S. D. WANLASS: *Phys. Rev.*, **86**, 426 (1952).

[5] R. ARMENTEROS, K. H. BARKER, C. C. BUTLER, A. CACHON and C. M. YORK: *Phil. Mag.*, **43**, 597 (1952).

[6] C. C. BUTLER: *Proceedings of the Bagnères Conference*, 1953.

[7] Y. B. KIM, J. R. BURWELL, R. W. HUGGETT and R. W. THOMPSON: *Phys. Rev.*, **96**, 229 (1954).

TABLE V. – *Analysis of 44 charged V-events observed by the Manchester group working at the Jungfraujoch.*

(J. S. BUCHANAN, W. A. COOPER, D. D. MILLAR and J. A. NEWTH: *Phil. Mag.*, **45**, 1025 (1954)). The momenta in the c.m.s. (p^*) are computed under the assumption that the primary particle has mass 1000 m_e.

Event	Primary Particle					Secondary Particle			
	Sign	p	%Error in $1/p$	Velocity	Mass	ϑ	p	%Error in $1/p$	p^*
AE 7	+	600	100	—	—	15 ± 2	—	—	—
JB 127	—	230	20	.40-.60	710-1 300	95 ± 7	—	—	—
JK 23	+	210	25	.31-.40	740-1 600	80 ± 7	—	—	—
JS 23	+	600	100	—	—	89 ± 3	41	10	—
NJ 93	—	350	15	.40-.60	790-1 900	53 ± 2	280	20	224^{+65}_{-37}
NN 13	?	900	100	—	—	35 ± 2	—	—	—
NC 75	+	550	100	—	—	57 ± 2	—	—	—
NS 61	—	950	100	—	—	11 ± 1	430	60	—
NT 249	+	1 000	100	—	—	28 ± 2	490	20	—
NR 194	+	1 100	300	—	—	18 ± 2	510	15	—
NZ 357	+	1 500	50	—	—	45 ± 5	—	—	—
OD 557	—	1 200	20	—	—	43 ± 3	430	40	387^{+343}_{-126}
OE 316	+	580	75	—	—	14 ± 1	—	—	—
OE 483	+	540	150	—	—	38 ± 3	310	70	—
OE 489	+	1 000	100	—	—	36 ± 1	580	100	—
PB 100	+	1 500	80	—	—	22 ± 2	—	—	—
PE 65	—	1 500	80	—	—	29 ± 1	—	—	—
PL 93	—	2 000	100	—	—	19 ± 3	260	25	—
QD 138	+	190	15	.37-.43	670-1 100	47 ± 3	230	15	182^{+39}_{-28}
QE 854	+	1 100	250	—	—	15 ± 1	500	20	—
QF 635	+	1 200	30	—	—	58 ± 2	300	50	444^{+670}_{-180}
QG 284	—	800	150	—	—	20 ± 2	—	—	—
QH 425	—	700	25	—	—	55 ± 2	140	15	161^{+55}_{-34}
QL 707	+	220	25	$>.46$	<1020	32 ± 2	300	10	209^{+38}_{-36}
QM 861	+	350	30	.43-.52	970-2 500	82 ± 2	67	15	102^{+40}_{-21}
QR 720	—	1 200	150	—	—	20 ± 3	530	15	—
QR 979	—	120	15	$<.31$	>610	89 ± 2	51	10	56^{+26}_{-4}
QT 937	+	120	10	.24-.34	600-1 000	31 ± 3	—	—	—
QU1046	+	320	30	.46-.60	580-1 600	57 ± 2	—	—	—
QW 557	+	800	100	—	—	41 ± 3	450	30	—
RC 290	+	320	100	—	—	62 ± 2	310	40	—
RC 886	+	2 900	100	—	—	11 ± 2	1 300	40	—
RC 941	+	1 300	100	—	—	18 ± 1	—	—	—
RD 25	+	800	100	—	—	31 ± 2	250	80	—
RD 264	—	600	70	—	—	14 ± 1	260	50	—
RD 473	—	700	14	—	—	40 ± 1	210	25	145^{+60}_{-29}
RE 410	+	2 100	100	—	—	11 ± 1	960	25	—
RF 254	+	1 140	50	—	—	37 ± 1	200	50	—

TABLE V (*continued*).

Event	Primary Particle					Secondary Particle			
	Sign	p	%Error in $1/p$	Velocity	Mass	ϑ	p	%Error in $1/p$	p^*
RF2000	+	2200	70	—	—	19 ± 1	1000	100	—
RG 585	+	320	16	$> .52$	< 1190	75 ± 1	120	16	133^{+33}_{-20}
RH 478	?	600	100	—	—	17 ± 1	—	—	—
RM 253	+	600	100	—	—	45 ± 2	360	10	—
RM 541	−	440	70	—	—	23 ± 1	200	30	—
RP 993(1)	+	210	5	.29-.40	920-1440	117 ± 2	250	8	329^{+30}_{-82}

(1) For this event, the assumption of a primary mass equal to 1000 electron masses is inconsistent with the measurements. Indeed, with the help of Eq. (4.5) the experimental data give a lower limit of $(1225 \pm 90)\ m_e$ for the mass of the primary particle.

TABLE VI. – *Analysis of* 14 *charged* V*-events observed by the group at the California Institute of Technology with the double magnet chamber.*

« *A* » signifies origin above the chambers and « *P* » origin in the plate between the chambers. The letter « *b* » indicates that p^* was computed assuming a mass of 1000 m_e for the primary particle. From a paper by YORK, LEIGHTON and BJORNERUD (*Phys. Rev.*, **95**, 159 (1954)) with corrections indicated in a private communication.

Event	Origin and Sign	Primary Particle		Secondary Particle			
		p	I/I_0	ϑ	p	p_T	p^*
7029	$A(-)$	185 ± 25	6.8-8.0 [a]	85°	150 ± 20	150 ± 20	125 - 190
17620	$A(-)$	1050 ± 470	< 1.5	8°	750 ± 200	109 ± 28	179 ± 40 [b]
25343	$P(+)$	185 ± 45	3.4-4.4 [a]	51°	215 ± 43	165 ± 27	130 - 210
26622	$P(-)$	—	1.5-2.5	33°	295 ± 65	160 ± 35	130 - 210
31589	$P(-)$	—	1.5-3.0	40°	265 ± 40	170 ± 25	150 - 210
32530	$A(-)$	465 ± 220	1.4-1.8 [a]	29°	590 ± 250	285 ± 120	316 ± 120 [b]
36726	$A(+)$	—	1.5-3.0	108°	104 ± 30	135 ± 30	180 - 320
40840	$P(+)$	95 ± 30	6-12	87.5°	184 ± 20	184 ± 20	170 - 220
52999	$A(+)$	165 ± 85	15-30	121°	215 ± 60	185 ± 50	180 - 290
54056	$P(-)$	—	1.5-3.0	13°	325 ± 75	73 ± 15	100 - 190
55482	$P(-)$	—	1.5-2.5	53.5°	182 ± 30	146 ± 25	125 - 210
60452	$A(+)$	255 ± 175	2.8-4.2 [a]	99°	212 ± 10	210 ± 10	220 -255
65550	$A(-)$	1500 ± 800	< 1.5	41.5°	120 ± 50	79 ± 35	213 ± 50 [b]
78113	$A(+)$	107 ± 15	10-15	133°	251 ± 20	182 ± 15	280 - 325

a) Ionization measured photometrically.
b) p^* calculated assuming a mass of 1000 m_e for the primary particle.

4·7. – Experimental evidence for the $K_{\mu 2}$-Decay.

The experimental evidence for a two-body decay process with a μ-meson secondary is less direct than the evidence for the three other kinds of decay processes discussed previously. Indeed, there is no individual event, observed either in cloud chambers or in photoemulsions, that could not be explained in terms of either a $K_{\pi 3}$-, a $K_{\pi 2}$-, or a $K_{\mu 3}$-decay. However, the following arguments seem to indicate that the experimental data, taken as a whole, require the assumption of an additional decay process.

The M.I.T. group, working with a multiplate cloud chamber, and the Paris group, working with a multiplate chamber and a magnet chamber placed one under the other, have reported examples of S-events that cannot be interpreted as $K_{\pi 3}$- or $K_{\pi 2}$-decays because the range of the secondary particle is greater than 60 g cm^{-2} Pb.

Some of these events are listed in Tables III and VII.

TABLE VII. – *S-events observed with the magnet chamber and multiplate chamber of the École Polytechnique.*

Plate material: carbon and lead or copper. Ranges in g cm^{-2} Pb equivalent. In the computation of the corrected range, the ionization in the last visible section of the track is taken into consideration. (GREGORY, LAGARRIGUE, LEPRINCE-RINGUET, MULLER and PEYROU: *Nuovo Cimento*, **11**, 292 (1954)).

Event	S-particle Sign	S-particle Mass	Charged Secondary: Uncorrected min. range	Charged Secondary: Corrected min. range	Charged Secondary: Max. range	Remarks
21162			58	—	—	large angle scattering of secondary
17804			60	63	—	—
27924			68	71	—	—
21073			80.5	82.0 *	95.5 *	secondary stops.
25845	+		85	94.5 *	108.1 *	secondary stops.
16192	+	885±50	12	22	—	—
16197	+	915±80	38	41	—	—
18094	+	1030±85	48.5	51.5	—	—
27170	+	926±45	69±7	—	—	—
19231	+	857±70	67±2	70±2	—	—
26320	+	939±50	75	—	—	—
22964	+	911±70	84±4	—	—	—
23473	+	968±52	0	—	—	photon secondary, possible $\tau \to \pi + 2\pi_0$
18805	+	918±50	9.8	—	20.6	possible τ
16307	+	965±50	12.5	—	15	$= \tau \to 3\pi$ probable

* Values corrected according to private communication by Dr. GREGORY to the author.

Other events have been described by LEPRINCE-RINGUET at the 1954 Varenna Summer School.

In 14 such cases the secondary particle stops in the cloud chamber; the corresponding range limits are listed below:

M.I.T.	Event	No.	81558	$R = 102.6 - 143.0$	g cm^{-2} Pb
»	»	»	85380	» 94.5 — 108.9	»
»	»	»	92329	» 101.9 — 105.9	»
»	»	»	96787	» 91.4 — 101.1	»
»	»	»	102209	» 102.8 — 103.5	»
Paris	Event	»	21073	» 82.0 — 95.5	»
»	»	»	25845	» 94.5 — 108.1	»
»	»	»	30248	» 88.0 — 104.0	»
»	»	»	38275	» 89.1 — 111.0	»
»	»	»	38797	» 86.2 — 112.2	»
»	»	»	40896	» 100.9 — 113.8	»
»	»	»	47066	» 97.7 — 113.6	»
»	»	»	47438	» 91.3 — 111.4	»
»	»	»	48813	» 64.7 — 102.0	»

In the computation of the above figures, no account was taken of range straggling and of possible errors of reconstruction. Considering these experimental uncertainties, one concludes that the secondary ranges are consistent with a unique value of about 100 g cm^{-2} Pb. This is clear indication for the existence of a particle undergoing two-body decay.

Direct measurements by the Paris groups on S-events whose primaries traverse both chambers show that the primary mass is certainly not greater, and is probably smaller than the τ-meson mass. This result is consistent with the experimental value of the secondary range if the secondary particle is a μ-meson and if the neutral particle is massless. On the other hand, the neutral particle could not be a photon because a photon would not have escaped detection in the multiplate chambers. It is thus natural to assume that the decay process under consideration is of the type: $K_{\mu 2} \rightarrow \mu + \nu$. Under this assumption, the mass corresponding to a secondary range of 100 g cm^{-2} Pb is 952 m_e.

Notice that, if one tries to interpret all experimental facts without assuming any other decay process in addition to the $K_{\pi 3}$-, $K_{\pi 2}$- and $K_{\mu 3}$-decays, one encounters several difficulties.

One of them is the high mass value that appears to be required in order to explain certain decay events (e.g. Manchester event RP993) setting a lower limit of 1225 ± 90 m_e to the primary mass). These events are certainly not $K_{\pi 3}$- or $K_{\pi 2}$-decays. If one interprets them as $K_{\mu 3}$-decays and if one also interprets as $K_{\mu 3}$-decays all S-events different from $K_{\pi 3}$- or $K_{\pi 2}$-decays, one runs into a contradiction to the direct mass measurements on the primaries of S-particles mentioned above.

Another difficulty lies in the apparent difference between the energy distribution of the secondary particles of S-events observed in multiplate chambers and in photoemulsions respectively. In the cloud chamber experiments, very few secondary particles have been observed to stop. One should notice, of course, that $K_{\mu 3}$-decays giving secondaries with ranges less than about 20 cm^{-2} Pb are not recorded as S-events except in the comparatively few cases were a reliable primary mass measurement is available. Even in those cases, they cannot be separated from $K_{\pi 3}$-decays. It is however, significant that in the experiments of M.I.T. and of the École Polytechnique, only few S-events with secondary ranges between 20 and 80 g cm^{-2}, were found and all of these can be easily interpreted as $K_{\pi 2}$-decays. One then recognizes that, if all S-events different from $K_{\pi 3}$- or $K_{\pi 2}$-decays are to be interpreted as $K_{\mu 3}$-decays, the secondary spectrum of the $K_{\mu 3}$-decay must be strongly peaked at the high-energy end. This conclusion, which is also supported by measurements of the scattering of the secondary particles in the M.I.T. multiplate chamber, appears to be in contradiction to the observations in photoplates indicating a fairly flat decay spectrum for the $K_{\mu 3}$-particles.

The hypothesis of a $K_{\mu 2}$-decay process helps in solving the difficulties mentioned above. One can then assume that the S-particles observed in cloud chambers are for the most part $K_{\pi 2}$-particles and $K_{\mu 2}$-particles with a small admixture of $K_{\mu 3}$-particles. One can ascribe to the $K_{\mu 2}$-particle a mass lower than 1 000 m_e, as indicated by the measurements of the Paris group, and to the $K_{\mu 3}$-particle a mass sufficiently large to account for the highest observed energies of the secondary particles. One can also explain the difference between the energy spectra of the K-particle secondaries detected with photoemulsions and with multiplate chambers by assuming that the number of $K_{\mu 3}$-particles relative to that of $K_{\mu 2}$-particles is greater for the S-events observed in photoemulsions than for the S-events obsesrved in cloud chambers. This might be due to a difference in the mean life (the $K_{\mu 3}$-particles having a shorter life than the $K_{\mu 2}$-particles), or to a difference in the production spectrum (the $K_{\mu 3}$-particles being produced with a smaller average energy than the $K_{\mu 2}$-particles).

More experimental data are needed to establish the identity of the $K_{\mu 2}$-decay unambiguously. In the meantime it may be well to keep in mind that several possible sources of error exist in the interpretation of any individual observation.

For example, an S-event observed with a multiplate cloud chamber may represent the decay of a particle that has not yet come to rest completely. Even a comparatively small velocity of the decaying particle might appreciably increase or decrease the energy of the secondary meson, depending on whether the meson is emitted in a forward or backward direction.

Also, an event classified as an S-decay may represent instead the nuclear absorption of a negative K-meson, in which most of the available energy

goes into a π-meson (see Part 7). In the observations with multiplate cloud chambers, any charged evaporation product may easily escape detection because of its inability to emerge from the plate. In the observations with photoemulsions one can mistake a process of nuclear absorption for a decay only when there are no other charged decay products in addition to the π-meson. Since this is a rare occurrence, one must conclude that the majority of S-events observed in photoemulsions are true decay processes.

4·8. – Further Considerations.

We shall now discuss, by necessity in a tentative and preliminary way, the question of the relationship between charged and neutral heavy mesons and the identity of the particles responsible for the different decay processes discussed above.

There appears to be a close kinship between the θ^0-particle and the χ- (or $K_{\pi 2}$)-particle). Their decay processes are similar:

$$\theta^0 \to \pi^+ + \pi^-$$

$$\chi^\pm \to \pi^\pm + \pi^0$$

and the Q-values are the same, within the experimental errors ($Q_{\theta^0} = 214 \pm 5$; $Q_\chi = 215^{+15}_{-10}$ according to the Princeton event, see Sec. 4·5; $Q_\chi = 217 \pm 7$ from M.I.T. event 105596, see also paper by DALLAPORTA in these *Proceedings*). If these results are confirmed and if the spins of the two particles also turn out to be the same, one would be led to consider the χ-particle as the charged counterpart of the θ^0-particle. Notice, however, that the mean life of the χ-particle appears to be about 10 to 100 times larger than that of the θ^0-particle.

It seems that both positive and negative χ-particles exist. The Princeton event described in Sec. 4·5 represents the decay of a positive particle. It is likely that the χ-particles responsible for the S-events associated with γ-rays are also positive, since negative χ-mesons would presumably undergo nuclear absorption rather than spontaneous decay upon stopping in the plates of a multiplate cloud chamber. On the other hand, the Paris group found many examples of negative charged V-events, whose secondary particles are π-mesons and which cannot be interpreted as $K_{\pi 3}$-decays because of the magnitude of the secondary transverse momenta. It is likely that these events represent decay processes of χ^--particles.

Another striking fact is that the masses of the τ-meson and of the χ-meson (as deduced from their respective Q-values) are equal within the experimental errors. This raises the question as to whether the $K_{\pi 2}$-decay and the $K_{\pi 3}$-decay could be alternate decay modes of the τ-meson.

If we do not consider spin values greater than 1, we find that the χ-particle can either have spin zero and even parity, or spin 1 and odd parity. In the first case the two decay products are in an S-state, in the second case in a P-state. On the other hand we find that if the τ-particle has spin zero, it must have either even or odd parity. We thus conclude that if the τ- and χ-meson are the same particle, this particle must have either spin 1 and odd parity, or it must have a value of the spin greater than 1.

The mass of the $K_{\mu 2}$-particle is still somewhat doubtful. It appears to be slightly smaller than the τ-meson mass, but the difference is still within the experimental uncertainty. If the decay scheme

$$K_{\mu 2} \rightarrow \mu + \nu$$

is correct, one might be inclined to regard the $K_{\mu 2}$-particle as closely related to the π-meson, which has a similar decay scheme. In other words the $K_{\mu 2}$-particle might be a higher mass state of the π-meson. One would then ascribe to it spin zero and odd parity. This would make the $K_{\mu 2}$-particle necessarily different from the χ-particle. Disregarding these very speculative considerations, one might possibly consider the $K_{\mu 2}$-decay as a third alternate decay mode of the τ-meson, along with the $K_{\pi 3}$- and the $K_{\pi 2}$-decay.

A very peculiar fact worthy of notice is that according to the observations of the Paris group the $K_{\mu 2}$-particle appears to be always positive.

There are some reasons to believe that the $K_{\mu 3}$-particle is not related to the other charged heavy mesons. The high-energy tail of its decay spectrum indicates that its mass is larger than the masses of the τ-, the χ-, or the $K_{\mu 2}$-particle. Moreover, if the decay scheme

$$K_{\mu 3} \rightarrow \mu + \nu + \nu$$

is correct, the $K_{\mu 3}$-particle is a fermion, while the other K-particles discussed previously are bosons. Indeed, the $K_{\mu 3}$-particle would seem to be closely related to the μ-meson, which also decays into one charged fermion and two neutrinos.

As a final remark, we note that $K_{\mu 2}$- and $K_{\mu 3}$-particles, as well as τ-mesons, have been seen to come out of nuclear stars. There is also some evidence, but not of a decisive nature, for the direct production of $K_{\pi 2}$-particles in nuclear interactions.

5. – Charged Hyperons.

5·1. – General Considerations.

The experimental evidence for the existence of charged hyperons rests on a number of pictures obtained with photographic emulsions and with cloud chambers, that are interpreted as showing the decay in flight or at rest of charged particles of superprotonic mass. The mass measurements on the primary particles are often sufficiently accurate to exclude the possibility that this particle might be a heavy meson. They are usually not sufficiently accurate to distinguish the particle from a proton, but the possibility that the particle may be a proton is ruled out by its behavior at the end of the track. Consider, for example, the event listed in Table VIII, under N.R.L.. Here the primary particle gives rise to a π-meson of 95 ± 25 MeV kinetic energy after coming to rest in the emulsion. The event represents probably the spontaneous decay of a positive particle, or possibly the nuclear absorption of a negative particle. In either case the particle is certainly not a proton.

Even though the existence of charged hyperons appears to be well established, there still is a great deal of uncertainty concerning the number of different hyperons and their modes of decay, as we shall discuss in the following sections.

5·2. – The Decay Process $Y^+ \to p + \pi^0$.

In analogy to the Λ^0-particle, which decays into a proton and a negative π-meson, the existence of a positive hyperon, with the decay mode

$$Y^+ \to p + \pi^0, \tag{5.1}$$

has been suggested. In support of this suggestion the following experimental evidence exists. The C.I.T. group reported cloud chamber observations of charged V-events indicating the existence of short-lived positive particles that are difficult to explain as K^+-mesons (ALFORD and LEIGHTON, 1953). In two cases the secondary of a V^+-particle was recognized as a proton, but no Q-value could be determined. It is difficult to explain these observations as spurious events, such as the decay of Λ^0-particles, or nuclear scatterings of protons in the gas (YORK, LEIGHTON and BJORNERUD, 1953; 1954).

The Paris group reported a positive charged V-event with a secondary

TABLE VIII. – *Decay of charged hyperons in photo-emulsions.*

The Q-values computed according to the decay schemes $Y^+ \to p + \pi_0$ and $Y^+ \to n + \pi^+$ are indicated.

S decay at rest
V decay in flight

E_π, E_p are given only for decays at rest
R range in photoemulsion
$p\beta$ in the laboratory system

Reference	Decay	Primary Mass	Secondary Particle: Mass or identity	Secondary Particle: $p\beta$	Secondary Particle: R (mm)	Secondary Particle: E_π	Secondary Particle: E_p	Q-values: $Y^+ \to p + \pi^0$	Q-values: $Y^+ \to n + \pi^+$	Remarks
Tata										
[1] No. 1	V	2200^{+600}_{-400}	330 ± 60	160 ± 13	—	—	—	—	135 ± 35	from star (τ also produced)
[7] No. 2	V	2460 ± 500	(π, μ)	—	—	—	—	—	110 ± 25	from star
No. 3	V	2610^{+300}_{-250}	950^{+600}_{-400} (p)	—	—	—	—	129 ± 11	—	poss. scatt.
No. 4	V	2775 ± 185	p	—	—	—	—	225 ± 25	—	poss. scatt.
No. 5	V	2470 ± 300	p	—	—	—	—	212 ± 22	—	poss. scatt.
[2] N.R.L.	S	2869 ± 850	330 ± 90	150 ± 35	2.2	95 ± 25	—	—	114 ± 32	
[3] Cornell	V	2500 ± 900	(π, μ)	90^{+18}_{-13}	—	—	—	—	72^{+12}_{-8}	from star; $p\beta$ deduced from grain density for an assumed π.
[4] Rochester	V	2390 ± 500	(π, μ)	195	—	—	—	—	116 ± 50	from star: $p\beta$ deduced from grain density for an assumed π.
Rome										
[5] Y_1	S	2520 ± 640	—	—	—	—	—	—	—	from star
Y_2	V	2600 ± 500	(π, μ)	—	—	—	—	—	—	from star

	J_6	V	$2\,700 \pm 1350$	(π, μ)	204 ± 21	—	—	—	—	95 ± 21	from K^--star
	J_7	V	$2\,700 \pm 600$	(π, μ)	166 ± 17	—	—	—	—	90 ± 20	from star
Padua											
[7]	Y_1	V	$2\,100 \pm 400$	286 ± 30	—	—	—	—	131 ± 24	—	from star
	Y_2	S	$1\,840^{+900}_{-600}$	$2\,200^{+600}_{-400}$	—	—	—	$18.5 \pm .3$	116 ± 2	—	from star
	Y_3	V	$2\,000 \pm 200$	p	—	—	—	—	125 ± 30	—	from star
Bristol											
[8]	No. 2	S	$2\,500 \pm 500$	p	—	—	—	50	~ 400	—	could be nuclear capture of Y^-.
	No. 3	V	$2\,200 \pm 300$	(π, μ)	—	—	—	—	—	65 ± 20	from star
[7]	No. 1	V	$2\,750 \pm 500$	(π, μ)	85 ± 5	—	—	—	—	100 ± 6	from star; $p\beta$ deduced from grain density for an assumed π.
	No. 4	V	$2\,500 \pm 500$	$\leqslant m_\pi$	160 ± 20	—	—	—	—	36 ± 10	from star
		V	$2\,300 \pm 350$	—	—	—	—	—	—	> 85	from star - associated with K-meson.
		V	—	(π, μ)	—	—	—	—	—	115 ± 10	from star - associated with K-meson.
Warsaw [7]		V	$1\,900^{+450}_{-300}$	2000^{+450}_{-300} (p)	—	—	—	—	—	146 ± 40	from star
Cosmotron [10]		S	$2\,300 \pm 1\,000$	p	—	$1.78 \pm .03$	—	$19.5 \pm .2$	117 ± 2	—	

REFERENCES

[1] D. LAL, Y. PAL and B. PETERS: *Proceedings of the Bagnères Conference*, 1953 (p. 141).

[2] D T. KING, N. SEEMAN and M. M. SHAPIRO: *Phys. Rev.*, **92**, 838 (1953).

[3] P. H. BARETT: *Phys. Rev.*, **94**, 1328 (1954).

[4] Private communication.

[5] C. CASTAGNOLI G. CORTINI and C. FRANZINETTI: private communication.

[6] A. BONETTI, R. LEVI-SETTI, M. PANETTI and G. TOMASINI: *Nuovo Cimento*, **10**, 1736 (1953).

[7] *Proceedings of the Padua Conference*, 1954.

[8] D. H. PERKINS: *Proceedings of the Duke Conference*, 1953.

[9] D. H. PERKINS: *Dublin Meeting*, 1954, reported in *ONRL*, 29, 54.

[10] W. F. FRY and M. S. SWAMI: *Phys. Rev.*, **96**, 235 (1954).

proton. A small blob is visible at the apparent point of decay suggesting that perhaps the event is a nuclear scattering (FRETTER, GREGORY, JOHNSTON, LAGARRIGUE, MAYER, MULLER and PEYROU, 1953). If it is a real hyperon decay, one finds $Q = 26 \div 28$ MeV.

The best evidence for the suggested decay process comes from observations with photoplates (see Table VIII).

Here one should consider separately cases where the primary particle appears to decay in flight, and where the primary particle appears to decay at rest. A charged hyperon decaying in flight into a proton is an event that sometimes cannot be easily distinguished from the nuclear scattering of a proton. Thus several of the charged V-events with proton secondary listed in Table VIII are probably cases of nuclear scattering. Indeed, the apparent energy releases, computed under the assumption that the events represent true decay processes, do not seem to cluster around a single value.

After coming to rest in the emulsion, a charged hyperon may give rise to a secondary proton either by spontaneous decay or (if it has a negative charge) by a process of nuclear absorption producing a one-prong star. However, Table VIII lists four events of the type under consideration, in which the secondary proton has the same energy (about 18 MeV) with a very small error (*) (Rome Y_3, Milan-Genoa J_{pl}, Padua Y_2, Cosmotron), and only one event in which the proton has a different energy (50 MeV; Bristol no. 2). It is thus very likely that the three former events represent the two-body decay process of a charged positive hyperon. Under the assumption of the decay scheme: $Y^+ \to p + \pi^0$ one obtains $Q = 116 \pm 2$ MeV.

5·3. – The Decay Process $Y^+ \to n + \pi^+$.

Table VIII lists a number of events in which charged hyperons appear to decay into light mesons. Here again one must distinguish between events where the primary particle disappears in flight, and events where it disappears at rest. In the latter case the event could be the result of the nuclear absorption of a negative hyperon rather than a true decay process. In the former case this interpretation is much less likely.

It is reasonable to assume that the positive hyperon discussed in the previous section has the alternate mode of decay:

$$Y^+ \to n + \pi^+ . \tag{5.2}$$

From the experimental value of Q for the process $Y^+ \to p + \pi^0$ one computes a value $Q = 111 \pm 2$ MeV for this alternate mode of decay.

(*) The first of these events was reported in 1953 by the Padua group.

Of the 12 events with a light meson secondary of measurable energy listed in Table VIII, 9 can be interpreted according to the decay scheme (2.5). However, the experimental errors in the determination of Q are quite large, so that the evidence for a group of events giving a unique Q-value is not very strong. Moreover, there are 3 events which, if interpreted according to (2.5) give Q-values significantly different from 111 MeV (Cornell, Bristol no. 3, Bristol no. 4). It is difficult to interpret these events as nuclear absorption processes, because the primary particle disappears in flight. Possibly they represent the decay of the negative hyperon discussed in Sec. 5·5 below.

5·4. – The Decay Process $Y^- \to n + \pi^-$.

The experimental evidence for a negative counterpart of the positive hyperon discussed in the two previous sections rests upon two cloud-chamber events observed at Brookhaven (Fowler, Shutt, Thorndike and Whittemore, 1954). Both events represent decays in flight.

In the first event the primary particle enters the cloud chamber from the outside. It has a negative charge and a momentum of $p = 1190 \pm 170$ MeV/c. There is no indication as to its mass. The secondary particle has a negative charge and a momentum $p = 83 \pm 3$ MeV/c. Its rest energy is from 110 to 150 MeV, thus it could be either a π-meson or a μ-meson. The angle of emission is 76°.

The Q-values compuetd for different assumptions on the decay scheme are:

(5.3)	$Y^- \to n + \pi^-$	$Q = 130^{+25}_{-15}$	MeV
(5.4)	$Y^- \to \Lambda^0 + \pi^-$	$Q = 98^{+25}_{-10}$	»
(5.5)	$K^- \to \pi^0 + \pi^-$	$Q = 430 \pm 70$	»
(5.6)	$K^- \to \mu^- + 2\nu$	$Q > 520 \pm 80$	»

The first of the four decay schemes listed provides the most likely interpretation. The Q-value is consistent with that of the Y^+-decay described in the previous section.

In the second event a π^--meson of 1.37 GeV/c momentum, on colliding against a hydrogen nucleus, appears to produce a K^+ and an Y^-:

$$\pi^- + p \to K^+ + Y^- .$$

The Y^- subsequently decays, and for an assumed decay scheme: $Y^- \to n + \pi^-$ one finds $Q \geqslant 50$ MeV (*).

(*) An event recently found in a photoemulsion confirms the existence of the decay process $Y^- \to \pi^- + n$ and gives a Q-value of 107 ± 15 MeV [De Benedetti, Garelli, Tallone and Vigone, *Nuovo Cimento*, **12**, 952 (1954)].

5·5. – The Decay Process $Y^- \to \pi^- + \Lambda^0$.

Experimental evidence for this decay process, usually referred to as *cascade decay*, was first presented by the Manchester group (ARMENTEROS, BARKER, BUTLER, CACHON and YORK, 1952). This group published a picture showing a negative charged V-particle and a neutral V-particle. The neutral V-particle appeared to originate from the point of decay of the charged V. It was not possible to identify the neutral V nor the secondary charged particle of the V^--decay. There was a slight chance that the V^0-particle might have originated from the nuclear interaction that gave rise to the V^--particle, rather than from the decay of the V^--particle.

More recently the C.I.T. group reported 4 additional cases of cascade decay (ANDERSON, COWAN, LEIGHTON and VAN LINT, 1953; COWAN, ANDERSON, LEIGHTON and VAN LINT, 1953; COWAN, 1954). In all these events the charged V-particles were negative. In two cases to V^0-particle was identified as a Λ^0-particle. In the other two cases, too, the V^0-particle was probably a Λ^0 because the positive decay product formed a smaller angle with the line of flight of the primary neutral particle than the negative one. In all cases the neutral V appeared to come from the point of decay of the charged V. Moreover, in the last case reported, the neutral V and the charged V could not have come from the same nuclear interaction, so that the event could not be interpreted as a chance association.

The two C.I.T. events that could be analyzed in some detail gave the following results:

	Event 1	Event 2
Charged decay product of V^--particle:	π or μ	π
Positive decay product of V^0-particle:	proton	$m = 2050 \pm 350$
Negative decay product of V^0-particle:	π or μ	π or μ
Q-value of V^0-particle assumed to be a Λ^0:	39 ± 10	40 ± 13
Q-value of V^- for assumed decay $Y^- \to \Lambda^0 + \pi^-$:	60 ± 15	67 ± 12

As already mentioned, the three V-events listed in Table VIII giving light meson secondaries with « anomalous » Q-values ($Q = 72^{+17}_{-8}$, 65 ± 20, 36 ± 10) may be examples of cascade decay. In the last case, however, one would have to assume an error in Q of slightly more than twice the standard deviation in order to make this interpretation possible.

5·6. – Conclusions.

a) There is evidence for a positive particle with the two alternate decay schemes

$$Y^+ \to p + \pi^0 ,$$

$$Y^+ \to n + \pi^+ ,$$

and with Q-values of about 116 and 111 MeV respectively. The corresponding values of the primary mass and for the energies of the secondary particles in the frame of reference where the primary particle is at rest are: $M_Y = 2332\ m_e$; $M_Y c^2 = 1189$ MeV; $E_p = 1.8$ MeV; $E_n = 18.1$ MeV; $E_\pi = 93$ MeV.

b) There is evidence for a negative particle with the decay scheme:

$$Y^- \to \pi^- + \Lambda^0$$

and a Q-value of about 67 MeV, from which one obtains: $M_Y \cong 2590\ m_e$; $E_\pi \cong 58$ MeV; $E_{\Lambda^0} \cong 9$ MeV.

c) There is some evidence for a negative particle with the decay scheme:

$$Y^- \to n + \pi^- ,$$

which could be the negative counterpart of the Y^+-particle described under *a*), and could have essentially the same Q-value as this particle.

d) The mean life of the charged hyperon $Y^+ \nearrow p + \pi^0$, $Y^+ \searrow n + \pi^+$ is considerably shorter than the mean lives of the charged heavy mesons discussed in Sect. 5·4, for most of the charged hyperons recorded in photoemulsions appear to decay in flight, whereas most of the heavy mesons appear to decay at rest. It appears to be of the order of 10^{-10} s, and therefore of the same order of magnitude as the mean life of neutral hyperons. In contrast to this, we recall that charged heavy mesons have a considerably longer mean life than neutral heavy mesons.

The question of the mean life of charged hyperons is discussed in detail in the paper by AMALDI in these *Proceedings*.

TABLE IX. – *Cloud chamber data on V⁰-particles different from Λ⁰ or θ⁰.*

The Q-value computed for an assumed decay scheme $K^0 \to \pi^+ + \pi^-$ represents also a lower limit for the Q-value corresponding to an assumed decay scheme $\tau^0 \to \pi^+ + \pi^- + \pi^0$.

Reference	Positive Secondary			Negative Secondary			ϑ	Q-value	
	p	I/I_0	m	p	I/I_0	m		$Y_0 \to p + \pi^-$	$K_0 \to \pi^+ + \pi^-$
Manchester									
[1] 1	300	—	—	120	—	—	85°	—	114^{+19}_{-14}
13	580	—	—	800	—	—	14°	—	64^{+30}_{-20}
—	—	—	$< m_p$	—	> 1	—	—	—	50 ± 10
[2] —	124^{+54}_{-29}	~ 10	> 800	176^{+29}_{-21}	$\lesssim 2$	π, μ	—	64^{+18}_{-13}	
Princeton									
[3] 79-166	372 ± 100	< 2	< 1200	87 ± 15	< 3	< 400	36.5°	—	66 ± 24
80-206	325 ± 100	< 2.5	< 1400	262 ± 40	< 2	< 800	32.5°	82 ± 24	45 ± 17
Indiana									
[4] 328	250	—	—	390	—	—	29.6°	—	50
R429	860 ± 40	—	—	490 ± 50	—	—	$19.7 \pm .1$	—	86 ± 6
C.I.T.									
[5] 8796	570 ± 130	1-1.7	< 1200	120 ± 5	1.5-3	220-420	44°	—	116 ± 30
56337	240 ± 65	1-1.7	< 600	390 ± 30	1-1.7	< 830	63°	—	148 ± 30
59824	124 ± 10	1-2	< 310	365 ± 55	1-1.7	< 780	61°	—	96 ± 16
12590	493 ± 33	< 1.4	< 840	249 ± 12	< 1.3	< 385	34°	—	79 ± 10
15329	940 ± 100	1-1.7	< 2000	1420 ± 300	1-2	< 3500	8°	343 ± 80	45^{+25}_{-12}
(*) 19143B	260 ± 20	1-2	< 640	87 ± 4.5	1.3-3	160-300	40°	—	41 ± 5

(*) Appearing together with a normal θ°. $Q > 165 \pm 20$ if K" originates from any of the observed nearby interactions.

REFERENCES

[1] K. H. BARKER: *Proceedings of the Bagnères Conference*, 1953.

[2] K. H. BARKER: *Proceedings of the Duke Conference*, 1953.

[3] G. T. REYNOLDS: *Proceedings of the Duke Conference*, 1953.

[4] R. W. THOMPSON, J. R. BURWELL, H. O. COHN, R. W. HUGGETT, C. J. KARZMARK and Y. B. KIM: *Proceedings of the Rochester Conference*, 1954.

[5] V. A. J. VAN LINT, C. D. ANDERSON, E. W. COWAN, R. B. LEIGHTON and C. M. YORK Jr.: *Phys. Rev.*, **94**, 1732 (1954).

6. – Neutral V-Particles Different from Λ^0 or θ^0-Particles.

6·1. – Experimental Evidence.

Table IX contains a list of neutral V-events observed in cloud chambers, which can be interpreted neither as Λ^0-decay, nor as θ^0-decays. In some cases there is evidence that the primary particle is a neutral hyperon, in some cases the interpretation in terms of a neutral heavy meson appears more likely, in other cases one does not find in the experimental data any indication in favor of either assumption.

6·2. – Neutral Heavy Mesons Different from θ^0-Particles.

Several V^0-events have been observed in which the two secondary charged particles are light mesons but which, if interpreted as two-body decays with π-meson secondaries, give Q-values considerably smaller than 214 MeV. Thus there is definite experimental evidence for the existence of neutral heavy mesons with a decay scheme different from the θ^0-decay described in Part 2. The apparent Q-values do not seem to cluster around any single figure. One is thus led to the assumption that the « anomalous » events correspond to a three-body decay process.

The possible existence of a neutral τ-meson, with the decay scheme:

$$\tau^0 \to \pi^+ + \pi^- + \pi^0 \tag{6.1}$$

has been suggested. If one assumes that this particle has the same mass as the charged τ-meson (an hypothesis obviously without any solid foundation) one finds a Q-value of 79 MeV for the above process. Seventy-nine MeV is also an upper limit for the apparent Q-value, computed under the (erroneous) assumption of a two-body decay (see Sec. 2·1*b*).

Examination of Table 6.1 shows that many of the « anomalous » V^0-events are actually consistent with the τ^0-decay. However, some events, if interpreted according to the decay scheme (6.1), give, as a lower limit for Q, a value considerably greater than 79 MeV. One could, of course, assume that the mass of the τ^0-meson is considerably greater than that of the charged τ-meson. The C.I.T. group, however, has suggested that some of the « anomalous » V^0-events may represent an alternate mode of decay of the θ^0-particle:

$$\theta^0 \to \pi^{\pm} + \mu^{\mp} + \nu\,. \tag{6.2}$$

From the value of the θ^0-mass, one finds a Q-value of 244 MeV for this decay scheme (VAN LINT, ANDERSON, COWAN, LEIGHTON, and YORK, 1954).

The C.I.T. group has also tentatively suggested the existence of a neutral particle decaying into a heavy meson and a light meson:

$$K^0 \to K^{\pm} + L^{\mp} . \tag{6.3}$$

The only experimental argument in favor of this decay scheme is a neutral V-event in which the negative secondary particle appears to be heavier than a π-meson but lighter than a proton (LEIGHTON, WANLASS and ANDERSON, 1953). However, according to a private communication from LEIGHTON, it now seems that this event can be interpreted as the decay of a K^+-particle travelling upward.

6·3. – Neutral Hyperons.

The following experimental evidence exists for neutral hyperons different from Λ^0-particles.

a) The C.I.T. group has observed a few neutral V-events in which the positive particle is heavier than a π-meson and which, if interpreted according to the decay scheme:

$$Y^0 \to p + \pi^- \tag{6.4}$$

yield Q-values considerably different from 37 MeV. According to a private communication from LEIGHTON, the two cases of highest quality give $Q = 22 \pm 3$ MeV, and $Q = 80 \pm 12$ MeV.

b) The C.I.T. group (COWAN, 1954) has also reported a neutral V-event with the following characteristics:

Positive secondary: $p = (165 \pm 25)$ MeV/c; undergoes π-μ decay in flight.

Negative secondary: $p = (875 \pm 80)$ MeV/c; $I/I_0 = 1.70 \pm .19$;

$$m = (1\,850 \pm 250)\ m_e .$$

(The angle between the secondary tracks is $\vartheta = 23°.2$).

If one assumes the existence of a negative proton and explains the event whith the decay scheme:

$$Y^0 \to p^- + \pi^+$$

one obtains

$$Q = 11.7 \pm 4 \text{ MeV} .$$

If one assumes the decay scheme:

(6.5) $$Y^0 \to Y^- + \pi^+$$

with a mass of 2 332 m_e for the Y^--particle (see Part 5), one obtains

$$Q = 15 \pm 6 \text{ MeV} .$$

Notice that if the decay scheme (6.4) is correct, the Y^0-particle would be an « anti-hyperon » in the sense of Dirac's theory, and should have been produced simultaneously with an ordinary hyperon by materialization of energy. If, instead, one interprets the event according to the decay scheme (6.5), the Y^0-particle would be an ordinary hyperon and could represent a « second excited mass state » of the neutron.

7. – Nuclear Absorption of Negative Heavy Mesons and Negative Hyperons.

There have been observed processes of nuclear disintegrations following the absorption of negative particles at rest, which cannot be explained as due to the nuclear absorption of π^--mesons because of one of the following reasons:

a) mass measurement on the primary particle;

b) energy release in star;

c) presence of π-mesons and/or Λ^0-particles among the disintegration products; in most cases the event appears to be due to the nuclear absorption of negative heavy mesons, but in some cases the primary particle seems to be a negative hyperon.

7·1. – Observations with Photoemulsions.

These are summarized in Table X. As already pointed out, some of the events listed in Table VIII as hyperon decays could well be cases of negative hyperon capture.

7·2. – Observations with Cloud Chambers.

The Manchester group (BARKER, 1953) has reported the following event: a primary, negative particle of mass 1 100-2 000 m_e stops in a plate in a magnet chamber. A V^0 appears to emerge from the plate in the backward direction.

TABLE X. – *Nuclear absorption of negative particles in photoplates.*

Star: p = proton, d = deuteron, α = α-particle, t = triton. r = recoil, f = unidentified fragment, π = π-meson, e = electron E_π is the kinetic energy of the π-meson. E_{tot} is the total kinetic energy of the charged decay products.

Reference		Primary Mass	Star	E_π	E_{tot}	Interpr.	Remarks
Tata							
[1]	K_1^-	1000^{+720}_{-400}	2p, 1π	28	185	K^- (Y^-)	from star
	K_2^-	—	3p, 1π	29	199	K^-, Y^-, excited fragment	from star
	K_3^-	1015 ± 120	4p, 1p or d	—	>246	K^-	
	K_4^-	850 ± 95	2p	—	> 31	K^-	
	K_5^-	540^{+290}_{-170}	2p	—	>140	K^-	
Manchester							
[2]	K_1^-	1900 ± 500	1p, 1π	54	> 69	K^-, Y^-	
	K_2^-	1260 ± 400	3p	—	> 9.5	K^-	
		1060 ± 150					
Paris (E. Pol.)							
[3]		—	5f, 1π^-	—	—	K^-	
[4]		530 ± 200	1p	—	130 ± 20	K^-	
		580 ± 150					
Paris (E. Norm.)							
[13]		1745 ± 100	π^+, e, f	27	> 29	Y^- (K^-)	π - μ
Padua							
[5]	K_1^-	1070 ± 160	2p, π^-	37	96	K^-	from star
[13]	K_2^-	985 ± 150	2p	—	24	K^-	from star
	K_3^-	987 ± 120	3p, α	—	149	K^-	from star
	Y_1^-	2000 ± 300	p, f, f	—	~ 60	Y^-	from star
Rome							
[6]	K_1^-	1060 ± 50	π^-	38.5 ± 2.5	38.5 ± 2.5	K^-	from star, could be the decay of K^- particle (See Table II).
[7]	Chicago	~ 1000	p, 2π ?	15 (?)	>15	K^-	
[8]	Israel	1310 ± 245	5f	—	—	K^-	

TABLE X (*continued*).

Reference	Primary Mass	Star	E_π	E_{tot}	Interpr.	Remarks
[9, 13] Dublin	2280^{+703}_{-480} 2100^{+600}_{-800}	2p	—	~21	Y^-	
Sweden						Some doubt on interpretation. Possible min. ion. sec. may have escaped detection.
[10] K_1	905 ± 70	no visible secondary			K^- ?	
K_2	900 ± 70	» » »			K^- ?	
K_3	890 ± 90	» » »			K^- ?	
Cosmotron						
[11] K_0	1200 ± 300	1 or t, π?	50	~100	K^-	
[12] K_1	970 ± 150	p, π	50	63	K^-	π makes star
Genoa, Milan						
[13] K_1^-	1170 ± 230	*f*, Y^+	—		K^-	
K_2^-	970 ± 90	2p, e	—	25	K^-	
[14] Cornell	940 ± 200	3p, $\varkappa$, π or μ	33 ± 4	69 ± 4	K^-	This K^- ie believed to be the decay product of a charhed hyperon heavier than the charged hyperon discussed in Part 5.
[13] Bristol	2680 ± 350	p	—	100	Y^-	poss. Y^+-decay
[13] Lund	985 ± 70	p, n, *f*	—	> 22	K^-	from star

REFERENCES

[1] D. LAL, Y. PAL and B. PETERS: *Proc. Ind. Acad. Sci.*, **38**, 398 (1953).
[2] J. V. MAJOR, I. MACPHERSON, O. PARHASK and G. D. ROCHESTER: private communication.
[3] L. LEPRINCE-RINGUET: *Rev. Mod. Phys.*, **21**, 42 (1949).
[4] J. CRUSSARD: *Proceedings of the Bagnères Conference*, 1953.
[5] M. BALDO, M. CECCARELLI, M. GRILLI and B. VITALE: private communication.
[6] E. AMALDI, G. BARONI, C. CASTAGNOLI, G. CORTINI, C. FRANZINETTI and A. MANFREDINI: *Nuovo Cimento*, **11**, 207 (1954).
[7] W. F. FRY and J. J. LORD: *Phys. Rev.*, **87**, 533 (1952).
[8] S. ROSENDORF, R. STAHL and G. YEKUTIELI: *Phys. Rev.*, **93**, 901 (1954).
[9] R. H. W. JOHNSTON and C. O'CEALLAIGH: *Phil. Mag.*, **45**, 424 (1954).
[10] S. VON FRIESEN, K. KRISTIANSSON and E. ALINDER: Private communication.
[11] J. HORNBOSTEL and E. O. SALANT: *Phys. Rev.*, **93**, 902 (1954).
[12] R. D. HILL, E. O. SALANT and M. WIDGOFF: *Phys. Rev.*, **94**, 1794 (1954).
[13] *Proceedings of the Padua Conference*, 1954.
[14] Y. EISENBERG: *Phys. Rev.*, **96**, 541 (1954).

The plane of the V^0 intersects the extension of the primary particle within the plate, so that the V^0 appears to come from the point of stopping of the primary particle. The V^0 is probably a Λ^0-particle (under this assumption, one obtains from the measurements $Q = 69^{+18}_{-13}$; thus the Q-value differs from the normal Q-value of a Λ^0-particle by two standard deviations).

The M.I.T. group, operating with a multiplate chamber, has discovered the following events (DESTAEBLER, 1954).

Event 81460. – An electron shower with an energy 400 ± 200 MeV originates from the point of stopping of a particle which, from ionization and scattering, appears to be heavier than a π-meson but lighter than a proton.

Event 86407. – An L-meson and a V^0-particle appear to come from the point of stopping of a particle. The plane of the V^0 contains the point where the tracks of the primary particle and that of the L-meson (extended into the brass plate) intersect. With an assumed decay scheme: $Y^0 \rightarrow p + \pi$ for the V^0-particle, one obtains $Q < 46$. Thus the V^0-particle could be a Λ^0. If this is the case, its kinetic energy is 30 ± 4 MeV. If the charged L-meson emitted simultaneously with the V^0-particle is a π-meson, its kinetic energy lies between 81 and 106 MeV. The trajectories of the V^0-particle and of the meson form an angle of 142°.

Event 81882. – A V^0-particle appears to come from the point of stopping of a charged particle in a brass plate. The V^0 is consistent with a Λ^0. If it is a Λ^0, it has a kinetic energy of 30 ± 7 MeV.

Event 93242. – A V^0-particles appears to come from the point of stopping of a charged particle in a brass plate. The V^0 is consistent with a Λ^0. If it is a Λ^0, it has a kinetic energy of 65 ± 20 MeV.

7·3. – Possible Interpretations.

The following are some of the processes that may occur when a K^--particle enters a nucleus:

(7.1) $\quad K^- + p \rightarrow p + \pi^-$

(7.2) $\quad K^- + (p, n) \rightarrow$ excited nucleus

(7.3) $\quad K^- + p \rightarrow n + \gamma$

(7.4) $\quad K^- + p \rightarrow \pi^0 + \Lambda^0$

(7.5) $\quad K^- + n \rightarrow \pi^- + \Lambda^0$

(7.6) $K^- + p \to \pi^- + \Lambda^+$

(7.7) $K^- + (p, n) \to \Lambda^0 +$ excited nucleus

etc. etc.

Processes 1, 2, 3 are unlikely if it is true that heavy mesons and hyperons interact strongly with nuclei only when they are in pairs. Processes 4, 5, 6, 7 are preferable from a theoretical point of view (GOLDHABER, 1953). They would be the reciprocal of the observed production process (see Sect. 2·3) $p + \pi^- \to \Lambda^0 + K^0$.

7·4. – Kinematics of the Process $K^- + n \to \Lambda^0 + \pi^-$.

The system (K^-, n) has a rest energy

$$(m_K + m_n)c^2 = 1432 \text{ MeV},$$

if we assume $m_K = m_\tau$. The combined kinetic energy of the two particles produced in the process

$$K^- + n \to \Lambda^0 + \pi^-$$

is

$$Q = (m_K + m_n - m_\pi - m_{\Lambda^0})c^2$$

or

$$Q = 179 \text{ MeV}.$$

The kinetic energies of the two secondary particles are

$$E_\pi = Q \frac{m_{\Lambda^0}c^2 + Q/2}{(m_K + m_n)c^2} = 151 \text{ MeV},$$

$$E_{\Lambda^0} = Q \frac{m_\pi c^2 + Q/2}{(m_K + m_n)c^2} = 28 \text{ MeV}.$$

These values can be changed because of the motion of the nucleons in the nucleus.

The dynamics of the process $K^- + p \to Y^+ + \pi^-$ are similar to the above, except for a somewhat smaller Q-value due to the larger mass of the Y^+.

M.I.T. event 86407 provides evidence for the process $K^- + n \to \Lambda^0 + \pi^-$. The fact that E_π appears to be too small and that the meson and the V^0 are

not colinear may be due to an interaction of the π-meson within the nucleus in which the process occurs.

In M.I.T. event 93242 the energy of the Λ^0 seems too large. This may be due to the motion of the nucleon in the nucleus in which the K^- is absorbed.

The Genoa event (Table X) provides evidence for the process $K^- + p \rightarrow \rightarrow Y^+ + \pi^-$.

In M.I.T. event 81460 the shower may be due to the decay photons of a π^0-meson arising from the process $K^- + p \rightarrow \Lambda^0 + \pi^0$.

8. – Unstable Nuclear Fragments.

Occasionally among the disintegration products of high-energy nuclear interactions one finds highly excited nuclear fragments that subsequently decay, giving rise to secondary stars. The remarkable features of these events are the large amount of energy released in the disintegration of the excited fragments and the frequent appearance of π-mesons among the products of this disintegration.

One would expect that a highly excited nuclear fragment has a very short life, and cannot travel far enough from the parent interaction to produce a separate star. In order to bypass this difficulty, it has been suggested that the unstable fragments are nuclei in which a Λ^0-particle has replaced a neutron. When the Λ^0-particle decays, the nucleus breaks up. The decay may occur in the normal fashion, with the production of a proton and a π^--meson (*mesonic decay*). Or the Λ^0 may change into a neutron without the emission of a π^--meson (non-mesonic decay). In this case a nearby nucleon must participate in the reaction to the extent of taking up some momentum.

Let Q be the Q-value of the Λ^0-decay (37 MeV), B_Λ the binding energy of the Λ^0-particle and B_n the binding energy of the neutron. Then the energy released in the mesonic decay is

$$Q - B_\Lambda + B_n = 37 \text{ MeV} + (B_n - B_\Lambda) ,$$

and the energy released in the non-mesonic decay is

$$Q + m_\pi c^2 - B_\Lambda + B_n = 176 \text{ MeV} + (B_n - B_\Lambda) .$$

A test of the above assumption is to determine whether or not one obtains reasonable values for the Λ^0 binding energy, B_Λ, from the observed energy releases. This appears to be the case in the events that can be analyzed in

some detail. It is, however, too early to determine whether or not the hypothesis of the bound Λ^0 can account satisfactorily for all decay processes of highly excited fragments.

In connection with the phenomenon here discussed, some preliminary results obtained with the Brookhaven cosmotron are worth mentioning. In a systematic search for unstable fragments, FRY found one event in 200 stars produced by 1.5 GeV π^--mesons, and 6 events in 10 400 stars produced by 3 GeV protons. The same author found 3 excited fragments in 4 400 cosmic ray stars.

BIBLIOGRAPHY

W. L. ALFORD and R. B. LEIGHTON: *Phys. Rev.*, **90**, 622 (1953).

B. M. ANAND: *Proc. Roy. Soc.*, **220**, 183 (1953).

C. D. ANDERSON, E. W. COWAN, R. B. LEIGHTON and V. A. J. VAN LINT: *Phys. Rev.*, **92**, 1089 (1953).

R. ARMENTEROS, K. H. BARKER, C. C. BUTLER and A. CACHON: *Phil. Mag.*, **42**, 1112 (1951).

R. ARMENTEROS, K. H. BARKER, C. C. BUTLER, A. CACHON and C. M. YORK: *Phil. Mag.*, **43**, 597 (1952).

M. BALDO, G. BELLIBONI, M. CECCARELLI, M. GRILLI, B. SECHI, B. VITALE and G. T. ZORN: private communication, 1954.

K. H. BARKER: *Proceedings of the Duke Conference* (1953), pp. 11-18.

H. S. BRIDGE, C. PEYROU, B. ROSSI and R. SAFFORD: *Phys. Rev.*, **91**, 362 (1953).

R. BROWN, U. CAMERINI, P. H. FOWLER, H. MUIRHEAD, C. F. POWELL and D. M. RITSON: *Nature (London)*, **163**, 82 (1949).

E. W. COWAN, C. D. ANDERSON, R. B. LEIGHTON and V. A. J. VAN LINT: *Phys. Rev.*, **92**, 1089 (1953).

E. W. COWAN: *Phys. Rev.*, **94**, 161 (1954).

R. R. DANIEL and D. PAL: private communication, 1954.

W. B. FOWLER, R. P. SHUTT, A. M. THORNDIKE and W. L. WHITTEMORE: *Phys. Rev.*, **93**, 861 (1954).

W. B. FRETTER, B. GREGORY, R. H. W. JOHNSTON, A. LAGARRIGUE, H. MEYER, F. MULLER and C. PEYROU: *Proceedings of the Bagnères Conference*, p. 113, 1953.

M. GELL-MANN and A. PAIS: *Proceedings of the Glasgow Conference*, 1954.

G. GOLDHABER: *Phys. Rev.*, **92**, 1279 (1953).

B. GREGORY, A. LAGARRIGUE, L. LEPRINCE-RINGUET, F. MULLER and C. PEYROU: *Nuovo Cimento*, **11**, 292 (1954).

R. D. HILL, E. O. SALANT and M. WIDGOFF: *Phys. Rev.*, **95**, 1699 (1954).

A. L. HODSON, J. BALLAM, W. H. ARNOLD, D. R. HARRIS, R. R. RAU, GEO. T. REYNOLDS and S. B. TREIMAN: private communication, 1954.

R. B. LEIGHTON, S. D. WANLASS and W. L. ALFORD: *Phys. Rev.*, **83**, 843 (1951).

R. B. LEIGHTON, S. D. WANLASS and C. D. ANDERSON: *Phys. Rev.*, **89**, 148 (1953).

C. O'CEALLAIGH: *Phil. Mag.*, **42**, 1032 (1951).

O. I. PAGE: *Phil. Mag.*, **45**, 863 (1954).

S. L. RIDGEWAY and G. COLLINS: *Chicago Meeting A.P.S.*, 1954.

J. M. ROBSON: *Phys. Rev.*, **83**, 349 (1951)

G. D. Rochester and C. C. Butler: *Nature*, **160**, 885 (1947).
G. D. Rochester and C. C. Butler: *Reports on Progress in Physics*, **16**, 364 (1953).
M. Schein, D. M. Haskin, R. G. Glasser, J. Fainberg and K. Brown: *Proceedings of the Bagnères Conference* (1953), p. 166.
F. M. Smith, W. Birnbaum and W. H. Barkas: *Phys. Rev.*, **91**, 765 (1953).
R. W. Thompson: *Proceedings of the Duke Conference* (1953), pp. 11-35.
R. W. Thomspn, J. R. Burwell, R. W. Huggett and C. J. Karzmark: *Phys., Rev.* **95**, 1576 (1954).
R. W. Thompson, A. V. Buskirk, H. O. Cohn, C. J. Karzmark and R. H. Rediker. *Proceedings of the Bagnères Conference* (1953), p. 30.
V. A. J. Van Lint, C. D. Anderson, E. W. Cowan, R. B. Leighton and C. M. York: *Phys, Rev.*, **94**, 1732 (1954).
V. A. J. Van Lint, G. H. Trilling, R. B. Leighton and C. D. Anderson: *Phys. Rev.*, **95**, 295 (1954).
M. Yasin: *Phil. Mag.*, **45**, 413 (1954).
C. M. York, R. B. Leighton and E. K. Bjornerud: *Phys. Rev.*, **90**, 167 (1954); **95**, 159 (1954).

Editors' Note.

As a complement to prof. B. Rossi's lectures on fundamental particles, several contributions in form of seminars were given by some european specialists, whose texts are published hereafter.

As to the results of the École Polytechnique and of the Bristol Group, respectively reported by Prof. L. Leprince-Ringuet and Dr. M. G. K. Menon, these were the object of recent extensive publications. Their text is therefore omitted here, but the results are comprised in the Tables of the above lectures by Prof. B. Rossi.

SUPPLEMENTO AL VOLUME II, SERIE X
DEL NUOVO CIMENTO

N. 1, 1955
2° Semestre

Results on Heavy Mesons.

M. CECCARELLI

Istituto di Fisica dell'Università - Padova
Istituto Nazionale di Fisica Nucleare - Sezione di Padova

We will discuss here briefly some results of the Padua nuclear emulsion group concerning the existence of a K-meson decaying into a charged π-meson and, probably, a π^0-meson. We will also present data on the nuclear capture of negative K-mesons (*).

1. – $K_{\pi 2}$-mesons (χ-mesons).

In the scanning of two large stacks of stripped emulsions, flown during the Sardinian Expedition, there have been found 13 K_1-meson events with « thin» secondaries.

TABLE I.

Event	PRIMARY			SECONDARY			
	Total length	Length /plate	Mass	Total length	Length /plate	$p\beta$ at emission	Mass
	mm	mm		mm	mm		
K-Pd_3	42.6	4.5	964±60	21	6.5	160±10	275±33
K-Pd_7	36.5	7.0	945± 50	24	17.0	159± 9	278±30
K-Pd_{11}	4.9	1.6	1132±100	45	10.0	172± 8	283±27
Average			962±40			164± 6	
K-Pd_8	27.0	1.7	1100±135	44.4	16.4	149± 8	197±25

(*) For a more ample discussion see M. BALDO, G. BELLIBONI, M. CECCARELLI, M. GRILLI, B. SECHI, B. VITALE and G. T. ZORN in *Nuovo Cimento*, 1, 1180 (1955).

Measurements have been carried out fully only on those events for which the primary track was long enough to exclude definitely the possibility of a hyperon, and in which the secondary track was longer than 20 mm with a path greater than 5 mm per plate.

In this way there have been selected four events the data of which are listed in Table I.

The masses of the primary particles have been determined with the standard methods (scattering and ionization versus range) which we will not discuss here in detail. We would like however to discuss briefly the method used for identifying the secondary particles.

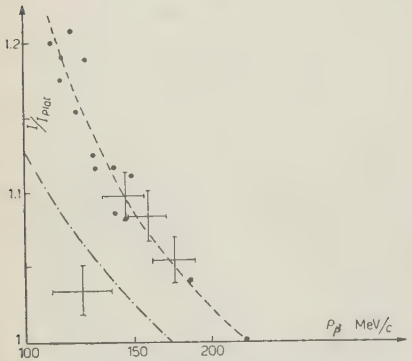

Fig. 1.

For this purpose we have chosen π-meson tracks coming out from nuclear disintegrations, traversing the same plates traversed by the secondary of each K-meson and having grain densities as close as possible to that of the secondary track. The calibration tracks had also to traverse at least 5 mm in each plate with a total path of at least 20 mm and had to be located less than 20 mm from the track to be identified.

Both, the secondary and the calibration tracks have been submitted to identical scattering and blob density measurements; the values of blob density have been normalized to the « plateau » value deduced from fast electron tracks.

We have noted that the points « $p\beta - I/I$plateau » belonging to the four sets of tracks used for the calibration of the four secondaries were consistent with a unique curve, enabling us then to present all the points on the same graph (Fig. 1).

The $p\beta$ value used for plotting each point has been deduced from the experimental $p\beta$ values for the different portions of the track, correcting them to correspond to the comparatively small region of track where the ionization measurements were made. For the secondary tracks the $p\beta$ values indicated in the Figure do not then necessarily correspond to the $p\beta$ values at the point of emission reported in Table I.

The errors of $p\beta$ quoted in the table are only statistical and they do not take into account the « scattering constant » fluctuations. This does not, however, increase the errors on the mass of the particles but only increases by some 8% the error on the Q-values.

The mass spectrum of all the analized particles is shown in Fig. 2. It is there evident that three secondaries are very probably π-mesons and the fourth a μ-meson.

If we assume that the first three K-mesons have suffered a two body decay with emission of a charged pion of 105 ± 9 MeV kinetic energy, we can compute the mass of the $K_{\pi 2}$-meson for different values of the mass of the neutral secondary.

We obtain

	Decay	Mass of the $K_{\pi 2}$-meson
1)	$K_{\pi 2} \rightarrow \pi^+ + \gamma$	870 m_e
2)	$K_{\pi 2} \rightarrow \pi^+ + \pi^0$	950 m_e
3)	$K_{\pi 2} \rightarrow \pi^+ + (600\ m_e)$	1180 m_e

Comparing these three mass values with the direct primary mass determination giving a value of 962 ± 40 m_e, we are led to consider the second decay process as the most probable.

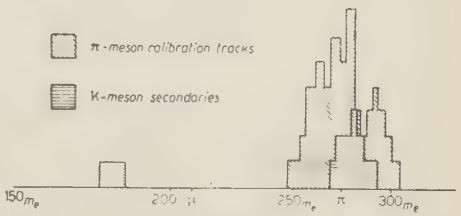

Fig. 2.

We would like to observe that the relatively high frequency of $K_{\pi 2}$-mesons in respect to the $K_{\mu 2}$ and $K_{\mu 3}$-mesons, which appears from our experiment, could be explained by the fact that with our low K_1-meson scanning efficiency ($\sim 20\%$) the $K_{\pi 2}$-mesons can be strongly favoured since they have secondaries at about 1,2 times the minimum ionization, in comparison with the K_1-mesons which have approximately minimum ionization secondaries.

2. – Negative K-mesons.

In Table II are summarized some of our results on the nuclear absorption of negative K-mesons.

TABLE II.

Event	Capture star products	Total visible energy including binding energy and π-meson rest masses
K^--Pd_1	$2P + 1\pi^-$	252 MeV
K^--Pd_2	$2P$	40 »
K^--Pd_3	$3P + 1\alpha$	178 »
K^--Pd_4	$3P$	75 »
K^--Pd_5	$1P + 1\pi$	250 »
K^--Pd_6	$1P + 1\pi$	210 »

The average mass value for the primary particles turns out to be $1007 \pm 74 m_e$.

It would seem to us premature to make any remark on the behaviour of K^--meson capture stars. We will just observe that in one of the stars a track is seen which is probably due to a 7 MeV α-particle, thus making it reasonable to assume that the capture has occurred in a light nucleus.

This may indicate that at least some of the K^--mesons are not very weakly interacting particles.

From our experiment we can tentatively deduce some frequencies for the different types of heavy mesons. The frequencies are deduced by estimating our scanning efficiency for the different particles; this was done using the results of an unbiased Bristol experiment (see MENON report).

The estimated frequencies are:

Events	K_1	$K_{\pi 2}$	$\tau+\tau'$	K^-
Number/cm³day	3	0.8	0.5	0.5

The numbers refer to a stack of $15 \times 10 \times 2.4$ cm³, not surrounded by absorber, flown at an altitude of 27 km and at 41° N (geomagnetic latitude).

These frequencies are of course approximate. We will only remark that if we assume, as is possibly indicated by some cloud chamber experiments, that the τ-mesons have a large positive excess it follows that not all of the K^- events can be ascribed to the nuclear capture of τ^--mesons.

SUPPLEMENTO AL VOLUME II, SERIE X
DEL NUOVO CIMENTO

N. 1, 1955
2° Semestre

On the Identification of Charged Hyperons and the Establishment of Their Decay Schemes in Nuclear Emulsions.

A. BONETTI

Istituto di Scienze Fisiche dell'Università - Milano
Istituto Nazionale di Fisica Nucleare - Sezione di Milano

1. – Introduction.

In September 1953 Prof. POWELL gave at this Summer School an account of the evidence for the existence of charged unstable particles of hyperprotonic mass (1). He discussed the nature of these hyperons and the various types of decay-schemes which had been proposed.

After one year the number of examples has considerably increased and on some of them it has been possible to make precise measurements. However our knowledge of charged hyperons is still largely conjectural.

In one of the preceding lectures Prof. ROSSI has given a general survey of the up-to-date information obtained both from Wilson chamber and nuclear emulsion. To this lecture I shall refer freely in the following, while discussing in detail the nuclear emulsion evidence. The experimental data are contained in Table VIII of ROSSI's lectures (2).

2. – Mass of the primary particles.

Mass measurements on the primary particles have supplied the essential information that there exists a group of unstable particles of mass definitely different from that of the other unstable particles observed up to now in

(1) *Proceedings of 1953 Varenna Summer School*, in *Suppl. Nuovo Cimento*, **11**, 165 (1954).

(2) See also the *Report of the Committee on Charged Hyperons*, in *Proc. of Padua Conf., Suppl. Nuovo Cimento*, **12**, 448 (1954).

nuclear emulsions. The mass measurements on the single particles give values which are widely spread between 1800 and 3000 m_e, around a mean of abour 2400.

On the other hand, it is well known that the accuracy and resolving power of the methods of mass measurements are rather low, and give neither a precise value of the mass of the primary particles, nor the possible fine structure of the mass distribution (the same difficulty is met in the case of K-particles). Indeed, it is easily shown [3] that, when the errors are large as is often the case in nuclear emulsions, the identification of a single particle with one or another of the known particles is not unambiguous even if the masses differ considerably. So, some of the events described as charged hyperons could be K-mesons, and viceversa.

3. – Mass of the secondary particles and possible decay-schemes.

More precise information is given by the analysis of the decay. It takes place both at rest and in flight. The fact that decays in flight are more frequently observed than those at rest suggests that charged hyperons have a mean life shorter than that of K-mesons [4], which decay mostly at rest. This fact is useful in the identification of hyperons decaying in flight.

The secondaries of charges hyperons in part are recognized as protons, in part are presumably of smaller mass. Following ASTBURY *et al.* [5], we distinguish the two cases with the symbols Y_p and Y_L respectively. Making use of the Wilson-chamber notation, we apply the prescript S and V to both symbols to indicate if the decay takes place at rest or in flight.

a) SY_p-*events*. – In these events a hyperon comes to rest and a proton emerges. In all the examples known to date, the range of the secondary is $\sim 1675\ \mu$.

These events could be interpreted either as decays or as interactions following the nuclear capture of the primary particle. This latter possibility is supported by the existence of σY-events [6], that is to say of low energy stars produced by the capture of negative hyperons. The fact that, apart from the above SY_p-events, no examples of either single proton or deuteron emission in a σY-events has been observed, might be explained by the difficulty in picking it out from the background of proton and deuteron scatterings, when the

---

[3] C. DILWORTH, S. J. GOLDSACK and L. HIRSCHBERG: *Nuovo Cimento*, **11**, 113 (1954).

[4] See paper by E. AMALDI, in these *Proceedings*.

[5] *Proc. of Padua Conference* (1954), loc. cit.

[6] *Proc. of Padua Conference* (1954), loc. cit.

secondary particle is a few hundred microns long. This difficulty would occur also in the case of hypothetical hyperons decaying to protons of very short range.

In fact, the uniqueness of the range of the secondary protons in the known examples of SY_p-particles hints very strongly at a 2-body decay into a proton and a neutral particle.

In this case we can make an assumption as to the nature of the neutral secondary. That the second particle is a π^0 is suggested by analogy with the well established decay-scheme of the neutral hyperon Λ^0 and by the presence of charged π-mesons among the secondaries of Y_L-particles (see **3-***c* and **3-***d*). With these assumptions we obtain from the conservation of momentum and energy:

(1)
$$Y_p \rightarrow p + \pi^0 + Q^{(1)}$$
$$p^{*(1)} = (190 \pm 2) \text{ MeV/c}$$
$$Q^{(1)} = (116 \pm 2) \text{ MeV}$$
$$M_{Y_p} = (2\,327 \pm 2)\ m_e .$$

b) VY_p-*events.* – They appear as 2-branch stars in which one of the particles (the secondary) is a proton, the other one (the primary) moves towards the centre of the star. This is assumed to be the point of decay.

It is useful to distinguish two cases:

i) the secondary proton has a velocity in the laboratory system greater than that of the primary near the centre of the star. In the 2 examples of this type which have been published, the mass and the velocity of the primary are such as to justify the interpretation of the events as decay processes. If we make use of decay-scheme (1), we find a value of the momentum p^* in the centre-of-mass system in fair agreement with that obtained from the analysis of events SY_p. So it seems reasonable to consider these VY_p-events as decays in flight of the same particle of mass 2327 defined above.

ii) When the secondary proton has a velocity smaller than that of the primary at the point of decay, it is not clear whether the event is a decay, a scattering, or an interaction. Three isolated events of this type have been reported by the Bombay Group. One of them could represent the decay in flight of a particle Y_p (scheme 1); the other gives a much higher value of p^*, and could suggest the existence of other types of hyperons. While a statistical analysis of all the particles of mass intermediate between that of the proton and of the deuteron, giving rise to apparent scatterings or interactions, could possibly solve the problem, such an analysis as to my knowledge has not yet been made.

Fig. 1*a* shows the values of p^* both for SY_p- and VY_p-events.

c) SY_L-*events*. – In the few examples reported up to now, the ionization of the secondary is near the plateau value. This fact, together with the experimental value of the mass of the primary, suggests that the secondary particle cannot be a proton.

In one case (see Table I) the secondary is an L-meson (possibly a π-meson) of $p\beta = (150 \pm 35)$ MeV/c.

TABLE I. – *Secondary Particles of* SY_L- *and* VY_L-*events*.

Event	No. of examples	Ionization relative to plateau	p at emission (MeV/c)	Mass (m_e)	Notes
SY_L	4	1	?	$< M_p$	short or dipping
	1	1.15±.07	150±35	330±90	Ws_1 - possible π-meson
VY_L	3	1	?	$< M_p$	short or dipping
	1	0.98±.05	160±20	$\leqslant M_\pi$	Br_4 - L-meson or electron
	7	1.25±.1	? (short)	$e < M \leqslant M_\pi$	Bo_2 } probable L-mesons
		1.34±.02	? (dipping)		Br_1
		1.15±.05	? (dipping)		Br_3
		1	? (dipping)		Br_6
		1.25±.08	170±30		Ro_2
		1.07±.02	204±20		$GeMi_6$
		1.1 ±.02	166±17		$GeMi_7$
	3	1.26	160	330±60	Bo_1 } Suggests presence of meson
		1.6 ±.1	91±40	300±75	It_1
		1.3	120	286±30	Pd_1
	1	ends in the emulsion	55.6±1	M_π	To_1 - π^--meson producing a 2-prong σ-star

Assuming that once again we are dealing with a 2-body decay, it is tempting to assume the existence of an alternative mode of decay of the particle Y_p into a neutron and a charged π-meson. Then from the scheme

$$Y_\pi \rightarrow n + \pi^\pm + Q^{(2)} \tag{2}$$

and from

$$M_{Y_\pi} = M_{Y_p} = (2\,327 \pm 2)\ m$$

we obtain

$$p^{*(2)} = (185 \pm 2)\ \text{MeV/c}$$

and

$$Q^{(2)} = (110 \pm 2)\ \text{MeV}\,.$$

We have also $(p\beta)_\pi = (148 \pm 2)$ MeV/c. This is fairly close to 167 MeV/c which is the $p\beta$ of the π-meson emitted in the disintegration of particle $K_{\pi 2} \equiv \chi$ (the corresponding p^* is 202 MeV/c). So there is always the possibility of confusion between SY_L^- and $K_{\pi 2}$-particles, if the only reliable measurements are the $p\beta$'s of the secondaries.

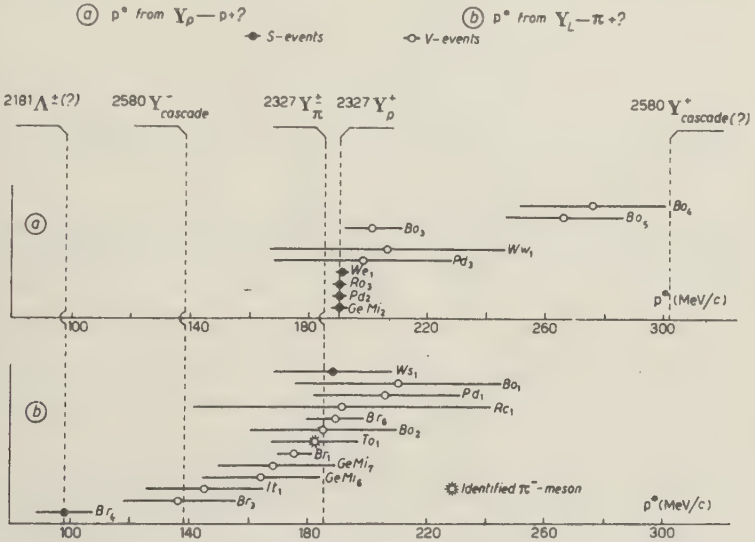

Fig. 1. – Values of p* from the decay of charged hyperons in nuclear emulsion.

d) VY_L-*events*. – Most of the hyperons known to-date belong to this group. The events appear as 2-branch stars in which one of the particles (the primary) moves towards the centre of the star; the other one is a fast singly charged particle. The available experimental data on the secondaries are given in Table I. Protons can be excluded on the basis of the mass of the primary. In one case the secondary is definitely a π^--meson (7); other cases also suggest the presence of π-mesons.

In all cases the velocities of the primary and secondary particles are such as to make improbable that some of these events represent nuclear interactions of, let us say, protons or deuterons. With the hypothesis that all these events represent the decay in flight of hyperons, a convenient way of comparing the experimental results is to calculate the momentum p^* in the centre-of-mass system, assuming a two-body decay. If we assume once again that the charged secondaries are all π-mesons, we get the distribution shown in Fig. 1*b*: we see that the single values of p^* are spread between 100 and 200 MeV/c, with

(7) A. De Benedetti, C. M. Garelli, L. Tallone and M. Vigone: *Nuovo Cimento*, **2**, 952 (1954).

rather large errors. This distribution does not give a clearcut evidence for a unique decay-scheme, nor does it give any cogent evidence for a 3-body decay.

On the other hand the observations both in Wilson chamber and in nuclear emulsions are such as to support the existence of more than one particle undergoing 2-body decay into a charged pion and particle of nucleonic or hypernucleonic mass:

i) Taking into account the large experimental errors, some or all of the VY_L-events can be explained with decay-scheme (2). It should be noted that also in this case (see 3-*c*) confusion could arise with $K_{\pi 2}$-particles decaying in flight, owing to the closeness of the values of p^*.

ii) A process which can be interpreted as the decay of a negative hyperon is the cascade process observed in Wilson chamber. It is represented by the decay scheme:

(3) $$Y^-_{\text{cascade}} \rightarrow \Lambda^0 + \pi^- + Q^{(3)}$$

with

$$Q^{(3)} = \sim 65 \text{ MeV},$$

whence

$$M_{Y^-_{\text{cascade}}} = \sim 2\,580 \text{ m}_e$$

$$p^{*(3)} = \sim 138 \text{ MeV/c}.$$

A certain number of VY_L-events with low p^* may fit this scheme.

Prof. DALLAPORTA has suggested a possible interpretation of Bombay VY_p-events with high p^* (see 3-*b* and Fig. 1*a*) which does not involve the existence of a new type of hyperon.

Indeed, if the positive counterpart of the particle Y^-_{cascade} exists, it could undergo an alternative decay of the type:

(4) $$Y^+_{\text{cascade}} \rightarrow p + \pi^0 + Q^{(4)},$$

where

$$M_{Y^+_{\text{cascade}}} = M_{Y^-_{\text{cascade}}} = \sim 2\,580 \text{ m}_e.$$

Then

$$p^{*(4)} = \sim 300 \text{ MeV/c}.$$

This hypothesis requires further experimental support.

iii) If the low value of p^* from event Y-Br$_4$ is a bona fide effect, the vent can be separated from the other low momentum examples. Then one ould introduce a hypothetical charged counterpart of Λ^0 with decay scheme

5) $$\Lambda^{\pm} \rightarrow \mathrm{n} + \pi^{\pm} + Q^{(5)}$$

$$M_{\Lambda^{\pm}} \cong M_{\Lambda^0} = \sim 2181 \ \mathrm{m_e}$$

$$Q^{(5)} \cong 36 \ \mathrm{MeV}$$

$$p^{*(5)} \cong 98 \ \mathrm{MeV/c} .$$

t has been already pointed out that a positive particle of this mass, decaying nto a proton, and a π^0, would be very difficult to observe.

. – Conclusion.

Four groups of particles of hyperprotonic mass have been observed in nuclear mulsions:

$$\mathrm{SY_p} , \quad \mathrm{VY_p} , \quad \mathrm{SY_L} , \quad \mathrm{VY_L} .$$

The p-secondaries are protons. The L-secondaries are certainly lighter han protons. In one case the L-secondary is definitely a π^-. In other cases he identification of the secondary with a π-meson is probable.

This phenomenological picture can be interpreted by means of two (or three) particles, undergoing 2-body decays into a nucleon, or a hyperon, and a pion:

$\mathrm{Y_{p,\pi'}}$	of mass (2327 ± 2) $\mathrm{m_e}$	(evidence from nuclear emulsions)
$\mathrm{Y_{cascade}}$	of mass ~ 2580 $\mathrm{m_e}$	(evidence from Wilson chamber)
($\Lambda^{\pm}$	of mass 2181 $\mathrm{m_e}$	hypothetical from nuclear emulsions)

The decay schemes are summarized in Table II.

TABLE II. – *Proposed types of charged hyperons and decay-schemes.*

Event	Particle	Decay-scheme and Q-value	Mass (m_e)	p^* (MeV/c)	Notes
SY_p	(Y_p (J_p, Ω_p)	$p+\pi^0+116$ MeV	2 327	190	very probable
VY_p	Y_p^+	»	»	»	very probable
	(Y^+ cascade)	($p+\pi^0+\sim 247$ MeV)	($\sim 2\,580$)	(~ 305)	hypothetical
SY_L	$Y_\pi^\pm$ (J_π, Ω_π)	$n+\pi^\pm+110$ MeV	2 327	185	alternative mode of Y_p; probable
VY_L	$Y_\pi^\pm$	»	»	»	alternative mode of Y_p; probable
	Y^- cascade	$\Lambda^0+\pi^-+\sim 65$ MeV	$\sim 2\,580$	~ 138	probable
	($\Lambda^\pm$)	($n+\pi^\pm+36$ MeV)	(2 181)	(98)	hypothetical

SUPPLEMENTO AL VOLUME II, SERIE X
DEL NUOVO CIMENTO

N. 1, 1955
2° Semestre

Comparison of Results on K-Particles Disintegrating at rest in Cloud Chambers and Photoemulsions.

C. DILWORTH

Istituto di Scienze Fisiche dell'Università - Milano
Istituto Nazionale di Fisica Nucleare - Sezione di Milano

B. ROSSI

Massachusetts Institute of Technology - Cambridge, Massachusetts

The amount of information available today on the mode of decay at rest of the heavy mesons, while not sufficient to allow a quantitative and unique picture to be drawn, is such as to justify a qualitative comparison between the results obtained by the two instruments most fruitful in the field, i.e., the multiplate cloud chamber and the photographic emulsion. The conclusions

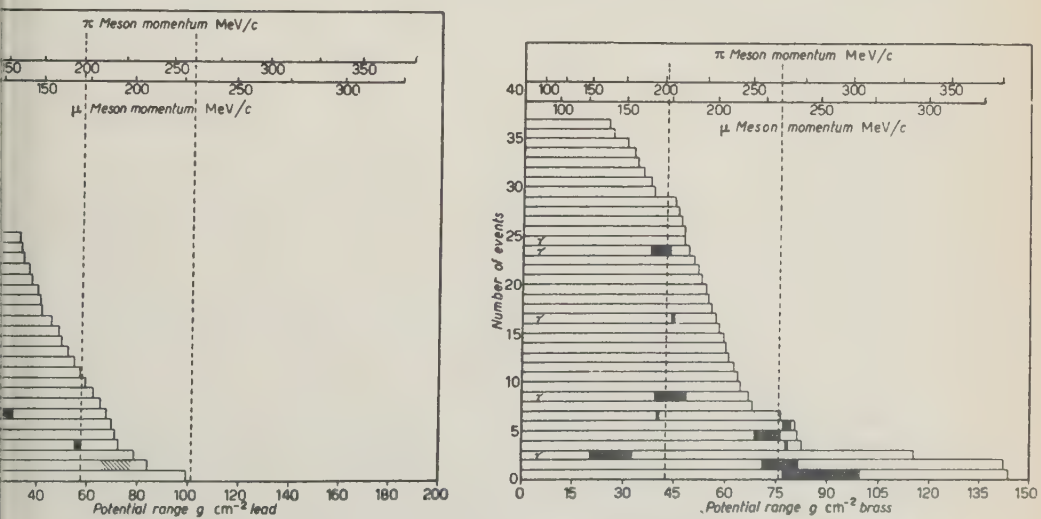

Fig. 1. – Distribution in potential and actual ranges of the secondary particles of events observed with the M.I.T. multiplate chamber: (*a*) lead plates; (*b*) brass plates: 1 g cm^{-2} Pb is equivalent to 0.75 g cm^{-2} brass.

drawn here from this comparison are, of course, subject to uncertainty due to the small statistics available.

Figs. 1 and 2 summarize some of the pertinent experimental data. Altough data on S-events are available both from the École Polytechnique and

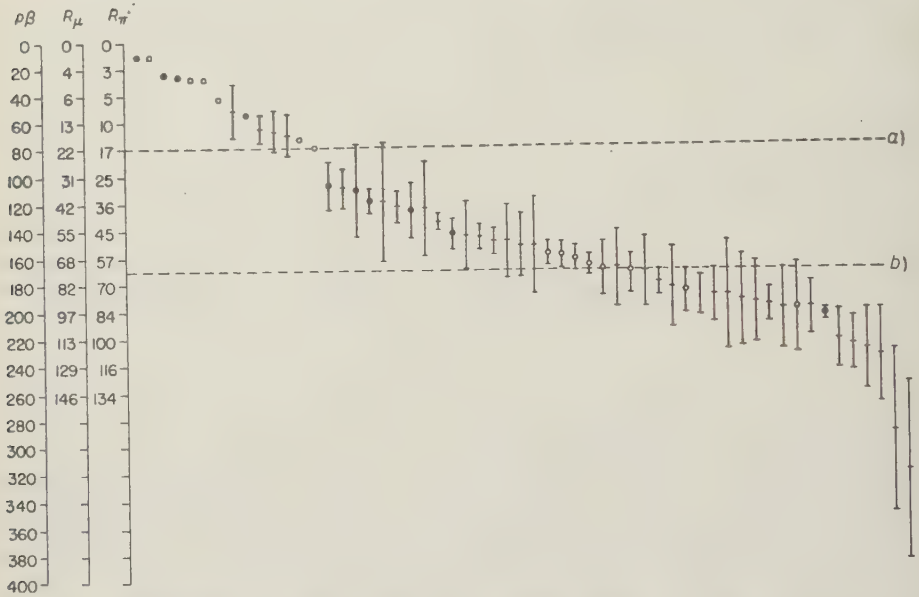

Fig. 2. – Distribution in $p\beta$ and range of the secondaries of K-particles observed to decay at rest in photoemulsions. Open dots: identified π-mesons; solid dots: identified μ-mesons.

M.I.T. chambers (see lectures of B. ROSSI in these *Proceedings*), only those of M.I.T. are represented in Fig. 1 because we have not sufficient data from E. P. to plot the potential range in their case. The two diagrams in Fig. 1 refer to S-events observed with the M.I.T. cloud chamber equipped (*a*) with lead plates and (*b*) with brass plates. Each event is represented by a rectangle of unit height, whose length indicates the potential range of the secondary particle.

Potential range is defined here as the minimum range at production that would allow the particle to escape from the chamber with nearly minimum ionization. We have taken it as equal to the thickness that the particle actually traverses (or would traverse if it were not stopped) augmented by six g cm^{-2} Pb. If the secondary particle comes to rest in the chamber, or if it is heavily ionizing at the point where it goes out of the illumination, the possible values of the actual range are shown by the black area (the shaded area in one of the Pb events refers to a case of questionable stopping). In the computation of

the range limits, no account was taken of statistical fluctuations in the ionization losses. The range straggling due to these fluctuations has a root mean square value of about three percent. The symbol (γ) indicates that an electronic shower appears to be associated with the decay. The events are arranged from the bottom to the top, in order of decreasing potential range. One thus obtains a histogram which, when properly normalized, gives the probability, $P(R)$, that, in an event taken at random, the potential range of the secondary particle has a value greater than R.

The data obtained by the group of the École Polytechnique are similar to those shown in Fig. 1. The striking feature in all cases is the small number of secondary particles stopping with ranges between 20 and 60 g cm^{-2} Pb, compared to the high proportion of particles stopping with ranges greater than 80 g cm^{-2} Pb.

Fig. 2 shows the distribution in $p\beta$ and in range of the measured secondaries of K-particles stopping in photographic emulsions. Black dots are identified μ-meson secondaries, open circles are identified π-meson secondaries. The other points represent unidentified secondaries. There appears to be here a considerable spread of values of $p\beta$, covering the whole range from zero to about 230 MeV/c, with a concentration in the region around 170 MeV/c.

We wish to interpret the evidence on the decay spectra given by the two instruments by postulating the least possible number of different decay schemes. Thus, leaving out events that give π-meson secondaries with $p\beta < 80$ MeV/c (*) and that are probably examples of the alternate mode of decay of the τ-meson ($\tau \to \pi^{\pm} + 2\pi^0$), we shall begin with the assumption of a:

One-Particle Scheme.

A decay process of the following type

$$K_{\mu 3} \to \mu + \nu + \gamma \qquad (\varkappa\text{-particle of MENON and O'CEALLAIGH})$$

would explain the spread in $p\beta$ values found in the emulsion work, the presence of μ-mesons (identified by the characteristic $\mu \to e$ decay) with $p\beta < 80$ MeV/c, and the evidence for γ-rays associated with the decay of S-particles in the multiplate chambers. It does not account for the presence of a monoenergetic π-meson group with $p\beta$ around 170 MeV/c, such as seems to be indicated by the emulsion and by the cloud chamber work.

Moreover, the assumption of a single decay process makes it very difficult

(*) The absolute maximum value of $p\beta$ for this mode of decay is 92 MeV/c.

to reconcile the $p\beta$-spectrum obtained in the emulsion work with the small number of short-range secondaries observed in the multiplate chambers. Indeed one can compute the expected number of particles that stop in a given multiplate chamber with ranges between R_1 and R_2 by means of the equation

$$N_{R_1R_2} = \int_{R_1}^{R_2} P(R)n(R)\,\mathrm{d}R\,,$$

where $n(R)$ represents the number of particles with ranges between R and $R+\mathrm{d}R$, and $P(R)$ the probability of a potential range to be greater than R. If one evaluates $n(R)$ from the $p\beta$ spectrum shown in Fig. 2 and if one takes $P(R)$ from Fig. 1*b* one finds, for example, that in the M.I.T. cloud chamber equipped with brass plates, there should have been 12 secondary particles stopping with ranges smaller than 90 g cm^{-2} Pb, and one particle stopping with range greater than 90 g cm^{-2} Pb, out of a total of 37 observed particles with ranges greater than 20 g cm^{-2} Pb (20 g cm^{-2} Pb is the μ-meson range corresponding to $p\beta = 80$ MeV/c). The actual numbers were five and five. One finds a similar inconsistency if one analyzes in the same manner the data obtained with the lead assembly in the M.I.T. chamber, or the data reported by the group at the École Polytechnique.

Such a discrepancy between the decay spectra of the same postulated particle observed with photoemulsions and cloud chambers could only be explained by the supposition that a given value of $p\beta$ corresponds to a range greater than that computed for the μ-meson; i.e., by the assumption that the secondary particles are sub-μ-mesons. For this there is no evidence, so we proceed to discuss a:

Two-Particle Scheme.

We postulate the existence of two particles:

$$\mathrm{K}_{\mu 3} \rightarrow \mu + \nu + ?\,,$$

$$\mathrm{K}_{\pi 2} \rightarrow \pi + \pi^0 \qquad (\chi\text{-particle of MENON and O'CEALLAIGH}).$$

(We refer the reader to the lectures of B. ROSSI in these *Proceedings*, as well as to the papers of CECCARELLI and DALLAPORTA, for a discussion of the experimental evidence for the existence of the $\mathrm{K}_{\pi 2}$-particle.) Notice that now the decay spectra observed with photoemulsions and with cloud chambers

ed not be identical because the two instruments may select $K_{\mu 3}$- and $K_{\pi 2}$-rticles in different proportions.

According to our new assumption, the γ-rays associated with the S-particles served in multiplate cloud chambers arise from the decay of the π^0-meson. ie $p\beta$ spectrum observed in photoemulsions is the superposition of a con-uous spectrum, corresponding to the $K_{\mu 3}$-particle, and a line spectrum cor-sponding to the $K_{\pi 2}$-particle. According to the best information available, e position of this line should be at about $p\beta = 170$ MeV/c. Because of the atively low accuracy of scattering measurements it is difficult to separate e two spectra unambiguously. However, with the explicit assumption that ere is no observational bias in scanning, and there are no large systematic ises of error in the scattering measurements, it appears difficult to escape e conclusion that the $K_{\mu 3}$-decay produces a substantial number of se-ndaries in the range of $p\beta$ between 80 and 170 MeV/c. In fact, Fig. 2 cludes 13 secondaries whose measured $p\beta$ lies between 80 and 170 MeV/c d differs from 170 MeV/c by appreciably more than one statistical error. e cannot attribute any large fraction of these low $p\beta$-values to fluctuations m the $K_{\pi 2}$-line for the following reasons:

a) Of these 13 particles the five on which mass measurements have been de tend all to be classified as μ's rather than π's (see Table I) if they are electrons.

TABLE I. – *Data on the secondaries of five* K*-particles observed in photoemulsions.*

Event	$p\beta$ (MeV/c)	I/I_0	Mass (m_e)	P_μ/P_π (*)
Br_{24}	119 ± 9	1 ÷ 1.2	203 ± 8	10^{28}
$GeMi_3$	108 ± 18	1.14 ± .03	190 ± 32	4
It_7	111 ± 35	1.1 ± 1	190 ± 60	1.5
O_1	126 ± 21	1.05 ± .03	200 ± 20	50
Br_3	144 ± 12	0.96 ± .026	170	?

(*) P_μ/P_π is the estimated relative probability that the particle should be a μ rather than π-meson.

b) The spectrum of identified π-meson secondaries (see Fig. 2) shows a r separation between the group attributed to the τ-decay and that corres-ding to the $K_{\pi 2}$-line. Of the 13 particles mentioned above, that are either tified as μ-mesons or not identified, only four carry an error in the deter-ation of $p\beta$ appreciably greater than that of the identified π's.

c) Consider the measured values of $p\beta$ in terms of their distribution in ber of standard deviations from the $K_{\pi 2}$-line (Fig. 3). If we take as cor-the errors cited (they are almost certainly underestimated) there are, for

18 particles lying within one standard deviation of the line, 13 at more than one standard deviation below it and 14 at more than one standard deviation above. Thus of the 13 particles lying below one standard deviation of the line, 10 must be considered as independent of it. If on the other hand, we believe that the errors on the scattering measurement have been underestimated (*), we still remain with the conclusion that there are as many secondaries of the $K_{\mu 3}$ with $p\beta$ less than 170 as with $p\beta$ greater than 170 MeV/c.

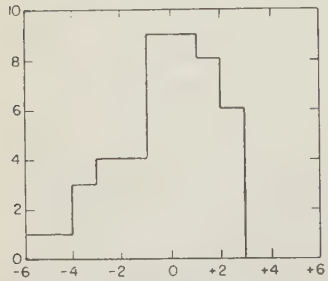

Fig. 3. – Distribution of $p\beta$ values in terms of standard deviations from the $p\beta$-line (observations with photoemulsions).

This is contrary to the cloud chamber evidence, as one can see, for example, with the following argument. The μ-meson range corresponding to $p\beta = 170$ MeV/c is 72 g cm^{-2} Pb. In the pictures taken with the brass assembly in the M.I.T. cloud chamber there are 16 events in which one can be practically sure that the potential range of the secondary particle is greater than 72 g cm^{-2}, because its measured value exceeds 72 g cm^{-2} Pb by more than twice the mean range straggling. In two cases the secondary particle comes to rest with a range of about 60 g cm^{-2} Pb; these events must be regarded as $K_{\pi 2}$-decays. In one of the remaining 14 cases the secondary particle comes to rest with a range less than 72 g cm^{-2}Pb. Its range lies between 27 and 44 g cm^{-2} Pb, and a γ-ray appears to be associated with the S-particle decay. It is natural to interpret this event too as a $K_{\pi 2}$-decay and assume that the secondary particle has undergone nuclear stopping. The other 13 cases must represent $K_{\mu 3}$-decays, according to the assumed two-particle scheme. On the other hand, from the photoplate work we have concluded that a $K_{\mu 3}$ secondary has a probability of at least $\frac{1}{2}$ to stop after traversing less than 72 g cm^{-2} Pb. Thus the probability that none of the 13 $K_{\mu 3}$ secondaries should come to rest with a range smaller than 72 g cm^{-2} Pb is $(\frac{1}{2})^{13} = 1/8\,000$. If, on the other hand, we assume that the 14 cases mentioned above are $K_{3\mu}$ decays, then there has been one secondary particle out of 14 with a secondary range less than 72. The probability for this to happen is $14\ (\frac{1}{2})^{14} = 10^{-3}$.

Thus the two-particle scheme does not solve the difficulty, and it seems necessary to consider a:

(*) Pushing to the extreme this scepticism we might be left with the conclusion that there are only $K_{\pi 2}$-secondaries in this $p\beta$ range in the emulsions. This however would still leave us to explain the μ-secondaries which stop in the emulsion, the long range particles in the Wilson chamber, and the lack of nuclear interactions in about 50 cm of K-secondaries observed to date in the photoemulsion.

Three-Particle Scheme.

If, in addition to the $K_{\mu 3}$- and the $K_{\pi 2}$-particles, one postulates the existence of a third particle, and if one further assumes that this particle appears much more prominently among cloud chamber events than among emulsion events, one can obviously explain the apparent discrepancy between the spectra observed with the two instruments. In particular, we wish to examine here the assumption that this third particle has a decay scheme of the type:

$$K_{\mu 2} \rightarrow \mu + \nu \qquad (K_\mu \text{ of the École Polytechnique}),$$

and thus produces a μ-meson of definite energy.

Altogether, the M.I.T. and the École Polytechnique groups reported 13 S-events in which the secondary particle comes to rest after traversing more than 80 g cm^{-2} Pb (see Rossi's lectures, Sec. 4·7). To decide how many of these events can be interpreted as $K_{\mu 2}$-decays we refer to Table II. The first

TABLE II. — *Consistency check of the assumption of a two-body decay for the* $K_{\mu 2}$*-particle*

Range (g cm^{-2} Pb)	90	95	100	103	105
Error (g cm^{-2} Pb)					
0	4	8	8	11	9
3	6	9	12	12	10
6	8	10	13	12	12

line in this table indicates various assumed ranges for the μ-meson from the $K_{\mu 2}$-decay; the second line shows the number of events that are compatible with each given range, if one does not make any allowance for errors due to straggling in range; the third and fourth lines show the corresponding numbers evaluated on the basis of a possible straggling error equal to one and two standard fluctuations respectively (3 and 6 g cm^{-2} Pb).

One sees that if the secondary of the $K_{\mu 2}$-decay range is near 100 g cm^{-2} Pb, all of the S-particles with long range secondaries observed in multiplate chambers can actually be interpreted as $K_{\mu 2}$-particles.

Notice that a secondary range of about 100 g cm^{-2} Pb implies a primary of about 940 m_e, close to that of the τ-meson mass.

From the foregoing, it appears that the relative numbers of $K_{\mu 3}$-, $K_{\pi 2}$-, and $K_{\mu 2}$-particles in plates and in cloud chambers must bear to one another the following relations:

in plates

$$n_{K_{\mu 3}} \gtrsim n_{K_{\pi 2}} \gtrsim n_{K_{\mu 2}},$$

in cloud chambers

$$n_{K_{\mu 2}} > n_{K_{\pi 2}} \gg n_{K_{\mu 3}} .$$

If one assumes that the difference between the relative abundances of the different particles in the two types of experiments is due to a difference in their mean lives, one arrives at the following tentative result:

$$\tau_{K_{\mu 2}} \gtrsim \tau_{K_{\pi 2}} > \tau_{K_{\mu 3}} .$$

In conclusion, it seems possible to explain the experimental evidence available today on the basis of the three-particle scheme suggested above. However, some difficulties that do not appear very significant at the present time, may become serious when more experimental information is available. They may require the consideration of other possible causes for the observed difference between the secondary spectra obtained with cloud chambers and photoemulsions. One of these causes could be a difference in the energy spectra at production of the $K_{\mu 3}$-, $K_{\pi 2}$-, and $K_{\mu 2}$-particles. Another could be the presence of an appreciable number of particles giving electron secondaries, a few examples of which have been reported recently. A fast electron may be very difficult to distinguish from a fast μ- or π-meson in the photographic emulsion, while in a multiplate chamber it can be recognized by its scattering or the cascades produced in the plates. Thus often in photoemulsion work a $K \to e$ decay will be mistaken for a $K \to \mu$ or a $K \to \pi$ decay. In cloud chamber work, on the other hand, such an event may be interpreted as a $\mu \to e$ or a $\pi \to \mu \to e$ decay and thus ignored.

Note added in proof. The data on which some of the arguments treated in this paper were based have changed since September 1954. We refer for the evidence up to date in cloud chamber to H. S. BRIDGE, H. DESTAEBLER Jr., B. ROSSI and B. V. SREEKANTAN (*Nuovo Cimento*, 1, 874, (1955)) R. ARMENTEROS, B. GREGORY, A. HENDEL, A. LAGARRIGUE, L. LEPRINCE-RINGUET, F. MULLER and C. PEYROU (*Nuovo Cimento* 1. 915 (1955)) and A. L. HODSON *et al.* (*Rochester Conf.*, 1955). For the emulsion technique some of the reasons which might have biased the early energies are set forward in A. BONETTI, R. LEVI SETTI, B. LOCATELLI and G. TOMASINI (*Nuovo Cimento* 1, 904 (1955)).

SUPPLEMENTO AL VOLUME II, SERIE X
DEL NUOVO CIMENTO

N. 1, 1955
2° Semestre

Statistical Evidence Concerning the χ-Meson Decay.

N. DALLAPORTA

Istituto di Fisica dell'Università - Padova
Istituto Nazionale di Fisica Nucleare - Sezione di Padova

I think that some more evidence may be gathered from plate work concerning the 2 body decay of the χ-meson ($K_{\pi 2}$) which was proposed already a couple of years ago by the Bristol school to occur according to the scheme:

$$\chi \rightarrow \pi + ?$$

In fact if we take from the complete table of K decays which has been collected during the Padua conference of last April, all the events for which there is some evidence, more or less strong, that the secondary is a π-meson, we obtain the following Table I.

TABLE I.

Name of event	$p\beta$ of secondary	Name of event	$p\beta$ of secondary
Br_7	170 ± 29	It_2	172 ± 26
Br_8	187 ± 17	Ko_3	223 ± 22
Br_9	162 ± 9	Ko_5	167 ± 8
Br_{15}	184 ± 30	Pd_3	160 ± 10
Br_{17}	172 ± 17	Pd_7	159 ± 9
Br_{22}	170 ± 20	Pd_{11}	172 ± 8
$GeMi_4$	200 ± 33		

If we except perhaps Ko_3 the evidence seems rather good for a unique $p\beta$ of the secondary of 167.5 ± 6 MeV/c.

Of course, in this way no account is taken of the real evidence of the secondary being a π, or of any systematical bias in the selection of the events.

If we now assume, on the evidence of the cloud chamber event in Prin-

ceton, that the secondary neutral particle of the decay is a π^0:

$$\chi \rightarrow \pi + \pi^0$$

we obtain for the Q-value of the reaction

$$Q = 215 \pm 8$$

and the mass of the χ turns out to be

$$m_\chi = 960 \pm 18$$

which seems to fit rather well with the mass of the θ^0-particle and suggests that the χ may well be the charged counterpart of it.

Prof. Rossi is of the opinion that the photons originating in his S-events in the Wilson chamber could be consistent as secondaries of the π^0.

The fact that the $\chi\theta$-particle could exist in both charged or neutral state and that the same could be said of the τ-particle (as some evidence now appears concerning the existence of the τ^0), increases the interest of considering the possibility that both decays in 2 or 3 π could be alternative modes of decay of the same particle. This of course depends on the spin and parity of the particle; the best indication concerning these data can be obtained by the energy distribution spectrum of the odd secondary π-decay product of the τ, which has been constructed with all the experimental material at the time available by the reporting Committee on τ-meson at the Padua conference; the actual evidence cannot up to now give any definite answer.

SUPPLEMENTO AL VOLUME II, SERIE X
DEL NUOVO CIMENTO

N. 1, 1955
2° Semestre

Two Examples of a Star Emitting Two Heavy Unstable Particles(*).

A. DEBENEDETTI, C. M. GARELLI, L. TALLONE and M. VIGONE

Istituto Nazionale di Fisica Nucleare - Sezione di Torino

Few examples of stars emitting either a hyperon and a heavy meson ([1,2]), or two heavy mesons ([1,3]) have been reported so far. During the regular scanning of a stack of stripped emulsions we have observed two additional cases of a star emitting two unstable heavy particles.

The first event ([4]) is a star of the type $21+7p$ from which a positive τ-meson and an excited fragment are emitted (Fig. 1). The Q value of the τ-meson is 71.4 ± 3.2 MeV and the data of the three π-mesons emitted are the following:

Charge		Energy (MeV)	Angles
π_1	$-$	$30{,}7 \pm 1{,}5$	$\varphi_{\pi_2\pi_3} = 102^\circ\,50' \pm 30'$
π_2	$+$	$17{,}06 \pm 0.85$	$\varphi_{\pi_1\pi_3} = 133^\circ\,35' \pm 30'$
π_3	$+$	23.61 ± 0.84	$\varphi_{\pi_1\pi_2} = 123^\circ\,34' \pm 30'$

The unstable fragment travels 1490 μ and disintegrates at rest in two charged particles whose tracks are collinear within experimental errors. The event can be interpreted as a two body decay according to the scheme

(*a*) $$^3H_1^* \rightarrow {}^3He_2 + \pi^- + Q \qquad Q = 42.06 \pm 4.2 \text{ MeV}$$

(*) Lecture given by C. M. GARELLI.

([1]) D. LAL, Y. PAL and B. PETERS: *Proc. Ind. Ac. Sci.*, **38**, 398 (1953).

([2]) W. B. FOWLER, R. P. SHUTT, A. M. THORNDIKE and W. L. WHITTERMORE: *Phys. Rev.*, **93**, 861 (1954).

([3]) E. AMALDI, G. BARONI, C. CASTAGNOLI, G. CORTINI, C. FRANZINETTI and A. MANFREDINI: *Nuovo Cimento*, **11**, 207 (1954).

([4]) A. DEBENEDETTI, C. M. GARELLI, L. TALLONE and M. VIGONE: *Nuovo Cimento*, **12**, 466 (1954).

this interpretation being supported by the following experimental data:

— the primary is singly charged, and mass measurements give the values

$$M_f = 4830 \pm 1400 \text{ m}_e \quad \text{(scattering-range with constant sagitta)}$$

$$M_f = 5300 \pm 900 \text{ m}_e \quad \text{(ionization-range)};$$

— the fast secondary goes out of the stack after a range of 17 300 μ.

From scattering and ionization we conclude that the particle is a light meson whose kinetic energy is

$$E = 39.8 \pm 4 \text{ MeV}.$$

The hypothesis that the heavy secondary is a $^3He_2$ nucleus is suggested by charge conservation and by the value of the mass of the primary. Under this assumption its energy is

$$E = 2.66 \pm 0.7 \text{ MeV} \quad \text{(from range)}$$

$$E = 2.26 \pm 0.26 \text{ MeV} \quad \text{(from momentum balance)}.$$

The good agreement of these figures strongly supports the interpretation (*a*).

In the second case ([5]) a K-meson and a neutral particle decaying in flight are ejected from a star of the type $27+9p$ (Fig. 2). The K-meson has a range of 5 700 μ and its mass results

$$M = 1020 \pm 270 \text{ m}_e \quad \text{(scattering-range)},$$

$$M = 1165 \pm 130 \text{ m}_e \quad \text{(ionization-range)}.$$

The secondary has an angle of dip of 29°; from ionization and scattering measurements over a range of 2 000 μ we obtained

$$b^* = 0.974 \pm 0.033,$$

$$p\beta = 104 \pm 24 \text{ MeV/c}.$$

from which we conclude that it is a light meson; from the $p\beta$ value it seems reasonable to assume the decay scheme

$$K(\mu) \rightarrow \mu + ? + ?$$

([5]) A. DEBENEDETTI, C. M. GARELLI, L. TALLONE and M. VIGONE: *Nuovo Cimento*, **12**, 369 (1954).

P
a
b
674
τ*
14.735
12.543
π1
π3
π2
8373
1593
300μ

Fig. 1.

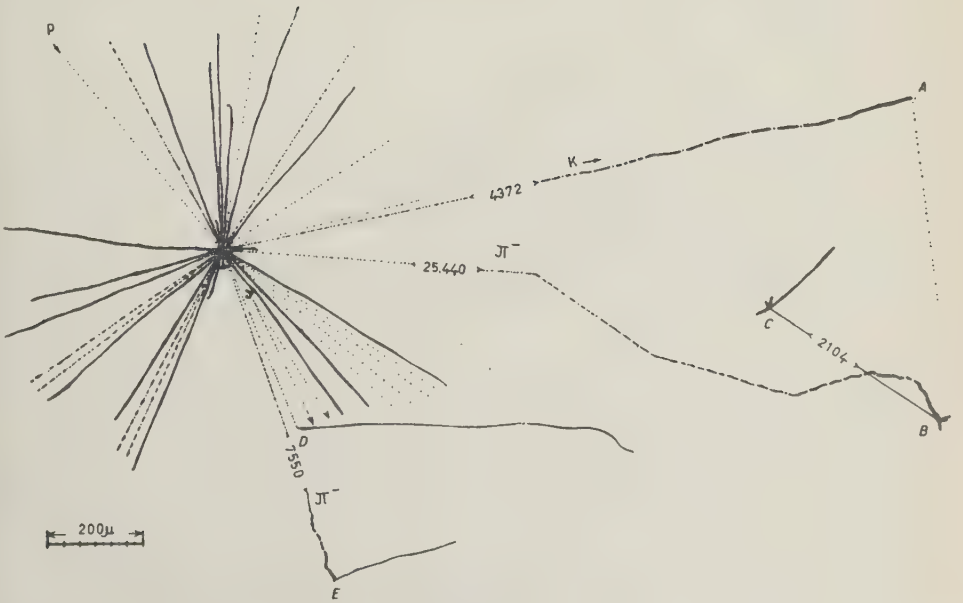
P
A
K
4372
π⁻
25.440
C
2104
B
D
7550
π⁻
E
200μ

Fig. 2.

Near the star a V-event consisting of a pair of lightly ionizing particles has been observed. The vertex of the pair is at a distance of 25 μm from the centre of the star, whose position has been determined from the intersection points of pairs of relativistic prongs. (The most probable uncertainty in this position is ± 0.18 μm). The two tracks are coplanar with the point thus determined.

We indicate by ϑ_{12} the angle between the two tracks, and by ϑ_{1p_0}, ϑ_{2p_0} the angles between each track and the assumed direction of motion of the neutral particle coming from the star:

$$\vartheta_{12} = 16^0\,43' \pm 30'$$

$$\vartheta_{1p_0} = 14^0\,52' \pm 45'$$

$$\vartheta_{2p_0} = \cdot 1^0\,53' \pm 45' .$$

From ionization and scattering measurements on the track of lower energy we can say that it is either an electron or a light meson; nothing can be said about the other track, because its ionization is very near minimum and the scattering measurements are disturbed by local distortions. We think very improbable that the V-event is an electron pair produced by a γ ray or by an abnormal decay of the type: $\pi^0 \to \beta^+ + \beta^-$. It seems more reasonable to interpret the event as a $\Lambda^0 \to p + \pi^- + 37$ MeV or as a $\theta^0 \to \pi^+ + \pi^- + + 216$ MeV.

In fact, if we assume that the measured track is a π-meson, from its momentum and from the assumed direction of motion of the neutral primary we can calculate the energy release in the two cases, and we obtain

$$Q_{V^0} = 36^{+67}_{-16} \text{ MeV} , \qquad Q_{\theta^0} = 216^{+150}_{-55} \text{ MeV} .$$

Unfortunately it is not possible to decide between the two schemes, as the identification of the more energetic particle lies in the doubtful possibility of distinguishing between the plateau and minimum ionization.

We can conclude that the hypothesis of the production of a K-meson and a neutral heavy particle (Λ^0 or θ^0) is not inconsistent with the experimental data.

SUPPLEMENTO AL VOLUME II, SERIE X
DEL NUOVO CIMENTO

N. 1, 1955
2° Semestre

On the Measurement of the Mean Life Time of Strange Particles.

E. AMALDI

Istituto di Fisica dell'Università - Roma
Istituto Nazionale di Fisica Nucleare - Sezione di Roma

1. – Introduction.

It is well known that one of the more peculiar properties of heavy mesons and hyperons consists in the fact that their mean life appears to be extremely long if compared with their rate of production.

The simple knowledge of the order of magnitude of their mean life is sufficient to prove the existence of such a difficulty whose solution probably needs the discovery of some very important feature of these new objects.

However, one can hope to learn something more about the structure of these particles and to get a hint to the solution of the above mentioned problem by establishing the values of the mean lives and the branching ratios of the various possible decay processes for each one of the species of particles.

It follows that the problem of the experimental determination of the mean life of strange particles has to be carefully considered with the double aim of extending the interval of time on which the measurements are possible, and of improving the precision of the corresponding results.

Starting from this point of view, we have devoted, during the last few months in Rome, a certain time to this problem, and I am reporting here our considerations and conclusions which refer mainly to the case of charged particles observed in nuclear emulsions.

The more direct method of measuring the mean life of a charged unstable particle is obviously that based on fast counters technique.

A first step in this direction has been made recently by MEZZETTI and KEUFFEL [1], who have given some evidence for the existence of K-particles with a mean life of about $8.7 \cdot 10^{-9}$ s.

---

[1] L. MEZZETTI and J. W. KEUFFEL: *Phys. Rev.*, in press.

This value however, is already very close to the limit than can be attained by such a technique: in fact, the resolving power of the experimental set-up of the preceding authors is of about $3 \cdot 10^{-9}$ s and it appears very difficult, at least in the immediate future, to improve it by more than a factor 2 or 3.

On the other hand, we know that many of the strange particles have life-times appreciably shorter than 10^{-9} s. For instance we know that the mean life of Λ^0 is

$$\tau = (3.7^{+0.8}_{-0.6}) \cdot 10^{-10} \text{ s},$$

and that of θ^0 is

$$\tau = (1.5^{+0.5}_{-0.3}) \cdot 10^{-10} \text{ s}.$$

It is well known that the measurements of these short life-times have been performed by means of cloud chamber observations.

On the other hand, no systematic work has been done until recently to explore the possibility of life-time determinations based on emulsion technique measurements.

Before going into the details of the methods that we have developed, I would like to draw attention to the fact that with emulsions still more than with cloud chambers and almost as well as with counters technique, the main difficulty is due to the uncertainty in the identification of the particles. Therefore, the lower limit of the life-time of charged particles that can be determined in emulsions, is imposed by the requirements for their identification. This last depends, of course, on the properties of the considered type of particles, in particular on the type of their decay process. If the decay process is so typical as to ensure the identification of the primary particle and to allow the determination of its velocity, one can push the measurements down to very short times: without going into the details of such a hypothetical case, it may be sufficient to notice that a mean life of 10^{-14} s in the laboratory frame of reference, corresponds to a mean free path of 30 μm, if the particle has a velocity close to the velocity of light.

Such a case however, is purely hypothetical and probably does not exist in practice. In general, the identification of the particle must be based on the determination of its mass, charge and velocity, apart from its decay process. This means that in general, it will be necessary to dispose of tracks of at least 1 mm lengths. It follows that for a particle of mass not very different from that of the proton and kinetic energy of about 1 GeV, the lower limit of the life-time that we can measure by means of emulsion observations, is of the order of 10^{-12} s. The existence of more than one type of particle of equal charge and very close masses, can make the identification very difficult also if their mean path is longer than 1 mm.

As regards long times, we will see in the following that in principle any life could be measured with emulsion technique, provided we dispose of a suffi-

ciently great number of identified particles. In practice, however, the intensity at disposal at present is so small that already life-times of the order of $10^{-8} \div 10^{-9}$ s are too long to be measured with any acceptable precision. This upper limit is of secondary importance because, as already stated above, other techniques can be used in these cases.

2. – The Method of Maximum Likelihood for Cloud Chamber Technique.

Before describing the methods that we propose to use with emulsion technique, I will recall very briefly one of the methods used in the case of cloud chambers, which appears to be by far the best one.

This method, developed by BARTLETT ([2]), can be presented as follows.

Let us assume that we have n identified particles of the same species, for each one of which the following quantities have been measured ([3]): the length l_r of the path crossed by the particle, between its appearence in the illuminated region and its decay, within the region where the observation of its decay is possible; the maximum length of path L_r available for the same particle, after its appearence in the illuminated region, within the region where the observation of its decay is possible, and finally the velocity β_r.

From these data, one can immediately derive their observed time of flight t_r which they spent in the frame of reference in which they are at rest, to cross the distance l_r, and their so called potential time T_r that they would have spent to cross, in the same frame of reference, the path L_r if they had not decayed.

If τ is the mean life of the species of particle under consideration, one can say that the probability that the r-th particle is observed to decay between t_r and $t_r + \mathrm{d}t_r$ having at our disposal for observation a potential time T_r, is simply given by

$$\frac{\exp[-t_r/\tau]}{1-\exp[-T_r/\tau]}\frac{\mathrm{d}t_r}{\tau}. \tag{1}$$

Therefore the probability that for fixed τ our n particles decay just at the observed moments, is given by the expression

$$G(\tau; t_1, t_2, \ldots, t_r, \ldots, t_n; T_1, T_2, \ldots, T_n)\,\mathrm{d}t_1\,\mathrm{d}t_2 \ldots \mathrm{d}t_r \ldots \mathrm{d}t_n = \tag{2}$$
$$= \prod_1^n \frac{\exp[-t_r/\tau]}{1-\exp[-T_r/\tau]}\frac{\mathrm{d}t_r}{\tau}.$$

The function G is called the « likelihood function »; according to R. A. FISHER

([2]) M. S. BARTLETT: *Phil. Mag.*, **44**, 249, 1407 (1953).
([3]) J. G. WILSON and C. C. BUTLER: *Phil. Mag.*, **43**, 993 (1952).

the best estimate of τ is the value that makes G a maximum for given values of t_r and T_r ($r=1, 2, ..., n$). This method calls for many comments and criticisms ([4]). But I will not go into any details nor will I give the final expression for the estimate of τ. In fact, discussing the case of emulsion technique, we will have the opportunity of writing down an expression of the mean life which includes, as particular case, that relative to the cloud chamber technique.

3. – The Method of Maximum Likelihood for the Emulsion Technique.

The simplest thing to do passing from cloud chambers to emulsions, consists in trying to extend the method previously described. This has been done by CASTAGNOLI, CORTINI and FRANZINETTI who have presented their report at the Padua Conference ([5]).

The main difference between these two cases is obviously due to the fact that while in a cloud chamber the particles fly keeping their velocity practically constant, in emulsions, the particles are rapidly slowed down on account of the much higher density of the medium. The time (in the frame of reference in which the particle is at rest) necessary for a particle of residual range R to be slowed down to thermal energies, is obviously given by the expression

$$t = \int_0^R \frac{\sqrt{1-\beta^2}}{c\beta} \mathrm{d}R \,. \tag{3}$$

Dividing both sides of eq. (3) by the mass M of the particle and recalling that R/M is a function only of the velocity β, one can write

$$\frac{t}{M} = f\left(\frac{R}{M}\right) = F(\beta) \,. \tag{4}$$

Making use of well known empirical expressions valid in the emulsion for the range-velocity relation, one obtains ([6])

$$\frac{t}{M} = 1.97 \cdot 10^{-13} \left(\frac{R}{M}\right)^{0.713} \tag{5}$$

for $\beta \leqslant 0.4$ (namely $R/M \leqslant 2 \cdot 10^4$ μm), where t is in seconds, M in protonic masses and R in microns, and

$$\frac{t}{M} = 2.76 \cdot 10^{-11} \left(\frac{R}{M}\right)^{0.708} \tag{6}$$

([4]) M. ANNIS, W. CHESTON and H. PRIMAKOFF: *Rev. Mod. Phys.*, **25**, 818 (1953).

([5]) C. CASTAGNOLI, G. CORTINI and C. FRANZINETTI: *Suppl. Nuovo Cimento*, **12**. 297 (1954).

([6]) E. AMALDI, G. BARONI, G. CORTINI, C. FRANZINETTI and A. MANFREDINI: *Suppl. Nuovo Cimento*, **12**, 181 (1954).

for $\beta \geqslant 0.4$, where t and M are in the same units and R in cm. By means of these two equations we can easily pass from range measurements to time measurements.

It is now clear that we can repeat the same statistical considerations that are valid for cloud chambers. Therefore equation (2) will be valid also in the case of emulsion observations.

Also in this case the lengths l_r and L_r and the corresponding times t_r and T_r refer to the region where the observation of the decay process is possible i.e., in this case, the volume actually scanned. Furthermore one has to distinguish between three types of events (5):

a) particles which are brought to rest in the emulsion and then decay;

b) particles which decay in flight inside the emulsion in such a position and with such a (vector) velocity that they would have been brought to rest in the emulsion, if they had not decayed;

c) particles which decay in flight in the emulsion and are not to be included in group *b*).

Both the events *a*) and *b*) are obviously associated with an infinite potential time; furthermore the events of type *a*) supply us different information from that supplied by events of type *b*) and *c*). While for these last groups of events we know at what instant the corresponding particles have decayed, for the particles of groups *a*) we can only state that the decay happened at a time not smaller than the corresponding moderation time t_r^0 ($r=1, 2, \ldots, n_a$) given by eq. (3).

It follows that we have to integrate equations (2) with respect to dt_1, $dt_2, \ldots, dt_{n_a}$ from the corresponding t_r^0 to infinity.

One can so find a new likelihood function whose maximum defines the best estimate of τ. One gets

$$\tau = \frac{1}{n_b + n_c}\left\{\sum_1^{n_a} t_i^0 + \sum_1^{n_b} t_k + \sum_1^{n_c}\left(t_l + \frac{T_l}{e^{T_l/\tau} - 1}\right)\right\}. \tag{7}$$

We note that in the case of cloud chambers only events of group *c*) exist and therefore the corresponding expression of τ reduces tc the last term appearing at the right hand side of equation (7).

For the expression of the statistical error by which the estimated value of τ is affected, we refer to the original paper (5).

We prefer to discuss here the systematic error which could affect our results in a substantial way.

In any measurement of the type of that considered here there are two

different sources of systematic experimental errors which are usually indicated as experimental bias.

The first one is of geometric nature, the second of kinematic origin.

With the expression geometric experimental bias we indicate the fact that as a consequence of the finite dimensions of the stack of emulsions, the percentage of particles which do not decay before excaping from the emulsion depends on their range.

The interesting feature of the method of maximum likelihood described above is that the geometric bias is eliminated by the introduction of the potential time T .

With the expression kinematic experimental bias we indicate the fact that the probability p of observation of a decay process, will be in general, a function of the velocity of the particle at the instant at which it decays. In fact, the faster is a particle, the smaller is the corresponding probability of detection of its decay. That is due, in part to the composition (in the laboratory frame of reference) of the velocity of the particle with the velocity of the corresponding decay products in its frame of reference, in part to the lower ionization of the particle itself which again is a function of the velocity.

If we could determine in some way the probability p_r of detection relative to each one of the considered events, we could obviously correct the estimated values of τ also from this source of systematic error.

In this case eq. (7) has obviously to be substituted by the following expression

$$\tau = \frac{1}{\sum_1^{n_b} \frac{1}{p_k} + \sum_1^{n_c} p_l} \left\{ \sum_1^{n_a} t_i^0 + \sum_1^{n_b} \frac{1}{p_k} t_k + \sum_1^{n_c} \frac{1}{p_l} \left(t_l + \frac{T_l}{e^{T_l/\tau} - 1} \right) \right\} \tag{8}$$

where we have made the reasonable assumption that the probability of detection of particles decaying at rest is equal to 1.

4. – The Method of Residual Time.

After the Conference of Padua where the preceding method had been presented, we tried to develop some method which would allow the evaluation and possibly the elimination of the kinematic experimental bias. This new method has the disadvantage that it does not allow a simple correction for the geometrical experimental bias.

The principle of the method is the following (7): let us consider for a mo-

(7) E. Amaldi, C. Castagnoli, G. Cortini and C. Franzinetti: *Nuovo Cimento*, **12**, 668 (1954).

ment a stack of emulsions of infinite dimension containing a source of monoenergetic particles of a well defined species. To the kinematic energy K_0 of the emitted particle will correspond a range R_0, a velocity β_0 and, according to equation (4), a moderation time t_0.

It is now obvious that in order to get some information on the mean life of the particles considered, it is convenient to describe their motion through the emulsion by means of the variable t related to the instantaneous residual range R by equation (4).

So we can say that the number of particles which decay between t and $t+\mathrm{d}t$ is given by

$$\mathrm{d}n = S \exp\left[-\frac{t_0 - t}{\tau}\right]\frac{\mathrm{d}t}{\tau} = N_0 \exp\left[\frac{t}{\tau}\right]\frac{\mathrm{d}t}{\tau} \tag{9}$$

where S is an inessential constant expressing the total number of particles emitted at the instant t_0 by our source. Equation (9) shows that the number of particles decaying per unit of time varies exponentially with t (Fig. 1). All particles which decay at instants between 0 and t_0 decay in flight, while the area enclosed by the exponential at the left of the ordinate axis (negative values of t) corresponds to particles that decay at rest. This simple exponential law holds not only if the particle source is monoenergetic, but also when a value t_0 of t exists, which leaves at its right all sources of particles.

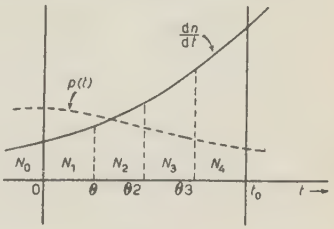

Fig. 1.

It is now evident that making use of representations of this type, we can deduce the mean life of the particles considered. For instance, we can divide the time t_0 in a certain number of intervals, all of length θ (in Fig. 1 $\theta = \frac{1}{4}t_0$) and call N_1, N_2, ... the numbers of particles decaying in each one of them.

Then one finds immediately that the following relations hold

$$1 + \frac{N_1}{N_0} = \exp\frac{\theta}{\tau}, \tag{10}$$

$$\frac{N_i}{N_{i-1}} = \exp\frac{\theta}{\tau} \qquad i \geqslant 2 \tag{11}$$

where N_0 is the number of particles decaying at rest.

In the ideal case of complete absence of any type of experimental bias, equations (10) and (11) can obviously be used to deduce τ. But also in the

case of a non negligible kinematic experimental bias we will be able not only to establish the value of τ but also to determine the probability of detections defined above in connection with the method of the maximum likelihood.

From what we have said, we have to expect that the probability of detection is a function of the ionization of the type

$$(12) \qquad \begin{cases} p(i) = 1 & \text{for } i > i_0 \\ p(i) = \left(\dfrac{i}{i_0}\right)^{\alpha} & \text{for } i \leqslant i_0 \end{cases}$$

where i_0 and α are two convenient empirical constants. Considering that i is a function of the velocity, one can express p as a function of t. We will get a curve of the tpye of that given in Fig. 1 (dotted line).

Let us assume now that we can choose such a small value of θ that all (or almost all) the particles decaying in the interval $0 \leqslant t \leqslant \theta$ have a probability of detection equal to 1.

Then equation (10) will be correct (or almost correct) and we can use it in order to calculate $e^{\theta/\tau}$ and τ. Once we know $e^{\theta/\tau}$ we can compare it with the experimental ratios n_i/n_{i-1} ($n_i = \eta_i N_i$) and deduce the average efficiency of detection relative to the successive intervals

$$(13) \qquad \frac{\eta_i}{\eta_{i-1}} = \frac{n_i}{n_{i-1}} \exp\left[-\frac{\theta}{\tau}\right] \qquad i \geqslant 2 ,$$

where

$$(14) \qquad \eta_i = \frac{\int_{(i-1)\theta}^{i\theta} \exp[t/\tau]\,\rho(t)\,\mathrm{d}t}{\int_{(i-1)\theta}^{i\theta} \exp[t/\tau]\,\mathrm{d}t} .$$

The knowledge of the η_i is sufficient to give some information on the experimental bias. But one can go further and introduce in equations (14) some well chosen expression for $p(t)$ containing a few parameters which can be adjusted to give the experimental values of the η_i.

For such a purpose one can make use of the expression (12) or, in order to have an expression still simpler in the sense that it contains a single adjustable constant T,

$$(14) \qquad p(t) = 1 \quad \text{for} \quad t \leqslant 0 ; \qquad p(t) = \exp[-t/T] \quad \text{for} \quad t > 0 .$$

Once we have determined the values of the constants appearing in the chosen expression of $p(t)$ we drop the assumption $\eta_1 = 1$, we calculate η_1 and repeat the preceding procedure.

In such a way, it is possible to get, by successive approximations, a value of τ which has been corrected for the kinematic experimental bias.

The above described procedure of successive approximations gives a correct result only if all the ranges of the particles involved in it are short with respect to the dimensions of the stack of emulsions. If this condition is not satisfied the geometrical experimental bias will affect the results.

In this case the best procedure consists in applying the method of residual time so as to determine by successive approximations $p(t)$, and once known the $p_k = p(\beta_k)$ for each one of the available events, estimate τ by means of equation (8).

Finally, I would like to note that, as long as the assumption that p is a function only of the velocity and therefore of the residual time t, the effect of the kinematic experimental bias on the estimate of τ with the method of maximum likelihood is in part compensated by the fact that in equations (7) and (8) appears only the observed time of flight and not the residual times.

5. – A few Examples of Application of the Preceding Methods.

We can now try to apply the preceding methods to the observations collected up to now on the strange particles.

The only case which allows an attempt to be made is that of the hyperons.

By making use of 20 cases in which particles of mass larger than that of protons have been observed to decay or to interact according to the scheme,

$$\begin{aligned} &Y^+ \to p + \pi^0 + 117 \text{ MeV} \\ &Y^\pm \to n + \pi^\pm + 115 \text{ MeV} \\ &Y^- + \text{nucleus} \to \text{star} \end{aligned}$$

and assuming that they are all due to the same type of particle, we obtain

$$3 \cdot 10^{-10} \geqslant \tau \geqslant 0.5 \cdot 10^{-10} \text{ s} ,$$

where the upper limit is deduced by means of the method of maximum likelihood, and the lower limit by means of the method of residual time estimating generously the kinematic experimental bias. The data available up to now are too scarce to allow any attempt at successive approximations. The value given above has to be taken, keeping in mind that we are not sure that all the events used are due to the same particle: therefore it must be considered only as a first attempt while the correct value will be deduced later when many more examples of well identified hyperons will be available.

In the case of τ-mesons it is not possible to apply either of the two methods

described above. Out of 43 well established examples of τ-mesons, no one has been observed, up to now, to decay in flight. On the other hand, the sum of all the corresponding moderation times is about $0.9 \cdot 10^{-8}$ s. Therefore we can conclude that probably the mean life of τ-mesons is not much shorter than 10^{-8} s, provided we can exclude that the lack of observations of τ-mesons decaying in flight might be due to the kinematic experimental bias. This seems to be the case because the decay process of τ-mesons is so typical that the probability of observation of decay processes in flight is expected to be close to 1.

One can add that also cloud chamber observations seem to indicate a mean life of τ-mesons not shorter than 10^{-8} s.

The situation is quite different for all other types of K-mesons known today, whose process of decay consists in the emission of a single charged particle. In these cases, the kinematic experimental bias can completely alter our observations and therefore any considerations of the type of that made for τ-mesons loses significance.

In spite of that, in occasion of a discussion held with B. Rossi at Varenna, Mrs. Scarsi and Vitale have calculated for various groups of K-mesons, the sum of the corresponding moderation times. Their data are collected in the following Table I.

Table I.

Number of events	Identification of the secondarv	$p\beta$ of the secondary	Total moderation time
82	unidentified L-meson		$11.4 \cdot 10^{-9}$
11	π-meson	—	$1.4 \cdot 10^{-9}$
13	μ-meson	50 MeV/c	$1.1 \cdot 10^{-9}$
9	μ-meson	50 MeV/c	$0.6 \cdot 10^{-9}$
Total 115	-	—	$14.5 \cdot 10^{-9}$

These 115 processes of decay at rest have to be compared with a single case of decay in flight. However, from this data no conclusion can be derived on the mean life of K-mesons unless at least some rough estimate of the kinematic experimental bias has been established.

SUPPLEMENTO AL VOLUME II, SERIE X
DEL NUOVO CIMENTO

N. 1, 1955
2° Semestre

Unstable Fragments.

R. Levi Setti

Istituto di Scienze Fisiche dell'Università - Milano
Istituto Nazionale di Fisica Nucleare - Sezione di Milano

The first example of delayed disintegration of a heavy unstable fragment was described by Danysz and Pniewski in 1952 [1]. The heavy splinter was emitted by a cosmic ray induced star and after a path length of 90 μ it seemed to stop in the emulsion and give rise to a secondary star of 4 branches. The high energy release visible in the secondary star ($\sim$ 90 MeV) was incompatible with any known reaction of delayed disintegration of excited nuclei. Danysz and Pniewski showed that the most simple interpretations of the event, in terms of familiar phenomena, were rather improbable:

a) the probability that the supposed secondary star was a random star in chance coincidence with the end of the fragment, was very small;

b) the fact that the fragment was practically stopped together with the high energy of the secondary star ruled out that the latter was produced by nuclear interaction of the fragment with a nucleus of the emulsion;

c) the long lifetime of the fragment made it very unlikely that the secondary star was due to the delayed deexcitation of a nuclear excited state of the fragment.

They therefore proposed two new explanations:

d) the fragment was emitted with a π-meson bound in a Bohr orbit and the secondary star was the result of the reabsorption of the π^-;

e) the secondary star was provoked by the decay of a Λ^0 bound to the fragment in place of a neutron.

Later observations have confirmed that *a*), *b*) and *c*) can be discarded and also *d*) has been ruled out in most of the cases, due to the fact that the energy release in many of the disintegrations is greater than the rest mass of the π^-. The remaining explanation *e*) (the Λ-fragment hypothesis), has received on the other hand great support from the evidence accumulated to date and seems the most appropriate to explain the greatest part of the known cases.

Since 1952, the increased knowledge of unstable particles has led to the formulation of two other possible interpretations:

f) capture of a K^-, bound to the fragment in a Bohr orbit;

g) association to the fragment of charged and neutral hyperons other than the Λ^0. (This possibility was also advanced by [1]).

While in some cases the events can be interpreted by *e*), *f*) or *g*), there is only one event, that of FRY and SWAMI [2], which seems incompatible with the hypothesis of the Λ-fragment and needs to be explained by either *f*) or *g*).

In what follows we shall assume the Λ-fragment hypothesis to be valid and in this light consider the experimental results. The terminology adopted is that of CHESTON and PRIMAKOFF [3, 4].

1. – Nature of the Disintegration Products.

The presence of a π-meson amongst the disintegration products of some examples of unstable fragments, suggests a first classification of these fragments into two classes; those which undergo mesonic and non-mesonic decay. Of the first type, 8 cases are known, and in 3 of them the meson was identified as a π^- from the σ-star produced at the end of its range.

Another 19 cases of decay in which visible (charged) mesons are not emitted are available from the literature. However, with the limitations suggested by [5], 5 of these are considered doubtful due to the shortness of the tracks of the fragments so that the number of more definite non mesonic decays reported up to now is about 14. The possibility cannot be excluded that some of these represent π^0-mesonic decays.

All the experimental data concerning primary and secondary particles are listed in Tables I*a* (mesonic decays) and I*b* (non-mesonic decays) (*).

Apart from π-mesons, the products of both mesonic and non-mesonic decays include protons, deuterons, tritons, α-particles and heavy recoil fragments.

The frequency of occurrence of the two modes of decay, mesonic or non mesonic, seems to depend on the mass number of the fragments. The 8 cases of mesonic decay are given by fragments of tritium and helium only, whereas the 14 cases of non mesonic decay, except two cases of helium disintegration, are all given by heavier fragments. The branching ratio mesonic/non-mesonic decay thus appears to be a rapidly decreasing function of the atomic number.

(*) The code-words suggested in *Supplemento* to *Il Nuovo Cimento*, n. 2, **12**, 1954, have been used to indicate the laboratories quoted in this paper. The following new code words have been introduced:

TABLE 1*a*. – *Mesonic Decay*.

Event	Parent Star	R_F (μ)	Z_F	Energy per nucl. (Mev)	Time of flight (s)	DISINTEGRATION PRODUCTS (Identity and Energy (MeV)) 1	2	3	4	Q (MeV)	Disintegration scheme	A (MeV)	B_n (MeV)	B_Λ (MeV)
$Ge\text{-}Mi_1$ [16]	22+3n	13000	1	32.7	$2.5\cdot10^{-10}$	π^- (σ5) 39.4±1.0	^{3}He 2.7±0.6			41.7±1.0	$^3H^* \rightarrow {}^3He+\pi^-+Q$	5.5±1.1	6.2	0.7±1.1
To_1 [17]	21+7p	1490	1	9.5	$5\cdot10^{-11}$	π 39.8±4	^{3}He 2.66±0.7			4.2±42	»	5.9±4.2	»	0.3±4.2
Pd_6 [18]	16+2 (?)	2200	1	11.9	$6.5\cdot10^{-11}$	π^- (σ1) 39.3±0.8	^{3}He 2.6±0.6			41.6±1.0	»	5.4±1.1	»	0.8±1.1
Ww_5 [6]	37+7p	520	1	5	$2\cdot10^{-11}$	π 50±15	^{3}He 2.6±0.2				»			
Bh_1 [19]	6+0π^- (π^-1,5GeV)	260	2	6.5	10^{-11}	π 26.0±0.7	p 5.3	^{3}He 3.5		35±0.8	$^4He^* \rightarrow {}^3He+p+\pi^-+Q$	18.5±1	20.5	2±1
Pd_3 [18]	12+3p	3380	2	28.3	$6\cdot10^{-11}$	π^- (σ1) 32.1±1.2	p 2.6	^{3}He 0.25		35±1.2	$^4He^* \rightarrow {}^3He+p+\pi^-+Q$	18.5±1.3	20.5	2±1.3
							d 3.3	^{4}He 0.27		35.8±1.2	$^6He^* \rightarrow {}^4He+d+\pi^-+Q$	−2±1.3	1.9	3.9±1.3
Mnn_2 [20]	4+0K$^-$	97	2	3.5	$5\cdot10^{-12}$	π^- (ρ) 24.2±0.5	p 8.9±0.2	^{3}He 1.1±0.2		34.2±0.9	$^4He^* \rightarrow {}^3He+p+\pi^-+Q$	17.7±1	20.5	2.8±1
Ep_1 [21]	30+30p	68	2-3	2.8	$>4\cdot10^{-12}$	π 25^{+4}_{-3}	p 2.7	^{3}He 0.55		28.2±4	$^4He^* \rightarrow {}^3He+p+\pi^-+Q$	11.7±4	20.5	8.8±4
								^{6}Li 0.9		28.6±4	$^7Li^* \rightarrow {}^6Li+p+\pi^-+Q$	−1.1±4	7.2	8.3±4

TABLE 1b. – *Non Mesonic Decay.*

Event	Parent star	R_F (μ)	Z_F	Energy per nucl. (MeV)	Time of flight (s)	DISINTEGRATION PRODUCTS (Identity and Energy (MeV)) 1	2	3	4	Q (MeV)	Disintegration scheme	Δ (MeV)	B_n (MeV)	B_Λ (MeV)
Ww_4 [15]	31+14p	190	2	5.3	$8\cdot10^{-12}$	p (prob.) 93	d (prob.) 17			140-180 150-185 140	$^3He^* \rightarrow 2p+n+Q$ $^4He^* \rightarrow p+d+n+Q$ $^4He^* \rightarrow 2p+2n+Q$			
Os_1 [21]	12+4p	243	2	6.2	10^{-11}	p 44	p 44			> 88	$^4He^* \rightarrow 2p+2n+Q$			
Loi_1 [22]	16+0p	219	2-3	5.8 (He)	$> 10^{-11}$	p (prob.) 48 ± 3	p-d-t-α 4 (p)	p-d-t-α 1.6 (p)						
Ww_2 [15]	18+14n	80	3-4	3.6 (Li)	$> 4\cdot10^{-12}$	p (prob.) 40	p-d-t-α 3.1 (p)	p-d-t-α 1 (p)		> 80				
Wsc_2 [2]	22+9p	192	3-4	6.2-7.5	$> 7\cdot10^{-12}$	π 45 ± 18 or p 300 ± 125	α 14	p-d-t 2.7 (p)	p-d-t 20-24 (p)	> 92 > 328	possible mesonic decay			
Pd_1 [9]	10+7p	170 ± 5	4	7	$6.5\cdot10^{-12}$	p 80	p 17	p (prob.) 10.5	p (prob.) 3.8					
Rc_1 [23]	18+4p	88.8	4	5	$4\cdot10^{-12}$	α 27.0	p 5.5	p 4.4			$^8Be^* \rightarrow {}^4He+2p+2n+Q$ $^9Be^* \rightarrow {}^4He+2p+3n+Q$			
Wsc_1 [24]	(17+5)?	55	4	3.6	$3\cdot10^{-12}$	α 43	α 39			170 ± 3 176 ± 3	$^8Be^* \rightarrow {}^3He+{}^4He+n+Q$ $^9Be^* \rightarrow {}^4He+{}^4He+n+Q$	15.7 ± 3 2.9 ± 3	19 1.7	3.3 ± 3 -1.2 ± 3
Go_1 [25]	27+4p	262	4	9.1	$9\cdot10^{-12}$	α 14	α 12			195 ± 3 > 104	$^9Be^* \rightarrow {}^4He+{}^4He+n+Q$ $^9Be^* \rightarrow {}^4He+{}^3He+2n+Q$			

							25 ± 5							
Mnn_1 [27]	24+10p	30	4-7	2.2-2.8	10^{-12} (^{14}N)	p (ass.) 125	p-d-t 5.2 (p)	$^{12}_{5}$B 10.4		140.5 ± 11	$^{14}_{7}N \rightarrow ^{12}_{5}B + 2p + Q$	-10 ± 11	10	20 ± 11
Pd_7 [18]	12+3p	70 ± 4	4-7	4-5.6	$> 2.5 \cdot 10^{-12}$	p-d-t 8.2 (p)	Recoil 4 μ							
Lu_1 [28]	out	1400	9	40	$2 \cdot 10^{-11}$ decay at 5-10 μ residual range	α 32	p (ass.) 10-15	$Z > 2$ (4-5) μ						
Pd_4 [18]	20+3p	65 ± 5	>3			d 34	p-d-t 23 (p)	p-d-t 3 (p)						
Pd_2 [9]	11+1p	9 ± 2			$8 \cdot 10^{-13}$ (Li)	p 32.5	d 21.5	p 11.7						
Ww_3 [15]	18+1p	13				p (prob.) 30	p (prob.) 3.8							
Mo_1 [29]	13+1n	2				p (ass.) 23.6	p (ass.) > 6.5	p (ass.) > 5.4	p (ass.) 5					
Ca_1 [30]	12+5p	~ 5				p (ass.) ~ 25	p (ass.) < 25	short	short					
Pd_5 [18]	12+0p	< 5				p-d-t 48-55 (p)	p-d-t 19 (p)	p-d-t 2.8 (p)						

2. – Relative Frequency of Emission of Unstable Fragments.

If it is assumed that a neutron is replaced by a Λ^0 in a fragment, the probability of finding a Λ^0 in a fragment might well be proportional to the number of neutrons in it. As suggested by DANISZ [6], one can compare the frequency vs. charge distribution of stable fragments, weighted accordingly to the number of neutrons in each type of fragment, with the frequencyvs. charge distribution of unstable fragments (see also GRILLI and LEVI SETTI [5]).

Fig. 1 shows a plot of the weighted frequency $N(A-Z)$ versus Z for stable fragments ejected from stars having $N_h \geqslant 8$ [7,8] normalized to the N vs. Z distribution of unstable fragments, including in the plot only the 8 mesonic decays and 13 of the better defined non-mesonic decays. Both stable and unstable fragments belong to a comparable velocity interval of emission, in the plot of stable fragments only stable Be nuclei are included. In several unstable fragments, the charge was estimated not only from direct measurements, but also from the complete charge balance of the decay products.

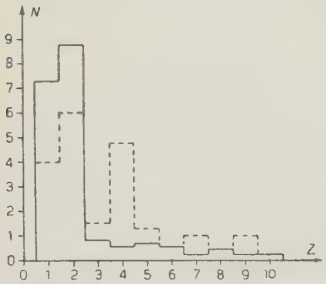

Fig. 1. – Normalized plots of the frequency vs. charge distribution of unstable fragments (broken line) and of the $N(A-Z)$ vs. Z distribution of stable fragments (full line).

The two distributions are sufficiently similar, considering the small statistics as yet available, to show that the assumption made is not incompatible with the experimental evidence. The lightest unstable fragments observed up to now are tritons, and no unstable deuterons have been observed.

3. – Lifetime of Unstable Fragments.

Since all the examples represent decays at rest or practically so, the lifetimes of excited fragments are longer or at least equal to their stopping times. Only inferior limits can therefore be assigned to mean lifetimes, and are 10^{-11} s for the lightest fragments of charge 1 and 2, and some units of 10^{-12} s for the heavier. The difference is simply due to the shorter time of flight of the heavier fragments taking into account the energy interval of emission, and therefore a dependence, if existing, on A of the lifetime would be likely to be masked by this effect.

In addition the detection of decays in flight, which could give a measure of the mean lifetime, is rendered difficulty by experimental bias [5].

4. – Energy Spectrum of the Nucleons Ejected in the Decay.

The energy of the nucleons emitted in mesonic decays is limited to a few MeV, while it extends from a few MeV to over 100 MeV, in non-mesonic decay. The bulk of the spectrum is in the low energy region in which the discrimination of protons from α-particles is difficult.

In the extended tail at the higher energies, the particles represented are largely protons. The presence of these high energy protons is of some interest in the study of non-mesonic decay. In fact, if one assumes that the non-mesonic decay is due to the reabsorption of the π^- liberated in the decay of the Λ^0, one should expect to observe an energy spectrum of protons similar to that arising in the capture of π^- in light nuclei. On the contrary, the frequencies of emission of protons of energy greater than 30 and 80 MeV from unstable fragment disintegrations, 9/14 and 4/14 respectively, are one and two orders of magnitude greater than the corresponding frequencies in π^- captures in light nuclei. Non mesonic decays must therefore be interpreted in terms of processes other than π^- reabsorption.

5. – Energy Releases and Binding Energy of the Λ^0 in the Fragments.

Non-mesonic decays are usually caracterized by a large energy release, often greater than 100 MeV, but always less than 175 MeV (except in the case of [2]), the upper limit to be expected in the case of complete conversion of the mass difference between the Λ^0 and the neutron into kinetic energy of the decay products.

The energy release in the mesonic decay has been found to lie close to the Q of the free Λ^0 (37 MeV). In some cases the Q could be determined accurately from energy and momentum balance and slight systematic differences revealed between the energy release in the break up of the fragment and that of the free Λ^0. The 8 cases of this type represent two typical decay processes:

1) $$^3\mathrm{H}^* \rightarrow {}^3\mathrm{He} + \pi^- + Q\,,$$

2) $$^4\mathrm{He}^* \rightarrow {}^3\mathrm{He} + \mathrm{p} + \pi^- + Q\,.$$

In process (1) one of the decay products of the Λ^0 is visible (π^-) while the second recoils bound to the other two nucleons into a ^{3}He nucleus; in process (2) both products are visible, together with the recoiling residual nucleus of ^{3}He.

The four tritium disintegrations in the 8 cases of mesonic decays, do not

leave alternative possibilities to the interpretation as they satisfy all conservation principles only by scheme (1); the observed Q values are 41.7 ± 1, 41.6 ± 1, 42 ± 4.2 and 52 ± 15 MeV. These figures strongly suggest that the energy release is unique and the weighted mean of the first three more accurate values gives $Q = (41.7 \pm 0.7)$ MeV.

Of the four remaining mesonic decays, one fits only scheme (2) (Mnn_2), with a Q of (34.2 ± 0.9) MeV, two also fit the same scheme with Q of (35 ± 0.8) MeV (Bh_1) and (35 ± 1.2) MeV (Pd_3), but they could also be interpreted in terms of less probable ^{5}He and ^{6}He disintegration respectively, the last (Ep_1) fits ^{4}He disintegration with a Q of (28 ± 4.2) MeV, but has an alternative explanation as ^{7}Li break-up. On the basis of what has been found in tritium, it is reasonable to assume that also helium fragments should have a unique energy of excitation. Relying on the most probable interpretation (process (2)), for the first three cases one finds that the energy release is in fact consistent with a unique Q-value, obtained from the average of them, of (34.7 ± 0.5) MeV.

From the knowledge of the Q of the Λ^0 [10] and of the energy release in the decay process, the binding energy of the Λ^0 in the fragment can be deduced.

For this it is convenient to introduce the quantity Δ defined by:

$$\Delta = \sum m_i + Q - M - (M_\Lambda - M_n) = B_n - B_\Lambda, \tag{3}$$

where B_n is the binding energy of a neutron in the fragment, B_Λ the binding energy of the Λ^0, m_i are the masses of the decay products, Q is the visible energy release of the disintegration, M is the mass of the stable fragment corresponding to the Λ-fragment, and $M_\Lambda - M_n$ the mass difference between the Λ^0 and the neutron.

A better understanding of the meaning of Δ in equation (3) is obtained by establishing an energy level scheme. This is done in Fig. 2*a* and 2*b* for tritium and helium respectively. The horizontal broken lines represent the levels which the Λ-fragments should occupy if the Λ^0 be-

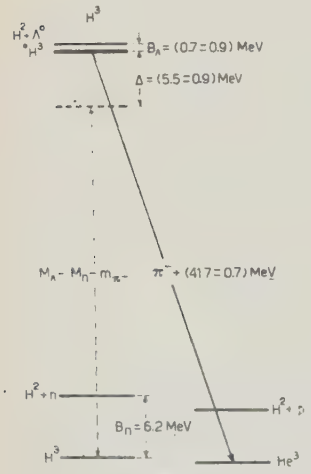

Fig. 2*a*.

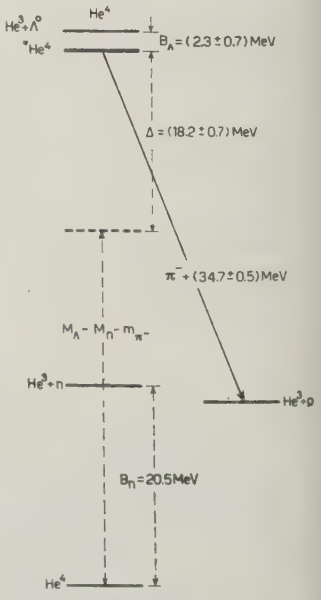

Fig. 2*b*.

haved as a neutron. It can be seen that Δ acquires the physical meaning of an excitation energy of the Λ-fragment, released during the decay in addition to $(M_\Lambda - M_n)\, c^2$.

For both tritium and helium disintegrations, Δ is positive and equal to (5.5 ± 0.9) MeV and (18.2 ± 0.7) MeV respectively. The binding energy of the Λ^0 is $(0{,}7 \pm 0{,}9)$ MeV in tritium and (2.3 ± 0.7) MeV in helium nuclei, to be compared with the binding energy of a neutron in these nuclei, equal to 6.2 and 20.5 MeV respectively.

It seems therefore established that the binding of the Λ^0 in Λ-fragments of tritium and helium is weaker than that of a neutron.

An evaluation of Δ and B_Λ can be made in only two cases of non mesonic decay; a precise determination of the Q of the reaction is rendered often impossible by the complexity of the disintegrations, when these decays are observed in nuclei heavier than ^{3}He and ^{4}He. The available data are insufficient to draw a definite conclusion on the binding energy of the Λ^0 in fragments of $Z > 2$. Moreover for this type of events, although there exists a general agreement with the Λ-hypothesis, it cannot be excluded that some individual case is due to one of the two possible processes *f*) or *g*).

6. – Origin of Unstable Fragments.

A clear cut picture of the mechanysm of production of unstable fragments is not yet available. The only information that transpires is the following.

All unstable fragments found to date arise from disintegrations of heavy nuclei of the emulsion, Ag or Br, as indicated by the number of heavy tracks in the parent stars. These stars seem to be induced mostly by charged primaries and are in general characterized by a large evaporation; the average number of dense tracks N_h is 19. The number of ejected shower particles is variable within wide limits.

The most interesting cases are the production of a Λ-helium by a 1.5 GeV π^- interaction (Bh_1), the ejection of a τ-meson by the parent star of a Λ-tritium (To_1), and the ejection of a Λ-helium in a σK star (Mnn_2).

Event Bh_1 could be due [12] to a production process of the type:

$$\pi^- + p \to \Lambda^0 + \theta^0 ,$$

the Λ^0 being ejected in a bound state to a fragment; event To_1 would suggest a production process:

$$\pi^+ + n \to \Lambda^0 + \tau^+ \quad \text{or} \quad p + n \to \Lambda^0 + \tau^+ + n .$$

Although one event of this type cannot provide evidence, as the ^3H and the τ-meson are ejected by a complex interaction, the probability of observing two independent rare phenomena in the same event is probably smaller than the probability of occurrence of a single process of double production, so that it seems quite reasonable to suppose that the two unstable particles are really associated. It can be pointed out that a number of events have been observed in which pairs of hyperons and K particles are produced in the same complex star.

Event Mnn_2 can be fitted [13] in one of the schemes:

$$K^- + p \to \pi^0 + \Lambda^0 ; \qquad K^- + (p, n) \to \Lambda^0 + \text{excited nucleus}$$

of which examples have been observed in cloud chamber experiments [14, 15].

7. – Discussion.

Some of these observations agree with the model of unstable fragments proposed by CHESTON and PRIMAKOFF [3] to account for the properties of the first observed examples.

This model, based on the Λ-interpretation, has been shown to hold if one of the two schemes of production in pairs holds too:

$$n + n \to \Lambda^0 + \Lambda^0 ; \qquad \pi + n \to \Lambda^0 + K$$

(a scheme of copious single production of Λ^0 cannot account in fact for life-times of Λ-fragments as long as 10^{-12} s or more as observed.

As pointed out by [3] and [16], a Λ-fragment can undergo either mesonic decay through the two reactions:

(1) $$\Lambda^0 \to p + \pi^- + 37 \text{ MeV}$$

(2) $$\Lambda^0 \to n + \pi^0 + 45 \text{ MeV},$$

or non-mesonic decay as the result of a two body interaction [16]:

(3) $$\Lambda^0 + n(p) \to n + n(p) + 175 \text{ MeV}$$

A decay through scheme (2) would give rise to apparently non-mesonic decays. Process (3) should give rise to an energy spectrum of the protons ejected with a maximum at about 80 MeV. CHESTON and PRIMAKOFF regard

the non-mesonic decay as a process formally analogous to the non-radiative transition to the ground state of an ordinary excited nucleus (internal conversion). In this case the spectrum should extend well above 80 MeV.

As we have seen in Sec. 1 and 4, both mesonic and non-mesonic decays are observed, and a high percentage of fast protons is present in the non-mesonic decays. GRILLI *et al.* [9] have shown that the greater part of the disintegrations not leading to π emission can be satisfactorily explained by the elementary process (3), however the present statistics do not exclude that the internal conversion analogy is the more suitable in certain cases.

The mean life for non-mesonic decay ought to be rather shorter (10^{-11}, 10^{-12} s) than the mean life of the free Λ^0. The branching ratio mesonic/non-mesonic decay was expected to decrease with increasing A, in accordance with the ratio of the mean life for non-mesonic decay to the mean life for mesonic decay. As shown in Sec. 1 and 3, from the experimental data only inferior limits can be assigned to the life times, which are however compatible with the above values. The dependence on A of the branching ratio for the two modes of decay is in agreement with that expected.

It was also suggested [3, 4] that Λ-deuterons should exist decaying mesonically and non-mesonically, with a life time of the order of 10^{-10} s. These have not yet been observed. Considering the low binding of the Λ^0 in nuclear matter, the absence of Λ-deuterons could be due to the absence of bound states of the $\Lambda^0 + p$ structure.

The fact that the binding energy of the Λ^0 in tritium and helium nuclei is definitely lower than that of the neutron would suggest that the interaction mechanysm between the Λ^0 and nucleons is probably different from that of nuclear forces between nucleons, since, if the forces acting between the Λ^0 and nucleons are supposed to be ordinary nuclear forces, one should expect the binding energy of the Λ^0 in a nucleus to be greater than that of a neutron, due to the greater mass of the Λ^0 and the non-operation of the Pauli exclusion principle between the Λ^0 and the neutron.

APPENDIX

In the computation of A and B_Λ in Table I, the following constants have been used:

a.m.u.	$= (931.162 \pm 0.024)$	MeV	[31]
m_e	$= (0.510984 \pm 16 \cdot 10^{-6})$	»	[31]
m_p	$= (938.232 \pm 0.024)$	»	[31]
m_n	$= (939.526 \pm 0.024)$	»	[31]
m_{π^-}	$= (139.24 \pm 0.15)$	»	[32]
m_{Λ^0}	$= (1114.45 \pm 0.5)$	»	[10]

The isotopic weights employed are those given by SEGRÉ [33].

REFERENCES

[1] M. Danysz and J. Pniewski: *Phil. Mag.*, **44**, 348 (1953).
[2] W. F. Fry and M. S. Swami: *Phys. Rev.*, **96**, 809 (1954).
[3] W. Cheston and H. Primakoff: *Phys. Rev.*, **92**, 1537 (1953).
[4] H. Primakoff and W. Cheston: *Phys. Rev.*, **93**, 908 (1954).
[5] M. Grilli and R. Levi Setti: *Suppl. Nuovo Cimento*, **12**, 466 (1954).
[6] M. Danysz: Private communication.
[7] J. Crussard: *Thésis, Faculté des Sciences, Université de Paris* (1952).
[8] D. H. Perkins: *Proc. Roy. Soc.*, A **203**, 399 (1950).
[9] M. Grilli, B. Sechi and G. T. Zorn: *Suppl. Nuovo Cimento*, **12**, 310 (1954).
[10] M. W. Friedlander, D. Keefe, M. G. K. Menon and M. Merlin: *Phil. Mag.*, **45**, 533 (1954).
[11] A. Bonetti, R. Levi Setti, M. Panetti, L. Scarsi and G. Tomasini: *Nuovo Cimento*, **11**, 330 (1954).
[12] W. B. Fowler, R. P. Shutt, M. Thorndike and W. L. Whittemore: *Phys. Rev.*, **93**, 861 (1954).
[13] K. Barker: *Duke Conference* (1953).
[14] H. De Staebler: *Phys. Rev.*, **95**, 1119 (1954).
[15] P. Ciok, M. Danysz and J. Gierula: *Nuovo Cimento*, **11**, 436 (1954).
[16] A. Bonetti, R. Levi Setti, M. Panetti, L. Scarsi and G. Tomasini: *Nuovo Cimento*, **11**, 218 (1954).
[17] A. Debenedetti, C. M. Garelli, L. Tallone and M. Vigone: *Nuovo Cimento*, **12**, 466 (1954).
[18] M. Baldo, G. Belliboni, M. Ceccarelli, M. Grilli, B. Sechi, B. Vitale and C. T. Zorn: *Nuovo Cimento*, 1180, (1955).
[19] R. D. Hill, E. O. Salant, M. Widgoff, L. S. Osborne, A. Pevsner, D. M. Riston, J. Crussard and W. D. Walker: *Bull. Am. Phys. Soc.*, **29**, 60 (1954).
[20] J. E. Naugle, E. P. Ney, P. S. Freier and W. B. Cheston: Private communication.
[21] J. Crussard et D. Morellet: *Compt. Rend.*, **236**, 64 (1953).
[22] D. A. Tidman, G. Davis, A. J. Herz and R. M. Tennent: *Phil. Mag.*, **44**, 350 (1953).
[23] J. Crussard, M. F. Kaplon, J. Klarmann and J. H. Noon: *Phys. Rev.*, **584**, 95 (1954).
[24] W. F. Fry and S. R. Whithe: *Nuovo Cimento*, **11**, 551 (1954).
[25] K. Gottstein: *Suppl. Nuovo Cimento*, **12**, 389 (1954).
[26] P. H. Barrett: *Phys. Rev.*, **94**, 1328 (1954).
[27] P. S. Freier, G. W. Anderson and J. E. Naugle: *Phys. Rev.*, **94**, 677 (1954).
[28] B. Waldeskog: *Ark. för Fys.*, **8**, n. 36 (1954).
[29] G. Lovera, L. Barbanti Silva, C. Bonacini, C. De Pietri, R. Perilli Fedeli and A. Roveri: *Nuovo Cimento*, **10**, 980 (1953).
[30] M. Ladu e N. Marongiu: Private communication.
[31] J. W. M. Du Mond and E. R. Cohen: *Rev. Mod. Phys.*, **25**, 691 (1953).
[32] F. M. Smith, W. Birnbaum and W. H. Barkas: *Phys. Rev.*, **91**, 765 (1953).
[33] E. Segrè: *Experimental Nuclear Physics* (New York, 1953), vol. 1.

Lectures on the Origin of Cosmic Rays.

B. ROSSI

Department of Physics and Laboratory for Nuclear Science
Massachusetts Institute of Technology - Cambridge, Massachusetts

1. – The Primary Cosmic Radiation.

1·1. – Geomagnetic Effects.

The primary cosmic radiation consists of protons: i.e., nuclei of hydrogen, and of nuclei of the heavier elements (*). As we shall see, there is evidence that these nuclei reach the neighborhood of the earth completely ionized.

In the neighborhood of the earth, but long before entering the atmosphere, cosmic-ray particles are deflected by the earth's magnetic field, which closely resembles that of a dipole. The theory of this effect has been developed by STÖRMER (1931, 1932, 1933), by LEMAÎTRE and VALLARTA (1933), and by VALLARTA's students. Recently, the trajectories of cosmic-ray particles have been studied experimentally, by means of a model experiment, by MALMFORS (1945) and by BRUNBERG (1953).

A particle of charge Ze and momentum p, travelling in a magnetic field B *at right angles to the lines of force*, describes a trajectory whose radius of curvature R, obeys the equation:

$$RB = pc/Ze\,,$$

where B is measured in gauss, e in e.s.u. and the other quantities in the CGS system. If we express p in eV/c, the above equation becomes:

$$300\,RB = p/Z \qquad (1.1)$$

(*) An account of the experimental work leading to this conclusion will be found in an article by B. PETERS in *Progress of Cosmic Ray Physics* (PETERS, 1952).

The quantity:

$$M = pc/Ze \tag{1.2}$$

has the dimensions of a voltage and is called the *magnetic rigidity*. Measured in volts, this quantity is numerically equal to p/Z where p is measured in eV/c, therefore, to 300 RB (R in cm, B in gauss).

The effect of a magnetic field on a particle depends only on its magnetic rigidity.

Liouville's Theorem (see Appendix II) plays an important part in the interpretation of geomagnetic effects. From this theorem it follows that if, for a particle of a given rigidity, M, there exists a trajectory reaching from infinity to a given point of the earth in a given direction, the differential directional intensity of cosmic rays at the given place, in the given direction and for the given rigidity is the same as if the magnetic field did not exist. (Differential directional intensity means number of particles per second, per unit area, per unit solid angle and per unit rigidity interval.) The above statement is valid under the assumption that *cosmic rays are distributed isotropically at large distance from the earth* (see Sec. 1·5).

The theory of geomagnetic effects shows the following.

For each point of the earth and for each direction of arrival, one can define a rigidity, M_1, such that all particles of rigidity greater than M_1 can reach from infinity to the given point in the given direction. From Liouville's theorem it follows that the intensity for rigidities greater than M_1 is the same as in the absence of the magnetic field. One can also define a rigidity, M_2, such that no particle of rigidity less

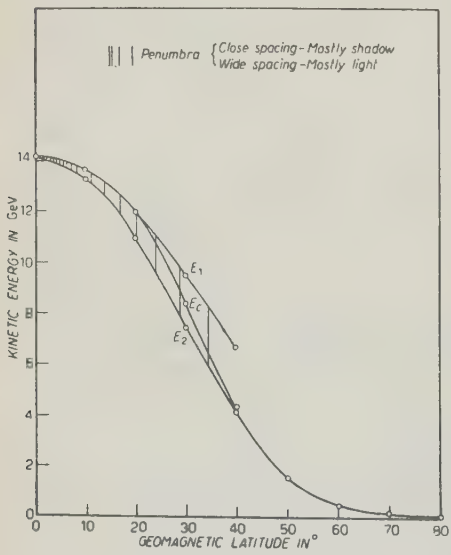

Fig. 1. – Effect of the earth's magnetic field on protons arriving in the vertical direction at various geomagnetic latitudes. The upper curve gives the kinetic energy, E_1, such that protons of energy $E > E_1$ arrive with the same intensity as if the magnetic field did not exist. The lower curve gives the kinetic energy, E_2, such that no protons of energy $E < E_2$ can reach the earth. The energy band between E_1 and E_2 is partially prevented from reaching the earth by the magnetic field. On a first approximation, however, one can assume, at each latitude, a sharp boundary, E_c between allowed and forbidden energies. The middle curve gives E_c as a function of latitude.

than M_2 can arrive from infinity. Thus the intensity is zero for $M < M_2$. For rigidities intermediate between M_1 and M_2 there are alternate « bands » of « forbidden » and « allowed » rigidities. The observable result is an « average » intensity smaller than the full intensity.

M_1 and M_2 are functions of the geomagnetic latitude, λ, and of the direction of arrival. Curves giving proton energies corresponding to M_1 and M_2 as functions of λ for different directions will be found in a paper by VALLARTA (1948). In the practical applications one often makes the simplifying assumption that the intensity is unaffected by the earth's magnetic field down to a cut-off rigidity, M_c, and is zero below M_c. M_c, of course, is intermediate between M_1 and M_2. The proton energies corresponding to M_1, M_2 and M_c in the vertical direction are shown in Fig. 1 as functions of λ.

For given zenith and azimuth angles, M_c is a decreasing function of latitude. This explains the increase of cosmic-ray intensity that one observes as one goes from the geomagnetic equator to the poles (latitude effect). For a given latitude and for a given zenith angle, M_c depends on the azimuth. For positive particles, M_c is greater in the eastern directions than in the western directions, and therefore the intensity of cosmic rays is greater in the western directions than in the eastern directions (East-West effect).

12. – Mass Spectrum of the Primary Radiation.

Most of the data on the mass spectrum of primary cosmic rays comes from observations with photo-emulsions (PETERS, 1952).

For a given velocity, the specific ionization and, therefore, to a first approximation, the grain density, are proportional to the square of the charge. Using electron-sensitive emulsions one can distinguish between protons and α-particles. Using less sensitive emulsions, one can identify somewhat heavier nuclei. The tracks of nuclei with large Z are too dense to permit grain counting. In this case, however, one can estimate the charge from the number of δ-rays, whose frequency increases as the square of Z.

Supplementary data on the relative abundance of different nuclei in the primary radiation were obtained by means of pulse ionization chambers (ELLIS, GOTTLIEB, VAN ALLEN, 1954) of cloud chambers, and of scintillation counters (STIX, 1954; reference to previous experiments will be found in this paper).

Most of the measurements were carried out with balloons, flying at altitudes where the residual pressure is about 15 g cm^{-2}. The mean free path for nuclear collisions varies from 44 g cm^{-2} for α-particles to 21 g cm^{-2} for nuclei with Z of the order of 14 (PETERS, 1952). Thus an appreciable number of nuclear collisions occur in the air layer above the balloon-borne equipment, and some of the observed light nuclei arise from fragmentation of the heavier

components. One must correct for this effect in order to determine the true composition of the primary radiation as it enters the atmosphere.

Observations at various latitudes have shown that, within the experimental uncertainties, the various nuclei of the primary radiation have similar spectra, *if these spectra are plotted as functions of the momentum per nucleon*:

$$\frac{p}{A} = \frac{Z}{A} M . \tag{1.3}$$

In other words, the *relative* abundance of nuclei for which p/A exceeds a given minimum value, $(p/A)_{\min}$, is approximately independent of $(p/A)_{\min}$. This relative abundance appears in Table I. The figures apply to the composition of the cosmic radiation in the neighborhood of the earth, but outside of the earth's magnetic field. It does not represent the composition of the radiation as it reaches the earth's atmosphere. Indeed, the minimum rigidity of the particles observed at a given place and in a given direction is the same for all nuclei. A/Z is 1 for protons but is approximately 2 for the heavier nuclei. Eq. (1.3) then shows that the geomagnetic cut-off, in terms of the momentum per nucleon p/A, is about twice as large for protons than for the heavier nuclei. Consequently, in the total radiation observed at a given place, the number of heavier nuclei relative to that of protons is greater than indicated in Table I.

TABLE I. – *Relative Abundance of Various Groups of Nuclei in Cosmic Radiation* (from PETERS, 1952, and KAPLON, 1952).

Atomic Number, Z	Percent of Particles	Percent of Nucleons
1 (protons)	91.5	69
2 (α-particles)	7.8	23
3-5	?	?
6-9	0.4	4.5
10-30	0.15	3.5
31 and over	< 0.001	—

Some uncertainty still exists as to the number of Li, Be and B nuclei in the primary radiation. These nuclei are more difficult to identify than either the lighter nuclei (H, He) whose tracks can be readily recognized from the grain density, or the heavier nuclei, whose tracks can be identified from the density of δ-rays. Moreover, the correction on account of the fragmentation of heavier nuclei is particularly large and uncertain for nuclei of the Li, Be, B group. From the recent data of KAPLON, NOON and RACETTE (1954) it would appear that these nuclei are present in the primary radiation, but are not as abundant as the nuclei of the C, N, O, F group, the abundance ratio between the two groups being 0.46 ± 0.16 (see also STIX, 1954).

One important result should be pointed out. It is possible to determine the energy of primary nuclei heavier than hydrogen from their penetration and, sometimes, from the appearance of their tracks in photo emulsions. One finds that the minimum energy of the particles observed at a given latitude coincides with the cut-off energy computed from the theory of geomagnetic effects, if the nuclei arrive upon the atmosphere completely stripped of the planetary electrons (PETERS, 1952). From this result one concludes: *a*) that the nuclei actually arrive in the neighborhood of the earth completely stripped, *b*) that the theory of geomagnetic effects is essentially correct. Notice, however, that no data of this kind have been obtained near the poles. Notice also that it has not been possible as yet to make any similar direct determination of the energy of protons.

1·3. – Absence of Electrons and Photons.

Various experimenters have looked for the possible existence of high-energy electrons and photons in the primary radiation, making use of the property of these particles of producing conspicuous electronic showers on traversing high-Z materials. Measurements with pulse ionization chambers surrounded by lead (HULSIZER and ROSSI, 1948) set an upper limit of 1 percent for the number of electrons or photons relative to that of protons at energies greater than 4.5 GeV. Cloud-chamber experiments (CRITCHFIELD, NEY and OLESKA, 1952) have reduced this upper limit to 0.6 percent for electrons above 1 GeV.

There is no information on the possible existence of electrons of energy considerably lower than 1 GeV (such electrons, of course, could be observed only near the poles).

1·4. – The Energy Spectrum of Primary Cosmic Rays.

The study of the latitude effect has provided data on the energy spectra of protons and of heavier particles at energies below 14 GeV per nucleon. Some of these data are summarized in Figs. 2, 3 and 4, compiled from the measurements of various authors (these curves are reproduced from a paper by MORRISON, OLBERT and ROSSI, 1954). In these figures, E_p is the kinetic energy *per nucleon* and J the *integral directional intensity* (number of particles of energy greater than E_p per cm^2, per s and per steradian).

The data relative to heavy particles (Fig. 4) were obtained by means of photo-emulsions flown at different latitudes. The total number of particles (Figs. 2 and 3) were measured with counter telescopes carried aloft by means of balloons or rockets. The number of protons is, at all energies, approx-

imately 10 percent smaller than the corresponding total number of particles. The solid line in Fig. 2 and the dashed lines in Figs. 3 and 4 are drawn according to a power law of the type:

$$J = \text{const} \cdot (M_p c^2 + E_p)^{-1.5}, \tag{1.4}$$

where $M_p c^2$ is the rest energy of the nucleon.

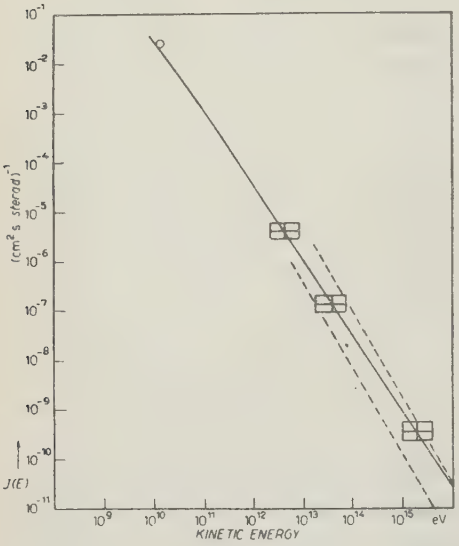

Fig. 2. – The integral intensity of cosmic rays, $J(E)$ at kinetic energies from 14 GeV to $2 \cdot 10^6$ GeV. The abscissa, E, represents the kinetic energy, E, of the particle which, for a nucleus of mass number A is A times the energy per nucleon, E_p. The experimental data indicated by squares are taken from BARRETT, BOLLINGER, COCCONI, EISENBERG, and GREISEN (1952). The point at 14 GeV corresponds to the vertical integral intensity at the geomagnetic equator. The band between the two dashed lines indicates results deduced from the observations on air showers. The solid line is the graph of the function: $J = \text{const} \cdot U^{-1.5}$ where $U = A(M_p c^2 + E_p) = (A M_p c^2 + E)$ is the total energy of the particle.

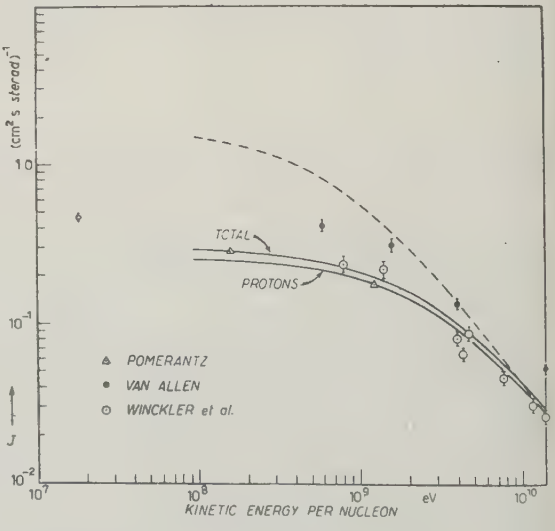

Fig. 3. – The integral intensity of primary cosmic rays at kinetic energies, E_p less than 14 GeV *per nucleon*. The upper solid curve is that suggested by BARRETT *et al.* (1952) and refers to all particles. The lower solid curve, deduced from the former by subtraction of the heavy particles, refers to protons. The circles and the triangles represent experimental determinations by WINKLER and POMERANZ, as summarized by PUPPI (1952). The dots represent measurements by VAN ALLEN (1953). The dashed line is drawn according to a power law of the type $J = \text{const}\ (M_p c^2 + E_p)^{-1.5}$.

Considering the results for the total number of particles, one sees that while the data between 2 and 14 GeV (Fig. 3) fit reasonably well the above law, those at lower energies deviate considerably from it. More recent measurements of NEHER, PETERSON, and STERN (1953) and of VAN ALLEN (1953) confirm this result. In fact, they are consistent with the assumption that the primary radiation does not contain any particle of rigidity, p/Z, less than 0.8 GeV. In any case, it appears that if particles of rigidity less than the 0.8 GeV exist, their number is less than 10 percent the number of particles above the same rigidity.

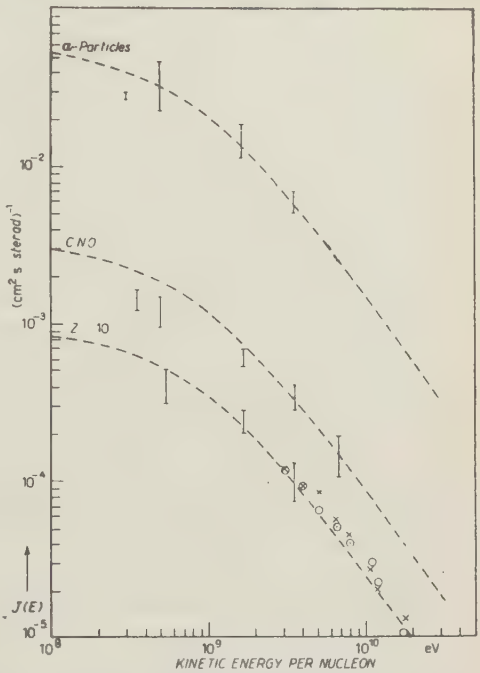

Fig. 4. – The integral intensities of heavy primary cosmic rays at kinetic energies, E_p, less than 20 GeV *per nucleon*. The experimental points refer to measurements by KAPLON, PETERS, REYNOLDS, and RITSON (1952). The dashed lines are drawn according to the power law $J = \text{const} \cdot (M_p c^2 + E_p)^{-1.5}$.

The above conclusions apply essentially to the proton component of the primary radiation, because most primary cosmic rays are protons. From the data shown in Fig. 4, it is not clear whether or not a similar low-energy cut-off exists also for the heavier components. However, recent results of ELLIS, GOTTLIEB and VAN ALLEN (1953) have shown that such cut-off actually exists. Indeed, it appears that the cut-off occurs for all particles *at the same value of the magnetic rigidity* (rather than, for example, at the same value of the momentum or the energy). This result strongly suggests that the low-energy cut-off is not a property of the source of cosmic rays, but is due rather to a shielding effect by a magnetic field in the space around the earth.

The data on the energy spectrum at energies greater than 14 GeV are more uncertain, and of a less direct character, than those at energies smaller than 14 GeV. From Fig. 2 one sees that, within the large experimental uncertainties, one can represent the integral spectrum from about 10 to about $2 \cdot 10^6$ GeV by means of the power law given by Eq. (1.4).

With reference to the experimental points we note the following. The point between 10^{12} and 10^{13} eV originates from observations by KAPLON, PETERS, REYNOLDS, and RITSON (1952) with photo-emulsions. In these experiments the energy of the primary particles was extimated from the appearance of the nuclear interactions that they were observed to produce. From the very limited number of observations available, it appears, that, in the region between 10^{12} and 10^{13} eV, the number of heavy nuclei is still roughly 10 percent of that of hydrogen nuclei.

The point at $4 \cdot 10^{13}$ eV was obtained by the Cornell group (BARRETT, COCCONI, EISENBERG, and GREISEN, 1952) from the frequency of mesons capable of penetrating to a depth of 1600 m water equivalent ($4 \cdot 10^{13}$ eV is the estimated value of the minimum energy of protons necessary to produce these mesons). The point at $2 \cdot 10^{15}$ eV also originates from experiments by the Cornell group. It is derived from the observed frequency of meson showers observed underground and associated with air showers observed above ground.

The dotted lines represent data obtained from the observation of air showers. An air shower results from a chain of interactions, nuclear and electromagnetic, initiated by a primary particle of high energy. Presumably the primary interaction gives rise mainly to charged and neutral π-mesons (even though one cannot rule out the possibility that a considerable fraction of the energy goes into the production of heavy mesons). The neutral π-mesons decay into photons, which then multiply into electronic showers. Most of the charged π-mesons interact again, producing additional charged and neutral π-mesons. The process continues for a number of generations, until the energy of the charged π-mesons becomes sufficiently small that the mesons will preferentially decay into non-interacting μ-mesons rather than undergo further nuclear collisions. One sees that a large fraction of the original energy is found eventually in the electronic component. Indeed, on a crude approximation, the number of electrons at the shower maximum is proportional to the energy of the initiating particle. However, the development of air showers is far from being fully understood in all its details, so that it would be difficult to compute the energy of a particle producing a given shower to better than a factor of two or three. Within this uncertainty, the primary energy in eV may be taken as 10^9 times the number of electrons at the maximum.

Air showers spread over large areas, with densities decreasing gradually from the shower center. When the total number of particles is sufficiently high, a shower can be detected at distances as large as 100 meters or more from the center. Thus, with a comparatively small number of detectors appropriately spaced, one can record showers whose axes strike within a large area. From the practical point of view, the large area of detection of air showers is their most important feature. It alone makes it possible to detect the high-energy particles of the primary radiation despite their exceedingly small rate

of arrival. It has been estimated, for example, that primary particles of energy greater than 10^{16} eV arrive at a rate of one per m^2 every 2 or 3 years. One needs, therefore, an area of detection of about 1000 m^2 in order to record one such particle per day.

It is not known as yet how far the cosmic ray spectrum actually does extend. Energies of 10^{16} eV appear to be fairly well established, even though it is not known whether such particles are protons or complex nuclei (in which case the energy per nucleon would be smaller in the inverse ratio of the atomic mass number). Energies greater than 10^{17} have been reported. However, one must use great caution in interpreting data on such rare events. It is always possible that, through some extreme fluctuation, a shower may exhibit abnormally high local concentrations at the places where the detectors are located, and may thus appear to have a much higher energy than it actually possesses. Only by using large numbers of detectors to sample the shower density at many different points will one succeed in minimizing the probability of such statistical errors.

One can obtain independent information on the intensity of primary cosmic rays by measuring the total energy dissipated in the atmosphere by the primary particles and by all of their secondaries. After correction for the energy disappearing in the form of neutrinos, one should obtain the total energy flux of the primary radiation.

This method yields primary intensities about two times smaller than those obtained from the direct measurements of the number of oncoming particles quoted before.

The discrepancy may indicate the existence of hitherto unknown secondary processes producing large numbers of neutrinos or of other unsuspected invisible rays. Or it may be ult mately accounted for by errors in the interpretation of our present data. For example, even at the top of the atmosphere one does not observe primary cosmic rays alone. Nuclear interactions occurring in the atmosphere below project upward particles that will be observed along with the primary radiation, if one does not use directional detectors. Moreover, some of these particles, deflected by the magnetic field, will be brought back to the earth after having gone some distance into space. They can be distinguished from truly primary rays only on account of their smaller energy. The corrections for these albedo effects are difficult to make. Even though arguments have been presented indicating that such effects are not very large, it is nevertheless possible that the primary intensity has been overestimated in their account (*). On the other hand, in estimating the energy dissipation

(*) Experiments by Perlow, Davis, Kissinger and Shipman (1952) and by Vernov and Charakhchyan (1953) appear to support this view. In both of these experiments the recording instrument was such as to discriminate effectively against

in the atmosphere it is difficult to compute the energy used to disintegrate nuclei and to produce low-energy neutrons. It is thus possible that the energy dissipation has been underestimated. In any case, the discrepancy shows that our present data on the absolute values of primary intensities may be in error by almost a factor of two.

1·5. – Time Fluctuations.

The intensity of cosmic rays in the lower atmosphere undergoes fluctuations of several percent. These fluctuations are correlated with and explained by changes in meteorological conditions (temperature and pressure of the atmospheric layer above the recording apparatus).

After correction for the meteorological effects, the intensity of cosmic rays in the lower atmosphere appears to be, on the whole, remarkably constant. In particular, daily fluctuations amount to less than 0.1 percent, indicating that cosmic rays responsible for the effects observed near sea level are isotropically distributed in the neighborhood of the earth to perhaps one part in 1000 (see Sec. 4·1). Occasionally, however, fluctuations of the order of several percent or even more have been detected. They will be discussed later (see Part 3).

Cosmic-ray effects observed in the lower atmosphere are due to primary particles with energies of the order of at least several GeV. There is some evidence that large fluctuations occur in the cosmic-ray intensity observed at high altitudes and latitudes, where the effect of primary particles with energies of the order of 1 GeV or less can be felt (*).

---

albedo rays as well as against α-particles and heavier nuclei. PERLOW and his collaborators found at 41° a proton intensity of $5.8 \cdot 10^{-2}$ cm^{-2} s^{-1} sterad^{-1}. The Russian workers found proton intensities of $1.5 \cdot 10^{-2}$ at 0°, $3 \cdot 10^{-2}$ at 31°, and $15 \cdot 10^{-2}$ at 51°. These values are considerably lower than those corresponding to the proton curve in Fig. 3.

(*) In a private communication to the writer, Dr. NEHER has pointed out that, at high latitudes and altitudes, the cosmic-ray intensity appears to fluctuate by at least a factor of 1.6 during the 11-year solar cycle. The maxima of cosmic-ray intensity seem to occur when the solar activity is a minimum. In Dr. NEHER's opinion, which is shared by the writer, these fluctuations, as well as the 27-day recurring variations and the magnetic storm effects, are « modulation » phenomena correlated with solar activity. Apparently electromagnetic fields, due to streams of ionized material emitted by the sun at all times, but with greater intensity during the periods of high solar activity, keep some of the incoming cosmic radiation away from the earth. Particles of both low and high magnetic rigidity are affected but those of low rigidity more than those of high rigidity.

6. – Energy Flux of Cosmic Rays.

From the data summarized in the preceding section, one can compute the energy flux of cosmic rays in the neighborhood of the earth, but outside the earth's magnetic field. With an uncertainty perhaps as large as a factor of two, this flux is

$$P \approx 2.2 \cdot 10^9 \text{ eV cm}^{-2} \text{ s}^{-1} \text{ ster}^{-1},$$

or

$$P \approx 3.5 \cdot 10^{-3} \text{ erg cm}^{-2} \text{ s}^{-1} \text{ ster}^{-1} \quad (*).$$

Since the cosmic radiation is practically isotropic, the corresponding energy density in the neighborhood of the earth is

$$\frac{4\pi}{c} P \approx 1.4 \cdot 10^{-12} \text{ erg cm}^{-3} \approx 1 \text{ eV cm}^{-3},$$

2. – Some Astronomical Data.

1. – The Structure of the Galaxy.

Stars are not scattered randomly through space, but are concentrated in comparatively dense groups, or *galaxies*.

Our galaxy contains approximately 10^{11} stars. It also contains diffuse matter, mainly in the form of gas, and to a much smaller extent in the form of dust (grain size of the order of 10^{-5} cm). There is about as much matter in interstellar gas as there is in stars. The gas in the neighborhood of bright hot stars is strongly ionized. The space between galaxies does not contain diffuse matter of density comparable to that of the interstellar matter in our galaxy.

Astronomers divide stars into two broad groups: Population I stars (young stars, associated with gas and dust) and Population II stars (old stars). The stars of Population I, the interstellar gas and the dust occupy a volume in the crude shape of flat grindstone with a slight bulge at the center. We shall refer to this volume as the *galactic disk*. The galactic disk is surrounded by a diffuse spherical haze of stars, mainly belonging to Population II.

Gas and dust occur in *clouds*, where the density of matter is much greater than in the surrounding space.

(*) 1 eV = $1.6 \cdot 10^{-12}$ erg.

Stars and clouds are not distributed uniformly through the galactic disk. There is a large concentration of stars near the galactic center. There are other local concentrations of gas, dust and Population I stars. In analogy with the observed structure of other galaxies, it has been suspected for some time that these concentrations of matter occur in the form of *spiral arms*. The recent methods of radio astronomy, which allow one to localize regions of highest hydrogen concentration through the observation of the 1420 megacycle radiation (*) appear to confirm this view. (Due to the differential rotation of the galaxy, the Doppler shift of the radiation is related to the distance of the source from the earth.) Fig. 5 shows the distribution of interstellar hydrogen in the galaxy, as it emerges from recent observations. The thickness of a spiral arm is supposed to be approximately 3000 l.y., and the distance between spiral arms about 6000 l.y. The solar system appears to lie near the edge of a spiral arm. Some numerical data on astronomical dimensions and on the distribution of matter in the galaxy are collected in Tables II and III.

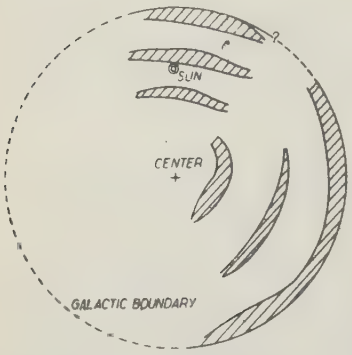

Fig. 5. – Rough sketch of the distribution of interstellar hydrogen in our galaxy (from data supplied by the staff of the Harvard Observatory).

TABLE II. – *Some Astronomical Dimensions* (l. y. = 1 light year = $0.95 \cdot 10^{18}$ cm).

Distance of our galaxy from nearest neighbor	$1.8 \cdot 10^5$ l.y.
Diameter of galactic disk	10^5 l.y.
Thickness of galactic disk:	
for gas clouds	$1.5 \cdot 10^3$ l.y.
for stars at large	$3 \cdot 10^3$ l.y.
for central bulge	$5 \cdot 10^3$ l.y.
Position of the sun:	
distance from galactic center	$2.8 \cdot 10^4$ l.y.
distance from median plane	30 l.y. (doubtful)
Distance of nearest star	4 l.y.
Radius of solar system (maximum distance of Pluto from Sun)	$0.74 \cdot 10^{15}$ cm
Distance of Earth from Sun	$1.5 \cdot 10^{13}$ cm
Radius of the Sun	$0.70 \cdot 10^{11}$ cm
Radius of the Earth	$0.64 \cdot 10^9$ cm
Range of observed star radii	from 1/400 to 3000 Sun radii

(*) This radiation corresponds to the transition between states in which the nuclear and electron spins are parallel and antiparallel respectively.

TABLE III. – *Distribution of Matter in the Galaxy.*

Mass of the Sun	$M_\odot = 2 \cdot 10^{33}$ g
Range of observed star masses	$M_\odot/10$ to 100 $M_\odot$
Density of smoothed out distribution:	
matter in stars	10^{-24} g cm^{-3}
matter in interstellar gas	10^{-24} g cm^{-3}
matter in interstellar dust	10^{-26} to 10^{-25} g cm^{-3}
Range of densities for interstellar gas	10^{-25} to 10^{-22} g cm^{-3}
Maximum density of interstellar dust	10^{-21} g cm^{-3}
Number of galactic stars	10^{11}

2·2. – Galactic Motions and Galactic Magnetic Fields.

The galaxy as a whole rotates around an axis perpendicular to its plane. The rotation does not correspond to that of a rigid body, the angular velocity being higher in the inner regions than in the outer regions. At the position of the solar system, the linear velocity due to the rotation of the galaxy is about 220 km/s. In addition to the general rotation of the galaxy, there are random motions of the gas clouds, with velocities spread over a wide range, around a mean value of 8 or 10 km/s (with a higher speed in central regions of the galaxy).

Several independent arguments suggest (but do not prove) the existence of magnetic fields in the galaxy. The most important piece of evidence is the partial polarization of light from distant stars, which appears to be due to a preferential orientation of elongated dust grains in interstellars space (see HILTNER, 1951). It is natural to ascribe the orientation of dust grains to a magnetic field. The required intensity is of the order of $6 \cdot 10^{-6}$ gauss. However, it has been suggested that it may be also possible to explain the alignment of dust grains by some hydrodynamic action. If the alignment is due to a magnetic field, one finds that the field is directed preferentially along the galactic arms. This suggests a fairly regular structure for the magnetic field, the galactic arms being essentially tubes of force. However, the observations are also consistent with the assumption of a magnetic field that varies irregularly from point to point, with a slight preferential orientation of the lines of force parallel to the galactic arms.

Another argument for the existence of a galactic magnetic field is the following. Ionized gas clouds are good conductors. If any magnetic field at all is present, the motion of the clouds in such a field will give rise to eddy currents, which enhance the existing field, while slowing down the motion. Thus kinetic energy is changed to magnetic energy. Under certain conditions, there is a tendency toward an equilibrium condition in which the density of kinetic

energy is equal to the density of magnetic energy:

$$\frac{1}{2}\varrho v^2 = \frac{1}{8\pi} B^2 . \tag{2.1}$$

With $\varrho \approx 10^{-24}$ g cm^{-3}, $v \approx 10$ km s^{-1}, one obtains $B \approx 4 \cdot 10^{-6}$ gauss. It is, however, impossible to prove that equipartition between magnetic and kinetic energies has been actually achieved in interstellar space (*).

2·3. – Solar and Stellar Magnetic Fields.

It is doubtful as to whether or not the sun possesses a general dipole field. If it does, the strength of this field is at present less than about 5 gauss at the poles. Strong and rapidly varying magnetic fields have been observed in sunspots (up to about $3 \cdot 10^3$ gauss). Other stars have magnetic fields much stronger than the sun. Fields as large as 10^4 gauss, reversing their direction every few days, have been observed.

2·4. – Radiation.

The flux of solar radiation at the earth is $1.4 \cdot 10^6$ erg cm^{-2} s^{-1}. The corresponding radiation density is $5.9 \cdot 10^{-4}$ erg cm^{-3}.

In the neighborhood of the solar system, the stellar radiation has a density about 10^9 times smaller, or $\sim 6 \cdot 10^{-13}$ erg cm^{-3}. There is a large uncertainty in the value of the mean density of stellar radiation in the galactic volume.

Some data on the distribution of energy in the galaxy are listed in Table IV.

(*) FERMI has presented the following argument based on the consideration of the energy densities, which supports the view that the magnetic field of the galaxy has a fairly regular structure. As noted above, the magnetic field strength necessary to explain the polarization of star light is of the order of 10^{-5} gauss, if the field is regular. If the field is irregular, however, the root mean square value of the field required to explain the polarization is considerably greater than 10^{-5} gauss. Therefore the density of magnetic energy is considerably greater than the density of kinetic energy associated with the turbulent motion. This conclusion appears to contradict the initial assumption of an irregular distribution of the magnetic field because if the density of magnetic energy is greater than the density of kinetic energy, then the hydrodynamic motion is dominated by the magnetic field and should therefore yield to the natural tendency of the lines of force to contract thus eliminating any strong irregularity of the field.

TABLE IV. – *Mean Energy Densities in the Galaxy in* eV *per* cm³ (1 eV = $1.6 \cdot 10^{-12}$ erg).

Rest-energy density of matter	10^9
Kinetic energy density of galactic rotation	10^3
Kinetic energy density of turbulent gas motion	1
Magnetic energy density	1
Stellar radiation	0.4
Cosmic rays	1
Solar radiation at the Earth	$3.7 \cdot 10^8$

2·5. – Distribution of Elements.

Hydrogen is the most abundant element in the universe. The abundance of the other elements is very uncertain, especially in the interior of stars, and varies greatly from star to star. A representative sample is shown in Table V.

TABLE V. – *Chemical composition of cosmic matter and of cosmic rays (relative numbers of atoms, taking the abundance of hydrogen equal* 1).

Element	H	He	Li	Be	B	C	N	O	$Z \geqslant 10$
Stars	1	?	?	?	?	10^{-4}	10^{-4}	10^{-3}	?
Interstellar matter	1	.1	0	0	0	$3 \cdot 10^{-3}$	0	10^{-2}	$2 \cdot 10^{-6}$
Cosmic rays	1	.08	?	?	?	$4 \cdot 10^{-3}$			$1.5 \cdot 10^{-3}$

3. – Cosmic Rays and the Sun.

3·1. – Correlations with Solar Phenomena.

The cosmic-ray intensity shows fluctuations that are definitely correlated with solar phenomena. The following effects have been established:

a) occasional large increases associated with solar flares,

b) frequent small increases associated with solar flares,

c) decreases associated with magnetic storms (magnetic storms are known to be correlated with solar activity),

d) periodic diurnal variations, correlated with the solar time,

e) 27-day recurring intensity variations, correlated with similar recurrent variations of solar activity.

In principle any one of these effects may be due 1) to a variable source of cosmic rays at the sun, or 2) to a « modulation » by solar phenomena of the intensity of a radiation originating outside of the solar system.

3·2. – Large Increases Associated with Solar Flares.

On four occasions (February 28, 1942; March 7, 1942; July 25, 1946; November 19, 1949 (for this latter see Table VI)) sudden large increases of the cosmic-ray intensity were observed to occur simultaneously with the appearance of a large flare at the sun (ELLIOT, 1952).

TABLE VI. – *List of stations operating during the large cosmic-ray increase on November 19, 1949.*

STATION	Geom. lat. (in degrees)	Altitude (*) (in meters)	Symbol used in Fig. 10
Amsterdam	54 N	—	A
Bagnères	46 N	550	B
Cheltingham	50 N	—	C
Christchurch	48 S	—	Ch
Climax	48 N	3500	Cl
Freiburg-Friedrichshafen	48 N	—	F
Godhavn	80 N	—	G
Huancayo	1 S	3350	H
Manchester	57 N	—	M
Nagoya	25 N	—	Na
Ottawa	56 N	—	Ot
Resolute	83 N	—	R
Teloyucan	30 N	2285	T

(*) Altitude listed only for mountain stations.

The following is the chronology of events associated with solar flares.

1. – *Light*: the luminosity of the flare rises to a maximum in 2 or 3 minutes, then decays gradually with a « mean life » of the order of 30 minutes.

2. – *Radio waves*: are received with only a slight delay after the visible light arrives.

3. – *Magnetic storms*: begin with a delay of the order of one day after the peak of the light flash; the magnetic field increases suddenly, then drops below normal and recovers to the normal value in a few days.

4. – *Cosmic rays*: the intensity rises to a maximum about one hour after the peak of the light flash, then decreases gradually over a period of about one day; sometimes it goes below normal during the subsequent magnetic storm.

The main characteristics of the cosmic-ray effect are listed below.

1) The intensity changes are occasionally very large. On November 19, 1949, for example, a cosmic-ray ionization meter at Climax, Colorado, recorded an increase of about 200 percent (FORBUSH, STINCHCOMB, and SCHEIN, 1950).

2) At a given location, the magnitude of the effect depends critically on the component of the cosmic radiation selected by the detector. For example, on November 19, 1949, a slow-neutron detector at Manchester, England, recorded an increase of intensity of about a factor of 6 (ADAMS, 1950), while a meson detector at the same location recorded an increase of only 11 percent. This important observation indicates that the low-energy component of the primary radiation is more strongly affected than the high-energy component, for it is well known that primary rays capable of producing mesons that are observed near sea level must have an energy of at least 6 GeV, whereas particles of energy considerably less than 6 GeV are still effective in producing slow neutrons.

3) The intensity increases observed with a given kind of detector are more pronounced at higher altitudes than at sea level; e.g., the 200 percent increase observed at Climax (3 500 m above sea level) on November 19, 1949, compares with a 43 percent increase observed at Cheltenham (sea level). This effect has presumably the same explanation as the effect mentioned under 2). One should mention in this connection that SCHEIN and his collaborators noticed for the first time, that large changes in the intensity of the primary radiation close to the top of the atmosphere may occur during solar outbursts. They reported an increase of 50 percent in the rate of star production on the occasion of a solar flare on May 11, 1949 (LORD, ELSTON, and SCHEIN, 1950). No changes at sea level or at mountain altitudes were observed at that time.

4) The intensity increase observed with a given detector and at a given altitude varies greatly with the geographical location. For example, the 200 percent increase observed at Climax (geographic latitude 39.4° N, 106.2° W, 3 590 m altitude) on November 19, 1949, contrasts with the absence of any observable increase at Huancayo, Peru (12.0° S, 77.3° W, 3 350 m altitude). On the same occasion, the increase was 70 percent at Ottawa (45° N, 76° W, sea level) and 12 to 15 percent at Resolute (75° N, 95° W, sea level).

It may be pointed out that on none of the four occasions was any increase detected at Huancayo. This station is located practically at the geomagnetic equator (geom. lat. 0.6° S) and the failure of observing the effect could be due to the magnetic field of the earth preventing the arrival of low-energy primaries near the equator.

The remarkable dependence of the effect on longitude will be discussed below.

There appears to be little doubt that the large increases associated with solar flares are due to the production of cosmic-ray particles at the sun or in the vicinity of the sun. The strongest argument is the magnitude of the effect, which one cannot possibly explain by any indirect « modulation » mechanism.

If one assumes that the extra radiation observed on the occasion of solar flares actually comes from the sun or from its neighborhood, one may inquire as to where the particles should strike the earth surface. The problem was investigated first by SCHLÜTER (1951) and later by FIROR (1954). One makes the assumption that the sun does not possess any magnetic field, so that the particles travel along straight lines from the sun to the neighborhood of the earth, and are then deflected by the earth's magnetic field. Figs. 6 and 7 show the results of FIROR. In deriving these results, FIROR made use of the trajectories computed by STÖRMER, DWIGHT and SCHLÜTER, as well as of data obtained from the model experiments of MALMFORS (1945) and BRUNBERG (1953). The curves refer to positive particles of various magnetic rigidity, coming from different regions of the sky and arriving upon the earth in the vertical direction. Fig. 8 explains the meaning of the angles plotted in Figs. 6 and 7. Notice that the longitude of the

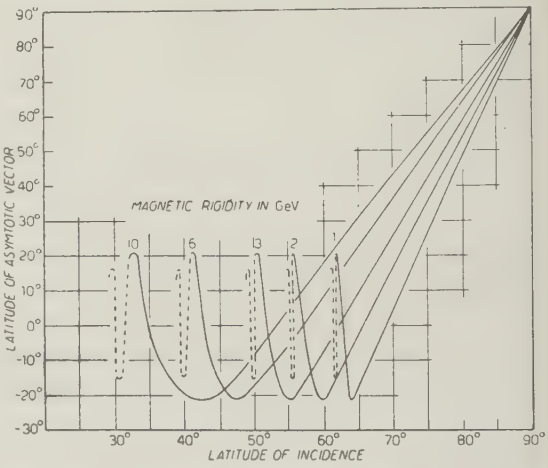

Fig. 6. – Relation between the geomagnetic latitude of impact on the earth of particles arriving vertically from the sun with magnetic rigidities of $1 \div 10$ GV, and the geomagnetic latitude of the source (from FIROR, 1954).

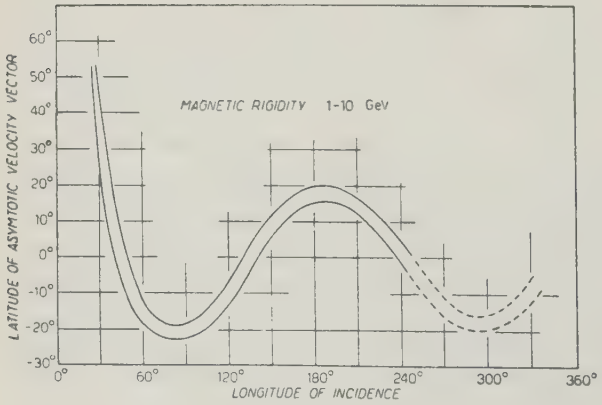

Fig. 7. – Relation between the geomagnetic longitude of impact on the earth of particles arriving from the sun with magnetic rigidities of $1 \div 10$ GV, and the latitude of the source. 0° corresponds to noon, 180° to midnight. Curves shown are the envelope of the individual curves for each rigidity (from FIROR, 1954).

point of incidence is measured with respect to the meridian plane containing the source.

One sees (Fig. 6) that for a given latitude of the source the latitude of incidence depends markedly on the rigidity. The longitude of incidence, however (Fig. 7), is almost independent of rigidity, at least for rigidities between 1 and 10 GV.

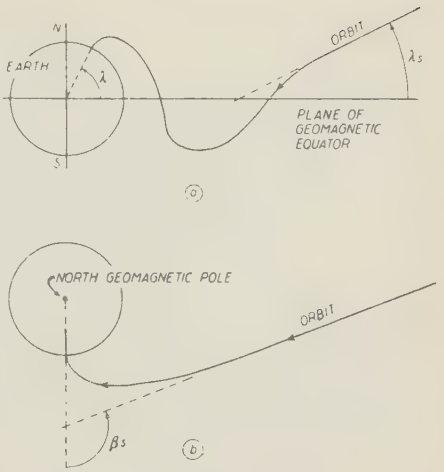

Fig. 8. – Angles used to describe orbits of cosmic rays coming from the sun and arriving vertically upon the earth, (from FIROR, 1954): *a*) orbit in a meridian plane that moves with particle, showing the latitude of incidence, λ, and the latitude of the asymptotic velocity vector, λ_s; *b*) projection of the orbit on the equatorial plane. The angle β_s is the longitude of impact relative to the source.

From Figs. 6 and 7 one can determine the *impact points* on the earth of particles of given rigidities originating from the sun, considered as a point source. The impact points corresponding to particles of different rigidities form *impact lines*. Notice, however, that many factors tend to produce a spread in the point of arrival of the particles (finite dimension of the source, detection of particles coming in directions other than the vertical direction, perturbation of the orbits by possible magnetic fields in the space between the earth and the sun). Thus, instead of impact lines, one should more appropriately consider *impact zones*.

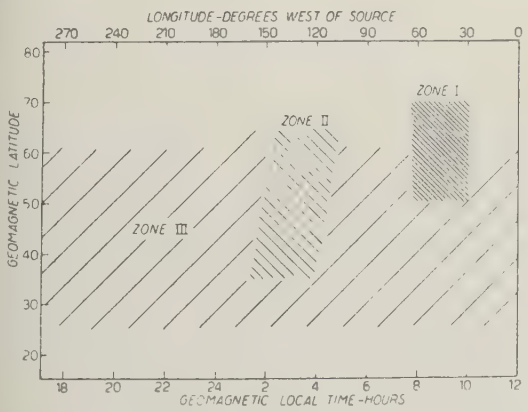
LONGITUDE-DEGREES WEST OF SOURCE
270 240 210 180 150 120 90 60 30 0
GEOMAGNETIC LATITUDE
60 70 60 50 40 30 20
ZONE I
ZONE II
ZONE III
18 20 22 24 2 4 6 8 10 12
GEOMAGNETIC LOCAL TIME-HOURS

Fig. 9 – Impact zones on the earth for particles arriving from the sun with magnetic rigidities between 1 and 10 GV at the time when the sun lies in the geomagnetic equator. For the definition of zones I, II, III, see Sec. 3·2. The density of crosshatching indicates roughly the relative intensities for different zones.

Considering particles of rigidity between 1 and 10 GV, one finds that there are essentially three impact zones. The first impact

zone refers to particles arriving to the point of observation without crossing the equatorial plane. This zone is in the shape of a band, a few hours wide in longitude, centered at around 9 am, ($\beta_t = 45°$), and extending in latitude from about 70° *to about* 50° (see Fig. 9). The second zone refers to particles arriving at the point of observation after having gone once through the equatorial plane. This zone is also in the shape of a band, centered at about 4 am, extending in latitude from about 65° *to about* 35° (see Fig. 9).

The third zone includes particles that have gone through the equatorial plane two or more times. The impact points of these particles spread over a zone extending in latitude from about 60° to about 25° and covering practically all longitudes.

The above results refer to the case that the sun lies in the geomagnetic equator. The position of the zones changes during the course of time as the position of the sun with respect to the geomagnetic equator changes.

In all three zones the rigidity of the particles increases with decreasing latitude. Thus at the high-latitude boundary of the zone one receives particles of 1 GV, at the low-latitude boundary one receives particles of 10 GV.

The intensity is different in the different zones For a detector located at the latitude of 50°, FIROR finds intensity ratios 7:3:1 for the three impact zones. FIROR summarizes his conclusions as follows:

« If the sun, while near the geomagnetic equator, emits a pulse of particles with rigidities up to 10 GV, identical detectors scattered over the earth's surface would see the following.

« 1. Detectors located at latitudes less than 25° would receive no new particles (*).

« 2. Detectors between 25° and 30° would see an increase in counting rate. This increase would be due to the background zone and would have no strong longitude (local time) dependence.

« 3. Detectors above 35° would see an increase as in 2, but in addition those detectors at local times around 0400 would see an increase about three times as large as in 2.

« 4. Detectors above 50° would see an increase as in 2, but detectors near 0400 or 0900 would see additional increases, up to seven times as large as in 2.

« The highest latitude at which detectors would see increases, either the background type as in 2 or the strongly local time dependent increase as in 3 and 4, would depend on the lowest rigidity particles to which the detector was sensitive. »

(*) The exact latitudes mentioned here are of course dependent on the assumption that there are no new particles with $M > 10$ GV.

The existence of limited impact zones explains, at least qualitatively, the large variation in the magnitude of the solar flare effects observed at different locations. On the whole, there seems to be some measure of quantitative agreement between the observations and the theoretical predictions, in that the larger increases occur, in general, within the impact zones where the computed intensity is greater. Notable exceptions are the two stations located near the geomagnetic north pole (GODHAVN and RESOLUTE). These stations are located outside of all impact zones, and yet recorded consistently considerable increases on the occasion of the solar flares.

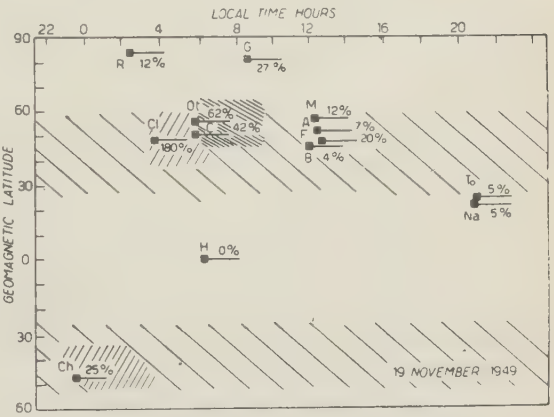

Fig. 10. – Impact zones on the earth at the time of the large cosmic-ray increase on November 19, 1949 (from FIROR, 1954). The cross-hatching indicates the positions of the zones with the density of cross-hatching giving roughly the relative intensities predicted for the different zones. The cosmic-ray stations are indicated by solid squares; the line attached to each station shows its motion during the increase. Near each station is an identifying letter (see Table VI) and the percentage increase observed.

Fig. 10 shows a comparison between theoretical predictions and the experimental results for the flare of November 19, 1949. Table VI gives the latitude and altitude of the stations. The impact zones are indicated by cross-hatching. The density of cross-hatching indicates roughly the relative intensities to be expected in the different zones. The lack of symmetry between the zones in the northern and the southern hemispheres is due to the fact that the sun was not on the geomagnetic equator at the time of the flare. The squares indicate the positions of the stations at the beginning of the flare, and the lines attached to the squares indicate the motion of the stations during the period of observation. The numbers indicate the observed percent increases.

3·3. – Small Increases Associated with Solar Flares.

Experiments by SIMPSON's group with slow-neutron counters (SIMPSON, FONGER and TREIMAN, 1953) have shown the existence of small increases of cosmic-ray intensity associated with the appearance of small solar flares on

the solar disk. The effect is similar to the large flare effect described previously, except for the fact that it is much smaller and that it occurs much more often. Neutron detectors are very appropriate for the study of this effect because *a*) they are sensitive to the low-energy component of the primary radiation, and *b*) they have high counting rates and therefore provide high statistical accuracy.

The observations were made at Climax. This station is located at 48° N geomagnetic latitude and is thus within the latitude range of the second impact zone and of the weaker third impact zone. It was found that when a solar flare occurs in the early morning (i.e., at such a time as to place Climax in the second impact zone) the average cosmic-ray intensity observed in a period of about 2 hours after the flare is about 0.5 percent above normal. No similar increase accompanies the appearance of flares at other times of the day.

The similarity between the large flare increases and the small flare increases strongly suggests that one should ascribe the latter effect, as the former, to the direct production of cosmic-ray particles on or near the sun. Under this assumption the particles arriving at Climax in the 4 am zone have magnetic rigidities of about 4 GV.

From the observed increases and from the average rate of occurrence of solar flares one can estimate the total number, $N_\odot$, of particles per second and per GV rigidity interval at an average rigidity of 4 GV, produced by the sun through the solar flare mechanism. Such an estimate was made by Simpson and his collaborators (Firor, Simpson and Treiman, 1954) who obtained

$$N_\odot \approx 2 \cdot 10^{23}\ \mathrm{s}^{-1}\ (\mathrm{GV})^{-1}\ . \tag{3.1}$$

The computation involves large uncertainties, so that an error of a factor of 10 in either direction is likely, and an even larger error cannot be ruled out. The experiment described provides no information on the production at the sun of particles with rigidities considerably greater or smaller than 4 GV.

3·4. – Solar Diurnal Variations.

In the preceding sections we have presented evidence for the existence of a mechanism operating on the sun and associated with solar flares that is capable of producing cosmic-ray particles. The computed production of rate of 4 GV particles at the sun is a lower limit for there may be solar sources not associated with visible flares.

One can, in principle, determine the rate of production of cosmic-ray particles at the sun from the diurnal variation of cosmic-ray intensity. For it is

clear that, if the sun produces cosmic-ray particles, the cosmic-ray intensity at the earth should be greater in the daytime than at night (of course the observations must be corrected for the effect of the earth's magnetic field).

It is convenient to define the following quantities

Density, ϱ, the number of particles per unit volume.

Directional intensity, j; $j\,\mathrm{d}\omega\,\mathrm{d}S$ is the number of particles per unit time incident upon the element of area $\mathrm{d}S$ within the element of the solid angle $\mathrm{d}\omega$ perpendicular to $\mathrm{d}S$.

Flux, I; $I\,\mathrm{d}S$ is the total number of particles per unit time traversing the area $\mathrm{d}S$ in a given sense.

Current vector, Ψ; the resultant of the velocity vectors of all particles contained in the unit volume.

Considering particles that move with the velocity v, the following relations exist.

$$\varrho = \int \frac{j}{v}\,\mathrm{d}\omega\,, \tag{3.2}$$

where the integral is extended over all directions.

$$I = \int j \cos\theta\,\mathrm{d}\omega\,, \tag{3.3}$$

where θ is the angle between the normal to $\mathrm{d}S$ and the direction of $\mathrm{d}\omega$, and the integral is extended over the upper hemisphere. For a nearly isotropic radiation, the above equations become:

$$\varrho = 4\pi j/v\,, \tag{3.4}$$

$$I = \pi j\,, \tag{3.5}$$

and therefore

$$I = \tfrac{1}{4} v\varrho\,. \tag{3.6}$$

The component of Ψ in a direction x has the expression

$$\Psi_x = \int j \cos\vartheta\,\mathrm{d}\omega\,, \tag{3.7}$$

where ϑ is the angle with the given direction x and the integral is extended over the whole sphere. If I_x and I_{-x} are the values of I in the positive and

in the negative x-direction respectively

$$\Psi_x = I_x - I_{(-x)} . \tag{3.8}$$

The above equations obviously hold irrespective of whether one considers the differential spectrum (i.e., particles per unit rigidity interval), the integral spectrum (i.e., all particles above a given rigidity), or the total radiation (i.e., all particles, irrespective of rigidity).

Consider now a sphere centered at the sun and of radius, R, equal to the distance of the earth from the sun. If the sun emits $N_\odot$ particles per unit time (and if we neglect the absorption of cosmic-ray particles by the sun) (*) we obtain the following equations, expressing the conservation of particles:

$$N_\odot = 4\pi R^2 \Psi_R = 4\pi R^2 (I_R - R_{(-R)}) . \tag{3.9}$$

Here Ψ_R is the radial component of $\mathbf{\Psi}$, I_R is the « midday » flux and $I_{(-R)}$ the « midnight » flux.

Measurements at sea level by FORBUSH, by ELLIOT and DOLBEAR, and by other observers (ELLIOT, 1952) indicate the existence of periodic changes of the order of 0.1 percent in the cosmic-ray intensity, that are related to the solar time (+). ALFVÉN has analyzed these data, taking into account the deflection of the particles in the earth's magnetic field (ALFVÉN, 1954). After correcting for this effect, he finds that the directional intensity of cosmic rays has a maximum in the afternoon, at times that vary between about 3 pm and 6 pm. This means that the current vector, $\mathbf{\Psi}$, has a *positive* radial component R_R. Thus there appears to be at the earth a net outgoing flux of variable magnitude. The variations appear to be related to the 11-years solar cycle.

One cannot determine more than an order of magnitude for the average value, Ψ_R, of this component. Nor is there a clear explanation for the tangential component of $\mathbf{\Psi}$. With ALFVÉN we shall take

$$\Psi_R = I_R - I_{(-R)} \approx 4 \cdot 10^{-4} I , \tag{3.10}$$

(*) The rate of capture of 4 GV particles by the sun is about $6 \cdot 10^{21}\ \mathrm{s}^{-1}\ (\mathrm{GV})^{-1}$, if the sun has no magnetic moment (FIROR, 1954).

(+) Notice that there may be considerably larger density fluctuations of the cosmic-ray intensity at high elevations. In this connection one might mention that LORD and SCHEIN (1950) found a day-to-night ratio of about a factor of two in the flux of heavy primaries near the top of the atmosphere. Some of the other experimenters, however, were unable to confirm this results (see summary of data in STIX, 1954).

where I is the average flux. Eq. (3.9) then gives:

$$N_\odot/4\pi R^2 = 4\cdot 10^{-4}\, I\,. \tag{3.11}$$

Considering Eq. (3.5) and the experimental value of the differential intensity at 4 GV one finds the following value for the number of particles originating from the sun in one second, per GV rigidity interval at 4 GV:

$$N_\odot \approx 10^{23}\ \mathrm{s}^{-1}\ (\mathrm{GV})^{-1}\,.$$

This value of $N_\odot$ is of the same order of magnitude as that estimated previously (Eq. (3.1)). This result, however, should be accepted with extreme caution because of the uncertainties in the experimental data, as well as in the corrections for the effect of the earth's magnetic field, and because of the arbitrary assumption that the anisotropy observed at the earth is representative of the average anisotropy at a distance from the sun equal to the radius of the earth's orbit.

3·5. – Possible Trapping of Cosmic-Ray Particles in the Vicinity of the Sun.

Eq. (3.11) shows that the particles coming *directly* from the sun contribute a negligible amount to the total radiation observed at the earth.

It is, however, conceivable that in the general vicinity of the solar system magnetic fields exist that prevent the free escape of particles of solar origin into space. These fields might bring the particles back toward the sun many times. They would thus increase the total flux of cosmic-ray particles of solar origin above the value $(N_\odot/4\pi R^2)$ corresponding to free escape. It has even been speculated that cosmic-ray particles of solar origin may be stored for a sufficient length of time as to account for the total intensity.

One can consider two models representing opposite idealizations for the structure of the trapping field:

A) The sun is surrounded by a trapping volume with «reflecting walls». Let R_t be the radius of this volume (conceived as spherical) and T the average trapping time. The average density of particles in the volume is then

$$\varrho_\odot = \frac{3N_\odot T}{4\pi R_t^3}\,, \tag{3.12}$$

and the average flux is

$$I_\odot = \frac{1}{4} v\varrho_\odot = \frac{3vN_\odot T}{16\pi R_t^3}\,. \tag{3.13}$$

If $I_\odot$ is of the same order of magnitude as the total flux, I, the following condition must be satisfied (see Eq. (3.11)):

$$4 \cdot 10^{-4} \frac{3vN_\odot T}{16\pi R_t^3} \approx \frac{N_\odot}{4\pi R^2},$$

or

$$\frac{vT}{R_t}\left(\frac{R}{R_t}\right)^2 \approx 3000 . \tag{3.14}$$

It would seem reasonable to assume that R_t is at least as large as the radius of the solar system ($7.4 \cdot 10^{14}$ cm) so that $R_t/R \approx 50$. Thus

$$vT/R_t \geqslant 7.5 \cdot 10^6 .$$

In other words, the average particle would have to «knock at the wall» many million times before it escapes. The total trapping time would be at least 5000 years. The suggested model would imply some sort of a general, fairly regular field permeating the whole solar system. Such a field could not be due to a magnetic dipole of the sun because if the sun possesses a magnetic dipole at all, this dipole field is certainly too weak for the purpose. One might perhaps speculate about the possible existence of a gigantic «ring current» circulating in the solar system. But, apart from the likelihood of such a current, it is doubtful as to whether it could produce such an impervious «wall» as required.

More realistically, perhaps, one might think of ionized clouds, emitted by the sun and carrying with them magnetic fields. These clouds would act effectively as «scattering centers» for cosmic-ray particles. We are thus led to consider our second limiting model.

B) The sun is surrounded by a scattering medium, characterized by a transport mean free path λ; λ is essentially the average distance traveled by a particle before it has lost recollection of the original direction of its motion. The current vector, $\mathbf{\Psi}_\odot$, has then the expression

$$\mathbf{\Psi}_\odot = -\frac{\lambda}{3} v \operatorname{grad} \varrho_\odot , \tag{3.15}$$

and, in the stationary state, the density $\varrho_\odot$ satisfies the diffusion equation

$$\nabla^2 \varrho_\odot = 0 . \tag{3.16}$$

If the diffusing medium occupies a sphere of radius R_1 around the sun (so that $\varrho_\odot = 0$ at $R = R_1$), the solution of Eq. (3.16) is

$$\varrho_\odot = k\left(\frac{1}{R} - \frac{1}{R_1}\right), \tag{3.17}$$

where k is determined by the condition

$$\Psi_{\odot_R} \times 4\pi R^2 = N_\odot . \tag{3.18}$$

The asymmetry in the radiation of solar origin is:

$$\frac{\Psi_{\odot R}}{I_\odot} = -\frac{4\lambda}{3\varrho_\odot}\frac{\partial \varrho_\odot}{\partial R},$$

or, if $R_1 \gg R$:

$$\Psi_{\odot R}/I_\odot \approx \lambda/R . \tag{3.19}$$

If a large part of the radiation is of solar origin, we obtain for Eqs. (3.10) and (3.19):

$$\lambda \approx 4\cdot 10^{-4} R \approx 6\cdot 10^9 \text{ cm} .$$

The radius of curvature of the trajectory of the particles in the regions of strongest field must be smaller than λ. Thus, considering an « average » cosmic-ray particle of about 10^{10} V rigidity, one obtains a lower limit of $10^{10}/(300\cdot 6\cdot 10^9) = 5\cdot 10^{-3}$ gauss for B in the regions of maximum field. While this value is high, it may not be completely unreasonable *a priori*. However, the existence of a scattering field of the type required by this model, with a transport mean free path several thousand times smaller than the distance of the earth from the sun, is contrary to the observation that occasionally there appear to be cosmic-ray trajectories reaching more or less directly from the sun to the earth. Indeed, as we have seen in Sections 3·2 and 3·3, only an essentially field-free region between the sun and the earth makes it possible to understand the observed increases of cosmic-ray intensity that accompany solar flares.

In conclusion, it appears, difficult to assume that cosmic-ray particles of energy of the order of 10^{10} eV may be trapped in the vicinity of the sun for a sufficient length of time as to make the sun an important source for the bulk of the cosmic radiation; and it seems impossible to realize the conditions that would be necessary to effectively trap particles with one million times the average energy, as are found at the tail end of the cosmic-ray spectrum.

3·6. – Magnetic Storm Effects.

Magnetic storms are world-wide events with the following characteristics. A sudden increase in the horizontal component of the earth's magnetic field, B, lasting for about an hour, is followed by a decrease below normal, reaching a minimum in 10 to 20 hours. A recovery period lasting from one to several days brings the value of B back to normal. The initial increase is rarely greater than 1 percent. The maximum negative value is usually somewhat greater than the positive peak (ELLIOT, 1952).

Severe magnetic storms are usually accompanied by marked decreases of cosmic-ray intensity (FORBUSH, 1938). The decreases are neither latitude nor altitude sensitive, and are of the order of 5 to 10 percent.

A magnetic storm is presumably due to a « ring current » circulating around the earth, at a distance of several times the earth's radius. This current is the residual effect of the passage of a cloud of ionized gas expelled by the sun. A clear explanation of the cosmic-ray decreases accompanying magnetic storms is still lacking. The observed decreases cannot be due to a change in the earth's magnetic field produced by the ring current. The strongest argument against such an explanation is that any change in the earth's magnetic field would merely change the geomagnetic cut-off. This would not produce any change of intensity at high latitude, where the magnetic cut-off lies well below the minimum rigidity of the cosmic-ray particles present in the primary spectrum.

There have been speculations that the magnetic storm effect may be due to changes in the geoelectric field. According to another view (MORRISON, 1954) the passage of the ionized cloud, which is responsible for the magnetic storm, would temporarily sweep the interplanetary volume free of cosmic-ray particles.

In any case, the following arguments lead one to believe that the cosmic-ray decrease is a « modulation » effect and is not caused by a change in the strength of a solar source of cosmic rays:

1) The effect is approximately simultaneous with the appearance of the magnetic storm, and not with the solar disturbance (occurring about a day earlier) that originates the cloud responsible for the magnetic storm.

2) Since the cosmic-ray intensity occasionally *decreases* by as much as 10 percent when a magnetic storm occurs, one would have to assume that there is at the sun a continuous source of cosmic rays which ordinarily accounts for at least 10 percent of the observed intensity. From the arguments developed in the preceding section it follows that a 10 percent contribution from the sun requires a mechanism capable of trapping cosmic rays for about 5000 years in the vicinity of the sun.

With such a long storage time, no appreciable variations can be produced by changes in the source strength lasting only for times of the order of one day.

3·7. – The 27-Day Recurring Variations.

The intensity of cosmic rays shows irregular variations, that have a tendency to recur with a 27-day cycle (ELLIOT, 1952). The variations appear with much greater amplitude in measurements with slow-neutron detectors than in measurements with meson detectors. In the first instance, the changes amount to 5 to 30 percent (SIMPSON, 1954). Thus the low-energy end of the primary spectrum is more strongly affected than the high-energy end by whatever phenomenon produces the 27-day recurring variation.

The effect is worldwide, and is correlated with magnetic disturbances.

Since the variations are observed at high latitudes, as well as at low latitudes, they cannot be produced by changes in the geomagnetic field (see preceding Section). No satisfactory interpretation can be found in terms of a variable geoelectric field. On the other hand, it seems unlikely that the variations are produced by changes in the strength of a solar source. The modulation mechanism suggested by MORRISON (see preceding Section) may offer a plausible interpretation.

4. – Galactic Theories of the Origin of Cosmic Rays.

4·1. – Mean Life of Cosmic-ray Particles in the Galaxy.

The assumption of a solar origin for the bulk of the cosmic radiation is the most economical in terms of energy requirements but, as we have seen, is difficult to reconcile with the high degree of isotropy of cosmic rays at the earth.

The isotropy would be easily understandable if the cosmic radiation came, for the most part, from galaxies other than our own, since the galaxies appear to be distributed with nearly uniform density around us (*). This hypothesis, however, requires prohibitively high source strengths. Indeed, since the light coming from extragalactic nebulae is about 1 percent of the light coming from galactic stars, and since the energy density of cosmic rays is about the same

(*) The rotation of the galaxy should produce a small asymmetry (of a fraction of 1 percent; the Compton-Getting effect), which is not observed. This asymmetry could be easily masked by a moderate amount of magnetic deflection of the cosmic-ray trajectories in the galactic space.

as that of starlight, one would have to conclude that the energy going into cosmic rays is about 100 times greater than that going into starlight. It is interesting to note that, if the energy density of cosmic rays in intergalactic space was the same as in the neighborhood of the earth, the energy present in the form of cosmic rays would be about 1/1000 of the total energy of the Universe, including the rest-energy of matter.

It thus appears likely that the majority of the observed cosmic rays comes from sources in our galaxy, but different from the sun. We shall now discuss this assumption in some detail.

In the galaxy, cosmic-ray particles travel presumably along curved paths, if the evidence for the existence of galactic magnetic fields has been correctly interpreted. Eventually they will escape from the galaxy, or will end their journey by colliding against a nucleus of interstellar matter. In such collision most of the energy of the particle changes into mesons. If the colliding particle is a complex nucleus, it will break up into simpler nuclei or into free nucleons. Notice that collisions with stars play a completely negligible role because of the extreme rarity of such events.

As we have seen in Part 2, interstellar matter consists almost entirely of hydrogen, spread through space with a mean density of about $\frac{1}{2}$ proton per cm^3; thus we only need to consider collisions of cosmic-ray particles with protons. We can estimate the mean free path for such collisions in interstellar space for the various components of the cosmic-ray beam, using a value of $4 \cdot 10^{-26}$ cm^2 for the nucleon-nucleon cross-section at cosmic-ray energies and computing the cross-sections of the heavier components on the basis of the semi-transparent model of nuclei. The mean free path in nuclear matter is taken as $2.7 \cdot 10^{-13}$ cm, and the nuclear radius as $1.4 \cdot 10^{-13} A^{\frac{1}{3}}$ cm. Table VII gives the results (*).

TABLE VII. – *Mean Free Paths for Nuclear Collisions* (density of interstellar hydrogen: $\frac{1}{2}$ proton per cm^3).

Cosmic-ray Particle	Proton	α-particle	C,N,O-group	Fe-group
Average A	1	9	14	30
Mean free path in 10^6 l.y. . .	50	20	7	4

(*) Of course some of the collisions will result only in a small change of the atomic number in the case of complex nuclei, or in a small change of the kinetic energy in the case of protons. Therefore the *effective* mean free paths may be appreciably larger than the actual collision mean free paths. However, our rudimentary knowledge concerning the density of interstellar matter, the cross-sections for high-energy collisions and the events following such collisions, does not justify a more detailed evaluation of the mean free path.

It is important to remark that, irrespective of the acceleration mechanism, any galactic theory of the origin must ascribe to cosmic-ray particles a mean free path before escape from the galaxy, L, which is long compared with the thickness of the galactic disk, but short compared with the collision mean free path. The upper boundary to L comes from the mass spectrum of the cosmic-ray beam. Considerations based on the relative abundance of protons and heavier nuclei in this beam, and on the numbers of secondary protons which a pure heavy primary beam would make by nuclear collisions with interstellar matter, shows that the mean path L of cosmic-ray particles (at least up to 10^{13} eV) cannot be appreciably larger than the collision mean free path of the heaviest components (PETERS, 1952). We thus obtain from Table VII:

$$L \leqslant 4 \cdot 10^6 \text{ light years} .$$

The lower limit to L comes from considerations of intensity and isotropy. The density of cosmic-ray energy near the earth is of the same order of magnitude as the energy density of starlight. A mean life of cosmic rays in the galaxy approximately equal to that of starlight would then imply a cosmic-ray source of about the same strength as that of starlight. In order to avoid this very unlikely conclusion we must thus assume that L is large compared to the thickness of the galactic disk.

The argument based on the observed symmetry was first given by COCCONI (1951) and is here presented in a somewhat different form. One can estimate a lower limit for the anisotropy of cosmic rays at the earth by taking into account only the fact that the solar system is off the median plane of the galaxy, considered as a disk of thickness $2h$ and infinite extension, and assume that cosmic-ray sources are distributed symmetrically with respect to the median plane. Consider two planes parallel to the median plane, at distances z_s and $-z_s$ from it. Let I_1 and I_2 be the numbers of particles per unit area and unit time which cross one of the two planes entering or leaving the intervening volume, respectively. Thus the net number of particles per unit area and unit time leaving this volume through *both* boundaries is $2(I_2 - I_1)$. If we neglect nuclear collisions, we then obtain the following equation expressing the conservation of particles:

$$I_2 - I_1 = \int_{-z_s}^{z_s} S(z)\, \mathrm{d}z , \tag{4.1}$$

where $S(z)$ is the source strength in particles per unit volume and unit time. On the other hand, for a nearly isotropic distribution the following equation holds (see Sec. 3·4):

$$I_1 + I_2 = \tfrac{1}{2} \varrho v , \tag{4.2}$$

where ϱ is the density of particles and v their velocity. The ratio between the total number of particles present in the galaxy at any particular time and the number of particles produced per unit time represents the mean life, L/v, of the particles in the galaxy; thus

$$L/v = \frac{\int_{-h}^{+h} \varrho \, dz}{\int_{-h}^{+h} S(z) \, dz} . \tag{4.3}$$

If we assume that the density of cosmic-ray particles near the earth is a fair sample of the mean density throughout the galaxy, the above equation becomes

$$L/v \approx \frac{2h\varrho}{\int_{-h}^{+h} S(z) \, dz} . \tag{4.4}$$

The asymmetry of cosmic rays with respect to the plane $z = z_s$ may be defined as

$$\delta = 2 \frac{I_2 - I_1}{I_2 + I_1} . \tag{4.5}$$

From Eqs. (4.1), (4.2) and (4.4) one then finds for δ the expression

$$\delta \approx \frac{\frac{4h}{L} \int_{-z_s}^{+z_s} S(z) \, dz}{\int_{-h}^{+h} S(z) \, dz} . \tag{4.6}$$

For example, in the case of a uniform distribution of sources through the galaxy, Eq. (4.6) reduces to

$$\delta \approx 4z_s/L . \tag{4.7}$$

At the mean energy of cosmic rays, about 10 GeV, $\delta \leqslant 10^{-3}$, and therefore:

$$L \gtrsim 4\,000\, z_s = 1.2 \cdot 10^5 \text{ l.y.}$$

Even at energies as high as about $4 \cdot 10^{13}$ eV, $\delta < 10^{-2}$, and thus $L > 12\,000$ light years (BARRETT, COCCONI, EISENBERG, and GREISEN, 1954). These limits would be higher except for the fact that the sun lies close to the galactic equator. It is not likely that the local distribution of the sources is really as sym-

metrical as the over-all galactic disk model which we use, so that the limits given above are probably conservative.

Very important in connection with the question concerning the mean life of cosmic-ray particles in the galaxy is the abundance of Li, Be, and B nuclei in the primary radiation. These nuclei presumably arise from fragmentation of the heavier nuclei since Li, Be, and B do not seem to appear with any appreciable abundance either in the stellar atmosphere or in interstellar matter (see Table V). If one accepts the recent results of KAPLON, NOON, and RACETTE (1954) giving an abundance ratio of 0.46 between the Li, Be, B group and the C, N, O, F group one concludes that the mean life is of the order of 10^6 years.

4·2. – Strength of Galactic Sources.

In a condition of steady state, the mean *energy density* of cosmic rays, the mean *power density* of cosmic-ray sources (energy emitted per unit volume and unit time) and the *mean life* of cosmic-ray particles in the galaxy are related by the equation:

(4.8) (energy density) = (source power density)·(mean life).

A similar relation holds for starlight. The energy densities of cosmic rays and of starlight are approximately the same. The mean life of starlight in the galaxy is of the order of magnitude of the thickness of the galactic disk (measured in light years) i.e., of the order of a few thousand years. If the mean life of cosmic rays is of the order of one million years, one concludes that the energy output of cosmic-ray sources is of the order of a few tenths of a percent of the energy output of light sources.

From the discussion in Sec. 3·4 we conclude that the cosmic-ray power output of the sun is of the order of magnitude of $4 \cdot 10^{-4}$ times the energy per unit time carried by all cosmic-ray particles that cross in the outward direction a sphere centered at the sun and of radius equal to the distance, R, of the earth from the sun. On the other hand, the energy flux per unit area equals $v/4$ times the energy density (Eq. (3.6)). Thus one can write the equation

(4.9) (solar power output) = $(4 \cdot 10^{-4}) \cdot (\pi R^2 v) \cdot$(energy density).

This equation, together with Eq. (4.8), yields

(solar power output) = $(4 \cdot 10^{-4}) \cdot \pi R^2 L \cdot$(source power density),

where L is the mean path before escape of cosmic rays from the galaxy. Taking $L \approx 10^6$ l.y. one obtains

$$\frac{\text{Solar power output}}{\text{Source power density}} \sim 3 \cdot 10^{-7} . \tag{4.10}$$

One can make two different assumptions on the mechanism responsible for the acceleration of cosmic rays: *a*) cosmic rays acquire their energy by processes occurring in stars or (more likely) in the immediate neighborhood of stars; *b*) cosmic rays acquire their energy gradually during their motion through galactic space.

a) In the first case we have

$$\text{(source power density)} = \text{(mean stellar power output)} \cdot \text{(density of stars)} .$$

The density of stars is of the order of 1 per 100 (l.y.)^3. Thus Eq. (4.10) yields

$$\frac{\text{Solar power output}}{\text{Mean stellar power output}} \sim 3 \cdot 10^{-9} . \tag{4.11}$$

We conclude that the cosmic-ray output of the average star must be enormously greater than the cosmic-ray output of the sun.

b) In the second case, cosmic rays presumably derive their energy from the variable electromagnetic field connected with the turbulent motion of ionized gas in interstellar space. The turbulent energy density of interstellar matter (both kinetic and magnetic) can be estimated roughly, and turns out to be of the same order of magnitude as the density of cosmic-ray energy, perhaps 1 to 10 eV per cm^3 (see Table IV). The energy presently stored in the interstellar turbulent motion could then supply the cosmic-ray power requirements only for a time equal to the mean life of cosmic-ray particles in the galaxy, i.e., a time very short compared to the age of the galaxy. This implies that cosmic rays represent an important load on the energy input to the turbulent motion, which presumably is the galactic energy of rotation. In our neighborhood the ordered rotational energy density is about a thousand times greater than the turbulent energy.

4·3. – The Propagation of Cosmic-ray Particles in Galactic Space.

In Sec. 4·1 we concluded that it is necessary to postulate a trapping mechanism capable of holding cosmic-ray particles in the galaxy for times long compared with the time for escape along straight-line paths.

A magnetic field appears to be the only agency capable of producing this effect. Indeed, we may regard the observed isotropy of cosmic rays as substantiating evidence for the existence of a galactic magnetic field.

Notice that in a magnetic field of the order of $6 \cdot 10^{-6}$ gauss (which is a lower limit for the magnetic field strength required to explain the polarization of starlight (see Sec. 2·2)) a particle with a momentum as great as 10^{16} eV/c has a radius of curvature of only 5 l.y. if it travels perpendicularly to the lines of force. This length is small compared with the thickness of the galaxy and it is thus at least conceivable that the galactic magnetic field may effectively trap even cosmic-ray particles of the highest observed energies.

It is impossible to make any realistic computation of the propagation of cosmic-ray particles in the galactic space before we have a better knowledge of the galactic magnetic fields. We may invert the problem and ask ourselves what the properties of galactic magnetic fields must be in order to account for the cosmic-ray observations. For this purpose it is useful to investigate the general consequences of some highly idealized models. But before undertaking this task, one may want to recall some general properties of the trajectories of charged particles in magnetic fields.

We shall assume here that the magnetic fields are static fields, so that the momentum of a particle is a constant.

In a uniform field B, a particle will describe a helicoidal trajectory on a cylinder of radius R_B. If ϑ is the angle of the trajectory with the lines of force (*angle of pitch*), R_B is given by the equation

$$R_B = \frac{p}{300B} \sin \vartheta , \tag{4.12}$$

(R_B in cm, B in gauss, p = momentum in eV/c). The velocity of propagation along the lines of force is, of course

$$v_B = v \cos \vartheta . \tag{4.13}$$

If the field is non-uniform, the trajectories are very complicated and, in general, cannot be computed analytically even if one knows the analytical expression of the field. There are, however, some useful theorems that hold approximately in the case of a slowly varying field, i.e., when the field changes only slightly in strength or direction over distances of the order of R_B.

a) The field strength changes gradually along the lines of force, but does not change appreciably in the perpendicular directions. Then the particle follows a quasi-helicoidal path around a tube of force, with an angle of pitch, ϑ, that

changes gradually according to the equation

$$\frac{\sin^2 \vartheta}{B} = \text{const}, \tag{4.14}$$

(see Appendix I). Thus a particle starting with an angle of pitch ϑ_0 at a point where the magnetic intensity is B_0, and moving toward a region of progressively increasing field, will reverse its motion at the place where B reaches the value, B_{max}, corresponding to $\vartheta = 90°$, i.e.

$$B_{max} = \frac{B_0}{\sin^2 \vartheta_0}. \tag{4.15}$$

b) The lines of force are slightly curved, but the field strength is constant. Then the particle spirals around a tube of force, but has a tendency to drift slowly in the direction perpendicular to the plane containing the lines of force. The drift velocity is

$$v_{Dr} = v \frac{\cos^2 \vartheta}{\sin \vartheta} \frac{R_B}{R_0}, \tag{4.15a}$$

where R_0 is the radius of curvature of the lines of force, and R_B is given by Eq. (4.12) (see Appendix II).

c) The field strength changes gradually in a direction perpendicular to the lines of force. Then the trajectory of the particle drifts slowly in the direction perpendicular to the lines of force and to the gradient of the absolute value of the field. The drift velocity is

$$v_{Dr} = \frac{1}{2} v \sin \vartheta R_B \frac{1}{B_0} \frac{\partial B}{\partial R}. \tag{4.15b}$$

(see Appendix III).

All of the above results apply, as stated, to the case of a slowly varying magnetic field. Regions of space with dimensions of the order of R_B or smaller, containing magnetic fields considerably different than that of the surrounding space, act, instead, as «scattering centers» that disturb the comparatively regular motion of the particles described above. The angle of deflection will depend critically on the point of incidence upon the inhomogeneous region, and may thus be quite different for neighbouring trajectories.

An important general property is expressed by Liouville's theorem, (see Appendix II), which states that in a static magnetic field, if the direct-

ional intensity of cosmic-ray particles is constant in time, it is also a constant along the trajectory of any individual particle.

The following is a consequence of the above theorem.

Consider an area $d\sigma$ and a narrow bundle of trajectories crossing $d\sigma$ in a nearly perpendicular direction (see Fig. 11). Let $d\omega$ be the solid angle of this bundle. The number of particles coming from a direction within $d\omega$ and crossing $d\sigma$ in the time interval between t and $t+dt$ is $j(t)\,d\omega\,d\sigma\,dt$. Consider now a cross-section of the bundle, $d\sigma'$, at a distance $l = v(t-t')$ from $d\sigma$. According to Liouville's theorem the directional intensity at this location is again j. Of the particles traversing $d\sigma'$, only those travelling within an appropriate narrow solid angle, $d\omega'$ will reach the area $d\sigma$. The number of such particles during the time interval from t' to $t'+dt'$ is $j\,d\sigma'\,d\omega'\,dt'$. These however, are the same particles that traverse $d\sigma$ in a direction within the solid angle $d\omega$, during the time interval from t to $t+dt$. We thus obtain

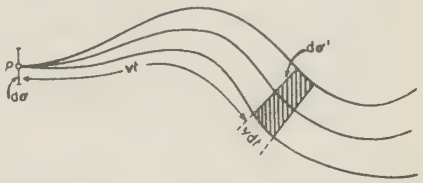

Fig. 11. – Illustrating the narrow bundle of trajectories discussed in Sec. 4·4.

$$j\,d\sigma'\,d\omega'\,dt = j\,d\sigma\,d\omega\,dt\,,$$

and therefore

$$d\sigma'\,d\omega' = d\sigma\,d\omega = \text{const}\,. \tag{4.16}$$

We are now in a position to write a general expression of the intensity of cosmic rays at a given point, O, of the galaxy and in a given direction. We invert the trajectory of the particle that arrives at the given point and in the given direction, and we follow it backward until it goes out of the galaxy. Let l_0 be the distance of P from the point of exit, measured along the trajectory.

The particles arriving at P in a direction within the solid angle $d\omega$ must have been produced within the « tube » occupied by the corresponding bundle of trajectories. Let s be the directional source strength (number of particles produced per unit time, per unit volume and per unit solid angle). We leave the possibility open that s may depend on position and direction. If the source is isotropic, and S is the omnidirectional source strength, then $s = S/4\pi$. Neglecting nuclear collisions, we then obtain for the directional intensity at P the following equation

$$j\,d\sigma\,d\omega = \int_0^{l_0} s\,d\sigma'\,d\omega'\,dl\,,$$

or, on account of (4.16),

$$j = \int_0^{l_0} s \, dl . \tag{4.17}$$

We thus conclude that the intensity observed at a given point and in a given direction is equal to the source strength, integrated along the trajectory passing through the given point, in the prescribed direction. If, in particular, the source is isotropic and of constant strength throughout the galaxy, Eq. (4.17) becomes

$$j = Sl_0/4\pi . \tag{4.18}$$

Notice that, if the magnetic field is irregular, the path lengths corresponding to nearby trajectories may be very different. Also, for a given direction, the path length may vary rapidly and irregularly with energy. Therefore l_0 should be understood as a mean value rather than a sharply defined quantity.

4·4. – The Diffusion Model (*).

We shall now make the assumption that the magnetic field varies very irregularly from point to point, being comparatively strong in small regions of space (presumably to be identified with ionized hydrogen clouds) and very weak in the rest of the space. In this case the propagation of cosmic-ray particles in the galactic space will resemble a random-walk motion, with the magnetic elements, acting as scattering centers. One can then define a *transport mean free path*, λ, as the average distance over which a particle loses all recollection of the original direction of its motion. λ will be of the order of magnitude of the distance between scattering centers and may thus, to a certain extent, be independent of the particle energy.

One can use the well-known diffusion theory to study the characteristic properties of the propagation of cosmic rays. Let us write $\varrho(\boldsymbol{r}, t, n)\,dn$ for the number of particles per unit volume, at position $\boldsymbol{r}$ and time t, which have undergone between n and $n+dn$ collisions since their ejection from the source, and let us define the function $\varphi = v\varrho$, where v is the velocity of the particles. For a nearly isotropic radiation, $\varphi/4\pi$ is the number of particles per second and per unit solid angle traversing a sphere of 1 cm² cross-sectional area. Fol-

(*) This section is a summary of the paper « The Origin of Cosmic Rays » by MORRISON, OLBERT and ROSSI (1954).

lowing the familiar methods of neutron diffusion and age theory, and neglecting nuclear collisions, we obtain the differential equation expressing the conservation of particles

$$\frac{\partial \varrho}{\partial t} = \frac{\lambda}{3} \nabla^2 \varphi - \frac{1}{\lambda} \frac{\partial \varphi}{\partial n} + S(\boldsymbol{r})\, \delta(n) \,. \tag{4.19}$$

Here λ is the transport mean free path, and $S(\boldsymbol{r})$ the source density function (assumed to be isotropic and constant in time). Notice that v, as well as λ, may be a function of n. The Dirac delta-function indicates that the injection is, of course with $n = 0$.

It is enough to treat the stationary case, with $\partial\varphi/\partial t = 0$, and S constant in time. For any finite n, we have:

$$\frac{\lambda}{3} \nabla^2 \varphi - \frac{1}{\lambda} \frac{\partial \varphi}{\partial n} = 0 \,. \tag{4.20}$$

Considering Eq. (4.19) in the neighborhood of $n = 0$, we have:

$$\varphi(\boldsymbol{r}, 0) = \lambda S(\boldsymbol{r}) \,. \tag{4.21}$$

No other boundary condition in the variable n is needed except the finiteness of φ for all n. The boundary condition to be set in ordinary space is less formal. It depends upon the reflectivity of the boundaries of the diffusing region. We shall set $\varphi = 0$ at the extrapolated boundaries, i.e., we shall assume no reflection. Note that a moderate amount of reflection would not substantially alter the present treatment. Only a practically total reflection from the galactic boundaries would invalidate our conclusions.

A simple mathematical discussion leads to the following results.

a) The solution of Eq. (4.20) or, more specifically, the functional dependence of φ on n at the location of the solar system, is not affected to any appreciable degree by the actual value of the galactic radius, R_0. This is easily understandable on physical grounds because $h \ll R_0$ and therefore the leakage through the cylindrical surface at $R = R_0$ is negligible compared to the leakage through the plane surfaces at $z = \pm h$. For this reason we can ignore the boundary condition $\varphi = 0$ at $R = R_0$.

b) Assume that the cosmic-ray sources are distributed uniformly in the radial direction, and symmetrical with respect to the equatorial plane of the galaxy. Unless the source strength varies rapidly in the direction perpendicular to this plane, one may write the solution of Eq. (4.20) as follows:

$$\varphi(z, n) = A \cos\left(\frac{\pi z}{2h}\right) \exp\left[-n/N\right] , \tag{4.22}$$

where z is the distance from the galactic equator, $2h$ the thickness of the galactic disk, N is given by the equation

$$N = \frac{12h^2}{\pi^2\lambda^2} \approx \left(\frac{h}{\lambda}\right)^2 , \tag{4.23}$$

and A by the equation

$$A = \frac{2\lambda}{h}\int_0^h S(z)\cos\left(\frac{\pi z}{2h}\right)\mathrm{d}z . \tag{4.24}$$

For the quantity

$$\Phi(r, n) = \int_n^\infty \varphi(r, n')\,\mathrm{d}n' \tag{4.25}$$

we obtain the expression

$$\Phi(z, n) = AN\cos\frac{\pi z}{2h}\exp\left[-n/N\right], \tag{4.26}$$

from which it follows that

$$\Phi(z, 0) = AN\cos\frac{\pi z}{2h} . \tag{4.27}$$

Notice that the solution given by Eq. (4.22) becomes less and less accurate as n decreases and cannot be trusted for $n < N$. Consequently, Eq. (4.27) represents only a crude approximation. Notice also that $\Psi(z, 0)/4\pi$ represents the directional intensity of all cosmic-ray particles, as defined in Sec. 3·4.

c) From Eq. (4.3) one obtains the following expression for the mean path of cosmic-ray particles before escape from the galaxy

$$L = \frac{v\int_{-h}^{+h}\varrho\,\mathrm{d}z}{\int_{-h}^{+h}S(z)\,\mathrm{d}z} = \frac{\int_{-h}^{+h}\Phi(z, 0)\,\mathrm{d}z}{\int_{-h}^{+h}S(z)\,\mathrm{d}z}$$

If $S(z)$ is constant one obtains from this equation, together with Eqs. (4.24) and (4.27), $L = (8/\pi^2)\lambda N$, or approximately

$$L \approx \lambda N \approx h^2/\lambda . \tag{4.28}$$

This approximate relation is valid for any reasonably smooth source distribution. It shows that the mean life of cosmic-ray particles in the galaxy is primarily determined by the leakage through the two boundary planes of the

galactic disk. If we take $h \approx 10^3$ l.y. and $L \approx 10^6$ l.y. (see Sec. 4·1) we obtain

$$\lambda \approx 1 \text{ l.y.} \tag{4.29}$$

d) In order to investigate the influence of the location of the source, one may solve Eq. (4.20) for the case of a source distributed along a line perpendicular to the plane of the galaxy. One finds the following solution:

$$\varphi(R, z) = \text{const} \times \cos\left(\frac{\pi z}{2h}\right) \frac{\exp[-n/N]}{n} \exp\left[-\frac{3R^2}{4n\lambda^2}\right], \tag{4.30}$$

where R is the radial distance of the point of observation from the line source. Integration with respect to n yields approximately

$$\Phi(R, z, 0) = \text{const} \times \cos\left(\frac{\pi z}{2h}\right) \sqrt{\frac{2h}{\pi R}} \exp\left[-\frac{\pi R}{2h}\right]. \tag{4.31}$$

Eq. (4.30) is derived under the assumption that the source strength is symmetric with respect to the equatorial plane and does not vary rapidly in the z-direction. Eq. (4.31) is valid if $\pi R/2h \gg 1$.

From Eq. (4.31) one sees that at distances larger than the thickness of the galaxy the contribution of a given source decreases rapidly with distance, the reduction factor being approximately $\exp[-\pi R/2h]$. Thus any theory postulating a three-dimensional random-walk propagation of cosmic rays through galactic space leads to the conclusion that cosmic rays are locally generated, in our galactic neighborhood, mostly within a few thousand light years from the sun. Any appreciable contribution to the total flux from sources further away than several times the thickness of the galactic disk would imply an extremely uneven distribution of the sources in the galaxy. It would also require an excessively large energy output from these sources. In particular, it seems difficult to assume, as it has been sometimes speculated, that most cosmic rays come from the dense concentration of stars at the center of the galaxy, 30 000 light years from the solar system. In our model the reduction factor for a source located at this distance relative to a local source is, approximately, 10^{-20}!

4·5. – The « White Box » Model.

We shall next consider a second highly idealized model, representing the opposite extreme of the model discussed in the previous section.

Assume that the magnetic field is extremely weak within the galaxy, but comparatively strong at the boundaries of the galactic disk, so that these boundaries act as highly reflecting surfaces for the cosmic-ray beam. One may think, for example, of the galactic disk as bounded by two double layers of electric current, producing strong magnetic fields within the layers, and practically zero field outside. A double layer 10 l.y. thick, with an internal field of 10^{-5} gauss would behave as a perfect reflector for particles of momenta less than $3 \cdot 10^{16}$ eV/c. Irregularities in the distribution of the currents would provide a possibility of escape. We shall assume that because of these irregularities, cosmic-ray particles undergo essentially diffuse reflection at the galactic boundaries.

The intensity observed in a given point and in a given direction may be written as the sum of two terms:

$$j = j_1 + j_0 , \tag{4.32}$$

where j_1 is an anisotropic component, representing the contribution to the observed intensity of the particles arriving directly from the sources, without reflection at the galactic boundaries, and j_0 is an isotropic component, representing the contribution of the particles arriving after diffuse reflection at the boundaries.

For a uniform distribution of the sources,

$$j_1 = Sl_1/4\pi , \tag{4.33}$$

where l_1 is the length of the straight or slightly curved trajectory reaching from the point of observation to the boundary of the galaxy.

The isotropic component j_0, which is much stronger than j_1, is given by the equation

$$j_0 = v\varrho/4\pi = SL/4\pi , \tag{4.34}$$

where L is the mean path before escape, and is related to the fraction, ε, of cosmic-ray particles leaking through the boundary at each reflection by the equation

$$\varepsilon L \approx 4h . \tag{4.35}$$

Thus the ratio of the anisotropic to the isotropic component is

$$j_1/j_0 = l_1/L . \tag{4.36}$$

Under the present assumption of very weak galactic fields, l_1 will be of the order of h for the direction perpendicular to the plane of the galactic equator,

and may be an appreciable fraction of the galactic radius for directions lying in the equatorial plane. Thus the model predicts an anisotropy of the order of many times h/L, with a maximum in the equatorial plane. Conversely, the absence of an anisotropy greater than about 0.1 percent implies that L must be many times 1000 h, according to the present model.

4 6. – Trapping in a Galactic Arm.

We have considered so far the galaxy as a more or less homogeneous medium as far as the production and propagation of cosmic-ray particles is concerned. As already mentioned astronomical data on the distribution of matter and magnetic fields in the galaxy, suggest that it would be perhaps more appropriate to consider a galactic arm, rather than the whole galaxy, as the relevant volume. Such an arm has a thickness, $2h$, a width perhaps somewhat greater ($3h$ or $4h$) and a length equal to several times the galactic radius, R_0.

A diffusion model, with the diffusing material confined to a galactic arm, gives nearly the same results as those obtained in the case of the disk. One should consider, however, that according to present information, the solar system lies at the edge of a galactic arm, or perhaps outside of the main concentration of matter that characterizes the arm structure. One may thus expect that, if any anisotropy is observed, the intensity should be a maximum in the direction of the nearest concentration.

Another possible model for the propagation of cosmic rays in a galactic arm is suggested by the astronomical observations indicating that the magnetic lines of force follow, in the main, the direction of the arm. Cosmic rays might thus propagate along helicoidal paths, spiralling around the lines of force of the galactic arm, until they eventually escape into extragalactic space.

If the magnetic field were perfectly smooth, the length of a trajectory connecting the point of observation with the galactic boundary would vary considerably with the direction of observation, which determines the angle of pitch of the helicoidal path. Thus one would expect a considerable degree of anisotropy in the cosmic radiation. However, some irregularities in the magnetic field, acting essentially as scattering centers, might easily randomize the directions to a sufficient degree as to account for the observed anisotropy.

4·7. – The Mechanism of Acceleration.

Some theories interpret the production of cosmic rays as a violent process of a nuclear character. Typical of this group of theories is the theory linking the origin of cosmic rays with supernovae. Supernovae are gigantic explosions.

One occurs every few hundred years in our galaxy. The explosion releases an amount of energy perhaps equivalent to the total mass of the sun. According to some theories, a star bursts into a supernova when it has exhausted its supply of hydrogen and its rotational velocity happens to be below a critical level. At this point gravitational attraction, no longer balanced by centrifugal force or by internal pressure, causes the star to collapse until its core is just one enormous lump of nuclear matter. The star blows up in a tremendous explosion whose end products are mainly nuclei of the heavy stable elements. It is speculated that cosmic rays may be secondary products of this outburst. In the initial phase of the explosion lumps of nuclear matter much heavier than the nuclei of any of the ordinary elements may be thrown into space with velocities approaching the speed of light. These fragments would be highly unstable and would disintegrate, ejecting protons, α-particles and other nuclei. The ejected particles, with energies further increased by electrostatic repulsion of the highly charged fragment from which they originated, would form the cosmic radiation. Even if cosmic rays were produced entirely in instantaneous bursts, several hundred years apart, we should still expect the observed cosmic-ray intensity to be constant, because of the long mean life of the particles in the galaxy.

Most theories, however, endeavor to explain the acceleration of cosmic-ray particles as an electromagnetic process. It would be difficult to locate the acceleration process in the interior of stars, or deep in the stellar atmosphere. In the first place, one cannot produce strong electric fields where there is a large density of highly ionized, and therefore highly conducting matter. In the second place, the presence of heavy nuclei in cosmic rays proves that very little matter has been traversed during the acceleration process. One could, however, assume that cosmic rays acquire their full energy in acceleration processes, occurring in the outer atmosphere, or at least in the general neighborhood of stars. On the other hand, one could assume that cosmic-ray particles are ejected from the stellar atmosphere with comparatively small energy — comparable to the energy of the ion beams that are responsible for the aurora borealis — and are then gradually accelerated during their motion through space.

As for the mechanism of acceleration, one may envisage the possibility of a unidirectional process, in which the particle energy increases continuously up to its final value, or one may consider some sort of a random process, in which particles sometimes gain and sometimes lose energy with, however, a net average gain.

a) Processes of the *first kind* would occur mainly in the vicinity of stars. The prototype of such processes is the so-called « betatron effect » suggested by SWANN (1933) long before the invention of the betatron. Swann's original

hypothesis linked the production of cosmic rays to sunspots. Sunspots are disturbances in the solar atmosphere that cover areas many thousands of miles in diameter. A sunspot is the seat of a magnetic field which increases gradually in strength as the spot develops, and then decays as the spot fades. This changing magnetic field produces an electric field, that can accelerate particles up to energies of the order of 10 GeV. It is natural to assume that similar processes occur also in other stars, and one may think of more violent disturbances capable of producing correspondingly higher energies.

Indeed, it is possible that the bulk of the cosmic radiation may come from a few types of stars with special electromagnetic characteristics. Double stars whose two partners possess strong magnetic moments and revolve rapidly around a common center of gravity, and variable stars whose exceedingly strong magnetic fields appear to reverse direction in a period of a few days have been singled out as possible important sources of cosmic rays.

MENZEL and SALISBURY (1946) proposed a different mechanism for the acceleration of cosmic-ray particles in the neighborhood of stars. They based their speculations on the assumption that stars emit radio waves of very large wavelength. Presumably these waves arise from mechanical turbulence in the highly ionized gases that form the stellar atmosphere. Any charged particle which finds itself along the path of a wave is accelerated by the electric field of the wave in a direction at right angles to the path of the wave. However, as soon as the particle acquires some velocity, the magnetic field associated with the wave deflects the particle in a forward direction. In this manner a particle may build up an energy of 10 or 100 GeV. Since the particle always lags behind the wave, it will find itself after a while in a position where the electric field of the wave is opposite to its velocity and it will begin to lose the energy it has accumulated. But if the wave field is disturbed at the right moment, as could easily happen under stellar conditions, the particle might escape with its maximum energy.

SWANN (1954) has recently suggested that cosmic-ray particles may have acquired their energy during their motion through galactic space, by a phenomenon of electromagnetic induction due to a gradual variation of the general magnetic field of the galaxy. He has shown that if, for example, the magnetic field of the galaxy has axial symmetry and if the particles are injected at a time when the magnetic field is zero, the particles acquire energy continously as the field increases. With the known size of the galaxy and with the assumed present strength of galactic fields, energies as high as the highest observed cosmic-ray energies could be easily accounted for.

b) Processes of the *second kind* were first suggested by FERMI (1949) who proposed the following concrete model. Consider a space filled with clouds of ionized magnetic plasma, such as we have pictured in Sec. 4·5 but assume, now, that

these clouds have a random motion. A particle colliding against a cloud will gain or lose energy depending on whether the cloud is approaching or receding. On the average, however, there will be a net gain of energy, in part because head-on collisions occur more often than overtaking collisions. One can prove that the fractional average energy gain per collision

$$\alpha = \frac{\Delta U}{U} \tag{4.37}$$

is independent of U and is proportional to the square of the velocity of the cloud. Indeed, if one assumes isotropic scattering in the collisions against clouds, one obtains

$$\alpha \approx \tfrac{4}{3}(V/c)^2 , \tag{4.38}$$

where V is the velocity of the cloud and c the velocity of light. Even though the theory in this form represents obviously an over-simplification of the problem, its results are probably characteristic of any theory in which cosmic rays gain energy through a random process of interaction with moving magnetic fields.

Such processes may occur in the whole galactic space, where wandering clouds of ionized gas are known to exist. Or they may occur in localized regions of space, possibly in the vicinity of certain kinds of stars, where perhaps conditions of exceptionally violent turbulence occur. It has been suggested that in these regions one may also find the main source of galactic radio noises.

4·8. – The Diffusion Model with Acceleration in Space.

We shall assume here that cosmic-ray particles are emitted from stars with comparatively small energies, U_0, and are then accelerated during their motion through space with a mechanism of the kind described under *b*) in the preceding section.

We use the diffusion model to describe the propagation through space. From this model we have obtained the following expression (Eq. (4.26)) for the number of particles per unit time, per unit area, and per unit solid angle that arrive at the point of observation having undergone more than n collisions since their emission,

$$\Phi(n) = \text{const} \cdot \exp\left[-n/N\right] . \tag{4.39}$$

Eq. (4.37) yields the following relation between the number of collisions and the energy of the particle

$$U = U_0 \exp\left[\alpha n\right]$$

or

$$n = \frac{1}{\alpha} \ln \left(\frac{U}{U_0} \right) . \tag{4.40}$$

If we call $J(U)$ the integral cosmic-ray spectrum (number of particles per unit area, per unit time, and per unit solid angle, with energy greater than U) we obtain:

$$J(U) = \frac{1}{4\pi} \Phi(n) = \text{const} \cdot \exp \left[- \frac{1}{\alpha N} \ln \frac{U}{U_0} \right]$$

or

$$J(U) = \text{const} \cdot \left(\frac{U_0}{U} \right)^{1/\alpha N} \tag{4.41}$$

One thus obtains an energy spectrum in the shape of a power law. As pointed out in Part 1, the experimental data on the primary spectrum can be fitted quite well to a power law for energies between 10^{10} and 10^{15} eV. The exponent is 1.5 ± 0.2. Comparing with the theoretical expression, we obtain

$$\frac{1}{\alpha N} \approx 1.5 , \tag{4.42}$$

or, remembering Eq. (4.23),

$$\alpha \approx 0.6 (\lambda^2 / h^2) . \tag{4.43}$$

It is somewhat difficult to reconcile Eq. (4.43) with astronomical observations. According to Eq. (4.29), λ is of the order of 1 l.y.. Notice that from the known size of gas clouds, one concludes that λ cannot be smaller than about 1 l.y. and, in fact, one would like to assign to λ a value somewhat greater than this value. With $\lambda \approx 1$, Eq. (4.43) yields $\alpha \approx 0.6 \cdot 10^{-6}$, which, together with Eq. (4.38), gives a velocity of about 200 km/s for the magnetic clouds. This velocity is greater by about a factor of 10 than the mean velocity of clouds obtained from astronomical observations.

The difficulty is a real one and should not be minimized. However, one cannot rule out the possible existence of diluted, hitherto undetected magnetic clouds, having high velocities. It is also conceivable that the model described may underestimate the rate of energy exchange between magnetic clouds and cosmic-ray particles.

FERMI (1953) has recently suggested a mechanism that would produce more rapid acceleration than the process based on random collisions with wandering

clouds. This mechanism is based on the assumption that the magnetic field is relatively regular along the galactic arms (see Sec. 4·7). Under this assumption cosmic-ray particles spiral around the lines of force. If the field strength along the line of force increases gradually, the angle of pitch, ϑ, of the spiral increases, until eventually the particle is reflected backwards (see Sec. 4·3). It is possible for a particle to be trapped between two regions of high field strength. The particle will then travel back and forth between the two «jaws» of the trap, gaining or losing energy depending on whether the jaws move away from or against one another.

Since only the component of the momentum parallel to the lines of force is changed, the product $p \sin \vartheta$ remains constant. Thus if a particle is caught in an accelerating trap, the angle of pitch will gradually decrease, until the particle escapes from the trap. Before this happens, however, the energy may have increased by a fraction of the order of 10 percent.

If the field were perfectly smooth, the particle, now traveling along a helix of small pitch, could not easily be trapped again, but would escape from the galaxy. Irregularities of the field, however, may bring the angle of pitch back to a large value and thus enable the particle to be trapped again.

A particle, of course, may be caught in a retarding as well as in an accelerating trap, so that in this model, too, the process of energy gain is of a statistical character. Here, however, the individual steps are larger than in the previous model, and thus the resultant rate of energy gain may be faster.

In the above computations, we have neglected the ionization loss of cosmic-ray particles in interstellar space. Considering this energy loss, we may define a *critical energy*, U_c, such that the rate of energy gain and the rate of energy loss become equal at this energy. Evidently, particles injected at energies below U_c cannot gain energy through a process of gradual acceleration. Table VIII lists the critical energies for the various components of the cosmic radiation, computed for the acceleration mechanism discussed at the beginning of this section, with $\lambda = 1$ l.y., $\alpha = 0.6 \cdot 10^{-6}$.

TABLE VIII. – *Critical Kinetic Energies of Cosmic-ray Particles.*

Cosmic-ray Particle	Proton	α-particle	C,N,O-group	Fe-group
Average charge	1	2	7	15
Critical kinetic energy (MeV) .	0.9	3.8	65	320

These energies are quite low compared with the cosmic-ray energies, which means that ionization losses are to a large extent negligible.

4·9. – The Low-Energy End of the Spectrum.

As stated in Part 1, the cosmic-ray spectrum deviates considerably from a power law at rigidities below 2 GV. Indeed, particles of rigidity less than about 1 GV seem to be almost totally absent.

This peculiarity of the spectrum is not easily explained on any of the various hypotheses discussed above.

As already mentioned, the scarcity of low-energy particles may be the result of the screening by a magnetic field surrounding the solar system. Such a field, however, could not be due to a magnetic moment of the sun because this moment, if it exists at all, is certainly too weak to explain the observed cut-off.

If cosmic rays gain their full energy in stellar phenomena, one may find the explanation of the low-energy cut-off in the peculiarities of the acceleration mechanism. For example, only particles above a certain rigidity may be able to escape from the region where the acceleration occurs.

The diffusion model with gradual acceleration in space discussed in the previous section may perhaps explain the depletion of the low-energy end of the spectrum with the additional assumption that very few cosmic-ray particles are injected into galactic space in the neighborhood of the earth. Under this assumption, all particles must have undergone a minimum number of collisions, and therefore must have gained a certain minimum amount of energy, before they reach our planet.

4·10. – Absence of Electrons and Photons in the Primary Radiation.

As stated in Part 1, the number of electrons and photons above 1 GeV arriving at the earth is less than 1 percent of the total particle flux. One can also compute an upper limit for the number of electrons in our galactic neighborhood taking into account the fact that these electrons, as they are deflected by the galactic magnetic field, should radiate radio-frequency waves whose polarization is related to the direction of the lines of force (Treiman and Blume, 1954). From the intensity and the character of the radio noises, and assuming a fairly regular magnetic field of the order $6 \cdot 10^{-6}$ gauss, one finds an upper limit of the order of 1/1000 for the fractional number of electrons in the total cosmic-ray flux.

Electrons in the primary cosmic rays may have two origins: initial production at the source, together with the protons and the heavier components, or subsequent collisions of nucleons in space, producing mesons or neutrons.

a) It has been estimated that a few percent of the energy lost in collisions will appear in the form of electrons and photons resulting from the decay of mesons and neutrons. Since we have concluded that the probability of a nuclear collision before escape from the galaxy is small, we can expect from this source a negligible number of electrons or photons.

b) As for the direct production, we must again distinguish the case that cosmic-ray particles acquire their full energy at the source or are accelerated during their motion through space.

In the first instance, the absence of electrons may be due to a peculiarity of the source. Or, possibly, one may explain it by postulating some mechanism capable of degrading the electron energy at a fast rate during the propagation in space. Collision with photons and, as already mentioned, radiation by deflection in magnetic fields have been suggested as possible processes leading to such energy losses.

In the second instance, the absence of electrons is easily understandable if we assume that the electron spectrum at injection is similar to that of the heavy particles in the kinetic energy scale, and that the energies of injection are of the order of, say, 10^7 or 10^8 eV. Since the rate of energy gain is proportional to the *total* energy (inclusive of rest energy) protons will gain energy at a rate from 10 to 100 times greater than electrons. Thus the final electron spectrum will be similar to the final proton spectrum, but with the energy scale reduced by a factor of 10 to 100. Because of the steep energy dependence of the intensity, such a shift in the energy scale implies a very large ratio between the numbers of protons and electrons above any given energy of the order of 10^9 eV or more.

4·11. – The High-Energy Portion of the Spectrum.

The mean life of cosmic-ray particles in the galaxy must be a decreasing function of their energy because as the energy increases the particles are less deflected by the magnetic fields and must therefore escape more easily.

Depending on the structure of the magnetic field, the mean life may decrease gradually with increasing energy, or it may remain practically constant up to some limiting energy, and then begin to decrease. The decrease may occur more or less suddenly. Suppose first that cosmic-ray particles do not gain their energy during the motion through space, but are injected into space with their full energy. The observed spectrum depends both on the source spectrum and on the energy dependence of the mean life. In fact, the intensity at a given energy is proportional to the product of the source strength and the mean life of the same energy (see Eq. (4.8)). At energies around 10^{10} eV

we know that the radiation is isotropic to better than 1 part in 1000. The mean life necessary to explain this high degree of isotropy depends on the model. As we have seen, 10^5 years is an absolute minimum, and 10^6 years a more likely lower limit. At energies around $4 \cdot 10^{13}$ eV the radiation appears still to be isotropic, but the accuracy of the measurements is only of about 1 percent (BARRETT, COCCONI, EISENBERG, and GREISEN, 1954; see Sec. 4·1). Thus the mean life could have decreased by a factor of the order of 10 or more from 10^{10} to $4 \cdot 10^{13}$ eV. At even higher energies the mean life could be shorter yet and quite appreciable anisotropy might occur.

Different models predict different kinds of anisotropy. Thus the disk diffusion model predicts a minimum and a maximum of intensity in the two opposite directions perpendicular to the plane of the galaxy. The « white box » model predicts a minimum of intensity perpendicularly to the plane of the galaxy, and a maximum in the directions parallel to this plane. If cosmic-ray sources are not distributed uniformly in the galactic plane and if there is no great amount of scattering in our galactic neighborhood, one would expect a maximum of intensity in the direction of the nearest concentration of sources.

Suppose now that cosmic-ray particles gain energy during their motion through space. We have seen in Sec. 4·8 that one obtaind from the theory the observed power spectrum if one assumes that both the mean life before escape and the fractional energy gain per unit time remain constant up to energies of the order of 10^{15} eV. If this is what actually happens, and if at a somewhat higher energy the mean life suddenly decreases, one would expect a sharp cut-off in the energy spectrum. Thus the intensity would drop to an unobservable low value before any appreciable asymmetry develops.

A measurable anisotropy at some high energy would indicate that the mean life before escape decreases gradually with energy and that, at the same time, the fractional energy gain per unit time increases, so as to offset the decrease in the mean life and produce the observed approximate power spectrum.

Experimentally, very little is known about the shape of the spectrum and the existence of possible asymmetries at high energies.

One of the most convincing pieces of evidence, perhaps, comes from some measurements on extensive air showers. From this experiment, performed recently in New Zealand (FARLEY and STOREY, 1954) there appears to be a maximum of the order of one percent in the direction pointing to the center of the galaxy. For the reasons developed before, however, it seems difficult to interpret this result as an indication that cosmic radiation observed at the earth is produced mainly near the galactic center.

Appendix I

Motion of Charged Particles in Non-uniform Magnetic Fields.

The motion of a charged particle in a non-uniform magnetic field is, in general, of a complex nature. Quite often, even with the knowledge of the explicit mathematical expression for the spatial dependence of the magnetic field, one is not able to solve the equations of motion in a closed form. However, in certain special cases one can derive simple theorems which give enough information about the motion of the particle in a confined region of space. In what follows, we shall consider three typical, idealized cases of non-uniform fields. Each of these cases emphasizes a different, singled-out feature of nonuniformity.

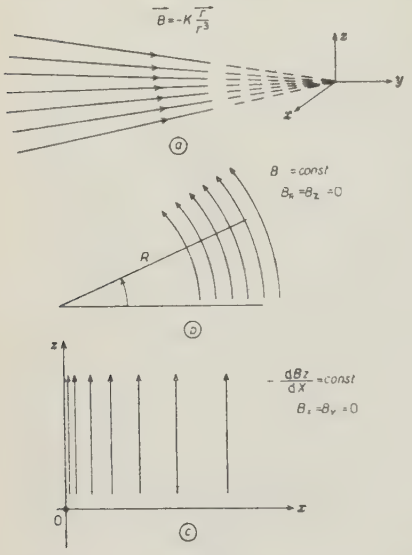

Fig. A.1. – Illustrating the three types of non-uniform magnetic fields, $\boldsymbol{B}$, discussed in Appendix I.

Case A. Consider a magnetic field, $\boldsymbol{B}$, which *increases* gradually *along the lines of force* but does not change appreciably in directions perpendicular to the lines of force. Such a field can be approximated, at least in a limited region of space, by a *central* field. Because of the zero-divergence condition for $\boldsymbol{B}$, this central field must necessarily be the of form

$$\boldsymbol{B} = -K\frac{\boldsymbol{r}}{r^3}, \tag{A.1}$$

where K is a constant, and $\boldsymbol{r}$ is the position vector from a suitably chosen origin of a fixed coordinate system. For slowly varying fields this origin will lie far away from the region under consideration (see Fig. A.1*a*).

The general equation for the motion of a particle of charge e in a magnetic field, $\boldsymbol{B}$, is

$$\frac{\mathrm{d}\boldsymbol{p}}{\mathrm{d}t} = \frac{e}{c}\boldsymbol{v} \times \boldsymbol{B}, \tag{A.2}$$

where $\boldsymbol{p}$ is the momentum and $\boldsymbol{v}$ the velocity respectively. In the case under consideration this equation becomes

$$\frac{\mathrm{d}\boldsymbol{p}}{\mathrm{d}t} = -\frac{eK}{cr^3}(\boldsymbol{v} \times \boldsymbol{r}), \tag{A.3}$$

The absolute values of $\boldsymbol{p}$ and $\boldsymbol{v}$ are constant in time because, according to Eq. (A.2), $\boldsymbol{v}\cdot\mathrm{d}\boldsymbol{p}/\mathrm{d}t = 0$. Multiplying vectorially both sides of Eq. (A.3) by $\boldsymbol{r}$, one gets

$$\frac{\mathrm{d}\boldsymbol{p}}{\mathrm{d}t}\wedge\boldsymbol{r} = \frac{eK}{cr^3}\boldsymbol{r}\wedge(\boldsymbol{v}\wedge\boldsymbol{r})\,.$$

Since $(\mathrm{d}\boldsymbol{p}/\mathrm{d}t)\wedge\boldsymbol{r} = \mathrm{d}(\boldsymbol{p}\wedge\boldsymbol{r})/\mathrm{d}t$ and $\boldsymbol{v}/r - \boldsymbol{r}(\boldsymbol{r}\cdot\boldsymbol{v})/r^3 = \mathrm{d}(\boldsymbol{r}/r)/\mathrm{d}t$, one has immediately the following integral of this equation

$$\boldsymbol{p}\wedge\boldsymbol{r} - \frac{eK}{c}\frac{\boldsymbol{r}}{r} = \boldsymbol{C}\,, \tag{A.4}$$

where $\boldsymbol{C}$ is a constant vector. Squaring both sides of Eq. (A.4) one obtains

$$p^2r^2\sin^2\vartheta + \left(\frac{eK}{c}\right)^2 = C^2\,, \tag{A.5}$$

where ϑ is the angle between $\boldsymbol{v}$ and $\boldsymbol{B}$ (« angle of pitch »). On account of Eq. (A.1), Eq. (A.5) may be also written as

$$\frac{\sin^2\vartheta}{B} = \text{const.}\,, \tag{A.6}$$

where $B \equiv |\boldsymbol{B}|$.

Eq. (A.6) implies that, if the particle moves toward the region in increasing B, the angle of pitch increases gradually until it reaches 90° at which point the particle will reverse its original direction.

Case B. Consider now a magnetic field, $\boldsymbol{B}$, which does not change appreciably in its magnitude but whose *lines of force* are *slightly curved*. In order to study the effect of this curvature, it is convenient to consider the motion of the particle in a system of cylindrical coordinates (R, φ, z) and assume that the lines of force coincide with the circles of constant R and point in the positive φ-direction (see Fig. A.1*b*). Since there is no acceleration along the lines of force

$$R^2\frac{\mathrm{d}\varphi}{\mathrm{d}t} = \text{const.} \tag{A.7}$$

On the other hand, the acceleration in the z-direction is given by

$$\frac{\mathrm{d}^2z}{\mathrm{d}t^2} = \omega\frac{\mathrm{d}R}{\mathrm{d}t}\,, \tag{A.8}$$

where

$$\omega = \frac{eBv}{cp}\,. \tag{A.9}$$

We take the origin of time at a moment when the velocity of the particle is perpendicular to the z-axis ($dz/dt = 0$ at $t = 0$). We call R_0 the value of R at this instant and ϑ_0 the angle of the trajectory with the lines of force. Then $R_0 d\varphi/dt = v \cos \vartheta_0$ at $t = 0$ and Eq. (A.7) becomes

$$R^2 \frac{d\varphi}{dt} = v \cos \vartheta_0 R_0 . \tag{A.10}$$

Upon integration, Eq. (A.7) becomes

$$\frac{dz}{dt} = \omega(R - R_0) . \tag{A.11}$$

Consequently, the (constant) square of the velocity may be written as

$$v^2 = \left(\frac{dR}{dt}\right)^2 + \left(\frac{v \cos \vartheta_0 R_0}{R}\right)^2 + \omega^2 (R - R_0)^2 . \tag{A.12}$$

One sees from Eq. (A.12) that $(R - R_0)$ is a bounded function of time. Due to our assumption that the lines of force are *only slightly* curved, one has

$$|R - R_0| \ll R_0 ,$$

so that the higher powers of $(R - R_0)/R_0$ can be neglected. Thus, by differentiating Eq. (A.12) with respect to time, one arrives at the following approximate equation

$$\frac{d^2}{dt^2}(R - R_0) + \omega^2 (R - R_0) = \frac{v^2 \cos^2 \vartheta_0}{R_0} . \tag{A.13}$$

This is the well-known differential equation of an harmonic oscillator. Its solution, satisfying our initial conditions ($R = R_0$ and $dR/dt = v \sin \vartheta_0$ at $t = 0$), is

$$R - R_0 = \frac{v \sin \vartheta_0}{\omega} \sin \omega t + \frac{v^2 \cos^2 \vartheta_0}{\omega^2 R_0} (1 - \cos \omega t) . \tag{A.14}$$

By integrating Eq. (A.11) with the aid of Eq. (A.14) one obtains (apart from an arbitrary integration constant)

$$z = -\frac{v \sin \vartheta_0}{\omega} \cos \omega t + \frac{v^2 \cos^2 \vartheta_0}{\omega^2 R_0} (\omega t - \sin \omega t) . \tag{A.15}$$

If we neglect terms containing powers of $(R - R_0)/R_0$ higher than one, we

obtain for Eq. (A.10)

$$\frac{\mathrm{d}\varphi}{\mathrm{d}t} = \frac{v\cos\vartheta_0}{R_0} + \frac{2v\cos\vartheta_0}{R_0^2}(R - R_0)\,.$$

Notice that v/ω is of the order of $R - R_0$ and therefore $v/\omega R_0 \ll 1$. Thus the second term in the expression for $R - R_0$ (Eq. (A.14)) is small compared to the first. Neglecting this term, one obtains

$$\frac{\mathrm{d}\varphi}{\mathrm{d}t} = \frac{v\cos\vartheta_0}{R_0} - \frac{2v^2\cos\vartheta_0\sin\vartheta_0}{R_0^2\omega}\sin\omega t$$

or, upon integration

$$\varphi = \frac{v\cos\vartheta_0}{R_0}t - \frac{2v^2\cos\vartheta_0\sin\vartheta_0}{R_0^2\omega^2}(1 - \cos\omega t)\,, \tag{A.16}$$

where we have taken $\varphi = 0$ at $t = 0$. Equations (A.14), (A.15) and (A.16) give the three coordinates of the particle as a function of time. In Eqs. (A.14) and (A.15) the second term on the right hand side is smaller than the first by a factor of the order of $(R - R_0)/R_0$, and thus represents a small correction. At the limit for very large values of R, the correction term becomes negligible and the equations indicate that the particle follows an helicoidal path on a cylindrical surface of radius $R_B = v\sin\vartheta_0/\omega = cp/eB$. For a finite but large value of R_0 the trajectory is still approximately an helix. $R - R_0$ varies between fixed values, i.e., the projection of the trajectory in the (R, φ)-plane oscillates around the circular line of force $R = R_0$: The expression for the coordinate z, instead, contains an oscillating term, and a term that increases linearly with time. This means that the trajectory drifts slowly in the z direction. The drift velocity is

$$v_{dr} = \frac{v^2\cos^2\vartheta_0}{\omega R_0} = \frac{v\cos^2\vartheta_0}{\sin\vartheta_0}\frac{R_B}{R_0}\,. \tag{A.17}$$

Case C. Consider finally a magnetic field whose lines of force are straight and parallel, but whose *magnitude decreases* gradually in one of the directions *perpendicular to the lines of force.* Choosing the cartesian coordinate system such that its z- and x-axes are parallel to $\boldsymbol{B}$ and grad$|\boldsymbol{B}|$, respectively (see Fig. A.1*c*) one has the following equations of motion:

$$\frac{\mathrm{d}^2x}{\mathrm{d}t^2} = \frac{ev}{cp}\frac{\mathrm{d}y}{\mathrm{d}t}B(x)\,, \tag{A.18}$$

$$\frac{\mathrm{d}^2y}{\mathrm{d}t^2} = -\frac{ev}{cp}\frac{\mathrm{d}x}{\mathrm{d}t}B(x)\,, \tag{A.19}$$

$$\frac{\mathrm{d}^2z}{\mathrm{d}t^2} = 0\,. \tag{A.20}$$

If one first neglects the dependence of B on x, i.e., if one puts $B(x) = B(0) = \text{const}$, one finds the « unperturbed » solution, representing a helicoidal path. With an appropriate choice of the origin of time, this solution is

$$\text{(A.21)} \qquad \begin{cases} x = \dfrac{v \sin \vartheta_0}{\omega_0} \sin \omega_0 t \,, \\ y = \dfrac{v \sin \vartheta_0}{\omega_0} \sin \omega_0 t \,, \\ z = (v \cos \vartheta_0) t \,, \end{cases}$$

where

$$\text{(A.22)} \qquad \omega_0 = \frac{ev B(0)}{cp} \,.$$

Considering now that $B(x)$ varies slowly with x, one can expand $B(x)$ around $x = 0$ and neglect terms containing the second and higher derivatives of $B(x)$. Writing for short

$$\text{(A.23)} \qquad \varkappa = -\frac{1}{B(0)} \left[\frac{\mathrm{d}B(x)}{\mathrm{d}t} \right]_{x=0} ,$$

we have

$$\text{(A.24)} \qquad B(x) = B(0)(1 - \varkappa x) \,.$$

Inserting (A.24) into (A.19) and integrating, one finds

$$\text{(A.25)} \qquad \frac{\mathrm{d}y}{\mathrm{d}t} = -\omega_0 \left(x - \frac{1}{2} \varkappa x^2 \right) ,$$

where we have chosen the integration constant so as to make $\mathrm{d}y/\mathrm{d}t = 0$ when $x = 0$, in agreement with the unperturbed solution (Eqs. (A.21)). Since $\varkappa$ contains the derivative of B, the term $\varkappa x^2$ is small compared to x and, we can compute this term by using for x^2 the value corresponding to the unperturbed solution. Thus we have

$$\frac{\mathrm{d}y}{\mathrm{d}t} = -\omega_0 x + \frac{1}{2} \varkappa \frac{v^2 \sin^2 \vartheta_0}{\omega_0^2} \sin^2 \omega_0 t \,.$$

Neglecting terms containing $\varkappa^2$, Eq. (A.18) then becomes:

$$\frac{\mathrm{d}^2 x}{\mathrm{d}t^2} + \omega_0^2 x = \frac{3}{2} \varkappa r^2 \sin^2 \vartheta_0 \sin^2 \omega_0 t$$

or

$$\frac{\mathrm{d}^2x}{\mathrm{d}t^2} + \omega_0^2 x = \frac{3}{4}\varkappa r^2 \sin^2\vartheta_0[1 - \cos 2\omega_0 t]. \tag{A.26}$$

This is the differential equation of a forced harmonic oscillation. Its solution enables one to integrate Eq. (A.23) and thus to arrive at the following final result

$$x = \frac{v\sin\vartheta_0}{\omega_0}\sin\omega_0 t + \frac{3}{4}\varkappa\frac{v^2\sin^2\vartheta_0}{\omega_0^2}\left(1 + \frac{1}{3}\cos 2\omega_0 t - \frac{4}{3}\cos\omega_0 t\right); \tag{A.27}$$

$$y = \frac{v\sin\vartheta_0}{\omega_0}\cos\omega_0 t - \frac{\varkappa}{2}\frac{v^2\sin^2\vartheta_0}{\omega_0^2}\left(\omega_0 t + \frac{1}{2}\sin 2\omega_0 t - 2\sin\omega_0 t\right); \tag{A.28}$$

$$z = v\cos\vartheta_0 t\,. \tag{A.29}$$

Eq. (A.27) shows that, similarly to case B, the particle suffers a gradual drift (see Fig. A.2). The direction of the drift is now in the $-y$ direction and therefore perpendicular to $\boldsymbol{B}$ and grad $|\boldsymbol{B}|$.
The drift velocity is given by

$$v_{dr} = -\frac{1}{2}\frac{v^2\sin^2\vartheta_0}{\omega_0}\varkappa, \tag{A.30}$$

where $\varkappa$ and ω_0 are defined by Eqs. (A.23) and (A.22) respectively.

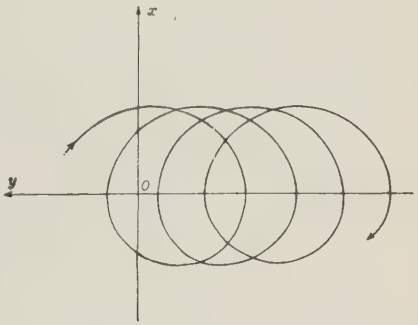

Fig. A.2. – Sketch of the trajectory described by a charged particle moving in the plane perpendicular to the lines of force of a magnetic field whose magnitude decreases slowly along the positive x-axis (see Fig. A.1c).

Appendix II

Liouville's Theorem for Charged Particles in a Static Magnetic Field.

The motion of charged particles in a magnetic field obeys the Hamilton equations

$$\left\{\begin{array}{ll} \dfrac{\mathrm{d}x}{\mathrm{d}t} = \dfrac{\partial H}{\partial \pi_x}\,; & \dfrac{\mathrm{d}\pi_x}{\mathrm{d}t} = -\dfrac{\partial H}{\partial x}\,; \\ \dfrac{\mathrm{d}y}{\mathrm{d}t} = \dfrac{\partial H}{\partial \pi_y}\,; & \dfrac{\mathrm{d}\pi_y}{\mathrm{d}t} = -\dfrac{\partial H}{\partial y}\,; \\ \dfrac{\mathrm{d}z}{\mathrm{d}t} = \dfrac{\partial H}{\partial \pi_z}\,; & \dfrac{\mathrm{d}\pi_z}{\mathrm{d}t} = -\dfrac{\partial H}{\partial z}\,; \end{array}\right. \tag{A.31}$$

where x, y, z are the cartesian coordinates, and π_x, π_y, π_z the components of the conjugate momentum

$$\boldsymbol{\pi} = \boldsymbol{p} + \frac{e}{c}\boldsymbol{A}\,. \tag{A.32}$$

In the above equation, $\boldsymbol{p}$ is the ordinary momentum and $\boldsymbol{A}$ the vector potential of the magnetic field.

From Eqs. (A.31) it follows that

$$\frac{\partial}{\partial x}\left(\frac{\mathrm{d}x}{\mathrm{d}t}\right) + \frac{\partial}{\partial y}\left(\frac{\mathrm{d}y}{\mathrm{d}t}\right) + \frac{\partial}{\partial z}\left(\frac{\mathrm{d}z}{\mathrm{d}t}\right) + \frac{\partial}{\partial \pi_x}\left(\frac{\mathrm{d}\pi_x}{\mathrm{d}t}\right) + \frac{\partial}{\partial \pi_y}\left(\frac{\mathrm{d}\pi_y}{\mathrm{d}t}\right) + \frac{\partial}{\partial \pi_z}\left(\frac{\mathrm{d}\pi_z}{\mathrm{d}t}\right) = 0. \tag{A.33}$$

One thus sees that the velocity vector in the six-dimensional phase space: $(\mathrm{d}x/\mathrm{d}t, \ldots, \mathrm{d}\pi_x/\mathrm{d}t, \ldots)$ has zero divergence, like the velocity vector in an incompressible fluid.

Suppose now that the phase space is filled with representative points with a density $N(x, y, z, \pi_x, \pi_y, \pi_z, t)$. Consider the representative points contained, at a certain instant, in a given element of phase space. As the representative points move along their trajectories, the element of phase space in which they are contained changes shape, but does not change volume, because of the zero divergence of the velocity vector. It follows that the density, N, of representative points in the neighborhood of a given representative point remains unchanged during the motion of the latter. If, in particular, N is independent of time (i.e., if one considers a condition of steady state), N is a constant along the trajectory of any representative point.

Let us now go from the phase space to the six-dimensional space formed by three space coordinates and the three components of the ordinary momentum, $\boldsymbol{p}$. By virtue of Eqs. (A.32) the Jacobian determinant $\dfrac{\partial(\pi_x, \pi_y, \pi_z)}{\partial(p_x, p_y, p_z)}$ is equal to one. Therefore the density, N', of representative points in the new space is equal to the density of representative points in the phase space

$$N'(x, y, z, p_x, p_y, p_z, t) = N(x, y, z, \pi_x, \pi_y, \pi_z, t)\,. \tag{A.34}$$

It follows that, in the steady state, N' is a constant along the trajectory of a representative point in the (x, y, z, p_x, p_y, p_z) space.

The number of particles per unit volume of ordinary space, that have a momentum between p and $p+\mathrm{d}p$ (in absolute value) and move in a direction included in the solid angle, $\mathrm{d}\omega$ is

$$N' p^2\,\mathrm{d}p\,\mathrm{d}\omega\,.$$

Therefore the number of particles with momentum between p and $p + \mathrm{d}p$ moving in a direction within the solid angle $\mathrm{d}\omega$, that traverse the unit area perpendicular to the direction of their motion, is

$$N' v p^2\,\mathrm{d}p\,\mathrm{d}\omega$$

where v is the velocity. Remembering the definition of directional intensity, j, we thus obtain

$$j = N' v p^2 . \tag{A.34}$$

Since, in the steady state, N' is constant along the traiectory of a representative point, and since v and p, in a static magnetic field, are also constant, we reach the following conclusion: *in the steady state the directional intensity of particles has the same value at all points of the trajectory of a particle.*

Appendix III

Acceleration of Cosmic-Ray Particles by Collisions with Moving Magnetic Clouds.

The following is a computation of the energy gain of cosmic-ray particles through the Fermi mechanism, under the assumption that the motion of the particles in the galactic space may be described as a random walk between moving magnetic clouds, behaving like scattering centers.

Consider a particle of energy U, momentum $\boldsymbol{p}$ and velocity $\boldsymbol{\beta}$ colliding with a cloud of velocity $\boldsymbol{B}$, the two velocities being measured in terms of the velocity of light, c. Let ϑ be the angle between $\boldsymbol{\beta}$ and $\boldsymbol{B}$. In the frame of reference of the cloud, the energy of the particle before the collision is

$$U^* = \frac{U - Bp\cos\vartheta}{\sqrt{1-B^2}} = U\frac{1 - B\beta\cos\vartheta}{\sqrt{1-B^2}} . \tag{A.35}$$

After the collision, the energy in the frame of reference of the cloud is the same as before the collision, because, in this frame of reference the magnetic field of the cloud is a static field. The momentum, however, is distributed at random in direction, and thus has an average value equal to zero. Thus, if one goes back to the frame of reference of the galaxy, one finds the following expression for the *arerage* energy U' of the particles that have collided with a cloud whose velocity forms an angle ϑ with the velocity of the particle

$$U' = \frac{U^*}{\sqrt{1-B^2}} = U\frac{1 - B\beta\cos\vartheta}{1-B^2} . \tag{A.36}$$

The probability for a particle to collide with a cloud whose velocity $\boldsymbol{B}$ forms an angle between ϑ and $\vartheta - \mathrm{d}\vartheta$ with that of the particle is proportional to both the number of such clouds and to the relative velocity of the particle with respect to them. With the appropriate normalization factor, this probability is (for $B \ll \beta$)

$$\frac{1}{2}\sin\vartheta\left(1 - \frac{B}{\beta}\cos\vartheta\right)\mathrm{d}\vartheta .$$

By computing the average of U' over all possible angles one then obtains

$$(A.37) \qquad (U')_{av} = \frac{1}{2}\,\frac{U}{1-B^2}\int_0^{\pi}(1-B\beta\cos\vartheta)\left(1-\frac{B}{\beta}\cos\vartheta\right)\sin\vartheta\,\mathrm{d}\vartheta = \\ = \frac{1+\frac{1}{3}B^2}{1-B^2}\,U \approx \left(1+\frac{4}{3}B^2\right)U.$$

Therefore the average energy gain per collision is:

$$(A.38) \qquad a = \frac{\Delta U}{U} = \frac{(U')_{av}-U}{U} = \frac{4}{3}B^2.$$

BIBLIOGRAPHY

N. Adams: *Phil. Mag.*, **41**, 503 (1950); N. Adams and H. J. J. Braddick: *Phil. Mag.*, **41**, 505 (1950).

H. Alfvén: private communication (1954).

P. H. Barrett, L. M. Bollinger, G. Cocconi, Y. Eisenberg, K. Greisen: *Rev. Mod. Phys.*, **24**, 133 (1952).

P. H. Barrett, G. Cocconi, Y. Eisenberg and K. Greisen: *Phys. Rev.*, **95**, 1571 (1954).

E. Brunberg: *Journ. Geophys. Res.*, **58**, 272 (1953).

G. Cocconi: *Phys. Rev.*, **83**, 1193 (1951).

L. Critchfield, E. P. Ney and S. Oleska: *Phys. Rev.*, **85**, 461 (1952).

H. Elliot in J. G. Wilson's: *Progress in Cosmic Ray Physics*, Amsterdam, Chap. VIII (1952).

R. A. Ellis, M. B. Gottlieb and J. A. Van Allen: *Phys. Rev.*, **95**, 147 (1954).

F. J. M. Farley and J. R. Storey: *Proc. Phys. Soc.*, **67**, 997 (1954).

E. Fermi: *Phys. Rev.*, **75**, 1169 (1949).

E. Fermi: *Galactic Magnetic Fields and the Origin of the Cosmic Radiation*, Russell Lecture at the Meeting of the American Astronomical Society at Boulder, Colorado (August 1953).

J. Firor: *Phys. Rev.*, **94**, 1017 (1954).

J. Firor, J. A. Simpson and S. B. Treiman: *Phys. Rev.*, **95**, 1015 (1954).

S. E. Forbush: *Terr. Magn. Atmos. Elect.*, **43**, 207 (1938).

S. E. Forbush, T. B. Stinchcomb and M. Schein: *Phys. Rev.*, **79**, 501 (1950).

W. A. Hiltner: *Astoph. Journ.*, **114**, 241 (1951).

R. I. Hulsize and B. Rossi: *Phys. Rev.*, **73**, 1402 (1948).

M. F. Kaplon, J. H. Noon and G. W. Racette: private communication (1954).

M. F. Kaplon, B. Peters, H. L. Reynolds and D. M. Ritson: *Phys. Rev.*, **85**, 295 (1952).

G. Lemaître and M. S. Vallarta: *Phys. Rev.*, **43**, 87 (1933); see also by the same authors: *Phys. Rev.*, **49**, 719 (1936); *Phys. Rev.*, **50**, 49 (1936).

J. J. Lord, A. W. Elston and M. Schein: *Phys. Rev.*, **79**, 540 (1950).

J. J. Lord and M. Schein: *Phys. Rev.*, **78**, 484 (1950); **80**, 304 (1950).

K. G. Malmfors: *Ark. f. Mat. Astr. Fys.*, **32** A, 8 (1945).
D. Menzel and W. W. Salisbury: *Nucleonics*, **2**, 67 (1946).
P. Morrison, S. Olbert and B. Rossi: *Phys. Rev.*, **94**, 440 (1954).
P. Morrison: *Washington Meeting of the American Physical Society* (1954).
H. V. Neher, V. Z. Peterson and E. A. Stern: *Phys. Rev.*, **90**, 655 (1953).
G. J. Perlow, L. R. Davis, C. W. Kissinger and J. D. Shipman: *Phys. Rev.*, **88**, 321 (1952).
B. Peters in J. G. Wilson's: *Progress in Cosmic-Ray Physics*, Chap. IV, Amsterdam (1952).
G. Puppi in J. G. Wilson's: *Progress in Cosmic-Ray Physics*, Chap. VI, Amsterdam (1952).
A. Schlüter: *Zeits. Naturf.*, **6** A, 613 (1951).
J. A. Simpson, W. Fonger and S. B. Treiman: *Phys. Rev.*, **90**, 934 (1953).
J. A. Simpson: *Phys. Rev.*, **94**, 426 (1954).
T. Stix: *Phys. Rev.*, **95**, 782 (1954).
C. Störmer: *Zeits. Astrophys.*, **3**, 31 (1931); **3**, 227 (1931); **4**, 290 (1932); **6**, 333 (1933); etc.
W. F. G. Swann: *Phys. Rev.*, **43**, 217 (1933).
W. F. G. Swann: *Phys. Rev.*, **96**, 240 (1954).
S. B. Treiman and M. Blume. *Washington Meeting of the American Physical Society* (1954).
J. A. Van Allen: *Nuovo Cimento*, **10**, 630 (1953).
M. S. Vallarta: *Phys. Rev.*, **74**, 1837 (1948).
S. N. Vernov and A. N. Charakhchyan: *Doklady SSSR*, **91**, 487 (1953).

SUPPLEMENTO AL VOLUME II, SERIE X
DEL NUOVO CIMENTO

N. 1, 1955
2° Semestre

The Energy Spectrum of the Primary Cosmic Radiation.

U. HABER-SCHAIM (*)

Physikalisches Institut der Universität - Bern, Switzerland

In the following I wish to discuss the energy spectrum of the primary cosmic radiation in the energy band 60-1000 GeV. This region lays above the magnetic cut-off but below that where extensive air showers are used to determine the primary spectrum. Two methods have been employed in this intermediate energy band. Both are very indirect and therefore if one states the results one should also mention all the assumptions made.

a) The primary spectrum can be deduced from the range spectrum of energetic muons under ground ([1,2]). Assuming that muons interact with matter only through their charge, the range spectrum can be translated into an energy spectrum. The next step is to correlate the muon energy spectrum to the primary spectrum by cascade mechanism. For primary energies below 1000 GeV the first step of the cascade will be a good approximation, i.e. one obtains a good estimate by considering only the simple process: primary → 1st generation pions → muons. Still one has to know the production spectrum of pions in a nuclear collision with given primary energy which at present is not experimentally known. One is forced to make an assumption taken from the theory. This is not very satisfactory since in a sense we obtain an equation with two unknown quantities. Yet the Fermi theory of pion production ([3]) has been applied to this problem using the experimental results for the muon spectrum ([4]). The result is that the integral primary spectrum (of protons and heavier nuclei combined) can be expressed by a power law E^{-s} with $s \sim 1.5$.

(*) Now of the Departmant of Physics, University of Illinois, Urbana Ill.

([1]) U. HABER-SCHAIM: *Phys. Rev.*, **84**, 1199 (1951).

([2]) U. HABER-SCHAIM and G. YEKUTIELI: *Nuovo Cimento*, **11**, 172, 683 (1954).

([3]) E. FERMI: *Elementary Particles*, p. 84.

([4]) P. H. BARRET, L. M. BOLLINGER, G. COCCONI, Y. EISENBERG and K. GREISEN: *Rev. Mod. Phys.*, **24**, 133 (1952).

It can be shown that the spectrum of the parent pions can be well approximated by a power law if the observed muon spectrum has such a form at least for muons below 100 GeV ([1]). Then if we denote the exponent of the pion spectrum by r, and assume that the number of pions produced in a collision is proportional to E^k and finally that the inelasticity of the collision is independent of energy then the following relation is obtained

$$s = r - k(r-1)\,. \tag{1}$$

In Fermi's theory $k = \frac{1}{4}$. If the multiplicity is independent of energy i.e. $k = 0$ then $s = r$ as is well known to be the case for the electron photon cascade. Since $r \sim 1.75$, s will not depend strongly on k within reasonable limits.

b) The second method is more direct and is based on the analysis of stars produced in photographic emulsions at high altitudes (30 km). Under favorable flight conditions i.e. a long and high plateau and with a small stack of plates one can safely assume the majority of the stars to be produced by primary particles. Thus there is no need to consider unknown cascade processes. Another advantage of this method is that one can obtain separately the energy spectra of primary protons and α-particles. The key problem is to determine the energy of a star producing particle by making measurements on the secondary tracks. Since scattering measurements of the fast secondaries are not possible in most cases in the energy region under consideration one is limited to measuring their angular distribution. Generally speaking the angular distribution is a result of the conservation of energy and momentum; the greater the energy the more collimated are the secondaries. But in order to have a quantitative relationship one has to make some specific assumptions about the nature of the collision. This has been done by several authors ([5,6]). The essential points are the following.

1) The great majority of secondary particles are produced in a single collision, so one can define a center of mass system for the whole process.

2) The angular distribution in the center of mass system is symmetrical with respect to the equatorial plane.

3) The velocity of the shower particles in the center of mass system is larger than the velocity of the center of mass relative to the laboratory system.

If these conditions are fulfilled there exists a one to one correspondence

([5]) H. L. Bradt, M. F. Kaplon and B. Peters: *Helv. Phys. Acta*, **23**, 24 (1950).
([6]) C. C. Dilworth, S. J. Goldsack, T. F. Hoang and L. Scarsi: *Nuovo Cimento*, **10**, 1201 (1953).

between the observed angles in the laboratory system and those in the c.m. system. Using the symmetry requirement one can obtain an approximate expression for the energy of the primary:

$$E = 2Mc^2 \cot^2\theta_{\frac{1}{2}}, \tag{2}$$

where $\theta_{\frac{1}{2}}$ is the median angle of the shower particles in the laboratory system and M is the nucleon mass. Eq. (2) implies that only one nucleon was hit in the meson producing collision. This restriction, however, is not essential as far as the form of the energy spectrum is concerned ([7]). The values of E obtained from (2) are then fitted into a E^{-s} curve by the maximum likelyhood method ([7,8]). The results obtained from 65 stars of $E > 60$ GeV found in a systematic scanning are shown in Table I (*).

TABLE I (*).

E	s	Number of stars
> 60	1.23 ± 0.14	65
> 100	$1.3\ ^{+0.22}_{-0.21}$	40
> 120	$1.45^{+0.26}_{-0.24}$	35

The errors represent those values of s which are less probable by a factor $e^{\frac{1}{2}}$ than the most probable one. This coincides with the standard deviation of a Gaussian distribution. The apparent monotonic change of s with E should be considered with caution. It cannot be ruled out that it is due to a small bias against stars of low energy.

([7]) A. ENGLER and U. HABER-SCHAIM: *Phys. Rev.*, **95**, 1700 (1954).

([8]) See also T. F. HOANG, L. JAUNEAU, J. JOUVIN et C. MABBOUX: *Nuovo Cimento*, **12**, 869 (1954) who used a similar approach at lower energies.

(*) The data given in Table I form a continuation of the work described in ref. ([7]). They have not been published elsewhere. I am indebted to Dr. A. ENGLER for the permission to quote them here.

PARTE SECONDA

Sezione I

Progetto di macchina acceleratrice per il Centro Europeo di Ricerche Nucleari

---

CERN, the European Council for Nuclear Research.

E. Amaldi

Istituto di Fisica dell'Università - Roma
Istituto Nazionale di Fisica Nucleare - Sezione di Roma

1. – Introduction.

Shortly after the war it was felt in various European scientific circles and in particular among the physicists of several European Universities and research institutions that, in order to regain a first rank position in nuclear science, it was necessary to make a common effort.

In fact, it was clear that in many European countries, still suffering from the very serious damages of the recent war, the problem of reconstructing their capacity and of developing their efficiency in the field of nuclear sciences could find an adequate solution from both the financial aspect and from the point of view of technical and scientific personnel through a collaboration among the European countries.

The need of costly equipment and of a rather large number of very specialized personnel limited in most of the European countries the development of the research work along important lines. On the other hand, it was stressed that even in the United States the progress of nuclear science was partly due to a wide collaboration among many universities distributed over large areas and to the existence of scientific teams which included research workers drawn from many countries.

It was at Lausanne, in December 1949, on the occasion of the European Cultural Conference, that the problem was publicly discussed at length for the first time and an important message of Louis de Broglie was read.

Although no special field of research and no particular geographical region were mentioned in this resolution, it was clear that among the various projects, which could be envisaged at that time, the establishment of an European

co-operation in fundamental research concerning the structure of matter was one of the most useful and promising tasks to aim at.

As a consequence, the project of an European nuclear research laboratory took shape under UNESCO's auspices during the year 1915. On invitation and under the chairmanship of Prof. P. AUGER, Director of the Department of Natural Sciences of UNESCO, a first meeting of a few European experts took place in Paris in the middle of May 1951, with the aim to prepare a first provisional programme.

As a result of a series of meetings, the experts recommended the constitution of a provisional international organization with a budget of about 1 million Swiss francs for a period of about 18 months, to prepare detailed technical plans and budgets which the European Nations could then use to set up a permanent organization endowed with considerable financial means.

2. – The Organizational and Legal Development of CERN.

All European Member States of UNESCO were invited in December 1951 to take part in a Conference of governmental representatives aiming to a study of the proposals of the experts. These last were approved by 10 European countries and on the 15th of Februar 1952 an Agreement setting up a « Council of Representatives of European States for planning an International Laboratory » was signed at Geneva by Belgium, Denmark, France, the German Federal Republic, Italy, the Netherlands, Norway, Sweden, Switzerland and Yugoslavia.

The main tasks of the provisional organization, called CERN (Conseil Européen pour la Recherche Nucléaire) were to prepare plans for the international laboratory and for the accelerators around which the future research would be centered, as well as a Convention to be submitted and signed by the representatives of the participating States which had to include the budget extending over the period of time necessary for the accomplishment of the construction.

Without going into the details of the structure and of the activities of CERN, I will recall the more important steps and decisions taken by the European Council for Nuclear Research.

Each Nation is represented in the Council by two delegates with a single vote, and as many experts as they deem necessary.

Among the delegates there are physicists as HEISENBERG for Germany, PERRIN for France, SCHERRER for Switzerland, WALLER and GUSTAFSON for Sweden, DE GROOT for the Netherlands. Besides these physicists there are representatives of leading national organizations of research in their countries such as BANNIER, Director of the Netherlands Organization for Pure Research; COLONNETTI, President of the Italian National Research Council and WIL-

LEMS, President of the Institut Interuniversitaire des Sciences Nucléaires at Brussels. There are also jurists and diplomates, particularly interested in the organization of international cultural relations such as Mr. VALEUR, of the French Ministry of Foreign Affairs and Mr. PENNETTA, legal consultant of the Italian Foreign Office.

The Council elects a chairman who remains in office for a period which depends in some way on the circumstances. First chairman has been Professor SCHERRER who was in office until the decision about the seat of the Laboratory was taken; the second has been Mr. BANNIER, who conducted the Council to the signature of the Convention and the third and actual chairman is Mr. VALEUR, who is working for the final step which will convert the provisional Organization into a permanent one. Vice-chairman of the Council have been HEISENBERG and PERRIN at the beginning and later, when Mr. VALEUR from France was nominated chairman, PERRIN — on his own request — was substituted by NIELSEN, from Copenhagen.

The position of the United Kingdom needs some special comments. Although the representatives of the United Kingdom did not sign the Agreement of the 15th of February 1952, Great Britain was, since December of the same year, collaborating very efficiently with the Council both with financial support and with highly qualified personnel. The representatives of the United Kingdom, Sir BEN BOCKSPEISER, Secretary of the Department of Scientific and Industrial Research, and Sir JOHN COCKCROFT took part in all CERN sessions formally as observers but practically in very close collaboration with the delegates of all other Nations.

The more important steps and decisions taken by CERN until now can be summarized as follows:

In its first session, held in Paris in May 1952, the Council set up specialized Study Groups and nominated its first international officers: the Secretary General E. AMALDI (Italy), responsible for presenting the reports as a whole; O. DAHL (Norway), Director of the Proton Synchrotron Group; C. J. BAKKER (Netherlands), Director of the Synchro-cyclotron Group; L. KOWARSKI (France), Director of the Laboratory Group and N. BOHR (Denmark), Director of the Theoretical Study Group.

These Officers, together with Prof. P. PREISWERK (Switzerland), Deputy-Director of the Laboratory Group, constitute the Executive Group which has to carry on the work according to the decisions taken by the Council.

The second session of the Council was held in June 1952, in Copenhagen, at the end of the Nuclear Physics Conference in which was discussed, with a wide participation of physicist of all European countries, the present situation in fundamental nuclear physics with a view to elucidate the problems which could be most fruitfully dealt with by international co-operation.

The programme of the Study Groups was adopted by the Council in the light of the results of the Conference.

In particular, it was decided to prepare the plans and to study the financial implications of a proton synchrotron for not less than 10 billion electron volts and of a synchro-cyclotron for about 600 million electron volts.

The third session was held in Amsterdam in October 1952, and was mainly devoted to the choice of the site where the Laboratory was to te built. At the end of a discussion in which four offers were considered (Arnhem, from the Netherland; Copenhagen, from Denmark; Paris, from France and Geneva, from Switzerland), it was unanimously decided to erect the Laboratory on a site at Meyrin, at 7 km from Geneva on the road to Lyon.

The fourth session, held in Brussels in January 1953, was mainly devoted to discuss the basic principles of the Convention and the rate to be adopted for the distribution of the expenses among the participating States.

Among various principles taken into consideration, that of the financial distribution in proportion with the corresponding national income, obtained from the beginning the favour of the majority of the representatives of Member States and was finally unanimously adopted at a later session (Table I).

TABLE I.

a) – Scale to serve as a basis for the assessment of contributions during the period ending on the 31st of December, 1956 (*).

Country	Percentage
Belgium	4.88
Denmark	2.48
France	23.84
German Federal Republic	17.70
Greece	0.97
Italy	10.20
Netherlands	3.68
Norway	1.79
Sweden	4.98
Switzerland	3.71
United Kingdom of Great Britain and Northern Ireland	23.84
Yugoslavia	1.93
TOTAL	100.00

b) – Staff distribution as at June 17th, 1954.

Country	Number
Belgium	3
Denmark	5
France	10
Great-Britain	10
Greece	2
Italy	8
Netherlands	8
Norway	5
Sweden	5
Switzerland	25
German Federal Republic	9
Yugoslavia	1
U.S.A.	1
TOTAL	92

(*) This Scale is revised every 3 years.

The fifth sessions was held in Rome in March 1953. The Convention for the establishment of a (permanent) European Organization for Nuclear Re-

search started to take shape and was completed during the sixth session held in Paris at the end of June 1953.

The first of July 1953, at the Quai d'Orsay, the Convention was signed by the representatives of all the above-mentioned States who had signed the Agreement of the 15th of February 1952, plus the United Kingdom and Greece.

I intend to come back later to some of the fundamental points stressed in the Convention; I shall only mention now that it will enter into force when seven States will have ratified it and provided that the total of their percentage contributions will amount to not less than 75% of the total.

From the beginning of July until now the Council held three more sessions (October 1953, January 1954 and April 1954) all in Ceneva, in which various important organizational and administrative matters were considered and decided.

At its last session, the Council unanimously voted a recommendation proposing the nomination of FELIX BLOCH as Director of the permanent Organization, coupled with the names, as other members of the Directorate, of E. AMALDI, in the capacity of Deputy-Director and of C. J. BAKKER, in the capacity of representative of the Scientific Group Leaders with special reference to the construction of the machines.

3. – The Present Legal Situation of CERN.

Until now, 9 countries have ratified the Convention. They are, in order of ratification:

United Kingdom, Switzerland, Denmark, Greece, Netherlands, Norway, Belgium, Sweden, German Federal Republic.

The following ratifications are still expected:

France, Italy, Yugoslavia.

Only the first of the two conditions required for the entering into force of the Convention has actually been fulfilled; namely: the one relating to the number of countries having ratified it.

The second condition providing that not less than 75% of the total percentage contributions of the Member States be obtained, has not yet been fulfilled. This will be achieved with ratification either by France or by Italy. There is no doubt that these countries will ratify within a short delay. In France, the Lower House has already given its approval and the Convention will be examined by the Upper House in September. In Italy, the Convention is now being examined by the Upper House, while the ratification procedure is fairly well advanced in Yugoslavia.

Therefore, although it will be necessary to waite some months in order to

have the legal position of the permanent organization definitively established, its practical existence and efficiency are clearly recognized (*).

As a consequence of such a situation the provisional organization is still into being but has started to perform some of the duties of the permanent organization. Following these lines and under the authorization of the Finance Committee of the Council, work on the site has started in the middle of May.

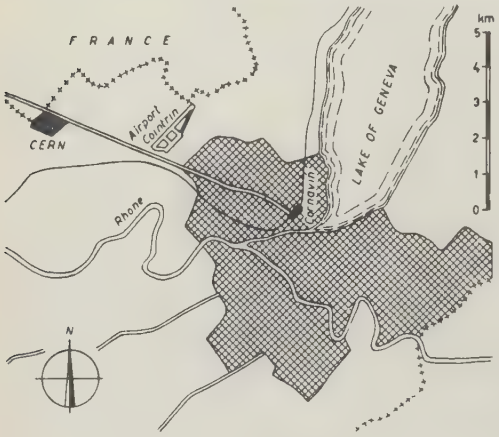

Fig. 1.

4. – The CERN Machines and the Laboratory at Geneva.

While the Organization developed along the above-mentioned lines, the design of the machines and of the laboratory as well as all other activities of CERN were in progress.

O. DAHL was directing the Proton-Synchrotron Group, supported by G. K. GOWARD who was made available to CERN by Great Britain. To the deepest

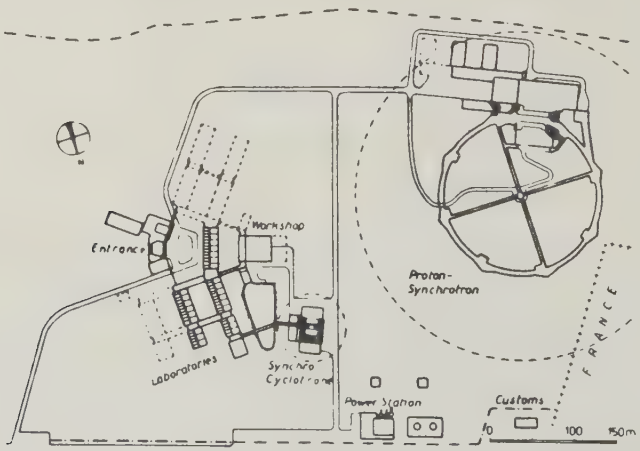

Fig. 2.

(*) *Note added in proof.*: – The Convention entered into effect the 29th of September 1954, and before the end of February 1955 the procedure of ratification in all 12 participating countries was accomplished.

concern of all the representatives and of the scientific and technical staff of CERN, GOWARD passed away in the middle of March of this year. He has been substituted in his work by J. B. ADAMS also from Great Britain.

The original project of the Proton Synchrotron was very similar to the Brookhaven cosmotron, only enlarged in order to produce 10 billion electron

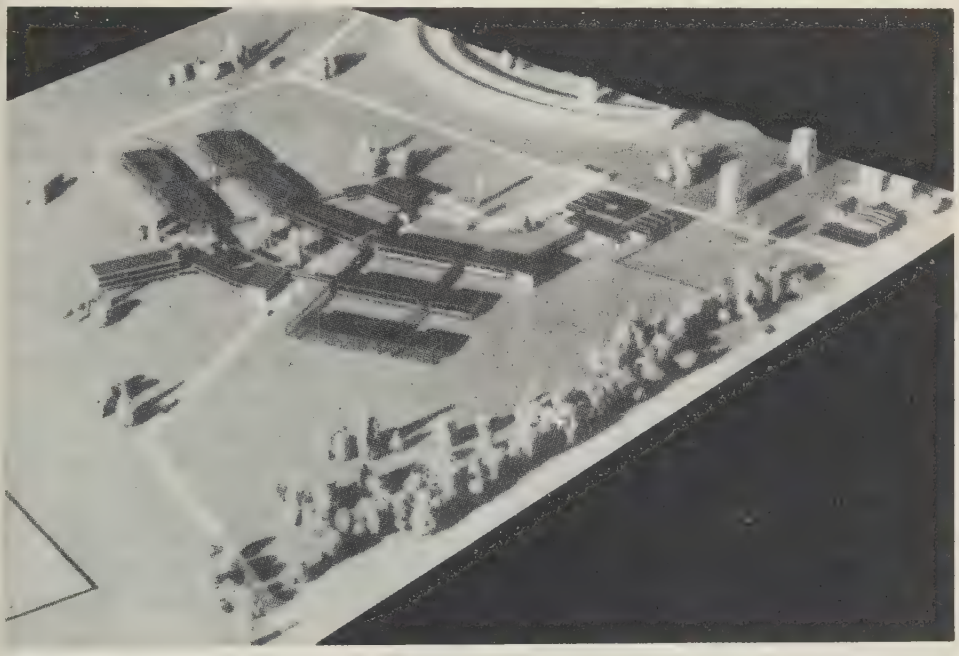

Fig. 3.

volts instead of 2.5. During the summer 1952 the strong focussing principle was discovered at Brookhaven and therefore the project of the Proton Synchrotron was changed from a conventional machine into an alternating gradient machine and it was possible, for about the same cost, to increase the energy up to 25 billion electron volts.

The progress of this project and of the theoretical investigations of the new principle will be presented in some detail in the lectures of ADAMS, LÜDERS and HINE.

C. J. BAKKER has in the meantime developed the project of a synchro-cyclotron for about 600 million electron volts. This machine is of a more conventional type and is very similar, apart from the higher energy, to those of Chicago and Pittsburg. The design of the magnet is now frozen and ready for final invitations for tenders, while experiments on a 1/10 scale model for determining details of the shimming are still going on.

The main difference of this machine with respect to the two above-mentioned, is the high frequency system in which vibrating reeds instead of rotating condensors are used. The system is very similar to that adopted in the enlarged synchro-cyclotron at Berkeley. Experiments on models of the vibrating reeds are now progressing satisfactorily. Details of this machine will be presented in the lecture of PICKAVANCE.

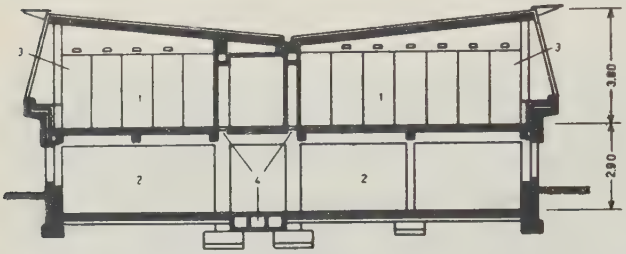

Fig. 4.

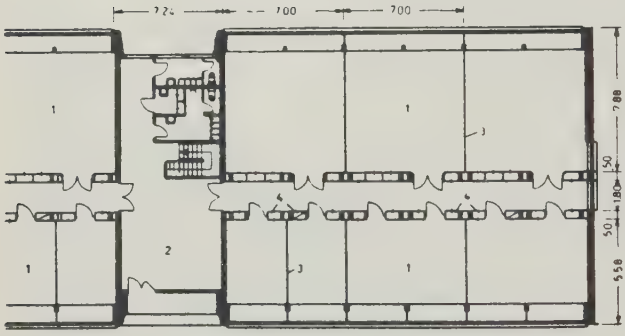

Fig. .5

KOWARSKI and PREISWERK have worked on various problems connected with the general organization and administration of the Laboratory, the instrumentation, the workshops and the buildings.

Fig. 1 shows the site at Meyrin, where the Laboratory will be constructed, with respect to the city of Geneva.

Fig. 2 shows the general lay-out of the Laboratory, while Fig. 3 is a picture of a model of the site with the building.

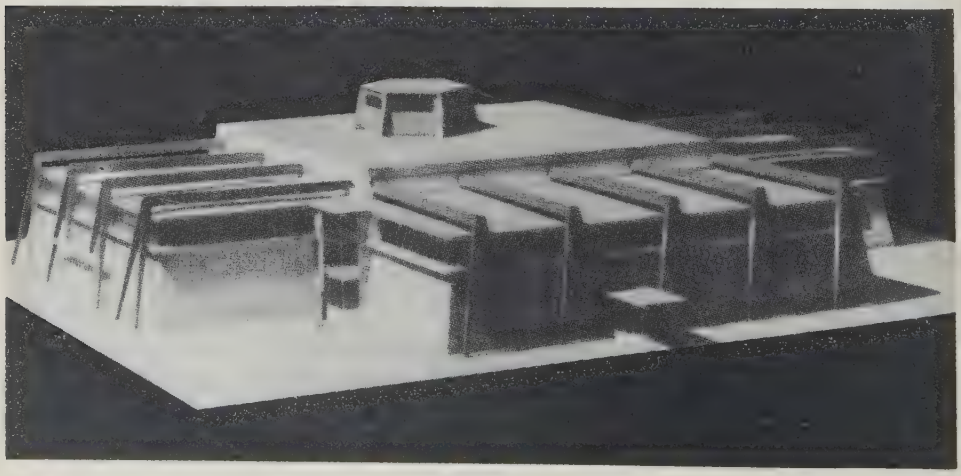

Fig. 6

Fig. 4 and 5 give sections and plans of the Laboratory while Fig. 6 shows a model of the building of the Synchro-Cyclotron.

5. – Other Activities of CERN.

The Theoretical Study Group set up in Copenhagen under the direction of Professor N. BOHR has been by now, active for 2 academic years. The Group consists, besides Professor BOHR and 3 other senior members, of 1 junior member from each one of the 12 participating countries. The Group has collaborated with the Proton-Synchrotron Group on various problems relating to the stability of the orbits of the machine. Its main task however, is that of developing an advanced training of junior theoretical physicists and offering them the opportunity to perform research work under the guidance of senior theoretical physicists. Regular course and frequent colloquia held by members of the group or by distinguished visitors invited by the Group-Director, are an essential part of the activity.

Numerous reports (29), papers (16), and lecture-notes (5) have been published by the members of the Group on various aspects of high energy physics including nuclear constitution and field theory.

Another important activity of CERN is the « Co-operation » which can, at least at present, be divided in the two following branches.

The first one, under the direction of Professor BOHR, refers to activities of CERN which are developed in connection with existing high energy machines which have been gratiously put at the disposal of CERN by various national institutions. Such a co-operation is quite active with the Laboratory of Liverpool where a synchro-cyclotron of 410 MeV has been recently completed and which is very close to operation. Four junior experimental physicists of various European countries will study there in close collaboration with the local British physicists, and under the authority of Professor SKINNER, director of the Liverpool Laboratory.

A similar arrangement is going on in Uppsala where two junior experimental physicists of CERN are doing research work with the local cyclotron of 200 million electron volts put at disposal of CERN by Professor SVEDBERG.

The second aspect of co-operation consists of sponsoring co-operative European research endeavours, such as cosmic rays investigation. Two international expeditions for launching balloons from Sardinia were organized in 1952 and 1953. In the second expedition, in which 18 European universities and institutions took part, about 10 liter (or 37 kg) of nuclear emulsions were exposed for about 8 hours at about 25 000 meters above sea level. The work on these emulsions is going on in all the participating laboratories (with

a total of about 100 microscopes) and interesting information is collected on new particles such as K-mesons and hyperons.

At a conference held in Padua in April last by members of the expedition the results of 6 months work have been presented; about half of all the τ- and K-mesons and about 2/3 of all the hyperons observed in emulsions until now, have been found in investigations of less than 1/4 of the emulsions exposed in this expedition (*).

Finally, during the next autumn two research teams will be established in Geneva, one working on Nuclear Induction, directly under Prof. BLOCH, the other working on some problem of cosmic rays connected with the development of experimental techniques, which later will be useful for the experiments with the machines.

The existence of these research teams will contribute to create the right spirit of research at Geneva.

6. – Questions Related with the Staff and the Finances.

The scientific and technical staff of CERN amounts, at the moment, to about 60 people plus 10 junior scientists working with the Theoretical Study Group for a period of several months, while the administrative staff amounts to about 20 people.

Table II shows the distribution of personnel among the Member States. When CERN will have achieved its full development, the total staff will amount to about 300 people.

While the Proton-Synchrotron Group and the Laboratory Group are already in Geneva, the Synchro-cyclotron Group is still scattered in the various towns of Europe and will move to Geneva next September; the Theoretical Group is located at Copenhagen, where they will remain for about three more years.

At Geneva, the Proton-Synchrotron is located in a wing of the Institute of Physics of the University and in a few hutments erected in its vicinity. The surface of the hutments amounts to about 600 m^2. The Group has also at disposal a concrete building annex to the Institute with a surface of 600 m^2.

The Central Administration, the Laboratory Group (and later on the Synchro-cyclotron Group) are placed in a Villa at the airport of Geneva (surface 360 m^2) and in a few hangars rented by CERN from the airport authorities (surface 325 m^2). A few more hutments will be erected there during summer.

(*) *Note added in proof.* – See the *Rendiconti del Congresso Internazionale sulle particelle instabili pesanti e sugli eventi di alta energia nei raggi cosmici*, Padova, 12-15 Aprile 1954, in *Suppl. Nuovo Cimento*, **12**, n. 2 (1954).

The work on the site has started in May in order to prepare the foundations for the machines before next winter.

At the beginning of 1956, construction on the site will be advanced enough to allow for the gradual transfer of the experimental activity from the provisional accomodations to the permanent ones.

The total budget amounts to 120 million Swiss francs to be spent in about 7 years.

7. – Some Information about the National Programmes of Construction of High Energy Accelerators in Europe.

In order to give a fair view of the activity going on in Europe in the field of high energy accelerators, one has to consider also the national programmes.

In Table III I have collected a few data about the machines (of an energy higher than 100 MeV) which are already completed in Europe.

One can see that, apart from the United Kingdom and Sweden, there are no other European countries where machines would allow for research in the field of high energy physics. Even in United Kingdom, where a very considerable effort in this direction has been made, there is still a delay of about 6 years when compared with the development in this field of research in U.S.A.

The situation will be remarkably improved during the next few years; this not only as a consequence of CERN's activities, but also because important projects of construction of high energy accelerators are going on in various national institutions.

Table IV contains data I was able to collect about the various national projects of this type.

The number and nature of all these projects ensure that in a few years the physics of π-mesons will be a highly cultivated field also in Europe. Although some of the national machines will produce particles of energy around and above 1 GeV, one may expect that, if work on artificial heavy mesons and hyperons will proceed satisfactorily, this will be mainly due to the Proton-Synchrotron of CERN.

8. – The Nature of the Aims of CERN.

Before ending this report, I would like to stress three points which are essential in order to understand the real nature of CERN.

The first refers to the relations between CERN and national institutions. The Convention constituting CERN establishes that CERN has to collaborate with the national research institutions — and this collaboration is already

TABLE III. – *Accelerators producing particles of en*

Country	Place	Institution of which the machine belongs	Organization supplying money	Director of laboratory	Director of project	Collaborato
Sweden	Uppsala	The Gustaf Werner Institute for Nucl. Chemistry, University	The late Gustaf Werner Institute and Swedish Atomic Energy Commission	TH. SVEDBERG	TH. SVEDBERG	H. TYRÉN B. HEDIN B. HELLSTR
United Kingdom	Harwell	Atomic Energy Research Establishment	Department of Atomic Energy	J. D. COCKCROFT	T. G. PICKAVANCE	H. SNOWDE J. B. ADAM
	Birmingham	Physics Department,	Department of Scientific and Industrial Research	M. L. OLIPHANT P. B. MOON	M. L. OLIPHANT P. B. MOON	J. S. GOODE L. V. HIBB J. L. SYMON H. H. TAYL and others
	Liverpool	Liverpool University	Department of Scientific and Industrial Research University Grant Committee	H. W. B. SKINNER	M. J. MOORE	J. R. HOLT W. J. G. GRE B. S. HALLI J. H. CRAIG Messrs. Met politan Vick Electr. Co.
	Glasgow	University	Department of Scientfic and Industrial Research	TH. I. DEE	M. MAC FARLAINE	Messrs. Met politan Vick Electr. Co., A.E.R.E.,

han 100 milion electron volt. Machines in operation.

e ine	Max. energy	Appr. date nf operation	Nr. of research groups	Beam intensity	Repe-tition time	Duration of pulse	Present stage
o- on	200 MeV	December 1951 ready for research 1952	6	Internal beam average 1 μA	240 pps	100-500 μs	Used for fundamental high energy physics, nuclear, chemistry spectroscopy etc.
on	180 MeV	September 1949	4	1-2 mA internal	50 pps	200 μs	—
otron	1 GeV	July 1953	4	$3 \cdot 10^9$ protons per pulse	0.1 pps	3 ms	—
o- on	410 MeV	August 1954	5-6	1 μA internal	about 200 pps	several hundred μs	Almost complete.
n- tron	320 MeV	April 1954	4		5 pps	10-1000 μs	—

pps = pulse per second.

TABLE IV. – *Accelerators producing particles of energy larger t*

Country	Place	Institution to which machine belongs	Organization supplying money	Director of laboratory	Director of project	Collaborat
France	Saclay	Commissariat à l'Énergie Atomique	Commissariat à l'Énergie Atomique	F. PERRIN	R. MAILLÉT S. D. WINTER	BERNIER, BRUCK, DEB LÉVY-MEND LUTZ, PODL PAUTHIER, VOST, TA
Germany	Bonn	Physicalisches Institut, University	Deutsche Forschungsgemeinschaft	W. PAUL	W. PAUL	Dr. BODEN Dr. EHREN Dr. STEINW
Italy	Rome	Nat. Institute for Nuclear Physics	C.N.R.N. and industry		G. SALVINI	E. PERSICO I. F. QUER M. AGENO
Netherlands	Delft	Department of Technical Physics, University	University of Delft	F. A. HEYN	F. A. HEYN	
Sweden	Stockholm	Swedish Atomic Energy Commission	Swedish Atomic Energy Commission	H. ALFVÉN	O. VERNHOLM	S. LUNDQV H. NYSÄTE E. SMÅRS, M. SEDLAC C. E. TÖRN A. HOLM
United Kingdom	Harwell	Atomic Energy Research Establishment	Department of Atomic Energy	J. D. COCKCROFT	T. G. PICKAVANCE	Mr. MULLE Mr. WELKI Mr. SNOWD

illion electron volt. Machines in drawing or constructing stage.

e ne	Max. energy	Appr. date operation	Nr. of research groups	Beam intensity	Repe-tition time	Duration of pulse	Present stage
tron g	1.75 GeV	January 1958			1 pps		Planning of the project
n- tron ng	500 MeV	1956 or 1957	1		50 pps		Planning almost finished. Started preliminary experiments
n- tron	1.0-1.2 GeV	1957 or later	about 10	possibly 10^{10} electrons per pulse	25 pps	1000 μs	Preparing model of synchrotron; no definitive orders to industry given
tron	1 GeV	1956			1.25 pps		
n- tron	1 GeV	1956		10^{9}-10^{10} electrons per pulse	12.5 pps		Dynamic measurement on full scale magnet sector
near tor	500 MeV	1958 or 1959	3-4	1 μA mean current	50 pps	200 μs	Design study completed up to 150 MeV; engineering design in progress

pps = pulse per second.

going on with many universities and other research institutions of the various European countries — and also when setting up the structure of the Organization itself and that of the Laboratory in Geneva, the Council limited its aims in order to avoid too large a concentration of European activities in one place, even if this should be the European Laboratory itself. The idea is rather to have a place, namely the Geneva Laboratory, where European physicists may go for special research which needs exceptional facilities not available n their own institutions and where, at the same time, they will have the opportunity of meeting their colleagues and exchanging their views so that, as a consequence, they will get a further stimulus for their activities in national institutions.

The second point concerns the organizational structure of the Laboratory which is determined by the principle expressed in the following form in the Minutes of the 7th session of the Council: « The new Laboratory at Geneva should resemble in its research characteristics the research laboratory of a university, through which there is a free flow of graduates », and therefore « most posts should be of a short duration to allow of the flow of scientists through the Laboratory so necessary to avoid stagnation. This will also increase the number of scientists who are able to use the unique facilities of the Laboratory ».

The third point relates to the purposes of the Organization which are established in Article II of the Convention, reading as follows: « The Organization shall provide for collaboration among European States in Nuclear Rsearch of a pure scientific and fundamental character, and in research essentially related thereto. The Organization shall have no concern with work for military requirements and the results of its experimental and theoretical work shall be published or otherwise made generally available... ».

SUPPLEMENTO AL VOLUME II, SERIE X
DEL NUOVO CIMENTO

N. 1, 1955
2° Semestre

The Alternating Gradient Proton Synchrotron.

J. B. ADAMS

Proton Synchrotron Group, CERN - Geneva

1. – Introduction and History of the CERN Proton Synchrotron Group.

The purpose of this paper is to describe in physical terms the new principle that has extended the maximum energy to which proton synchrotrons can be built nowadays. By using the principles of the constant gradient machines, of which the Cosmotron at Brookhaven and the Bevatron at Berkeley are examples, I will try to outline the differences between the old and new type machines and the facts that have been discovered in developing the new idea.

But first I would like to outline the history of the Group which has carried out most of this development work in Europe. In June of 1952 at a conference in Copenhagen the newly formed CERN Council decided to start an engineering design study for the construction of a 10 GeV proton synchrotron that was to be a scaled up version of the Cosmotron. The principles of this machine were well known at this time and so the design study was thought to be a simple extrapolation of engineering design. By July 1952 a design group of three people was set up with Dr. O. DAHL in charge and they were asked to have the study ready by November 1953.

In August of 1952 DAHL, WIDERÖE and GOWARD visited Brookhaven to see the Cosmotron at first hand and to talk to the staff that had built it. They found not only the Cosmotron but a new idea for making cheaper and higher energy machines. This idea was so attractive that in October 1952 the CERN Council decided to drop the engineering study for a 10 GeV proton synchrotron and ask the group to undertake a theoretical study on the new idea. The energy of the new machine was fixed at about 30 GeV since it seemed at that time that a 30 GeV new style machine would cost about the same as a 10 GeV old style machine.

In December 1952 the Proton Synchrotron (PS) group was formed to augment the original staff of three and, for convenience, the group was split up into four subgroups charged with investigating the main features of the

new idea. The theoretical study group, working mainly on questions of orbit stability, had its headquarters in Harwell, England, and some of its staff in Copenhagen. The magnet studies were concentrated in Paris in Professor GRIVET's laboratory. The radio frequency problems were studied at Heidelberg in Professor BOTHE's institute, and the headquarters of the whole group was at Dr. DAHL's Institute at Bergen. For the next ten months the group worked on the various problems and met together from time to time to discuss results.

By October 1953 enough was known about the machine to make it possible to present a tentative design to the Council of CERN. In America meanwhile the Brookhaven team and another at M.I.T. Boston had been working on the same problems. So at the end of October a conference was held at the Institute of Physics of the University of Geneva to which were invited representatives of Brookhaven, Berkeley, M.I.T. and the Mid-Western Universities. The PS group of CERN gave a series of lectures on its researches over the previous year and presented a consistent and, I think, practical design for a 30 GeV Alternating Gradient (A. G.) Proton Synchrotron. The Brookhaven team had also covered the same ground and had arrived at an almost identical design.

At the time of this conference the CERN Council agreed that the PS group should centre itself in Geneva as this was going to be the final home of CERN and the State of Geneva and the University kindly offered temporary accommodation for the group. By December 1953 most of the group had moved to Geneva and the real work of designing the machine started.

We plan that the construction of the machine will take about six years. A start has already been made on the final site at Meyrin which is near the French frontier, west of Geneva. We hope to have our final laboratories and main buildings for the machine completed at the beginning of 1956 when we will move to the permanent site. The manufacture of the magnet, which is the most important part of the machine and the one which determines the time scale for construction, will start in the middle of 1955 and parts will arrive on the site in the middle of 1956. The whole machine should be installed by the end of 1959 and the first trials started at that time.

We hope to build up the staff from the present 50 to about 70 by the end of 1954, 120 by the end of 1955 and reach our peak staff of 130 during 1956. Thereafter there will be a fall off in staff as the machine reaches completion and finally a large part of the design staff will be replaced by nuclear physics staff using the machine for high energy nuclear physics experiments.

2. – Principles of the Constant Gradient Proton Synchrotron.

Although the principles of the constant gradient (C. G) machine are well known it is useful to have these in mind when considering the differences between the two types of machines. The Cosmotron is taken as an example of a C. G.

machine. Protons are accelerated from an energy of 3.5 MeV, at which energy they are introduced into the machine from an electrostatic generator, to about 2.5 GeV. The acceleration is at a constant radius of 10 metres in a ring shaped magnetic field. The magnetic field is increased from the injection field of 270 gauss to a peak field of 14 000 gauss in 1 s so keeping the particles at constant radius as their energy is increasing.

We first consider the stability of the free transverse oscillations, or betatron oscillations, at constant energy. If the lines of magnetic field are bowed outwards from the centre of the machine so that there is a fall off in the magnetic field with radius then for a particle displaced above or below the horizontal plane of symmetry there is a restoring force towards this median plane. Therefore for all negative values of the field gradient $\mathrm{d}B/\mathrm{d}r$ there will be some focusing force in the vertical direction. If we define,

$$n = -\frac{r}{B}\frac{\mathrm{d}B}{\mathrm{d}r},$$

then the condition for vertical stability is that $n > 0$. In the horizontal plane there is an equilibrium radius for a particle defined by its energy as,

$$B_0 r_0 = \frac{\sqrt{E^2 - E_0^2}}{ec},$$

that is, a particle at energy E in a magnetic field B_0 will describe a circle of radius r_0 round the machine. A particle placed at some greater radius r_1 in a slightly decreased field B_1 will oscillate about the equilibrium orbit circle providing the product $B_1 r_1$ is greater on the outside of the circle than $B_0 r_0$ and smaller on the inside. The limit of stability is reached when the product $B_1 r_1$ is the same as $B_0 r_0$ or when,

$$\frac{\mathrm{d}(Br)}{\mathrm{d}r} = 0 .$$

In terms of the field gradient n this is,

$$n = 1 .$$

So we find that for stability of the free oscillations in both vertical and horizontal directions we must have,

$$0 < n < 1 .$$

We now consider the oscillations of particles at different energies in the machine. As already noted there is a certain circle of radius r_0 where the

magnetic field is B_0 and round which particles of a certain energy E_s will circulate without oscillation. E_s is called the equilibrium energy. Now the magnetic field is increasing with time and to keep particles at a constant radius their energy must be increased by a certain amount eV per revolution. The method of increasing their energy is usually by acceleration in an electric field fed by a radio frequency power generator making available more than the required energy gain per revolution. We assume that the frequency of this generator is sympathetically matched to the magnetic field so that particles going round the equilibrium orbit at a velocity corresponding to their ever increasing energy always take a revolution time equal to the periodic time of the accelerating voltage. Then at some phase of the accelerating voltage waveform particles can find a voltage that will give them the correct energy gain per revolution providing the peak voltage available is greater than that required by the particles. There are of course two phases, one on either side of the sinusoidal accelerating voltage waveform, where the correct energy gain per revolution can be found. The stable one, called the equilibrium or stable phase, is discovered as follows. A particle at an energy greater than the equilibrium energy will describe a circle of larger radius than the equilibrium radius and so take longer to go round one revolution. But on the other hand it is going at a greater velocity than the equilibrium particle and so takes less time to go round. It happens in a synchrotron that the increase in revolution time due to the larger radius is greater than the decrease in revolution time due to the increased velocity, so the radius effect wins. Now if this particle at greater energy takes longer to go round then it finds itself after one revolution at a different phase of the accelerating waveform. The stable phase angle is then on that side of the sinewave that makes this new phase angle correspond to less energy gain per revolution for this particle. Then as the particle goes round it gains less energy than the equilibrium particle and finally has the same energy. A similar argument applies to particles with less initial energy than the equilibrium particle and consequently at smaller radius than the equilibrium radius. In this way particles oscillate in energy, phase and radius about the equilibrium values. The frequency of this oscillation is very slow compared with the free oscillations so that the analyses for the free oscillation can be carried out assuming constant energy.

It is of interest to note that if the frequency of the accelerating voltage is not correct for the equilibrium particle at its equilibrium radius then there must exist some new equilibrium radius at which the particle can pick up the correct amount of energy without oscillating in phase. Providing this new equilibrium radius is inside the vacuum chamber then some particles will be accelerated, but if at any time during the 1 second accelerating period the equilibrium orbit goes outside the vacuum chamber then all particles are lost. This condition determines a frequency tolerance on the accelerating voltage

frequency throughout the cycle and means that elaborate arrangements have to be made to keep the frequency and the magnetic field in step.

3. – Principles of the Alternating Gradient Proton Synchrotron.

In recent years the cost of proton synchrotrons has mounted rapidly until nowadays a machine whose energy satisfies a nuclear physicist costs as much as a modern jet bomber. It became increasingly clear that if further progress was to be made in high energy nuclear physics by experiments using artificially accelerated particles some new principle must be found that would cheapen the cost per GeV. It was lucky for CERN that just at the time a European machine was being considered this new principle was discovered. The problem was simple enough. A cheaper machine could be built if the amplitudes of the free and forced oscillations of the accelerating particles could be decreased in some way so that the vacuum chamber size and the cross-section of the magnet ring could be reduced. The simplest way to reduce the amplitude of the free oscillations is to increase the frequency by increasing the restoring force, and although this is easy to achieve in the vertical direction by increasing the magnetic field gradient, the condition for horizontal stability is violated if n exceeds unity.

The new principle discovered by CHRISTOPHILOS and COURANT, LIVINGSTON and SNYDER increases the frequency of the betatron oscillations by alternating the sign of the gradient of the magnetic field. The structure of the magnet is no longer uniform round the ring with a constant gradient but is broken up into sectors whose gradient is alternatively positive and negative.

Equations of motion: $\ddot{\varrho} = \omega_0^2 n \varrho$, $\ddot{z} = \omega_0^2 n z$

Solutions for radial motion:

focusing field, $n = -$

$$\varrho = A \sin \omega_0 n^{\frac{1}{2}} t + B \cos \omega_0 n^{\frac{1}{2}} t$$

defocusing field, $n = +$

$$\varrho = C \sinh \omega_0 n^{\frac{1}{2}} t + D \cosh \omega_0 n^{\frac{1}{2}} t .$$

Particle motion (sector length $= \pi/2$).

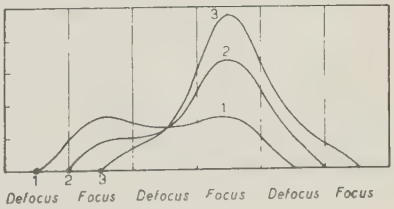

Fig. 1. – Motion of particles in an A.G. machine.

In Fig. 1 are given the magnetic field equations and the differential equations for particles circulating in these fields. The solutions to these equations in the case of the horizontal motion for instance show that when n is negative the sector is focusing for this motion, but that when n is positive the solutions give an exponential divergence of the particle away from the equilibrium orbit. Nevertheless under certain conditions it is possible to achieve overall focusing properties over a number of sectors as is shown in the lower

illustration. Since the old restriction of $n=1$ no longer applies n can now be a very large number so that the wavelength of the oscillation can be reduced to the length of a few sectors and the number of cycles of betatron oscillation per revolution can be increased from 0.7 to the order of 10. There is now no difference in the focusing conditions for horizontal and vertical motions since what is a focusing sector for horizontal motion is a defocusing sector for vertical motion and vice versa so that the magnet structure looks the same for both motions with a phase shift of one magnet sector.

We can divide up the magnet structure into identical periods consisting in the simplest case of a focusing followed by a defocusing sector which repeat an integral number of times round the magnet ring. A general transfer matrix can be written for this magnet period relating the end values for the displacement and derivative of a particle to the starting values,

$$\begin{pmatrix} y_1 \\ \dot{y}_1 \end{pmatrix} = T \begin{pmatrix} y_0 \\ \dot{y}_0 \end{pmatrix}.$$

There also exists a special solution, called the Floquet solution, which can be written,

$$\begin{pmatrix} y_{f_1} \\ \dot{y}_{f_1} \end{pmatrix} = \lambda \begin{pmatrix} y_{f_0} \\ \dot{y}_{f_0} \end{pmatrix}$$

where λ is the Floquet multiplier. It can be shown that the only possible oscillary solutions are when,

$$\lambda = e^{\pm i\mu},$$

where μ is the phase shift of the oscillation per magnet period. Applying these solutions to the general matrix gives,

$$\mathrm{Tr}\,(T) = (T_{11} + T_{22}) = 2\cos\mu,$$

from which the stability limits are,

$$\cos\mu = \pm 1 \quad \text{or} \quad \frac{\mathrm{Tr}\,(T)}{2} = \pm 1.$$

In Fig. 2 these limits have been drawn on a plane with axis n_1 and n_2 which are the n values in the focusing and defocusing sectors. Outside the two lines $\cos\mu_z = +1$ and -1 there is vertical instability and outside the other two lines $\cos\mu_r = -1$ and $+1$ there is horizontal instability. The final stable area for both motions is shaped like, and in fact called, a « necktie ». The waveforms of free oscillation drawn in Fig. 1 are for a machine operating in the middle of this stable area where $\mu_z = \mu_r = \pi/2$, i.e. where there is a

phase shift of $\pi/2$ radians every magnet period and so four magnet periods per betatron wavelength.

We now come to the stability of the energy oscillations. A particle with the equilibrium energy or momentum goes round the machine in a circle as in the constant gradient machine. But due to the rapid fall-off of the magnet field with radius in a defocusing sector, and the equally rapid increase in magnet field with radius in a focusing sector, the equilibrium radius for a particle with say greater momentum than the equilibrium particle is no longer a smooth curve along the sectors but a discontinuous series of straight lines as is shown in Fig. 3. The radial position of these straight lines corresponds to where the product $B \cdot r$ is appropriate to the energy of the particle and they lie either side of the continuous equilibrium orbit for the particle of correct energy. The particle cannot of course follow these discontinuous lines and particles on the new equilibrium orbit are found to describe a nearly sinusoidal motion of wavelength equal to the magnet period displaced outwards at a greater radius than the old equilibrium orbit in the case of particles with greater energy. The important fact now emerges that the displacement of the equilibrium orbit in the alternating gradient machine for a given energy difference is far smaller than in a constant gradient machine and the term used to express this effect is « momentum compaction ». For a constant gradient machine we have

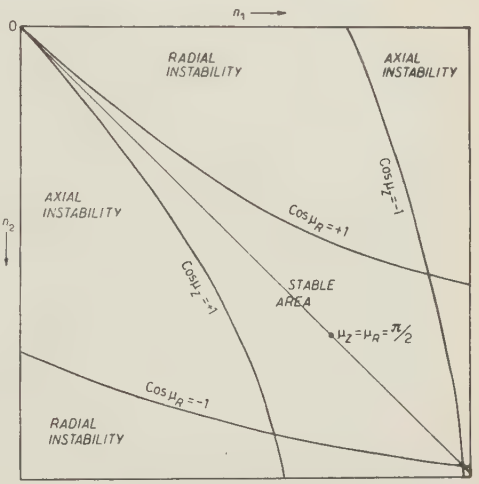

Fig. 2.

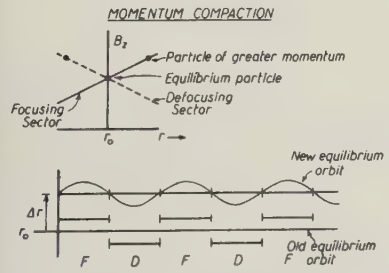

Momentum compaction factor: =

$$= \frac{\Delta r/r_0}{\Delta p/p_0} = \frac{1}{n} \cdot \frac{2}{\varphi} \left[\frac{1}{\coth \varphi - \cot \varphi} \right]$$

where, $\varphi = \frac{\pi}{2M} \cdot n^{\frac{1}{2}}$,

M = magnet periods per revolution.

Fig. 3. – Momentum compaction.

$$\frac{\Delta r/r_0}{\Delta p/p_0} = \frac{1}{1-n} \cong 2.5,$$

but for the alternating gradient machine we have

$$K = \frac{\Delta r/r_0}{\Delta p/p_0} = \frac{1}{n} \cdot \frac{2}{\varphi} \left(\frac{1}{\coth \varphi - \cot \varphi} \right),$$

where $\varphi = (\pi/2M) \cdot n^{\frac{1}{2}}$ and M is the number of magnet periods per revolution. For a typical A.G. machine the « momentum compaction factor » $K = 0.04$ gives an improvement of about 60 to 1 over the C.G. machine and this is just as important as the reduction in the betatron oscillation amplitude already noted in favour of the new principle.

However this improvement brings with it certain difficulties or at least differences in the conditions of stability of the energy oscillations. It has already been described how particles in a C.G. machine oscillate stably about a certain phase of the waveform of the accelerating voltage. It was pointed out that the increased radius of a particle with greater energy than the equilibrium particle caused the particle to take longer to go round one revolution, and that this effect more than offsets the decrease in revolution time due to the greater velocity of this particle. In the A.G. machine, due to the momentum compaction effect, the increase in radius is so small for a particle with greater energy than the equilibrium particle that the velocity effect wins in the non-relativistic region and the stable phase is on the other side of the accelerating voltage waveform, as it is in a Linear Accelerator where there is only a velocity effect. However, when the particles reach relativistic velocities the velocity effect becomes smaller and smaller and finally the radius effect wins again. Thus at some time during the acceleration cycle the stable phase angle changes from one side of the accelerating voltage waveform to the other, from the Linac stable phase angle to the synchrotron stable phase angle. The particle energy at which this change over takes place is called the « Transition Energy » and in order to preserve the full beam intensity it is essential to shift the phase of the accelerating voltage waveform by π radians fairly quickly at this critical energy.

This summary completes the main physical features of the new idea and the differences in principle between A.G. machines and C.G. machines. We must now look at the difficulties that rise when the new idea is examined in greater detail and an attempt is made to realise an alternating gradient machine in practice. What has been described above was covered in the original paper of COURANT, LIVINGSTON and SNYDER. What follows was uncovered by the development work of the American groups at Brookhaven and at M.I.T. and independently by the CERN PS group in Europe.

4. – Modifications to the Stability Criteria due to Errors of Construction.

In an A.G. proton synchrotron the magnet is divided up into a number of supposedly identical sectors. These sectors are physically separate units and have to be arranged round a circle. If the units are perfect in themselves there will still be some error in the alignment of the units round a perfect circle. Also the n values in the various sectors will not be identical, as manufacturing

and material tolerances will cause random variations about the correct value.

In Fig. 4 these sorts of errors are analysed into equivalent perturbations that act on a particle as it goes round the machine. It can be seen that the mechanical errors of alignment give rise to perturbations that are independent of the displacement and derivative of the particle as it goes by the incorrectly placed sector whereas an error in the n value of a sector or in its physical length gives rise to a perturbation that is linearly proportional to the displacement of the particle or its derivative, or both. There is one other type of error not shown in Fig. 4 which is of importance in the operation of the machine. If one sector is twisted out of the plane of the orbit, then coupling terms arise between the horizontal and vertical betatron oscillation which in some circumstances can produce serious effects.

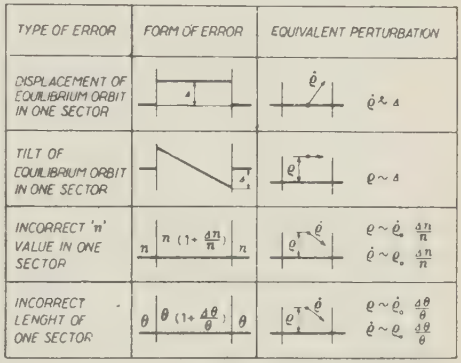
TYPE OF ERROR
FORM OF ERROR
EQUIVALENT PERTURBATION
DISPLACEMENT OF EQUILIBRIUM ORBIT IN ONE SECTOR
TILT OF EQUILIBRIUM ORBIT IN ONE SECTOR
INCORRECT 'n' VALUE IN ONE SECTOR
INCORRECT LENGHT OF ONE SECTOR

Fig. 4.

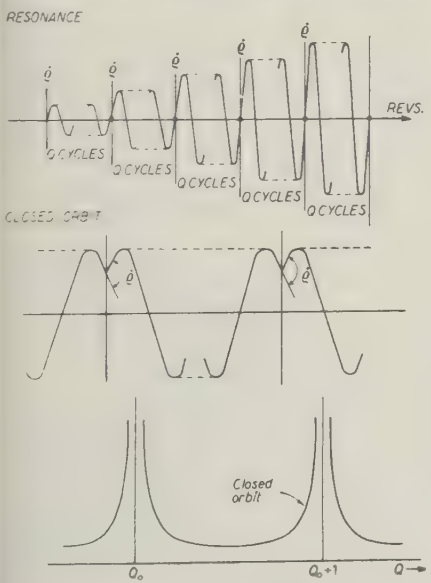

Fig. 5. – Resonance in a linear system. Perturbation $\dot{\varrho}$ = constant.

The effect of the first « constant » type of perturbation, due to misalignments is shown in Fig. 5 for the simple case of one perturbation per revolution. If there are an integral number of betatron cycles per revolution (called Q) then the perturbation excites a resonance since it occurs at the same phase of the betatron oscillation each turn. If we adjust the parameters of the machine so that it operates between these resonant points, then there exists an orbit for a particle that repeats itself each revolution allowing for the perturbation. This is illustrated for this simple case in the second diagram of Fig. 5. This special orbit is called the « Closed Orbit » and it can be shown that all other orbits are free oscillations about the closed orbit. At a resonant value the displacement of the closed orbit from the ideal orbit becomes infinite as is shown in the last picture.

The second type of perturbation, illustrated in Fig. 6, amplifies the free oscillations about the closed orbit. At the resonant values, that is integral

Q values, the perturbations excite oscillations whose amplitude becomes infinite, and the same thing happens when there are an integer plus a half cycles per revolution, at the so-called « Sub-resonances ». It can be shown that these resonances and sub-resonances do not occur at single values of Q but that there is instability over a narrow band of Q values about the resonant ones. At the edge of these « Stop Bands » the amplitude of oscillation rises linearly to infinite values and inside the stop bands the increase in amplitude is exponential. Between the stop bands the amplitude of oscillation beats up and down quite stably at a maximum amplitude shown in the last illustration of Fig. 6.

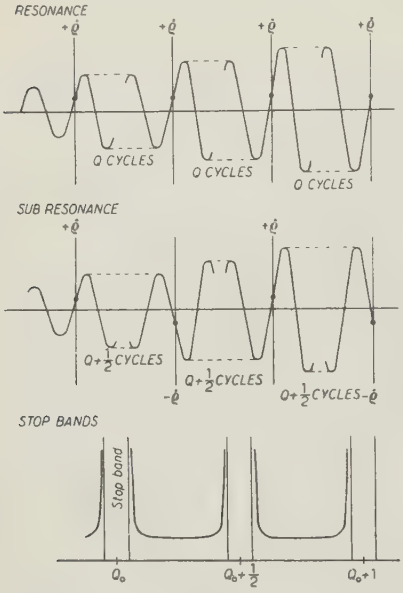

Fig. 6.

It is clear from these physical features that an A.G. machine must work between the stop bands with a Q value of integer plus a quarter or three quarters. If for any reason during the acceleration cycle the Q value approaches a stop band then most of the particles will be lost by collision with the vacuum chamber walls due to « blow up » of the betatron oscillations. As in the C.G. machine the closed orbit must, of course, lie within the vacuum chamber throughout the whole acceleration cycle.

We can now illustrate all these effects on the original stability diagram of Fig. 2. In Fig. 7 only the main resonances have been drawn in for a typical machine. In Fig. 8 the small black diamond shown in Fig. 7 is magnified and the sub-resonances drawn in. Also illustrated in this figure are the resonances due to the effect of twisted sectors mentioned above that occur when,

$$Q_R + Q_V = \text{integer}\,,$$

where Q_R and Q_V are the number of betatron cycles per revolution in the horizontal and vertical directions respectively. Finally in Fig. 9 the largest of the available safe areas called the « Working Diamond » is further magnified

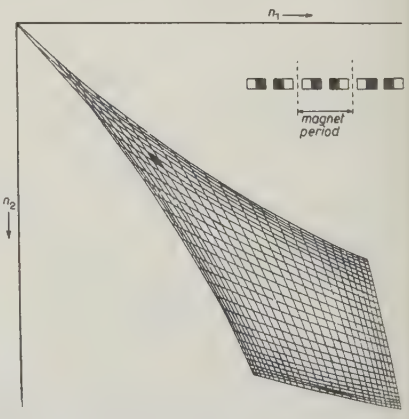

Fig. 7. – Stability diagram (resonance lines drawn in).

and all the stop bands drawn in. The working point is then in the centre of this working diamond and it must stay near the centre during the whole of the acceleration cycle.

Now the question of stability of the betatron oscillations looks very different from the original picture given in Fig. 2. The large stable area has been subdivided by unstable bands until only a very small area is really safe and the tolerances imposed on the errors of construction of the machine are very tight indeed.

For a typical machine the length of the working diamond expressed as a ratio of the mean n value at the working point is

$$\frac{\Delta n_1}{n} = 5\ \%$$

and the width of the diamond in the same units is

$$\frac{\Delta n_2}{n} = 1\ \%\ .$$

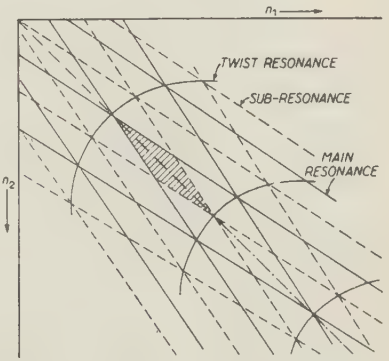

Fig. 8. – Part of stability diagram (main, sub and twist resonances).

The width of the stop bands is determined by the random errors in the sector n values or in sector lengths and to keep the stop bands reasonably narrow, so that the safe area of the working diamond is not further reduced, it is necessary to limit the random n errors to less than 1% of the mean n value.

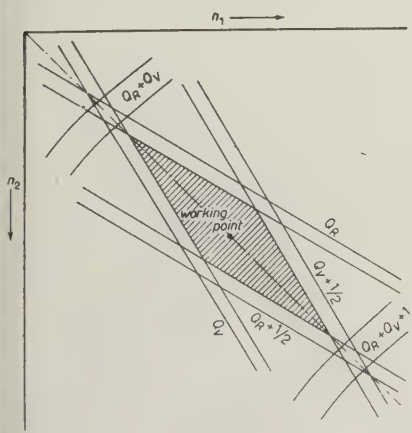

Fig. 9.

The A.G. machine is very sensitive to mechanical misalignment errors. If in a C.G. machine we displace one sector of the magnet of length l by an amount a then the peak amplitude of oscillation due to this displaced sector is approximately

$$\hat{y}_{CG} = \frac{l \cdot a}{r_m} \cdot \sqrt{1 - n}\ ,$$

where r_m is the mean radius of the magnet ring. The same length sector displaced by the same amount in an A.G. machine gives a peak amplitude of oscillation of

$$\hat{y}_{AG} = \frac{l \cdot a}{r_m} \cdot \sqrt{n} \cdot W\ ,$$

where W is a waveform correction factor due to the non-sinusoidal waveforms in A.G. machines. For a typical machine where $\mu = \pi/3$, W is about 4. Allowing for the much higher n of the A.G. machine compared with the C.G. machine and the different waveforms the ratio

$$\frac{y_{AG}}{y_{CG}} \cong 100 .$$

In practice to keep the peak deviation of the closed orbit within 0.5 cm of the centre of the vacuum chamber the magnet units of an A.G. machine have to be aligned to within $\pm$ 0.05 cm of a perfect circle. Since the mean radius of a 25 GeV machine is about 100 metres this means measuring the position of the magnet units to within 1 part in 10^5. As has already been emphasized if the closed orbit at any time wanders outside the vacuum chamber then all particles are lost, not just a fraction of them.

5. – Design Data and Layout of a 25 GeV Proton Synchrotron.

In Table I are listed the significant parameters of the most recent CERN design of a 25 GeV machine. The energy is only limited by financial consi-

TABLE I. – *Parameters of a* 25 GeV *proton synchrotron.*

Maximum energy	E	= 25	GeV
Maximum magnetic field on the orbit	B_0	= 12 000	gauss
Radius of curvature of magnet units	r_0	= 7178	cm
Mean radius of orbit	r_m	= 9490	cm
Field index	n	= 278	
Phase shift of betatron oscillations per magnet period	μ	= 0.8	
Number of betatron cycles per revolution	Q	= 6.25	
Transition energy (total)	E_{TR}	= 6.0	GeV
Injection energy (kinetic)	E_1	= 50	MeV
Injection magnetic field	B_1	= 140	gauss
Time of rise of magnetic field	t	= 1	s
Pulse repetition	T	= 5	s
Harmonic order of radiofrequency	m	= 32	
Radiofrequency range	5.1 to 16.3		MHz

derations and the peak magnetic field by reasons of constancy of n during the acceleration cycle. The values of n and μ have been chosen as the result of a comprehensive study of all the limitations imposed by the physical features of such a machine. The transition energy is determined by the need to get passed the rapid change in the velocity of the particles while they are ap-

proaching relativistic velocities and the need to allow the energy oscillations to be damped down so that discreet bunches of particles are formed before the phase of the accelerating voltage is shifted. The injection energy is chosen as high as is practical using known Linac design information. The Cosmotron of 10 m radius can use an electrostatic generator giving 3.5 MeV protons and inject at a magnetic field of 270 gauss. With our machine of 100 m radius the injection energy is 50 MeV at a magnet field of 140 gauss which is only half the Cosmotron value. Bearing in mind that the remanent fields in the magnet are about 40 gauss and that eddy current effects are of the order of tens of gauss this injection field is rather low. But without constructing a very high energy Linac similar to the new Harwell Linac it is not possible to go any higher. The rise time of the magnetic field is determined by the peak kVA of the generator supplying the power which for a 1 s rise time is about 28 000 kVA. The rise time could be as long as 2 s without any detrimental effect. The repetition rate of the magnet cycle is a question of the mean generator power and more importantly of the rate of the output pulses from a nuclear physics point of view. If we ask for at least one pulse every 5 s, as is delivered by the Cosmotron, then the mean generator power is about 1.7 MW. Finally the harmonic order of the accelerating voltage frequency is chosen

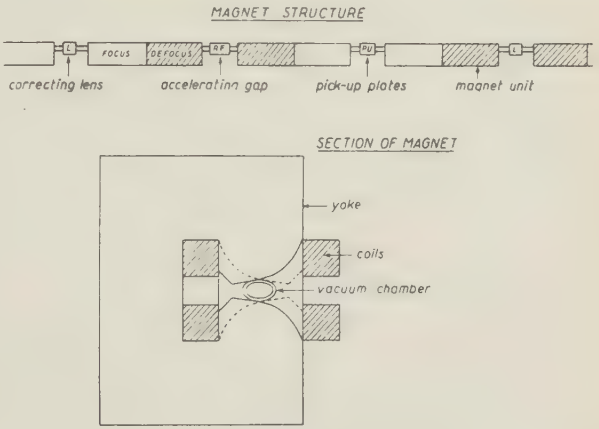

Fig. 10. – Magnet structure.

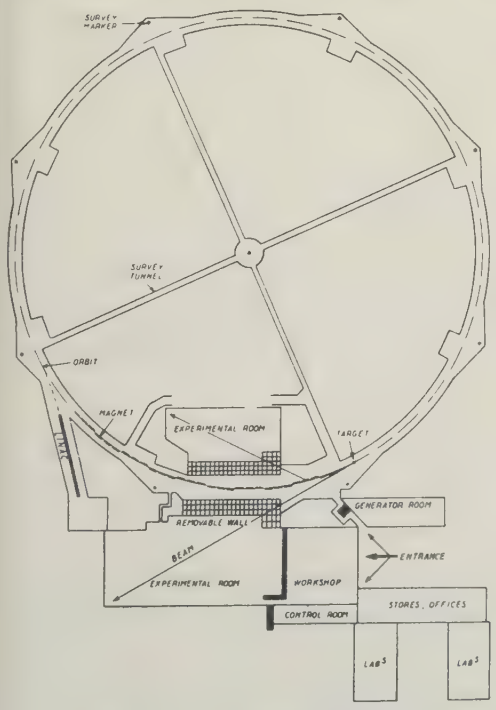

Fig. 11. – Building layout.

as high as possible so that the amplitude of the energy oscillations is as small as possible consistent with the practical performance of the material used in the accelerating cavities whose properties deteriorate at frequencies much higher than 20 MHz.

In Fig. 10 the structure of the magnet is shown diagramatically with breaks between the magnet units for placing the accelerating cavities and other correcting lenses. The cross-section of the magnet is also illustrated.

Fig. 11 shows the shape of the buildings to house the proton synchrotron.

6. – Conclusions.

This completes an introduction to the new A.G. proton synchrotron showing how the idea started, the original optimism and the subsequent disenchantment as the development work proceeded. We are left with a new type of machine that offers a method of getting very high energy particles cheaper than by any other artificial means but at the expense of imposing very tight tolerances in the construction of the machine. Nevertheless the fact that both Brookhaven and CERN are going ahead with this type of machine shows that there are reasonable hopes that the tolerances can be met in practice.

Appendix

1. – Comparison between the Beam Intensities of an Alternating Gradient Proton Synchrotron and a Constant Gradient Proton Synchrotron of the same Vacuum Chamber Aperture.

It is of general interest to calculate the beam intensity accepted into a constant gradient proton synchrotron of the same aperture and therefore roughly of the same cost as the present CERN design of alternating gradient proton synchrotron. At least such a study will answer the question why do we proceed with the A.G. design despite all the difficulties with construction tolerances rather than make a more established and better understood machine.

There are certain common features with either machine. The injection energy cannot be any different from 50 MeV since it is determined by the injection field which should not go lower than the present 140 gauss. Similarly there is no reason to suppose that the vacuum pressure will be any different in the two machines if the same size chamber is used.

2. – Injected Beam Diameter Inside the Vacuum Chamber.

We will take the same value for the « Acceptance » of the injection Linac that has been used for the A.G. machine, namely

$$A_L = 0.5 \cdot 10^{-3} \text{ cm radians}$$

(e.g. spot radius of 0.5 cm and incoherent half angle of divergence of 10^{-3} radians).

The cross-section of the beam, if it is correctly introduced inside the vacuum chamber of the C.G. machine, is given by

$$\text{vertical height of beam} = \hat{y}_v^2 = \frac{r_m}{n^{\frac{1}{2}}} \cdot A_L ,$$

$$\text{horizontal width of beam} = \hat{y}_r^2 = \frac{r_m}{(1-n)^{\frac{1}{2}}} \cdot A_L ,$$

where r_m is the mean radius of the vacuum chamber.

Substituting appropriate values for the C.G. machine, we find

$$\hat{y}_v = 2.4 \text{ cm} \quad \text{and} \quad \hat{y}_r = 2.95 \text{ cm} .$$

These are amplitudes so the peak to peak beam dimensions are

$$\text{height} = 4.8 \text{ cm} \quad \text{and} \quad \text{width} = 5.9 \text{ cm}$$

and the cross-section is elliptical.

Remembering that the vacuum chamber has internal dimensions of height $\times$ $\times$ width = 8 cm $\times$ 12 cm, we see that the beam will nicely fit inside with some room to spare all round.

In the case of the A.G. machine the equations giving the beam cross-section are more complicated and for a machine with $n = 278$, $\mu = 0.8$ the beam dimensions work out to be

$$\text{height} \times \text{width} = 2 \text{ cm} \times 2 \text{ cm} .$$

3. – The Possibility of Multiturn Injection.

The beam current in the Cosmotron is greatly increased by using multi turn injection so that particles are accepted into the machine during several revolutions. It is obvious that with a beam 5.9 cm wide in a vacuum chamber of 6 cm half width there is no question of more than one turn injection. However, it is worth while to calculate the rate at which the equilibrium orbit shrinks in each revolution if the particles are not being accelerated. The

shrinkage per revolution is given by

$$\frac{\Delta r}{r_0} = \frac{\mathrm{d}B}{\mathrm{d}t} \cdot \frac{2\pi \cdot r_m}{c\sqrt{2(E_K/E_0)}} \cdot \frac{1}{B_0} \cdot \frac{1}{(1-n)},$$

where E_K is the kinetic energy of the injected particles,

B_0 is the magnetic field at injection,

E_0 is the rest energy of the proton.

For $\mathrm{d}B/\mathrm{d}t = 14000$ gauss/s, $r_m = 9490$ cm, $B_0 = 140$ gauss and $E_K = 50 \cdot 10^6$ eV, we find

$$\Delta r = 9.3 \text{ cm}.$$

4. – Comparison of the Current Accepted by the Two Machines.

We can write the proton intensity accepted by a machine in terms of the injected intensity as

$$I = \eta_s \cdot \eta_{\mathrm{gas}} \cdot \eta_T \cdot \eta_R \cdot I_0,$$

where the η are dimensionless coefficients due to the following reasons,

η_s is the loss coefficient due to the combined synchrotron and betatron oscillation amplitudes losing particles to the vacuum chamber walls;

η_{gas} represents the loss of particles due to gas scattering;

η_T is the loss coefficient due to passing through the transition energy in the case of the A.G. machine;

η_R is the loss coefficient due to deviations in the « closed orbit » at injection due to starting magnetic field errors.

We now proceed to calculate these coefficients for each machine.

5. – η_s, the Synchrotron Oscillation Coefficient.

The amplitude of radial oscillation during the synchrotron phase oscillation in a C.G. machine is given by

$$\frac{\Delta r_s}{r_0} = 1.18 \left[\frac{r_0 \cdot r_m \cdot \dot{B}}{E_k \cdot m \cdot n(1-n) \cdot 10^8} \right]^{\frac{1}{2}},$$

where r_0 and r_m are the radius of curvature and mean radius of the particles; $\dot{B} = \mathrm{d}B/\mathrm{d}t$; $m =$ harmonic order of the accelerating voltage frequency. The units are gauss, cm, eV.

If we use the fundamental frequency of the accelerating voltage, i.e. $m = 1$,

then $\Delta r = 236$ cm. If we use $m = 32$, the 32nd harmonic as in the A.G. machine, then $r = 40$ cm. In either case the oscillation amplitude is much larger than the vacuum chamber width.

To calculate η_s we imagine that particles are injected continuously at the correct energy and radius during one revolution. Working with a stable phase angle of 30°, half of these particles fall outside the stable phase swing in both machines. At one quarter cycle later in the synchrotron period all the particles that originally lay at one radius, but distributed round π radians in angle, have rotated so that they are bunched into a narrow angle around the machine, but spread out in radius. The peak value of the radial spread is just the synchrotron swing Δr_s calculated above. All those particles that now lie outside the vacuum chamber are of course lost and some allowance has to be made for the extra radial swing of the betatron oscillations set up at injection and already calculated above as $\hat{y}_r = 2.95$ cm.

From this model we find

$$\eta_s = \frac{a - \hat{y}_r/2}{\Delta r_s}$$

(where a is the horizontal half width of the vacuum chamber), and for the values already calculated $\eta_s = 0.1$. Even using the high harmonic order of 32, then 90% of the particles are lost during the first synchrotron oscillation cycle.

In the case of the A.G. machine, due to the momentum compaction, the synchrotron oscillation amplitude is only 0.5 cm and all the particles are held inside the vacuum chamber.

6. – η_{gas}, the Gas Scattering Coefficient.

Injecting at 50 MeV instead of 3.5 MeV as in the Cosmotron, the gas scattering losses are very much smaller even though the vacuum chamber is small and the pressure, $1 \cdot 10^{-5}$ mm Hg, rather worse. The method of calculating the gas scattering amplitudes and the probability of survival of a particle is given in *Rev. Sci. Instr.*, **24**, no. 9, p. 836. Using this method we find that

$$\eta_{gas} = 0.5$$

if we assume that the median plane of the particles at injection can lie up to 1 cm away from the geometric plane and that this effect gives an effective vertical half aperture of 3 cm for the vacuum chamber. Thus due to gas scattering at injection we lose about 50% of the injected particles.

In the A.G. machine there is virtually no loss due to gas scattering.

7. – η_T, the Transition Energy Loss Coefficient.

This coefficient only applies to the A.G. machine and must be a guess at this stage. We guess that perhaps half of the particles may be lost going through the transition energy, but we have reason to believe that very few will be lost

in practice. Nevertheless we take

$$\eta_T = 0.5 .$$

8. – η_R, the Injection Magnetic Field Error Coefficient.

The injection field is 140 gauss and we assume that we can measure this to ± 0.5 gauss, i.e. about $\pm 0.3\%$ accuracy. The equivalent radial shift of the equilibrium orbit due to this field is given by

$$r_R = \frac{r}{n}\frac{\mathrm{d}B}{B_0},$$

and for the C.G. machine $\Delta r = 37$ cm (for the Cosmotron it is only 5 cm). If we construct the magnet ring out of individual sectors of length l, as was done for the Cosmotron magnet, then the equilibrium radius in these sectors will be distributed at random about the correct radius within the limits ± 37 cm.

We can now work out the peak amplitude of betatron oscillation due to a shift of the equilibrium orbit in one of these sectors. For the C.G. machine,

$$\hat{y} = \frac{2\pi}{\lambda}\cdot l\cdot \Delta r_r = \sqrt{1-n}\,\frac{l\cdot r_r}{r_m}$$

and for $l = 25$ cm, $\Delta r = 37$ cm, we find $\hat{y} = 0.054$ cm. For N such sectors in the complete magnet ring in which the injection fields are distributed at random, we can simply write that the peak amplitude of oscillation after one revolution is

$$|\hat{y}|, = \hat{y}\sqrt{N} = \hat{y}\sqrt{\frac{2\pi r_0}{l}}$$

and for the C.G. machine $|\hat{y}|, = 2.27$ cm.

After one revolution all the errors repeat again and there is no randomness between successive turns. If the machine is working with one cycle of betatron oscillation (i.e. $n = 1$) per revolution, then the amplitude builds up linearly to infinity. If on the other hand $n = 0.75$, then there is one half betatron cycle per revolution and the amplitude built up on the first revolution is reduced again to zero on the next revolution and the closed orbit deviation is half the amplitude after one revolution. Since in C.G. machines $n = 0.6$, we assume that the closed orbit deviation is roughly equal to the amplitude after one revolution.

The net result of the errors due to injection field is to make the effective size of the vacuum chamber smaller than the actual size in the horizontal plane.

We can therefore calculate a new value for the synchrotron loss coefficient,

η_s, and call it η_s' and define the loss coefficient due to the errors in the injection field as

$$\eta_\kappa = \frac{\eta_s'}{\eta_s}.$$

For the C.G. machine values already assumed we find that

$$\eta_\kappa = 0.5 .$$

In the case of the A.G. machine similar errors in the injection field give a peak closed orbit deviation of 0.5 cm and this does not cause any loss of the beam.

9. – Mechanical Errors in Aligning the Sectors of the Magnet.

It has been shown that the A.G. machine is about 100 times as sensitive to errors in the alignment of the magnet sectors to a perfect circle as is the C.G. machine. Alignment errors present no great problems with the C.G. machine, but if the specified tolerance is not kept on these misalignments in the A.G. machine, then the closed orbit quickly approaches the vacuum chamber walls and all the particles are lost. It is difficult to express this idea as a loss coefficient since it's value is either 1 if the tolerances are maintained or 0 if they are not. All one can express is an alignment coefficient η_A for the C.G. machine which is $0.01\eta_A$ for the A.G. machine. The A.G. machine has just got to be aligned correctly by some means.

10. – Conclusion.

In Table II the various loss coefficients calculated for the two machines have been tabulated and the final accepted current worked out. We see with the rather optimistic conditions and simple methods used in this evaluation that a C.G. machine with the same size vacuum chamber as the latest CERN A.G. machine will only accept about 5% of that current accepted by the A.G. machine. This surely is sufficient justification for going ahead with the A.G. machine.

As a matter of interest the loss coefficients have been calculated for a C.G. machine with twice the horizontal aperture of the present A.G. machine. The accepted current is still only 36% of that accepted by the A.G. machine. The C.G. machine magnet cost for this double aperture would be over twice that for the A.G. machine magnet and the vacuum chamber and vacuum pump costs are also doubled. Furthermore the magnet generators cost more to supply the extra field. In fact such a machine would be appreciably more expensive than the A.G. machine, but not by a factor of 2.

TABLE II.

Kind of Machine	Alternating gradient	Constant gradient	Constant gradient
Vacuum chamber dimensions . . .	8 cm × 12 cm	8 cm × 12 cm	8 cm × 24 cm
Injected beam dimensions (for $A_z = 0.5 \cdot 10^{-3}$ cm radians)	2 cm × 2 cm	4.8 cm × 5.9 cm	4.8 cm × 24 cm
Injection time (revolutions)	1	1	3
Injected current	I_0	I_0	$3I_0$
Synchrotron oscillation amplitude (32nd harmonic)	0.7 cm	40 cm	40 cm
Synchrotron oscillation coefficient η_s	1	0.1	0.15
Gas scattering coefficient: η_{gas} (pressure = 10^{-5} mm Hg)	1	0.5	0.5
Transition energy coefficient η_{Tr}	0.5	1	1
Injection field coefficient η_B (error = 0.5 gauss in 140)	1	0.5	0.8
Alignment coefficient η_A	$0.05\eta_A$	η_A	η_A
Accepted current (normalised to that for A.G. machine)	1	0.05	0.36

Lastly, quite apart from comparisons of intensity between the two types of machines, there is an important practical difficulty with C.G. machines of large radius. For $n = 0.7$ and $r_0 = 100$ m, $dB/dr = 0.01$ gauss cm^{-1} at an injection field $B_0 = 140$ gauss. Over a vacuum chamber 10 cm wide therefore the field variation at injection time is only 0.1 gauss and if we ask that n should be constant to 10% over the aperture of the vacuum chamber, then we have to be able to measure and guarantee magnetic fields to better than 0.01 gauss.

This is far from possible and represents probably the greatest practical reason for abandoning C.G. machines at these high energies.

SUPPLEMENTO AL VOLUME II, SERIE X
DEL NUOVO CIMENTO

N. 1, 1955
2° Semestre

Experimental Facilities of the CERN Proton Synchrotron.

A. CITRON and M. G. N. HINE (*)

Proton Synchrotron Group CERN - Geneva (Switzerland)

The purpose of this lecture is to describe the building layout and provision for experiments which are planned for the CERN proton synchrotron. The general design of this machine has been considered by many people, and the plans proposed are the result of much discussion between members of the CERN P.S. group and the CERN architect, Dr. STEIGER of Zürich. The shielding calculations were made by Professor GENTNER and Dr. CITRON in Freiburg, and Dr. CITRON has since considered in detail various arrangements for targets and ejection of beams which will be described later in this lecture. I should also say that we have tried to keep in mind all the time that the machine is to be used for nuclear Physics, and that we are anxious to receive, and use, any criticism or suggestions from people with experience in using large machines, or who think that some kinds of experiments are not properly provided for.

When planning for a machine which will not be in full use for seven years or more, and for an energy ten times greater than that obtainable now, the main difficulty is, of course, one's ignorance of the course of physics in the intervening time, and of what will be the focus of interest when the machine actually works. There are, however, a few general considerations one can find from past experience which help in deciding what to include or leave out, and which we have tried to satisfy in our plans.

a) If a machine is to have a useful life of, say, ten years, the vast majority of the experiments done on it will not be of the kind which stimulated the desire for the machine before it was built, the qualitative, exciting work which discovers new particles and wins Nobel Prizes; the machine must also be

---

(*) Lecture given by Dr. HINE.

designed for the hundreds of experiments which are done to explore systematically the whole range of energies and nuclear properties and which are essential for proper testing of theories.

b) Past experience shows that machines usually fail in these latter types of experiments because of lack of intensity, which may, for example, rule out multiple scattering experiments, or which may prevent adequate analysis and collimation of the wanted particles to reduce backgrounds; because of lack of facilities to observe some energies or kinds of particles at all; and because of lack of experimental space round the machine, both close to the orbit and behind shielding walls.

c) With a good machine, the demand to use it can be so high that the machine should be running most of the time, so the shielding must be adequate for some people to be preparing their apparatus near the machine while other people are doing experiments, and also the targets must be arranged so that as many experiments as possible can run simultaneously, even if requiring different energies and intensities.

Before I describe how we have tried to meet these requirements in the CERN machine, I will have to recall some facts and figures about the machine, and about nuclear events at these energies. The machine is designed to give protons up to 25 GeV kinetic energy, with the possibility of getting somewhat higher if the behaviour of the magnets permits. The output is in pulses once every five seconds, whose duration might vary between 2 μs, if all the protons suddenly hit a thick target, and perhaps some tens of milliseconds if more elaborate target arrangements are successful. The beam current we shall actually obtain is less accurately predictable, but if figures which could reasonably be aimed at, of a 1 mA injected beam with 20 % capture and acceleration efficiency, are realized, then there would be $6 \cdot 10^9$ protons per pulse after acceleration, or a flux of about 10^9 per second. This is the figure on which our shielding calculations are based, though we have space in general for more shielding if it is later found necessary.

Nuclear Physics information for shielding and target design has been collected by Dr. CITRON in several CERN reports, both from published cosmic ray data, and from information found with the Brookhaven Cosmotron; the latter is of course for energies of about 2 GeV, but if extrapolated sensibly it agrees reasonably with the cosmic ray results. In the 25 GeV region it seems binding of nucleons in the target atoms can be neglected, that being all events treated as nucleon-nucleon collisions, and that the total cross-section for nuclear events is rather less than the geometric nuclear cross-section.

When a 25 GeV proton enters a thick target, the final result is always a

star, usually before the proton has lost more than one or two percent of its energy. The star particles, in an average case will amount to about

$$\left.\begin{matrix} 6 \text{ charged mesons} \\ 2 \text{ neutral mesons} \end{matrix}\right\} \text{ top energy 6 GeV}$$
$$2 \text{ neutrons} > 1 \text{ GeV}$$
$$2 \text{ neutrons} > 1 \text{ GeV}$$
$$26 \text{ neutrons} < 1 \text{ GeV}$$
$$2 \text{ protons} > 1 \text{ GeV}$$
$$26 \text{ protons} < 1 \text{ GeV}$$

On its way through the target the proton will undergo a certain amount of scattering from both electromagnetic and nuclear forces, including the effects of diffraction, and may also turn into a neutron in a charge exchange process before finally forming a star.

If the target is really thick, that is part of a shielding wall, the more energetic of the star particles can make another generation of small stars. Further thickness of shield gives exponential absorption of the degraded radiation. The absorption length of about 200 g/cm² can be derived by suitable modification of cosmic ray absorption data for the atmosphere. The result of these calculations, which are given in detail in Dr. CITRON's reports, and in the Report of the A.G. Synchrotron Conference in Geneva, are that a thickness of 5.5 metres of Barytes loaded concrete is necessary to shield workers against the full beam intensity.

The total attenuation factor of such a wall is about 10^4, so it is clear that if the intensity of particle beams into the experimental hall is more than one ten thousandth of the main beam in the machine, it may not be possible for people to work near unshielded experimental apparatus with the beam on.

This fact, with our requirement, stated earlier, that the machine must be able to run nearly continuously without affecting assembly and testing of apparatus, is one of the reasons we have experimental space both inside and outside the magnet ring (Fig. 1).

The length of the hall outside the ring was chosen to allow room for experiments to be set up at several points along the beams of highest energy which run diagonally across the hall, and also to allow time for a reasonable fraction of the highest energy π-mesons to decay to μ-mesons inside the hall. The width of the outside hall, and the size of the hall inside the ring give, we hope, enough room for the apparatus to stretch out at right angles to the direction of the main beams, or to the main shielding wall.

The other parts of the building, the workshops, laboratories and offices, are physically as close as they can be to the experimental area, but are shielded from the radiation in the outside hall by a subsidiary shielding wall 2 metres

thick and 5 metres high, running across the main hall and outside across the end of the control room wing (Fig. 1).

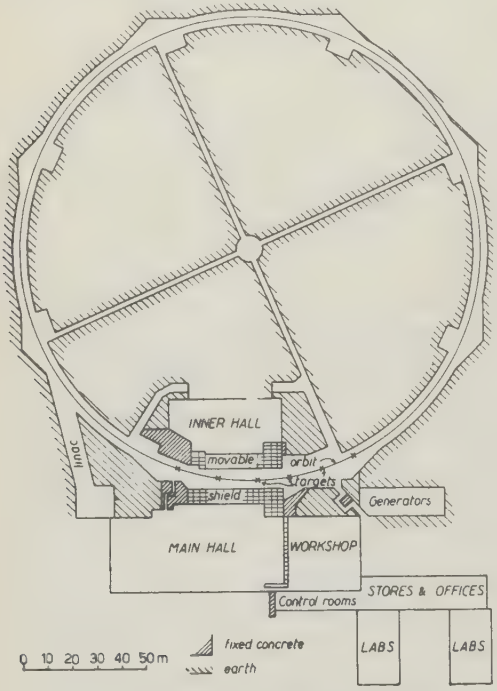

Fig. 1. – CERN Proton Synchrotron.

With this building and shielding layout we hope we can satisfy all the principles outlined above: the layout is flexible, with room for experiments either close to the magnets or behind the main walls. Targets can be seen from all angles, both in the inside and outside experimental areas. The shield is demountable if necessary, and the floor will carry any amount of extra shielding if, for example it, is needed for a high intensity ejected beam. The whole floor area is free from obstructing pillars, and is spanned by overlapping 20 ton cranes.

The best kind of output from a particle accelerator is of course one where all the circulating beam is extracted with good geometry over a long period of time, to improve counting efficiency and reduce background: unfortunately this has not been achieved in any circular high energy machine, and we must first consider the behaviour and yields of targets introduced into the circulating beam. After that the possible use of a Piccioni type ejector scheme will be discussed, but although this seems promising it cannot be regarded as a replacement for more conventional internal targets before it has been tried practically.

To help in evaluating methods of using internal targets, necessary physical data for some target material, and the effect on the proton motion in passing through a target of one nuclear mean free path thickness are given in Table I.

The column « shift of closed orbit » gives the inward radial displacement of the closed orbit in the proposed CERN Machine due to the loss of energy in one passage through the target. The « mean scattering angle » is that due to coulomb forces, and the last column is the amplitude of betatron oscillations produced by the protons being scattered through the mean angle.

It can be seen that a target thick enough to absorb most of the incident protons is large and unwieldy if made of a light element, and that the resulting large emitting area of the target will result in low particle fluxes into exper-

imental apparatus. This performance can be compared with that of a very thin foil target, where the energy loss is perhaps 50 keV rather than 200 MeV.

Table I.

Material	Nuclear Mean free Path		Energy loss in one m.f.p.		Shift of closed orbit cm	Mean Scattering Angle in one m.f.p.		Amplitude of free oscillations cm
	g/cm²	cm	MeV	%		radians	degrees	
H_2	35	500	140	0.56	1.6	$0.58 \cdot 10^{-3}$	0.033	1.2
Li	50	94	145	0.57	1.6	$0.70 \cdot 10^{-3}$	0.040	1.4
H_2O	77	77	154	0.62	1.8	$1.16 \cdot 10^{-3}$	0.067	2.3
Al	105	39	210	0.84	2.4	$1.7 \cdot 10^{-3}$	0.097	3.4
Pb	206	18	412	1.65	4.7	$4.75 \cdot 10^{-3}$	0.27	9.4

In this case, if the target is pushed into the beam after the magnetic field has stopped rising, the energy loss in one passage through the target is made up by energy gain from the radio frequency accelerators during the next revolution. Some small phase oscillations may be set up as a result, but the amplitude of the corresponding radial oscillation is of the order of a few millimeters. Otherwise the proton will continue to revolve in the machine neither gaining nor losing energy until it makes a nuclear collision in the target foil. During this time small angle scattering will have built up free oscillations to about the amount given in the last column of Table I, as the angle of scatter is the same whether the proton makes one transit through a thick target or many transits through the same total thickness of foil. As can be seen from the Table, the resulting oscillation can be comfortably held in the vacuum chamber for all but very heavy targets, and for light elements it is small enough to allow a total target thickness of two mean free paths, in which time almost all the protons will have caused a nuclear event.

There is one source of loss in this way of using targets, that if an appreciable nuclear scattering or a charge exchange occurs, the proton will be lost from the circulating beam and will not cause a star. In a single thick target, of course, these processes do not interfere with the final fate of the proton. This loss of star production is, however, a gain if one wants to use the scattered protons or the charge exchange neutrons, and this use of thin targets is the most efficient way of producing them The proportion of protons which will undergo a serious scattering, or turn into neutrons is difficult to estimate from existing data, but taking some Brookhaven information (Quarterly and Annual Progress Reports, 1953) on the tracks of 2.2 GeV protons from the Cosmotron in photographic plates, and on neutron and proton cross-sections, it might be that about one fifth of the protons are significantly scattered, and that of these

a fraction, probably between one quarter and one tenth, will lose their charge and appear as neutrons.

Several advantages follow from the use of very thin targets in this manner:

a) The duration of the bombardment is longer than if a thick target is used, and can be controlled fairly easily, by varying either the thickness of the foil, or its shape and cross sectional area. In using this latter method, the target would be a small disc or even a piece of wire, whose thickness is still kept about 50 keV, but whose area is so small that only a fraction of the particles in the beam hit it on each revolution, so that more revolutions are needed before every proton has been absorbed.

If the energy loss per traversal is 50 keV, and the total loss, from Table I, is 200 MeV, the whole process will last about 4000 revolutions, or 8 milliseconds. By using a target with small cross-section area this could perhaps be increased to 1/10 second, which would be very satisfactory from the nuclear physicist's point of view. During such a time the magnetic field and hence the proton energy might change by a few percent, but this would not be objectionable in most cases.

b) This system will work equally well if the 50 keV foil is split up into several thinner foils, and put at different places round the circumference. Thus, by choosing foil materials, thicknesses and areas, several experiments can be run simultaneously with different intensities and types of reaction, provided they can all put up with the same proton energy.

c) With such small targets the ease of handling is greatly increased, and they could be moved in and out of the beam very rapidly. Further, materials only obtainable in small quantities can be used, and it might be possible to use a liquid hydrogen target in the form of a thin wall tube a few mm in diameter with the hydrogen flowing through it.

d) Targets with small cross-section area form sources with low acceptance, (the product of size and angular divergence), which are much easier to use with lenses to transfer large fluxes of particles into counter systems or cloud chambers some distance away. This point will be elaborated later on.

Something can be said about the angular distribution of the particles leaving the machine. The high energy neutrons and protons come mainly from the scattering and charge exchange mentioned above, and these are essentially two body elastic processes. In that case the variation of energy with angle of scatter is a known function. In our case, for 25 GeV protons, whose total energy in centre of mass space is 3.8 times rest mass, the energy is given by

$$E = \frac{25}{1 + (3.8 \operatorname{tg} \theta)^2} \text{ GeV} .$$

This gives energies of 22.6, 17.2, 12.3 GeV at 5, 10, 15°.

The yield from a process which is isotropic in centre of mass space, which might be roughly true of some of the scattering, is given by

$$N(\theta) \propto \frac{1}{\cos^3\theta\,(1+(3.8\,\mathrm{tg}\,\theta^2))^2}.$$

This shows half intensity at about 10°. For charge exchange, the process is known to occur predominantly at small angles in the centre-of-mass space, with a half width of about 22° both at 400 MeV and at 2 GeV, and if this holds at higher energies, the corresponding angle in the Laboratory will be about 2.5° for half intensity and 5° for one tenth.

Diffraction scattering occurs at even smaller angles, possibly with a half width of $\sim 30'$, so that these protons are unfortunately too much scattered to remain trapped in the machine, but not enough to get clear of it before the fringing field of the next magnet unit disturbs them.

The fastest particles which come out of the stars are the π-mesons, and a few fast protons and neutrons, which cannot easily be distinguished from them in photographic plates. The angular distribution of such particles from cosmic ray created stars have been measured (Camerini, Lock, Perkins) and the yield curve is predominantly in the forward direction. The energy is not a unique function of angle, but the energy distribution of the π-mesons in centre of mass space is known to extend up to about 800 MeV from cosmotron experiments, and this upper limit does not seem to depend much on energy of the proton creating the star. The corresponding upper limit of energy in laboratory space, and the yield, at various angles are given in Table II.

Table II.

Angle in Laboratory Space	Meson/sterad per proton	Upper limit of Energy (kinetic) for 800 MeV in C.M. space
0°	12	6.0 GeV
5°	10	5.6 »
10°	7	4.4 »
15°	5	3.2 »
20°	3	2.3 »
30°	1.5	1.3 »
60°	0.5	330 MeV
90°	0.25	90 »
180°	0.2	20 »

In addition to the charged π-mesons, there will be also perhaps one third that number of neutral π-mesons, which decay within a few centimetres into a pair of high energy photons, which will go in essentially the same direction as the parent meson. Thus as well as the charged meson distribution given above there will be a similarly distributed flux of photons, of about one half the intensity, and whose upper energy limit is about one half the figures in the last column of Table II.

The other, lower energy, particles from the stars are distributed more isotropically, especially those with energies only of the order of 10 MeV. which will be by far the most common particles leaving the targets at angles of 90° or more.

It would be unwise to expect to find any other types of particles at a useful distance from the machine, as the lifetimes of most mesons are too short for flight paths of more than a few centimetres. There does seem to be some evidence that the τ-meson's lifetime might be as long as 10^{-8} s, so an energetic meson of this kind might survive a flight of 20 metres, allowing for the effect of time dilatation. This would still not be able to reach the far side of the main shield, but could be detected in apparatus in the inner target areas.

The possibility of observing the various classes of particles that have been discussed can be seen in Fig. 2, which shows the possible positions of targets

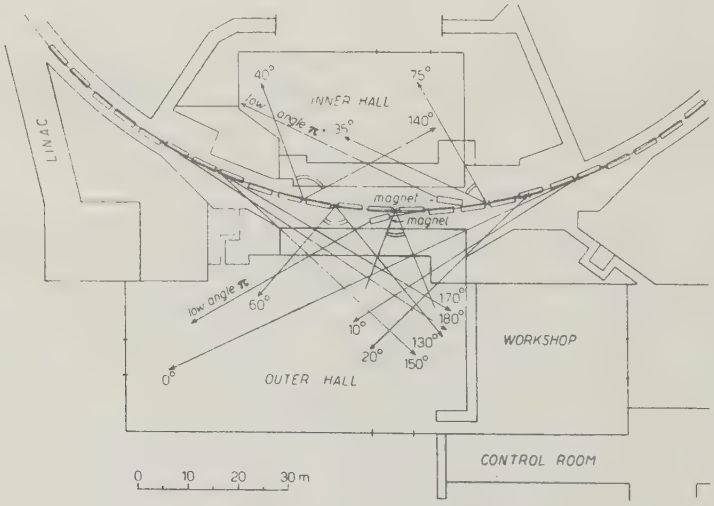

Fig. 2. – Target arrangements.

in the straight sections between the magnet units, and the ranges of angle over which each target can be seen, either from the outside or inside experimental hall. Obstruction to emerging particles from the iron return yoke of

the magnet is avoided to a great extent by arranging the magnet units in groups of three, with the yokes alternately outside and inside the proton orbit.

Some of the low angle beams of π-mesons are shown emerging not from the target, but further down the following magnet unit. It seems possible, to judge from some tracing of trajectories, to allow this to happen, and to use the magnets to do some energy analysis, and to bend the beams, especially those of π^+-mesons on the inside of the ring, so that they hit the shielding wall at a greater angle than otherwise. There is space between the magnets and the shield for other extra bending or analysing magnets. These may have to be quite large and heavy, since it needs a magnet about 5 metres long to deflect a 5 GeV meson through 30°.

The estimates of yields of different kinds of particles we have made can now be combined with the geometry of the targets and shielding to estimate the fluxes of different kinds of particles on the safe side of the shield. No extra focusing is considered at the moment.

a) High energy protons.

About 1/10 incident protons scattered with half width 5°.
Target distance, from outside shield, 35 metres.
Angle of scatter 5°.
Energy of scattered proton 22 GeV.
Flux emerging from shield $5 \cdot 10^2$ protons/pulse cm^2.

b) High energy neutrons.

About 1/40 incident protons send neutrons into a beam 2.5° half width, which, of course, can be used at its angle of highest intensity.
Target distance 40 metres.
Energy of neutrons 25 GeV.
Flux emerging from shield $8 \cdot 10^2$ neutrons/pulse cm^2.

c) High energy π-mesons.

About 6 π-mesons/steradian per proton, at 10° to beam.
Target distance 20 metres.
Energy of mesons 4.4 GeV upper limit.
Flux emerging from shield $7 \cdot 10^3$ mesons/pulse cm^2.

d) High energy photons.

About 4 π^0-mesons/steradian per proton along the tangential direction, with the exchange neutrons.

Target distance 40 metres.
Energy of photons 3 GeV upper limit.
Flux emerging from shield $8 \cdot 10^3$ photons/pulse cm^2.
There will be, as well, a large flux of lower energy photons and electrons from cascades in the wall of the channel through the shield.

e) Low Energy π-mesons.

About 0.5 π-mesons/steradian per proton at 60° to the beam.
Target distance 10 metres.
Energy of mesons 300 MeV upper limit.
Flux emerging from shield $2 \cdot 10^3$ mesons/pulse cm^2.

f) Low Energy Protons and Neutrons.

About 40 low energy nucleons (< 30 MeV) per proton isotropically distributed.
Target distance 10 metres.
Flux emerging from shield $1.6 \cdot 10^4$ nucleons/pulse cm^2.

These fluxes may or may not be adequate for qualitative experiments; the high energy proton beam would certainly be too intense for a cloud chamber, a few pulse would fully load a photographic plate, the neutron beam would probably be reasonable for cloud chamber work. For work involving scattering, and counter telescopes or analysers of low efficiency these yields would be regarded as far too low for work in the cyclotron energy range. The beams in general contain particles of a wide range of energy, and the backgrounds are very high. Further, it will be difficult to detect short lived particles from the targets in the main proton beam itself, where the targets are inaccessible and the background probably high.

To counter these difficulties, two improvements can be asked for, a high current ejected beam of protons, clean and well collimated, outside the main shield; and some general techniques for improving the efficiency of collecting particles emitted from targets, so that either intensities can be raised, or the same counting rates maintained but with a much smaller circulating beam or thinner targets, and a corresponding reduction in background.

This problem of how to form and transport beams of particles about the laboratory has been greatly eased by the use of the alternating gradient focusing principle, in just the same way as the design of synchrotrons has been. Some special cases can be discussed to show that the use of A.G. lenses and channels for this purpose seems quite practical.

Two conditions should be fulfilled, or at least aimed at, in the design of an economical focusing channel: the focusing and bending forces should be

spread out evenly along the length of the channel, and no part of the channel should have a larger aperture than is needed to carry the beam of particles safely. The first requirement is well known, and easy to demonstrate: the focusing or bending forces are proportional to some electric or magnetic field strength, whereas the stored energy, and cost, are proportional to the square of the field. The field distribution along the particle trajectory which minimizes the cost while keeping the product of field strength and length of focusing regions constant is the uniform distribution.

The first condition looks very obvious, but its point is usually obscured by a common way of describing beams of particles simply by their angular

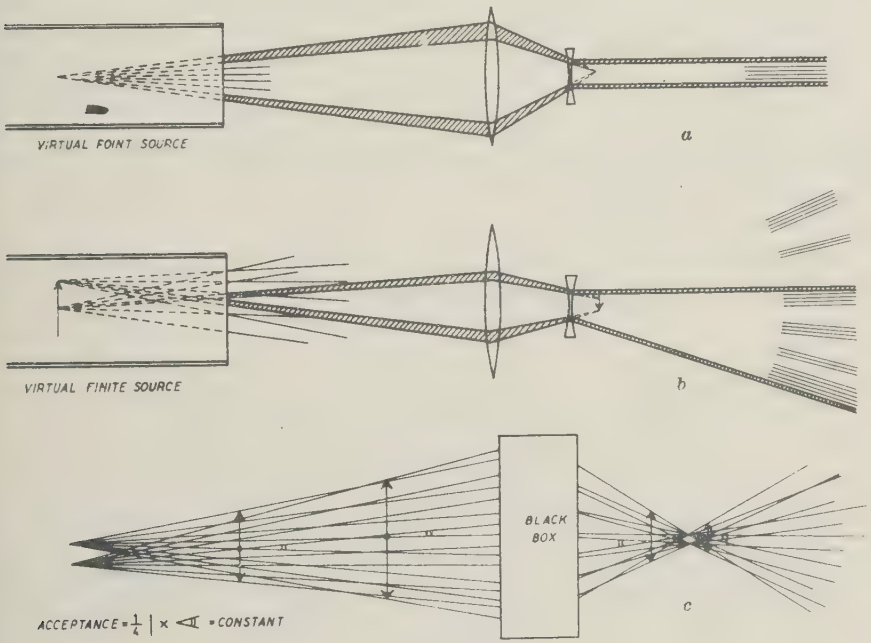

Fig. 3.

divergence, as though all the particles had come from a point source. If that were so the diverging beams could be made to converge onto an exact point image by a lens, and then the rays could be bent by a diverging lens, placed just before the new focal point into a parallel pencil with as small a diameter as one wished (Fig. 3*a*). Such a pencil beam could then travel indefinitely with no further focusing. The absurdity of this conclusion comes from the neglect of the finite size of the original source of the particles; from any point on the surface of the source comes a whole bundle of diverging rays, and any optical systems which attempt to make a small beam by forming a reduced

size image of the source will at the same time form an image from whos surface the ray divergence is by the same factor larger (Fig. 3*b*).

This is a consequence of a general theorem of wide range, in optics th Helmholz-Lagrange law, in dynamics Liouvilles theorem, which says, in ray optical terminology, that the product of the radius of a pencil of rays an the incoherent part of the angular divergence (half angle) is a constant alon the pencil (Fig. 3*c*). In CERN accelerator work this constant product is calle Acceptance; pieces of apparatus, such as counter telescopes or focusing channel or holes through a shield can all be given an acceptance by drawing the extrem rays which can just pass through them and calculating the radius and angl of divergence of the pencil so formed. The most economical optical systen for bringing particles to an experimental apparatus is one where the acceptanc of the focusing lenses and apertures etc., are all equal to that of the experiment If the lenses are properly arranged all the parts of the system will just carr the pencil of rays, and the maximum possible flux of particles will be take from the target to the experiment. This maximum flux can be calculated b finding the effective angle over which the source emits, from the source siz and the acceptance of the experimental apparatus. No knowledge of the inte vening channel is necessary.

As an example, the acceptance of the structure in Fig. 4*a*, which migh be a counter telescope, or a hole through a shielding wall, or the sensitive regio

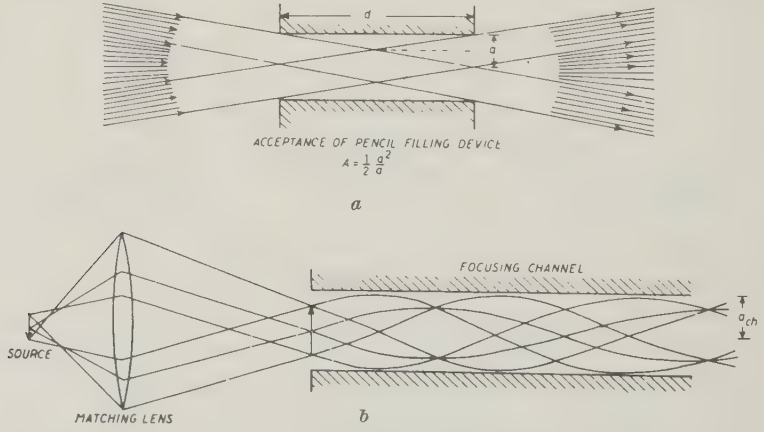

Fig. 4.

of a cloud chamber, of length d and radius a, is $\frac{1}{2}(a^2/d)$. If the source the spot at the target, has radius a_s, and emits a total flux of Φ particle per steradian, then the number N of particles emitted in a pencil of hal angle θ is $N = \Phi\pi\theta^2 = \Phi\pi A^2/a_s^2$, where A is the acceptance of the pencil

and which is determined by the counter geometry. This shows that the flux of particles into the counters can be increased by decreasing the spot size on the target, until the angle at the source becomes too large for practical lenses to handle. If m.k.s. units are used the unit of acceptance is the metre radian, with subdivisions mm rad and μ rad. This latter is the same as 1 mm 10^{-3} rad, a unit already used for describing the properties of beams from accelerating machines.

For some typical cases, the acceptance might vary from 2 mm rad for a cloud chamber of 40 cm diameter and 8 cm thick sensitive region to 0.1 mm radi for a counter telescope 5 cm diameter and 3 m long. The simple target arrangement with no focusing 30 m from a 20 cm diameter hole in the shield will have an acceptance of 0.03 mm rad for a 1 cm radius target spot, so such a size of shield channel will seriously limit the possible intensity which might be put into these detectors.

A focusing channel, formed from a string of A.G. quadrupole lenses can be made with quite a high acceptance by these standards. The equation of transverse motion for a particle in such a channel is

$$\frac{\mathrm{d}^2 y}{\mathrm{d}s^2} + \left(\frac{e}{p}\frac{\hat{B}}{a_{\mathrm{ch}}}\right) y = 0,$$

where P is the particle's momentum
a_{ch} the radius of the channel
$\hat{B}$ the maximum magnetic field (at radius a_{ch})
} mks units

Putting $m = (e/p)\hat{B}/a_{\mathrm{ch}}$ the equation has the same form as that for particles in the A.G. Synchrotron, and the theory of that machine can be used to find the acceptance of such a channel. If the channel is designed for highest acceptance A for a particular energy, then

$$A = 0.24\, a_{\mathrm{ch}}^2 \sqrt{m} \quad \text{m rad.}$$

For a big channel, for 10 GeV particles, with radius 10 cm and peak field 10^4 gauss, $m = 0.3$ and the acceptance

$$A = 1.35 \cdot 10^{-3} \text{ m rad} = 1.35 \text{ mm rad}.$$

This is 45 times as large as the acceptance of the hole-in-the-wall considered above, and as the flux of particles is proportional to A^2, its use would permit an increase in intensity of two thousand times into a suitably designed piece of apparatus.

If the energy of the wanted particles were lower A will remain unchanged if $\hat{B}$ is decreased by as much as p the momentum; for 2 GeV particles only 2 000 gauss is needed at the edge of the aperture.

For the highest energies, the acceptance needed is lower, as the half angle of the high energy beams does not exceed 1/20 radian ($2\frac{1}{2}°$), so, for a 1 cm radius target spot, the acceptance is 0.5 mm rad, and a 10 cm radius channel for 25 GeV will need only 3 000 gauss at the edge. It is worth noticing that although a channel with the same acceptance could be made with only about 6 cm radius by raising the field at the edge to 10 000 gauss, such a channel would have more stored magnetic energy and cost more. The stored energy per unit length of channel, E_s, is proportional to $a^2\hat{B}^2$.

Now

$$A^2 \propto a^4 m \propto a^3 \frac{\hat{B}}{p} \propto \frac{a^3\hat{B}}{(\mathrm{GeV})} \quad \text{for relativistic energies.}$$

So

$$a^2 \propto A^{4/3}\,(\mathrm{GeV})^{2/3}\hat{B}^{-2/3}$$

and

$$E_s \propto A^{4/3}\,(\mathrm{GeV})^{2/3}\,\hat{B}^{4/3}\,.$$

An advantage of A.G. channels is that they will not pass particles of low energy. There is a complete cut off at an energy of about half that for maximum acceptance, and a strong fall off for energies much above the chosen value. The energies in the pass band can be varied simply by the level of magnetic field ($\hat{B}/p$ is a constant for a given channel) which gives a convenient way of making a crude monochromator and of reducing background.

The ability of the channel to separate energies can be much increased by adding some uniform bending field to the quadrupole type focusing field in the channel, and arranging the channel on a circular arc rather than on a straight line. Since the bending field occupies a large part of the particles path between the target and the experiment, it is much lower for a given energy resolution than if a conventional bending magnet is used, and the cost and engineering design do not seem to be very worrying.

There is one more problem in the use of these channels, that of injecting the particles into the channel and of guiding them out properly into the experimental apparatus. This can be done by extra lenses at the beginning and end of the channel. The source is imaged onto the entry of the channel, with sufficient magnification to give an image whose size is $1/\sqrt{2}$ the aperture of the channel. The lens aperture is made sufficient to take that angle of beam which gives, with the particular source size, the same acceptance as that of the channel, and the resulting (demagnified) angular divergence of rays from the image at

the entry to the channel uses up the remainder of the aperture (Fig. 4*b*). This condition, in which the apertures needed for the size and angular deviation of the virtual source are equal, can be called the »« matched » condition (*). The lenses which are used for this matching process can also be alternating gradient units, though if the magnification needed is not unity, different lengths or m values must be used in the two parts of the lens to get proper focal lengths for the horizontal and vertical directions, as these lenses are in general not astigmatic.

The other way in which the effectiveness of the CERN synchrotron could be increased would be to secure an efficient ejector for the main proton beam. The efficiencies of the plain « hole in the wall », and a good channel, using low angle scattered protons, are of the order $0.3 \cdot 10^{-4}$, $2 \cdot 10^{-3}$ respectively, which leaves a long way to go.

A good ejector should have three qualities:

a) it should eject a high proportion of the circulating beam;

b) the ejected beam should have reasonable geometry;

c) the ejection process should last a long time, at least a millisecond.

From these criteria it follows that whatever is used to kick particles out of the focusing region of the machine must have an or-all-nothing property; if a particle is at all affected it must be given a full size kick and not merely given an oscillation of large amplitude in the synchrotron which will probably lead to its loss rather than its successful ejection. This rules out a simple kicking magnet, whose fringing field has just this troublesome property if the circulating beam is moved slowly into the magnet gap: slowly, as it must be to satisfy rule *c*).

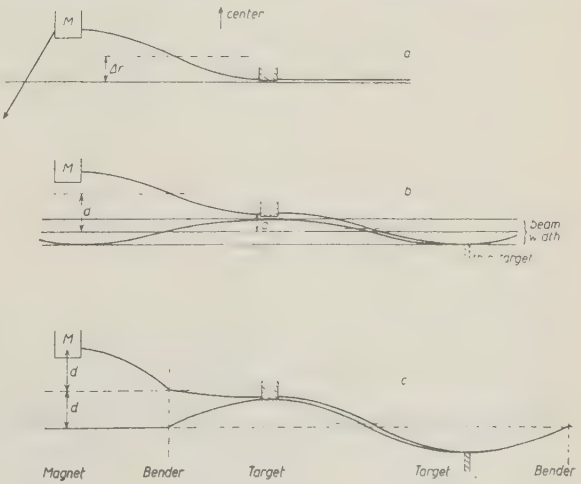

Fig. 5.

The only successful device to date even on paper is that used in the Piccioni type ejector, where the energy loss of a particle in passing through a fairly thick target is used

(*) *Note added in proof.* – This is too simple a discussion of the matching problem Other methods can be used which do not involve forming images of the source.

to start a large free oscillation about a new equilibrium orbit displaced towards the centre of the machine (Fig. 5*a*). This oscillation is large enough half a wavelength further round the machine to take the particle into a kicking magnet which can now be far enough from the remaining beam of undisturbed particles not to affect it appreciably. The effective « fringing field » of such an « energy losing » target is due to scattering of the particles out of the side of the target before they have passed through and lost the full amount of energy.

From the data in Table I, it is clear that although a heavy element target would be best for high efficiency, since an energy loss corresponding to a closed orbit shift of 2 cm can be obtained by a thickness of less than one half a nuclear mean free path, the amplitude of oscillation caused by the scattering in the target is too large for the vacuum chamber at a point one quarter of a wavelength further round the machine, so a lighter element target about one mean free path long must be used, with only about 30 % of the incident protons coming out on the far side. The angular divergence is then quite small, and at the kicking magnet half a wavelength away the particles come to a focus again, so that the magnet aperture needed is only about 1.5×3 cm, to hold the initial width of the beam and the radial spread caused by energy straggling in the target.

A kicking magnet 1 metre long with a field of 20 000 gauss will give enough sideways momentum to the protons to take them clear of the main magnetic field about one magnet period later, and the kicker can be so placed that the subsequent motion and the fringing fields of the main magnets allow the ejected beams to come out with a very reasonable size and angular divergence i.e. a reasonable acceptance (Fig. 6). The acceptance of the beam in the kicking magnet is about 0.02 mm rad and the aberrations in the subsequent magnetic fields should not increase this beyond 0.1, which is easily handled by lenses and A.G. channels to take the beam across the experimental hall.

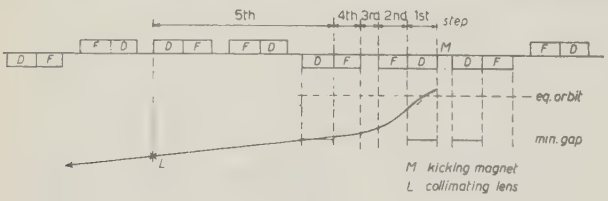

Fig. 6.

To generate a long output pulse it is necessary to move the circulating beam very slowly onto the target. Under practical conditions the reis then a considerable loss due to protons being scattered out of the side of the target rather than passing right through. To avoid this, a further, quite thin, target, can be used half a wavelength furtherback, on the outside of the beam this time, to give a displacement of, say, 2 mm to the protons hitting it, which will

ensure their staying inside the main target for the whole of its thickness. This thin target will not have sufficient scattering in it for its « fringing field » to be serious (Fig. 5*b*).

The movement of the beam onto the targets can be accomplished by a pair of small bending magnets spaced one wavelength apart, as in Fig. 5*c*, which induce and then cancel an oscillation of growing amplitude as the exciting current in the magnet is increased.

The principal losses of protons in this scheme occur in the main target, where perhaps 60-70 % will be lost by nuclear collisions, and some further losses from fringing fields. One might however hope for an overall efficiency of 10-20 %, which gives a gain in intensity of nearly 1000 over the simple scattering ejector.

This use of focusing channels and ejectors may seem too complicated and expensive, and so it will be for a year or so after the machine starts to operate. In practice, however, within a few years experimentalists are always clamouring for ever higher intensities, and it is usually found possible to get money and staff to build an untried type of machine even in an energy range which is fairly well covered, if its intensity is increased by a factor of several hundreds or more for some types of experiment. As an example, Gt. Britain has started building a proton linear accelerator for 600 MeV even before the cyclotron for a similar energy at Liverpool is fully operative. Viewed in this light, the cost, perhaps a million francs or so, of a set of channels is a very cheap way of staving off of the inevitable day when this proton synchrotron becomes a reason for nuclear physicists avoiding instead of visiting Geneva.

SUPPLEMENTO AL VOLUME II, SERIE X
DEL NUOVO CIMENTO

N. 1, 1955
2° Semestre

Theory of Particle Orbits in the Alternating Gradient Synchrotron.

G. LÜDERS

Proton Synchrotron Group, CERN - Geneva
Max-Planck-Institut für Physik - Göttingen

In this paper the theoretical aspects of the particle behaviour in the alternating gradient synchrotron shall be outlined. For a description of the situation in more physical terms the reader is refered to the paper of Dr. ADAMS.

The considerations shall be confined in two respects,

1) Only the behaviour of particles of the proper momentum shall be analysed. So we shall only be concerned with the stability of deviations of the position of particles from the equilibrium orbit, i.e. deviations which are essentially perpendicular to this equilibrium orbit. Nothing shall be said about stability of the phase with respect to the accelerating radio frequency.

2) We shall only be concerned with linear effects, viz. we shall drop all non-linear terms in the kinematic part of the equations of motion (Coriolis forces, centrifugal terms) and neglect all intrinsic non-linearities of the magnetic field. This approximation means that the results can be valid only for small deviations from the equilibrium orbit and for a sufficiently high degree of linearity of the magnetic field. The reasons for the limitation to « linear theory » are twofold: no general theory for the non-linear behaviour is available, and the non-linear considerations made so far by the CERN Proton Synchrotron Group are in a rather preliminary stage.

In Part 1 of this paper the theory of the perfect machine will be sketched which treats the proton synchrotron proposed by COURANT, LIVINGSTON and SNYDER in their classical paper. In this machine, the magnet structure repeats itself in strictly identical periods along the circumference. This perfect machine can never be realized in practice and so one meets with several types

of imperfections the influence of which will be outlined in part 2. The theory of these imperfections has been developed at several places but not much has yet been published.

1. – Perfect Machine.

In Fig. 1 a cross-section of the beam is shown, taken perpendicularly to the equilibrium orbit. The centre of the machine may be imagined far to the left. Vertical deviations of the particles from the equilibrium orbit may be expressed by a coordinate, z, horizontal ones by another coordinate, r. Measuring the arc length along the equilibrium orbit in a unit (angle) θ, which increases from 0 to 2π over one revolution and assuming symmetry of the magnetic field with respect to a horizontal plane, one derives the following equation of motion for, e.g., the vertical deviations

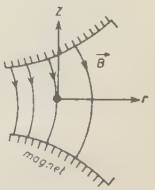

Fig. 1.

$$z''(\theta) + n(\theta) z(\theta) = 0 \,. \tag{1.1}$$

In this equation, the dashes mean derivatives with respect to the arc length θ and the quantity $n(\theta)$ (field index) is defined by

$$n(\theta) = \begin{cases} -\dfrac{R}{B_z} \dfrac{\partial B_z(\theta)}{\partial r}, \\ -\dfrac{R^2}{\varrho B_z} \dfrac{\partial B_z(\theta)}{\partial r}. \end{cases} \tag{1.2}$$

The first line is valid if the equilibrium orbit is simply a circle with radius R. The second one refers to the general case, the quantities R now being defined by

$$\text{circumference} = 2\pi R \tag{1.3}$$

and $\varrho(\theta)$ being the local radius of curvature (magnetic radius) of the equilibrium orbit (notice that the product ϱB_z is a function of the particle momentum only).

In Eq. (1.1) the acceleration and, consequently, the change of the magnetic guiding field B with time have been neglected. Taking them into account, one finds that the particle orbits following from Eq. (1.1) are then damped down in amplitude proportionally to the reciprocal square root of the particle momentum. So all these oscillations about the equilibrium orbit (which are called « betatron oscillations ») become smaller and smaller in the course of acceleration.

The following two mathematical statements are true for the solutions of Eq. (1.1).

1) Provided a pair $z_a(\theta)$, $z_b(\theta)$ of linearly independent solutions of the Eq. (1.1) has been found, the most general solution (particle orbit) can be expressed as a linear combination of those two basic solutions.

2) For every pair of solutions, the Wronskian

$$W_{ab} = z_a(\theta) z_b'(\theta) - z_a'(\theta) z_b(\theta) \tag{1.4}$$

is independent of θ and is different from 0 if $z_a(\theta)$ and $z_b(\theta)$ are linearly independent.

According to COURANT, LIVINGSTON and SNYDER, the field index $n(\theta)$ (Eq. (1.2)) has to be chosen as a strictly periodical function, viz.

$$n(\theta+\theta_0) = n(\theta) \tag{1.5}$$

where the period θ_0 has to be an integral fraction of 2π,

$$\theta_0 = 2\pi/M\,, \tag{1.6}$$

(M = number of periods of the magnet structure). Assumption (1.5) means that the differential Eq. (1.1) is of the so called Floquet type. According to Floquet's theorem, one can normally choose two solutions (Floquet solutions) which somehow reflect the periodicity of the coefficient $n(\theta)$

$$z_1(\theta+\theta_0) = \lambda_1 z_1(\theta)\,, \qquad z_2(\theta+\theta_0) = \lambda_2 z_2(\theta), \tag{1.7}$$

where λ_1, λ_2 are constants independent of θ.

For the Floquet multipliers λ_1, λ_2 one finds: what follows:

1) since $n(\theta)$ is a real quantity, λ_1 and λ_2 are both real or they form a complex conjugate pair;

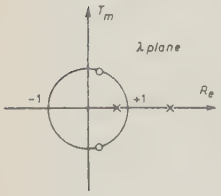

Fig. 2.

2) by application of the constancy of the Wronskian to θ and $\theta + \theta_0$ one sees that

$$\lambda_1 \cdot \lambda_2 = 1; \tag{1.8}$$

consequently, in the complex λ plane (Fig. 2), the locus of λ_1 and λ_2 is given by the real axis and the unit circle, and the position of the pair λ_1, λ_2 is either that indicated by $\times$ or that indicated by $\circ$. In the first case ($\lambda_{1,2}$ on the real axis), one of the multipliers has a modulus bigger than one. Assume this to be the case for λ_1; then $z_1(\theta)$ will formally grow in amplitude indefinitely in the course of the time and one therefore has instability of the betatron oscillations in this case. If λ_1

and λ_2 both lie on the unit circle their modulus y is equal to one and one has stability.

Let us assume now that the distribution of the field index (i.e. the function $n(\theta)$) is changed continuously everywhere. Then, if we have stable working conditions in the beginning (if, consequently, λ_1 and λ_2 are situated on the unit circle) these points will move continuously on the circle in some direction and finally approach the points ± 1 where the two branches of the locus intersect. Then normally they will no longer continue on the circle but move for a while on the real axis. This shows that, in the alternating gradient scheme, a sufficiently big change of $n(\theta)$ brings one from stable to unstable working conditions and that, on the border between stability and instability, there is an orbit which is periodical either over one period ($\lambda = +1$) or over two periods ($\lambda = -1$) of the field index.

Normally one puts

$$\lambda_{1,2} = \exp[\pm i\mu] \tag{1.9}$$

and the « mode » μ is a real quantity under stable conditions. Although the foregoing discussion was confined to one direction of oscillation only, one should keep in mind that for the successful performance of the synchrotron actually stability of all kinds of betatron oscillations is needed or, what is the same, stability both of vertical and horizontal oscillations.

2. – Influence of Imperfections.

There are, within the frame of linear theory, three types of imperfections which were already mentioned in Dr. ADAMS' paper.

1) Imperfections of the *guiding field* $B_z(\theta)$ on the equilibrium orbit (due to geometrical displacements of magnets perpendicular to the equilibrium orbit, remanent fields, etc.).

2) Imperfections of the *field index* $n(\theta)$ (individual differences of the magnets, different lengths, different saturation behaviour).

3) *Coupling* between vertical and horizontal oscillations (geometrical twists about the equilibrium orbit).

All these imperfections do, of course, act simultaneously on the particles but for systematical reasons they shall be treated separately.

The *guiding field* determines the equilibrium orbit. If it deviates from its proper value, a particle can no longer travel along the original equilibrium path. But one can show that, also in this case, there is one orbit in the ma-

chine which is closed in itself after one revolution and that all particles starting off this closed orbit just perform ordinary betatron oscillations about it.

Mathematically, the equation of motion (1.1) is now modified by an inhomogeneous term

$$z''(\theta) + n(\vartheta)z(\theta) = \delta f(\theta) . \tag{2.1}$$

In the case that the imperfection is caused by the vertical displacement $\delta\zeta(\theta)$ of the magnets, it is almost evident that

$$\delta f(\theta) = n(\theta)\,\delta\zeta(\theta) . \tag{2.2}$$

In the more general case that there is some small horizontal component $\delta B_r(\theta)$ of the guiding field on the original equilibrium orbit, one can show that

$$\delta f(\theta) = \frac{R^2}{B_{z0}}\,\delta B_r(\theta) . \tag{2.3}$$

The « closed orbit » $\hat{z}(\theta)$

$$\hat{z}(\theta + 2\pi) = \hat{z}(\theta) \tag{2.4}$$

can be expressed in a closed form in terms of $\delta f(\theta)$ and the Floquet solutions for the perfect machine as follows:

$$\hat{z}(\theta) = \int_{\theta-2\pi}^{\theta} d\theta'\,\delta f(\theta') \left\{ \frac{z_1(\theta')z_2(\theta)}{W(1-\exp[-2\pi i Q])} - \frac{z_2(\theta')z_1(\theta)}{W(1-\exp[+2\pi i Q])} \right\} . \tag{2·5}$$

(Notice that in the arguments of $z_{1,2}$ there appears θ as well as the variable of integration θ'!). In this equation, W represents the Wronskian constructed from the Floquet solutions ((1.4) for $z_a = z_1$, $z_b = z_2$) and Q is the number of (vertical) betatron oscillations along the circumference. This quantity is, in terms of M (1.6) and μ (1.9), given by

$$Q = \frac{M\mu}{2\pi} . \tag{2.6}$$

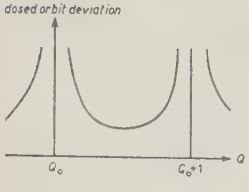

Fig. 3.

From (2.5) one sees that the closed orbit deviates more and more from the original equilibrium orbit the nearer one approaches working conditions which lead to integral Q. One has a typical phenomenon of resonance. In Fig. 3 the beahvior of the peak deviation of the closed orbit (for given space) is shown qualitatively. The different values of Q on the abscissa are thought to be produced by some modification of $n(\theta)$ inside each period. Q_0 represents some integral value of Q.

Since the whole beam follows the closed orbit and has to stay inside the

vacuum chamber everywhere one has to make sure that this closed orbit does never deviate too much from the original equilibrium orbit. That means

1) $\delta f(\theta)$ has to be sufficiently small;

2) one may not work too close to a resonance.

If there are imperfections of the *field index*, the condition of periodicity (1.5) will normally not be valid any longer. Instead, one has only periodicity over one revolution, i.e.

$$n(\theta + 2\pi) = n(\theta)\,. \tag{2.7}$$

The orbits are therefore still given by an equation (1.1) of the Floquet type. But now, Floquet's theorem has to be applied to one revolution 2π. In general, there is a pair of Floquet solutions with the properties

$$\tilde{z}_1(\theta + 2\pi) = \tilde{\lambda}_1 \tilde{z}_1(\theta)\,, \qquad \tilde{z}_2(\theta + 2\pi) = \tilde{\lambda}_2 \tilde{z}_2(\theta)\,, \tag{2.8}$$

and all that has been said about the properties of λ_1 and λ_2 holds unchanged for $\tilde{\lambda}_1$, $\tilde{\lambda}_2$. If there were no imperfections, one would simply have

$$\tilde{\lambda}_1 = \lambda_1^M = \exp[2i\pi Q]\,, \qquad \tilde{\lambda}_2 = \lambda_2^M = \exp[-2\pi i Q] \tag{2.9}$$

and, in the complex plane, the points $\tilde{\lambda}_1$ and $\tilde{\lambda}_2$ would, under a change of the working conditions, pass over the critical points $\tilde{\lambda}$ $\pm$ 1 without noticing it. If, however, only the weaker periodicity condition (2.7) holds true, they will in general not pass over those critical points without deviating for a while onto the real axis. So, in the presence of imperfections of the field index, the region of stable working conditions is split up by unstable bands which are called « stopbands ». These stopbands lie close to those working conditions where, for a perfect machine, one would have

$$Q = \text{integer}\ (\tilde{\lambda} = +1) \quad \text{or} \quad Q = \text{half an integer}\ (\tilde{\lambda} = -1)\,. \tag{2.10}$$

A mathematical solution of the problem in a closed form is not possible. In most cases of practical interest, one can apply a perturbation treatment. For this purpose one splits $n(\theta)$ into a perfect part and imperfections

$$n(\theta) = n_{\text{perf}}(\theta) + \delta n(\theta) \tag{2.11}$$

with

$$n_{\text{perf}}(\theta + \theta_0) = n_{\text{perf}}(\theta)\,. \tag{2.12}$$

(That this splitting is not uniquely defined does not affect the result). Having performed the splitting (2.11) one finds for the stopband width (distance between the edges in terms of the value of Q for the corresponding perfect ma-

chine)

$$\delta Q_{\text{stop}} = \left| \frac{1}{\pi W} \int_0^{2\pi} \mathrm{d}\theta \, \delta n(\theta) \, (z_1(\theta))^2 \right| . \tag{2.13}$$

Here, $z_1(\theta)$ is one of the Floquet solutions for the corresponding perfect machine and W is the Wronskian formed from $z_1(\theta)$ and $z_2(\theta) = z_1^*(\theta)$.

The centre of a stopband does normally not coincide exactly with an integral value of Q for the perfect machine, but neighbouring stopbands are shifted by practically the same amount. So, the position of the stopband centre is not a quantity of practical interest.

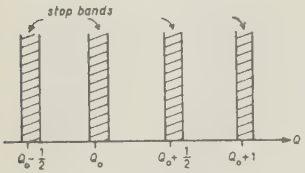

Fig. 4.

The stopbands, occurring at integral and half integral values of Q, are shown in Fig. 4. We emphasize that, inside a stopband, the beam shows a monotical blow up whereas imperfections of the guiding field lead to a displacement of the beam as a whole. The blow up inside the stopbands is anticipated by beatings in amplitude inside the « windows » but close to a stopband border. There any orbit increases in amplitude over a number of revolutions, decreases again and so forth. The physical reason is that, near to a stopband, the orbits are almost periodical (or antiperiodical) over one revolution. So, imperfections of the field index which initially may act as to blow up the beam, finally come out of phase and act in the opposite direction, come again out of phase and so on. Fortunately, these « shoulders » of the stopbands are rather narrow.

In the presence of imperfections both of the guiding field and of the field index, the peak deviation of the closed orbit goes to infinity at both edges of those stopbands which lie near to integral numbers of Q. The behaviour of the betatron oscillations about the closed orbit is not influenced by imperfections of the guiding field and, therefore, is described correctly by the foregoing considerations.

Two requirements must be fulfilled to have the machine still working successfully in presence of an imperfect field index.

1) The stopbands must be sufficiently narrow to have reasonably wide windows between the stopbands.

2) The working point must not be too close to a stopband to avoid troubles from the beatings in amplitude (and, of course, from a big displacement of the closed orbit).

In the case of *coupling* the considerations can no longer be confined to one component of oscillation. Now the orbits are described by a system of two

coupled equations

$$z''(\theta) + n_{zz}(\theta)\, z(\theta) + n_{zr}(\theta)\, r(\theta) = 0\,, \quad r''(\theta) + n_{rz}(\theta)\, z(\theta) + n_{rr}(\theta)\, r(\theta) = 0\,. \tag{2.14}$$

Geometrical twists of the magnets also lead to a horizontal component of the guiding field but this affects only the closed orbit and not the betatron oscillations about it which are correctly described by (2.14).

Every solution of (2.14) is given by a pair of functions, $z(\theta)$ and $r(\theta)$. Further, any solution (orbit) is a linear combination of four linearly independent ones.

By expressing the coefficients $n_{jk}(\theta)$ explicitely in terms of derivatives of the guiding field, one can show that

$$n_{rz}(\theta) = n_{zr}(\theta)\,. \tag{2.15}$$

From this it follows that for any pair of solutions, $z_a(\theta)$, $r_a(\theta)$ and $z_b(\theta)$, $r_b(\theta)$, the following bilinear expression

$$W_{ab} = z_a(\theta) z_b'(\theta) - z_a'(\theta) z_b(\theta) + r_a(\theta)\, r_b'(\theta) - r_a'(\theta)\, r_b(\theta) \tag{2.16}$$

does not depend upon θ.

The coefficients $n_{jk}(\theta)$ are obviously periodical over one revolution

$$n_{jk}(\theta + 2\pi) = n_{jk}(\theta)\,. \tag{2.17}$$

This means that again we have a mathematical problem of the Floquet type. Normally, one therefore can find four Floquet solutions which after one revolution simply take up a numerical factor

$$\begin{pmatrix} \tilde{\tilde{z}}_1(\theta + 2\pi) \\ \tilde{\tilde{r}}_1(\theta + 2\pi) \end{pmatrix} = \tilde{\tilde{\lambda}}_1 \begin{pmatrix} \tilde{\tilde{z}}_1(\theta) \\ \tilde{\tilde{r}}_1(\theta) \end{pmatrix} \tag{2.18}$$

(and in an analogous manner for the other solutions). The following statements are true for the Floquet multipliers $\tilde{\tilde{\lambda}}_1$, $\tilde{\tilde{\lambda}}_2$, $\tilde{\tilde{\lambda}}_3$, $\tilde{\tilde{\lambda}}_4$.

1) Since $n_{jk}(\theta)$ are real quantities, either all four multipliers are real or, for a complex multiplier the complex conjugate number is also among these multipliers.

2) By applying (2.16) to the Floquet solutions one finds that the four multipliers can be ordered in pairs so that the product of the two members of each pair is equal to one.

If we are interested in only those working conditions which would be stable in the absence of coupling, one has to distinguish between two entirely dif-

ferent configurations of the Floquet multipliers in the complex plane (Fig. 5). The pairs of complex conjugate multipliers may either be identical with the pairs of those giving product one (configuration 1) or they may not (configuration 2). In the first case one obviously has stability, in the second one instability, since there are multipliers with a modulus bigger than one. The limiting case between both configurations where, in the presence of coupling, one possibly might pass from stability to instability, appears whenever two multipliers approach each other. Then, two overall phaseshifts become equal. So one might expect instability due to coupling, whenever in the corresponding perfect machine (with no coupling) one is near to working conditions with

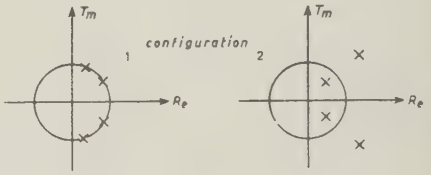

Fig. 5.

$$Q_z + Q_r = \text{integer} \quad \text{or} \quad Q_z - Q_r = \text{integer}. \tag{2.19}$$

Fortunately, a closer analysis shows that actually only one of these two possibilities does lead to instability. Under conditions normally considered one has instability only if Q_z+Q_r is an integer but not if $Q_z - Q_r$ is.

The situation shall be explained in somewhat more detail by considering the working diamond in the $n_1 - n_2$ plane (cf. the paper by Dr. ADAMS). This working diamond is shown in Fig. 6. The borders of the working diamond are given by stopbands due to an imperfect field index which are only slightly modified by the coupling. These stopbands lie in the vicinity of the lines, Q_z, Q_r = integral or half integral number, in the n_1–n_2 plot for the corresponding perfect machine. At the line Q_z+Q_r=integer, which is outside the working diamond, one has a coupling stopband. Inside such a stopband, one again has a monotical blow up of the beam but now as a two dimensional effect rather than as a one dimensional one as in the case of stopbands due to an imperfect field index. A line $Q_z - Q_r =$ integral crosses the diamond as a diagonal. Also on this line there is a strong interaction between vertical and horizontal oscillations but this does not lead to instability but to some exchange between the amplitudes of vertical and horizontal motion. One may describe this fact by saying that one here has beatings, not in amplitude but in direction of oscillation.

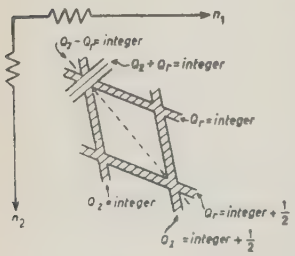

Fig. 6.

The theory outlined so far allows us to predict, for known imperfections, their influence on the orbits. But this is not the situation one meets in

practice. One rather wants to obtain predictions for the behaviour of a machine which has not yet been built and the imperfections of which one does not know. This leads one to try some kind of statistical approach in the sense that one imagines an ensemble of machines being built as actual realizations of the same perfect machine by identical procedures. These machines will all be slightly different from each other and one of them — but we do not know which one — will be the machine we are actually building. To construct such an ensemble mathematically one has to make assumptions (which have to be justified by considering the actual procedure of building the machine) about the probability distributions of the several types of imperfections and especially of the statistical interdependence of imperfections in different parts of the machine.

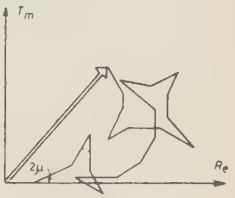

Fig. 7.

The general procedure of this *statistical treatment* shall be shown in the case of the stopband width given by equation (1.13). For the sake of simplicity it shall be assumed that the imperfections $\delta n(\theta)$ are constant inside each sector and are statistically independent of each other in different sectors. Further, it shall be assumed that positive and negative values of δn are equally likely. Then, the integral appearing in the cited equation, shall be split into a sum with each term giving the integral over just one period θ_0. This sum can be represented by a chain of lines in a complex plane (Fig. 7). The stopband width is then given, apart from a constant factor, by the vector connecting beginning and end of that chain. Between two subsequent lines there is an angle of 2μ as easily follows from

$$(z_1(\theta + \theta_0))^2 = \exp[2i\mu](z_1(\theta))^2 . \tag{2.20}$$

Under the assumptions made one just has a random walk problem with M steps in two dimensions and it is well known that the root mean square value of the distance between start and end of the walk is proportional to the square root of the number, M, of steps. Quantitatively one has in this case, as can easily be deduced from (2.13)

$$\langle \delta Q_{\text{stop}} \rangle_{\text{rms}} = \sqrt{M} \langle \delta n \rangle_{\text{rms}} \left| \frac{1}{\pi W} \int_0^{\theta_0} \mathrm{d}\theta' (z_1(\theta'))^2 \right| , \tag{2.21}$$

where, by definition, for any quantity η

$$\langle \eta \rangle_{\text{rms}} = \sqrt{\langle \eta^2 \rangle} . \tag{2.22}$$

Further, the probability distribution of the length of the vector in question ($\propto \delta Q_{\text{stop}}$) is well known for such a random walk problem. Writing x instead

of δQ_{stop} one has for the probability $p(x)$ of finding an x between x and $x + \mathrm{d}x$ the following Rayleigh distribution

$$p(x)\,\mathrm{d}x = \frac{2}{\langle x^2 \rangle} \exp\left[-\frac{x^2}{\langle x^2 \rangle}\right] x\,\mathrm{d}x\,. \tag{2.23}$$

Statistical considerations of this kind have been used for determining sets of possible machine parameters.

SUPPLEMENTO AL VOLUME II, SERIE X
DEL NUOVO CIMENTO

N. 1, 1955
2° Semestre

Synchrocyclotrons, and the CERN 600 MeV Machine.

T. G. PICKAVANCE

Atomic Energy Research Establishment - Harwell

1. – Introduction.

The reasons for the presence of the synchrocyclotron in the CERN programme, in addition to the 25 GeV proton synchrotron, may be summarised as follows:

1) It is intended to provide facilities for research in high energy nuclear physics at the earliest possible time. The 600 MeV synchrocyclotron is almost the most powerful machine which can be reduced to normal engineering practice. Rather little development work is required, whereas the alternating gradient proton synchrotron needs long and difficult development which must not be rushed if disaster is to be avoided.

2) The synchrocyclotron will not, in any case, be obsolete when the machine has been built, since in its own energy range it will be a much more powerful machine (by at least a factor 1000). The role of the synchrocyclotron in present-day research is to make more detailed studies of the fields opened up by cosmic ray research and by the use of the very large machines.

2. – Particle Stability in the Synchrocyclotron.

The synchrocyclotron is a variant of the phase-stable closed orbit accelerator. Particles are admitted at practically zero velocity in the centre of a cylindrical magnet gap. The magnetic field is kept constant, and the frequency of the RF accelerating field is slowly reduced during acceleration to take account of the fact that the « cyclotron frequency ».

$$f_0 = \frac{eB}{2\pi mc},$$

diminishes with increasing energy. Part of this decrease is caused by the rela-

tivistic increase of mass of the particles, and the remainder by a reduction of the magnetic field strength with increasing radius, deliberately introduced for the purpose of focusing the particles. It is necessary to operate all large accelerators in conditions of phase stability and directional stability. We have the usual condition for directional stability:

$$1 > n > 0\,, \qquad \text{where} \qquad n = \frac{-r}{B_z}\frac{\partial B_z}{\partial r}$$

For $n < 1$ there is radial stability (closed orbits), and associated with the radial focusing forces there are the « radial betatron oscillations » of frequency

$$f_r = (1 - n)^{\frac{1}{2}} f_0\,.$$

With $n > 0$ there are forces restoring the particles towards the median plane of the magnet gap, and the corresponding « vertical betatron oscillations » of frequency

$$f_r = n^{\frac{1}{2}} f_0\,.$$

For the phase-stable particles, there are oscillations of phase, radius and energy with respect to the particles in the equilibrium orbit. These oscillations have much lower frequency than the betatron oscillations and the orbital motion, and their radial extent is of no consequence in the synchrocyclotron except at the very beginning of the acceleration. Moreover there is no difficulty analogous to that caused by the « forcing » of the phase oscillations by frequency — tracking errors in the proton synchrotron, because here there is nothing to track—only the frequency is varied. Thus the law of frequency variation with time is uncritical, and may be varied over wide limits without loss of phase stability.

The RF accelerating voltage may be quite small (a few kilovolts), since even under such conditions the total path length is only a few hundred kilometres. The loss of particles by gas scattering or charge exchange is quite negligible at pressures of the order of $5 \cdot 10^{-6}$ mm Hg except, again, near the beginning of the acceleration. There are, therefore, none of the difficulties from RF breakdown which characterised our earlier struggles with conventional cyclotrons.

From the point of view of the user, the synchrocyclotron may be summed up as follows:

Advantages.

1) *No critical operating conditions.* The synchrocyclotron is the least critical in operation of all high energy machines yet developed.

2) *High intensity.* Mean currents of about 1 microampere are readily obtained, with about 100 pulses per second of a few hundred microseconds duration.

Disadvantage.

Costly magnet. The magnetic field has to be applied over a large, cylindrical volume, and the weight and cost of the magnet increase very rapidly with the particle energy required. The useful upper energy limit of the synchrocyclotron is limited, by consideration of cost, to about 1 GeV or so. At higher energies, the smaller intensity and greater difficulty of the proton synchrotron have to be accepted.

3. – Components of a Large Synchrocyclotron.

The CERN machine will be used as an example to illustrate the main features of a practical accelerator.

3·1. *The magnet.* – Table I gives the design parameters of the CERN synchrocyclotron magnet.

TABLE I. – *CERN synchrocyclotron magnet.*

Pole diameter	5.00 m
Maximum orbit radius ($n = 0.2$)	2.28 m
Field at this radius	17.8 kgauss
Field at the centre	18.8 kgauss
Maximum gap	45 cm
Minimum gap	36 cm
Steel weight	2 500 ton

The maximum energy obtainable is determined by the product of the maximum radius for particle stability and the magnetic field at that radius, and the maximum economically obtainable field is limited by saturation effects. It follows that, with the cylindrical geometry of the synchrocyclotron magnet, the rate of fall of magnetic field with increasing radius should be made as small as possible consistent with adequate vertical focusing. In other words, a small value of n is used. There are certain resonance effects which cause the loss of most of the particles from the beam at certain values of n: the first of these occurs at $n=0.2$, where the frequency of radial oscillation is twice the frequency of vertical oscillation. Moreover, there is little or no contribution from electric focusing at any time in the acceleration process (some of the phase-stable particles are actually defocused at injection), so

that a finite value of n must be used to give magnetic focusing at all radii. Consequently the magnet is shimmed in such a way as to give a small, positive value of n from a small to as great a radius as possible, and in particular the radius where $n=0.2$ is made as large as possible. A compromise has to be made at the outer edges of the poles, where the gap has to be reduced in order to compensate for loss of flux by fringing, since sufficient space has to to be left for insertion of the accelerating electrode.

The CERN magnet has been designed on the basis of scale model tests made at Uppsala by members of the CERN Synchrocyclotron Group. The engineering design is now complete and detailed specifications of the frame and windings, and corresponding erection schedules, have been drawn up for tendering purposes. We are satisfied that the manufacture of the magnet as specified is within the capacity of European industry.

3·2. *Radiofrequency system.* – It is necessary to apply an RF peak potential of about 10 kV to the accelerating electrode, the accelerating field being concentrated between the electrode and a grounded « dummy dee ». The frequency variation required in the CERN machine is over the approximate range 30-16 MHz, and the repetition rate of the frequency-modulation cycle has been chosen to be 50 Hz.

We have chosen the three-quarter wave system originally developed by McKenzie at Berkeley, and also used in the large synchrocyclotrons at Chicago and Liverpool. These machines, and all other existing synchrocyclotrons known to the author, use a motor-driven rotating condenser to vary the resonant frequency of the system. However, the physical dimensions of the CERN machine are such that the rotary condenser would have to be mounted rather close to the magnet poles in order to achieve the desired resonant frequency and eddy current effects and assembly difficulties would be very troublesome. Moreover, the rotating condenser in the RF system is a formidable device from the engineering point of view. The same difficulties had been encountered earlier at Berkeley during the design work for the conversion to 730 MeV of the 184-inch synchrocyclotron, and the Berkeley engineers accordingly evolved a different type of condenser. This consists of a vibrating reed system, so that the condenser becomes a parallel plate device with variable separation between the plates. The plates are excited in a tuning-fork type of resonance by an A.C. solenoid.

We have adopted the same system for the CERN machine, with detailed differences. The Berkeley system uses plates of nitride-hardened steel, clamped rigidly at the nodal points of the mechanical movement and copper plated. It was necessary to use several plates, vibrating in phase, to obtain the required total width. The RF subgroup of the CERN team working at Amsterdam were attracted by the possibilities of a one-piece aluminium alloy vibrator

machined from the solid. No plating would be needed, since the RF losses of aluminium are sufficiently small for this purpose. The success of the method would depend upon the provision of a sufficiently good block of aluminium alloy, free from flaws, and the avoidance of deep scratches during manufacture and assembly. The manufacturing schedule of the synchrocyclotron is determined largely by the magnet and building programme is such that a final decision between these two systems can wait for some time yet — in particular, it can probably await practical experience at Berkeley with the built-up steel system.

In the meantime, experimental work has been proceeding on scale models at the Eindhoven works of Messrs. Philips. Two kinds of scale models have been used. One is a quarter-scale model in all dimensions, and the other has full-size dimensions in section (i.e. the correct mechanical resonant frequency) but reduced width. Results so far are promising. Fatigue failure has not occurred after many millions of vibrations, except for one early failure attributed to a flaw in the metal visible under the microscope. It has proved possible to maintain the required amplitude of oscillation without trouble from undesirable transverse modes. Development is proceeding satisfactorily on devices to control the amplitude within the required close limits.

Some attention has been given to the design of the RF circuits associated with the system, and it is probable that a full-scale mock-up of the system will be made for RF experiments on feeder lines, coupling problems and the suppression of unwanted modes of oscillation. One mode which will probably be troublesome is the transverse mode in which the dee edge is half a wavelength long.

This is the only part of the synchrocyclotron on which appreciable development work is needed. Much has already been done, and the Berkeley group have generously kept us informed of the results of their work, but we shall probably strengthen our RF team shortly.

3·3. *Vacuum system.* – The stainless steel vacuum chamber will be of the conventional kind in which the upper and lower magnet pole type form two of the walls, with a rubber vacuum seal extending around each pole tip. Two 80 cm diameter oil diffusion pumps will be used, with the usual auxiliaries and mechanical pumps. The system is completely designed, and we are ready to invite tenders.

Much thought has been given to the shape of the vacuum chamber in order to facilitate the experimental use of the machine. It is planned to extract the proton beam on one side of the machine, and neutron and meson beams on the other. All the RF and pumping equipment will be on the « proton » side. This arrangement, which was used with the Harwell cyclotron, has been found most convenient in avoiding congestion in the experimental space. On the

« neutron » side there will be an absolute minimum of cyclotron equipment and a single large, removable faceplate will be placed as close to the magnet poles as possible. This plate is roughly equal in length to the magnet pole diameter, and there will be no fixed vertical supports crossing the magnet gap behind it. The object is to allow the extraction of neutron and meson beams in as wide as possible a range of positions and directions.

3·4. *Shielding.* – The shielding problem of a large accelerator is a formidable one. Almost all the protons in the beam will come to rest somewhere in the machine, and previous experience warns us that there will be high energy neutron fluxes at 1-2 metres distance of at least 10^7 neutrons cm^{-2} s^{-1}. The health tolerance dose is about 10 neutrons cm^{-2} s^{-1}, and the tolerance for experimental background is about the same. It is necessary to use heavy shielding; with high energy neutrons the thickness of a shield to produce a given absorption is roughly inversely proportional to the density of the shielding material.

The layout has to be carefully considered in relation to the experimental utility of the machine. In the CERN layout, the synchrocyclotron will be

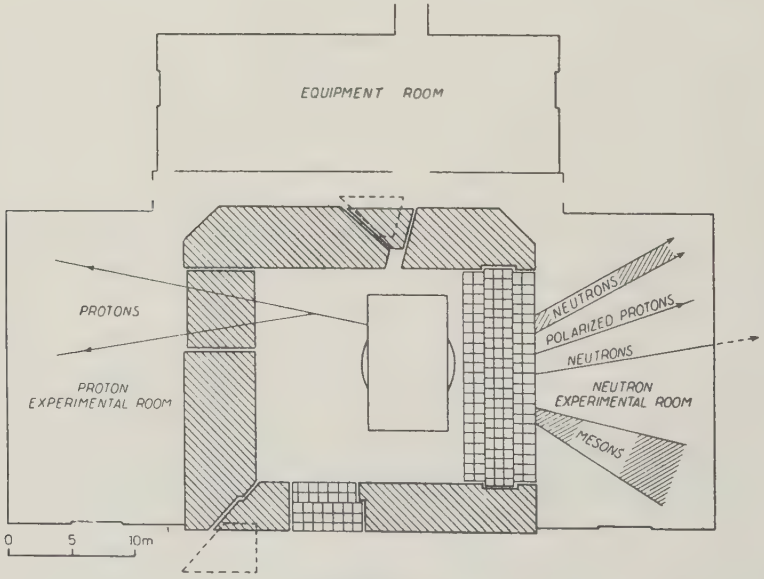

Fig. 1.

enclosed in a compact shield, above ground level, containing just enough space to perform the vital assembly and maintenance operations. Collimated beams of particles will be allowed to emerge from this enclosure as required, and,

after passing through an experiment target, the beams will be absorbed in local shields outside the enclosure.

The arrangement is shown in the Fig. 1. Two experimental rooms are provided, one for experiments with the external proton beam (« proton room ») and one for experiments with neutrons and internally produced meson beams (« neutron room »). In those parts of the main enclosure which are not partially screened by the magnet yoke there is provision for a maximum thickness of 5.7 metres of loaded concrete (density about 3.5). As is customary those parts of the experimental walls near the magnet median plane, through which the collimated beams will emerge, will be built up with steel bars for better absorption of high energy neutrons.

3·5. *Neutron room.* – The neutron and meson experimental room is 14 metres deep by 25 metres wide, and is separated from the cyclotron room by a wall built up from rectangular heavy concrete blocks. This wall is placed very close to the cyclotron (about 60 cm from the outer edge of the magnet coils) and is 17 metres wide. Collimating channels may be placed at any place in the 17 metres width, and the wall is adjacent to the long vacuum chamber faceplate already mentioned. The wall is mounted on a platform which may be retracted into the floor by means of a screw jacking arrangement. This will facilitate the adjustment and alignment of beam channels, and ensure that no large gaps will remain between the top of the wall and the ceiling of the cyclotron rooms. It is intended to load the individual shielding blocks on to the platform with the help of a fork-lift truck, adapted as a mobile crane.

A 20 ton travelling crane will be installed in the neutron room, and the floor will be strong enough to carry heavy magnets, local shielding walls, etc.. A long-flight neutron beam may be allowed to escape from the room, and the site has been planned so that no buildings will be erected in the path of this beam.

3·6. *Proton room.* – This room is also 14 metres deep by 25 metres wide, and has similar floor and crane arrangements. A similar, but smaller, adjustable wall is provided on the side adjacent to the cyclotron room. It is intended to allow two or more proton beams to pass through channels in this wall into the proton room, the different beams being selected with the help of a bending and focusing magnet. Rather less experimental space is needed here than in the neutron room, since the possible number of beams is much less. Nevertheless, it is always found that large amounts of bulky apparatus make their appearance after an accelerator has been running for some years, and the surplus space in the proton room is intended for the storage of such items.

There is easy communication between the two experimental rooms, through a broad corridor which passes around the outside of the main shielding and

also connects with a corridor to the control room. Counting rooms for the experiments are situated near the control room.

3·7. *General.* – There are two entrances to the cyclotron room, which are sealed off during operation by moveable heavy concrete wedges. One of these openings can be made big enough, by removing concrete blocks, to permit the passage of the largest parts of the machine.

The roof is of concrete, 1.5 metres thick, and the main cyclotron room contains only that equipment which has to be close to the magnet (e.g. vacuum and RF equipment). The remaining equipment, such as the magnet generator and the high voltage rectifier, will be housed in a large equipment room which also has space for cloud chamber and particle bending magnet generators. The equipment room will have a 10 ton crane.

It is anticipated that research staff will be able to work in whichever of the experimental rooms is not being irradiated at a given time. It may be safe, with the help of auxiliary shielding blocks in the experimental rooms, to work near an experiment actually being performed but this would be permitted only in very rare cases and after careful radiation surveys has shown that there was no health hazard. These machines are extremely lethal, and it is better to suffer some inconvenience and delay by remotely controlling experiments than to take even a slight risk.

The CERN synchrocyclotron buildings are almost completely designed; only details need to be settled. Preliminary excavation has started at the site.

4. – Output of a Typical Synchrocyclotron.

Synchrocyclotrons have proved to be very reliable machines, and the probable output of a new machine can be predicted with reasonable confidence. Typical values are shown in Table II.

Some general remarks may be made on some of the numbers listed in Table II. The broad energy spread of the beam striking an internal target is a consequence of the rather large radial oscillation amplitudes which have so far occurred in synchrocyclotrons. Some success has been achieved in reducing this spread, but at the expense of intensity. Similarly, the good spectrum of the external beam is a result of momentum dispersion as the protons pass through the fringing magnetic field, and, therefore, also occur at the expense of intensity. The regenerative beam extraction system, originally proposed by TUCK and TENG in Chicago and developed theoretically by LE COUTEUR in Liverpool, may give a substantially increased yield in the external beam. The maximum improvement expected is by about a factor 100. Since the lecture was delivered, experiments on this system have been started on the

new Liverpool synchrocyclotron, and it is reported that about 2% of the internal beam has reached the entrance of the magnetic shielding channel. This would represent an improvement over the scattering method used at Harwell and elsewhere by about a factor 30 (J. M. CASSELLS, private communication) (*).

TABLE II. – *Synchrocyclotron output characteristics.*

Mean proton current (internal)	~ 1 μA
Pulse duration	~ 200 μs
Pulse repetition rate	~ 50 Hz
Energy spread of internal beam (radial oscillations.)	5-10 %
Flux of external proton beam (useable in experiments, in a shielded enclosure, as reported from various laboratories.)	10^5-10^7 proton cm^{-2} s^{-1}
Energy spread of external beam	~ 1 %
Neutron flux close to machine	$\sim 10^7$ neutrons cm^{-2} s^{-1}
Useful neutron flux (Collimated beam in a shielded enclosure.)	$\sim 10^5$ neutron cm^{-2} s^{-1}
Meson flux	$\sim$ 10-1 000 π-mesons cm^{-2} s^{-1} depending on meson energy with $\sim \pm 10$ MeV energy spread.
Meson energy (For 600 MeV protons as at CERN.)	Up to 400 MeV π^- Up to 200 MeV π^+ by $p+p \rightarrow \pi^+ + d$ in external beam with $\sim \pm 5$ MeV spread.

The neutron fluxes given in Table II are very rough and are extrapolated from measurements made by the author and others on the Harwell synchrocyclotron. They refer to « high energy » neutrons (i.e. in the case of the CERN machine, to neutrons over about 200 MeV). Much of the flux is contained in a peak of the energy distribution near the bombarding proton energy and most of the width of the peak in this region is attributable to the spread in energy of the internal beam together with the additional spread caused by multiple traversal of the target by the beam (this latter effect has been called « recirculation » by some American workers). The effective number of traversals can be predicted theoretically, and the results agree well with experiment over a fairly wide range (say, from 2 to 20 traversals). The two effects which have to be considered are the multiple scattering of the beam by the target material

(*) *Note added in proof.* – Still more recently, 20% of the internal beam of the Liverpool synchrocyclotron has been made to reach the entrance of the channel, and 2% has been focused into a small area (about 5 cm^2) at a point remote from the accelerator.

and the axial focusing caused by the magnetic field distribution. The particles are eventually lost by striking the dee, and if all other conditions are kept constant the effective number of traversals is roughly proportional to the square of the vertical dee aperture. The number of traversals may therefore be reduced, and the spectrum somewhat improved at the expense of intensity, by artificially reducing the dee aperture, and this is often done. Similarly, the effect may be exploited to obtain high specific activities by bombarding a very thin target using the full aperture.

In addition to the yield of high energy neutrons, large numbers of « evaporation » neutrons of average energy 2-3 MeV may be expected whenever heavy elements are bombarded.

There is room for considerable improvement in the yields of external protons and of mesons produced in internal targets, by development of improved focusing systems. However, it must be borne in mind that the internal energy spread and the effect of the fringing field are serious obstacles and are bound to cause loss of intensity compared with the ideal situation which one would like to have.

The CERN synchrocyclotron is being designed by an international group under the direction of Professor C. J. Bakker.

PARTE SECONDA

Sezione II

Progetto inglese di macchina acceleratrice.

Proton Linear Accelerators for Nuclear Research, and the A.E.R.E. 600 MeV Project.

T. G. Pickavance

Atomic Energy Research Establishment (AERE) - Harwell

1. – Introduction.

A certain proportion of our work at Harwell is devoted to fundamental research, and we already have one high energy machine which is used in a part of this programme. This is the 110-inch synchrocyclotron, which has been operating for nearly 5 years, producing 175 MeV protons. When planning our future programme we took into account the existence of CERN, with its plans to construct a 25 GeV proton synchrotron and a 600 MeV synchrocyclotron, in addition to the national requirements of the United Kingdom itself. In these circumstances, with access by British physicists to particles of the highest energies assured by our participation in CERN and with a considerable variety of accelerators already existing in Great Britain, we were attracted by the possibilities offered by a large proton linear accelerator. Such a machine would be designed to give high intensity of real events in the experiments, and would be complementary to the CERN programme and to our own existing facilities.

In what follows it is the intention to discuss the project in general terms and from the point of view of the user of the machine and not the constructor. We assume that protons are required, and do not attempt to discuss the relative merits of protons and electrons in nuclear physics.

2. – General Features of Linear Accelerators.

The linear accelerator has certain obvious advantages over other type of machines:

1) There is no beam extraction problem, so that flexibility and high intensity should be assured.

2) The machine can be built in stages, and can be extended to higher energies if the nuclear physics situation appears to justify this at any time.

We first have to consider the energy range in which a linear proton accelerator appears to be a sensible proposition. This is largely an economic question; economics rather than technology have for some time determined the useful energy range of large accelerators. The cost of high energy accelerators may be summarised very roughly as follows in Table I.

TABLE I.

Large synchrocyclotron ($\sim$ 600 MeV) . . . . . (The cost of a synchrocyclotron varies non-linearly with energy)	\$ 8.00 per keV
Conventional proton synchrotron	\$ 3.00 per keV
Large alternating-gradient proton synchrotron . .	\$ 1.00 per keV

The cost of a large proton linear accelerator is not yet known with any accuracy, but it may be assumed to be of the same order as that of a synchrocyclotron of the same energy — perhaps somewhat higher. In the present stage of development the A.G. proton synchrotron is the best machine for the highest energies, and we have to compare the proton linear accelerator with the synchrocyclotron, in the energy region of a few hundred MeV.

3. – π-Meson Physics.

If we are correct in assuming that π-mesons are closely concerned with the nature of nuclear forces, we shall need to compile a great deal of precise experimental data on the particles for a long time to come. Two kinds of experiments are involved:

1) *Studies of production phenomena.* We have to determine production cross-sections, angular distributions, energy dependence, and so on. These are « primary beam » experiments and the intensity of existing machines appears to be sufficient for such work.

2) *Experiments in which π-mesons are the bombarding particles.* Here we are concerned with such quantities as differential scattering and reaction cross-sections of nucleons and nuclei, and we have first to produce the π-mesons in nucleon-nucleon collisions. These are « secondary beam » experiments, and the intensity offered by existing machines is insufficient for really precise work. There is a case for building an accelerator with an increased useful yield of π-mesons.

3·1. *Meaning of « useful yield ».* – We always mean number of particles $cm^{-2}\ s^{-1}\ MeV^{-1}$ entering the experimental equipment, with the proviso that the total number per second per MeV interval must also be large, since a large flux in a vanishingly small area is not useful! We need for precise experiments:

a large number of events to observe	*good statistics*
small energy spread, since most of the phenomena which we investigate are energy dependent . . .	*good spectrum*
a well-collimated beam, since most of the phenomena which we investigate are dependent upon the angle of observation with respect to the beam	*good geometry*

4. – Comparison of Proton Linear Accelerator and Synchrocyclotron.

4·1. *Experiments in which an external beam must be used.* – The flux of protons, available as a collimated beam in a well-shielded enclosure, reported from various cyclotron laboratories, varies over the range

$$10^5 \div 10^7 \text{ protons cm}^{-2}\ \text{s}^{-1}\ .$$

A proton linear accelerator giving a mean current of 1 μA, which is a typical internal beam current for a synchrocyclotron, in an area of 5 cm^2 would give a useful flux of

$$\sim 10^{12} \text{ protons cm}^{-2}\ \text{s}^{-1}\ .$$

There would therefore be an enormous gain, by at least a factor 10^5, over *present* synchrocyclotron yields. For example at 450 MeV where the cross-sections have been determined, the reaction

$$\text{p} + \text{p} \rightarrow \pi^+ + \text{d}$$

would yield a flux of π^+-mesons in an experimental target of

$$\sim 4 \cdot 10^5\ \pi^+\ \text{cm}^{-2}\ \text{s}^{-1}\ ,$$

with good energy resolution. Corrected for energy spread, this represents an improvement by nearly a factor 10^4 over existing π^+ yields.

The external beam of synchrocyclotrons may be greatly improved if a new method, not yet fully tried, should prove successful. The expected maximum improvement is by about a factor 100. Moreover, the optics of beam focusing devices could undoubtedly be improved. But even allowing an additional factor 100 for improved focusing, and both these estimated possible factors

of improvement are optimistic, the external beam of the proton linear accelerator would still be greater by one or two orders of magnitude (*).

The final comparison would depend upon the relative beam currents of proton linear accelerators and synchrocyclotrons after continued development of both types of machine but the linear accelerator would always produce a much higher ratio of real events: background events since the whole beam would be available externally.

4·2. *Experiments in which the internal beam of the synchrocyclotron may be used.* – All synchrocyclotron experiments with beams of high energy neutrons are performed with the internal beam, since the highest possible intensity is required. There would be two advantages to be gained by using a proton linear accelerator:

i) *The energy distribution would be better.* The energy spread (width at half height) of the beam of a high energy linear proton accelerator would be about 1%, whereas the internal synchrocyclotron beam has a spread of 5-10% as a result of radial oscillations of the protons. Smaller energy spread has been achieved with synchrocyclotrons, but only with great loss of intensity. Hence there would be a larger yield per unit energy interval of the high energy neutrons.

ii) *The background radiation would be lower.* All the protons in the synchrocyclotron, except for the small number (a few per cent) which make nuclear interactions in the internal target, stop somewhere inside the machine and produce unwanted neutrons. The beam of the proton linear accelerator could be brought intact through a hole in a shielding wall, passed through the target and led away for a considerable distance before being stopped. Moreover it should be possible to bring experimental apparatus much closer to the neutron-producing target, since there are no magnet poles and coils to intrude. A factor of at least 10 should be gained, in useable intensity, by the use of a linear accelerator producing the same beam current as a synchrocyclotron.

The internal synchrocyclotron beam is also much used in experiments with π-mesons, and at present time fluxes $10 \div 1000$ π^--mesons cm^{-2} s^{-1} are available, the value in this range depending upon the meson energy.

It is estimated that 1 μA of protons at 450 MeV, from a linear accelerator, would produce from a carbon target a flux $\sim 10^5$ π^--mesons cm^{-1} s^{-1} with a similar energy spread to that at present available in the synchrocyclotron meson beams. The gain is simply due to better geometry. The mesons produced by a synchrocyclotron have to travel rather a long distance from the internal

(*) *Note added in proof.* – The regenerative beam extraction system has now been put into operation at Liverpool, with spectacular success. 2% of the internal beam of the Liverpool synchrocyclotron is now available externally.

target to the experiment, passing through the fringing field of the magnet on the way. Some focusing is produced by the fringing field, but only over a rather small solid angle. Undoubtedly this focusing could (and should) be improved; perhaps it would pay to use specially shaped magnet pole pieces near the internal cyclotron target. Nevertheless it appears to us that the linear accelerator, for the same beam current, would always have a useful factor in hand, and the factor of improvement over existing sources of π^--mesons is very striking. For π^+-mesons the gain is very great. π^+-mesons are rather weakly produced by the internal beam of the synchrocyclotron since they must be emitted near the backward direction; for the same reason they have rather low energy.

These considerations, together with the possibility of future extensions, have led us to make a serious study of high energy proton linear accelerators.

5. – Fundamental Difficulty of the Proton Linear Accelerator.

It is well known that phase stability of the particles in a linear accelerator, with respect to the accelerating RF field, requires that the particles be accelerated in an electric field rising with time (or, in the case of a travelling wave, ahead of the wave crest). This condition is also the condition for radial electric defocusing of the particles by the RF field. No high energy accelerator has a hope of success unleess it is operated in conditions of directional and phase stability. There is no serious stability problem with linear electron accelerators, since at extreme relativistic velocities, which occur at quite low electron energies, the radial and longitudinal oscillations virtually disappear. With protons, however, we are dealing with, « slow » particles throughout the accelerator, in the energy range which we are considering here. Moreover, long RF wavelengths have to be used with slow particles, for reasons associated with transit time and the minimum hole size required for the particle beam. For protons of a few MeV, the minimum wavelength is about 1 metre, whereas the electron accelerator can use a wavelength of 10 cm.

These facts explain the comparative neglect of the proton linear accelerator and the success of the electron linear accelerator (notably at Stanford University, where 600 MeV electrons have been produced with good yield). The biggest proton linear accelerator at present operating is the 32 MeV machine constructed some years ago at the University of California by ALVAREZ and his collaborators. A bigger machine, for 68 MeV, is nearing completion at the University of Minnesota. The Alvarez machine produces a mean current of a few tenths of a microampere, with an energy spread of about 100 keV and with very good collimation. 85% of the beam passes through a 3 mm

aperture, with an angular divergence of 10^{-3} radian. The corresponding proton flux is very high, about $2 \cdot 10^{13}$ protons cm^{-2} s^{-1}.

5·1. *Solution of the focusing problem by Alvarez.* – The Alvarez accelerator consists essentially of a long cylindrical resonator excited in the E_{010} mode at about 200 MHz, and the protons are accelerated by the longitudinal electric field along the axis. Many RF cycles are occupied in the passage along the resonator, and axial drift tubes are introduced to shield the particles from the reverse half-cycles of the electric field. In this mode of operation the particles travel the distance between the centres of successive drift tubes in one RF cycle. The electric field distribution in the accelerating gaps between the drift tubes is distorted, to produce an inward radial component for focusing, by placing a conducting grid of high transparency across the entrance of each drift tube. Foils were originally used but they had to be very thin in order to avoid excessive loss of particles by scattering, and they were destroyed by sparking.

5·2. *Focusing in a large machine.* – The grids could not be used in a very long machine, with hundreds of drift tubes, since the resulting exponential loss of beam current would be prohibitive. It appears from work done by Bell at Harwell that foils of 10 times the thickness used by Alvarez could be used from 50 MeV upwards, without excessive loss due to scattering. It is not known whether the foils would successfully resist damage by RF sparking but they might be placed well inside the drift tubes, shielded from the RF field, and made to carry a suitable DC potential for focusing. Other methods have been considered by various people. An intense axial beam of electrons could be used to introduce charge on the axis (Chick and Petrie) but this method has not yet been tried. A 1 ampere beam of 75 keV electrons would be needed to focus 22 MeV protons, and the method does not appear promising for very large linear accelerators. In another method the proton beam would be made to spiral around a charged axial conductor.

The most promising method at present appears to be alternating gradient focusing, similar to that planned for the big proton synchrotrons. Quadrupole electrostatic or magnetic lenses would be placed inside the drift tubes, with electrodes or pole pieces arranged to produce zero field on the axis of the drift tube and constant field gradients, equal in magnitude and opposite in sign, across two perpendicular planes crossing on the axis. These would be similar to the quadrupole correcting lenses proposed for the proton synchrotron, and would be mutually oriented in successive drift tubes in such a way as to produce the desired radial dynamics of the particle motion. The electrodes or pole pieces would be shaped in section as rectangular hyperbolae, and adjacent poles would have opposite polarity. Magnetic focusing appears

to be preferable, since there are no breakdown problems and the field may be progressively reduced along the accelerator, as $1/v$. The gradient required is of the order of 1 kilogauss per cm, which is easily obtainable.

As with the proton synchrotron, it is necessary to study the changes in radial motion induced by random misalignment of the magnetic centres and by non-linearities in the focusing fields. The problem should be less serious here, since each particular disturbance is encountered only once, but it appears to be necessary to align the magnetic centre-lines of the lenses to within a few thousandths of an inch. This will not be easy.

6. – Radiofrequency Problems.

A 600 MeV proton linear accelerator will need 100/150 MW of peak RF power at a relatively long wavelength ($\sim$ 1 metre), and the provision of suitable power sources obviously constitutes one of the major problems. In the interests of reliability and simplicity it is desirable to use a fairly small number of individual sources, so that valves capable of giving at least 1 MW each are required. Suitable valves are not yet commercially available, and a valve development programme is an essential part of a big proton linear accelerator project. Maintenance of the correct RF phase along the whole accelerator, within narrow limits, is necessary in order to preserve phase stability for a useful fraction of the injected particles, and this involves the use of power amplifiers rather than oscillators. Elaborate tuning and phase-shifting devices, automatically controlled, are needed, and close dimensional tolerances and temperature control of the RF-heated surfaces have to be maintained.

There are also RF structure problems. The Alvarez structure is very efficient at low particle velocities, but becomes less efficient as the drift-tube dimensions and resonator diameter are changed to take account of the increasing particle velocity. Ultimately a resonance effect in the drift tubes causes very high RF losses, at about $v/c=2/3$ with the geometry usually adopted. It is necessary, therefore, to change to a different structure at some stage, and a suitable energy at which to make this change appears to be about 150 MeV. The structure used at the higher energies would have dividing walls at the centre of each drift tube, so that it would take the form of a series of individual « pill-box » resonators. In order to reduce multiplicity of components and power sources, many of these unit cells would be contained in a single tank excited by a single RF source. The aperture of the drift tubes would be too small to provide sufficient RF coupling between the individual unit cells, and some form of coupling through the dividing walls would have to be devised. One structure which may be suitable is the π-mode structure, where it is known that sufficient coupling can be achieved by placing loops in each unit

cell, adjacent loops being connected together through a hole in the dividing wall. In the π-mode structure the protons travel the distance between centres of adjacent drift tubes in one half of the RF cycle. A structure operating in the $\pi/2$ mode could be operated in either resonant or travelling wave form, and in either case we believe that sufficient coupling between unit cells could be achieved simply by cutting holes in the dividing walls. A choice between these three structures can only be made after careful studies of power losses, liability to RF breakdown, optimum section length, feedback problems (in the case of travelling wave system), dimensional tolerances, and so on. Such studies are being made at Harwell, both experimentally and theoretically.

7. – Outline of the Harwell Project.

The Harwell project is still in an early stage, but the main characteristics can be discussed in general terms. Injection will be at 0.5 MeV, the protons being produced by an RF ion source and accelerated by a potential difference obtained from a Cockcroft-Walton generator. The usual system of electrostatic lenses is incorporated, and it is anticipated that several milliamperes of protons in the pulse will be produced within the acceptance conditions of the linear accelerator. Suitable ion sources and focusing systems have been built and tested.

The first linear accelerator tank, 20 feet long, will be very similar to the Bevatron injector at Berkeley and the first tank of the Minnesota accelerator. It will be of Alvarez type and will use grid focusing initially, because at these low velocities the drift tubes are extremely short and therefore contain little space for focusing magnets, and because the defocusing forces are stronger at the lower velocities. The second and third tanks will each be 40 feet long and will each add 20 MeV to the proton energy. They will also be of Alvarez type, but will use alternating gradient focusing provided by electromagnets inside the drift tubes. The resonant frequency of these three tanks will be nominally 200 MHz.

After the third tank, i.e. at an energy of 50 MeV, it will be an advantage to reduce the wavelength. The phase oscillation amplitudes will have diminished sufficiently by this time to ensure that no particles will be lost from the stable bunches if the wavelength is halved (in an ideal machine with no phase « jitter »), and the use of the shorter wavelength enables the diameter of the resonators to be halved. Since the vacuum envelopes of the early resonators will be about $4 \div 6''$ in diameter, the saving achieved in this way will be considerable. A further advantage is that it is found that a higher accelerating rate may be used at the shorter wavelength, without risk of breakdown. The next series of tanks, then, will operate at approximately 400 MHz.

They will still be of the Alvarez pattern, and this system will continue until an energy of about 150 MeV has been reached.

Beyond 150 MeV it will be necessary to change the structure for one with dividing walls, for reasons already discussed. However, the wavelength will remain the same, and from this point on the tanks will be identical save for a slow change of the dimensions of the unit cells to account for the increasing velocity of the protons.

The 10 MeV tank is now completely designed, and all important physical characteristics and much engineering design have been established for the second and third tanks. The main features of that part of the machine from 50 MeV to 150 MeV are settled, and serious engineering design will start soon. Beyond 150 MeV the basic physics is well understood, and experiments and calculation have been under way for some time to establish the main features of a practical machine.

In all the waveguide work, and also in the work which is proceeding on modulators, controls and general RF problems, we are collaborating with Messrs. Metropolitan-Vickers who will manufacture the appropriate equipemnt.

The valve programme has to be divided into two parts on account of the change of wavelength at 50 MeV. Rather little power will be required at 200 MHz (about 4 or 5 valves), and our valve development group will produce grounded-grid triode power amplifier valves of a type which they are now developing. A similar type of valve of modified design suitable for operation at 400 MHz with a power output of $1 \div 2$ MW peak, is being developed for us by the English Electric Valve Company. Finally, we are collaborating with a group at London University who are developing a $1 \div 2$ MW klystron for operation ad 400 MHz. A choice will ultimately be made between these two 400 MHz valves.

The overall design parameters of the accelerator are listed in Table II.

Table II.

Final proton energy	600 MeV
Mean beam current	1 μA
Duty cycle	1 %
Pulse duration	50 Hz
Length	270 m

It is intended to instal beam bending stations at intervals, so that protons of intermediate energy may be extracted. Shielding will be by earth banks, and the site has been chosen to allow extension to several times the length corresponding to 600 MeV.

The project is being approved in stages, so that at present we are engaged in a large scale exercise to determine whether a 600 MeV proton linear acce-

lerator of acceptable reliability and output is economically feasible. Certainly there appear to be no fundamental scientific objections to the construction of such an accelerator, and we are convinced of the advantage to nuclear physics which would result from its satisfactory operation.

One remark may be made on the subject of electron machines. In the region of a few hundred MeV, 1 proton is the equivalent of approximately 2 000 electrons in terms of useful meson production per unit interval of meson energy. Electron linear accelerators are easier to build than proton machines, and indeed may be the machines of the future even for the very highest energies when electrons are specifically required, but for the particular purpose which we have in mind the proton linear accelerator appears to be a much better proposition, despite the difficulties.

PARTE SECONDA

Sezione III

Progetto francese di macchina acceleratrice

Sur le projet du synchrotron à protons de Saclay.

H. Bruck et R. Lévy-Mandel

Commissariat à l'Énergie Atomique, France

Le plan quinquennal 1953-1957 du Commissariat à l'Energie Atomique prévoyait l'édification d'un grand accélérateur dont les caractéristiques n'avaient pas été arrêtées.

Au cours de l'année 1954, sous l'impulsion de son Haut-Commissaire, le Professeur F. Perrin, la décision a été prise de construire sur le terrain du Centre d'Études Nucléaires de Saclay, un synchrotron à protons. L'énergie que les particules accélérées doivent atteindre a été fixée à 1.75 GeV, à un premier stade, avec possibilité de pouvoir dépasser cette valeur ultérieurement. L'énergie des particules accélérées a été ainsi choisie, à la suite d'informations de Brookhaven, afin qu'elle soit suffisante pour la création de particules V.

La responsabilité de la réalisation de cette machine est assumée par M. R. Maillet. L'établissement du projet, ainsi que la surveillance technique de son exécution est à la charge du Service des Accélérateurs, dirigé par M. S. D. Winter.

Les auteurs, membres de ce Service, ont l'honneur de présenter, ci-dessous, quelques remarques sur le choix du type et les dimensions de cette machine, sur la conception de son aimant, ainsi que sur le bâtiment et la mise en œuvre pratique du projet.

1. – Choix du type de la machine.

1·1. *Tableau comparatif des caractéristiques de l'orbite.* – A la suite d'études comparatives, une machine du type conventionnel, à la manière du Cosmotron de Brookhaven, a été adoptée, écartant ainsi le principe de la focalisation intense.

Cette décision s'appuie sur les études suivantes:

1) Un rapport etabli sous la direction de M. A. ABRAGAM [1] et consacré essentiellement aux possibilités de la focalisation intense.

2) Un avant-projet de machine conventionnelle par M. P. DEBRAINE [2].

3) Des déterminations de caractéristiques d'aimants et de dimensions d'entrefer à partir de mesures à la cuve rhéographique.

4) Une étude économique comparative par M. S. D. WINTER [3].

Le Tableau I, extrait du rapport cité de A. ABRAGAM, reproduit quelques caractéristiques calculées de deux machines à 1.75 GeV, respectivement conventionnelle et à focalisation intense, ainsi que les caractéristiques d'une machine de 30 GeV, à focalisation intense.

TABLEAU I.

N° du projet (cf. note *CEA* n. 41)		Conv. 2	Foc. int. 4	Foc. int. *a*
Energie en fin d'accélération . . .		1.75 GeV		30 GeV
Induction sur l'orbite en fin d'accélération $(B_0)_{max}$		10 kgauss		12 kgauss
Rayon de courbure magnétique de la trajectoire	r_0	8.40 m		86 m
Type de la machine . . .		conventionnel	foc. intense	foc. intense
Mailles — nombre		4	18	57
Mailles — type		*F O*	*D O F O*	*F O F D O D*
Mailles — longueurs		*F*: 13.2 m *O*: 3.3 m	*D, F*: 146 cm *O* : 73 cm	*F, D*: 237 cm *O* : 143 cm
Indice du champ	n	0.6	$\pm$ 36	$\pm$ 392
Fréquence betatron	Q_r	0.71	3.78	7.25
Déphasage de l'oscillation par maille (mode σ) . .		—	$2\pi/4.76$	$2\pi/7.88$
Energie cinétique de transition		—	2.39 GeV	$\sim$ 5.8 GeV
Energie d'injection		4 MeV	4 MeV	50 MeV
Vitesse de montée de l'induction	B_0	22.2 kG/s	18.9 kG/s	12 kG/s
Harmonique de la H.F. . .		2	2	38
Hauteur de la chambre . .	$2A_z$	50 mm	58 mm	49 mm
Largeur de la chambre . .	$2A_r$	365 mm	73 mm	70 mm

On a supposé pour les trois machines comparées dans ce Tableau la même pression résiduelle d'air de $p = 2 \cdot 10^{-6}$ tor dans la chambre, les mêmes erreurs

---

[1] A. ABRAGAM, C. BLOCH, M. PAUTHIER et I. SOLOMON: *Étude de la focalisation intense dans le Synchrotrons à Protons, Note CEA*, n. 41 (Janvier 1954.

[2] P. DEBRAINE: *Cosmotron à gradient constant, Note CEA*, n. 62 (Avril 1954).

[3] S. D. WINTER: *CEA*, Note AC 273, du 27 Avril 1954.

quadratiques moyennes sur l'alignement des blocs magnétiques de $\langle \xi \rangle = 0.25$ mm, et sur l'induction rémanente de $\langle \delta B \rangle = 0.2$ gauss.

Parmi les informations produites par ce tableau, on note, particulièrement, les hauteurs $2A_z$ peu différentes entre les machines conventionnelle et à focalisation intense de 1.75 GeV; on note, ensuite, les dimensions $2A_z \times 2A_r$ presque identiques de la chambre des deux machines à focalisation intense, dont les rayons sont pourtant différents d'un facteur 10, et finalement, la valeur de l'énergie de transition, de la machine à focalisation intense de 1.75 GeV, valeur assez mal placée à 2.39 GeV.

1·2 *Commentaires sur les dimensions de la chambre de circulation.* – On sait que, dans une machine à grand rayon, le principe de la focalisation intense ou du gradient alterné permet une réduction notable de la section nécessaire de la chambre, ce qui permet de réduire en conséquence les dimensions et le prix de l'aimant.

On est tenté de concevoir une machine plus petite à rayon $r_0 \approx 10$ m, comme simple réduction homothétique d'une machine à grand rayon de l'ordre de 100 m. Cela serait permis s'il y avait invariance des trajectoires par rapport à une telle homothétie. Cependant:

a) une telle invariance n'est pas vérifiée par rapport au gas scattering dont l'amplitude croît quand le rayon et, de ce fait, l'énergie d'injection diminuent;

b) les défauts d'alignement des éléments de l'aimant ne peuvent pas être réduits dans la même proportion que le rayon;

c) l'énergie de transition n'est pas atteinte à la même fraction du cycle.

Le fait que les défauts d'alignement ne peuvent pas être réduits dans la même proportion que le rayon et que l'amplitude du gas scattering augmente quand le rayon diminue, conduit à une section de chambre sensiblement égale pour une machine de 10 m et de 100 m de rayon.

L'inclinaison des pièces polaires sera aussi sensiblement la même dans les deux cas, étant donné que l'induction ne doit pas varier de plus d'un facteur 3 d'une extremité de la zone utile radiale à l'autre, sinon, les champs deviendraient, du côté des champs faibles, à l'injection, trop sensibles à des effets perturbateurs et, du côté des champs forts, en fin de cycle, trop saturants pour le fer.

En réduisant le rayon, on est donc obligé de laisser le gradient du champ pratiquement constant, et ce faisant, l'indice $n = (r_0/B_0)(\mathrm{d}B/\mathrm{d}r)$ du champ baisse environ comme r_0. La forte convergence de la machine qui fait sa supériorité faiblit donc simultanément, rapprochant ses caractéristiques de celles d'une machine conventionnelle.

Il s'avère, ainsi, qu'à $r_0 \approx 10$ m le bénéfice de la focalisation intense est

déjà quasi nul, en ce qui concerne la hauteur $2A_z$ requise pour la chambre. Seule, la réduction de l'amplitude des oscillations synchrotron est encore importante, autorisant une réduction sensible de l'extension radiale de la chambre.

Par ailleurs, le peu de liberté que l'on a dans le choix du gradient du champ, c'est-à-dire de la convergence de la machine, ne laisse au constructeur aucun paramètre pour situer convenablement dans le cycle l'énergie de transition.

On sait que l'énergie cinétique de transition est approximativement $T_{tr} \approx (Q_r^2 - 1)E_0$, Q_r et E_0 étant respectivement la fréquence bétatron radiale et l'énergie au repos du proton. Il faut accepter que l'énergie de transition se place, pour une machine de $r_0 \approx 10$ m, très peu au delà de la fin du cycle, rendant assez délicat tout projet d'extension future de l'énergie maximum.

Une machine conventionnelle permet, en outre, de réaliser des champs magnétiques plus forts au centre de la chambre, et, déjà de ce fait, d'atteindre, à rayon égal, des énergies supérieures.

1·3. *L'intensité de pulsation.* – Dans les machines à focalisation intense, le pas de spiralisation est très petit. En plus, l'existence d'un gradient élevé du champ, ainsi que le phénomène de la saturation du fer, limitent l'extension radiale de la partie utilisable du champ magnétique. Dans ces conditions, il est avantageux de faire l'injection sur un tour unique. Cependant, grâce à la faible amplitude synchrotron qui caractérise la machine à focalisation intense, on conserve la majorité des particules introduites à l'intérieur de cette section relativement faible de chambre. Le fait que pour deux machines à focalisation intense de rayons respectivement grand et petit les sections de chambre soient approximativement égales, entraîne aussi l'égalité des sections maxima des faisceaux que l'on peut y injecter. La densité des protons, contenus dans ce faisceau, est limitée par la charge d'espace. Cette densité limite s'avère pratiquement indépendante des caractéristiques de la machine. Le nombre total des particules que l'on peut introduire dans une machine à focalisation intense diminue donc environ linéairement avec le rayon, rendant le problème de l'intensité plus ardu à rayon faible.

Dans une machine conventionnelle, afin de conserver les particules injectées, l'importance de l'amplitude des oscillations radiales synchrotron impose une extension radiale beaucoup plus grande de l'entrefer. Mais on peut mettre à profit ce fait en injectant sur plusieurs tours. On peut ainsi gagner aisément un ordre de grandeur sur le nombre total des particules injectées par cycle comparé à une machine à gradient alterné de même rayon.

1·4. *Considérations économiques.* – A rayon égal, les dimensions de l'aimant d'une machine à focalisation intense sont inférieures à celles d'une machine conventionelle. Cependant, l'économie qui en résulte n'est plus très importante

dans le cas présent d'un rayon d'orbite relativement faible. Contrairement à la situation pour une machine à grand rayon:

1) la différence des dimensions de l'entrefer ne porte plus que sur la largeur;

2) la différence du prix de l'aimant et de son alimentation ne constitue plus qu'une fraction relativement faible du prix total.

Tableau II.

Rayon de courbure magnétique des trajectoires . .	r_0	8,40 m		
Vitesse de montée de l'induction	B	20 kG/s		
Type de la machine . . .		conventionnel		foc. intense
Énergie en fin d'accélération		1,75 GeV	2,7 GeV	1,75 GeV
Induction sur l'orbite en fin d'accélération	$(B_0)_{max}$	10 kgauss	14 kgauss	10 kgauss
Dimensions de la chambre .	$2A_z$	100 mm		90 mm
	$2A_r$	300 mm		110 mm
Poids de l'aimant . . .	fer	580 t		~365 t
	cuivre	50 t		41 t
Puissance d'alimentation		10 000 kVA	19 800 kVA	5 800 kVA
Perte moyenne		250 kW	498 kW	275 kW
Prix de l'aimant		362		250
Prix de l'alimentation		131	220	101
Prix aimant + alimentation . . .		493	582	351
Total (approx.) des dépenses (bâtiment et main d'œuvre compris) (prix en millions de francs français).		1 750	2 100	1 800

Afin de pouvoir apprécier numériquement cette situation, nous extrayons au Tableau II quelques résultats d'une étude économique menée par S. D. Winter [4]. Ces données se rapportent à deux machines, conventionnelle et à focalisation intense, semblables aux deux premières du tableau I, à la différence près que:

1) la pression résiduelle a été supposée de $p = 10^{-5}$ tor (au lieu de $2 \cdot 10^{-6}$ précédemment);

---

[4] S. D. Winter: l. c. Les dimensions d'aimant à la base de cette étude sont éventuellement à majorer pour prévoir un espace supplémentaire dans les entrefers pour des enroulements correcteurs. La valeur comparative des chiffres de ce tableau ne serait pas affectée par ces rectifications.

2) la largeur de la chambre de la machine conventionelle a été réduite à une valeur moindre résultant d'un compromis entre le facteur intensité et le facteur prix.

Cependant, l'intensité de cette machine conventionnelle est encore estimée d'un ordre de grandeur supérieur à celle du projet comparé à focalisation intense [5].

Quant à la dépense totale, on constate qu'il y a pratiquement égalité entre les deux machines comparées.

1·5. *Conclusion.* – Pour un synchrotron à protons de 8,40 m de rayon, c'est-à-dire dont l'énergie des particules serait de 1,75 GeV à une induction de 10 kgauss sur l'orbite, la comparaison des deux types de machines conduit finalement aux appréciations suivantes, en faveur de la machine du type conventionnel, qui ont motivé son adoption:

1) plus grande facilité d'extension vers des énergies plus élevées;

2) intensité par cycle d'un ordre de grandeur supérieur;

3) différence des dépenses — en principe favorable à la machine à gradient alterné — extrêmement faible sinon nulle dans le cas d'une machine d'un rayon de 8.40 m seulement.

Les arguments suivants s'ajoutent en faveur d'une machine conventionnelle:

4) précision d'alignement des éléments de l'aimant moins critique;

5) avantages pratiques d'accessibilité et de facilité d'extraction du faisceau que procurent les sections droites plus longues et l'entrefer plus large;

6) garanties plus grandes — surtout à l'heure où la décision fut prise — concernant la réussite en général et le délai de réalisation dans le cas d'une machine dont déjà plusieurs prototypes fonctionnent aux Etats-Unis et en Angleterre.

2. – Valeurs numériques envisagées des paramétres

Les paramètres de la machine ne sont pas encore définitivement fixés.

Nous reproduisons, ci-dessous, un ensemble de caractéristiques envisagées. Le choix définitif en différera éventuellement, mais en tout cas, de très peu et par exemple par une section de chambre ou une longueur des sections droites légèrement supérieures.

---

[5] On obtient un facteur 10.8 dans l'hypothèse d'un faisceau injecté de même intensité dans les deux cas et en déterminant le rendement de la capture d'après E. Persico; voir ces *Comptes rendus.*

Ainsi, le Synchrotron de Saclay se différenciera de celui de Brookhaven essentiellement par une chambre dont les dimensions ont été substantiellement réduites: la hauteur sera plus petite compte tenu de l'expérience faite à Brookhaven sur ce point, ainsi que du choix d'une vitesse de montée du champ un peu plus élevée dans notre cas. De plus, la largeur de la chambre sera plus faible; ceci en rapport avec l'emploi d'un harmonique plus élevé — probablement le second — de la H.F.

Géométrie de l'entrefer et énergies de début et de fin de cycle.

— Énergie de fin d'accélération	1,75 GeV
— Champ sur l'orbite en fin d'accélération	$(B_0)_{max} = 10$ kG
— Rayon de courbure de la trajectoire	$r_0 = 8.4$ m
— $\dfrac{\text{Longueur totale des sections droites}}{\text{Longueur totale des secteurs magnétiques}}$	$x = 0.25$
— Longueur de l'orbite centrale	$C = 66$ m
— Énergie d'injection	4 MeV
— Champ sur l'orbite à l'injection	$(B_0)_i = 344$ G
— Vitesse de montée du champ à l'injection	$\dot{B}_0 = 20000$ G/s
— Longueur d'une section droite	$L_s = 3.36$ m
— Indice du champ	$n = 0.6$
— Pression à l'intérieur de la chambre	$p = 5 \cdot 10^{-6}$ mmHg

Oscillation bétatron.

— Fréquence de l'oscillation bétatron		horizontale	$Q_H = 0.77$
		verticale	$Q_V = 0.87$
— Paramètre β de la matrice de transfert	β_M	horizontal	$\beta_M^H = 1.82$
		vertical	$\beta_M^V = 1.47$
	$\overline{\beta}$	horizontal	$\overline{\beta^H} = 1.74$
		vertical	$\overline{\beta^V} = 1.43$

Caractéristiques du faisceau injecté.

— Admittance (linéaire)	$A = 2\alpha d = 2.5 \cdot 10^{-4}$ cm rad
— Diamètre horizontal	$2J_H = 8.7$ mm
— Diamètre vertical	$2J_V = 8$ mm

Excursion de l'orbite.

On admet qu'il y a 288 blocs magnétiques dont la position par rapport au centre obéit à une loi de Gauss d'écart quadratique moyen $\langle \xi_H \rangle = 2.5$ mm, et la position par rapport à un plan horizontal de référence obéit à une loi de Gauss $\langle \xi_V \rangle = 0.5$ mm.

On admet, en outre, que les blocs magnétiques sont groupés par paires de façon à réduire l'écart quadratique moyen de leur champ magnétique à l'injection à $\langle \Delta B \rangle = 0.2$ gauss.

On en déduit:

— Écart quadratique moyen de l'excursion verticale de l'orbite fermée . . . . . $\langle f_V \rangle = 0.15$ mm

— Écart quadratique moyen de l'excursion horizontale de l'orbite fermée . . . . . $\langle f_H \rangle = 1.44$ mm

Gas scattering.

— Moyenne quadratique de l'amplitude due à la diffusion par les gaz résiduels pour une pression résiduelle d'air de $p = 5 \cdot 10^{-6}$ tor $b_0^H = 33$ mm, $b_0^V = 29$ mm

— Fraction de particules non perdues par gas scattering contre les parois supérieure et inférieure de la chambre à la dite pression . 37 %

Pour ces chiffres, la hauteur utile de chambre est supposée égale à 65 mm pour une hauteur intérieure réelle de 80 mm.

Oscillations synchrotron.

— Fréquence de révolution de la particule:
à l'injection . . . . . $F_i = 0.42$ MHz
à la fin de l'accélération . . . . . $F = 4.3$ MHz

— Ordre de l'harmonique utilisée 2

— Phase optimum pour une chambre de 30 cm de largeur (d'après E. Persico, l. c.) . . . . . $\varphi_s = 41°$

— Dispersion maximum initiale d'impulsion des particules susceptibles d'être accrochées par la H.F. . . . . $(\Delta p/p)_{max} = \pm 1.55$ %

— Amplitude d'oscillation synchrotron correspondante . . $(\Delta r_s)_{max} = \pm 258$ mm

— Rendement de la capture (d'après E. Persico, l. c.) . . $\mathcal{E}(\alpha) = 27$ %

— Gain d'énergie par tour . . . . . 1112 eV

— Tension de crête de la H.F. . . . . 1680 V

— Contraction de l'orbite par tour pendant l'injection . . $\sigma = 2.95$ mm

— Déplacement radial de l'orbite pour une erreur de fréquence de 10^{-3} . . . . . $\partial_r = 21$ mm

— Durée de l'injection (approximative) . . . . . 120 μs

Entrefer.

— Largeur utilisable par le faisceau		300 mm
— En hauteur: Enroulement correcteurs		$2 \times 10 = 20$ mm
Paroi de la chambre (porcelaine)		$2 \times 25 = 50$ mm
Hauteur interne de la chambre		$= 80$ mm
Total		150 mm

Electro-aimant.

— Poids fer . . . . . 800 t

— Poids cuivre . . . . . 40 t

Induction maximum sur l'orbite	10 kG	14 kG	
Flux maximum	36.6	51.2	Wb
Induction moyenne dans la culasse	13200	18500	G
Ampère-tours maximum	134000	200000	
Energie électromagnétique maximum emmagasinée	2440	5200	kJ
Perte Joule par cycle	405	1280	kJ
Puissance de l'alimentation	10300	16100	kVA

3. – Sur l'aimant.

3·1. *Dimensions et structure.* – La Fig. 1 montre une moitié du profil en C des blocs qui composent l'aimant. Les dimensions de l'aimant représenté sont légèrement supérieures à ce qui serait nécessaire pour le projet décrit au chapitre précédent. Les dimensions de la Fig. 1 correspondent sensiblement à la limite supérieure de la gamme des possibilités envisagées.

Les dimensions d'un tel aimant sont conditionnées par les dimensions et l'induction maximum d'entrefer que l'on désire réaliser. La fraction de la section de l'entrefer utilisable par le faisceau est limitée radialement par la qualité du champ et en hauteur par l'encombrement à réserver à des enroulements correcteurs et à la paroi de la chambre. La section d'entrefer utilisable de l'aimant, représenté à la Fig. 1, est ainsi d'environ 373 mm radialement sur 110 mm en hauteur.

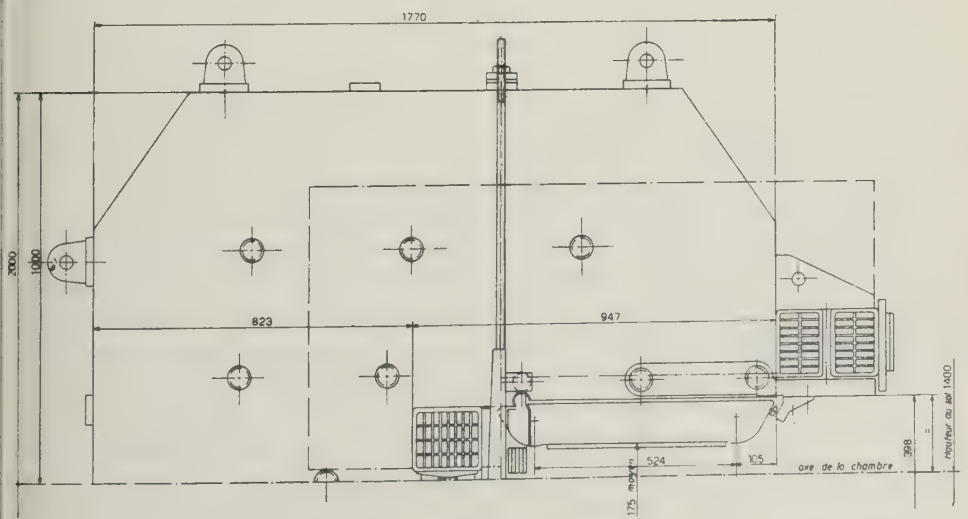

Fig. 1.

Comme à Brookhaven, l'aimant est constitué par 288 blocs pour un cercle complet. Chaque bloc couvre azimutalement $(2\pi/288)r_0 = 184$ mm au droit de l'orbite d'équilibre qui, pour l'exemple d'aimant décrit ici, a dû être porté à $r_0 = 8\,450$ mm.

Chaque bloc de culasse comporte 14 à 15 tôles d'environ 10 mm d'épaisseur chacune. L'épaisseur totale du bloc est de 149 mm avec une épaisseur utile d'acier de 145 mm.

La section de culasse, visible sur la Fig. 1, est dimensionnée de telle manière que l'induction moyenne dans chaque coupe traversée par le flux soit au maximum de $1.34B_0 = 18\,700$ gauss pour une induction dans l'entrefer de $B_0 = 14\,000$ gauss.

Les tôles de la culasse sont assemblées par tirants et par soudure à la périphérie.

Les pièces polaires sont rapportées. Chaque pièce polaire se compose de 82 à 83 tôles de 2 mm, l'épaisseur totale étant de 170 mm. Ces tôles sont assemblées par collage à l'araldite.

L'induction moyenne dans les pièces polaires est de $1.12B_0 = 15\,700$ gauss pour une induction dans l'entrefer de $B_0 = 14\,000$ gauss.

Le fait d'avoir séparé les pièces polaires de la culasse procure les avantages suivants.

1) La possibilité d'introduire un petit entrefer supplémentaire entre la culasse et les pièces polaires, entrefer dont il sera question d'une manière plus détaillée par la suite.

2) La possibilité d'entreprendre l'édification de la culasse sans devoir attendre la fin de l'étude de la forme exacte des pièces polaires; ceci procure un gain précieux de temps dans le cadre de l'ordonnancement de l'édification de la machine.

3) La possibilité de donner des épaisseurs différentes aux tôles de la culasse et des pièces polaires. L'épaisseur de la tôle de la culasse peut être choisie suffisamment grande pour amortir par courant de Foucault la répercussion des harmoniques élevés de l'ondulation du courant d'alimentation de l'aimant sur la courbe de la montée du champ. Par contre, la tôle des pièces polaires peut être suffisamment mince, rendant faible l'influence sur le champ dans l'entrefer des perturbations provenant et des courants de Foucault et des fluctuations statistiques des propriétés des tôles de la pièce polaire.

4) Finalement, le fait de séparer les pièces polaires de la culasse simplifie le profil des tôles de la culasse et rend ainsi l'usinage plus économique, tout particulièrement dans le cas présent où la fenêtre de la bobine intérieure est plus haute que l'entrefer.

3·2. *Sur le champ dans l'entrefer.* – On sait que la carte du champ dans l'entrefer de l'aimant doit rester pratiquement invariante à partir de l'injection jusqu'à la fin du cycle; même le rétrécissement de l'extension radiale de la zone utile du champ vers la fin du cycle doit être évité, car les procédés actuellement connus pour faire sortir le faisceau accéléré de l'entrefer en fin de cycle, s'accompagnent de larges oscillations radiales dans l'entrefer. Lors de

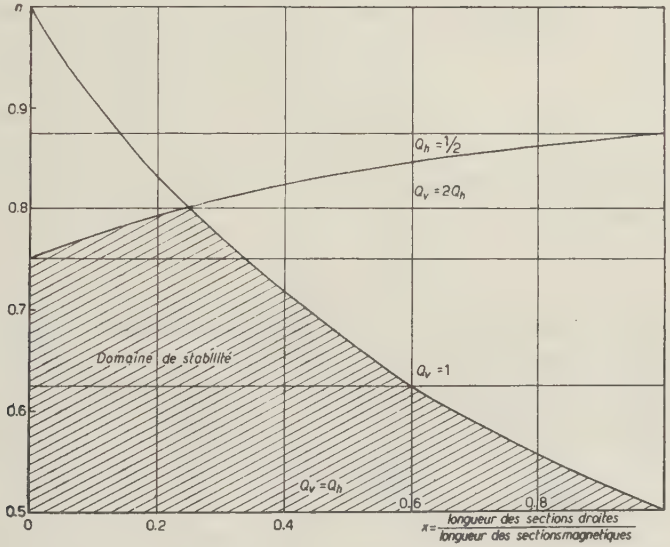

Fig. 2. – Extrait d'un rapport de M. PAUTHIER.

la montée du champ, on peut éventuellement tolérer une variation de l'indice du champ n'atteignant pas des valeurs limites pour lesquelles une résonance se produit. Ces valeurs limites sont fonction de la longueur des sections droites du synchrotron (voir Fig. 2) et se resserrent quand les sections droites s'allongent. L'ordre de grandeur de la tolérance est de $\delta n \approx \pm\ 0{,}1$.

La carte du champ dans l'entrefer est définie par la géométrie des surfaces polaires qui bordent cet entrefer. L'invariance du champ suppose que ces surfaces restent équipotentielles pendant tout le cycle. Une différence radiale de potentiel ΔP dans les surfaces polaires entre deux points distants de $\Delta r = AB$ (voir Fig. 3) entraîne une variation δn de l'indice du champ

$$\delta n = \frac{\Delta P}{P_0}\,\frac{r_0}{\Delta r} \tag{1}$$

Dans cette formule, P est la chute du potentiel magnétique entre une surface polaire et le plan médian de l'entrefer.

La différence de potentiel ΔP est l'expression de la différence de consommation d'ampère-tours (AT) dans la culasse le long de deux lignes de flux passant, respectivement, par A et B. Les AT en question peuvent avoir leur origine dans les AT normaux de la bobine d'excitation, dans la magnétisation rémanente et dans des courants de Foucault.

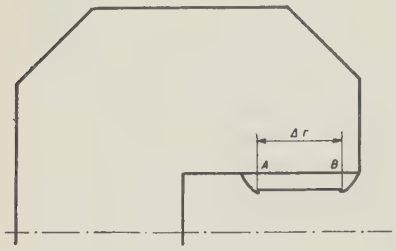

Fig. 3.

L'apparition de différences dans la consommation d'AT est particulièrement favorisée par la forme dissymétrique en C de la culasse qui crée des inégalités de chemins magnétiques pour les différentes lignes de flux.

On peut exprimer ΔP comme fraction γ de la chute de potentiel P_0 moyenne dans la demi-culasse:

$$\Delta P = \gamma P_c .$$

Pour des estimations numériques grossières, on peut considérer γ comme peu variable en fonction du degré de saturation de la culasse.

Pour la culasse considérée représentée aux Figs. 1 et 3, on trouve, à l'aide de mesures à la cuve rhéographique [6] entre les points A et B, sensiblement,

$$\frac{\Delta P}{P_c} = \gamma \approx \frac{1}{5} .$$

Par ailleurs, les AT consommés dans la culasse sont une fraction,

$$\eta = \frac{P_c}{P_0 + P_c} ,$$

des AT totaux.

On peut donc écrire:

$$\frac{\Delta P}{P_0} = \frac{\gamma\eta}{(1-\eta)} , \tag{2}$$

et respectivement, en tenant compte de (1),

$$\delta n = \frac{\gamma r}{(1-\eta)} \frac{r_0}{\Delta r} . \tag{3}$$

[6] Ces mesures ont été faites à l'aide d'une cuve à fond modelé, et par approximations successives. Il est ainsi possible de tenir compte du fait que la permeabilité magnétique de la culasse est une fonction variable du lieu.

La Fig. 4 représente la fraction η (théorique, calculée) des AT totaux, consommée dans la culasse, en fonction de l'induction B_0 dans l'entrefer.

D'autre part, sur la Fig. 5, la courbe *a* représente le défaut $\Delta P/P_0$, respectivement δn résultant de la courbe de η (Fig. 4) avec les relations (2) et (3).

Aux inductions faibles, la courbe δn ne représente pas l'erreur totale, réellement observable, étant donné qu'elle ne tient pas compte de la magnétisation rémanente, ni des courants de Foucault. Par contre, aux inductions fortes, elle est valable et en assez bon accord avec l'erreur δn observée à Brookhaven [7].

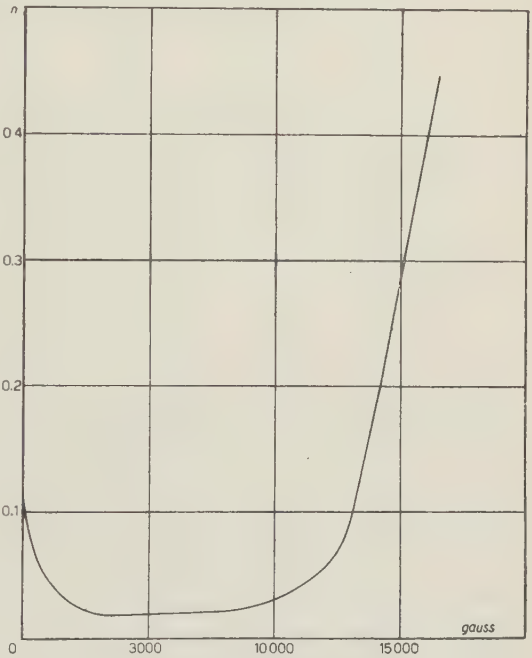

Fig. 4.

3·3. *Entrefer d'amortissement d'épaisseur constante.* – Le trait qui fait l'originalité de l'aimant du Synchrotron de Saclay est sans doute l'entrefer d'amortissement suggéré par M. Ricateau [8]. Cet entrefer supplémentaire, situé entre la culasse et chaque pièce polaire (Fig. 6) doit aisément permettre de réduire l'erreur δn sur l'indice du champ à une valeur $\delta n'$ plus faible d'un ordre de grandeur.

La théorie de cette idée a reçu quelques compléments par la suite et a fait l'objet de quelques premières mesures sur modèle [9].

Cependant l'exposé ci-dessous ne fait pas allusion aux mesures et les formules et courbes données sont purement théoriques.

On admet facilement l'action de cet entrefer dans l'analogie entre les relations fondamentales:

$$\boldsymbol{H} = \text{grad } P = \mu \boldsymbol{B}$$

$$\text{div } \boldsymbol{B} = 0$$

---

[7] *Rev. Scient. Instr.*, **24** (1953), p. 752, fig. 12 et p. 773, fig. 1.

[8] M. Ricateau: *Perturbations magnétiques dues au rémanent, perturbations magnétiques aux inductions élevées, Note CEA*, n. 72, Juin 1954.

[9] H. Bruck: *Sur l'aimant du Synchrotron*, note *CEA* à paraître.

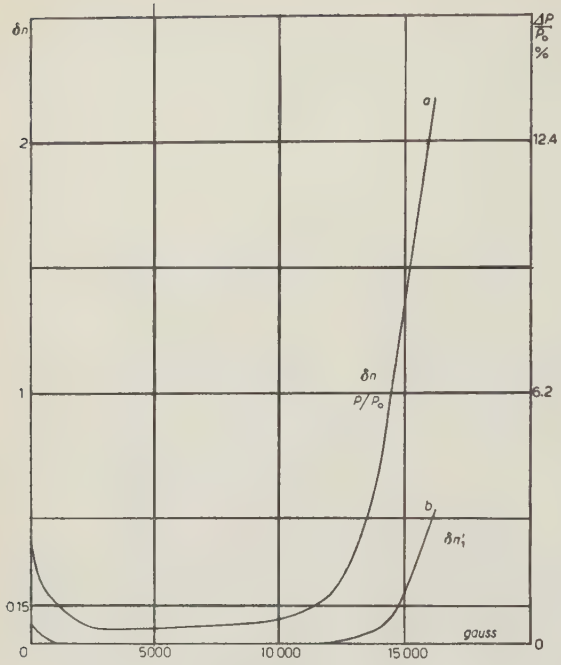

Fig. 5.

du magnétisme et les relations

$$\text{grad } P_e = cj$$

$$\text{div } j = 0 ,$$

régissant les répartitions de courant électrique dans un milieu de conductibilité spécifique c, fonction du lieu. Dans le langage de cette analogie, la pièce polaire est un bon conducteur (μ grand) comparé à l'entrefer d'amortissement.

Par conséquent (voir Fig. 6), sur un trajet $AA'B'B$, traversant d'abord l'entrefer, cheminant ensuite radialement dans la pièce polaire et retraversant encore une fois l'entrefer, la différence de potentiel ΔP s'épuise essentiellement dans les deux traversées de l'entrefer. La fraction $\Delta P_1'$ de différence de potentiel subsistant entre les extrémités $A'B'$ de la pièce polaire sera donc très petite.

On établit aisément les relations approximatives:

(4) $$\Delta P_1' = \frac{\Delta P}{1+K} \quad \text{respectivement} \quad \delta n_1' = \frac{\delta n}{1+K} \cdots ,$$

le nombre

$$K = \frac{8\mu_p h_f h_p}{\Delta r^2} = \frac{R_f}{R_p}$$

étant un'expression approximative pour le rapport de la réluctance R_f de la double traversée de la fente à R_p, réluctance du trajet dans la pièce polaire, et

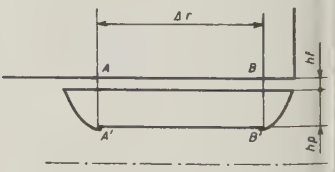

Fig. 6

μ_p la perméabilité magnétique de la pièce polaire,

h_f l'hauteur de l'entrefer d'amortissement,

h_p l'hauteur de la pièce polaire,

et $\Delta r = \overline{A'B'}$ (cf. Fig. 6).

Sur la Fig. 5, la courbe pour $\delta n_1'$ est représentée à côté de celle pour δn. La courbe pour $\delta n_1'$ a été calculée pour $h_f = 6$ mm, $h_p = 105$ mm, $\Delta r = 524$ mm.

Aux inductions élevées auxquelles l'effet atténuateur de l'entrefer est le plus nécessaire, l'efficacité du principe baisse rapidement à cause de la baisse rapide simultanée de la perméabilité μ_p de la pièce polaire.

3·4. *Entrefer d'amortissement d'épaisseur non constante.* – Il est possible de remédier quelque peu à cette situation en inclinant la face arrière de la pièce polaire par rapport à la face limite de la culasse. Une inclinaison d'un angle α fera varier linéairement en fonction de r l'épaisseur h_f de la fente (cf. Fig. 7).

On admet l'action d'une telle inclinaison de la manière suivante:

Supposons d'abord $\Delta P = 0$, entre A et B; la chute radiale de potentiel dans la pièce polaire sera en tout cas également petite par rapport à celle à travers l'entrefer d'amortissement. Ainsi les deux faces limites de l'entrefer d'amortissement peuvent être comparées aux faces — chacune equipotentielle — d'un condensateur à plaques planes mais non parallèles, à l'intérieur duquel le champ est donc non uniforme et en particulier plus fort du côté de l'écartement minimum des plaques. Dans la pièce polaire, le flux venant de la culasse est donc non uniformément réparti, tandis que le flux ressortant de la pièce polaire du côté de l'entrefer principal est pratiquement uniforme. A l'intérieur de la pièce polaire s'opère le réarrangement des lignes de flux, ce qui implique l'existence d'une composante radiale du champ, c'est-à-dire d'un gradient du potentiel.

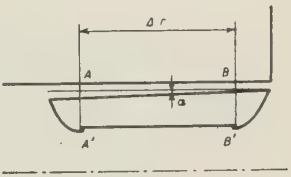

Fig. 7.

On est maître de la valeur et du signe de cette composante radiale, par le choix de la valeur et du signe de l'inclinaison α.

On trouve aisément une expression analytique approximative pour la chute radiale de potentiel dans la pièce polaire due à l'inclinaison α en supposant $\Delta P = 0$:

$$(6)\qquad \begin{cases} \Delta P_2' = -\dfrac{\Delta r \cdot H_0' \alpha}{1 + K}, \\ \delta n_2' = \dfrac{\Delta P_2' r_0}{P_0 \Delta r}. \end{cases}$$

H_0' est le champ magnétique moyen dans l'entrefer d'amortissement. Dans le cas général ($\Delta P \neq 0$; $\alpha \neq 0$) on a entre les points A' et B' la différence

de potentiel

$$(7)\qquad \begin{cases} \Delta P' = \dfrac{\Delta P - \Delta r H'_0 \alpha}{1 + K}, \\ \delta n' = \dfrac{1}{P_0} \dfrac{r_0}{\Delta r_0} \dfrac{\Delta P - \Delta r H'_0 \alpha}{1 + K}. \end{cases}$$

On peut choisir l'angle α de sorte que $\delta n' = 0$ pour l'induction maximum envisagée. Ce cas est représenté sur la Fig. 8 pour une induction maximum de $(B_0)_{max} = 14\,000$ gauss dans l'entrefer. Dans ce cas, comme la figure le montre, il y a surcompensation aux inductions moyennes; mais l'entrefer d'amortissement joue aisément son rôle d'atténuateur à ces valeurs d'induction moyenne pour lesquelles μ_p est élevé.

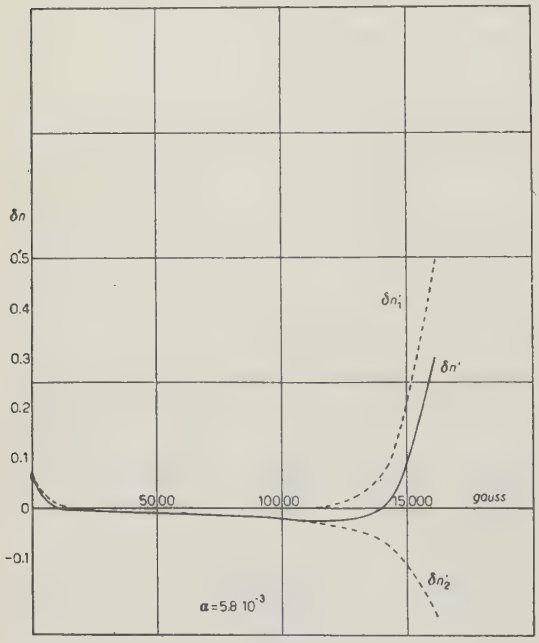

Fig. 8.

La conditions $\delta n' = 0$ ou $\Delta P = \Delta r H'_0 \alpha$ signifie que la différence de potentiel ΔP existant entre les extrémités radiales de la surface limite de la culasse est exactement absorbée par la surépaisseur $h_f(A) - h_f(B) = \Delta r \cdot \alpha$ de la fente; le chemin magnétique supplémentaire que représente cette surépaisseur compense exactement l'inégalité des chemins magnétiques de la culasse.

3·5. *Anneau de garde aux extrémités des pièces polaires.* – Cependant, pour que la face de la pièce polaire côté entrefer principal soit réellement équipotentielle, il faut encore considérer le flux de fuites venant du plan médian et qui pénètre radialement de part et d'autre dans les extrémités de la pièce polaire. Pour ce flux, l'entrefer d'amortissement joue un rôle néfaste, c'est-àdire le même que précédemment mais en sens inverse: la réluctance de la pièce polaire étant faible, comparée à celle de l'entrefer d'amortissement, les variations de potentiel provoquées par ce flux dans la pièce polaire seront également faibles, comparées à celles à travers l'entrefer. Le flux pénétrant radialement dans la pièce polaire ressortira dans l'entrefer d'amortissement uni-

formément réparti sur toute la largeur Δr de ce dernier. Le réarrangement de ces lignes de flux à l'intérieur de la pièce polaire implique à nouveau de fortes composantes radiales dirigées vers le centre de part et d'autre en tous points de la pièce polaire.

Pour parer à cette sensibilité accrue de la pièce polaire au flux de fuites radial, on est conduit:

1) à donner aux pièces polaires un profil en forme de bateau afin de réfracter les lignes du flux de fuites à l'intérieur de la pièce polaire vers la verticale;

2) à séparer les extrémités radiales des pièces polaires de la zone centrale par une fente verticale; les extrémités ainsi séparées joueront un rôle d'anneaux de garde par rapport à la partie centrale.

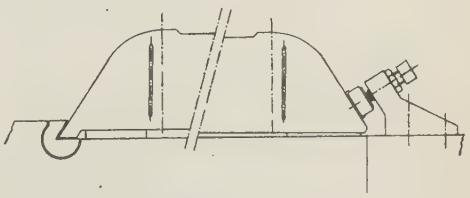

Fig. 9.

La Fig. 9, en reproduisant à une échelle plus grande que sur la Fig. 1 les extrémités radiales d'une pièce polaire, fait mieux ressortir la forme en bateau des extrémités, les fentes de séparation verticales, ainsi que la technique envisagée d'accrochage des pièces polaires à la culasse.

* * *

Les conceptions développées ci-dessus garantiront probablement dans les limites indiquées de tolérance, l'invariance de la carte du champ entre 340 gauss et 14000 gauss, c'est-à-dire du début jusqu'à la fin du cycle. Elles rendront, de ce fait, probablement ([10]) inutile l'emploi d'enroulements correcteurs.

Nous insistons cependant sur le fait qu'il ne s'agit, en ce moment, que d'un projet théorique dont la vérification expérimentale n'est pas encore entièrement achevée, tant en ce qui concerne les principes que les solutions technologiques de réalisation envisagées.

4. – Bâtiment destiné au synchorotron.

Nous avons cru pouvoir dégager de l'expérience acquise ailleurs un certain nombre de conditions qu'il serait bon d'introduire dans le projet d'un bâtiment:

1) construire sur un seul plan, ce qui simplifie la protection et, partant, l'expérimentation;

([10]) Il convient de formuler des réserves, en particulier sur une influence éventuelle en début de cycle, des courants de Foucault se produisant dans les parois de la chambre.

2) dégager la machine pour l'utiliser sur le maximum de sa périphérie et prévoir au départ des zones d'extension de l'expérimentation;

3) dégager pour l'expérimentation l'aire comprise à l'intérieur de l'aimant;

4) les moyens de levage doivent desservir à la fois la machine et la zone expérimentale.

La disposition du projet de Saclay telle qu'elle est répresentée par la Fig. 10 s'inspiré de ces conditions.

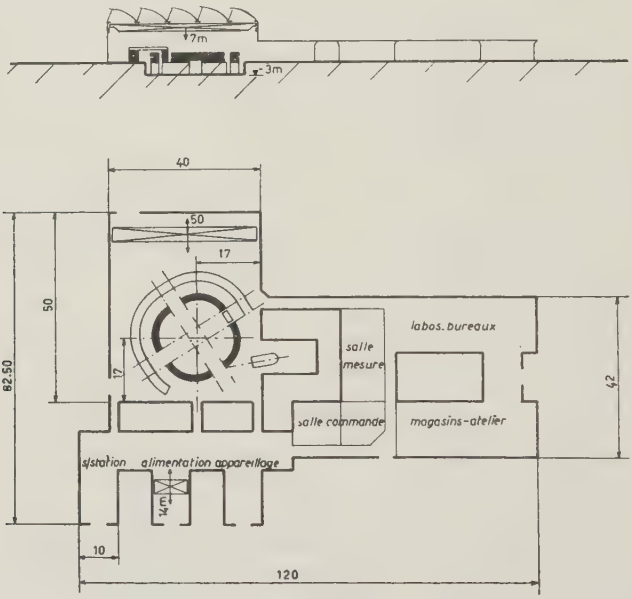

Fig. 10.

5. – Délais et moyens d'exécution du projet.

5'1. *Délais.* – Le choix du type de machine a été arrêté au cours du mois de Mai 1954. Les grandes lignes de l'ordonnancement de la réalisation sont les suivantes.

— Au cours du deuxième semestre de 1954, les études de réalisation sont entreprises.

— Au cours de 1955, l'aimant, son alimentation et l'injecteur sont lancés en fabrication. La construction des fondations de l'aimant et du bâtiment est commencée.

— Au cours du premier semestre de 1956, les blocs constituant l'aimant arrivent de fabrication et sont soumis à des contrôles magnétiques individuels. La chambre et le pompage sont lancés en fabrication.

— Au cours du deuxième semestre, le montage de l'aimant est commencé. La Haute Fréquence est lancée en fabrication.

— Au cours du premier semestre de 1957, le montage de l'aimant est terminé, son alimentation est mise en place et les essais magnétiques commencent. La chambre et le pompage sont achevés de fabrication et l'injecteur installé.

— Au cours du deuxième semestre de 1957, la chambre est mise en place avec le pompage et les essais avec faisceau commencent.

— La première étape de 1.75 GeV doit être atteinte au début de 1958.

5·2. *Moyens.* – Le personnel du Service des Accélérateurs, auquel l'exécution de ce programme a été confié, se décompose de la manière suivante:

Physiciens et ingénieurs, dont 4 ingénieurs mécaniciens et 7 ingénieurs électroniciens . .	22
Agents techniques	21
Dessinateurs	7
Ouvriers mécaniciens	15
Total	65

Ce chiffre doit être porté progressivement à 80 ou 90 personnes, mais les effectifs définitifs dépendront essentiellement de l'apport industriel plus ou moin important, tant pour les études que pour la réalisation.

SUPPLEMENTO AL VOLUME II, SERIE X
DEL NUOVO CIMENTO

N. 1, 1955
2° Semestre

The Italian Design of a 1000 MeV Electronsynchrotron: a Comparison between the Strong and the Weak Focusing.

G. SALVINI

Istituto di Fisica dell'Università - Pisa

1. – The Choice of the Injector.

Once the final energy is established, one of the most important decisions which has to be taken in the design of an electrosynchrotron is the choice of the injector; in fact not only the entire design will heavily depend upon the quality of the injector, but also some basic decisions, for instance the choice between weak and strong focusing, will depend on the injector.

This sentence may seem too extreme to him who considers the problem of the design of an electronsynchrotron with the same spirit of the old days (1946), when the injector was an almost isotropic furnace of low energy electrons (1), but the opinion will change when one considers the high energy injectors of today, which pour in the magnet a well-collimated beam of relativistic electrons through an inflector of high precision in the large space of one of the straight sections.

Let's try to demonstrate this statement considering three of the main characteristics of an injector (we will limit us to the electronsynchrotrons, but of course, some of the considerations apply to the machines for protons too). These characteristics are: the energy, the momentum spread and the geometrical dimensions of the injected beam.

Let's start with the energy of the injected beam: a high energy is generally to be preferred. With an injector of high energy we will inject at a higher induction field of the magnet. This will lessen the fondamental difficulty of controlling and shaping the induction field near the injection, because of the reduced percent effect of the remanence and the eddy currents at injection.

---

(1) CORNELL UNIVERSITY: *Synchrotron progress Report* (1949).

As we know, the injection at low fields—for instance 20 gauss—is a much greater difficulty in the electronsynchrotrons than in the protonsynchrotrons, where the injection field easily is 5-10 times higher due to the heavier mass of the proton.

Another advantage of the high injection energy is the reduced effect of the scattering in the residual gas inside the donut: the growth of the betatron oscillations induced by this scattering will be smaller than at low energies, with the behavior that we will consider in the following.

All these arguments indicate that the dimensions of the gap of the magnet may be smaller when the injection energy is higher. This assumption, which we will try to define more quantitatively later, is certainly right.

Another important advantage of the injection at high energy is the fact that the construction of the radiofrequency system may become easier: in fact, if we inject electrons of an energy of a few MeV ($2 \div 4$ MeV total energy) the velocity of the electrons differs from the velocity of the light by $3 \div 1$ percent and therefore we may not even need the frequency modulation: the instantaneous equilibrium orbit will remain inside the donut also if a constant value of the radiofrequency is assumed. For instance we remember that the 550 MeV electronsynchrotron of Cal. Tech., which has a very large gap, accelerates electrons injected from a pulse transformer of 1 million volt, and does not use frequency modulation. Electronsynchrotrons of a more economic structure could avoid frequency modulation only with electrons of a kinetic energy of at least 3 MeV.

The second quality of the injector that we are going to consider is the momentum spread of the electrons; a quantity which we may for instance define as the momentum interval inside which half the electrons emerging from the inflector are contained.

Let's indicate with Δp this quantity and with $\Delta p/p_0$ the percent spread around the nominal value p_0.

A magnet with weak focusing will generally [admit] only a small value of Δp, in the sense that all the electrons differing from p_0 for more than say $\pm 1\,\%$ will be lost against the walls. A strong focusing machine, on the contrary, has an higher momentum admittance, for instance by a factor 10. Therefore the choice of the type of focusing in the magnet may depend on the quantity $\Delta p/p_0$, characteristic of the injector.

The third important quality of the injector, is the geometrical dimension of the electron beam.

The dimensions of the beam (diameter and angular spread) are of great importance for the value of this efficiency: by improving the geometry of the injected beam, we may have the same final intensity of high energy electrons with a gap of the magnet which is considerably smaller.

2. – Types of Injectors

So, we begin to see that the ideal injector is a machine giving electrons of the highest energy (compatible with the inflecting system) and the minimum momentum spread, with a beam of a very high geometrical definition. Let's give a glance to what the market or the laboratory offer, keeping in mind that only after this inspection we will decide on the characteristics of the magnet.

In Table I we give a list of the injectors which may be taken in consideration

TABLE I.

Type of injector	Admittance	$\Delta p/p_0$	Max. Energy	Electrons/pulse
Van de Graaf . . .	$10^{-3} \div 10^{-4}$	$10^{-2} \div 10^{-3}$	~ 3 MeV	$10^{11} \div 10^{12}$
Cockcroft-Walton . .	$10^{-3} \div 10^{-4}$	$10^{-2} \div 10^{-3}$	~ 2 MeV	$(3 \div 5) \cdot 10^{12}$
Linear Accelerator [3]	$10^{-3} \div 10^{-4}$	$(3 \div 5) \cdot 10^{-2}$	~ 8 MeV	$10^{12} \div 10^{13}$
Pulse transformer . .	$10^{-3} \div 10^{-4}$	—	~ 1 MeV	$\sim 10^{12}$
Microtron	10^{-3} (?)	—	~ 6 MeV	$\sim 10^{11}$

for our purpose, with some of their characteristics. The numbers given in Table I may only constitute a rough indication of the possibility of these injectors, which should be discussed one by one.

With the quantity « admittance » we mean the value of the product: diameter of the beam times its angular spread at the exit from the inflector. This number does not give much more than an order of magnitude.

3. – Comparison between the Strong Focusing (Alternate Gradient) and the weak Focusing (Constant Gradient).

a) At this point, we have to go from the general to the specific: I do not think it is possible to give general rules for the choice of the injector, or for the choice of the magnet, and it is perhaps better for you if I present here the results we reached until now in the comparative study of two different designs, one of an e.s. of 1000 MeV maximum energy, employing weak focusing the other of an e.s. of the same energy but with strong focusing.

These results are those obtained from the Italian group (Sezione Acceleratore) working at the construction of a nuclear machine.

The program of the Sezione Acceleratore is to build an electronsynchrotron of 1000 MeV for the benefit of all the Italian Universities interested in nuclear physics and in quantum electrodynamics. The project is supported by the Istituto Nazionale di Fisica Nucleare. Therefore I am reporting here the re-

sults which were obtained with the contribution of all the members of our group.

Recent years are rather critical, for taking decisions on the design of an electronsynchroton of $0.8 \div 1.5$ GeV, and this mainly arises from the alternative in the choice between the strong focusing and the weak focusing solution for the magnet.

In order to make our decision as responsible as possible, we are calculating two designs: one electronsynchrotron with alternate gradient focusing (strong focusing) and one with constant gradient (weak focusing). This lecture is an invitation to you, and particularly to the French group who had to resolve a similar problem in the design of their protonsynchrotron of 2 GeV, to discuss the choice.

The two designs are not complete yet, and we will speak of them with this in mind. They have in common some basic dimensions which are the following:

the radius	~ 3.50 metres
the field at maximum . .	10 000 gauss
the injection energy . . .	2.5 MeV, total
the type of injector . . .	Cockcroft-Walton
the R.F. system	two resonant cavities.

In § 6 we give the exact data for the two designs; all the numerical calculations in the following were developed starting with the data of § 6.

The main problem is to obtain the intensity of the 1000 MeV electrons versus the cost, or better versus a certain nominal cost which takes into account also the time which the realization of the machine will require. Therefore we have to resolve the question of the dimensions of the gap in the two cases.

These dimensions depend as we already said on the choice of the injector, and we wish to justify our choice of a Cockcroft-Walton before all. The choice of the injector was made by prof. AGENO of the Istituto Superiore di Sanita, who will direct the construction with the help of the other members of his laboratory.

b) Looking again at Table I, we consider that the Cockcroft-Walton injector is more convenient thak the Van de Graaf and the pulse transformer. In fact, in comparison with the pulse transformer, the C.W. can give more intensity, for it has an higher capacitance (for instance ~ 1000 cm against ~ 100 cm), in pulsed operation. In comparison with the pulse transformer the C.W. can reach an higher energy, for the pulse transformer was never

operated at more than 1 MeV, as far as we know, and a pulse transformer of two MeV or so would probably be a difficult and large machine: the injector of the Cal. Tech. electronsynchrotron is a pulse transformer and reaches 1 MeV kinetic energy.

On the contrary, as we see from Table I, the C.W. is as good as the two others in respect of the admittance, and the $\Delta p/p_0$ value.

And now we ask, why not a linear accelerator or a microtron? Linear accelerators are better for intensity and maximum energy, so that we could even hope to avoid frequency modulation. But linear accelerators [2] have a large $\Delta p\ p_0$ value and this is certainly bad, at least with the weak focusing. Moreover, we have to rememebr that the use of an injection energy much higher than 2 MeV kinetic would make the problem of the inflector very hard: we should probably give up the usual electrostatic inflectors and study some new type employing magnetic fields. Another fact in favour of the C.W. is this: the Istituto di Sanità has a long experience with C.W. accelerators, while we never built in Italy a linear accelerator. Of course we could buy a l.a. in England [3], where they are commercially constructed, but we consider it to be of advantage to have a many years experience on the injector.

Going now to the microtron, we have to admit that we considered the microtron inconvenient for admittance and intensity, but we recently learnt that the swedish group [4] is planning to use the microtron as an injector in their strong focusing 1000 MeV electronsynchrotron, and we will try to know more on this machine.

With these points fixed, let's go back to the question of the dimensions of the gap, and therefore of the magnet, in the two cases of the strong focusing (alternate gradient, A.G.) and the weak focusing (constant gradient (C.G.).

c) Case of the alternate gradient (A.G.). The minimum gap dimensions for a 1000 MeV A.G. machine are, as it was already pointed out by doctor Bruck of Saclay in his lecture, hard to estimate we are mainly limited by pure mechanical precision and by the physical dimensions of the other pieces of the equipment: otherway the theoretical trend would be just to make n very large, and the gap as small as possible.

The question may be put in the following way. In order to have a linear induction field in the gap we have to make a gap with pole profiles which are in first approximation sections of an hyperbola; then the equipotentials have

---

[2] *Annual Review of Nuclear Science*, **1**, 199 e segg. (1952), M. Chodrow: *Rev Sci. Instr.*, **26**, 134 (1955).

[3] Two English factories are building l.a. of $3 \div 8$ MeV. The following considerations particularly refer to these types.

[4] Private communication.

to obey a law of the type (see Fig. 1)

$$A(x_0 \mp x)z = \text{constant} \equiv K\,, \tag{1}$$

where z is the vertical coordinate, x is the coordinate along the axis.

The pole profiles of the magnet will be described by this curve, with the sign — and + alternately. The central orbit of the electrons is perpendicular the the plan of Fig. 1, in the point $X = Z = 0$.

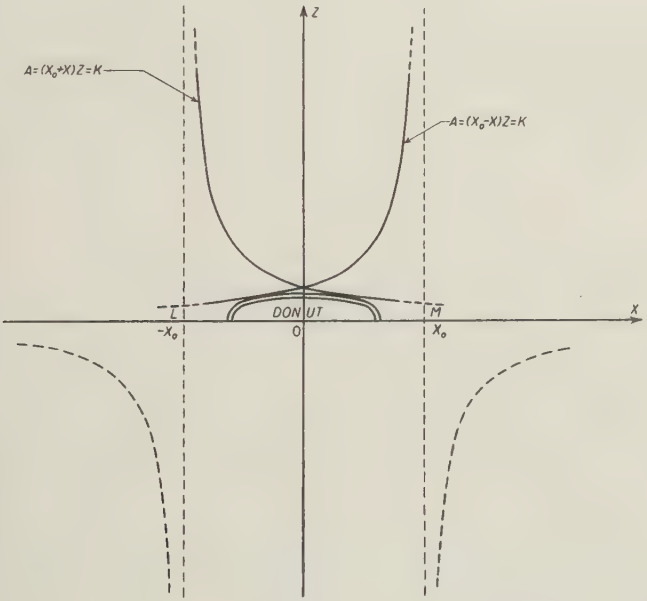

Fig. 1.

The value of the constant K determines the dimensions and the shape of the gap, and $\pm x$ is the distance of the vertical asymptots of the hyperbolae from the origin,

The component B_z of the magnetic induction is given by

$$B_z = \frac{\partial}{\partial z} A(x_0 \mp x)z = A(x_0 \mp x) \tag{2}$$

and this is evidently a field linear in respect of x.

On the other side, we can say that in an alternate gradient machine we need a field of the type

$$B_z = B_z^0\left(1 \mp \frac{nx}{R}\right), \tag{3}$$

where n is the field index, and R is the radius of the machine. By comparison between (2) and (3) we have:

$$B_z^0 = Ax_0, \quad n = \frac{R}{x^0}. \tag{4}$$

This means that if the radius R, which in both our projects is ~ 3.50 metres, is kept constant, the n value determines, at least to a certain extent, the dimensions of the donut. In fact in the conventional design of an alternative gradient magnet the useful region of the donut (see Fig. 1) will have a horizontal dimension not larger than the distance l between the asymptotes (length of the segment LM of Fig. 1) with the relation:

$$l = 2x_0 = \frac{2R}{n}.$$

In order to have a small gap, and therefore a small magnet, we have to increase for a given R the n value of the field.

Then we have to balance between two contrasting exigencies. On one side, if we want to take all the advantages of the strong focusing over the weak focusing solution we have to choose a high n value; on the other hand we cannot reduce the dimensions of the gap below certain values, which are imposed by other exigencies (dimension of the beam at the injection, dimension of the inflector, space for an useful spiralization etc.), and we cannot choose too high an n value, otherway the requirements on the mechanical precision of the parts of the magnet and on the precision in the measurement of the magnetic field become very hard or impossible to be fulfilled.

If we make reasonable assumptions of all these quantities, we conclude that in an A.G. e.s. with $R \cong 3.50$ metres n has to be chosen in the region of the tens (for instance $n = 15 \div 50$) rather than in the region of the hundreds. As you know, n is of the order of $200 \div 400$ in the case of the giant proton-synchrotrons with a radius of $50 \div 100$ metres.

In our design of the alternate gradient magnet we take $n = 21$. The main reason for this choice is that the new e.s. of the University of Cornell which is now going in operation has this value, and so we will have an opportunity of comparing our theoretical previsions with the experimental results.

d) Case of a constant gradient machine. – The choice of n is in this case simpler, for n has to be in the limits $0 < n < 1$ and you cannot expect large advantages from a particular choice: the betatron oscillations will have frequencies proportional to $n^{\frac{1}{2}}$ (vertical oscillations) and to $(1 - n)^{\frac{1}{2}}$ (horizontal oscillations) and you cannot hope to reduce one mode of oscillation if you don't enlarge the other.

The dimensions of the gap will then depend from the rather standard procedure of calculating the injection mechanism, the gas scattering, the radio frequency capture and so on.

4. – The Mechanism of Injection and Acceleration. Some General Remarks.

In the following part of this lecture we will compare the theoretical results of our two designs, the alternate gradient and the constant gradient. This comparison is not complete yet, and other calculations are in progress. The results come from the work of Prcfessor PERSICO and his theoretical group (doctors CARLO BERNARDINI, SONA and TURRIN).

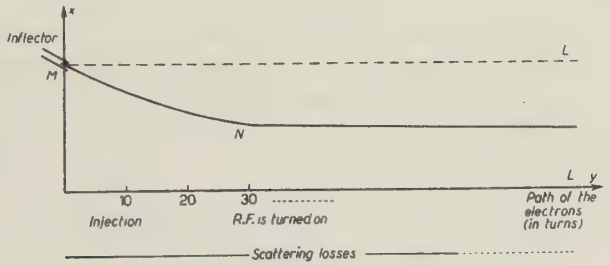

Fig. 2.

a) *We will outline the general procedure, before giving the numerical results.* – The electrons are injected in one of the four straight sections of the donut through the electrostatic inflector I (see Fig. 2). In Fig. 2 we represent the rectified path of the electrons, so that the abscissa gives the path of the electrons, and the distance between the two straight lines L and L' is the horizontal dimension of the donut. The sketch of Fig. 2, of course, is not at all in scale.

The beam emerging from the inflector will have certain geometrical dimensions (angle θ_0, width A) and a certain spread in momentum $\Delta p/p_0$. This is an electronsynchrotron, and we have to inject for many turns: in fact the period of revolution is of the order of 0.1 μs, which is a very short time, while an injection of $1 \div 2$ μs is what appears more convenient for us. There is therefore the problem of spiralizing the electrons inside the donut in such a way that we obtain the maximum efficiency.

The injection efficiency is something which we may define as the ratio between the number of electrons circulating inside the donut after the injection, until the R.F. is turned on, and the number of electrons which were injected. This efficiency (which we indicate with Q) is a function of many para-

meters:

$$Q = Q\left(\theta, \Delta p, A, \frac{\mathrm{d}B_z}{\mathrm{d}t}, n, \ldots\right),$$

which we have already defined.

If we disregard the possible inhomogeneities of the magnetic field, the simplest path of the electrons during the injection is a linear spiral in the case of the weak focusing (this path is represented with the line MN in Fig. 2), but it is a more complicated spiral curve in the alternate gradient case, due to the complicated nature of the instantaneous equilibrium orbits.

In the real case, the electrons will make betatron oscillations around the spiral orbit, with the behaviour which has been studied and exposed in his lecture by professor PERSICO.

Toward the end of the injection, at the proper moment, we will turn on the R.F. Of course, only a fraction of the electrons will be in the right phase relation with the R.F. system: we have therefore to define a F.R. capture efficiency, which we indicate by S. The function S is, directly or not, a function of the same variables than before, plus the rate of rise $\mathrm{d}V/\mathrm{d}t$ of the voltage of the R.F. at least:

$$S = S\left(\theta_0, \Delta p, A, \frac{\mathrm{d}B_z}{\mathrm{d}t}, n, \frac{\mathrm{d}V}{\mathrm{d}t}, \ldots\right).$$

The scattering of the electrons by the residual gas in the donut is important from the very beginning, up to an energy which more or less is three times the injection energy. This scattering will certainly produce a loss of electrons. We may indicate the efficiency for scattering in the gas with ϱ: this efficiency (probability that an electron survives the death for scattering from the residual gas on the walls of the donut) will be a function of many parameters: in particular it will depend on the mechanism and momentum p of injection, on the velocity of rise of the magnetic field, on the residual pressure P in the donut:

$$\varrho = \varrho\left(p, \frac{\mathrm{d}B_z}{\mathrm{d}t}, P, \ldots\right).$$

We remember that the value of $\mathrm{d}B_z/\mathrm{d}t$ at the injection is

$$\left(\frac{\mathrm{d}B_z}{\mathrm{d}t}\right)_{\mathrm{in}} = \frac{n\sigma}{RT_0}\,(B_z)_{\mathrm{in}},$$

where σ is the radial distance between two successive turns of our spiral MN, $B_{z\mathrm{in}}$ is the field at injection, T_0 is the period of revolution of the electrons.

Q, S, ϱ, are the « efficiencies » that an electron has to pass before feeling reasonably safe. After these examinations it will not meet difficulties for quite a long time, until when the R.F. will switch from one cavity to the other (a problem which we did not completely resolve yet), and later when radiation losses and coherence phenomena become important.

With this history in mind, we will now sketch our results for our two designs, the one costant gradient, alternate gradient the other. We have to underline the preliminary character of these results.

The main characteristics of the two machines for which the numerical calculations were made are given in § 6.

5. – Results of our Numerical calculations for the Constant Gradient and for the Alternate Gradient Design.

a) *Estimate of* Q ([5]). – In the constant gradient case the efficiency Q was calculated with the following assumptions:

$$A = 0.8 \text{ cm}$$

$$\theta_0 = \pm 3 \cdot 10^{-3} \text{ rad}$$

$$\Delta p/p = \pm 10^{-2} \text{ (which means } \Delta p = 2 \cdot 10^{-2} p) .$$

In the calculation the inhomogeneities of the magnetic field were neglected. We indicate by I the electron current (number of electrons per second) from the injector, and we define the time of injection Δt:

$$\Delta t = \frac{T_0 a}{2\sigma},$$

where a is the horizontal width of the donut which may be considered at disposal for the injection; Δt is therefore the time which an electron spends to spiralize from the inflector to the center of the donut. T_0 and σ were already defined in § 4.

Then we have:

$$Q = \frac{\text{electrons iniected in the time } \Delta t, \text{ and who survived}}{\text{electrons injected in the time } \Delta t} \simeq 0.4 .$$

([5]) A. TURRIN: *Rapporto Teorico della Sezione acceleratore* n. 3.

As we see, the time Δt depends on σ and a. The best value of σ, considering the probability for the spiralizing electrons of missing the inflector, is of the order of a few millimetres. The efficiency goes down fast for $\Delta p/p > \pm 10^{-2}$.

In the alternate gradient case the problem of estimating Q is harder and not completely resolved. We will provisionally assume, with the same definitions as before and with the same numerical values of A, τ_0, $\Delta p/p$, that Q is still 0.4. But we have to consider that the time Δt is probably shorter for a is reduced by a factor of the order of 2, (see § **6**) and therefore the number of electrons circulating in the donut after the injection is smaller than in the C.G. case.

One important remark is that in the A.G. case Q remains about the same also for $\Delta p/p$ as large as $\pm 3 \cdot 10^{-2}$. Some type of injector which may be inconvenient for the C.G. focusing (for instance the linear accelerator) could be successfully employed in the A.G. magnets.

b) *Estimate of S.* – Calculations were performed in the two cases (Professor PERSICO, Doctor BERNARDINI (6)), when the R.F. is turned on instantly (ideal case), and when the R.F. is turned on « slowly », for instance in 1-2 μ s. The two cases do not differ too much.

With the assumption $\sigma = 0.2$ cm we have:

Weak focusing: $S = 0.15$

Strong focusing: $S = 0.1$

S (weak)/S (strong) $= 1.5$. .

c) *Estimate of* ϱ. – We give here our numerical results for the C.G. case as they were obtained by Doctors SONA and C. BERNARDINI (7):

$\sigma = 0.1$ mm	pressure $= 10^{-5}$ mm_{Hg}	$\varrho = 0.15$
$\sigma = 0.2$ mm	pressure $= 10^{-5}$ mm_{Hg}	$\varrho = 0.3$
$\sigma = 0.6$ mm	pressure $= 10^{-5}$ mm_{Hg}	$\varrho = 0.8$.

In the A.G. case the calculation is more difficult, for we cannot be sure that it only depends on the maximum amplitude of the betatron oscillations and not on their particular shape. On the basis of some qualitative arguments we consider it reasonable to assume the same values of ϱ than in the C.G. case. An argument in favour of the strong focusing in respect to ϱ is the fact that fi

(6) E. PERSICO: *Rapporto Teorico della S. A., n.* 4; E. PERSICO and C. BERNARDINI: *Rapporto Teorico della S. A.*, n. 12.

(7) C. BERNARDINI: *Rapporto Teorico della S. A.* n. 11; P. G. SONA: *Rapporto Teorico della S. A. P.T.*, V.

the same value of σ the value of $\mathrm{d}B_z/\mathrm{d}t$ is higher in the A.G. case, and ϱ obviously increases with $\mathrm{d}B_z/\mathrm{d}t$. On the other side we should not forget that the increased value of $\mathrm{d}B_z/\mathrm{d}t$ may constitute a difficulty in the A.G. case for the increased difficulty of controlling the shape of the magnetic field and the rate of change of the R.F..

d) Final comparison between C.G. and A.G. focusing. – At this point, a comparison of the efficiencies of the two designs may be made by estimating the quantity $Z = Q \times S \times \varrho$ in one case and the other. The ratio of the values of Z should give more or less the ratio of the final intensities (number of electrons of high energy per second) of the two machines, which we will indicate by T. More exactly, we have to consider the values of Δt in the two cases, and then the value of T is given by:

$$T = \frac{\text{C.G. intensity}}{\text{A.G. intensity}} = \frac{Z_{\text{C.G.}} \times (\Delta t)_{\text{C.G.}}}{Z_{\text{A.G.}} \times (\Delta t)_{\text{A.G.}}} \approx 3 .$$

Our results are summarized in Table II.

TABLE II. – *Comparison of the efficiency of our two designs.*

	Q	S	ϱ	$Z = Q \cdot S \cdot \varrho$	T
Weak focusing (C.G.) . .	0.4	0.15	0.3	0.018	3
Strong focusing (A.G.) . .	0.4	0.1	(0.3)	0.012	

If we strictly stick to these results, we should conclude that our weak focusing machine promises three times more electrons than the strong focusing. But considering the present uncertainties of our calculations, expecially in the A.G. case, and remembering that a factor 3 in the final intensity is not very significant in a nuclear machine, I prefer to say that the final intensities in the two cases are not significantly different.

6. – Some Other Numerical Results.

We will briefly report in the following some theoretical results which were of importance in the calculation of the quantities Z and T.

a) Betatron oscillations in weak focusing and strong focusing. – We will give here as an example the results in one particular case [8].

---

[8] A. TURRIN: *Rapporto Teorico della S. A.*, n. 14.

Let's define:

x, the horizontal distance of the electrons from the axis of the donut;

$\mathrm{d}x/\mathrm{d}s = \alpha$, the angle between the tangent of the trajectory of the electron and the axis of the donut (s is the coordinate along the axis of the donut);

M, the maximum value assumed by x (maximum displacement from the axis).

With these hypotheses we have, for an electron of initial conditions $x = 0$ and $\mathrm{d}x/\mathrm{d}s = \alpha$:

$$\text{constant gradient:} \left(\frac{M}{R}\right)_{x=0} = 1.67\alpha$$

$$\text{alternate gradient:} \left(\frac{M}{R}\right)_{x=0} = 1.3\alpha\,.$$

This is an indication that the amplitude of the betatron oscillations are not too different in the two cases, with a ratio $1.67/1.3 \approx 1.3$.

This result may surprise a little, but we have to consider the peculiar character of the strong focusing betatron oscillations, whose hyperbolic part strongly contributes to increase the maximum displacement M.

b) *Momentum spread.* – We give here the maximum displacement $X_{\max}$ from the axis for an electron injected along the axis ($x = 0$, $\mathrm{d}x/\mathrm{d}s = 0$) with a momentum $p = p_0 + \Delta p$, where p_0 is the momentum corresponding to the axis of the donut:

$$p_0 = eB_z R\,.$$

The ratio of the two values of $X_{\max}$ in the two cases, weak and strong focusing, is:

$$\frac{(X_{\max})_{\text{weak}}}{(X_{\max})_{\text{strong}}} \cong \frac{5R(\Delta p/p_0)}{0.5R(\Delta p/p_0)} = 10$$

for $\Delta p/p_0 = \pm 10^{-2}$.

From this ratio we may conclude that an injector with too large a $\Delta p/p_0$ value is more inconvenient to the weak focusing.

c) *Amplitude of the synchrotron oscillations.* – Doctor C. BERNARDINI calculated the ratio K between the synchrotron oscillation amplitudes in the C.G. and in the A.G. design, for electrons of the same energy and which were captured in the same phase in the two cases.

The results are:

$$K = \frac{X_{\max}\ (\text{strong})}{X_{\max}\ (\text{weak})} = 1.75 + 5.97\left(\frac{E_0}{E}\right)^2 + \ldots$$

E_0 is the rest energy of the electron, and E is the electron's total energy.

7. – The Basic Data of our Two Designs. Our R.F. System.

a) *Constant gradient* (*weak focusing*).

Injector:

Type	Cockcroft-Walton
Maximum voltage	$2 \cdot 10^6$ V
pulses/s	$\leqslant 50$/s
electrons/pulse	$\sim 5 \cdot 10^{12}$ (hope)
$\Delta p/p$	$10^{-2} \div 10^{-3}$

Pressurized with nitrogen and freon.

Magnet:

4 quadrants, with straigth sections of 100 cm;
$n = 0.6$
Excitation: resonant CL circuit with a bias of direct current;
Dimensions of the gap: 21×8 cm^2 ($\sim 16 \times 6$ useful);
injection field: 24.5 gauss;
maximum field: 10^4 gauss.

Radius of equilibrium orbit: 333 cm.
Maximum energy of the electrons: 1000 MeV.
R.F. system: two resonant cavities in 4th harmonic, with a final frequency of 48.1×10^6 Hz (see § 7-*c*).

b) *Alternate gradient* (*strong focusing*). – The data of our a.g. machine are, as we already said, very close to those of the e.s. which is under construction at the Cornell University. We are grateful to Prof. WILSON for his kind supply of data and informations.

Injector: the same than in the C.G. design.

Magnet:

4 quadrants, with straight Sections of 90 cm;
$n = 21$;
Excitation: resonant CL circuit with a bias of direct current;
Dimensions of the gap: $\sim 9 \times 4$ cm^2 (8×3 useful);
structure of the gradients: see Fig. 3;
injection field: 21.5 gauss;
maximum field: 10^4 gauss.

Radius of the equilibrium orbit: 381 cm.
Maximum energy: 1 000÷1 200 MeV;
R.F. System: the same than in the C.G. design.

c) *The R.F. system.* – The radiofrequency has been studied by Professor QUERCIA, who is responsible of all the electronics of the Sezione Acceleratore, and by Ing. PUGLISI, who specialized on the problems of the Radio Frequency. What here follows is a summary from their reports.

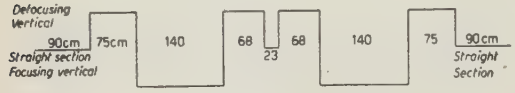

Fig. 3.

The frequency of revolution of the electrons, (which is of about 10 MHz at injection) increases of 2.1% as their energy increases from the injection energy (2.5 MeV total energy) to the final value of 1 GeV. In the present design the R.F. system employs two cylindrical resonant cavities which are located in two straigth sections. The first cavity drives the electrons from the energy of injection to about 10 MeV.

During this time the revolution frequency of the electrons increases by about 2.1%, and therefore the frequency of the electric field in the gap of the cavity has to increase by the same percent. The peak voltage of the cavity varies from about 3 to 7 kV.

The second cavity has to rise the energy of the electrons from ~ 10 MeV up to the final value. The peak voltage has to change during the process of acceleration from 7 kV to about 50 kV; this high value, as well known, is required to compensate for the radiation losses, which reach up to 27 kV at the maximum energy.

In Fig. 4 we give a block diagram of the apparati who feed and control the first cavity.

A pilot oscillator 4 guides the power amplifier 7 through the frequency multiplier 5 and the buffer amplifier 6. The power amplifier is directly connected to the cavity 19, which is the anodic resonant circuit of 7.

The frequency of the system, as we already said, has to change by $\sim 2.1\%$ and the rate of this change is a function of the energy of the electrons and therefore of the value $B_z(t)$ of the induction field at the equilibrium orbit. To control the frequency by the value $B_z(t)$, a coil is posed in the gap of the e.s.; the voltage induced in the coil is proportional to $\mathrm{d}B_z/\mathrm{d}t$; it is electronically integrated and this information goes to a function forming network 2 which controls the polarization current of an inductance with a ferroxcube nucleus. This inductance is a part of the circuit of the pilot oscillator 4, whose frequency is therefore controlled by the magnetic field in the gap and becomes a proper function of $B_z(t)$.

The precision required for this function is $\pm 1‰$.

The modulators 16 ad 20 perform the control in amplitude of the electric field of the cavity 19.

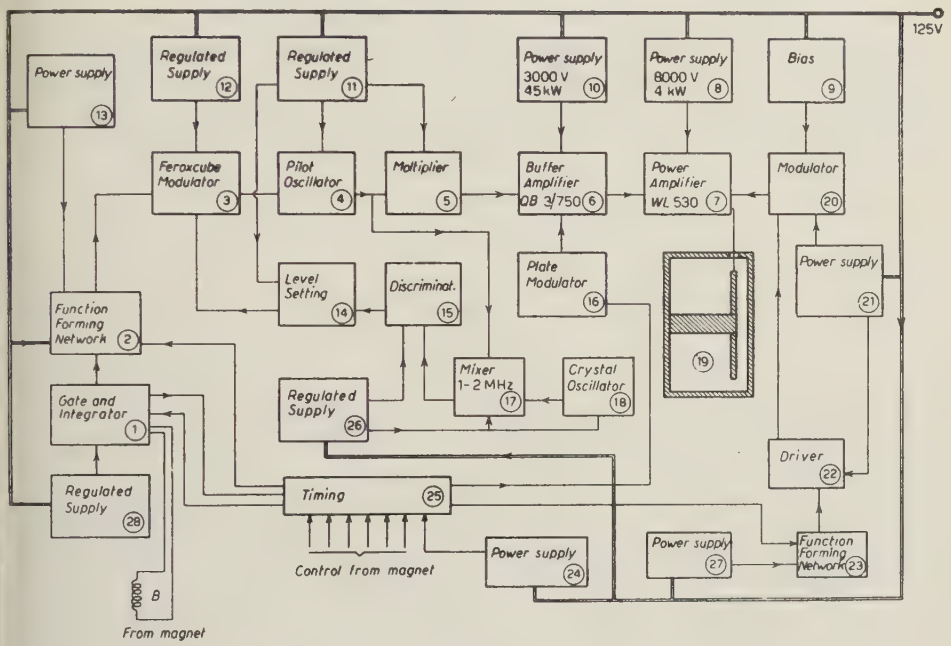

Fig. 4.

The R.F. system for the second cavity is not given in Fig. 3. This second cavity oscillates with a constant frequency, and the amplifiers feeding it are driven by the buffer amplifier 6.

8. – Conclusions.

From what we said we conclude that for an electronsynchrotron of about 1000 MeV a magnet employing strong focusing does not probably constitutes a definite advantage compared with the classical weak focusing design. On the contrary our numerical calculations for a comparison between the final intensities of two particular designs indicate the advantage of the Constant Gradient solution.

It certainly appears that in the C.G. case the problems connected with the injection of the electrons are more easy to resolve and understand, and probably we may have at disposal an injection time Δt larger than in the A.G. case.

To make our discussion more complete, we should compare the technical difficulties connected with the realization of the magnet in one case and the other: for instance the limits in the mechanical precision the tolerances on the magnetic properties of the iron etc. We will only observe that probably in our two designs these kind of difficulties are of the same order, may be with some advantage of the A.G. solution near the injection: in fact the distance Δn of the field value n_0 from the closest n values which lead to resonances is somewhat larger in the alternate gradient case.

SUPPLEMENTO AL VOLUME II, SERIE X
DEL NUOVO CIMENTO

N. 1, 1955
2° Semestre

A Theory of the Capture in a High Energy Injected Synchrotron.

E. PERSICO

Istituto di Fisica dell'Università - Roma

1. – Introduction.

In all synchrotrons for protons and in most of the modern electrosynchrotrons the particles are injected with a kinetic energy of the order of at least one MeV while the r.f. oscillating cavity is not yet excited, or is oscillating at a negligible amplitude. The particles accumulate in the donut, spiraling inwards because of the rising magnetic field, until the radio-frequency cavity starts oscillating, as suddenly as possible. At this instant, the particles that happen to be in a favourable phase are « captured » by the radio-frequency, and form one or more bunches that start being accelerated, while those that are caught in unfavourable phases are lost against the walls.

We will now expose an attempt to calculate the number of captured particles as a function of the radio-frequency peak voltage (and therefore of the initial equilibrium phase), of the width of the donut and other parameters of the machine. This calculation, although made under several simplifying assumptions, should give a criterium for choosing the initial equilibrium phases (for which we find an optimum value) and for evaluating the influence of the donut width on the output of the machine.

The simplifying assumptions are the following. We suppose that all the injected particles have the same energy and the same direction (parallel to the equilibrium orbit). The theory could be extended to the case of an injected beam having an energetic and angular spread by subdividing it in elementary beams.

We suppose also that the radio-frequency peak voltage across the cavity rises *istantaneously* from 0 to a given value U. By this we mean that the rise time should be short compared with the period T_ν of the phase oscillations *and* with $\sqrt{T_0\theta}$, where T_0 is the rotation period for the velocity c and θ is the duration of the injection.

When the rise of the radio-frequency voltage cannot be considered istantaneous, the theory needs a numerical integration of the phase equation for each set of parameters, which has been worked out only for a few typical cases. It seems that the results are not very different from those of the istantaneous rise, even for a rise time of T_r/h and of $4\sqrt{T_0\theta}$.

2. – Betatron Oscillations.

Let t be the time and

$$B(r, t) = B_0(t)(R/r)^n , \tag{1}$$

be the vertical magnetic induction at radius r. Here R is the radius of the so called « principal orbit » (running approximately in the middle of the donut section) and $B_0(t)$ is the magnetic induction on it: during the injection $B_0(t)$ can be considered a linear function.

The equilibrium orbit (e.o.) at time t is defined by

$$r_i = 3.335 \cdot 10^{-3} \frac{\beta E}{B(r_i, t)} = \tag{2}$$

(r_i in cm, B, B_0 in gauss)

$$= \left(3.335 \cdot 10^{-3} \frac{\beta E}{B_0 R^n}\right)^{1/(1-n)} \tag{2'}$$

where E is energy of the particles (included the rest energy) in eV, and β is the velocity divided by c. The e.o. contracts at each tour approximately by

$$\sigma = \frac{R}{1-n} \frac{\dot{B}_0}{B_0} T , \tag{3}$$

(T being the duration of the revolution).

We take as origin of time the instant at which the e.o. passes through the injection point: so at time t the e.o. will pass at a distance $\sigma t/T$ from that point.

We suppose that the radio-frequency cavity starts oscillating at the time θ at which $r_i = R$, and that during the interval from $t = 0$ to $t = \theta$ the injector keeps injecting at a constant rate of I particles per second. We consider this interval as the « injection interval »: probably some particles injected before $t = 0$ or after $t = \theta$ can still be captured but we neglect them. So the duration of the injection is

$$\theta = \frac{aT}{2\sigma} , \tag{4}$$

where $a/2$ is the distance of the injection point from the principal orbit (and therefore a is the useful donut width).

Of course, part of the particles injected between 0 and θ will be lost, before time θ, owing to collision against the injector or the walls. We introduce therefore a quantity $\varrho(t) \leqslant 1$, representing the « *instantaneous injection efficiency* », such that $I\varrho(t)\,\mathrm{d}t$ is the number of particles injected between t and $t + \mathrm{d}t$ still surviving at time θ. The calculation of ϱ does not belong to this paper. We can only say that, as a rule, it will increase from ε to almost 1 during the first few revolutions and then remain near unity for most of the time θ.

Now, a particle injected at time t will be injected at a distance

$$x_M = \frac{\sigma t}{T}, \tag{5}$$

from its e.o.: so it will start betatron oscillations of this amplitude about the e.o. These oscillations will continue, practically undamped, following the e.o. while it contracts, so that at time θ, when the radio-frequency is excited, the particle will oscillate about the principal orbit.

So, at time θ, all surviving particles will be oscillating, with various amplitudes, about the principal orbit. Those, which have an amplitude between x_M and $x_M + \mathrm{d}x_M$ will be those injected between t and $t+\mathrm{d}t$, and their number will be

$$I\varrho(t)\,\mathrm{d}t = I\varrho T \frac{\mathrm{d}x_M}{\sigma}. \tag{6}$$

3. – Synchrotron Oscillations.

As soon as the radio-frequency is excited, synchrotron oscillations are superimposed on betatron oscillations. This means that the e.o., about which the betatron oscillations take place, is no longer slowly contracting, but contracting and expanding alternately about the principal orbit. Besides, the e.o. is no longer the same for all particles because each particle, at each revolution, will pick up a different (positive or negative) amount of energy according the the *phase* φ in which it happens to cross the radio-frequency cavity.

Let us recall the law of synchrotron oscillations [1]. The phase φ varies according to the equation

$$\ddot{\varphi} = M\left(1 - \frac{U}{u}\sin\varphi\right), \tag{7}$$

---

[1] D. Bohm and L. Foldy: *Phys. Rev.*, **70**, 249 (1946).

where U is the peak value of the radio-frequency voltage across the cavity (in volt); u is the energy (in eV) which must be supplied at each revolution to the particle in order that it keeps the same radius R notwithstanding the rise of the magnetic field: it is given by

$$u = (1-n)\beta^2 E \frac{\sigma}{R}, \tag{8}$$

M is defined by

$$M = 2\pi \frac{kK}{T^2} \frac{u}{E} = 2\pi\beta^2(1-n) \frac{kK}{T^2} \frac{\sigma}{R}, \tag{9}$$

where

$$K = 1 + \frac{1}{\beta^2}\left[\frac{1}{A(1-n)} - 1\right]. \tag{10}$$

A is the total length of the principal orbit divided by the length of the curved parts; k is an integer (usually called the « harmonic order ») giving the ratio between the radio-frequency and the frequency of revolution.

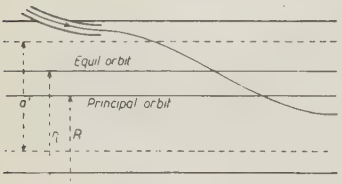

Fig. 1.

To the variations of the phase φ are related the oscillations of the e.o. through the relation

$$X = \frac{-R}{(1-n)\beta^2 K\omega_e}\dot{\varphi}, \tag{11}$$

where: $X = R_i - R$ is the displacement of the e.o.;
$\omega_e = k(2\pi/T)$ is the pulsation of the radio-frequency field.

During the injection, that is when $U = 0$, eq. (11) and (7) give, of course, the well known contraction of the e.o. at the rate σ/T.

After time θ, U has a constant positive value (greater than u). Equation (7) can be integrated once and gives

$$\dot{\varphi}^2 = 2MF(\varphi) + \text{const.}, \tag{12}$$

where

$$F(\varphi) = \frac{U}{u}\cos\varphi + \varphi. \tag{13}$$

If we define the « equilibrium phase » (or « synchronous » phase) φ_s by

$$\sin\varphi_s = u/U, \qquad 0 \leqslant \varphi_s \leqslant \pi/2 \tag{14}$$

equation (13) can be written

$$F(\varphi) = \frac{\cos\varphi}{\sin\varphi_s} + \varphi \,. \tag{13'}$$

The function $F(\varphi)$ is plotted in Fig. 2 [1].

It has obviously a maximum at $\varphi = \varphi_s$.

Equation (12) permits plotting $\dot{\varphi}$ (and therefore X) as a function of φ (Fig. 3). If we consider the « *synchronous particle* » running on the principal orbit at an angular velocity ω_e/k with the constant phase φ_s, and call $\theta_s(t)$ its azimut, we have

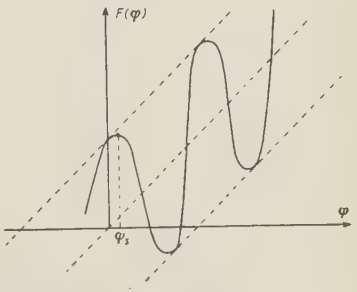

Fig. 2.

$$\theta - \theta_s = (\varphi - \varphi_s)/k \,,$$

(since $\dot{\varphi} = k\dot{\theta}$) and so the abscissa in Fig. 3 represents, in a convenient scale, the azimuth of a generical particle referred to that of the synchronous particle. On the other hand the ordinate, through equation (11), represents its radial displacement (apart from betatron oscillations). Therefore the curves of Fig. 3 represent the mouvement of any particle, apart from betatron oscillations, with respect to the synchronous particle.

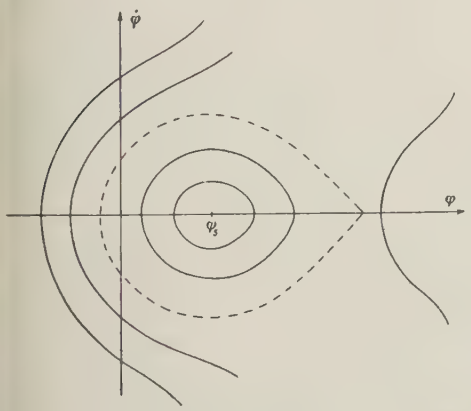

Fig. 3.

These curves fall into two classes, according to the value of the constant in eq. (12). Some of them are open curves, and represent particles that, sooner or later, collide with the walls and are lost. The remaining, and more interesting, curves, are closed, and represent particles oscillating around the synchronous particle.

Let us consider one of these closed curves. If we call φ_m and φ_M ($\varphi_m < \varphi_s < \varphi_M$) the extreme values of φ, we can assume one of these quantities, f.i. φ_M, as a parameter to label the curve. The other extreme, φ_m, is related to φ_M by a universal function

$$\varphi_m = g(\varphi_M, \varphi_s) \,,$$

defined by $F(\varphi_m) = F(\varphi_M)$, which has been numerically calculated for different

values of φ_s. The widest of all closed curves (dotted line in Fig. 3) corresponds to $\varphi_M = \pi - \varphi_s$.

Equation (12) can now be written

$$\dot{\varphi}^2 = 2M[F(\varphi) - F(\varphi_M)] . \tag{15}$$

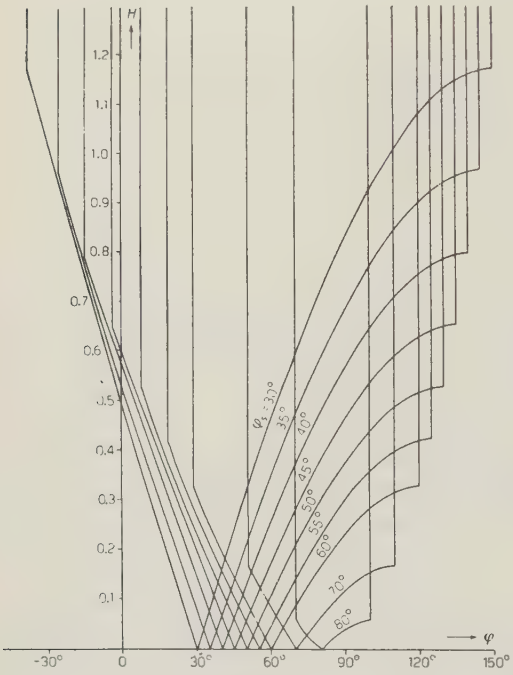

Fig. 4.

Now we are interested in the amplitude X_M of the synchrotron oscillation, and therefore (eq. (11)) in the maximum ordinate φ_M of the curve. It is seen immediately that it corresponds to $\varphi = \varphi_s$ and is given by

$$\dot{\varphi}_M = \sqrt{2M}\,\sqrt{F(\varphi_s) - F(\varphi_M)} .$$

We have plotted, in Fig. 4, the universal function

$$H(\varphi) = \sqrt{F(\varphi_s) - F(\varphi)} ,$$

for several values of φ_s. By means of these curves, we can immediately determine the amplitude X_M of the synchrotron oscillation as a function of one of the extremes (φ_m or φ_M) of the phase oscillation. In effect, from (11) and (15) we get

$$X_M = CH(\varphi_m) = CH(\varphi_M) , \tag{16}$$

where

$$C = \sqrt{\frac{\sigma R}{\pi k K (1-n)\beta^2}} . \tag{17}$$

4. – Theory of Capture.

Since the cavity starts oscillating at the instant θ at which $X = \dot{\varphi} = 0$ the initial conditions for the synchrotron oscillations are: $\dot{\varphi}_0 = 0$, and φ distributed with uniform probability [2] between $-\pi$ and π. This initi

[2] The phase of the particle at time θ is related to the instant of its injection t by $\varphi_0 = \text{const.} - \omega_0 t$. So the particles injected in an interval $\Delta t = T/k = t\pi/\omega_l$ have phases spread uniformely between $-\pi$ and π, and since $T/k \ll \theta$ we can practically assume Δt as an elementary interval $\mathrm{d}t$.

value φ_0 will be the φ_n or the φ_M of the phase oscillations, according whether it is $< \varphi_s$ or $> \varphi_s$.

Those particles, whose φ_0 happens to be in the region of closed curves, i.e. between $\pi - \varphi_s$ and $g(\pi - \varphi_s)$, initiate their oscillations around the synchronous particle, while the others are thrown against the walls. But only a part of the former group of particles can really perform their oscillations without hitting the walls, namely those for which the *total* amplitude of oscillation (synchrotron amplitude X_M plus betatron amplitude x_M) is less than the *useful* half width of the donut. We consider as « useful » width a' the radial width a diminished by a certain amount to take into account the gas scattering and the distortion of the orbit due to field irregularities and frequency errors. Therefore, once chosen the value of a', the capture condition can be written

$$X_n + x_n \leqslant \frac{a'}{2}. \tag{18}$$

Now we want to calculate how many particles satisfy this condition.

Let us consider first only the particles injected between t and $t+\mathrm{d}t$. They are $I\varrho\,\mathrm{d}t$ and perform betatron oscillations given by (5): so the capture condition for them is

$$X_M \leqslant \frac{a'}{2} - \frac{\sigma t}{T},$$

or, because of (16)

$$H(\varphi_0) = \frac{1}{C}\left(\frac{a'}{2} - \frac{\sigma t}{T}\right).$$

If, in Fig. 4, we draw an horizontal line of ordinate

$$H = \frac{1}{C}\left(\frac{a'}{2} - \frac{\sigma t}{T}\right) \tag{19}$$

and call $\Phi(H)$ the length intercepted on it by the curve of given φ_s, divided by the abscissa length corresponding to 360°, this Φ represents the captured fraction of the particles injected in $\mathrm{d}t$. So the total number of captured particles will be

$$N = \int_0^\theta \Phi\left(\frac{a'}{2C} - \frac{\sigma t}{CT}\right) I\varrho\,\mathrm{d}t. \tag{20}$$

Let us take H (eq. (19)) as integration variable and remark that for $H < 0$

we must assume $\Phi(H) = 0$, because these particles have $x_M > a'/2$. Then equation (20) becomes

$$N = \frac{CT}{\sigma} \int_0^{\alpha} \Phi(H) I \varrho \, dH , \tag{21}$$

where

$$\alpha = \frac{a'}{2C} . \tag{22}$$

We shall discuss later the factor ϱ, for the moment let us call $\bar{\varrho}$ a convenient average of ϱ and suppose that I is constant.

Then

$$N = I\bar{\varrho} \frac{CT}{\sigma} \int_0^{\alpha} \Phi(H) \, dH . \tag{23}$$

The integral represents the area between the curve of Fig. 4 and the horizontal line of ordinate α. It has been calculated numerically as a function of α for different φ_s and is plotted in Fig. 5. Remark that these curves represent universal functions, not depending on the parameters of the machine.

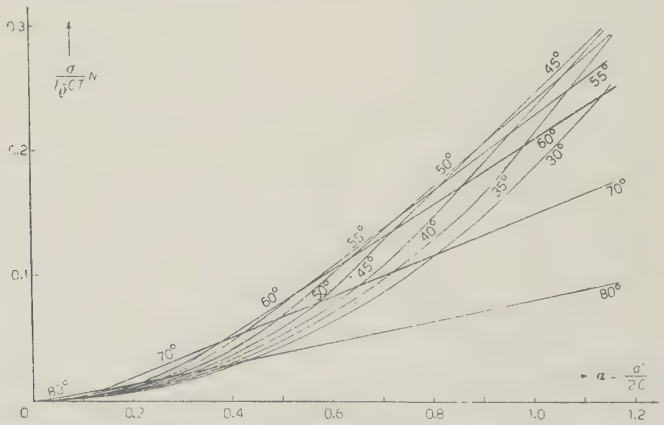

Fig. 5.

Now, this diagram shows that the family of curves has an envelope on the upper side. Therefore, for each value of α there exists a value of φ_s for which the number of captured particles is a maximum: it is the value belonging to that curve, which is tangent to the envelope at the point of abscissa α. So, if we call $J(\alpha)$ the ordinates of the envelope, the number of captured part

icles corresponding to the optimum φ_s is

(24) $$N_{\max} = I\bar{\varrho}\,\frac{CT}{\sigma}\,J\left(\frac{a'}{2C}\right)$$

or, using (22)

(24′) $$N_{\max} = I\bar{\varrho}\,\frac{a'T}{2\sigma}\,\frac{J(\alpha)}{\alpha}\,.$$

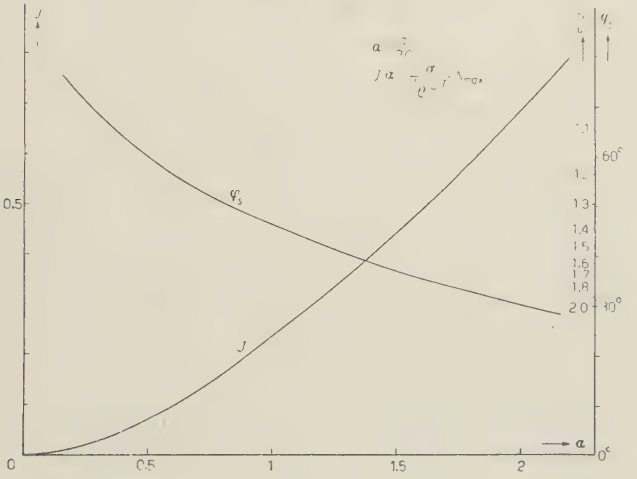

Fig. 6.

The function $J(\alpha)$, numerically calculated, is given in Table I. The same table gives also the optimum φ_s and $U/u = \operatorname{cosec}\varphi_s$ as functions of α. This table enables one to find immediately the most convenient radiofrequency voltage and the corresponding number of captured particles. For $\alpha < 2$ one can also use the diagram (Fig. 6) where the functions J, φ_s, U/u are plotted against α.

Table I.

α	$J(\alpha)$	$\varphi_s(\alpha)$	U/u
0.0	0.000		
0.5	0.072	59.5°	1.16
1.0	0.234	46.0	1.39
1.5	0.447	36.8	1.67
2.0	0.687	30.6	1.96
2.5	0.952	26.3	2.26
3.0	1.24	23.1	2.55
3.5	1.55	20.4	2.87
4.0	1.87	18.4	3.17
4.5	2.20	16.6	3.50
5.0	2.53	15.1	3.84

5. – Discussion of the Results.

To discuss the influence of various parameters on the number of captured particles it is convenient to approximate the function $J(\alpha)$ by an empirical formula. A good one is

$$J(\alpha) = 0.242\alpha^{\frac{3}{2}}. \tag{25}$$

Then eq. (24′) becomes

$$N_{\max} = 0.11 \cdot I\bar{\varrho}T\left(\frac{kK(1-n)\beta^2}{R}\right)^{\frac{1}{4}} \frac{a'^{\frac{3}{2}}}{\sigma_r^{\frac{5}{4}}} \tag{26}$$

In the case of an electrosynchrotron we can assume $\beta = \sim 1$; then we get

$$N_{\max} = 0.11 \cdot I\bar{\varrho}T\left(\frac{k}{AR}\right)^{\frac{1}{4}} \frac{a'^{\frac{3}{2}}}{\sigma_r^{\frac{5}{4}}}. \tag{26′}$$

This formula can be written (expressing all lengths in cm)

$$N_{\max} = 0.23 \cdot 10^{-10} I\bar{\varrho}k^{\frac{1}{4}}(\Lambda R)^{\frac{3}{4}} \frac{a'^{\frac{3}{2}}}{\sigma_r^{\frac{5}{4}}}.$$

The most interesting result contained in these formulae is the proportionality of $N_{\max}$ to $k^{1/4}a'^{3/2}\sigma^{-5/4}$. It is, however, based on the assumption that the « injection efficiency » $\varrho(t)$ is practically constant over most of the injection time.

If the r.f. voltage U is not given its optimum value, the number of captured particles decreases in a measure that can be easily calculated from the curves of Fig. 5.

6. – Influence of the Injection Losses.

Let us now discuss the influence of the variation of the injection efficiency $\varrho(t)$ during the injection time.

If the spiral pitch ϱ is very small, a good deal of particles will be lost against the deflector or the walls in the first two or three revolutions, while in the subsequent revolutions these losses will be negligible. That means that the integral in (21) represents now a sort of « weight » of the shaded area of Fig. 4 with a density which is < 1 in a strip near the upper border and almost $= 1$ in the remaining part of the area.

This suggests dividing the injection time θ in a first, short interval θ_1, (corresponding to the upper strip) in which $\varrho < 1$, while in the remaining inter-

val $\theta - \theta_1$ it can be assumed $\varrho = 1$. The two parts may give comparable contributions to the integral, because the low density corresponds to the wider part of the area, that is, because the early injected particles have lesser betatron amplitude and so are captured in a wider phase interval.

Putting

$$\alpha_1 = \frac{1}{C}\left(\frac{a'}{2} - \sigma\frac{\theta_1}{T}\right), \tag{27}$$

equation (21) becomes

$$N = IC\frac{T}{\sigma}\left[\int_0^{\alpha_1}\Phi(H)\,\mathrm{d}H + \int_{\alpha_1}^{\alpha}\Phi(H)\varrho\,\mathrm{d}H\right].$$

The first integral can be calculated be means of the curves of Fig. 5. The second integral, in most cases, will extend over an interval of α in which the curve ot Fig. 4 is vertical, that is Φ is constant. In such cases it will be

$$N = IC\frac{T}{\sigma}\int_0^{\alpha_1}\Phi(H)\,\mathrm{d}H + I\theta_1\bar{\varrho}_1\Phi(\alpha),$$

where $\bar{\varrho}_1$ is now the average of $\varrho(t)$ during the interval θ_1.

The determination of the optimum φ_s and of the corresponding N_{max} must be done in this case by trial and error.

This theory has been extended, by I. Solomon, to a strong focusing synchrotron. The final formulae are the same, provided K and C are replaced by

$$K = 1 + \frac{1}{\beta^2}\left[\frac{1}{AQ^2} - 1\right],$$

$$C = \frac{1}{\sqrt{Q^2 - 1}}\sqrt{\frac{R\sigma}{\pi k}},$$

where Q is defined by

$$\frac{\mathrm{d}r}{r} = \frac{1}{Q^2}\frac{\mathrm{d}p}{p},$$

p being the momentum of the particle.

PROPRIETÀ LETTERARIA RISERVATA

Direttore responsabile: G. POLVANI

Tipografia Compositori - Bologna

Questo fascicolo del *Supplemento* è stato licenziato dai torchi il 2-VIII-1955

SUPPLEMENTO
AL VOLUME II, SERIE X, DEL
NUOVO CIMENTO
A CURA DELLA SOCIETÀ ITALIANA DI FISICA

1955 — 2° Semestre — N. 2

Commemorazione di Enrico Fermi

tenutasi a Varenna e a Como il 6 Agosto 1955.

I

Cronaca delle cerimonie.

G. C. Dalla Noce
Segretario della Società Italiana di Fisica

Il 6 Agosto 1955, ricorrendo l'anniversario dell'ultima lezione tenuta da Enrico Fermi al Corso estivo, che la Scuola Internazionale di Fisica della Società Italiana di Fisica svolse nel Luglio-Agosto del 1954 nella Villa Monastero di Varenna, l'Ente Villa Monastero e la Società Italiana di Fisica vollero ricordare il grande Estinto con una breve cerimonia alla quale presenziarono la consorte e la sorella di lui, Signore Laura Fermi Capon e Maria Sacchetti Fermi, i docenti e gli alunni del Corso Internazionale di Fisica tenutosi quest'anno nella stessa Villa Monastero, e molte personalità del mondo culturale e politico.

La cerimonia si svolse in due momenti successivi: alle ore 15.30 a Varenna, alle ore 18 a Como.

A Varenna il Sottosegretario di Stato alla Pubblica Istruzione, on. Giovan Battista Scaglia, venuto in rappresentanza del Ministro, scoperse l'epigrafe marmorea, che, per iniziativa dell'Ente Villa Monastero e della Società Italiana

di Fisica, è stata posta in memoria e in onore di FERMI nella Villa Monastero, proprio nell'Aula dove Egli tenne le sue lezioni: la lapide, murata su una parete, appare come fosse appoggiata su un tappeto, opera di fine mosaico, ed è sormontata da un medaglione in bronzo recante l'effigie del grande Estinto.

La pietra è di porfido rosso antico, donato e lavorato dal Laboratorio delle pietre dure di Firenze; l'epigrafe è stata dettata dal prof. padre GIOVANNI PIGATO del Collegio « Gallio » di Como; il medaglione è stato modellato dal prof. GIANNINO CASTIGLIONI di Milano e fuso nelle Officine Johnson di Milano; il mosaico è stato composto da GENNARO BERNASCONI di Como su disegno rinascimentale; e tutta la composizione è opera dell'architetto FEDERICO FRIGERIO di Como.

Davanti alla lapide è posto un antico bacile su colonna in pietra scolpita, recante un perpetuo omaggio di verdi rami reclinati in basso.

Dopo lo scoprimento il Presidente della Società Italiana di Fisica, prof. GIOVANNI POLVANI, lesse e tradusse in italiano l'epigrafe aggiungendo alcune parole d'occasione; l'on. SCAGLIA pronunciò un breve discorso; e lo scultore CASTIGLIONI offerse in dono alla signora LAURA FERMI copia in bronzo del medaglione.

Indi tutti i partecipanti alla cerimonia si trasferirono a Como.

A Como, nel Tempio Voltiano, dopo brevi parole del Sindaco della città, comm. PAOLO PIADENI, e del Presidente dell'Ente Villa Monastero, avv. GILBERTO BOSISIO, il prof. ISIDOR ISAAC RABI, Premio Nobel per la Fisica e docente al Corso Internazionale di Fisica di quest'anno a Varenna, pronunciò l'orazione ufficiale in memoria di ENRICO FERMI (*).

Indi il Presidente della Società Italiana di Fisica, prof. GIOVANNI POLVANI, a nome della Società stessa offerse in dono alle Signore LAURA FERMI e MARIA SACCHETTI, al rappresentante del Ministro, on. SCAGLIA, e al Presidente dell'Ente Villa Monastero, avv. BOSISIO, copia del fascicolo del *Supplemento* al *Nuovo Cimento* contenente tutte le lezioni svolte a Varenna nel Corso internazionale di Fisica dell'anno passato e quindi anche quelle di FERMI.

Il Presidente della Società stessa prese infine occasione per comunicare pubblicamente che, per deliberazione del Consiglio di Presidenza, la Scuola Internazionale di Fisica della Società Italiana di Fisica s'intitolerà d'ora in avanti al nome di ENRICO FERMI.

(*) Il discorso tenuto in inglese fu simultaneamente trasmesso in italiano con impianto di cuffie telefoniche organizzato gentilmente dalla Soc. Siemens di Milano, alla quale va quindi il più cordiale ringraziamento.

HIC
ANIMO TOT INTER REIVM MIRA PACATO
ARCANA NATVRAE PRIMOR
IPSIS IN ATOMIS VOLVENTIA
DOCTORVM COETVI POSTREMVM APERVI
MEVM VNDE NOMEN IAM IMMORTALE FECERAM

Lapide e medaglione posti nell'Aula di Villa Monastero a Varenna,
in memoria e in onore di Enrico Fermi.
(6 Agosto 1955)

Il medaglione, con l'effigie di ENRICO FERMI,
sovrastante la lapide posta nell'Aula di Villa Monastero, a Varenna,
in memoria e in onore di lui.

SUPPLEMENTO AL VOLUME II, SERIE X
DEL NUOVO CIMENTO

N. 2, 1955
2° Semestre

II

Davanti alla lapide posta nell'Aula di Villa Monastero a Varenna, in memoria e in onore di Enrico Fermi.

G. Polvani
Presidente della Società Italiana di Fisica

(*leggendo l'epigrafe*)

HENRICUS FERMI
MCMLIV – AETATIS SUAE LIII

—

HIC
ANIMO TOT INTER RERUM MIRA PACATO
ARCANA NATURAE PRIMORDIA
IPSIS IN ATOMIS VOLVENTIA
DOCTORUM COETUI POSTREMUM APERUI
MEUM UNDE NOMEN IAM IMMORTALE FECERAM

(*traducendo*)

« ENRICO FERMI »
« 1954 - 53° della sua vita »

—

« Qui »
« l'animo quietato in fra tante bellezze naturali »
« disserrai per l'ultima volta a una schiera d'uomini di scienza »
« gli elementi ultimi e più riposti »
« che s'agitano entro gli atomi »
« onde immortale avevo già reso il mio nome. »

Con queste parole, che il porfido imperiale imagina aver sorpreso dire

dallo spirito di ENRICO FERMI, e con l'effigie di lui fusa nel bronzo, l'Ente Villa Monastero e la Società Italiana di Fisica hanno voluto ricordare che qui, a Varenna, ENRICO FERMI tornò a godere delle bellezze della sua terra, e in questa Aula fece, per l'ultima volta, dono agli altri del suo sapere.

A quanti qui verranno, possa questa memoria essere al tempo stesso suscitatrice di ammirazione per il grande italiano che essa ricorda, e testimonianza di gratitudine verso di lui per il bene e il beneficio ricevuti da tutti coloro che ai problemi della scienza appuntano la forza dell'intelletto.

SUPPLEMENTO AL VOLUME II, SERIE X
DEL NUOVO CIMENTO

N. 2, 1955
2° Semestre

III

Parole di omaggio a Enrico Fermi pronunciate nell'Aula di Villa Monastero.

G. B. Scaglia

Sottosegretario di Stato alla Pubblica Istruzione

La sobria austerità di questa cerimonia e le parole ispirate e nobilissime che il prof. Polvani ci ha testè letto fanno apparire veramente superfluo ogni discorso. Nè io oserei rompere il raccoglimento solenne di questa ora, se non fosse per adempiere l'incarico, che mi è stato affidato, di recare qui, a nome del Governo Italiano, con l'espressione della commossa solidarietà per la Consorte e per la Sorella, la cui presenza dà a questa cerimonia un carattere particolare di intimità, l'omaggio dell'Italia al grandissimo scienziato, che proprio qui per l'ultima volta ha voluto essere Maestro.

Qui tutto ci parla di lui; tutto si anima del suo ricordo; e per quanti, fra i presenti, hanno avuto il privilegio, or è un anno, di incontrarlo qui, di udire la sua voce, di incrociare il suo sguardo, di godere, sia pure per breve tempo, della sua conversazione arguta e schiva, non era certamente necessaria l'opera, pur tanto pregevole, dell'artista che ha modellato il medaglione che noi ammiriamo, perchè il suo sguardo penetrante e la sua immagine un po' assorta e — oggi solo lo avvertiamo — quasi presaga, ci rimangano fissi nell'anima, immedesimati per sempre con le linee stesse di questo ameno paesaggio.

Ma ben oltre il nostro ricordo durerà la fama di Enrico Fermi. E anche coloro che non furono qui lo scorso anno, anche coloro che qui passeranno negli anni e nei secoli che verranno, ai quali certo non sarà ignoto il nome di colui cui la Provvidenza riserbò di contemplare primo, e senza vertigini, gli orizzonti sconfinati dell'era atomica, riunendosi a studiare e a meditare qui, su questo lembo incantato del Lago che vide le prime esperienze di Alessandro Volta, non potranno non sentire aleggiare su di loro, stimolo e conforto, l'estremo messaggio scientifico che, a pochi mesi dalla morte, qui Egli ha affidato a discepoli convenuti da ogni continente.

SUPPLEMENTO AL VOLUME II, SERIE X
DEL NUOVO CIMENTO

N. 2, 1955
2° Semestre

IV

Brevi parole pronunciate nel Tempio Voltiano di Como alla cerimonia commemorativa di Enrico Fermi.

P. PIADENI
Sindaco di Como

Eccellenze, Signore e Signori,

la Città di Como porge, per il tramite della mia voce, il saluto e il benvenuto alle Autorità e agli illustri docenti e discenti del III Corso estivo di alta Fisica svoltosi in questi giorni a Villa Monastero, e ringrazia quanti son qui venuti in questo Tempio per ricordare e onorare ENRICO FERMI.

Un'espressione particolare di riconoscenza rivolgo poi, a nome di Como stessa, al prof. RABI per aver assunto l'incarico di commemorare ENRICO FERMI, e ai Congiunti dell'Estinto per avere accolto l'invito di presenziare a questa cerimonia.

La Città di VOLTA — mi rivolgo con particolare reverenza ai Congiunti di ENRICO FERMI — partecipa dolorosamente commossa, ma con orgoglio, alla solenne odierna commemorazione dell'illustre Scienziato, che un anno fa, già adombrato dall'ala imminente della morte, e forse presago della sua fine terrena, venne nella sua Patria, qui, sulle rive stupende del nostro Lario, per dettare le ultime sue lezioni di scienziato italiano in terra italiana.

Come Sindaco di Como considero altissimo onore la sorte che, in virtù di questo anniversario, oggi ci tocca: di esaltare cioè, proprio nel Tempio sacro ad ALESSANDRO VOLTA, antesignano delle moderne scoperte scientifiche, la memoria e la gloria di uno studioso che pienamente e degnamente simboleggia la continuità del decisivo contributo italiano al progresso delle scienze fisiche e dell'umana civiltà.

SUPPLEMENTO AL VOLUME II, SERIE X
DEL NUOVO CIMENTO

N. 2, 1955
2° Semestre

V

Allocuzione pronunciata nel Tempio Voltiano di Como alla cerimonia commemorativa di Enrico Fermi.

G. Bosisio

Presidente dell'Amministrazione Provinciale di Como e dell'Ente Villa Monastero

All'Onorevole Rappresentante del Governo, alle Eccellenze, Autorità, Signore, Signori qui tutti raccolti nel Tempio Voltiano per commemorare solennemente Enrico Fermi, laureato del Premio Nobel per la Fisica, il deferente omaggio dell'Ente Villa Monastero di Varenna che ho l'onore di presiedere.

Ai Congiunti rinnovati sensi di cordoglio e di profondo rimpianto per l'irreparabile perdita.

Ai fisici in lutto la Provincia di Como inchina reverente il suo labaro nel mesto e glorioso ricordo dell'Uomo cui la Scienza è tanto debitrice.

Nel cenacolo di Varenna e precisamente nell'Aula in cui per l'ultima volta Fermi rivolgendosi ad elette menti ammaestrò con dovizia di erudizione e con calore di conquistatore, da poche ore i lineamenti del suo volto forgiati nel bronzo da valente mano di artista, rammenteranno ai posteri come Varenna ebbe l'alto onore di raccogliere l'ultima lezione del Fisico che illustrò il nome italiano e aprì alla scienza nuovi orizzonti con le meraviglie della pila atomica, portando l'umanità a nuove conquiste. Egli stesso avvicinò la sua scoperta, come termine di paragone, alle Piramidi, perchè l'una e l'altre imponenti vittorie dell'uomo sopra la nateria bruta.

L'Ente Villa Monastero ritenne suo dovere di rinunciare alla solenne commemorazione nella sua Sede di Varenna, perchè più degno, onorifico e significativo reputò fosse il Tempio Voltiano, dove sono custodite le memorie del grande Comasco che trasformò la faccia del mondo, aprendo con le sue scoperte e le sue invenzioni l'era dell'elettricità.

A Como, ove tutto parla di Alessandro Volta — la casa avita, la chiesa

ove fu battezzato e sentì la grandezza della Fede che egli stesso divulgò ai fanciulli, il mausoleo che raccoglie le sue spoglie mortali, il marmoreo monumento, il Tempio che conserva gelosamente tutti i suoi ricordi — non poteva mancare la commemorazione ufficiale del più grande fisico contemporaneo congiungendola idealmente alla gloria del suo illustre concittadino.

Nuovo argonauta, FERMI spinse arditamente l'uomo a nuove cognizioni e a nuovi assoggettamenti delle forze fisiche, raggiungendo progressi e conoscenze fino a pochi anni fa impensati.

Come tutte le maggiori conquiste si affermano nell'umiltà, così il rogito del fatidico esperimento della pila atomica con la reazione a catena del 2 Dicembre 1942 venne redatto sull'impagliatura di un autentico fiasco di Chianti ove furono apposte con quella di FERMI altre firme illustri, note nel campo scientifico moderno.

Un nuovo navigatore italiano era arrivato nel nuovo mondo. Un nuovo mondo era scoperto.

Due pietre miliari nel progresso scientifico: la pila di VOLTA e quella di FERMI. Due nomi acquisiti alla storia della scienza, due italiani, due glorie di nostra gente che sono divenute gloria delle genti.

Il Tempio Voltiano doveva essere ed è la vera degna sede della commemorazione di chi avviò con metodo e tenacia la Scienza fisica verso inesplorate regioni e a nuove conquiste.

SUPPLEMENTO AL VOLUME II, SERIE X
DEL NUOVO CIMENTO

N. 2, 1955
2° Semestre

VI

In memoria di Enrico Fermi: discorso letto nel Tempio Voltiano a Como.

I. I. Rabi

Premio Nobel per la Fisica

Eccellenza, Ladies and Gentlemen,

It is my sad privilege today to come to speak to you about my friend and colleague Enrico Fermi. I left Italy a week ago after spending two extraordinary interesting and pleasant weeks at the Scuola Internazionale di Fisica at the Villa Monastero in Varenna. Last year Enrico Fermi gave a series of lectures, which now became famous, at the same school. In fact, today is the anniversary of his last lecture.

We are gathered today in this charming building which is the Alessandro Volta Memorial and I find it especially fitting that we should commemorate Enrico Fermi in this memorial building dedicated to his illustrious predecessor Volta, the great pioneer in electrical science more than a century ago. I recall with great pleasure the delightful Volta Conference of 1949 here in Como where were gathered a brilliant international group of physicists to discuss problems of cosmic rays. Enrico Fermi was naturally one of the leading lights of this Conference. Little did one imagine that a short six years later we would hold a commemorative meeting in this same building for this man who was so healthy vigorous and energetic and in the prime of life.

Enrico Fermi was a true son of Italy who spent sixteen very active and fruitful years as a resident in the United States. As such I hope he will become a symbol of the close collaboration and mutual respect and friendship between the people of Italy and those of the United States. His loss, I can assure, has been as deeply felt in the United States, by scientists, by government, by people, as it has been here in his native Italy. The phrase in which I heard of his mortal illness was: « The great Italian Navigator has made his last journey ».

Today, I wish to explain as clearly as I can the contribution of ENRICO FERMI to science and his influence as a personality and as a teacher. You have all read, I am sure, Mrs' LAURA FERMI charming book which describes FERMI from the domestic point of view. The great success of this book gave FERMI more pleasure than anything else as he consciously and heroically faced the last days of his life. It is unnecessary for me to recount FERMI's life history since LAURA FERMI has done it so much better than I could possibly hope to do. I will therefore confine myself to the more professional side of FERMI's career.

FERMI was extraordinary not only for the power of his genius, his great imagination and intellect, his tremendous vigor and endurance, his clarity and objectivity. It was almost unique that in an age of narrow specialization he was a generalist. He was neither just a theoretical physicist or an experimental physicist, a nuclear physicist or a solid state physicist, a pure physicist or an applied physicist. More than almost any other of his contemporaries he was a physicist and no branch of the subject from thermodynamics to relativity was foreign to him and he contributed importantly to almost every field. As an experimenter he also covered the whole field from spectroscopy to cosmic rays. To find an analogous figure in the history of science one must go back to the earlier days of physics, to ARCHIMEDES, and GALILEO, ISAAC NEWTON and HEINRICH HERTZ. For this reason I believe it will be generations before his equal will again be born.

One of FERMI's earliest and most important contributions was to the subject of statistical mechanics, where he discovered the statistics which bears his name forever, the FERMI statistics. Basing himself on Pauli's exclusion principle for electrons in atoms FERMI applied this idea quite generally in that no two electrons or particles of the appropriate properties could be in the same state. This idea led to statistical distribution laws which are entirely different from the classical laws of Maxwell and of Boltzmann. This idea of FERMI's was later developed by PAULI, by SOMMERFELD and by BLOCH and many others, till it is now the keystone of the theory of metals, semi-conductors and insulators.

With the Fermi statistics the specific heat and the electrical and thermal conductivities of metals can now be understood and predicted. The applications go even further into the statistics which lie at the basis of the chemical properties and specific heats of gases like hydrogenon and deuterium.

In the Fermi statistics only one particle such as an electron or at most two if their spins are opposite can occupy a particular energy state. After the lowest state is occupied by two particles the next one must go to a higher state and so on. As a result at sufficiently high particle density the states are all filled up to a level known as the top of the Fermi sea. On this picture only the few particles at the top of the Fermi sea have energy levels close by which are unoccupied and to which they go by collision. Then particles of the top

have a high energy and move very fast. The others are almost inert unless they receive large amounts of energy. It is clear how different this distribution is from the classical where the distribution is like a probability curve and all particles can change their energy by any minute amount. It is also clear that the Fermi distribution will lead to consequences very different from the classical distribution, which was inadequate to explain the properties of electrons in metals.

FERMI pursued the same idea to build a statistical theory of atomic structure. An atom with nuclear charge of Z units will be surrounded by Z electrons which are attracted to the nucleus and repel one another. In addition they are in very rapid motion. Clearly it is beyond the power of mathematics to solve a problem with large Z directly. The mathematics is too complicated. FERMI and independently THOMAS applied the Fermi statistics to this problem and obtained an expression for the charge density of the electron as a function of the distance from the nucleus. By further analysis he was able to show the existence of shells within the atom corresponding to the chemical picture of the period table of the elements. The Fermi-Thomas distribution is verified by the scattering of X-rays from atoms.

FERMI made this statistical theory for a purpose. He was at that time also interested in the effects of nuclear spin and magnetic moment on the spectra of atoms. By means of his statistical model he was able to calculate these effects more accurately and to evaluate the nuclear properties from spectroscopic information.

The very same ideas of the Fermi statistics are also applicable to nuclear structure and played a very important role in the early days of nuclear theory.

To digress to a period more than twenty years later, present theories of nuclear structure rely to a great extent on the independent particle model proposed independently by FERMI's colleague Prof. MARIE MAYER at the University of Chicago and Prot. JENSEN in Heidelberg. The essential ideas of this model are that the protons and neutrons in the nucleus move independently of each other under the influence of their mutual forces and that each proton and each neutron occupies a certain energy level. This idea is not sufficient to explain certain regularities in nuclear structure such as the so-called magic numbers at which the nuclei are particularly stable. What makes this model successful is the addition of spin-orbit forces which alter the energy of the proton or neutron depending on the direction which the spin points in with reference to the orbit of the particle in the nucleus. Prof. MAYER told me that she was working on this problem of nuclear structure with little success until FERMI suggested that she try the effect of the spin-orbit forces.

Before I turn to give some account of FERMI's contribution to nuclear science for which he received the Nobel prize and his greatest popular fame I

must mention one other contribution of his earlier days. That is his explanation of the radioactive emission of electrons and positive electrons known as positrons. This phenomenon is known as β-ray emission.

This phenomenon was one of the great mysteries of physics for years because the nucleus starts from a state of definite energy and ends with a state of definite energy and yet the β-rays themselves which are supposed to carry away this definite energy difference have a wide spread of energies. PAULI suggested that an additional unobserved particle of no electric charge is emitted at the same time and that the energy is shared between the β-ray particle and this new particle. FERMI made a mathematical theory of this idea and named this new particle the neutrino. This Fermi theory has been greatly developed since his original work and a great deal of experimental detail has been uncovered on the behavior of β-rays. This particle the neutrino has as FERMI originally suggested zero mass when it is at rest, just like a light quantum but a spin equal to that of an electron spin. It is so penetrating that it could pass through the mass of the sun without being stopped. To this day its direct action on matter, outside of the nucleus where it is spontaneously born, has not yet been observed with certainty. Fermi's solution of the mystery of the β-rays is one of his great contributions to physical science.

We now turn to that phase of FERMI's career which holds so much promise and so much dread for the future of mankind. It started in Rome shortly after the discovery of the neutron by Sir JAMES CHADWICK of the Cavendish Laboratory in Cambridge, England. FERMI immediately realized the great importance of the neutron as a means of making nuclear reactions. Since the neutron has no electric charge it is not subject to the repulsion of the nuclear charge. A neutron of even very low kinetic energy can enter the nucleus whereas a proton or α particle would be repelled and never get close to the nucleus.

After the discovery of artificial radioactivity by JOLIOT and CURIE in Paris FERMI and his brilliant group in Rome started a series of experiments on nuclear reactions with neutrons which made the *Ricerca Scientifica* one of the most prized journals in physics and caused all physicists interested in nuclei to learn enough italian to follow these fascinating researches. One of the most important observations was the slowing down of neutrons by collisions with hydrogenous material and the very interesting properties of these slow neutrons. This procedure was patented by the Rome group and the patent has recently been bought by the United States government for the sum of $ 300 000.

I will not go into detail of these interesting discoveries except to mention the only great and fortunate error which FERMI and his group made in their studies of the reactions of neutrons and uranium. The phenomena they observed were most curious and puzzling, which they tried to interpret as properties of nuclei heavier than uranium. Although such nuclei were certainly formed in their experiments they overlooked the possibility of nuclear fission

in spite of the suggestions of IVAN NODDACK that this phenomenon was not ruled out in their experiments. I shudder to think what would have happened to the world if nuclear fission had been discovered five years earlier and atomic weapons had fallen into the hands of a HITLER.

FERMI received the Nobel prize for his work with nuclear reactions with neutrons and by the time nuclear fission was discovered by HAHN and STRASSMANN in Germany in late 1938, FERMI and his family were already living in New York and FERMI was a professor of Physics at Columbia.

As in Rome, FERMI immediately attracted a brilliant group of young physicists around and proceeded with his experiments with larger means that he had in Rome, since we at Columbia already had an operating cyclotron.

In early 1939 the discovery of HAHN and STRASSMANN became known at Columbia. In fact I myself brought the news to FERMI since I had heard it from Prof. NIELS BOHR in Princeton. FERMI immediately realized the great energy released in this process and by the next day he had calculated the size of the crater which would be produced by the energy released from the fission of a kilogram of uranium.

Immediately the very interesting question arose as to whether the abundant isotope of uranium ^{238}U or the other isotope which is present to only one part in 140 was responsible for the phenomenon of fission. Experiment soon settled that it was the less abundant isotope ^{235}U which produced fission with slow neutrons.

The interesting question then arose, could one produce a self perpetuating chain reaction with normal uranium. This question resolved itself into a series of questions:

1) Did the fission reaction produce more than one neutron? If it did, a chain reaction was possible in principle.

2) Could one slow down these neutrons with available materials and in such a geometry that enough neutrons would be left to maintain the chain reaction?

3) Could such a chain reaction be controlled it it were once started, or would it always result in an explosion?

FERMI attacked these problems with characteristic energy, enthusiasm and insight. The fundamental physical constants were unknown, the theory was unknown, and the whole group felt that they were working against time with Hitler Germany as the formidable competitor.

Ever increasing means were put at FERMI's disposal by the government of the United States and by the end of 1942 FERMI had demonstrated the feasibility of the chain reaction in Chicago where the whole project had been transplanted from Columbia. The atomic age had begun, nuclear energy was

now a reality and the history of mankind had turned a sharp corner. Like many other great discoveries and inventions nuclear energy is not an unmixed blessing, because hand in hand with nuclear energy is the possibility of making nuclear weapons which increase man's destructive power by a factor of over a million. The destruction of mankind was already too large for safety before the discovery of nuclear energy and now mankind faces the possibility of wars of destruction which could bring our whole culture down in ruins and even endanger the future of the human race on this globe. To control this powertul but wild force will require all the wisdom, sympathy and restraint of which mankind is capable. The problem is fully realized by all mankind but the solution is as yet beyond our grasp. We can only hope that the wisdom of the nations is equal to the dread problem which confronts all equally.

It has turned out in the eventuality that the problem of constructing practical economical power reactors was much more difficult that had been anticipated. The new conditions were far beyond previous engineering experience. Now more than twelwe years after the first operating reactor was completed peaceful nuclear energy does not yet play an important role in our country. However, the most important problems have been solved and we can expect that the history of the next decade will show that nuclear energy will take on the expected role of contributing to the increasing demand for energy which is so characteristic of our century.

It is of the essence of the spirit of FERMI to always become interested in new and challenging problems. Soon after he showed that the chain reaction was a reality he left this field and joyned the new group at Los Alamos whose task was to make a weapon out of nuclear fission. Here again very little was known. Plutonium and Uranium 235 were not available except in microgram amounts. The factories for their production were being built by imagination and bold projection from poorly known data. The task of Los Alamos was to be ready with atomic weapons as soon as the material for their construction was available. That this formidable task was accomplished with spectacular success is now a matter of history. The Los Alamos Laboratory was such a tightly knit organization that the apportionment of individual credit is impossible. Here FERMI proved that he could also work in an organization where he was not the responsible leader but a leading participant in a group effort. For a man of FERMI's spirit and claim this way of working was a matter of great self discipline.

Perhaps never before in history has such a brilliant group of scientists been gathered together to accomplish a given task as at Los Alamos. A recital of the names of the scientists who where gathered there under the inspired leadership of Dr. J. K. OPPENHEIMER is like reading the Almanac of Gotha of Science. Many of the brilliant young people who were comparatively unknown at the time have since become famous. In spite of the dread nature of the task, I

believe that FERMI spent some of the happiest times of his life at Los Alamos. There, surrounded by brilliant and sympathetic colleagues and co-workers he enjoyed the stimulation of minds of equal agility and profundity. The beautiful setting on a mesa rising more than 700 meters above the desert with the Rio Grande at the foot of the mesa and the Jernez mountain rising up behind was extraordinarily beautiful and wild. In the distance through the clear air more than 60 kilometers away and always in view could be seen the Sangre de Cristo mountains which he would climb at every opportunity during the week-ends. In the winter there was skiing in the mountains and long walks at all seasons. This combination of intellectual stimulation, an important task and the beautiful and accessible outdoors gave him very great satisfaction. Even after the war he returned to Los Alamos summer after summer.

After the war was over, FERMI, much to our regret at Columbia, decided to move to the University of Chicago which seemed to offer better facilities for his work. In doing this he took with him some of the best people from Columbia and left me with the difficult task of reconstructing the Physics department. Our success in this effort is partly due to the fact that he was such a stimulating teacher that we could attract some of his pupils who where even more brilliant than those he kept by him in Chicago.

At Chicago FERMI again showed his versatility by entering the field of cosmic rays and high energy physics, particularly physics of mesons, the strange new particles which have been discovered in the post-war period.

Time will not permit me to recount his great achievement in this field. I will only mention that he gave for the first time, I believe, a reasonable account of the origin of the high energy of the cosmic rays which depends on the collision of particles with huge clouds of attenuated cosmic matter and with the weak magnetic fields which are trapped in them.

The beautiful experiments which he had in progress on the properties of mesons are now left for others to finish but his name will always be associated with this most interesting new field of physics.

The war caused many changes in the United States as elsewhere in the world. One of the most interesting was the close relation between scientists and government which started during the war because of the scientific and technological sophistication of modern warfare. The great laboratories which were started during the war like Los Alamos were stuffed largely by scientists from Universities who had no previous connection with government. After the war most of these men returned to their universities and their peacetime pursuits of teaching and research. In leaving they carried with them the most advanced knowledge and experience.

When the Congress of the United States enacted the Atomic Energy Act of 1946, it provided for a General Advisory Committee to be appointed directly by the President of the United States and responsible to him to advise the

Atomic Energy Commission of scientific and technologic policy. Amongst the original members of this Committee were men of such stature and influence as Dr. J. K. OPPENHEIMER, Dr. J. B. CONANT, the president of Harvard University and now U.S. Ambassador to Germany, Dr. L. A. DUBRIDGE the President of the California Institute of Technology and others of similar stature. FERMI, although he was a fairly recent citizen of the United States, was so highly regarded for his scientific and personal qualities of loyalty and judgement that he was appointed to be one of the original members of this group. He served for four years, during which time he had a voice in some of the most important decisions which affect the future of the world, since this committee possessed complete access to some of the most highly secret items of national policy. His advice was always calm and judicial, based on a profound scientific knowledge and an equally profound understanding of the response of people in critical situations. Those who disagreed with him on any point did so with great misgiving because of their respect for the soundness of his judgement. Events rarely proved him to be wrong. As in everything else he undertook he evoked the confidence and admiration of all with whom he was associated. He was about to be reappointed to this Committee by President EISENHOWER but his illness and death deprived the United States of one of its wisest counselors.

Here in Italy where his memory is so alive and where so many have heard FERMI lecture I do not have to describe the remarkable fascination he could induce in any audience. He used no histrionics in his delivery. It was always calm and deliberate. The fascination lay in the feeling of clarity and simplicity he could impart to the audience. They felt illuminated and had the sense of partecipating in profound and beautiful insight.

With his students FERMI was friendly but not soft. He never asked them to do less than they could accomplish. In them he inspired a feeling which was very close to worship. What greater memorial can a teacher, a scholar leave behind him than a group of students who will keep his memory alive and carry out his dreams and insight for generations to come? It is a greater memorial than any monument in marble because it is alive in the hearts and minds of men.

Not only in the history of science in books and periodicals but in living men and women all over the globe irrespective of race, creed or color the memory of FERMI will live on. FERMI, a son of Italy, will live on as an inspiration for scientists for generations to come.

SUPPLEMENTO AL VOLUME II, SERIE X
DEL NUOVO CIMENTO

N. 2, 1955
2° Semestre

VII

Il fascicolo delle lezioni svolte a Varenna, nella Villa Monastero, nel Corso Internazionale di Fisica del 1954.

G. POLVANI

Presidente della Società Italiana di Fisica.

La Società Italiana di Fisica, quando costituì la Scuola Internazionale di Fisica, deliberò che le lezioni che nella Scuola si sarebbero svolte, fossero ogni anno pubblicate in un numero speciale del *Supplemento* al *Nuovo Cimento*, e ciò non solo perchè rimanga documentata l'attività della Scuola, ma ancor più perchè possano giovarsi di quelle lezioni anche quanti non abbiano partecipato ai Corsi.

Fu così l'altr'anno pubblicato il fascicolo relativo al Corso del 1953 ed ora esce quello relativo al Corso dell'anno passato.

Il fascicolo, di ben quattrocentosettanta pagine, rispecchia fedelmente l'attività svolta; e nelle sue prime ottanta pagine raccoglie le sedici lezioni che ENRICO FERMI dettò, iniziandole la mattina del 19 Luglio e terminandole, un anno fa preciso, il venerdì 6 Agosto 1954.

La sera di quel venerdì, vigilia della sua partenza, ricordo che egli mi confidava di essere molto preoccupato per la pubblicazione delle sue lezioni. Il testo di queste, raccolto sui registratori magnetici e steso dagli allievi, risentiva troppo della forma originaria discorsiva tanto diversa da quella normalmente seguita nelle opere a stampa. ENRICO FERMI, che pure aveva riguardato in gran parte gli appunti stesi dagli allievi, avrebbe tuttavia desiderato rimaneggiare e sistemare il testo, e si rammaricava di non averne tempo nè modo. Pareva presentisse la sua prossima fine.

Con trepido rispetto e grande amore il prof. BERNARD T. FELD del Massachusetts Institute of Technology di Cambridge, il prof. GIANPIETRO PUPPI, Direttore del Corso del 1954 e noi tutti della Direzione, Redazione ed Editoria del giornale abbiamo curato la pubblicazione di queste lezioni di FERMI, conservandole, così, quanto è possibile, fedeli alla sua parola pronunciata. Esse

pertanto sono veramente l'estremo dono che con la sua voce egli ha dato ai fisici di tutto il mondo.

Leggendole, chi lo ha conosciuto, chi lo ha ascoltato, lo rivede là, sulla cattedra, nell'Aula di Villa Monastero, sotto la luce tagliente che scende dall'alto delle tre lavagne, parlare deciso con quel caratteristico suo caldo entusiasmo, che il partecipare agli altri il suo sapere gli conferiva.

Da oggi, per suscitare la presenza del suo spirito ed ammonire al dovere di maestro, là a Varenna, nell'Aula, sono una fredda pietra e un livido bronzo. Purtroppo la consumata perizia dell'artista e l'ispirazione del letterato non riescono, in quanti avevano sperato — come FERMI stesso aveva fatto sperare — di riavere lui con noi e per noi là a Varenna, ad attutire il dolore dell'irreparabile perdita: anzi più acerbo lo rendono.

A noi rimangono, ultimo bene, queste sue lezioni. E come atto di gratitudine e come testimonianza di ammirazione per il Maestro e per lo Scienziato, abbiamo voluto che tutto il fascicolo fosse dedicato alla memoria di lui, ENRICO FERMI.

A loro, gentili Signore, congiunte del grande Estinto, torni gradito dono questo fascicolo che, prezioso per il contributo da lui dato, è materialmente ben poca cosa di fronte al beneficio che noi da lui stesso ricevemmo.

E grazie anche di aver gradito, come gradiranno quanti hanno a cuore la nostra scienza e amano i nostri scienziati, che la Scuola Internazionale di Fisica della Società Italiana di Fisica s'intitoli, giusta una deliberazione del Consiglio di Presidenza, al nome immortale di ENRICO FERMI.

E anche a lei, on. rappresentante del Ministro, e a lei, Presidente dell'Ente Villa Monastero, torni ugualmente gradito questo dono in riconoscente testimonianza di quella stretta collaborazione che è al sommo delle nostre menti e nel profondo dei nostri cuori.